Mathematical Problems in Engineering

Recent Advances in Many-objective Optimization for Mathematical Complex Problems

Lead Guest Editor: Amandeep Kaur
Guest Editors: Shivani Goel and Wattana Viriyasitavat

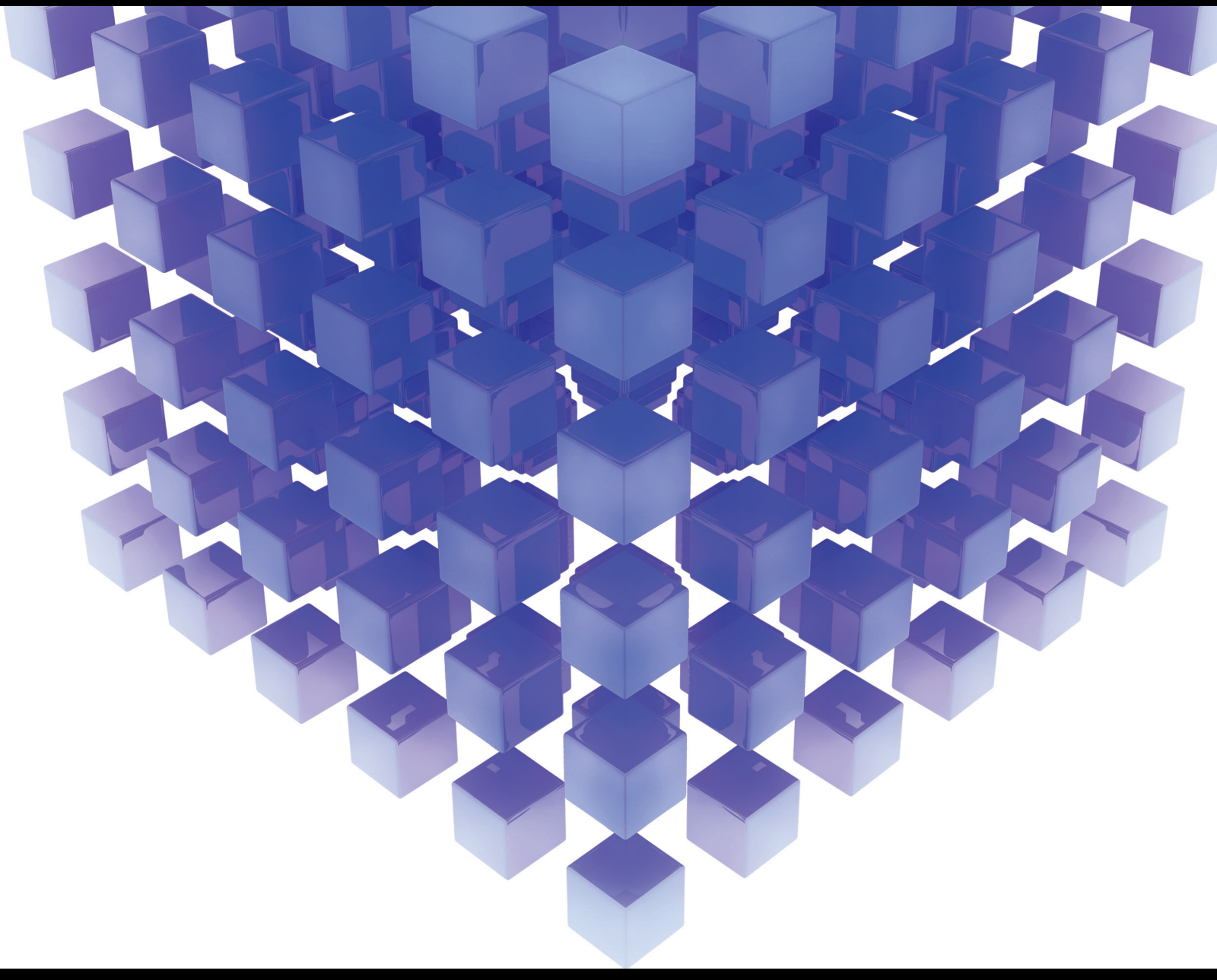

Recent Advances in Many-objective Optimization for Mathematical Complex Problems

Mathematical Problems in Engineering

Recent Advances in Many-objective Optimization for Mathematical Complex Problems

Lead Guest Editor: Amandeep Kaur
Guest Editors: Shivani Goel and Wattana Viriyasitavat

Chief Editor

Academic Editors

Contents

Contents

Hindawi
Mathematical Problems in Engineering
Volume 2022, Article ID 4825212, 13 pages
https://doi.org/10.1155/2022/4825212

Research Article

Optimization and Simulation of Monitoring Technology of Blasting Rock Movement Trajectory Based on the Improved SVM Algorithm

Jianyang Yu,[1,2] **Xiaobo Liu**,[2,3] **Liancheng Wang**,[2] **and Hao Wu**[2]

[1]*Key Laboratory of Ministry of Education on Safe Mining of Deep Metal Mines, Northeastern University, Shenyang 110819, China*
[2]*Intelligent Mine Research Center, Northeastern University, Shenyang 110819, China*
[3]*Civil and Environmental Engineering School, University of Science and Technology Beijing, Beijing 100083, China*

Correspondence should be addressed to Jianyang Yu; yujianyang310@126.com

Received 30 May 2022; Accepted 27 July 2022; Published 4 October 2022

Academic Editor: Amandeep Kaur

In most cases, the blasting object is the rock mass. Because the rock mass has the characteristics of anisotropy and inhomogeneity, there are often structural surfaces such as joints, fissures, faults, and weak interlayers, but details are basically impossible. Compared with the rock, these structural surfaces are weak parts, and the explosive energy required for breaking is smaller. It is difficult to take into account the existence of each weak side when the explosives are arranged in the blasthole. Therefore, after the explosive explodes in the rock mass, the explosive gas will first rush out from these weak parts, entraining individual fragments to form flying rocks. Aiming at the problem that it is difficult to accurately obtain the rock motion information in the blasting process of open-pit mines, this paper selects the kernel function to establish the support vector machine model and optimizes the parameters of the support vector machine model to obtain the optimal blasting rock trajectory prediction model. Under the protection of special protection devices, the information of the rock movement during the blasting process is collected at a higher frequency, and the analysis algorithm of the rock movement characteristics is researched on the basis of inertial navigation technology. The algorithm is used to analyze and output the rock movement. The curve of velocity, position, and kinetic energy provides a theoretical and technical basis for the study of rock movement law in the blasting process of open-pit mines. Through the experimental analysis, based on the cross-validation method, through the support vector machine model parameter optimization and comparison evaluation parameters, the optimal prediction model of the blasting rock trajectory is obtained as the support vector machine model based on the radial basis kernel function. The mean value of root mean square error and mean absolute error of this model are 0.102 and 0.0674, respectively, and the performance is the most robust among the three types of models.

1. Introduction

Blasting is an important means of open-pit mine production. The blasting process releases huge energy, a part of which is used to break the rock mass, and a part of it is used to throw the broken ore rock. The movement speed changes and movement trajectories of the ore rock at different positions during the blasting process are studied. The characteristics and laws can reflect various situations such as energy efficiency, ore depletion, and safety risks in blasting production and provide a scientific basis for the evaluation of blasting effects [1, 2]. Relevant scholars have done a lot of research work on the movement characteristics and laws of ore rock during the blasting process, mainly using the following methods. One is the high-speed photography method combined with the theoretical analysis method. By monitoring the blasting process and combining the blasting funnel theory, the velocity distribution of ore and rock and the proportion of explosive energy in each part of the blasting process are established, so as to provide a basis for

the adjustment and optimization of blasting parameters. One is to use color marking to mark the ore and rock before blasting and pass the mark after blasting the ore to measure the movement of ore and rock and combine the empirical formula to establish a ore-rock movement model, so as to determine the amount of waste rock mixed into the ore during the blasting process. The rock movement is more convenient to measure [3]. With the development of computer technology, more and more scholars use model experiments and numerical simulations on the basis of theoretical research to study the movement characteristics and laws of blasting ore and rocks, so as to provide reference for the safety protection of flying rocks during blasting. In recent years, with the emergence of machine learning and artificial intelligence, some scholars have used different learning algorithms to learn from previous blasting data and established rock movement models based on different blasting parameters to predict the movement of blasted rock [4, 5].

However, the environment of the blasting site is very harsh. The high-speed photography method is affected by the blasting smoke at the blasting site and cannot completely monitor the movement process of the ore rock. Due to the uniqueness and complexity of rock masses at different blasting sites, the accuracy and authenticity of methods such as model experiments, numerical simulations, and machine learning based on theoretical methods are insufficient [4]. Since the inertial sensor can collect and store the corresponding motion information at a higher frequency when it moves with the object, and has a built-in independent power supply, it can work normally without relying on the outside world [6–9], so it has special protection. In the case of the device, the movement information of the ore rock can be collected during the blasting process. Therefore, this paper proposes an experimental research method based on the inertial navigation technology to study the characteristics and laws of the blasting rock movement. It is proved by field experiments that this research method has obvious advantages compared with other research methods, which can accurately obtain the real movement characteristics of ore-rock movement.

As an important technology for mining, blasting technology has an indispensable position. In the underground ore mining of mines, blasting technology is almost always used regardless of tunneling or rock-breaking mining. The rational application of blasting technology can not only improve production efficiency but also help to improve the safe production environment in the well. In view of different mine environments, selecting reasonable blasting parameters is the key to safe and efficient production, so the optimization of blasting parameters is a topic that has received much attention. There are many ways to optimize the selection of blasting parameters mainly through comparison with the mature experience of similar mines and calculation of formulas. With the rapid development of computer technology, the optimization and selection of parameters in recent years has gradually been combined with intelligent algorithms, which has also become the blasting parameter. The method of obtaining blasting parameters through the on-site blasting test is reliable, but the cost is high and the efficiency is poor. For the research of blasting parameter optimization that requires a large amount of statistical data, the on-site test is not suitable. In order to improve the optimization efficiency of blasting parameters, the research of blasting parameter optimization in this paper mainly selects the means of combining the support vector machine model with the practice.

The innovations of this paper are as follows: Since rock blasting is a complex nonlinear system affected by multiple factors, the prediction of blasting rock trajectory is a multivariable prediction problem. This paper improves on the basis of the support vector machine model and establishes the prediction model of blasting ore, and the rock trajectory is verified, and the validity of the model prediction is verified by the cross-validation method.

The paper is arranged as follows: Chapter 1 introduces the related research on rock blasting parameters by relevant scholars and makes a summary based on the above research; Chapter 2 introduces the support vector machine and improves it based on the traditional model; Chapter 3 explains the blasting experiments carried out in this study which is cross-validated based on the experimental results; and the fourth chapter is the total of the full text.

2. Related Work

The damage degree and process control of explosives to rock are mainly realized by blasting parameters. Regarding the determination of blasting parameters, many scholars at home and abroad have conducted a lot of research on it, and some scholars have tried to give clear and unified conclusions. Therefore, there is no theory and conclusion about the calculation of blasting parameters that can be adapted to all production environments [10].

Gilbride successfully applied photography and related analysis techniques to parameter optimization research and successfully improved production efficiency and reduced production costs at the same time [11]. Taylor and Firth in order to study the influencing factors of blasting rock fragmentation applied the principal component analysis methodand also used the multivariate statistical method [12]. Yennamani used artificial neural network to study the relationship between blasting backflush and its related rock and explosive and hole network parameters. After optimization, very good results are obtained [13]. La Rosa and Thornton applied multiple flash imaging technology to the statistics of blasted ore-rock trajectory, which not only improved its measurement accuracy but also saved a lot of manpower and greatly improved the efficiency of related research [14]. Amini et al. used Kuz-Ram and Monte Carlo simulations to predict blasting parameters, and the final results were proved to be reasonable and efficient [15]. Manoj and Monjezi proposed to select seven factors such as the angle of internal friction, severity, in-situ leaching, injection strength, cohesion of the topsoil layer, and fully weathered ore layer to conduct orthogonal experiments. The experimental results were analyzed using the principle of response surface methodology, and established a model to

predict the stability of the in-situ leaching slope of ionic rare Earth ore [16]. Ohadi et al. intelligently optimized the blasting parameters using the KCO model, the Bond-Ram model, the Kuz-Ram model, and the EBT model and optimized the blasting parameters [17]. Yu et al. used the empirical formula method to optimize and adjust the number of blasting holes in railway tunnels and, at the same time, used the comparative research method to optimize and adjust the hole spacing and row spacing, and the optimization effect was obtained for improvement [18]. Sastry et al. used the existing blasting design, according to their existing data, combined with new requirements and new technology, and well completed the drilling and blasting method parameter optimization research [19]. Kourepenis et al. calculated and determined the blasting parameter design scheme based on experience and actual engineering needs when the blasting design scheme was uncertain [6]. Aggarwal et al. used empirical formulas to optimize blasting parameters such as blasthole row spacing, minimum resistance line, blasthole density coefficient, and bottom distance in a mine and achieved good results [7]. Shaeffer used the empirical formula to determine the charge consumption and the number of blastholes in the optimization study of blasting parameters for ore and rock excavation [8]. Perlmutter and Breit proposed to use the limit equilibrium method and discrete element numerical simulation to analyze the stability and failure mode of the open-pit mine slope on the basis of determining the relevant parameters of the slope stability. The problem is widespread, and the situation of high, steep, and complex rock slopes in large open-pit mines is particularly prominent [9].

In summary, intelligent computing and numerical simulation technology will be more and more frequently used in blasting parameter optimization research and future development direction. The previous research results have promoted the development of rock blasting to a certain extent, but the research on the prediction model of mineral rock blasting in some literatures has a small number of data samples, and the data selection is subject to a certain degree. The sample is not generated by random sampling; in addition, most of the models in the literature are tested only once, and the chance is large, which cannot prove the universality of the model.

3. Support Vector Machine Model Introduction and Algorithm Improvement

3.1. The Basic Idea of SVM. A support vector refers to the input x for some training points in the training set. The support vector machine method is a supervised learning method; that is, the category of the training point is known, and the correspondence between the training point and the category is obtained so as to separate the training set according to the category or predict the category corresponding to the new training point. In a nutshell, the support vector machine method is a classification method that firstly transforms the input space into a high-dimensional space through the Philippine linear transformation defined by the inner product function and then finds the optimal classification surface in this space. It shows many unique advantages in nonlinear and high-dimensional pattern recognition and can be extended to other machine learning problems such as function fitting.

The idea of support vector machine is created based on the optimal classification surface on the basis of linear separability, and its principle is shown in Figure 1.

In Figure 1, the optimal classification surface is relative to the multidimensional space. In the two-dimensional space, the optimal classification surface is the optimal classification line, which can accurately separate two types of data samples under the premise of ensuring the minimum empirical risk and make it the largest interval, that is, the largest classification interval.

Suppose there are two types of linearly separable sample sets (x_i, y_i), $i = 1, \ldots, n, x_i \in R^d, y_{i\in}[1, -1]$, then define $f(x) = \omega x + b$ as the form of the discriminant function. This form has parameters that need to be adjusted but must be linear. The response equation is shown as

$$\omega x + b = 0. \tag{1}$$

The first job to be done is to normalize the discriminant function to ensure that all samples under different classifications must meet the constraints. It can be deduced that all classification straight lines must be within the range represented by the following equation and make the correct classification, as

$$y_i[(\omega x_i) + b] - 1 \geq 0, \quad i = 1, \ldots, n. \tag{2}$$

The distance from the sample point to the hyperplane is

$$d = \frac{wx + b}{\|w\|}. \tag{3}$$

The distance of the classification line from which the response is obtained can be expressed as $2/\|w\|$, and the largest classification distance is equivalent to the smallest value of $\|w\|^2$, that is, the optimal classification hyperplane. In the case of a given sample, the selection of SVM parameters will first affect the learning ability of its model. Some scholars pointed out that the parameter selection of support vector machine not only determines its learning performance but also the size of the parameters which has a great influence on the scale of the hypothesis space and the search method of the space. In the support vector machine, it can be seen from the above description that the accuracy of the model is a contradictory community for the parameters, and the relationship between its own complexity and the parameters is also the same. For different situations, the selection of parameters is also different, and a trade-off needs to be made. The choice of parameters determines the performance of the support vector machine model. How to use the algorithm to obtain the optimal parameter combination is a problem that the support vector machine must consider. Parameter selection is the key to the quality of the support vector machine model. Manual selection is not only time-consuming and labor-intensive but also the found parameter group may not be optimal, but parameter selection can be treated as an optimization problem. Therefore, this paper

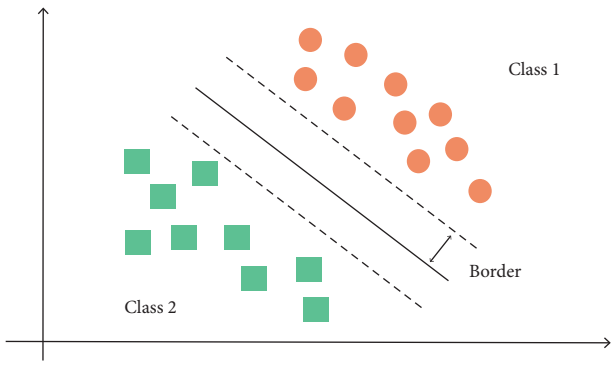

Figure 1: Basic idea of support vector machine.

considers the intelligent optimization algorithm and introduced the optimization of support vector machine parameters.

3.2. Improvement of the Support Vector Machine Algorithm Based on the Kernel Function. In order to make the support vector machine model have the best generalization ability, it is mainly necessary to do two things: the first thing is to choose a kernel function; the second thing is to choose an intelligent optimization algorithm to let the model obtain a set of optimal parameter combination. At present, the selection of the kernel function is generally a single kernel function. Based on the summary of the advantages and disadvantages of the polynomial kernel function and the Gaussian radial basis function, this paper forms a mixed kernel function of the polynomial kernel function and the Gaussian radial basis function. At the same time, the intelligent optimization algorithm used in this paper is an improved differential evolution algorithm. Finally, an improved support vector machine model is established.

In the support vector machine, to select the kernel function to map the nonlinear input to the high-dimensional feature space, this paper defines the characteristics of the kernel function based on the calculation requirements of the blasting rock trajectory as

$$K(u,v) = \sum_{k=1}^{\infty} \alpha_k \phi(u)\phi(v). \tag{4}$$

It is guaranteed that the symmetric function $K(u,v)$ under L_2 is expanded with a positive coefficient $\alpha_k > 0$ as

$$\int g^2(u)\mathrm{d}x < \infty. \tag{5}$$

Due to the complex factors affecting the blasting rock trajectory in the mining area, a single kernel function is often unable to achieve satisfactory prediction results. However, there are many types of kernel functions, and there is no good experience on how to choose the kernel function well. But if the kernel function is classified, it can be roughly divided into two types: the first type is the global kernel function, and the second type is the local kernel function. The polynomial kernel function is an excellent representative of the first type of global kernel function. Its advantages are that it has a strong generalization ability and a good globality in extracting data. Among them, the excellent representative of the second largest type of local kernel function is the Gaussian kernel function, which has the advantage of good learning effect, and the disadvantage is its poor generalization ability.

The first type of global kernel function and the second type of local kernel function have different performances; therefore, in terms of their performance, the first type of global kernel function and the second type of local kernel function should be considered. These two kernel functions construct a new type of kernel function according to a certain proportional relationship, as shown in Figure 2.

Although support vector machines and neural networks are both nonlinear classification models, support vector machines consist of single hidden layer, which mainly realize nonlinear classification through the trick of kernel function. The direction of the line of least resistance is the direction with the least rock resistance, and it is also the direction which is most likely to generate flying rocks. When the minimum resistance line is too small, after the explosive explodes, only a part of the energy is enough to break the rock in the direction of the resistance line, and the excess energy throws the broken rock forward, producing more and farther flying stones. When the minimum resistance line is selected is too large, the energy generated by the explosive is not enough to overcome the resistance of the rock in the direction of the resistance line, but the energy of the explosive needs to be released, so it is easy to produce rush guns at this time, which is followed by flying stones. Since the foundation of SVM is statistical theory, it has rigorous theoretical and mathematical ideas, which can overcome the unavoidable problems of neural network. At the same time, the SVM also has relatively strong approximation ability and generalization ability.

4. Experimental Design and Analysis

4.1. Experimental Site. In order to analyze the movement law of ore rock in the process of slag blasting in the open pit and the influence of the residual blasting pile on the movement of nearby ore rock, this paper selects the 31st bench blasting in the south mining area of Qidashan open pit as the experimental site, and the bench elevation is −120 m–105 m, section height is 15 m, blasting step length is 132 m, step width is 20 m–28 m, slope angle is 65°, step area is 3168 m^2, total volume is 47520 m3, and step rock volume is 104664 tons. The steps mainly include migmatites such as gray-white or flesh-red gneiss-like structure, anisotropic full-crystalline structure, and massive structure. The blasting type of the experimental blasting area is slag blasting, with a total of 62 blastholes. The rectangular hole arrangement is adopted, the hole spacing is 7.5 m, the row spacing is 6 m, and the blasting is carried out hole by hole. The stage height is 15 m, the explosive types are emulsion explosives and ammonium explosives, the maximum charge per hole is 650 kg, and the total designed charge is 37000 kg. The filling height is 8.5 meters, and the blasthole is filled with gravel. The length of the bus used for detonation is 600 m, and the

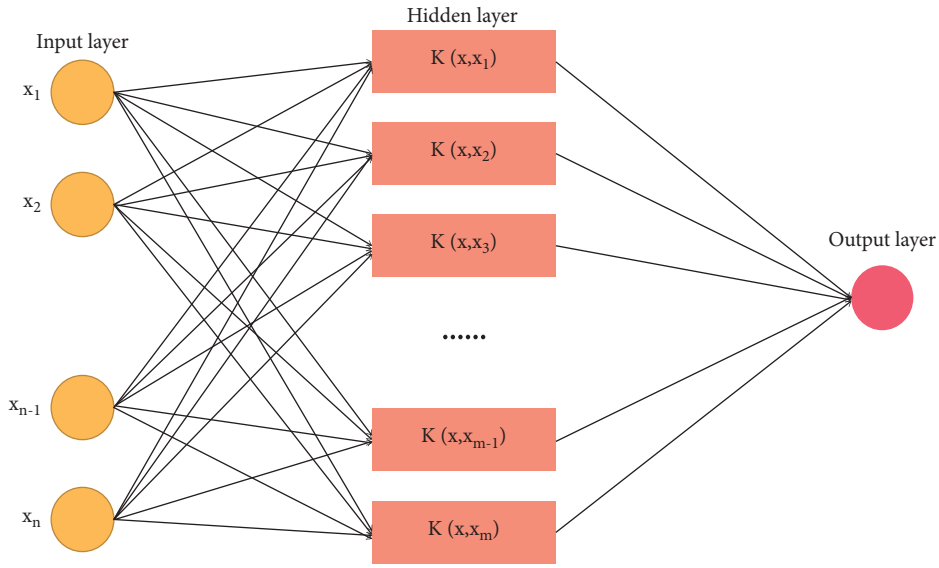

Figure 2: Structure diagram of the improved support machine.

combination of series and parallel connection is adopted. There are 130 detonating bombs, and 210 400 ms detonators are used in the hole, and 4 detonators of 25 ms, 20 detonators of 42 ms, and 41 detonators of 65 ms are used on the ground to detonate the entire blasting area for connecting.

4.2. Experimental Equipment. In this study, a high-precision MEMS inertial navigation sensor with automatic storage function is selected. The sensor size is 51.3 mm ∗ 36 mm ∗ 15 m and has an SD card slot. When the SD card is inserted, it will automatically turn on and work. There is an independent power supply inside, which can continuously, completely, and independently work for up to 5 hours, and the sensor records the acceleration and angular velocity of the three axial directions, respectively, at a frequency of 200 Hz. Among them, the acceleration accuracy is 0.01 g, and the angular velocity accuracy is 0.05°/s. The details of the sensor are shown in Figure 3.

According to the actual size of the sensor and the hole diameter of the blasthole, the design scheme of the special protection device for the sensor is determined. According to the design, the protection device is divided into two layers: inner and outer layers. The inner layer is a cuboid structure, which chooses PE pearl cotton material for production and uses soilworks software to carry out mechanical numerical simulation of the design protection device before production to determine its protection effect on the sensor, and the design diagram of the protection device is shown in Figure 4.

The protection device is made according to the design plan. In order to facilitate recycling and weighting, a color protection bag with better quality is equipped on the outside of the protection device, and the weight is placed in the protection bag to make its weight similar to the weight of the rock. The physical protection device is shown in Figure 5.

Figure 3: Inertial sensor for the experiment.

4.3. Experimental Process Design. In this paper, the support vector machine is used to predict the blasting rock trajectory. First, the rock pressure monitoring data sequence is normalized, then the embedded parameters of the phase space are determined, and then the phase space of the rock pressure monitoring data sequence is reconstructed. Then, the training sample set is established, then the test sample is set, and the prediction model is trained with the training sample set, and finally, the validity of the trained prediction model is verified with the test sample set. In order to avoid the too different magnitudes of each variable in the input variables affecting the training effect, the training data samples of the support vector machine should be normalized. When using the support vector machine to predict the mine pressure monitoring data, the radial basis function is used with the kernel function, and the cross-validation

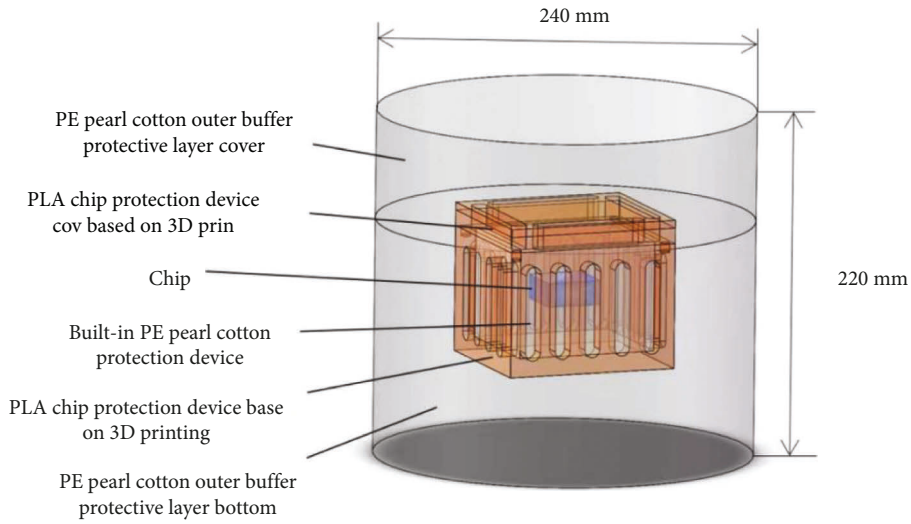

Figure 4: Design of the protection device.

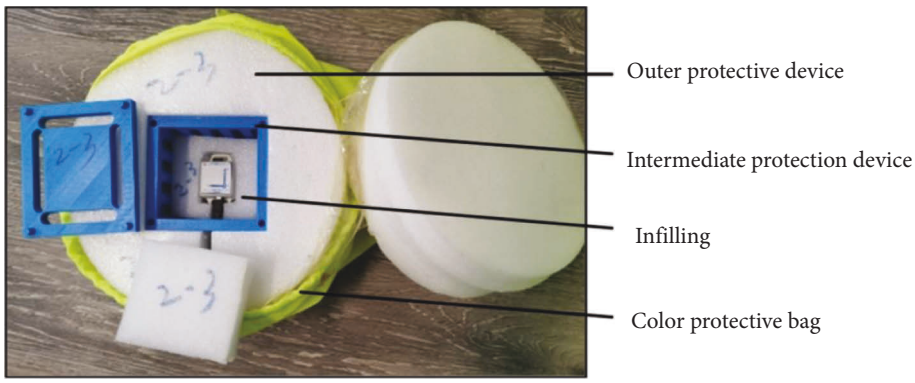

Figure 5: Entity diagram of the protection device.

method is used to optimize the parameters of the penalty parameter X_i and the kernel function y_i as

$$X_i = \overline{x}_i + \int X^2(x)\mathrm{d}x, \tag{6}$$

$$\begin{aligned} y_i &= f(X_i) \\ &= x_{i+1+(m-1)\tau}. \end{aligned} \tag{7}$$

The data collected on-site are analyzed and divided into training set and test set. The training set that needs to be trained is input into the neural network prediction model, the network is trained, and then the test set is input into the neural network prediction model. The effects are compared, and a more appropriate method is selected to predict the blasting effect. In the mining area, six blastholes were selected as experimental blastholes, and inertial sensors were embedded near the surface of each blasthole (not embedded in the blasthole packing). The sensors were placed horizontally, and the positive direction of the X axis was in the vertical slope in outward direction, and the sensor numbers are 1-1, 1-2, 2-1, 2-2, 3-1, and 3-2. According to the blasting design, the blasting sequence of the blastholes where each sensor is located is from morning to night: 2-2 (149 ms), 3–2 (157 ms), 3–1 (237 ms), 2–1 (298 ms), 1–2 (42 ms), and 1–1 (592 ms). The layout of the sensor is shown in Figure 6.

The main idea of the experimental method design is to embed the high-precision inertial sensor in the open stope according to the blasting site layout plan under the condition of special protection devices. In the end, recover the sensor and extract the sensor data, and then finally study the relevant data analysis to analyze the movement data of the ore rock during the blasting process so as to obtain the movement speed, kinetic energy, and trajectory of the ore rock, and study the movement law of the ore rock and technical process as shown in Figure 7.

The specific process of the experiment is as follows: (1) Insert the SD card into the inertial navigation sensor (automatically turn on after insertion); (2) place the sensor horizontally in the protection device according to the calibration direction of the protection device; (3) use the computer to communicate with the inertial navigation device through the data cable connecting the sensors, and then calibrate and adjust the sensor parameters; (4) embed the

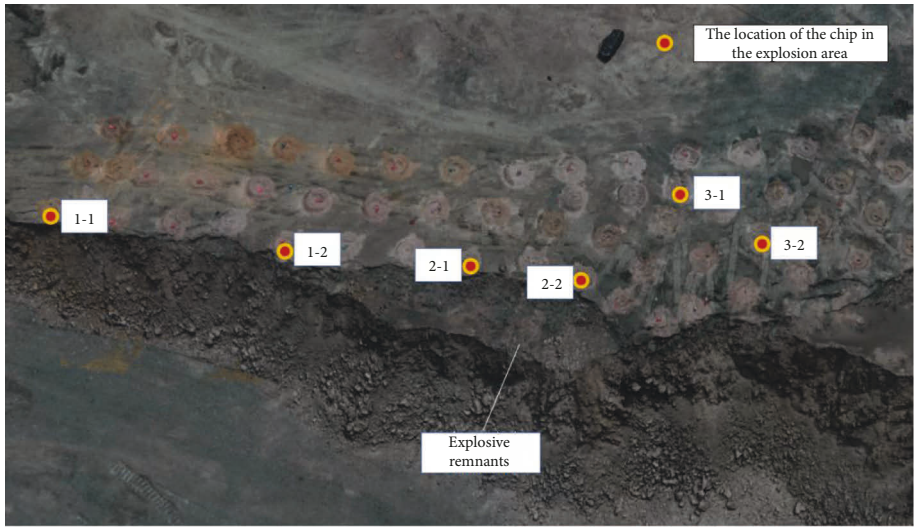

Figure 6: Sensor arrangement scheme.

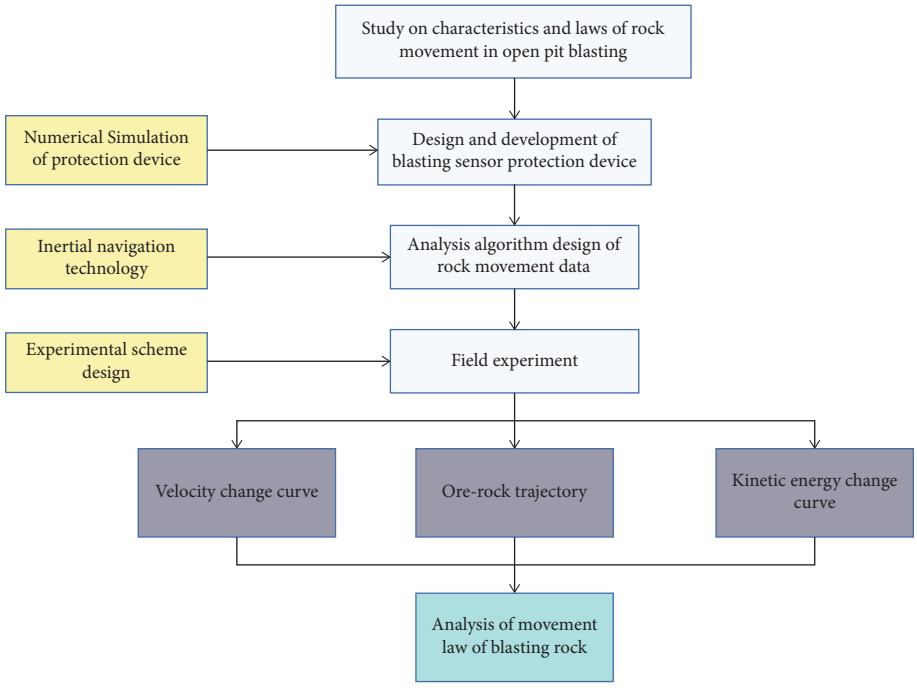

Figure 7: Experimental technical process.

protection devices in the blasting site according to the design plan; and (5) after the blasting, recover the inertial navigation sensor, take out the SD card, and extract the data.

During the blasting process of the mine, there are many factors that affect the blasting effect. All the known influencing elements are screened through the support vector machine algorithm, and the important influencing parameters are obtained as the input parameters of the support vector machine model. Support the use of the feature attributes in the support vector machine algorithm model to filter the main influencing factors, randomly give each feature a random weight, and select a certain number of features each time, with the previous intersection for training and learning, after continuous cycles, finally. The degree of influence of the remaining factor features on the classification task can be determined.

4.4. Prediction Based on the Improved Support Vector Machine Model. The reasons that affect the blasting rock trajectory mainly include four categories: one is blasting parameters, the second is explosive blasting parameters, the third is rock mass structure characteristics, and the fourth is physical and mechanical properties of intact rock and discontinuity. Among them, the blasting parameters include diameter of blasthole, blasthole depth, blasthole spacing, charge length,

blasthole angle, blasthole filling length, minimum resistance line, and step height. The above indicators are all controllable, while blasthole diameter is the most important indicator of the above parameters. Explosion parameters of explosives include type of explosive, density of explosives, power, and intensity. The physical and mechanical properties of intact rock and discontinuity include rock mass density, dynamic compressive strength, dynamic tensile strength, shear strength, dynamic elastic modulus, hardness, and mineral composition. The influence of the above factors on the distribution characteristics of the blasting rock trajectory is nonlinear, and it is difficult to obtain a universal empirical formula that includes all parameters. For the establishment of the ore rock trajectory prediction model for ore blasting, on the basis of fully considering the above four types of influencing factors, seven important indicators are selected, which are the ratio of blasthole spacing to resistance line, the ratio of step height to resistance line, the resistance line to shot, the ratio of hole diameter, the ratio of blasthole filling length to resistance line, the unit consumption of explosive, and in-situ block size and elastic modulus.

The data collected at the mine blasting site is analyzed and divided into training set and test set. The training set that needs to be trained is input into the neural network prediction model, the network is trained, and then the test set is input into the neural network prediction model. Then it is compared with the actual effect, and a more appropriate method is chosen to predict the blasting effect. The effective blasting data are obtained by selecting 10 groups of ore rocks, as shown in Table 1. Among them, 0 means that the blasting effect is good, 1 means that the blasting effect is good, and 2 means that the blasting effect is average.

When evaluating the blasting rock trajectory prediction model, two indicators, root mean square error (RMSE) and mean absolute error (MAE), are selected. Among them, RMSE is used to measure the deviation between the observed value of the model and the true value. The MAE can better reflect the actual situation of the predicted value error. Generally speaking, the smaller the value of the two, the more robust the model, and the better the performance. The calculation formulas of the two evaluation indicators are (9)

$$\mathrm{RMSE} = \sqrt{\frac{\sum_{i=1}^{n}\left(x_i - \widehat{x}_i\right)^2}{n}}, \tag{8}$$

$$\mathrm{MAE} = \frac{\sum_{i=1}^{n}\left|x_i - \widehat{x}_i\right|}{n}. \tag{9}$$

4.5. Analysis of Experimental Results. Put the data in the inertial sensor SD card on the computer, read the data through the sensor host computer and save it in txt text format, then convert the txt format data into Excel format and then perform data interception, and remove a large amount of useless data recorded before and after blasting and keep blasting. Useful motion data during the period contains the data content which includes the acceleration of the three axes (ax, ay, az), the angular velocity of the three axes (ωx, ωy, ωz), and the inertial navigation trajectory solution written in MATLAB software. The algorithm program performs data calculation, and the motion trajectory of each sensor is shown in Figures 8, 9, 10, 11, 12, and 13.

Table 1: Sample data sheet.

Minimum blasting resistance line/m	Unit explosive consumption/ (kg/m^3)	Blasting funnel angle/(°)	Working face width/ m	Real effect
3.927	1.256	125.37	32.5	0
3.476	0.894	140.24	34.6	0
4.569	0.884	135.36	29.5	1
4.326	1.324	134.63	30.6	0
3.326	1.136	142.58	33.5	0
2.969	0.836	125.51	33.3	2
2.453	0.967	123.36	38.5	0
3.656	1.013	133.85	36.6	0
3.337	0.804	137.93	29.9	1
2.969	0.934	129.81	30.9	0

Since the experimental stope is blasting with loose slag, sensors 1-1 and 1-2 are located near the outermost row of blastholes, that is, near the slope, and there is no blasting pile left from the previous blasting outside the slope, which is a normal slope; sensor 2-1 and 2-2 are located near the side slope but compared with the first group, and there are explosive piles left from the previous blasting outside the slope; sensors 3-2 and 3-2 are located near the middle blasthole of the stope, and the slope is far away.

Figure 14 and 15 show the distribution diagrams of the root mean square error and the mean absolute error generated by different kernel functions in the prediction process through multiple experiments.

It can be seen from Figures 14 and 15 that the radial basis kernel function is the kernel function with the highest recognition rate and the best performance, and the mean value of the root mean square error and the mean absolute error of the blasting rock trajectory prediction model is the lowest, which are 0.102 and 0.0674, respectively. The evaluation indexes of linear kernel function and radial basis kernel function are relatively similar. In the fifth experiment, the performance of the linear kernel function is slightly higher than that of the radial basis kernel function, but the other nine experiments have proved the superiority of the radial basis kernel function. This shows that the optimal model is determined by only one random experiment, and the random error is large, and it is more scientific and reasonable to use the mean value of the evaluation parameters as the criterion for the optimal model through multiple random experiments.

The motion trajectory of each sensor as a whole shows that it is thrown up and then dropped. During this period, there is a certain horizontal displacement. The direction and size of the horizontal displacement of each sensor are different. The direction of the horizontal displacement shows a certain randomness, and the horizontal displacement is the largest. The sensor 1-2 is about 11.5 m, the direction is along

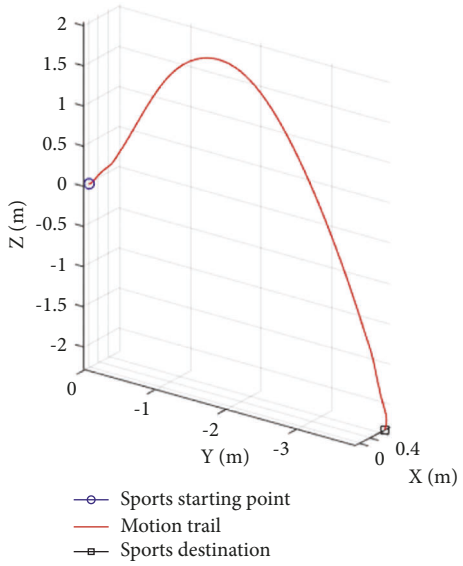

Figure 8: Movement track of sensor 1-1.

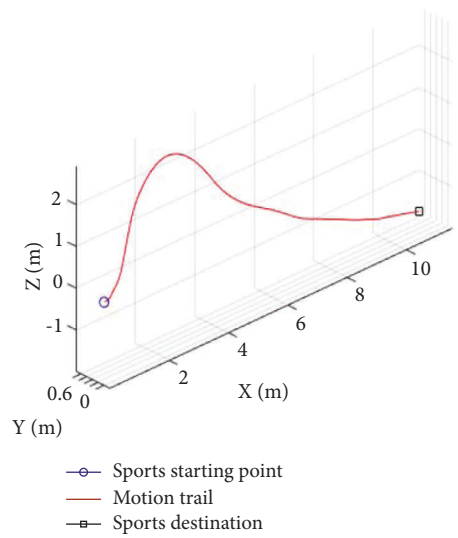

Figure 9: Movement track of sensor 1-2.

the positive direction of the X-axis, the horizontal displacement of other sensors is about 3 m, and the direction is random, indicating that when the X-axis; in the vertical direction, the largest upward displacement is sensor 3-1, which is about 5.3 m, and the smallest upward displacement is sensor 1-1, which is about 2 m; the largest downward displacement is sensor 2-2, which is about 4.8 m, and the smallest downward displacement is sensor 2-1, which is about 0.2 m. By comparing the three-dimensional models before and after the stope blasting, the placement of all sensors conforms to the actual situation on-site.

By analyzing the direction and size of the horizontal displacement of the sensor, it is shown that the movement direction of the sensor near the slope position is mainly along the direction perpendicular to the nearest free surface, and the smaller the distance from the free surface, the greater

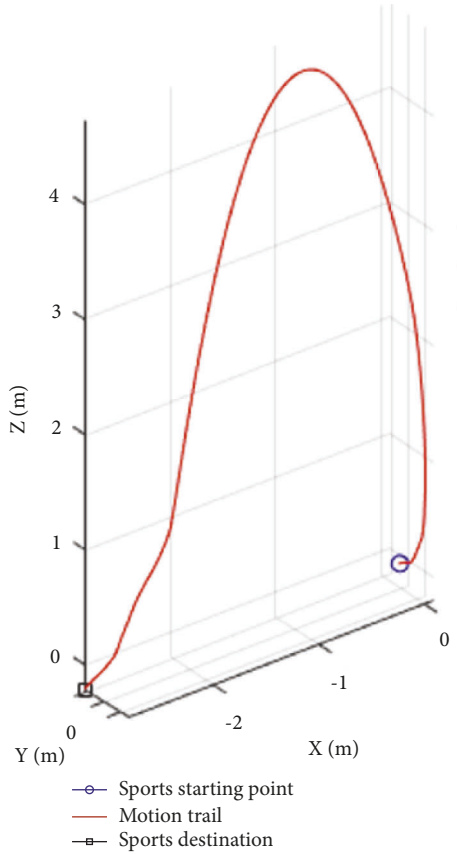

Figure 10: Movement track of sensor 2-1.

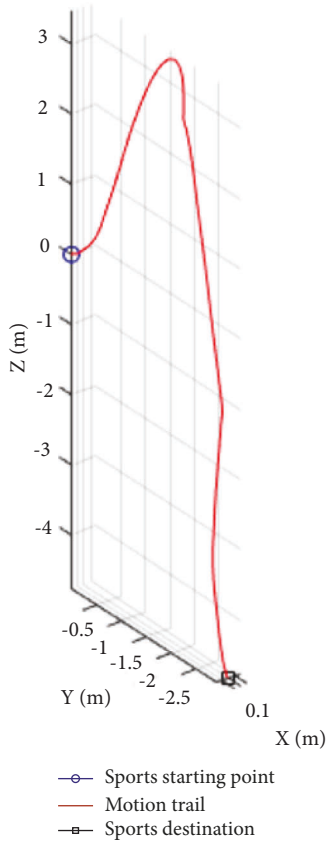

Figure 11: Movement track of sensor 2-2.

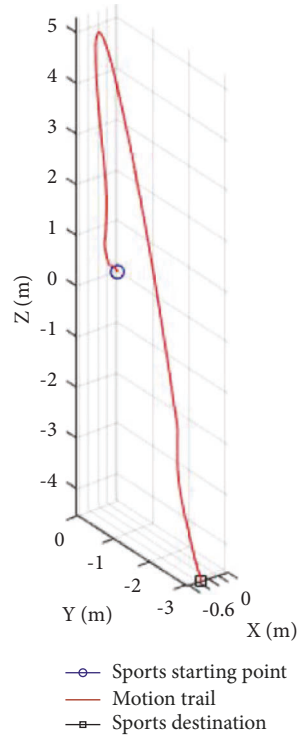

Figure 12: Sensor 3-1 motion track diagram.

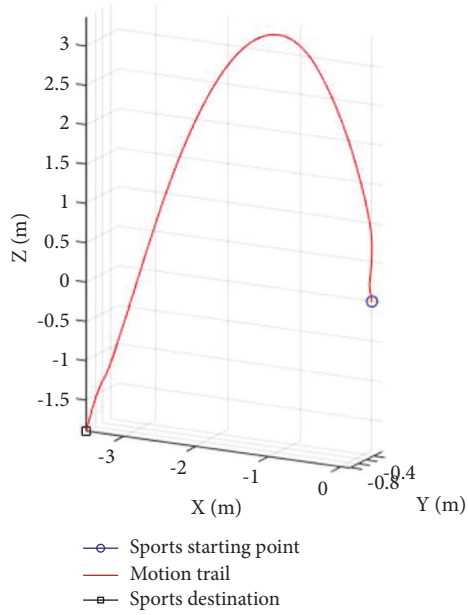

Figure 13: Movement track of sensor 3-2.

the horizontal displacement of the sensor. Among them, when the sensor is located at the edge and corner of the stope, such as sensor 1-1, its movement direction will be affected by the nearby blastholes and shifted to the direction without blastholes; for sensors 2-1 and 2-2, the free surface with the shortest distance will be changed by the influence of the residual explosion, and the movement direction will show randomness. By analyzing the uplift height of the sensor, it is found that the uplift height of the sensor at the slope position is lower than that of the sensor in the middle of the stope and the uplift height of the sensor near the slope, where there is an external explosion that is greater than that

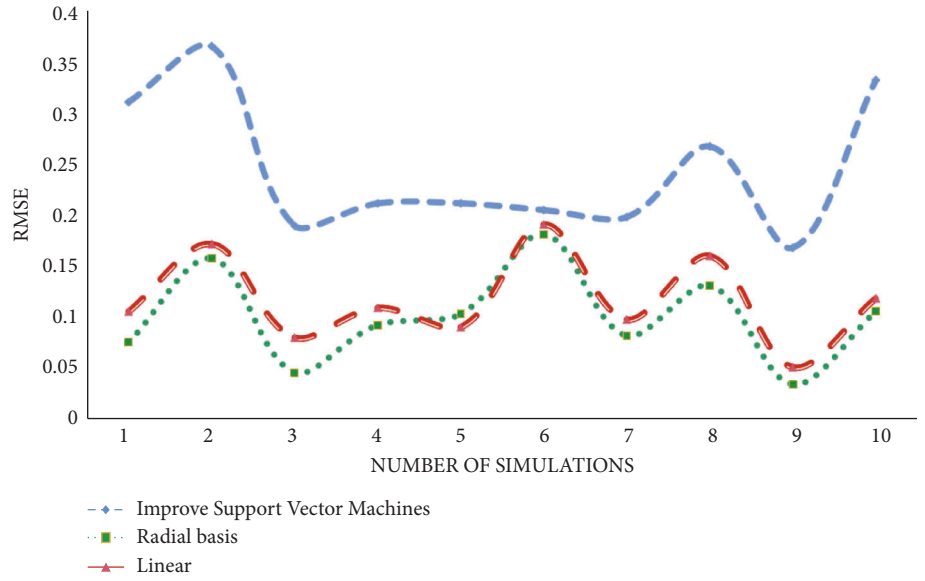

Figure 14: Root mean square error distribution of different kernel functions.

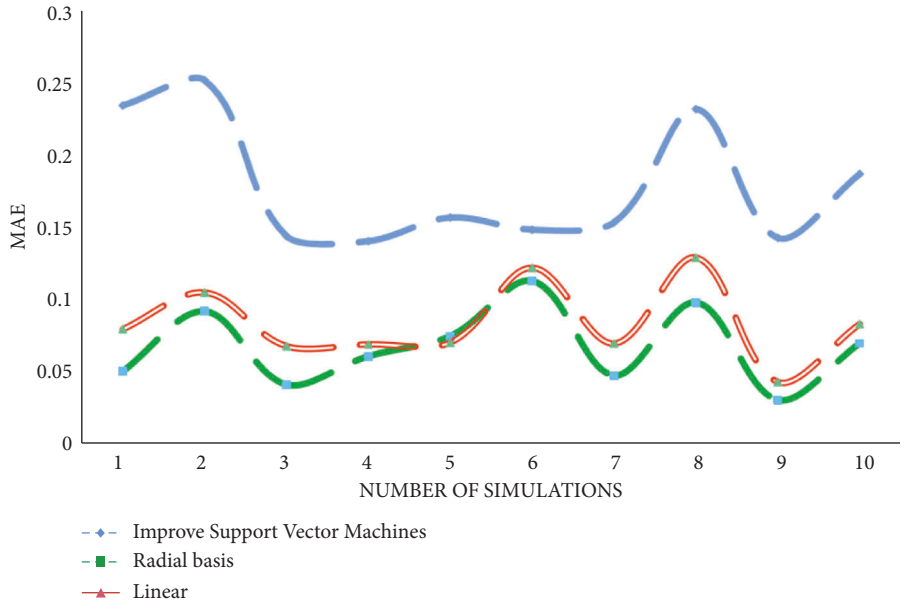

Figure 15: Distribution of the mean absolute error of different kernel functions.

of the sensor without the external explosion, indicating that the farther the blasting hole is from the free surface during the blasting process, the higher the energy acting on the vertical direction.

5. Conclusions

The main conclusions are as follows:

(i) This paper innovatively proposes a research method that uses high-precision MEMS inertial navigation sensors to monitor the movement characteristics of ore and rocks during stope blasting. The results obtained through field experiments show that this method can record more realistically and accurately. The movement state and characteristics of ore rock during blasting.

(ii) The change process of the movement speed of ore rock is divided into five stages, and each stage has a different shape; many collisions will occur during the initial acceleration process, and few collisions occur in other stages.

(iii) The movement trajectory of the ore rock shows that it is thrown up and then dropped; accompanied by a certain horizontal displacement during the period,

the ore rock at the slope position generally moves in the direction of the vertical nearest free surface, and the movement direction of the ore rock in the middle of the stope has a certain movement direction and randomness.

(iv) During the blasting process, the energy generated by the explosive mainly acts on the vertical direction, and the farther the blasthole is from the free surface position, the more energy acts on the vertical direction. The action efficiency of blasting energy is higher than that of the slope, and the action efficiency of blasting energy is higher than that of the ordinary slope.

(v) Under the full consideration of various influencing factors of ore rock blasting trajectory, the ratio of blasthole spacing to resistance line, the ratio of step height to resistance line, the ratio of resistance line to blasthole diameter, and the length of blasthole filling and resistance are selected. The ratio of the line, the unit consumption of explosives, the size of the in-situ block, and the elastic modulus, and a total of seven types of important indicators carry out research on the prediction model of the ore-rock trajectory for ore-rock blasting.Based on the cross-validation method, through the support vector machine model parameter optimization and comparative evaluation parameters, the optimal prediction model of the blasting ore and rock trajectory is obtained as the support vector machine model based on the radial basis kernel function. The mean value of root mean square error and mean absolute error of this model are 0.102 and 0.0674, respectively, and the performance is the most robust among the three types of models.

The field experiment results show that according to the characteristics of inertial sensors that can work completely independently, it is feasible to use high-precision inertial sensors to monitor the movement characteristics of ore and rock during stope blasting and the state and characteristics of rock movement during blasting. However, since the inertial sensor needs to use the median method to integrate the data once or twice with respect to time in the solution process, there is a certain error in this method, and the error will gradually accumulate with the increase of time. Therefore, in the future, in the process of research, the calculation method of the inertial sensor should be further optimized so as to make the obtained experimental data more real and reliable [20].

Data Availability

All data, models, and code generated or used during the study are included in the article.

Conflicts of Interest

The authors declare that they have no conflicts of interest.

References

[1] M. Sazid, M. R. Saharan, and T. N. Singh, "Effective explosive energy utilization for engineering blasting–initial results of an inventive stemming plug, SPARSH," in *Proceedings of the 12th ISRM Congress*, Beijing, China, October 2011.

[2] J. Park and K. Kim, "Use of drilling performance to improve rock-breakage efficiencies: a part of mine-to-mill optimization studies in a hard-rock mine," *International Journal of Mining Science and Technology*, vol. 30, no. 2, pp. 179–188, 2020.

[3] Y. h. Huang, Z. l. Mao, Z. y. Zhang, X. h. Li, and L. Yan, "Building the intelligent transportation systems based on the computation of driving velocity law of blasting fly-rock," *Cluster Computing*, vol. 22, no. S1, pp. 759–768, 2019.

[4] J. A. Sanchidrián, P. Segarra, and L. M. López, "Energy components in rock blasting," *International Journal of Rock Mechanics and Mining Sciences*, vol. 44, no. 1, pp. 130–147, 2007.

[5] E. M. Patterson, "Photography applied to the study of rock blasting," *Journal of Photographic Science*, vol. 5, no. 6, pp. 137–143, 1957.

[6] A. Kourepenis, J. Borenstein, J. Connelly, R. Elliott, P. Ward, and M. Wein, "Performance of MEMS inertial sensors," in *Proceedings of the IEEE 1998 Position Location and Navigation Symposium (Cat. No. 98CH36153)*, pp. 1–8, IEEE, Palm Springs, CA, USA, April 1996.

[7] P. Aggarwal, Z. Syed, X. Niu, and N. El-Sheimy, "A standard testing and calibration procedure for low cost MEMS inertial sensors and units," *Journal of Navigation*, vol. 61, no. 2, pp. 323–336, 2008.

[8] D. K. Shaeffer, "MEMS inertial sensors: a tutorial overview," *IEEE Communications Magazine*, vol. 51, no. 4, pp. 100–109, 2013.

[9] M. Perlmutter and S. Breit, "The future of the MEMS inertial sensor performance, design and manufacturing," in *Proceedings of the 2016 DGON intertial sensors and systems (ISS)*, pp. 1–12, IEEE, Karlsruhe, Germany, September 2016.

[10] S. Zhang, *Rock Movement Due to Blasting and its Impact on Ore Grade Control in Nevada Open Pit Gold mines*, University of Nevada, Reno, NV, USA, 1994.

[11] L. J. Gilbride, *Blast-induced Rock Movement Modelling for Bench Blasting in Nevada Open-Pit mines*, University of Nevada, Reno, NV, USA, 1995.

[12] D. L. Taylor and I. R. Firth, "Utilization of blast movement measurements in grade control," *Application of Computers and Operations Research in the Mineral Industry*, pp. 243–247, 2003.

[13] A. L. Yennamani, *Blast Induced Rock Movement Measurement for Grade Control at the Phoenix mine*, University of Nevada, Reno, NV, USA, 2010.

[14] D. La Rosa and D. Thornton, "Blast movement modelling and measurement," in *Proceedings of the 35th APCOM Symposium*, pp. 297–310, Melbourne: Australasian Institute of Mining and Metallurgy, Wollongong, Australia, September 2011.

[15] H. Amini, R. Gholami, M. Monjezi, S. R. Torabi, and J. Zadhesh, "Evaluation of flyrock phenomenon due to blasting operation by support vector machine," *Neural Computing & Applications*, vol. 21, no. 8, pp. 2077–2085, 2012.

[16] K. Manoj and M. Monjezi, "Prediction of flyrock in open pit blasting operation using machine learning method," *International Journal of Mining Science and Technology*, vol. 23, no. 3, pp. 313–316, 2013.

[17] B. Ohadi, X. Sun, K. Esmaieli, and M. P. Consens, "Predicting blast-induced outcomes using random forest models of multi-year blasting data from an open pit mine," *Bulletin of Engineering Geology and the Environment*, vol. 79, no. 1, pp. 329–343, 2020.

[18] Z. Yu, X. Shi, J. Zhou et al., "Feasibility of the indirect determination of blast-induced rock movement based on three new hybrid intelligent models," *Engineering with Computers*, vol. 37, no. 2, pp. 991–1006, 2021.

[19] V. R. Sastry, B. Raasekar, and G. R. Candra, "Assessing the explosive energy utilization in mine blasting–role of high speed videography," *Advanced Trends in Civil Engineering and Sustainable Development*, 2015.

[20] Z. Dingxiang, "A three dimensional mathematical model in calculating the rock fragmentation distribution of bench blasting in the open pit," *Explosion and Shock Waves*, vol. 3, 1984.

Hindawi
Mathematical Problems in Engineering
Volume 2022, Article ID 8101024, 10 pages
https://doi.org/10.1155/2022/8101024

Research Article

Multiattribute Group Decision-Making Method Based on Quaternary Connection Number of Cloud Models

Huabin Cheng,[1] **Yingchun Chen**,[2] **and Ping Xiong**[3]

[1]*Department of Basic Science, Wuchang Shouyi University, Wuhan 430064, China*
[2]*Science and Technology on Underwater Antagonizing Laboratory, Zhanjiang 524022, China*
[3]*College of General Education, Guangdong University of Science and Technology, Dongguan 523083, China*

Correspondence should be addressed to Ping Xiong; xiongping@wic.edu.cn

Received 9 June 2022; Revised 15 August 2022; Accepted 2 September 2022; Published 30 September 2022

Academic Editor: Amandeep Kaur

Based on the advantages of cloud theory and the connection number approach in handling uncertain information, this paper established a new quaternary connection number using the domain of interval corresponding to the centroid of a cloud model's expectation curve. Consequently, based on the cloud model theory of transformation between qualitative and quantitative uncertainties, this study suggests a model describing uncertain information more precisely by combining the advantages of quaternary connection numbers with three digital aspects of the cloud model. We defined the weighted nearness degree of the new connection number and gave a solution for finding the weight of the weighted nearness degree given that a three-parameter interval number can more precisely represent the expert's true intention than a classical interval number. The method of multiattribute group decision-making based on a cloud model's quaternary connection number was developed using a novel methodology to find the evaluation-index weight. According to a comparative analysis, the existing membership cloud gravity center (MCGC) method is nothing more than an exception to our proposed decision-making technique. It was also demonstrated that the proposal may present a more complete picture of experts' overall evaluations and communicate their preferences by adjusting the quaternion's uncertain parameters, making the group decision-making approach more widely applicable to a certain extent. The method was used to test a vessel's counterflooding capabilities to ensure its practicality and supremacy.

1. Introduction

Multiattribute decision-making (MADM) is one of the most important and ubiquitous real-life activities for selecting a suitable alternative among those required to achieve a certain goal. The information about accessing the alternatives has always been considered to be in the form of real numbers. However, in everyday life, ambiguity and insufficient knowledge make it difficult for a decision-maker to make an appraisal of an object. Zhao [1] created the set pair analysis (SPA) theory, in which certainty and uncertainty are examined as one system, to better handle uncertainties. The essential notions of SPA theory were addressed by Jiang et al. [2]. The fundamental idea behind SPA is to look at the characteristics of a set pair and create a connection number (CN) for them. To address MADM problems with a specified criteria weight and a criteria value that is an interval random variable, Wang and Gong [3] suggested a decision-making approach based on the SPA. Based on cumulative prospect theory and SPA, Hu and Yang [4] suggested a dynamic stochastic MADM. Using the TOPSIS approach, Xie et al. [5] demonstrated a CN under an interval-valued fuzzy set. Aside from this, some academics [6–9] used the SPA to handle fuzzy decision-making problems. Shen et al. [10] defined binary connection numbers (BCN) in SPA and utilized BCN to multiattribute decision-making issues in an interval-valued intuitionistic fuzzy set environment. Cloud theory, proposed by Li [11], an academician of the Chinese Academy of Engineering, is a method for resolving the fuzziness-randomness problem. The theory reveals the intrinsic relationship between fuzziness and randomness, which presented a unique algorithm architecture that simplifies the conversion between qualitative concepts and their quantitative representations. A cloud model is defined by three

digital properties (E_x, E_n, H_e), in which E_x is the primary, or most representative, value of a qualitative idea in the domain. The entropy E_n measures a qualitative concept's fuzziness and reflects the concept-accepted value range in the domain. As the entropyE_n, the hyperentropy H_e indicates the dispersion of cloud drops [11, 12].

A cloud model-based multiattribute decision-making (CM-MADM) with Monte Carlo technique is developed to address several challenges occurring in MADM problems [13]. Based on the probability theory and fuzzy set theory, the cloud model can study the detail of fuzziness of a qualitative concept membership function as well as the stochasticity by three numerical characteristics.

Currently, the cloud model is widely applied in the comprehensive evaluation, systemic decision-making, and data mining [14–16]. Many researchers have had positive outcomes in their research areas using the membership cloud gravity center (MCGC) [17], which is a common approach of evaluating a cloud model. In the study on the distribution of earnings from natural resource development, for example, Li and Zhou employed the MCGC model to show that a novel earning distribution strategy may make such distribution fair and square [18]. Combining the fuzzy extended analytical hierarchy process with the MCGC method, Zheng found a better way to manage enterprise knowledge [19]. To accurately evaluate the performance of portable devices, Peng et al. came up with an MCGC-based method [20]. Likewise, Zheng et al. put forward an MCGC-based approach to cybersecurity evaluation by introducing a cloud model to assess the cybersecurity situation [21]. Large-sample group decision-making is now made possible by the boom in big-data and computer technologies. Cloud theory is effective in presenting the opinions of large groups, whereas the dialectic set pair analysis can competently manage a matter's uncertainties on a macrolevel.

The fact that CNs and interval numbers are isomorphic is one of the key reasons why SPA can be utilized frequently in MADM with interval numbers. The CN is characterized by both certainty and uncertainty. The interval number has upper and lower bounds that have been specified, as well as uncertainty that can be arbitrarily valued within its scope. In the CN, the uncertainty coefficient might range with in the interval [−1, 1].

The particle swarm optimization (PSO) is a relatively new notion of combinatorial metaheuristic algorithm which is based on a metaphor of social interaction, namely, bird flocking or fish schooling. In [22], Chatterjee and Siarry considered nonlinear inertia weight variation for dynamic adaptation in particle swarm optimization, where a new variation of PSO model is considered which introduced nonlinear variation of inertia weight along with a particle's old velocity to improve the speed of convergence and fine-tune the search in the multidimensional space.

In this study, we developed cloud model's connection numbers, by utilizing three parameters' interval number containing upper and lower bounds as well as center of gravity. By integrating CNs in SPA, the production of a cloud model's connection numbers reveals how cloud theory renders data expression understandable within a big-data context and exposes the laws governing the uncertainty of overall information. On the theoretical basis of a cloud model and the connection numbers in set pair analysis, we proposed the following: (1) a cloud model-based method determines quaternary connection numbers, which have three digital features (E_x, E_n, H_e) of the cloud model and fully express the model's fuzzy information; (2) we coined an arithmetic weighted average nearness of quaternary connection numbers and put forth an approach to determination of the nearness's weight; (3) we raised a new method of determining the evaluation-index weight, given that the interval number expressed by three parameters can more accurately express an expert's real intention; (4) we leveraged the results from the above three steps to develop a multiattribute group decision-making method based on the connection numbers of a cloud model and through comparative analysis proved that the MCGC model is merely an exception to our proposed decision-making technique; and (5) we verified our method's practicality and superiority by adopting it in the evaluation of a vessel's counterflooding capabilities.

To do so, the rest of the manuscript is summarized as follows: Section 2 gives some overview on the cloud model and CNs. In Section 3, a cloud model's CN method for MADM has been presented under the SPA in which the assessments related to the attributes are taken in the form of quaternary connection numbers (QCNs). This section also reveals that the following: (i) the definition of weighted nearness degree of a QCN, (ii) determination method of weight of a QCN's nearness degree, (iii) determination method of index weight based on three parameters interval number, and (iv) steps of multiattribute group decision-making based on cloud theory for QCNs; and Section 4 gave the comparison of the proposed model and Section 5 studied a numerical example as a case study.

2. Basic Theories on the Cloud Model and Connection Numbers

2.1. Cloud Model Basics. The cloud model is a type of model investigating the uncertain conversion between the qualitative concepts of natural language and their quantitative representations.

Definition 1. Assume that U is a quantitative domain $U = \{x\}$ expressed by precise numerical values; C is the linguistic value connected to U; the membership $\mu_C(x)$, which shows how the x element in U falls under the qualitative concept expressed by C, represents a random number with steady tendency, and its distribution in the domain U is called a membership cloud, or simply "cloud," which can be expressed as

$$\forall x \in U, \exists \mu_C(x) \in [0,1], f: x \longrightarrow \mu_C(x). \quad (1)$$

As a critical cloud model, the normal cloud is most effective in expressing linguistic values.

Definition 2. If the random variable x satisfies $x \sim N(E_x, E_n'^2)$ and $E_n' \sim N(E_n, H_e^2)$ and $\mu(x)$ satisfies $\mu(x) =$

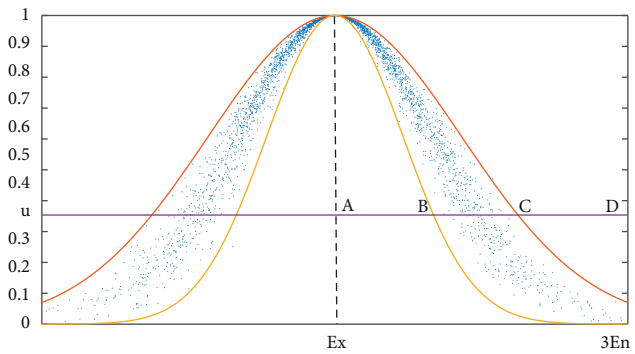

Figure 1: A sketch map of a cloud model.

$e^{-(x-E_x)^2/2E_n'^2}$, then the membership cloud of x in the domain is normal. When $E_n \neq 0$, $y = e^{-(x-E_x)^2/2E_n^2}$ is known as the expectation curve for the normal cloud.

Given that the normal cloud follows the 3σ rule governing the normal distribution, more than 99.73% of cloud drops of the normal random number fall under the $[E_x - 3E_n, E_x + 3E_n]$ range, and the overall features of the cloud model are not affected by the cloud drops outside the range.

As is displayed in Figure 1 (where $u = \sqrt{2}/4$), the digital features of a membership cloud have the following implications [1].

(1) The domain value corresponding to the centroid $A(E_x, \sqrt{2}/4)$ in the membership cloud-covered area reflects the central value of information about fuzzy concepts.

(2) The bandwidth of a membership cloud model's expectation curve indicates the fuzziness of fuzzy concepts.

(3) The randomly distributed variance of a membership corresponding to the point $B(E_x + \sqrt{\ln 8}\, E_n, \sqrt{2}/4)$ on a membership cloud-based expectation curve, or the hyperentropy H_e, suggests the dispersion of the membership cloud.

2.2. Backward Cloud Generator. The backward cloud generator is designed to identify the three digital features (E_x, E_n, H_e) of a cloud model by using the given cloud drops. A variety of ideas about the generator's algorithm have been provided by scholars. Having considered the scale of data for multiattribute group decision-making in practical issues, we offered an optimized Algorithm 1 of the backward cloud generator.

2.3. Connection Number Basics. The connection number is a major instrument in set pair theory. It serves as a connector between a certain number and its range and between macroscopic certainties and microscopic uncertainties. Also, it is a structure function that reflects the relationships of studied subjects under various conditions. Its commonly used form is the ternary connection number.

In [22], Chatterjee and Siarry introduced the concept of an interval number **a** on real number **R** as follows:

$\widehat{a} = [a^L, a^U] = \{a: a^L \prec a \prec a^U, a \in R\}$, where a^L and a^U are the lower bound and upper bound of the interval, respectively. Sengupta and Pal [23] defined a three-parameter interval as $\widehat{a} = [a^L, a*, a^U]$, where a_L is the lower bound, a^* is the center of gravity (the number that has the highest possibility), and a_U is the upper bound of the interval. If $a_L = a^* = a_U$, then the three-parameter interval number is reduced to a real number.

Definition 3. Assuming that A, B, C are real numbers and $i \in [-1, 1]$, $j = -1$, then

$$U = A + Bi + Cj, \tag{2}$$

which is called a ternary connection number and A, B, and C denote the identity, difference, and opposite degrees of any two researched subjects.

Let $A+B+C=N, \mu = U/N, a = A/N, b = B/N, c = C/N\mu$ be regarded as the ternary connection degree:

$$\mu = a + bi + cj, \quad \text{where } a, b, c \in R, a + b + c = 1. \tag{3}$$

Particularly, $U = A + Bi$ is called the binary or identical-different connection number.

In practical decision-making scenarios, the actual identity and difference degrees can be determined on a case-by-case basis, making possible the generation of all forms of the connection number, such as quaternary or quinary connection numbers.

3. Multiattribute Decision-Making Method Based on Cloud Model's Connection Numbers

3.1. Creation of Cloud Model's Connection Numbers. Various uncertain and fuzzy pieces of information must be dealt with in a practical decision-making process. In processing such information, many scholars have created connection numbers according to the expression of information [15]. However, the existing methods of establishing connection numbers find it hard to express the overall features of large-sample data. The creation of a cloud model's connection numbers demonstrates how cloud theory renders data expression reasonable within a big-data context and shows the laws governing the uncertainty of overall information by combining connection numbers in set pair analysis. According to the three implications of a cloud model's digital features mentioned in Section 2.1, the domain value corresponding to the centroid A of the cloud model's expectation curve reflects the central information of fuzzy concepts; that is, the domain value range can be used to develop quaternary connection numbers for the cloud model, which can express the model's uncertain information more accurately. The specific process is as follows.

Step 1: develop the equations for the internal and external envelopes by involving the standardized cloud model (E_x, E_n, H_e):

Input: the quantitative location of N cloud drops in the number field and the certainty of the quantitative concept represented by each cloud drop.
Output: the expectation value E_x, entropy E_n and hyperentropy He of a quantitative concept.
The detailed algorithm is as follows.
Step 1: solve $\hat{E}_x$ and $\hat{E}_n$ through the given cloud drop and the fitting using the least-squares method and the equation of the cloud model's expectation curve $\mu(x) = e^{-(x-E_x)^2/2E_n^2}$;
Step 2: remove the points satisfying $\mu(x) > 0.999$ and mark the remaining number of cloud drops as m;
Step 3: solve $_{En_i'}$ using the equation $_{En_i'} = \sqrt{-(x_i - \hat{E}_x)/2\ln(\mu_i)}$;
Step 4: solve $\hat{H}_e$ with the standard deviation function $\hat{H}_e^{\,2} = 1/m - 1\sqrt{\sum_{i=1}^{m}(_{En_i'} - \hat{E}_n)^2}$;
Step 5: output $\hat{E}_x$, $\hat{E}_n$, and $\hat{H}_e$, which are the expectation value E_x, entropy E_n , and hyperentropy H_e of a certain qualitative concept.

Algorithm 1: The process of reverse cloud generator

$$\begin{cases} y = e^{-\left((x-E_x)^2/2(E_n-H_e)^2\right)}, \\ y = e^{-\left((x-E_x)^2/2(E_n+H_e)^2\right)}. \end{cases} \tag{4}$$

Step 2: given the cloud model's asymmetry, the right half of the internal and external envelopes was extracted for calculation of the corresponding abscissa value when $u = \sqrt{2}/4$:

$$\begin{cases} x_B = E_x + \sqrt{\ln 8}\,(E_n - 3H_e), \\ x_C = E_x + \sqrt{\ln 8}\,(E_n + 3H_e). \end{cases} \tag{5}$$

In light of the 3σ rule, the abscissa of the D point was $x_D = E_x + 3E_n$.
Step 3: ensure that the quaternary connection number satisfies $U = A_1 + B_1 i_1 + C_1 i_2 + D_1 i_3$ and make $i_1, i_2, i_3 \in [-1, 1]$, where

$$\begin{cases} A_1 = E_x, \\ B_1 = \sqrt{\ln 8}\,(E_n - 3H_e), \\ C_1 = 6\sqrt{\ln 8}\,H_e, \\ D_1 = (3 - \sqrt{\ln 8})E_n - 3\sqrt{\ln 8}\,H_e. \end{cases} \tag{6}$$

Upon normalization, it was found that the quaternary identical-different connection number for the cloud model was $\mu = a + bi_1 + ci_2 + di_3$ and $i_1, i_2, i_3 \in [-1, 1]$:

$$\begin{cases} a = \dfrac{A_1}{N}, \\ b = \dfrac{B_1}{N}, \\ c = \dfrac{C_1}{N}, \\ d = \dfrac{D_1}{N}, \\ N = A_1 + B_1 + C_1 + D_1. \end{cases} \tag{7}$$

Built on the research on the abscissa interval of an expectation curve's centroid, the method of creating the quaternary connection number fully takes into account the implications of the cloud model's three digital features, thus expressing the model's uncertain data in a more comprehensive way.

3.2. Definition of the Weighted Nearness Degree of a Quaternary Connection Number. As a concept in fuzzy mathematics, nearness degree measures the extent to which two fuzzy subsets are similar to each other.

Definition 4. Assume $A, B, C \in F(U)$, if the mapping T: $F(U) \times F(U) \longrightarrow [0, 1]$ satisfies the following conditions:

(1) $T(A, B) = T(B, A)$.
(2) $T(A, A) = 1, T(U, \varphi) = 0$.
(3) If $A \subseteq B \subseteq C$, then $T(A, C) \le T(A, B)$ and $T(A, C) \le T(B, C)$.

Then, $T(A, B)$ is known as the nearness degree of A and B fuzzy sets, and T is the nearness function in $F(U)$.

Based on the aforementioned definition of the fuzzy set nearness and the importance of fuzzy information contained in all parts of a quaternary connection number, the nearness of the quaternary connection number is defined.

Definition 5. Assuming that (μ_1, μ_2) are quaternary connection numbers, $\mu_1 = a_1 + b_1 i_1 + c_1 i_2 + d_1 i_3$ and $\mu_2 = a_2 + b_2 i_1 + c_2 i_2 + d_2 i_3$, where $a_1 + b_1 + c_1 + d_1 = 1$, $a_2 + b_2 + c_2 + d_2 = 1$, and $a_1, b_1, c_1, d_1, a_2, b_2, c_2, d_2 \in [0, 1]$; then the nearness of the two connection numbers is

$$\begin{aligned} T(\mu_1, \mu_2) = 1 - \{ & w_a \|a_1 - a_2\| + w_b \|b_1 - b_2\| + w_c \|c_1 - c_2\| \\ & + w_d \|d_1 - d_2\| \}, \end{aligned} \tag{8}$$

where $0 \le w_a, w_b, w_c, w_d \le 1$ and $w_a + w_b + w_c + w_d = 1$. The definition can be straightforwardly proved to meet the three conditions in Definition 3.

3.3. Weight Determination in Definition of a Quaternary Connection Number's Nearness Degree. This section provides

a new method of determining the weight in the definition of a quaternary connection number's nearness.

Assuming that, after standardizing the evaluation information of the evaluation index $j(j = 1, 2, \ldots, m)$ for all plans $\{A_1, A_2, \ldots, A_n\}$, the cloud model's connection number is $\mu_{ij} = a_{ij} + b_{ij}i_1 + c_{ij}i_2 + d_{ij}i_3$ and $i_1, i_2, i_3 \in [-1, 1]$, where $i = 1, 2, \ldots, n$, $j = 1, 2, \ldots, m$. Let the ideal cloud model's connection number of the indexes $j(j = 1, 2, \ldots, m)$ in the model be $\mu_j^0 = a_j^0 + b_j^0 i_1 + c_j^0 i_2 + d_j^0 i_3$ and its average cloud model's connection number be $\frac{j}{\mu} = \frac{j}{a} + \frac{j}{b}i_1 + \frac{j}{c}i_2 + \frac{j}{d}i_3$, where

$$\begin{cases} \overline{a}_j = \dfrac{1}{n}\sum_{i=1}^{n} a_{ij}, \\ \overline{b}_j = \dfrac{1}{n}\sum_{i=1}^{n} b_{ij}, \\ \overline{c}_j = \dfrac{1}{n}\sum_{i=1}^{n} c_{ij}, \\ \overline{d}_j = \dfrac{1}{n}\sum_{i=1}^{n} d_{ij}. \end{cases} \tag{9}$$

The optimized model is developed as follows:

$$\begin{aligned} \min H &= w_{aj}^2\left(a_j^0 - \overline{a}_j\right)^2 + w_{bj}^2\left(b_j^0 - \overline{b}_j\right)^2 + w_{cj}^2\left(c_j^0 - \overline{c}_j\right)^2 \\ &\quad + w_{dj}^2\left(d_j^0 - \overline{d}_j\right)^2 \\ \text{s.t.} & w_{aj} + w_{bj} + w_{cj} + w_{dj} = 1, 0 \le w_{aj}, w_{bj}, w_{cj}, w_{dj} \le 1. \end{aligned} \tag{10}$$

The Lagrange function $L = H - \lambda(w_{aj} + w_{bj} + w_{cj} + w_{dj} - 1)$ is created and solved:

$$\frac{\partial L}{\partial \lambda} = 0, \frac{\partial L}{\partial w_{aj}} = 0, \frac{\partial L}{\partial w_{bj}} = 0, \frac{\partial L}{\partial w_{cj}} = 0, \frac{\partial L}{\partial w_{dj}} = 0. \tag{11}$$

Then, we obtain

$$\begin{cases} w_{aj} = \dfrac{1}{\left[G \cdot \left(\overline{a}_j - a_j^0\right)^2\right]}, \\ w_{bj} = \dfrac{1}{\left[G \cdot \left(\overline{b}_j - b_j^0\right)^2\right]}, \\ w_{cj} = \dfrac{1}{\left[G \cdot \left(\overline{c}_j - c_j^0\right)^2\right]}, \\ w_{dj} = \dfrac{1}{\left[G \cdot \left(\overline{d}_j - d_j^0\right)^2\right]}, \end{cases} \tag{12}$$

where

$$G = \frac{1}{\left(\overline{a}_j - a_j^0\right)^2} + \frac{1}{\left(\overline{b}_j - b_j^0\right)^2} + \frac{1}{\left(\overline{c}_j - c_j^0\right)^2} + \frac{1}{\left(\overline{d}_j - d_j^0\right)^2}. \tag{13}$$

The weight determination method is designed to develop a nonlinear planning model using the objective function or the quadratic sum of the difference between the expected and ideal values. The smaller the objective function, the more reasonable the corresponding plan for assigning the weight. In this method, the difference between the expected and ideal values of group decision-making information is fully considered, which can objectively show how each part of the connection number is prioritized in group opinions by specific evaluation indices.

3.4. Method of Determining the Index Weight Based on the Interval Number Expressed by Three Parameters. In the practical decision-making process, decision-makers tend to evaluate information in the form of interval numbers, given that experts find it complicated and uncertain to describe the importance of indices. When a parameter is expressed by an interval number expressed by two parameters, the opportunity to obtain a value within the whole interval is believed to be equal, which would produce a result far from the real intention of experts. Hence, the section offers a novel method of determining the index weight based on the interval number expressed by three parameters.

Assume that, in the hundred-mark system, the score of the index $j(j = 1, 2, \ldots, m)$ given by the expert $S_i(i = 1, 2, \ldots, n)$ is $[V_{ij}, \widetilde{V}_{ij}, \overline{V}_{ij}]$; then the estimated weighted value of the interval number expressed by three parameters $[\underline{w}_{ij}, \widetilde{w}_{ij}, \overline{w}_{ij}]$ can be obtained upon normalization through the following equation:

$$\underline{w}_{ij} = \frac{\underline{V}_{ij}}{\sum_{j=1}^{m}\underline{V}_{ij}}, \widetilde{w}_{ij} = \frac{\widetilde{V}_{ij}}{\sum_{j=1}^{m}\underline{V}_{ij}}, \overline{w}_{ij} = \frac{\overline{V}_{ij}}{\sum_{j=1}^{m}\underline{V}_{ij}}, \tag{14}$$

where $\widetilde{w}_{ij}$ is the gravity center of the interval number. Let $d_j^{\pm} = \overline{w}_j^{+} - \underline{w}_j^{-}$ be the maximal measure of the upper and lower bounds of the index j's estimated weights, where $\underline{w}_j^{-} = \min\left\{\underline{w}_{1j}, \underline{w}_{2j}, \ldots, \underline{w}_{nj}\right\}$ represents the minimal value of the lower bound of the index's $j(j = 1, 2, \cdots m)$ estimated values, while $\overline{w}_j^{+} = \max\left\{\overline{w}_{1j}, \overline{w}_{2j}, \ldots, \overline{w}_{nj}\right\}$ is the maximal value of the upper bound of the index's $j(j = 1, 2, \ldots, m)$ estimated values.

Let the weighted preference deviation of the expert s_i be h_{si}:

$$\begin{aligned} h_{si} &= \frac{w_{ij}^* - \widetilde{w}_{ij}}{d_j^{\pm}} = \frac{w_{ij}^* - \widetilde{w}_{ij}}{\overline{w}_j^{+} - \underline{w}_j^{-}} = \frac{\sum_{j=1}^{m}\left(w_{ij}^* - \widetilde{w}_{ij}\right)}{\sum_{j=1}^{m}\left(\overline{w}_j^{+} - \underline{w}_j^{-}\right)} \\ &= \frac{\sum_{j=1}^{m} w_{ij}^* - \sum_{j=1}^{m}\widetilde{w}_{ij}}{\sum_{j=1}^{m}\left(\overline{w}_j^{+} - \underline{w}_j^{-}\right)} = \frac{1 - \sum_{j=1}^{m}\widetilde{w}_{ij}}{\sum m\left(\overline{w}_j^{+} - \underline{w}_j^{-}\right) j = 1}, \end{aligned} \tag{15}$$

where w_{ij}^* is what the expert S_i believes the real weight of the index $j(j = 1, 2, \ldots, m)$ is and h_{si} is the ratio of the index j's weight error to $d_j^{\pm}$ given by the expert s_i. (Note: the expert's weight error is measured by the difference between the gravity center of the interval number expressed by three parameters and the real weight.) Each evaluating expert may

regard h_{si} consistently with each evaluation index, expressed as $j\,(j = 1, 2, \ldots, m)$. Therefore, the estimated value of j's weight, expressed as $w_j^*\,(j = 1, 2, \ldots, m)$, is

$$\hat{w}_j^* = h_s\left(\overline{w}_j^+ - \underline{w}_j^-\right) + \widetilde{w}_j, \tag{16}$$

where $\widetilde{w}_j$ is an aggregation of $\widetilde{w}_{ij}\,(i = 1, 2, \ldots, n)$ and h_s is an aggregation of h_{si} involving all participating experts. The equation $\sum_{j=1}^{m} \hat{w}_j = 1$ can be easily proved.

Definition 6. Assuming that f_k: $R^n \longrightarrow R$ is an n-element function, $k = (k_1, k_2, \ldots, k_n)^T$ is a weighted vector associated with f_k and satisfies $\sum_{i=1}^{n} k_i = 1, k_i \geq 0$ and $i = 1, 2, \ldots, n$. If $f_k(a_1, a_2, \ldots, a_n) = \sum_{i=1}^{n} k_i b_i$, where b_i is the number of i in $a_1, a_2, \ldots, a_n$, a progression that goes from largest to smallest, then the function f_k denotes the orderly weighted average (OWA) operator in the n dimension.

The definition suggests that the weighted coefficient k_i of the OWA operator is associated with the i spot in $a_1, a_2, \ldots, a_n$, rather than the number a_i. When $k = (1/n, 1/n, \ldots, 1/n)^T$, the OWA operator can be reduced to a simple arithmetic average operator. Thus, the aggregation can be conducted by using the following simplified equation.

$$h_s = \frac{1}{n}\sum_{i=1}^{n} h_{si}, \widetilde{w}_j = \frac{1}{n}\sum_{i=1}^{n} \widetilde{w}_{ij}. \tag{17}$$

And, after they are substituted into (14), the estimated aggregated value of the index weight, expressed as $\hat{w}_j^*$, can be calculated.

3.5. Steps of Multiattribute Group Decision-Making Based on Cloud Model's Quaternary Connection Number. Plan sorting has always been of critical importance in multiattribute decision-making methods. The section provides a method of this kind by ranking plans based on the calculation of the weighted arithmetic average nearness of the quaternary connection number and ideal connection number in different cloud models. The specific steps are as follows.

Step 1: have experts score of all plans in light of the evaluation-index system and standards, generate standardized cloud drops by indices oriented to benefits and costs, translate these cloud drops into a cloud model by using the backward cloud generator constructed according to Section 2.2, and subsequently create digital features.

Step 2: use the method of creating a cloud model's connection numbers, as indicated in Section 3.1, to construct the quaternary connection number for a cloud model founded on scoring by experts, and obtain a connection number-based decision-making matrix.

Step 3: develop the ideal cloud model by each index for the creation of the quaternary connection number, and, as instructed in Section 3.3, calculate the weight of each part of the cloud model's quaternary connection number.

Step 4: calculate the weight of all indices in the given index system as suggested in Section 3.4.

Step 5: measure the nearness of all proposed plans and the ideal plan by using (8) and (12), respectively, and calculate T_{ip}, the overall nearness of all these plans, through the following equation, where $i = 1, 2, \ldots, M$ (M is the total of plans):

$$T_{ip} = \sum_{j=1}^{t} w_j T_j\left(\mu_{ij}, \mu_{pj}\right). \tag{18}$$

In this equation, T is the total number of evaluation indices, w_j indicates the weight of each index, and μ_{pj} denotes the quaternary connection number of each index for the ideal plan.

Step 6: rank plans based on their overall nearness T_{ip}.

4. Comparative Analysis between the MCGC Model and the Decision-Making Method Based on Cloud Model's Quaternary Connection Number

The MCGC method is typical for evaluating a system using a cloud model. Specifically, if the system status of m evaluation indices is described by the m-dimensional comprehensive cloud, then a changing system status would make the comprehensive cloud and its gravity center altered. Therefore, a possible evaluation way is through the weighted deviation of the comprehensive cloud gravity center and ideal cloud gravity center under a certain status. Also, proposed plans can be sorted based on the weighted deviation between their comprehensive cloud gravity center and that of the ideal plan. The detailed process is as follows [5].

(1) For a system to be evaluated, calculate the gravity center vector G^0 of the m-dimensional comprehensive cloud for the ideal plan A_0 through

$$G^0 = \left(G_1^0, G_2^0, \ldots, G_m^0\right) = \mathbf{a}^0 \times \mathbf{b}^0, \tag{19}$$

where $\mathbf{a}^0 = (E_{x1}^0, E_{x2}^0, \ldots, E_{xm}^0)$ is the position vector of the m-dimensional comprehensive cloud gravity center and its component is the expectation value of each index; $\mathbf{b}^0 = (b_1^0, b_2^0, \ldots, b_m^0)$ represents the altitude vector of the comprehensive gravity center, which is a determined value in a to-be-evaluated system and is commonly known as the weight value of each index [8].

(2) For a given proposed plan A_i, provide its corresponding m-dimensional cloud gravity center vector, expressed as G^i, through the equation $G^i = (G_1^i, G_2^i, \ldots, G_m^i) = \mathbf{a}^i \times \mathbf{b}^i$, where $i = 1, 2, \ldots, n$.

(3) Give the definition of deviation of G^i and G^0 in the proposed plan A_i, calculate the deviation using equation (17), and evaluate A_i based on the weighted deviation.

$$\theta_i = \sum_{j=1}^{m} w_j \theta_j^i, \quad i = 1, 2, \ldots, n, \tag{20}$$

where

$$\theta_j^i = \begin{cases} \left(G_j^0 - G_j^i\right)/G_j^0 G_j^i < G_j^0 \\ \left(G_j^i - G_j^0\right)/G_j^i G_j^i \geq G_j^0 \end{cases} \quad j = 1, 2, \ldots, m. \tag{21}$$

Building on the aforementioned MCGC logic and steps, we found the following.

Theorem 1. *For a cloud model's quaternary connection number $\mu = a + bi_1 + ci_2 + di_3$ and $i_1, i_2, i_3 \in [-1, 1]$, when $i_1 = i_2 = i_3 = 0$, the evaluation method based on a cloud model's quaternary connection number is equivalent to the MCGC model.*

Proof. As is known in the method of creating a cloud model's quaternary connection number (see (7)), $a = A_1/N, N = A_1 + B_1 + C_1 + D_1, A_1 = E_x$. When $i_1 = i_2 = i_3 = 0$, the quaternion needs not to be normalized, meaning that it is reduced to $\mu = E_x$. And, for the proposed plan A_i, all its indices are reduced to the cloud model's expectation values, expressed as $E_{x1}^i, E_{x2}^i, \ldots, E_{xm}^i$.

As to the cloud gravity center's structure, A_i's position vector $\mathbf{a}^i = (E_{x1}^i, E_{x2}^i, \ldots, E_{xm}^i)$ is, in essence, the expected value of each index, and the altitude vector $\mathbf{b}^i = (b_1^i, b_2^i, \ldots, b_m^i)$ is the determined weighted value of each index. For a particular evaluation system, the index weight, once generated, is a determined value. Hence, each component of A_i's cloud gravity vector $G^i = (G_1^i, G_2^i, \ldots, G_m^i) = \mathbf{a}^i \times \mathbf{b}^i$ is the constant multiple of an expected value or $G^i = (w_1 E_{x1}^i, w_2 E_{x2}^i, \ldots, w_m E_{xm}^i)$, where $w_1, w_2, \ldots, w_m$ are weights of indices.

As shown in (18) and (21), θ_j^i is determined by investigating the extent to which the two weighted vectors, namely, $(w_1 E_{x1}^i, w_2 E_{x2}^i, \ldots, w_m E_{xm}^i)$ and $(w_1 E_{x1}^0, w_2 E_{x2}^0, \ldots, w_m E_{xm}^0)$, deviate from each other. In the evaluation method based on a cloud model's connection number, the overall nearness T_{ip} is determined by observing the deviation between $(E_{x1}^i, E_{x2}^i, \ldots, E_{xm}^i)$ and $(E_{x1}^0, E_{x2}^0, \ldots, E_{xm}^0)$. Therefore, when $i_1 = i_2 = i_3 = 0$, the two evaluation approaches are in practice equivalent.

The abovementioned theorem and proof indicate that the following.

(1) The MCGC method is an exception to the evaluation method based on a cloud model's connection number, where $i_1 = i_2 = i_3 = 0$. For the latter, the quaternary identical-different connection number demonstrates how the expectation value plays its role in index evaluation information and takes into account the full impact of the model's entropy and hyperentropy on evaluation.

(2) The steps of evaluation based on a cloud model's quaternary connection number showed that, in a practical decision-making process, expressing expert preferences through appropriate adjustments to (i_1, i_2, i_3) can offset the evaluation error arising from how the quaternary connection number's weight relies merely on objective numerical values rather than expert preferences.

(3) Compared with the MCGC approach, the evaluation method based on a cloud model's quaternary connection number collects more information from experts, thus producing more science-based results. Beyond that, (i_1, i_2, i_3) in the connection number can be tailored to the needs of the application context, which makes results better aligned with the operating condition of the evaluation system. That is how the proposed method can be further applied across different scenarios. □

5. Case Study

Among the damage control capabilities of a vessel, counterflooding is vital. There are four indices to evaluate a ship's overall counterflooding performance, namely, the cabin's capabilities of leak stoppage, bearing, drainage, and balancing. All these indices are oriented to benefits. Eight experts were invited to score the importance of these four evaluation indices in the hundred-mark system using the interval number expressed by three parameters, as is displayed in Table 1.

Table 1 is then normalized using (14), as shown in Table 2.

Using (13), we calculated the determined weight deviation degrees of experts, which were [−0.2186 −0.1976 −0.3100 −0.1524 −0.1993 −0.2141 −0.1706 −0.1857]. And upon the aggregation of the OWA operator, we input these values into (15) and obtained

$$\begin{aligned} h_s &= -0.2060, \widetilde{w}_1 = 0.1808. \widetilde{w}_2 = 0.2286. \widetilde{w}_3 \\ &= 0.3121, \widetilde{w}_4 = 0.3184. \end{aligned} \tag{22}$$

Lastly, with (16), we measured the estimated weight value of these four counterflooding indices, which were

$$\hat{w}_1^* = 0.1727, \hat{w}_2^* = 0.2193, \hat{w}_3^* = 0.2996, \hat{w}_4^* = 0.3084. \tag{23}$$

In addition, we had these experts' score of the counterflooding performance of three vessels, and each of them was required to provide the score and corresponding membership degree of the four indices in ideal and actual scenarios. Then, the backward cloud generator, as instructed in Section 2.2, was employed to translate the cloud drops offered by experts into a cloud model, whose digital features

Table 1: Scoring of the importance of a vessel's counterflooding indices.

Expert no	Cabin leak stoppage capability	Cabin bearing capability	Cabin drainage capability	Cabin balancing capability
s_1	[40, 42, 46]	[51 53 54]	[71 74 80]	[74 77 82]
s_2	[39, 41, 44]	[54 55 60]	[71 75 79]	[71 73 80]
s_3	[43, 44, 46]	[50 56 57]	[69 72 77]	[71 75 79]
s_4	[40, 42, 45]	[51 52 55]	[70 73 75]	[76 77 78]
s_5	[38, 40, 43]	[49 51 56]	[74 76 83]	[72 75 81]
s_6	[40, 43, 47]	[53 55 58]	[73 74 82]	[75 79 84]
s_7	[44, 45, 49]	[53 56 57]	[72 74 81]	[73 75 82]
s_8	[45, 48, 50]	[55 58 59]	[75 77 84]	[75 76 83]

Table 2: Normalized scoring of the importance of a vessel's counterflooding indices.

Expert no.	Cabin leak stoppage capability	Cabin bearing capability	Cabin drainage capability	Cabin balancing capability
s_1	[0.1695 0.1780 0.1949]	[0.2161 0.2246 0.2288]	[0.3008 0.3136 0.3390]	[0.3136 0.3263 0.3475]
s_2	[0.1660 0.1745 0.1872]	[0.2298 0.2340 0.2553]	[0.3021 0.3191 0.3362]	[0.3021 0.3106 0.3404]
s_3	[0.1845 0.1888 0.1974]	[0.2146 0.2403 0.244]	[0.2961 0.3090 0.3305]	[0.3047 0.3219 0.3391]
s_4	[0.1688 0.1772 0.1899]	[0.2152 0.2194 0.2321]	[0.2954 0.3080 0.3165]	[0.3207 0.3249 0.3291]
s_5	[0.1631 0.1717 0.1845]	[0.2103 0.2189 0.2403]	[0.3176 0.3262 0.3562]	[0.3090 0.3219 0.3476]
s_6	[0.1660 0.1784 0.1950]	[0.2199 0.2282 0.2407]	[0.3029 0.3071 0.3402]	[0.3112 0.3278 0.3485]
s_7	[0.1818 0.1860 0.2025]	[0.2190 0.2314 0.2355]	[0.2975 0.3058 0.3347]	[0.3017 0.3099 0.3388]
s_8	[0.1800 0.1920 0.2000]	[0.2200 0.2320 0.2360]	[0.3000 0.3080 0.3360]	[0.3000 0.3040 0.3320]

Table 3: Digital features of a cloud model for evaluating a vessel's counterflooding performance.

Vessel no.	Cabin leak stoppage capability	Cabin bearing capability	Cabin drainage capability	Cabin balancing capability
V_0	[85.20, 18.70, 1.20]	[83.40 17.90 1.30]	[86.50 19.20 2.10]	[82.40 11.30 1.70]
V_1	[83.70 19.10 1.50]	[84.10 18.90 1.41]	[83.20 14.50 3.11]	[81.70 10.10 1.54]
V_2	[85.70 18.20 2.10]	[81.50 16.50 1.00]	[85.70 17.10 2.30]	[82.60 12.10 1.60]
V_3	[84.50 17.80 1.80]	[82.90 18.20 1.20]	[87.30 21.10 1.40]	[80.70 12.30 1.43]

Table 4: Connection numbers of the cloud model for evaluating the ideal counterflooding capabilities of vessel V_0.

Evaluation indices	Cloud model's connection number values by indices
Cabin leak stoppage capability	$0.6030 + 0.1541i_1 + 0.0735i_2 + 0.1694i_3$
Cabin bearing capability	$0.6083 + 0.1473i_1 + 0.0820i_2 + 0.1624i_3$
Cabin drainage capability	$0.6003 + 0.1291i_1 + 0.1261i_2 + 0.1445i_3$
Cabin balancing capability	$0.7085 + 0.0769i_1 + 0.1265i_2 + 0.0881i_3$

Table 5: Connection numbers of the cloud model for evaluating the ideal counterflooding capabilities of vessel V_1.

Evaluation indices	Cloud model's connection number values by indices
Cabin leak stoppage capability	$0.5936 + 0.1493i_1 + 0.0920i_2 + 0.1650i_3$
Cabin bearing capability	$0.5973 + 0.1502i_1 + 0.0866i_2 + 0.1658i_3$
Cabin drainage capability	$0.6567 + 0.0588i_1 + 0.2124i_2 + 0.0721i_3$
Cabin balancing capability	$0.7295 + 0.0706i_1 + 0.1190i_2 + 0.0810i_3$

Table 6: Connection numbers of the cloud model for evaluating the counterflooding capabilities of vessel V_3.

Evaluation indices	Cloud model's connection number values by indices
Cabin leak stoppage capability	$0.6108 + 0.1223i_1 + 0.1295i_2 + 0.1374i_3$
Cabin bearing capability	$0.6221 + 0.1486i_1 + 0.0660i_2 + 0.1632i_3$
Cabin drainage capability	$0.6174 + 0.1122i_1 + 0.1434i_2 + 0.1270i_3$
Cabin balancing capability	$0.6947 + 0.0885i_1 + 0.1164i_2 + 0.1003i_3$

Table 7: Connection numbers of the cloud model for evaluating the ideal counterflooding capabilities of vessel V_4.

Evaluation indices	Cloud model's connection number values by indices
Cabin leak stoppage capability	$0.6128 + 0.1297i_1 + 0.1129i_2 + 0.1446i_3$
Cabin bearing capability	$0.6029 + 0.1531i_1 + 0.0755i_2 + 0.1685i_3$
Cabin drainage capability	$0.5797 + 0.1618i_1 + 0.0804i_2 + 0.1781i_3$
Cabin balancing capability	$0.6862 + 0.0982i_1 + 0.1052i_2 + 0.1103i_3$

are shown in Table 3. Among others, V_0 represents the ship equipped with ideal counterflooding capabilities.

Adopting the method of establishing a cloud model's connection number, as displayed in Section 3.1, we obtained

Table 8: Weights of the connection number's identical and three difference degrees in each evaluation index.

Evaluation indices	w_a	w_b	w_c	w_d
Cabin leak stoppage capability	0.9604	0.0174	0.0050	0.0172
Cabin bearing capability	0.8677	0.0587	0.0183	0.0553
Cabin drainage capability	0.2732	0.2574	0.2281	0.2412
Cabin balancing capability	0.5622	0.1811	0.0847	0.1720

the following decision-making tables, as shown in Tables 4–8.

The weights of the connection number's identical and three difference degrees in each evaluation index were calculated, as instructed in Section 3.3, and are shown as follows.

According to (18), the nearness degrees between the three vessels' counterflooding capabilities and their ideal performance were $T_1 = 0.9902$, $T_2 = 0.9682, T_3 = 0.9780$, respectively. That suggested that vessel V_1 boasted the strongest counterflooding capabilities, followed by vessel V_3 and vessel V_2, consistently with the practical scenario.

6. Conclusions

The quantitative analysis of uncertain and fuzzy information has always been important in information processing. Quantifying such information in group decision-making would lead to reasonable and science-based results. Cloud theory and set pair analysis have made great contributions to the research area. In this paper, based on the strengths of a cloud model and the connection number method in processing uncertain data, we (1) proposed a new cloud model-based method of establishing a quaternary connection number, which has the model's three digital features (E_x, E_n, H_e) that render the expression of the model's uncertain information more accurately and comprehensively; (2) we defined a new weighted arithmetic average nearness degree of the quaternary connection number and provided specific steps to determine the weight of such a nearness degree; (3) we offered a novel method of determining the weight of an index based on interval numbers expressed by three parameters, given the fact that the deviation degree remains unchanged when each expert determines the index weight; (4) we proposed an innovative multiattribute group decision-making method built on a cloud model's connection number and through comparative analysis proved that the MCGC method is an exception to our proposed decision-making method. The proposed approach can provide a fuller picture of the overall evaluation made by experts and express their preferences through adjustments to the quaternary connection number's uncertain parameters, which makes the group decision-making method more broadly applicable. Also, the technique can be applied to decision-making involving large-sample data and to the decision-making context where evaluation values are measured through modal particles. Nonetheless, when it comes to an application context, it awaits more research efforts to find out how to translate these particles into a cloud model reasonably and make sensible adjustments to the values (i_1, i_2, i_3) in the model's connection number, so that the resulting decisions better suit the context [24–29].

Abbreviations

MCGC: Membership cloud gravity center
MADM: Multiattribute decision-making
SPA: Set pair analysis
CN: Connection number
BCN: Binary connection number
E_n: Entropy
H_e: Hyperentropy
CM-MADM: Cloud model-based multiattribute decision-making
PSO: Particle swarm optimization
QCNs: Quaternary connection numbers
U: Quantitative domain
$\mu_C(x)$: Membership
$F(U)$: Set of fuzzy sets
$T\backslash(A, B)$: Nearness degree of A and B
M: Total number of planes
V_0: Ideal counterflooding capabilities.

Data Availability

All data, models, and codes generated or used during the study are included within the submitted article.

Conflicts of Interest

The authors declare that they have no conflicts of interest.

Acknowledgments

This word is supported by PhD Foundation of Wuchang Shouyi University (B20200206), National Key R&D Program of China (2021YFC3100202-1).

References

[1] K. Zhao, "Set pair and set pair analysis-a new concept and systematic analysis method," in *Proceedings of the National Conference on System Theory and Regional Planning*, pp. 87–91, Zhengzhou, China, May 1989.

[2] Y. L. Jiang, C. F. Xu, Y. Yao, and K. Q. Zhao, "Systems information in set pair analysis and its applications," *Proceedings of 2004 international conference on machine learning and cybernetics*, vol. 3, pp. 1717–1722, 2004.

[3] J. Q. Wang and L. Gong, "Interval probability stochastic multi-criteria decision-making approach based on set pair analysis," vol. 24, pp. 1877–1880, 2009.

[4] J. Hu and L. Yang, "Dynamic stochastic multi-criteria decision-making method based on cumulative prospect theory and set pair analysis," *Systems Engineering Procedia*, vol. 1, pp. 432–439, 2011.

[5] Z. Xie, F. Zhang, J. Cheng, and L. Li, "Fuzzy multi-attribute decision making methods based on improved set pair analysis," *Sixth international symposium on computational intelligence and design*, vol. 2, pp. 386–389, 2013.

[6] W. ChangJian, "Application of the set pair analysis theory in multiple attribute decision-making," *Journal of Mechanical Strength*, vol. 6, p. 029, 2007.

[7] S. Fu and H. Zhou, "Triangular fuzzy number multi-attribute decision-making method based on set pair analysis," *Journal of Software Engineering*, vol. 11, no. 1, pp. 116–122, 2016.

[8] R. Yue, Z. Wang, and A. Peng, "Multi-attribute group decision making based on set pair analysis," *International Journal of Advancements in Computing Technology*, vol. 4, no. 10, pp. 205–213, 2012.

[9] J. Yang, J. Zhou, L. Liu, Y. Li, and Z. Wu, *Similarity Measures between Connection Numbers of Set Pair Analysis*, Springer, Berlin, pp. 63–68, 2008.

[10] Q. Shen, X. Huang, Y. Liu, Y. Jiang, and K. Zhao, "Multi-attribute decision making based on the binary connection number in set pair analysis under an interval-valued intuitionistic fuzzy set environment," *Soft Computing*, vol. 24, no. 10, pp. 7801–7809, 2020.

[11] D. Y. Li, H. J. Meng, and X. M. Shi, "Membership clouds and membership cloud generators[J]," *Journal of Computer Research and Development*, vol. 32, no. 6, pp. 16–21, 1995.

[12] D. Y. Li, "Uncertainty in knowledge representation[J]," *Engineering and Science*, vol. 2, no. 10, pp. 73–79, 2000.

[13] L. Ren, L. He, Y. Chen, P. Tian, and J. Liu, "A cloud model based multi-attribute decision making approach for selection and evaluation of groundwater management schemes," *J Hydrology*, vol. 555, 2017.

[14] G. R. Su, B. S. Jia, P. Wang et al., "Risk identification of coal spontaneous combustion based on COWA modified G1 combination weighting cloud model[J]," *Scientific Reports*, vol. 2, no. 1, pp. 1–7, 2022.

[15] M. Guo, J. W. Zhao, D. Pan, M. Sun, Y. Zhou, and B Yan, "Normal cloud model theory-based comprehensive fuzzy assessment of wooden pagoda safety," *Journal of Cultural Heritage*, vol. 55, no. 3, pp. 1–10, 2022.

[16] S. L. Wang, D. R. Li, W. Z. Shi, and W. Xinzhou, "Cloud model-based spatial data mining," *Geographical Information Science*, vol. 9, no. 2, pp. 67–78, 2003.

[17] W. J. Wu, H. J. Cheng, and N. Cao, "The application of cloud barycenter theory to air defense forces operational capability evaluation model," *Fire Control and Command Control*, vol. 30, no. 4, pp. 82–84, 2005.

[18] T. Li and J. S. Zhou, "Study on the distribution of mineral resources development revenue based on Shapley value of cloud center of gravity," *China Mining Magazine*, vol. 29, no. 12, pp. 55–60, 2020.

[19] J. L. Zheng, "Enterprise knowledge management application evaluation based on cloud gravity center model and fuzzy extended AHP," *Journal of Computers*, vol. 6, no. 6, pp. 1110–1116, 2011.

[20] W. S. Peng, W. Wu, C. Li, and Q. Li, "Performance evaluation of man-portable devices based on the cloud center of gravity," *Journal of Physics: Conference Series*, vol. 1955, Article ID 012124, 2021.

[21] R. J. Zheng, W. Y. Wei, M. C. Zhang, and W. Qingtao, "Network security situation evaluation strategy based on cloud gravity center judgment," *Journal of Networks*, vol. 9, no. 2, pp. 283–290, 2014.

[22] A. Chatterjee and P. Siarry, "Nonlinear inertia weight variation for dynamic adaptation in particle swarm optimization," *Computers & Operations Research*, no. 3, pp. 859–871, 2006.

[23] A. Sengupta and T. K. Pal, "On comparing interval numbers," *European Journal of Operational Research*, vol. 127, no. 1, pp. 28–43, 2000.

[24] L. Kuai, X. Y. Fei, J. s Jiang et al., "A novel evaluation system of psoriasis curative effect based on bayesian maximum entropy weight self-learning and extended set pair analysis," *Evidence-based Complementary and Alternative Medicine*, pp. 1–13, 2021.

[25] X. Li, W. Q. Zhang, X. Wang, Z. Wang, and C Pang, "Evaluation on the risk of water inrush due to roof bed separation based on improved set pair analysis–variable fuzzy sets," *ACS Omega*, vol. 7, no. 11, pp. 9430–9442, 2022.

[26] X. M. Liu and K. Q. Zhao, "Quadratic-connection-number-based method and its applications for multiple attributes decision-making with interval numbers," *Fuzzy Systems and Mathematics*, no. 5, pp. 115–120, 2011.

[27] W. J. Wang, "Connection numbers method for ranking interval number," *Computer Engineering and Design*, no. 8, pp. 2055–2057, 2009.

[28] K. Kumar and H. Garg, "Connection number of set pair analysis based TOPSIS method on intuitionistic fuzzy sets and their application to decision making," *Applied Intelligence*, no. 8, pp. 2112–2119, 2018.

[29] D. Luo and X. Wang, "The multi-attribute grey target decision method for attribute value within three-parameter interval grey number," *Applied Mathematical Modelling*, vol. 36, no. 5, pp. 1957–1963, 2012.

Hindawi
Mathematical Problems in Engineering
Volume 2022, Article ID 7255653, 8 pages
https://doi.org/10.1155/2022/7255653

Research Article

Optimized Demand Information Sharing Model of Dual-Channel Supply Chain in E-Commerce

Yiming Song,[1] Shun Wu,[2] Yang Zhou,[1] Yiting Pan ,[3] and Kumar Sudhir [4]

[1]*Business School, Hohai University, Nanjing, China*
[2]*College of Economics and Management, Shanghai Ocean University, Shanghai, China*
[3]*Admission Office, Wenzhou Business College, Wenzhou, China*
[4]*Patan College for Professional Studies (PCPS), Kathmandu, Nepal*

Correspondence should be addressed to Yiting Pan; panyitingwbs@outlook.com and Kumar Sudhir; sudhir.kumar@patancollege.org

Yiming Song and Shun Wu contributed equally to this work.

Received 10 May 2022; Revised 18 June 2022; Accepted 1 July 2022; Published 30 September 2022

Academic Editor: Amandeep Kaur

In the dual-channel supply chain, the relationship between the electronic direct selling channel and the traditional selling channel is situated in an antagonistic game. The present study used the master-slave game model to analyze the dual-channel supply chain structure, where the manufacturer is the leader of the game, and the seller is the follower of the game. Based on the game analysis theory, the game order of manufacturer and seller is analyzed in the state of demand information sharing. The decision model of each member in the dual-channel supply chain is constructed, and the optimal production decision and product price decision under the demand information sharing between the seller and the manufacturer are determined by the reverse induction method. The expected economic benefits of both are calculated, respectively. The experimental results showed that the economic benefit of the model is higher than that of the traditional demand information nonsharing model, which could enhance the economic benefit of the manufacturer and the seller at the same time and alleviate the contradiction between the electronic direct selling channel and the traditional selling channel.

1. Introduction

With the rapid development of the globalization and the intensive popularization of the Internet technology and logistics industry, e-commerce has become one of the main forms of business trading [1]. In the field of e-commerce, relevant research has proposed dual-channel supply chain strategies to study the development trend of economy. Dual channel refers to two approaches to link the manufacturers with the consumers, that is, the traditional selling channels (i.e., products are sold by manufacturer to consumers through sellers) and electronic direct selling channels (i.e., products are directly sold by manufacturers to consumers) [2, 3]. This strategy has a significant advantage in both improving the market share of enterprises and meeting the needs of consumers. However, most of the sellers in traditional selling channels have a hostile attitude toward electronic direct selling channel. At the same time, different information in the dual-channel supply chain (such as consumers' information, selling information of the products, and product demand forecast information) may have a great impact on the producing decisions of stakeholders involved in this process. Moreover, the information held by each member is not comprehensive, and therefore, every stakeholder hopes to obtain relevant information held by other stakeholders to improve the reliability of their own producing decisions. Therefore, the opposing and antagonistic game relationship between members has becoming increasingly concerning [4].

Several well-known companies in developed countries have applied dual-channel supply chain strategies to actual business operations. For example, Nike, IBM, and Estee

Lauder have used different methods to deal with the conflicts between electronic direct selling channels and traditional selling channels, aiming to reach a harmonious state between the two different approaches. In this way, they tend to increase the market share of the products while also brings a new value transfer model for the company [5]. More specifically, the "demand information sharing" among members in a dual-channel supply chain is the main solution to solve the abovementioned problem [6]. The accuracy of predicting the amount of product sold can be improved through the sharing of demand information. Therefore, manufacturers and sellers in traditional selling channels can quickly and flexibly arrange the amount of production and increase the inventory according to the actual number of sold products. Thus, the operating performance of each member in the dual-channel supply chain can be effectively improved. Based on the abovementioned discussion, it is important to explore a dual-channel supply chain demand information sharing model in e-commerce, as it would provide scientific suggestions for the decision making of members in the dual-channel supply chain.

Previous literature has extensively discussed this topic, especially about Chinese markets. Reference [7] analyzed the impact of reducing costs for research and development in dual-channel supply chain on information sharing of retailers and considered the situation when manufacturers reduced the costs for research and development and when they did not. The study found that no matter whether the manufacturer invested in research and development to reduce production costs, and the profits of the manufacturer would always increase if retailers shared their market demand information with manufacturer. However, if manufacturers do not invest in research and development to reduce production costs, retailers would not share their market demand information with manufacturers, which was in line with existing ideas in this field. If the manufacturers invest in research and development to reduce production costs and when their research and development efficiency is high, the retailer will share their market demand information with the manufacturers. Otherwise, the retailers will still not share their market demand information with the manufacturer. In addition, the Nash information compensation mechanism is designed to encourage retailers to share their market demand information with manufacturers.

Chi et al. [4] further included the variable service level and established a Stackelberg game model based on the two-level optimization theory. It estimated the equilibrium pricing and optimal service level of manufacturers and retailers, and based on the optimal results, it studied the impact of changes of the free rider coefficient on deciding the price and service level, dual-channel demand, and profit of members in the supply chain. The study found that the free-riding phenomenon inhibited retailers' enthusiasm in providing services, lowered market demand, and negatively affected the profits of manufacturers and retailers. Based on the negative impact of the free riding, a coordination mechanism model based on revenue sharing was established, and the conditions for finding equilibrium solutions were given. The statistical results showed that under certain conditions, the adoption of the revenue sharing mechanism would increase the level of services provided by retailers, expand market demand, and improve profits for both manufacturers and retailers.

He [5] conducted relevant analysis and research on the supply chain management of large global circulation organizations and summarized the advantages of the current retail manufacturing industry. According to the limitations of the retail manufacturing industry, it combined the intermediate demand for reverse integration of the supply chain and analyzed the specific significance and mechanism of the division of labor and cooperation in improving the overall efficiency of the circulation industry. From the perspective of supply chain channel, it analyzed the solutions for differentiation and transformation of circulation organizations and restructured the circulation organizations. Furthermore, a new circulation manufacturing model was proposed to supplement and optimize traditional circulation organizations. Reference [6] proposed the information disclosure strategy of manufacturers in a dual-channel supply chain, considering the impact of information acquisition. This study described the demand for branded and nonbranded products in markets where consumers of different quality preference were involved. It concluded the final pricing and pricing strategy of the wholesale products of the brand manufacturer with or without information acquisition, and further come put with the quality information disclosure strategy and analyzed the impact of information acquisition on brand manufacturer pricing and information disclosure decisions. This study found that brand manufacturers were more willing to disclose information to high-type consumers than low-type consumers; the willingness of brand manufacturers to disclose information decreased as retailers increased the cost of acquiring nonbranded products; information acquisition was not beneficial for retailers, and its impact on brand manufacturers was related to market capacity; and taking information acquisition actions would increase brand manufacturers' willingness to disclose information to high-type consumers, whereas their disclosure willingness to low-type consumers depended on market capacity.

Fu et al. [8] studied the impact of economies of scale on information trading decisions in supply chain. On the one hand, supply chain information sharing enabled manufacturers to adjust wholesale prices based on demand information, resulting in an increasement in the double marginalization effect in supply chain; on the other hand, both parties making decisions based on symmetrical demand information would increase the stability of retailer's order. If the manufacturer is a producer of economies of scale, its average production cost decreases with an increase in order stability. When the manufacturer's basic cost is high, the cost-saving effect of information sharing would be greater than the double marginalization effect, and the supply chain profits would increase; information sharing can be achieved through information transactions. However, if the manufacturer's marginal production cost is constant, the average cost does not change with changes in order stability; information sharing therefore cannot be implemented due

to reduced supply chain profits. Reference [9] proposed a manufacturing supply chain information interaction method. Through the application of Handle logo analysis, this study tried to find a breakthrough in the intelligent supply chain management model, where the system information interaction drives the efficient coordination of supply chain business. This could help the manufacturing industry achieving the value-adding in the whole supply chain and would improve the overall competitiveness of the supply chain.

Liu et al. [10] studied the impact of retailer information sharing on the corporate social responsibility (CSR) of enterprises in the supply chain, as well as their CSR performance and economic performance under an uncertain market demand. The CSR configuration was described based on whether manufacturers and retailers actively implement CSR behaviors, and a dynamic game model was established and solved for a total of 8 situations, including information sharing and different CSR configuration combinations. The study found that under equilibrium conditions, both manufacturers and retailers would actively implement CSR behaviors, and this CSR configuration was optimal for the CSR performance and economic performance of related enterprises. Both parties conducting CSR behaviors would keep the CSR implementation efficiency at a high level, and retailers would voluntarily share predicting information. In this case, information sharing would be considered as a "win-win strategy" (i.e., information sharing would simultaneously improve the economic performance of manufacturers and retailers); at a low level of CSR implementation efficiency, retailers would have little incentive to voluntarily share predicting information [11–15].

However, there are many deficiencies in the current research, which are mainly reflected in the low expected economic benefits of sellers and manufacturers when the model adopts dual-channel supply chain strategy to make product sales decisions [16–21]. For example, scholars in developed countries such as Batarfi et al. [22], Modak and Kolle [23], and Soleimani et al. [24] explored and studied the demand information sharing of dual-channel supply chain after a long time of analysis and discussion. References [14, 25] applied Stackelberg game and designed an outsourcing contract between a supplier and a buyer, and determined the optimal outsourcing price, retail price, and outsourcing quality under the condition of uncertain demand. In the design of outsourcing contracts, the demand prediction of both supply and demand parties is private, resulting in information asymmetry. Three different prediction scenarios were studied, including noninformation sharing, information sharing, and buyer prediction, and the optimal values of outsourcing price, retail price, and outsourcing quality level were obtained. Furthermore, it compared the best strategies in the three scenarios and drew some insights for management. Reference [26] discussed the impact of three different methods on demand prediction and pricing decision making for combining the products of national brands and store brands in the era of big data. Based on the demand prediction under three different scenarios, that is, noninformation sharing (N), information sharing (I), and retailer prediction (R), the balanced wholesale price and retail price of national brand products and the balanced retail price of store brand were derived. The effects of information collection, information sharing, and prediction accuracy on prices and profits of enterprises in the era of big data were comprehensively discussed.

Based on above discussion, scholars have also found that the existing supply chain strategy has the deviation of expected economic benefits and manufacturers expected economic benefits. Meanwhile, in the context of China, through literature review, it can also be found that information sharing is of great help to optimal production decision making, product price decision making, and economic benefit calculation. Therefore, this paper believes that further discussion is necessary. Therefore, this paper proposes and constructs a dual-channel supply chain demand information sharing model under the e-commerce environment.

2. Methodology

2.1. A Framework of Demand Information Sharing Model of Dual-Channel Supply Chain. By referring to the dual-channel model proposed in previous studies [27–29], the following dual-channel supply chain is presented in this paper includes a manufacturer and a seller [8], as shown in Figure 1. The manufacturer acts as the leader of the game, and the seller is the follower of the game [9]. The following assumptions are made: each member is rational; each member undertakes neutral risk; each member independently determines the decision variables to maximize its economic benefits; and both the demand function and the benefit function are positive.

In model estimation, h and g refer to the production cost of each product of the manufacturer, and the price of each product sold to the seller that is determined by the bargaining ability of the manufacturer, respectively. In addition, p_e and p_r refer to price of each product sold to the consumers by the manufacturer through the electronic direct selling channel, and the price of each product sold to the consumers by the seller through the traditional selling channel. Therefore, the strategy of dual-channel supply chain can be describe as [10]: the manufacturer sold products with a unit price of h to the seller with the price of g, and meanwhile sold the product directly to the consumers with the price p_e through e-commerce; the seller sold the products to the consumers through a traditional selling channel with a price of p_r, based on the price of g and p_e.

Based on the above analysis, equations (1) and (2) can be used to calculate the demand function x_r (through traditional selling channel) and x_e (through electronic selling channel), respectively:

$$x_r = \theta m - p_r + np_e, \tag{1}$$

$$x_e = (1-\theta)m - p_e + np_r, \tag{2}$$

where $\theta(0<\theta<1)$, $m(m>0)$, and $n(0<n<1)$ refer to the market share of traditional selling channel, total market

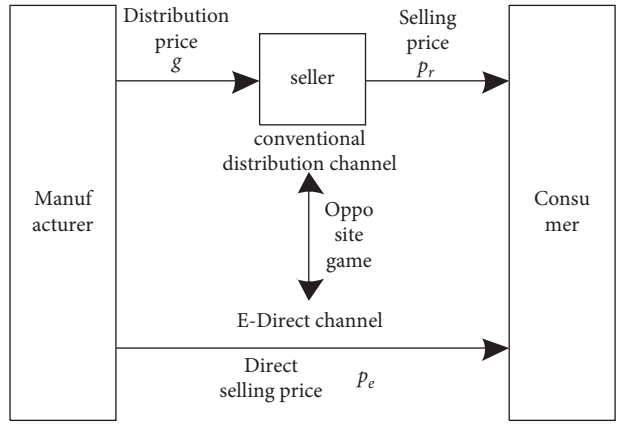

Figure 1: Structure of the dual-channel supply chain.

demand, and the cross-price elasticity coefficient between traditional selling channel and electronic direct selling channels under the dual-channel supply chain strategy. The total market demand is volatile due to the influences of different factors [25], and therefore, m is a random variable, represented by $m = m_0 + \delta$. In this equation, m_0 is constant and represents the fixed part in the market demand, that is, the seller's prediction of the total t market demand; and δ is a random variable representing the random factors in market demand (i.e., factors that stably affect market demand). The expected value and variance of δ are 0 and v, respectively (a higher v value indicates a lower stability of market demand).

Meanwhile, in the abovementioned equation, both $\theta m - p_r$ and $(1-\theta)m - p_e$ are higher than 0, indicating that these two different selling channels both have their own consumer loyalty.

2.2. Decision-Making Model of Dual-Channel Supply Chain. One of the pioneers of game theory is Gintis [30], whom analyzed the consciousness, habits, behaviors, interests, and psychological states of market designers, predators, and prey from a game perspective, and furthermore analyzed the nature of the market. The game theory proposes to apply well-developed theories in fields such as gambling, art of war, and psychology to find out the internal laws of the market and analyze the problems in trading concept, mentality, and habits, so that traders can trade calmly and produce stable income [31, 32]. Therefore, based on the game analysis theory, this paper analyzed the gaming order in the dual-channel supply chain strategy where the manufacturer and the seller share demand information [26]: (1) the manufacturer decides the prices through direct selling channel (decision variable) after negotiating with the seller when they share demand information (e.g., the sellers' prediction for total market demand) with the manufacturer; (2) the seller decides the prices for traditional selling channel and sells products (decision variable) based on the manufacture's bargaining ability and the private information the seller have.

According to the game between the members under different information sharing states of the dual-channel supply chain strategy, the decision-making model of the members in the dual-channel supply chain is constructed, and the optimal production decision and product price decision under the information sharing between the seller and the manufacturer are determined by the reverse induction [33]. Within the game order (2), y and ∂ refer to the sellers' overall potential demand for the market (seller's private information) and the proportionate relationship between g and p_e (i.e., manufacturers' bargaining ability). The value of ∂ ranges between 0 and 1, and a higher value indicates a higher bargaining ability of the manufacturer. When the value of ∂ is higher than 1, the manufacturer could sell all the products to the seller and there is no need to conduct electronic selling. Based on the above discussion, the following equation could be used to describe the seller's optimal production decision and product price decision in traditional selling channel:

$$\max_{p_r} E(\lambda_r | y) = (p_r - \partial p_e)[E(m|y) - p_r + p_e], \tag{3}$$

$$p_r = \frac{p_e + (1-s)m_0 + sy + \partial p_e}{2}. \tag{4}$$

In the above equation, λ_r, $E(m|y)$, and $s \in (0, 1)$ refer to the economic efficiency function of the seller, the predicting results of market demand, and measuring indicator of prediction of market demand, among which a higher value of s indicate a higher accuracy in predicting market demand [34].

Within the game order (1), manufacturers employ demand information sharing to understand the seller's prediction of market demand before setting the selling price in electronic direct selling channel [35]. ∂ refers to the manufacturer's bargaining power, with a value ranged between 0 and 1. A smaller value indicates that a lower bargaining power of the manufacturer. When the value is less than 1, the manufacturer can sell all products to the seller, and there is no need to conduct electronic direct selling. Based on the above discussion, the following equations are used to describe the manufacturer's optimal production decision and the product decision price in the electronic direct selling channel:

$$\max_{p_e} E(\lambda_e) = g[E(m) - E(p_r) + p_e] + p_e[E(m) - p_e + E(p_r)], \tag{5}$$

$$p_e = \frac{[(1-s)m_0 + sy]\left(2\partial^2 + 6\partial\right) - 1}{4\partial^3 - 6\partial^2 + 2\ \partial}, \tag{6}$$

where λ_e refers to the function of economic benefits of the manufacturers.

Combining equations (6) with (4), the sellers' selling price can be calculated as follows:

$$p_r = \frac{(1-t)m_0 + sy}{2} + \frac{[(1-s)m_0 + sy]\left(2\partial^2 + 6\partial\right) - 1}{4\partial^3 - 6\partial^2 + 2\partial} + \frac{\partial\left\{[(1-s)m_0 + sy]\left(2\partial^2 + 6\partial\right) - 1\right\}}{4\partial^3 - 6\partial^2 + 2\partial}. \tag{7}$$

Combining equations (6) with (3), and combining equations (7) with (5), the expected economic benefits of manufacturer and seller can be calculated, respectively:

$$\begin{aligned} E(\pi_r) &= \frac{m_0^2 + vs}{4} + \frac{\left(1+\partial^2\right)\left(m_0^2 + vs\right)\left(2\partial^2 + 6\right)^2 + 2 - 2m_0\left(2\partial^2 + 6\right)(1+\partial)}{4\partial^3 - 6\partial^2 + 2\partial} \\ &\quad - \frac{\left(m_0^2 + vs\right)\left(2\partial^2 + 6\right)(1+\partial)}{2\left(4\partial^3 - 6\partial^2 + 2\partial\right)}, \\ E(\pi_e) &= \frac{3\left(2\partial^2 + 6\right)\left(m_0^2 + vs\right) - 3m_0/2 + \left[\left(m_0^2 + vs\right)\left(2\partial^2 + 6\right)^2 + 1 - 2m_0\left(2\partial^2 + 6\right)\right](\partial - 1)/2\left(4\partial^3 - 6\partial^2 + 2\partial\right)}{4\partial^3 - 6\partial^2 + 2\partial} \\ &\quad + \frac{\partial\left\{\left(2\partial^2 + 6\right)\left(m_0^2 + vs\right) - m_0/2 + \left[\left(m_0^2 + vs\right)\left(2\partial^2 + 6\right)^2 + 1 - 2m_0\left(2\partial^2 + 6\right)\right](\partial - 1)/2\left(4\partial^3 - 6\partial^2 + 2\partial\right)\right\}}{4\partial^3 - 6\partial^2 + 2\partial}. \end{aligned} \tag{8}$$

3. Experimental Analysis

In order to evaluate the effectiveness of demand information sharing model of the dual-channel supply chain proposed in this paper, an experiment was designed in the present study to compare the traditional demand information nonsharing model with the model proposed in this paper. Company A is a manufacturer in food industry with a dual-channel market and is in the forefront of the industry, ranking third in the industry and first in Sichuan province. It has high-quality product power, C-end channel power, and management capabilities for upstream and downstream. In recent years, the company has continuously launched new products, putting around 1–5 new products in market every year, and half of the increase in profit comes from selling new products. Therefore, taking Company A and Company B, one of its fixed sellers, as the research object, the traditional nonsharing model of demand information and the model proposed in this article are used to simulate the process of selling products through the dual-channel supply chain strategy. Furthermore, the expected economic benefit and the manufacturer's expected economic benefit are analyzed. The estimated parameters of the economic benefit of the research objects are shown in Table 1.

Figure 2 shows the changes in economic benefits when sellers' manufacturers make decisions with using our proposed model and when they make decisions with traditional demand information nonsharing models. Figure 2(a) shows the seller's economic benefits from making decisions based on our model and based on the traditional demand information nonsharing model under the conditions of different prediction accuracy of market demand. Adopting our model in decision making led to a decline in the economic benefits of the seller as the accuracy of market demand prediction declines. For decision making using the traditional nonsharing model of demand information, the economic benefits of the sellers tend to decline first and rise afterward as the prediction accuracy of market demand decreases, and the economic benefits are generally lower than benefits from the model proposed in this paper. One of the reasons is that in the selling market, the traditional selling channel has a higher market share than the electronic direct selling channel. Therefore, without sufficient information in decision making, manufacturers tended to predict the market demand based on the amount of sold products from electronic direct selling channel. When the accuracy of the sellers' prediction for market demand is higher/lower than that of the manufacturer, their economic benefits would show a decline/rising trend as the prediction accuracy decreases. At the same time, under the condition that the sellers accurately predict the market demand, the economic benefit of using the traditional demand information nonsharing model in decision making is higher than the economic benefit obtained by using our model. The explanation is that the market share of the traditional selling channel is higher than the electronic direct selling channel, and therefore, the prediction accuracy of sellers is higher than the prediction accuracy of manufacturers. However, due to the

Table 1: Estimated parameters of economic benefits.

Fixed parameters in market demand during the calculation of economic benefits	Value
The market share of traditional selling channel	60% (range 10%–100%)
Cross-channel price elasticity coefficient between different channels	1
Producing cost per product/RMB (also called: Yuan)	10
Price of each product sold to the seller by the manufacturer/RMB	16
Price of each product sold through electronic direct selling channel/RMB	17.5
Price of each product sold by sellers through traditional selling channel/RMB	19
Accuracy of prediction for market demand by the seller	(Range 0%–100%)
Variance of market demand	50 (range 0–800)

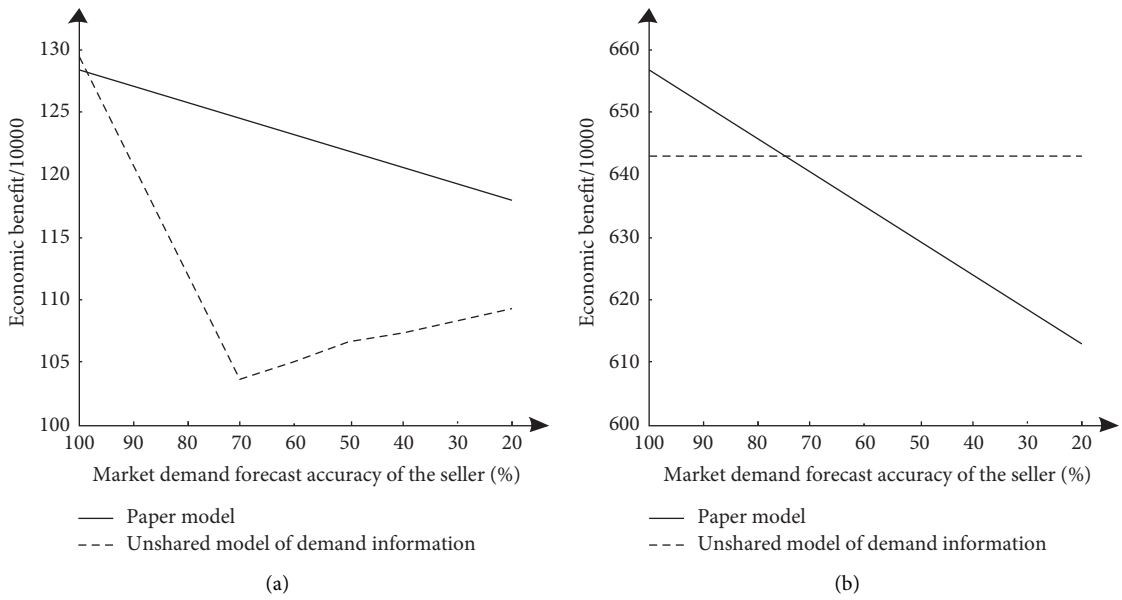

Figure 2: Changes in the expected economic benefits of members in the dual-channel supply chain: (a) expected economic efficiency of sellers; (b) expected economic benefits of manufacturer.

presence of various uncertainties in predicting the market demand, it is unrealistic to predict the market demand with a 100% accuracy.

Figure 2(b) shows the economic benefits of the manufacturer and how it is influenced by sellers' decisions made based on our model, and traditional demand information nonsharing model under the conditions of different prediction accuracy of market demand. The seller adopting the traditional demand information nonsharing model in decision making did not have an effect on the manufacturer's economic benefit, indicating that there is no significant correlation between the manufacturer's economic benefit and the seller's prediction. The reason is that under the condition of the traditional demand information nonshared model, manufacturers predict market demand based on the amount of sold products through electronic direct selling channel and make decisions accordingly, which has nothing to do with the predicting accuracy of the market demand of the sellers. In case that the sellers adopting our model in decision making, there was a positive relationship between the manufacturer's economic benefit and the seller's prediction accuracy for market demand, which was significantly higher than the economic benefits in the traditional demand information nonsharing model. This is because in our model, manufacturers use the demand information shared by sellers as the main reference for decision making. A lower predicting accuracy of market demand by the sellers would lead to a decrease in the economic benefits of the manufacturers.

Combining the results from Figures 2(a) and 2(b), it can be found that using the model proposed in this paper in decision making would, the economic benefits of both sellers and manufacturers were higher than those obtained by using traditional demand information nonsharing models for decision making. The effectiveness of the model proposed in the present study is therefore proved.

4. Conclusion

In the era of e-commerce, the dual-channel supply chain strategy, where the traditional selling channels and electronic direct selling channels co-exist, has become the main selling strategy in the field of processing and manufacturing commerce. The gaming and conflicts between channels raised by competition for prices also bring problems for the theoretical research and practical application of the theory in management in the field of e-commerce. Based on this, the present study developed a dual-channel supply chain

demand information sharing model under the e-commerce environment. Based on the structure of dual-channel supply chain, game analysis is used to calculate the expected economic benefits of the seller and the manufacturer under the condition of sharing sellers' prediction for market demand. By comparing the model proposed by the present study with the traditional demand information nonsharing model in an experimental design, the economic benefits of sellers and manufacturers were estimated. The results showed that using our proposed model in decision making of producing and deciding prices would increase the economic benefits of both sellers and manufacturers.

However, there are still some problems in implementing the proposed model as follows:

First, sufficient information sharing of market demand in dual-channel supply chain is a prerequisite for establishing an information control platform of product supply chain. However, in practice, each member of the supply chain would deliberately hide their cost, output, purchase price, and other information for their own benefit. Sales data, especially detailed data for each transaction, are considered as highly confidential business data. Even for staff inside enterprises, access to these data is monitored, let alone disclosing such information to individuals outside the enterprise. Under this circumstance, there are still risks in sharing demand information in the dual-channel supply chain, and the willingness of the members in the supply chain to share information timely may be doubted.

Second, one of the characteristics of the product supply chain is the large number of participants and that each participant differs in economic strength and production capacity. This has caused two phenomena. First, the share of the cost of using advanced predicting technology and information technology may differ across members. Second, there are uneven distributions of profits due to information sharing and information control. In the product supply chain, information is mainly controlled by downstream companies, and the increase in costs is mainly undertaken by downstream companies as well, whereas the increase in profits mainly goes to upstream companies. This situation results in the resistance of some of the enterprises toward building a cooperative relationship between members of the supply chain and may therefore increase the difficulty of running the platform.

Last, the establishment and application of the abovementioned platforms are supported by advanced management concepts and information technology, and at the same time, it requires the corresponding technology application level and market capacity. Although the aforementioned information sharing technologies have been developed to a certain extent, the application of these technologies in industry in China is still relatively weak. Furthermore, the source of the product supply chain is generally small-scale, and the related product information technology is relatively at infancy. The demand for information sharing and control platforms is also relatively weak as well. These are issues that need to be considered in actual application.

However, this paper is based on information sharing in the e-commerce environment of dual-channel supply chain members how to develop information sharing strategy and investigate the influence mechanism of supply chain members' decision and profit. However, there are some shortcomings in our work. First, due to space constraints, we did not delve into other ways to achieve information symmetry in a two-channel supply chain. In addition, this paper only considers retailers in a single industry, but in a real business environment, the variety of manufacturers is often diverse. Therefore, in the future research, the situation of adding multiple industries can be comprehensively considered for comparison.

Data Availability

The datasets used during the current study are available from the corresponding author on reasonable request.

Disclosure

Yiming Song and Shun Wu are co-first authors.

Conflicts of Interest

The authors declare that they have no conflicts of interest.

Authors' Contributions

Yiming Song and Shun Wu contributed equally to this paper. Yiming Song and Shun Wu performed conceptualization and formal analysis and developed the methodology. Yang Zhou collected data and performed the formal analysis. Yiting Pan performed the formal analysis and wrote the original draft and performed the supervision. Sudhir Kumar performed conceptualization, wrote the final draft, performed the supervision, and reviewed and edited the article.

References

[1] M. P. Rodríguez Bolívar, "Policy makers' perceptions on the transformational effect of Web 2.0 technologies on public services delivery," *Electronic Commerce Research*, vol. 17, no. 2, pp. 227–254, 2017.

[2] S. Y. Shi and J. C. Sun, "Pricing decisions of a dual-Channel supply chain with a risk-averse supplier and a budget constraint retailer," *Forecasting*, vol. 38, no. 02, pp. 90–96, 2019.

[3] J. Wei, S. Seedorf, P. B. Lowry, C. Thum, and T. Schulze, "How increased social presence through co-browsing influences user engagement in collaborative online shopping," *Electronic Commerce Research and Applications*, vol. 24, pp. 84–99, 2017.

[4] F. Y. Chi, Q. Xu, and T. T. Chen, "Two - channel supply chain benefit sharing contract design under hitchhiking effect," *Practice and Understanding of Mathematics*, vol. 18, pp. 39–53, 2018.

[5] Y. He, "Double channel supply chain based on 'pull' model research on reverse integration," *Business and Economic Research*, vol. 1, pp. 38–40, 2017.

[6] L. Deng, J. G. Zheng, and R. J. Zhao, "Double channel supply chain manufacturer information disclosure strategy considering the influence of information acquisition," *Industrial Engineering & Management*, vol. 23, no. 4, pp. 137–144, 2018.

[7] C. L. Shi and J. J. Nie, "The effect of dual channel supply chain on retailer information sharing," *Industrial Engineering & Management*, vol. 4, pp. 81–89, 2018.
[8] H. Fu, M. Jian, and Y. F. Fan, "Study on the influence of scale economy on supply chain information transaction decision," *Journal of Systems Science*, vol. 2, pp. 111–116, 2018.
[9] T. T. Wang and Q. Q. Ji, "Handle system in manufacturing supply chain information interaction," *Technology Innovation and Application*, vol. 8, pp. 66-67, 2019.
[10] J. Liu, J. J. Nie, and H. P. Yuan, "The influence of information sharing on corporate social responsibility allocation in supply chain," *Industrial Engineering & Management*, vol. 3, pp. 164–170, 2019.
[11] J. N. Wu, N. X. Wang, and Z. N. Wang, "Impact of information technology capability on financial performance during the period of economic downturn: the case of Chinese listed companies," *Electronic Commerce Research*, vol. 17, no. 3, pp. 403–423, 2017.
[12] M. Vanderroost, P. Ragaert, J. Verwaeren, B. De Meulenaer, B. De Baets, and F. Devlieghere, "The digitization of a food package's life cycle: existing and emerging computer systems in the pre-logistics phase," *Computers in Industry*, vol. 87pp. 1–14, C, 2017.
[13] Y. Li, "Predictions model of customer churn in E-commerce based on online sequential optimization extreme learning machine," *Journal of Nanjing University of Science and Technology*, vol. 43, no. 01, pp. 108–114, 2019.
[14] Z. J. Kong and Z. Y. Li, "Pricing decision in dual-Channel supply chain with the retailer's E-market," *Industrial Technology & Economy*, vol. 36, no. 3, pp. 116–122, 2017.
[15] J. H. Gerdes, C. T. Huang, and M. A. Sharaf, "Incorporating biometrics into veiled certificates: preventing unauthorized use of anonymous certificates," *Electronic Commerce Research*, vol. 17, no. 2, pp. 289–316, 2017.
[16] A. Khalid, P. Kirisci, Z. H. Khan, Z. Ghrairi, K. D. Thoben, and J. Pannek, "Security framework for industrial collaborative robotic cyber-physical systems," *Computers in Industry*, vol. 97, no. 4, pp. 132–145, 2018.
[17] A. Huang, "A risk detection system of e-commerce: researches based on soft information extracted by affective computing web texts," *Electronic Commerce Research*, vol. 18, no. 1, pp. 143–157, 2018.
[18] X. Tian and L. Liu, "Does big data mean big knowledge? Integration of big data analysis and conceptual model for social commerce research," *Electronic Commerce Research*, vol. 17, no. 1, pp. 169–183, 2017.
[19] R. Alguliyev, Y. Imamverdiyev, and L. Sukhostat, "Cyber-physical systems and their security issues," *Computers in Industry*, vol. 100, no. 1, pp. 212–223, 2018.
[20] F. Huang and X. G. Zheng, "Incentives of logistics service lever in retail drop-shipping double channel supply chain," *Computer Integrated Manufacturing Systems*, vol. 25, no. 05, pp. 1296–1306, 2019.
[21] K. Sun, Z. F. Wang, and Z. H. Yan, "Classification and theoretical models of sharing economy business models: based on studies of three typical cases," *Management Review*, vol. 31, no. 07, pp. 97–109, 2019.
[22] R. Batarfi, M. Y. Jaber, and S. Zanoni, "Dual-channel supply chain: a strategy to maximize profit," *Applied Mathematical Modelling*, vol. 40, no. 21-22, pp. 9454–9473, 2016.
[23] N. M. Modak and P. Kelle, "Managing a dual-channel supply chain under price and delivery-time dependent stochastic demand," *European Journal of Operational Research*, vol. 272, no. 1, pp. 147–161, 2019.
[24] F. Soleimani, A. Arshadi Khamseh, and B. Naderi, "Optimal decisions in a dual-channel supply chain under simultaneous demand and production cost disruptions," *Annals of Operations Research*, vol. 243, no. 1-2, pp. 301–321, 2016.
[25] X. W. Zhu, "Outsourcing management under various demand Information Sharing scenarios," *Annals of Operations Research*, vol. 257, no. 1-2, pp. 449–467, 2017.
[26] T. Zhang, X. Zhu, and Q. Gou, "Demand forecasting and pricing decision with the entry of store brand under various information sharing scenarios," *Asia Pacific Journal of Operational Research*, vol. 34, no. 02, Article ID 1740018, 2017.
[27] D. Fang and Q. Ren, "Optimal decision in a dual-channel supply chain under potential information leakage," *Symmetry*, vol. 11, no. 3, p. 308, 2019.
[28] Y. Dai, L. Dou, H. Song, L. Zhou, and H. Li, "Two-way information sharing of uncertain demand forecasts in a dual-channel supply chain," *Computers & Industrial Engineering*, vol. 169, Article ID 108162, 2022.
[29] R. Qiu, L. Hou, Y. Sun, M. Sun, and Y. Sun, "Joint pricing, ordering and order fulfillment decisions for a dual-channel supply chain with demand uncertainties: a distribution-free approach," *Computers & Industrial Engineering*, vol. 160, Article ID 107546, 2021.
[30] H. Gintis, *The Bounds of Reason: Game Theory and the Unification of the Behavioral Sciences*, Princeton University Press, Princeton, New Jersey, 2014.
[31] X. Pan, W. Zhang, and L. Chou, "The theory on the environmental emission trading under the concept of two-tired earning," *Ekoloji*, vol. 28, no. 107, pp. 1659–1663, 2019.
[32] G. Pu, Y. Zhang, and L. C. Chou, "Estimating financial information asymmetry in real estate transactions in China-An application of two-tier Frontier model," *Information Processing & Management*, vol. 59, no. 2, Article ID 102860, 2022.
[33] V. Turkulainen and M. L. Swink, "Supply chain personnel as knowledge resources for innovation a contingency view," *Journal of Supply Chain Management*, vol. 53, no. 3, pp. 41–59, 2017.
[34] M. R. Gholamian and A. H. Taghanzadeh, "Integrated network design of wheat supply chain: a real case of Iran," *Computers and Electronics in Agriculture*, vol. 140, pp. 139–147, 2017.
[35] G. M. P. Wanderley, M. H. Abel, E. C. Paraíso, and J. P. A. Barthes, "MBA: a system of systems architecture model for supporting collaborative work," *Computers in Industry*, vol. 100pp. 31–42, C, 2018.

Hindawi
Mathematical Problems in Engineering
Volume 2022, Article ID 6802967, 11 pages
https://doi.org/10.1155/2022/6802967

Research Article

An Internet of Things (IoT)-Based Optimization to Enhance Security in Healthcare Applications

Ali M. Al Shahrani,[1] Ali Rizwan,[2] Manuel Sánchez-Chero,[3] Carmen Elvira Rosas-Prado,[4] Elmer Bagner Salazar,[5] and Nancy Awadallah Awad[6]

[1]*Faculty of Computer Studies, Arab Open University, Saudi Arabia*
[2]*Department of Industrial Engineering, Faculty of Engineering, King Abdulaziz University, Jeddah 21589, Saudi Arabia*
[3]*Universidad Nacional de Frontera, Sullana, Peru*
[4]*Universidad Alas Peruanas, Lima, Peru*
[5]*Universidad César Vallejo, Piura, Peru*
[6]*Department of Computer and Information Systems, Sadat Academy for Management Sciences, Cairo 11742, Egypt*

Correspondence should be addressed to Ali Rizwan; arkhan71@kau.edu.sa

Received 27 June 2022; Revised 29 July 2022; Accepted 5 August 2022; Published 30 September 2022

Academic Editor: Amandeep Kaur

The Internet of Things (IoT) is a network that connects a large number of items. Each thing uses sensors to create and gather data from its surroundings and then sends to other objects or a central database through a channel. Keeping and transforming this created data is one of the most difficult tasks in IoT today, and it is one of the top worries of all enterprises that deploy IoT technology. Sensing equipment together with communication, storing, and display devices get benefit from technological advancements in the healthcare sector. Moreover, medical parameters and postoperative days require close observation. Therefore, the most cutting-edge approach to healthcare communication is adopted, which makes use of the Internet of Things (IoT). We can use the Internet of Things to speed changes in the healthcare environment, such as enhancing patient involvement and outcomes and shifting healthcare from reactive to proactive accessibility. Nonetheless, the growth of IoT exposes healthcare practitioners and their patients to new vulnerabilities, risks, and security concerns. However, there is currently a scarcity of research on how to improve IoT security in healthcare. Existing studies tend to concentrate only on the installation of IoT peripherals in a healthcare setting and to include a secure application solution. Because healthcare data and information are extremely sensitive, it is critical to have a secure health IoT application in place. As the IoT gets more widely used in healthcare, there will inevitably be more instances of sensitive patient information being made public. This paper proposes an optimized hashing algorithm with digital certificates to enhance the security. Initially, the health data are collected and preprocessed using normalization. The data are then stored in the IoT device. Here, the digital certificates are used for authentication purpose. The proposed discrete decision tree hashing algorithm (DDTHA) with ant colony optimization (ACO) hashes the unsigned digital certificates. The blowfish algorithm is used for encryption, and the signed digital certificate is obtained which is used for authentication purpose. The performance of the proposed system is evaluated and compared with conventional methodologies to prove the efficiency of the system.

1. Introduction

Today, IoT is an interesting topic in communication networks because it has the power to link the Internet with nearly endless kinds and numbers of sensors and devices and has a direct influence on our daily lives. There have been a lot of studies done in this area on the integration of various applications with the Internet of Things (IoT) [1, 2]. Although this technology has lately been intensively considered in the field of mobile healthcare, it has not yet been broadly implemented. To put it another way, m-health, or mobile healthcare, is the use of mobile devices to gather and store real-time health data from people and then make it available to healthcare practitioners, hospitals, and

insurance companies over the Internet. In recent years, m-health has been a major emphasis in the healthcare industry, with the most prominent example being portable diabetes management systems [3]. Figure 1 depicts the general framework of the IoT healthcare system.

Data gathered by sensing devices are the cornerstone of IoT systems and applications; nevertheless, the fact is that such data obtained by the sensor network are unreliable. To execute a wide range of difficult duties, sensor nodes are randomly placed in harsh environments and deserted regions, and they play a vital role in many different industries such as surveillance systems and smart cities, health monitoring, and intrusion detection. The underlying sensor network is more susceptible to assaults because of its complicated surroundings. There are many forms of assaults that may occur on network systems and resources; therefore, it is important to keep them safe. Attacks on WSNs may be classified as either internal or external, depending on where they originate. Existing research shows that assaults on the IoT network from the inside are significantly more damaging than attacks from the outside. To make matters worse, the security techniques for encrypted identification as well as routing protocols are efficient against external assaults but ineffective against internal ones. If a network has any network users, a quick and easy way to deal with them is to use trust assessment. Security on the other hand is a vital building block of modern systems [4]. Every once in a while, security mechanisms for authentication compel both classical and comment occurrences to be rigorously scrutinized, and they also call for cutting-edge security solutions for IoT devices with limited resources and performance to continue using IoT-based services in the real universe. Access control techniques that are computationally safe are thus an absolute need with the ever-computational craze. As a result, hash-based signature (HBS) schemes are a strong contender, as they provide security assurances based on reasonable hash features and are now the subject of cutting-edge certification activities [5]. Figure 2 depicts wearable healthcare devices.

The memory controller, on the other hand, oversees the network and ensures that only a single sensor node is ever in use. Carrier sensing may then be used by the master to minimize collisions with other networks running in the same frequency range as the master. Using the controller prevents problems. Either the memory controller selects the network devices as needed for information, or the sensor networks contact the controller for authorization to send data. A sensor network must also continuously listen for the next signal when it loses sync with the network master. Because of its greater power source, the master can send more power and serve as a portal to the surrounding world [6]. Healthcare services management has recently been regarded as an information-driven subject. Healthcare services management can only be improved via the use of information systems [7]. Despite ongoing breakthroughs in this field, the existing healthcare system faces several difficulties. There are technological advances like haze and the IoT capable of providing new services to the patients and adapting individuals from conventional healthcare control techniques to fresh technology processes due to growing life

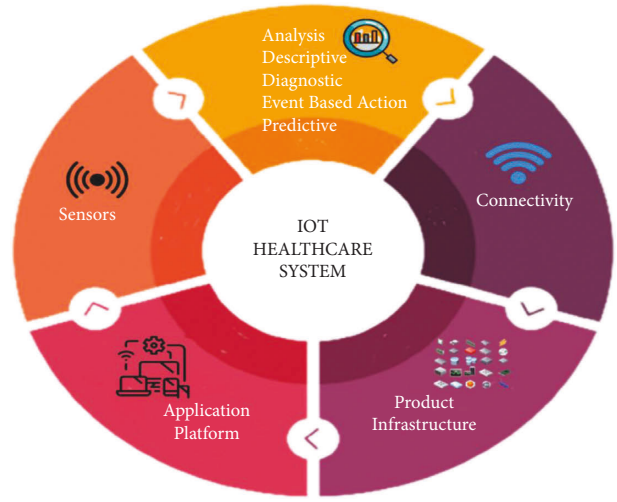

Figure 1: General framework of IoT healthcare system.

Figure 2: Wearable healthcare devices.

span, aging process citizens, and irreversible rapid population difficulties. There is possible cooperation between staff and service users (or those seeking support to improve overall comfort and wellbeing) at several levels in the administration of healthcare services. Lack of frequent and continuous usage has often resulted in the failure of innovative healthcare systems based on unique concepts like the Internet of Things [7].

1.1. Contribution of the Paper. The paper's main contribution is the security enhancement model in IoT using an optimized hashing algorithm with digital certificates for healthcare applications.

(i) To eliminate the unrelated or duplicated data from the raw datasets, the normalization approach is used.

(ii) The proposed DDTHA is used to boost the security of data, and ACO is also used to optimize the DDTHA's performance.

(iii) To convert the data into encoded data, the blowfish algorithm is used.

2. Literature Review

In this study, we provide a system for employing a secure IoT network to store, exchange, and transmit healthcare data. Here, we provide a summary of recent studies that are pertinent to our strategy and implementation. Share creation techniques and secret sharing methodology combined with improvement models are widely applied approaches to address several issues like impact of security and effectiveness of the plan. The shortcomings caused by the length and form of the secret target key have been expressly addressed by these improvement models. As mentioned in the study's major findings, distinct enticing ideal outcomes with changes based on the secret target key's varying lengths were shown. The study went further in addressing the drawbacks of the counting-based secret sharing generating techniques that were first developed [8]. The author [9] suggested using a unique algorithm to increase picture transmission security. Here, every input picture is resized, transformed into an audio file, and then delivered as an audio recording rather than being directly encrypted. The wav input is once more shrunk at the recipient's end to recover the output picture. It is far more challenging to identify any data contained in the audio because the data are in the form of audio. Information may be altered, data can be introduced that are not verified and are fake, etc., through intrusion. Using smart machines and blockchain technology, a contract is created to prevent these sorts of assaults from occurring. Several AI-based intelligent agents and blockchain are used throughout this suggested architecture. Adding biometric-based solutions for increased security may be a future improvement to this work. Again for purpose of identifying weaknesses in current security and privacy-preservation methods of EHR sets of data and developing a fresh approach for improving them, this study is being conducted [10]. Electronic health records, which store medical data electronically, have taken the role of older paper-based methods. The electronic health information system's susceptibility to attack vectors that adversely impact the security and privacy of medical information is one of the most crucial elements. We will discuss various security models and data privacy with e-health information in this essay. E-healthcare networks are often threatened by unauthorized availability of electronic devices, manipulation of data, denial-of-service assaults, and phishing. It is critical to developing a position access control because of the wide range of people obtaining this critical information from electronic health systems [11]. This research [12] examines how changing centralized databases to corner ones might reduce data manipulation. Cloud, fog, blockchain, and IoMT are all parts of the system. An IoMT was self-contained. The network standard method was also tested with public cloud resources. Several research initiatives use this encryption for its privacy benefits. Building a privacy-preservation mechanism to protect classified data transfers is difficult. Data transfer via an IoT network must be secure and maintain data integrity. It is tricky. Adaptive IoT security makes it difficult to distinguish between routine and attack events. The author [13] recommended using blockchain and public key infrastructure to limit patient access to electronic medical information. Information communication is hindered by an incompatible provider and hospital systems. Since the focus here is on the preservation of privacy in smart healthcare, this article has focused on the topic of electronic prescription transmission privacy assurances (ETP). Another flaw in the healthcare industry's strategy is there is no way to provide individual users' rights well beyond those granted to the group [14]. To sustain patients' credibility and confidence in digital healthcare, a major scientific improvement is needed. This paper examines the e-health cloud's cryptographic and noncryptographic security techniques to safeguard privacy components and their limitations in the growing digital world. ABE's downside is requiring data owners to utilize an authorized user's public key for encryption. KP-ABE has limited scalability, and the data owners cannot pick who decodes the encrypted data since they must trust the key issuer [15]. For the sake of this study [16], they enhanced FL with a new, more lightweight security and privacy mechanism. As part of the federation training, they target devices powered by IoHT that required a privacy guarantee for privately owned health information. Each node in the federation employed DP to prevent data leaking. It is still impossible to have fully decentralized FL since no federation nodes have training capability, there are not enough good trained data, and training data must be traced back to their source. The goal of this study [17] is both COVID-19 and non-COVID-19 blockchain applications and services. Medline, SpringerLink, IEEE Xplore, ScienceDirect, arXiv, and Google Scholar were searched till July 29, 2021. Prototypes of clinical and technical designs were featured. Distributed databases are a well-established platform in healthcare organizations. However, systems have major disadvantages, including not being able to exchange data among peers, being vulnerable to outside threats (such as hacking), and not having an unchangeable data model. The healthcare system can sustain the trade-off between security and cost for prompt sickness diagnosis since security and cost problems are handled in this research. To prevent the compromising of private medical data on open networks, Schnorr signature encryption utilizing HECC was developed. When employed for accurate health diagnosis, sensor nodes that communicate data to the medicine server (MS) via the base station (BS) provide privacy and security risks to users [18]. The security and privacy of IoT in healthcare and issues with developing security standards, including security and privacy alternatives, are all covered in this article [19]. Homomorphic encryption allows computation on encrypted data. Due to IoT devices' limited processing capacity, low battery, and other restrictions, smart healthcare systems' security architecture is disregarded, resulting in countless security breaches. The author [20] reviewed EHS security considerations. EHS data protection is a hot topic. Various security measures have been developed for preventing threats and assaults. Due to EHS's sensitivity and openness, the proposed solutions do not ensure total security [21]. They

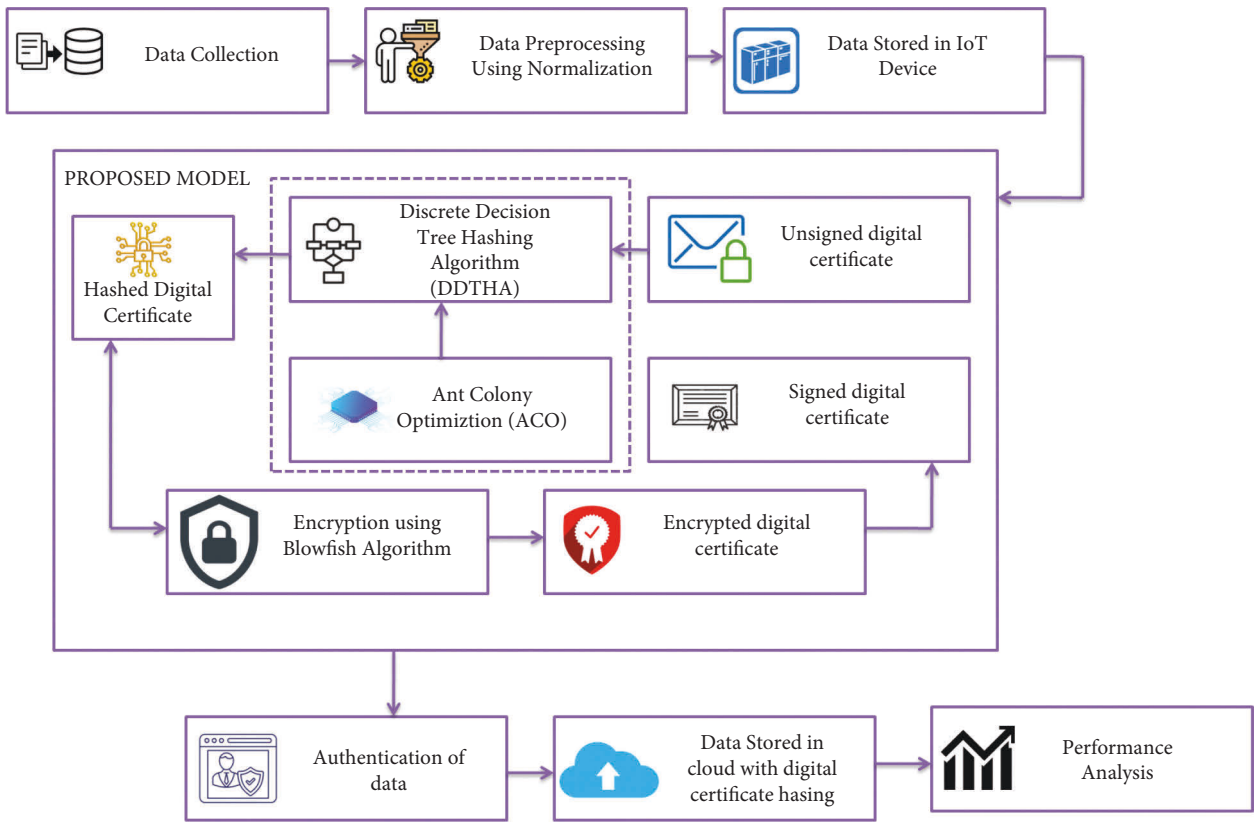

Figure 3: Proposed methodology of this research.

explored EHS security in this article. The most study focuses on protecting EHS data. Several security solutions have been offered for various threats and assaults. Due to EHS's sensitivity and openness, the provided methods are insufficient for total security. This paper [22] presents a cloud computing overview and reviews recent security concerns and solutions. Encrypting data in the cloud offer protected data access. They also faced certain cloud security engineering problems. Identifying these issues is the first step in addressing them; subsequent research must propose more practical answers. Due to solution protocol intricacies, they could not explain. To let others address and work on the concerns, they omitted certain solution specifics and procedures.

3. Proposed Methodology

IoT data management is one of the most challenging jobs in IoT today, and it is a major concern for all businesses that use IoT technology. This study suggests a digital certificate-enabled, optimized hashing technique to increase security. The health information is first gathered and normalized as part of the preprocessing. Digital certificates are used in this situation for authentication. Digital certificates that have not been signed are hashed using the proposed discrete decision tree hashing algorithm (DDTHA) with ant colony optimization (ACO). A signed digital certificate is acquired, and the blowfish technique is used to encrypt data for authentication. Figure 3 depicts the proposed methodology of this research.

Two datasets [23] on cardiovascular disease from Cleveland and Hungary were used to evaluate the proposed methodology. Those sets of data originate from the "University of California, Irvine (UCI)." There are 303 cases all in the original Cleveland database. There are a total of 294 cases in the Hungarian database.

3.1. Data Preprocessing Using Normalization. Typically, healthcare databases are made up of a range of heterogeneous data sources, and the data extracted from them are different, partial, and redundant, all of which have a significant impact on the final mining outcome. As a result, healthcare data must be preprocessed to guarantee that it is accurate, full, and consistent, as well as has privacy protection. Data normalization is a preprocessing procedure that scales or changes data to ensure an equitable contribution. Normalization enables us to construct a unique range from an existing one. It can anticipate or foresee advantages. Normalization adjusts raw data, so each characteristic contributes consistently. It solves dominant features and outliers, two fundamental machine learning data issues. Many methods for normalizing raw (un-normalized) data within a specified range have been devised. This research normalizes. These techniques are categorized by how they normalize raw data's statistical properties. It retains information relationships. It is a basic approach for fitting information inside predefined bounds.

As per this normalization method,

$$A' = \left(\frac{A - \min \text{value of } A}{\max \text{value of } A - \min \text{value of } A}\right) * (B - C) + C. \quad (1)$$

A represents real data, while D represents mapped data.

Parameter normalization uses mean and standard deviation to normalize unstructured data. (2) shows how to normalize unstructured data using the z-score variable:

$$f_i' = \frac{f_i - \overline{Y}}{\text{std}(Y)}, \quad (2)$$

where f_i' illustrates normalized values and f_i illustrates rate of the row Y of the *ith* column

$$\text{std}(Y) = \sqrt{\frac{1}{(m-1)} \sum_{i=1}^{m} (f_i - \overline{Y})^2}, \quad (3)$$

$$\overline{Y} = \frac{1}{m} \sum_{i=1}^{m} f_i \text{ or mean value.}$$

This method may be used to normalize each row above. Imagine a row where every value is the same, the standard deviation is 0, and every value is 0. Normalization indicates 0-1 values. Decimal scaling ranges from −1 to 1. This strategy

$$f_i = \frac{f}{10^q}. \quad (4)$$

Here, f_i represents the scaled values, f denotes the range of values, and q illustrates the smallest integer $\text{Max}(|f_i|) < 1$.

The data that have been preprocessed are subsequently saved to an IoT device. Then, the stored data are subsequently transmitted to a procedure called hashing, which is used for authentication purposes.

3.2. Discrete Decision Tree Hashing Algorithm (DDTHA). A discrete decision tree hashing algorithm is used to hash the unsigned digital certificate. The following is a definition of DH's objective function:

$$\min_{V,C,E} \|V - JE\| C2 + \lambda \|E\|_C^2 + b\|V - C(I)\|_C^2 d.p.V \int \{-1, 1\}^{m \times h}. \quad (5)$$

There are two ways to look at this: DH looks at the relationship between the two variables and the relationship between the two variables and the other. To speed up the procedure, we believe that regressing J into V is equivalent to regressing J into V. As long as there is no third term in DH, binary codes for each class will be unique. There are two types of binary code differences: one is across classes, and the other is between all samples.

There are three unknown variables in the mixed binary integer program of the problem. To get around this, we are going to repeatedly solve the issue using alternating optimization. The optimization of SDH in that each iteration alternately updates E, T, and V. We have got all the information right here.

S-step

$$T = \left(\phi(I)^P \phi(I)\right)^{-1} \phi(I)^P V. \quad (6)$$

Q-step may be rewritten as

$$\begin{aligned} &\min_e pq\left((JE - V)^P (JE - V) + \lambda pq\left(E^P E\right)\right) \\ &\quad = \min_e pq\left(E^P \left(J^P J + \lambda X\right) E\right) - 2pq\left(E^P J^P V\right). \end{aligned} \quad (7)$$

E can be solved using a closed-form solution if the derivative concerning E is set to zero:

$$E = \left(J^P J + \lambda X\right)^{-1} J^P V. \quad (8)$$

T-step: let us rework the story when S and E are repaired

$$\begin{aligned} &\min_V pq\left(\left(V - JE\right)^P (V - JE)\right) + bpq\left(V - C(I)\right)^P \\ &\quad \cdot (V - C(I)) d.p.V \int \{-1, 1\}^{m \times h}. \end{aligned} \quad (9)$$

$pq(V^P v)$ is a constant and has the same meaning as (B).

$$\min_V -pq\left(V^P (JE + bC(I))\right) d.p.V \epsilon \{-1, 1\}^{m \times h}. \quad (10)$$

To get a closed-form solution to T, use the formula below.

$$V = sgn(JE + bC(I)). \quad (11)$$

DH's T-step uses cyclic coordinate descent to learn the hash code bit by bit. Instead of using many steps to solve each bit, the T-step of DH uses just one, making it significantly quicker than DH. Algorithm 1 explains how to solve the DH problem. Algorithm 1 depicts the DDTHA.

A convex surrogate loss is often used to replace the zero-one loss in binary classification. Exponential loss is often used in boosting strategies like this one. Learning the f-th hash function is a challenge because of this difficulty. As a result, we use AdaBoost to overcome this issue. A decision tree and its weighting coefficient are learned in each boosting iteration. A binary decision tree has a decision stump at every node. The goal of training a stump is to minimize the weighted classification error by determining the optimal feature size and threshold. The next step is to simultaneously choose features and learn the hash function. In the literature, several effective decision tree learning strategies may considerably speed up the training process.

3.3. Ant Colony Optimization (ACO). Ant colony optimization is a technique that is used to improve the efficiency of the hash function operation. The first version of the ACO has historical relevance since it serves as the prototype for many different ant algorithms that, when combined, implement the ACO paradigm. ACO already matches the preceding subsection's framework, with the parts listed below:

$$t_{n\psi}^s = \begin{cases} \dfrac{\tau_{n\psi}^\alpha + \eta_{n\psi}^\beta}{\sum_{(n\zeta) \notin tabu_s} \left(\tau_{n\zeta}^\alpha + \eta_{n\zeta}^\beta\right)}, & \text{if } (n\psi) \notin tabu_s, \\ 0, & \text{otherwise.} \end{cases} \quad (12)$$

Inputs: training examples $\{i_x, j_x\} = 1$; code length h; maximum iteration number p; parameter λ
Output: binary codes $\{v_x\}_{x=1}^{m} \epsilon \{-1, 1\}^{m \times 1}$
Randomly select n examples $\{z_y\}_{x=1}^{n}$ from the trainingexamples and get the $\phi(x)$;
Initialize v_x as a $\{-1, 1\}$l vector randomly;
Initialize J as $J = \{J_{xy}\} \epsilon Q^{m \times f}$ where $J_{xy} = \begin{cases} 1, & if\ y_i = j \\ 0, & \text{otherwise} \end{cases}$;
Use (9) to initialize W;
Use (7) to initialize P;
Repeat
    T-step: Use (12) to solve T;
    K-step: Use (9) to solve E;
    S-step: Use (7) to solve T;
To acquire the hash function q_f, we must first train trees
Until convergence

Algorithm 1: DDTHA.

{Initialization}
Initialize $\tau_{n\psi}$ *and* $\eta_{n\psi}, \forall (n\psi)$
{Construction}
For each ant s (currently in state n) do
repeat
choose in probability the state to move
append the chosen move to the s-th ant's set $tabu_s$
until ant s has completed its solution.
end for
{Trail update}
For each ant move $(n\psi)$ *do*
compute $\Delta\tau_{n\psi}$
update the trailing matrix.
end for
{Terminating condition}
If not (end test) go to step

Algorithm 2: ACO.

$\begin{cases} \tau_{n\psi}^{\alpha} + \eta_{n\psi}^{\beta} / \sum_{(n\zeta) \notin tabu_s} (\tau_{n\zeta}^{\alpha} + \eta_{n\zeta}^{\beta}) & \text{if } (n\psi) \notin tabu_s \\ 0 & \text{otherwise} \end{cases}$ used in formula (10) indicates the effect of trail and attraction on $tabu_s$.

Formula (10) is used to update the trails after each iteration of the algorithm, i.e., after all ants have finished a solution.

$$\tau_{n\psi}(\tau) = \rho \tau_{n\psi}(\tau - 1) + \Delta\tau_{n\psi}. \tag{13}$$

For each step that an ant makes, (nψ), it contributes an equal amount of trail contributions, based on how well it solves its problem. This means that a better solution means a bigger contribution.

Using the TSP as an example, movements correspond to graph arcs; thus, a route ending at node x may correspond to the state n, while the state would correspond to the same path but with the arc (xy) added at the end (xy). Formula (12) becomes $\tau_{xy}(p) = \rho \tau_{xy}(p - 1) + \Delta\tau_{xy}$, if the length N_S of the tour discovered by the ant is used to measure the quality of the ant's answer to s.

$$\Delta\tau_{xy} = \sum_{s=1}^{f} \Delta\tau_{xy}^{s},$$
$$\Delta\tau_{xy}^{s} = \begin{cases} \dfrac{W}{N_s}, & \text{if ant } s \text{ uses are } (xy) \text{ initstour,} \\ 0, & \text{otherwise.} \end{cases} \tag{14}$$

W is a constant parameter in this example.

Ants build solutions in parallel and then update the trail levels in the main loop of the ant system. Various parameters must be tuned correctly for the algorithm's performance to be at its best τ_{xy} (0). These parameters include α, β, f, the number of insects used to define the quality of the solution, and W (which is used to define the relative relevance of ρ, trail, and attraction). Algorithm 2 depicts the ACO.

The process of hashing turns an unsigned digital certificate into a hashed one, which is subsequently changed

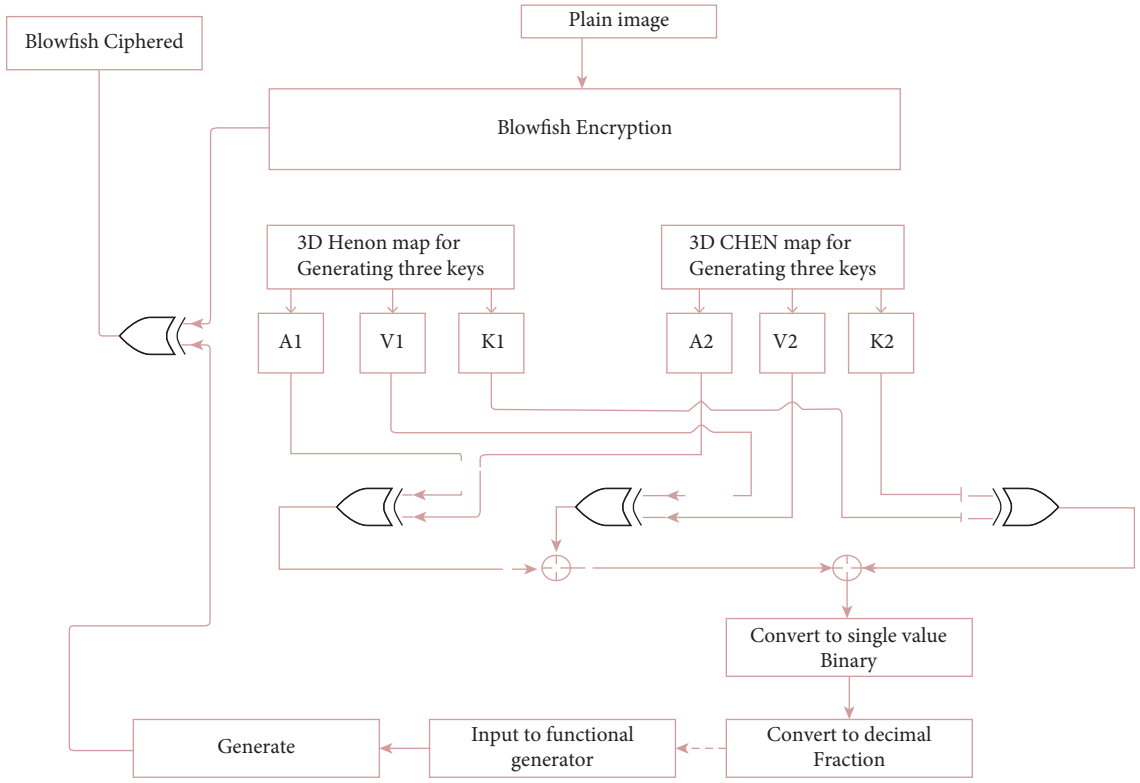

Figure 4: Framework of blowfish algorithm.

into an encrypted one via encryption. Finally, a signed digital certificate may be produced after the final encryption step.

3.4. Encryption Using Blowfish Algorithm (BA). During the process of encryption, the blowfish technique is used in our study to transform the plain text into cipher text. After the certificates have been encrypted, the hashed digital certificate then converts them into an encrypted digital certificate from which the final signed digital certificate is obtained.

In the BA framework, 3-dimensional Henon (Hn) and Chen (Ch) maps for encryption provide a supplement to numerical formulations and encrypted variables. BA is used to preprocess data from cloud databases. Figure 4 depicts the BA framework.

The mathematical expression for Hn map was provided as

$$\begin{aligned} x_{i+1} &= a - y_i^2 - bz_i, \\ x_{i+1} &= x_i, \\ y_{i+1} &= y_i. \end{aligned} \tag{15}$$

In comparison with the maps made out of extra current chaotic attractors, the stated attractor creates more challenging Hn maps. The following numerical equations serve as representations for the iterative map of Ch:

$$\begin{aligned} x_{i+1} &= a(y_i - z_i), \\ y_{i+1} &= (c-a)x_i - x_i z_i + cy_i, \\ z_{i+1} &= x_i y_i + bz_i. \end{aligned} \tag{16}$$

The unusual three-dimensional complexity of the dynamic attribute, in addition to the dimensionality, makes the system rather challenging. At last, the digital certificate that has been encrypted is saved in the cloud together with the digital certificate hashing.

4. Results and Discussion

In this paper, we investigate the security enhancement model in IoT using an optimized hashing algorithm with digital certificates for healthcare applications. "Waikato Environment for Knowledge Analysis (Weka)" and Java were used to establish this system's back end. To start this study, the datasets are collected from UCI. There are 303 cases all in the original Cleveland database. There are a total of 294 cases in the Hungarian database. The parameters are encryption time, decryption time, execution time, avalanche effect, and energy consumption. The existing methods are Lamport Merkle Digital Signature [LMDS (25)], Lightweight Mutual Authentication and Key Agreement [LMAKA (26)], PIRATE [PIRATE (27)], and Proxy Re-Encryption using RSA [PRER (28)].

Figure 5 depicts the encryption time. Encryption time discusses and indicates the average time needed to encrypt input media content files. It is measured in seconds. When it comes to encryption, the amount of time it takes to encrypt a given media data is directly related to the input media content file size. The LMDS was evaluated with an encryption time of 98 seconds. LMAKA was evaluated with an encryption time of 90 seconds. PIRATE was evaluated with an encryption time of 80 seconds. Proxy Re-Encryption

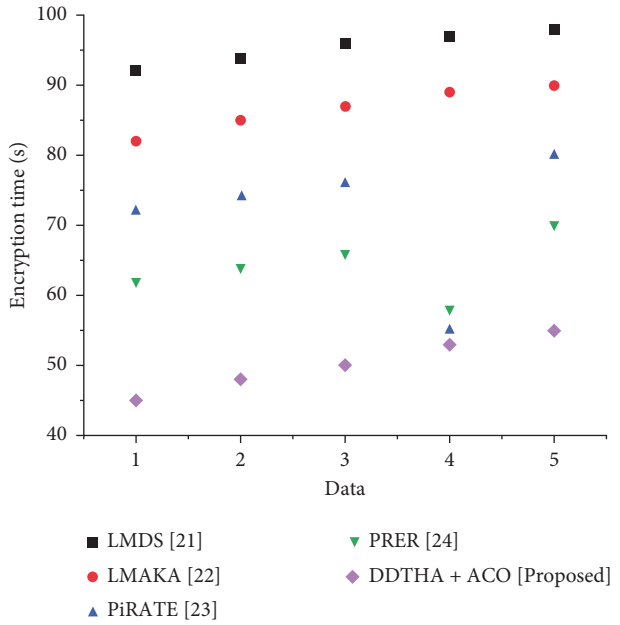

Figure 5: Comparative analysis of encryption time in suggested and traditional methods.

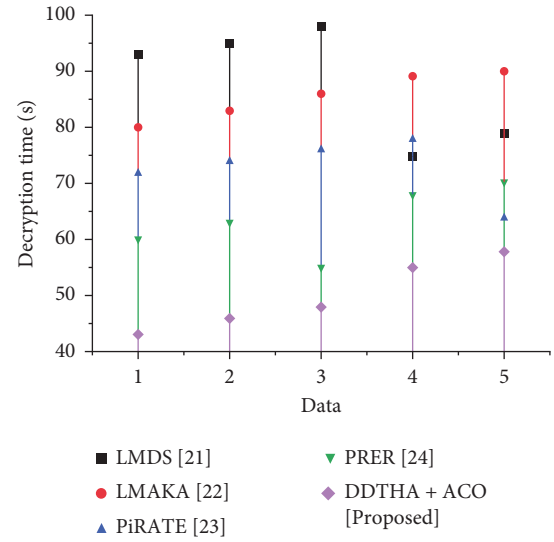

Figure 6: Comparative analysis of decryption time in suggested and traditional methods.

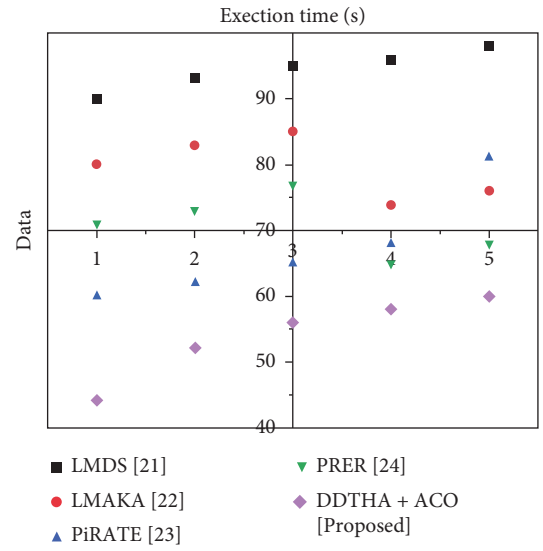

Figure 7: Comparative analysis of execution time in suggested and traditional methods.

using RSA was evaluated with an encryption time of 70 seconds. The proposed method discrete decision tree hashing algorithm with ant colony optimization (DDTHA + ACO) was evaluated with an encryption time of 55 seconds. Time taken by the proposed DDTHA + ACO technique for encryption was lesser compared to existing approaches like LMDS, LMAKA, PIRATE, and PRER. Thus, the proposed method encrypts data efficiently.

Decryption refers to the process of converting encrypted data back to its original state. Reverse encryption is often used. It decodes encrypted data so that only authorized users can do so since decryption needs a secret key or password.

Figure 6 depicts the decryption time. The Lamport Merkle Digital Signature was evaluated with a decryption time of 79 seconds. LMAKA was evaluated with a decryption time of 90 seconds. PIRATE was evaluated with a decryption time of 64 seconds. Proxy Re-Encryption using RSA was evaluated with a decryption time of 70 seconds. The proposed method discrete decision tree hashing algorithm with ant colony optimization (DDTHA + ACO) was evaluated with a decryption time of 58 seconds. Time taken by the proposed DDTHA + ACO technique for decryption was lower when compared with existing approaches like LMDS, LMAKA, PIRATE, and PRER.

The amount of time the system spends executing runtime or system operations on its behalf is taken into account when calculating the execution time of a job. The implementation determines the technique for calculating execution time.

Figure 7 depicts the execution time. The Lamport Merkle Digital Signature was evaluated with an execution time of 98 seconds. LMAKA was evaluated with an execution time of 76 seconds. PIRATE was evaluated with an execution time of 81 seconds. Proxy Re-Encryption using RSA was evaluated with an execution time of 68 seconds. The proposed method discrete decision tree hashing algorithm with ant colony optimization (DDTHA + ACO) was evaluated with an execution time of 60 seconds. Time taken by the proposed DDTHA + ACO technique for execution time was less when compared with existing approaches like LMDS, LMAKA, PIRATE, and PRER.

Using the avalanche effect, it is possible to compare the effectiveness of suggested and traditional algorithms in assuring media data security. It is estimated based on the algorithm's resilience to threats and on-the-fly attacks during media data transfer. The avalanche effect in encryption methods is defined as the proportion of changed bits in the cipher text to the total number of bits in the cipher text.

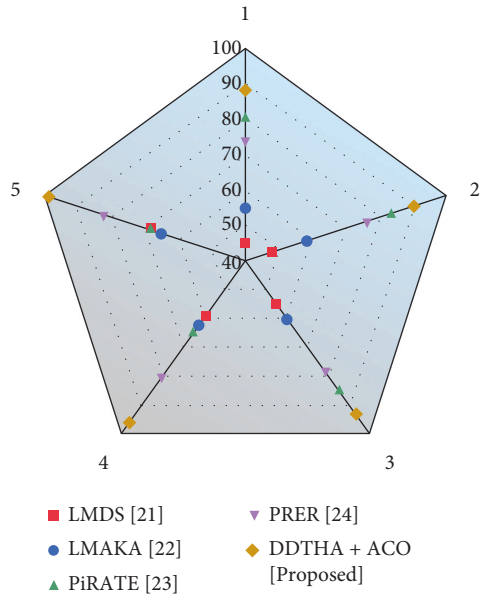

Figure 8: Comparative analysis of avalanche effect in suggested and traditional methods.

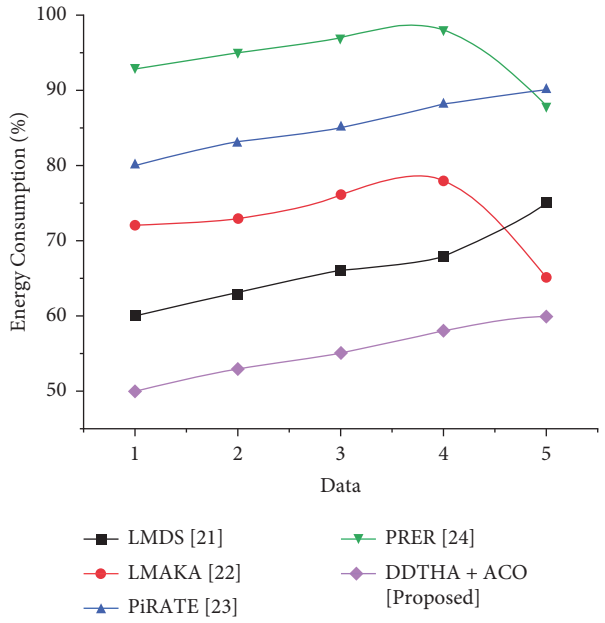

Figure 9: Comparative analysis of energy consumption in suggested and traditional methods.

Figure 8 depicts the avalanche effect. The Lamport Merkle Digital Signature was evaluated with the avalanche effect of 68 percent. LMAKA was evaluated with the avalanche effect of 65 percent. PIRATE was evaluated with the avalanche effect of 68 percent. Proxy Re-Encryption using RSA was evaluated with the avalanche effect of 82 percent. The proposed method discrete decision tree hashing algorithm with ant colony optimization (DDTHA + ACO) was evaluated with the avalanche effect of 98 percent. Compared to the current approaches, the suggested method exhibits more significance. When compared to the suggested technique, the current methods LMDS, LMAKA, PIRATE, and PRER reveal less effectiveness.

Energy consumption refers to the amount of power or energy consumed to encrypt data.

Figure 9 depicts energy consumption. The Lamport Merkle Digital Signature was evaluated with an energy consumption of 75 percent. LMAKA was evaluated with an energy consumption of 65 percent. PIRATE was evaluated with an energy consumption of 90 percent. Proxy Re-Encryption using RSA was evaluated with an energy consumption of 88 percent. The proposed method discrete decision tree hashing algorithm with ant colony optimization (DDTHA + ACO) was evaluated with an energy consumption of 60 percent. The suggested method shows less than the current approaches. The existing approaches, LMDS, LMAKA, PIRATE, and PRER, demonstrate high efficacy when compared to the proposed technique.

Precision is the resolution of the representation, often determined by the number of decimal or binary digits, whereas accuracy is the proximity of a computation to the true value.

The ability of a classifier to identify all positive samples is referred to as recall. Value (%) for recall, precision, and accuracy is shown in Figure 10. The Lamport Merkle Digital

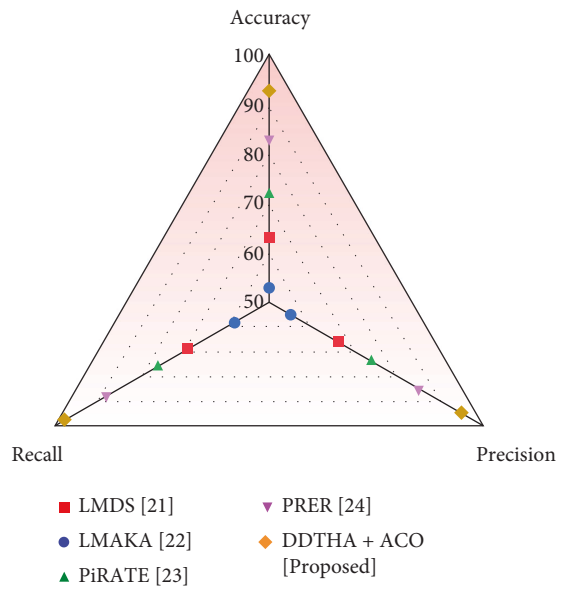

Figure 10: Comparative analysis of suggested and traditional methods.

Signature was evaluated with recall, precision, and accuracy of 69, 66, and 63 percent, respectively. LMAKA was evaluated with recall, precision, and accuracy of 58, 55, and 53 percent, respectively. PIRATE was evaluated with recall, precision, and accuracy of 76, 74, and 72 percent, respectively. Proxy Re-Encryption using RSA was evaluated with recall, precision, and accuracy of 88, 85, and 83 percent, respectively. The proposed method discrete decision tree hashing algorithm with ant colony optimization (DDTHA + ACO) was evaluated with recall, precision, and accuracy of 98, 95, and 93 percent, respectively. The

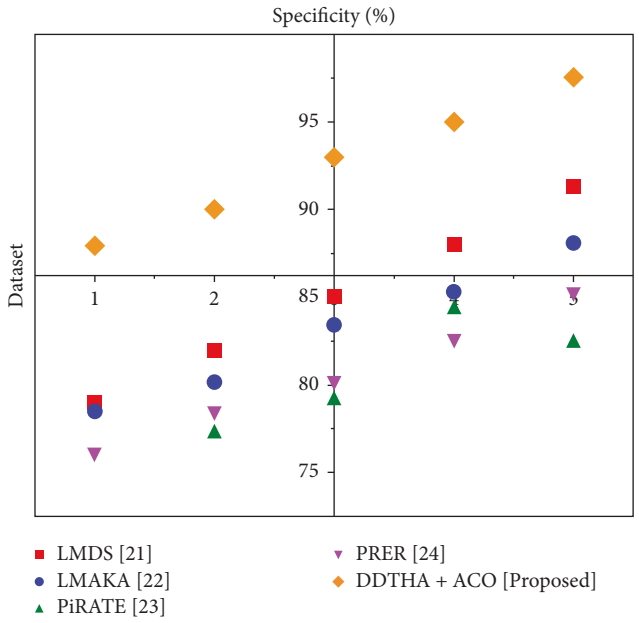

Figure 11: Comparative analysis of specificity.

suggested method shows higher than the current approaches. The existing approaches, LMDS, LMAKA, PIRATE, and PRER, demonstrate less when compared to the proposed technique.

LMDS specificity was 91.3%. LMAKA had 88.1% specificity. PIRATE's specificity was 82.4%. PRER was 85.3% specific. The DDTHA + ACO technique was 97.6% specific. The suggested method is better than the current approaches. The existing techniques are less successful than the suggested technique.

Figures 5 to 11 depict comparison of comparing the suggested approach with the current models. Existing methods used in this study are LMDS [21], LMAKA [22], PIRATE [23], and PRER [24]. Figures clearly show that the suggested approach performs better than the current techniques because of the existing method's drawbacks. The following are the drawbacks of the existing methods. LMDS requires more processing time, LMAKA is less secured, PIRATE requires high computational cost, whereas PRER has the issue of a processed lag brought on by dumping a major amount of computing work to the proxy for re-encryption, as well as the computationally intensive data in transit encryption as well as users' decryption procedures brought on by asymmetric cryptographic usage.

5. Conclusion

It is exceedingly challenging to guarantee the safety and confidentiality of an IoT-based health service. It is considerably more challenging by the fact that IoT is frequently used to link clients to healthcare organizations among a wide network of services who are dispersed across several domains and with various trust authorities. This makes it more difficult to secure patient information. A lot of researchers have come up with a variety of authentication and authorization strategies in order to avoid and preserve the sensitive data that are acquired with the assistance of wearable Internet of Things devices. However, there is a need for end-to-end security solutions in order to protect and control the data on patients' health. For this reason, it is crucial to implement stringent safety measures to protect this patient's information. In light of this, the research presented here suggests an improved hashing method that makes use of digital certificates in order to increase security. The unsigned digital certificates can be hashed using the discrete decision tree hashing algorithm (DDTHA) with ant colony optimization (ACO) that has been developed. In order to encrypt the data, the blowfish method is utilized, and then a signed digital certificate is created for subsequent usage in the authentication process. The proposed approach was analyzed and compared with existing approaches, as well as the proposed approach attained the greatest performance in terms of encryption time (55 s), decryption time (58 s), execution time (60 s), avalanche effect (98%), and energy consumption (65%) than those existing approaches.

5.1. Future Scope. However, there are still some restrictions on how quickly data may be encoded and decoded according to this study. That means it will have to be improved soon. The efficiency of this study could be greatly improved with the use of optimization methods for the problem of improving encryption and decryption speeds. Furthermore, the focus of this study is on only heart problems. More disease observation is needed in the future to help this field advance. As a result, we advise that, in the near future, a novel security method be developed in order to identify misbehaving greedy nodes in IoT networks.

Data Availability

The data that support the findings of this study are available on request from the corresponding author.

Conflicts of Interest

The authors declare that they have no conflicts of interest.

Acknowledgments

The authors would like to thank Arab Open University, Saudi Arabia, for supporting this study.

References

[1] A. Rizwan, D. A. Karras, J. Kumar, M. Sánchez-Chero, M. M. Mogollón Taboada, and G. C. Altamirano, "An internet of things (IoT) based block chain technology to enhance the quality of supply chain management (SCM)," *Mathematical Problems in Engineering*, vol. 2022, Article ID 9679050, 12 pages, 2022.

[2] A. Rizwan, D. A. Karras, M. Dighriri et al., "Simulation of IoT-based vehicular ad hoc networks (VANETs) for smart traffic management systems," *Wireless Communications and Mobile Computing*, vol. 2022, Article ID 3378558, 11 pages, 2022.

[3] A. Choudhuri, J. M. Chatterjee, and S. Garg, "Internet of Things in healthcare: a brief overview," *Internet of Things in Biomedical Engineering*, pp. 131–160, 2019.

[4] M. Usak, M. Kubiatko, M. S. Shabbir, O. Viktorovna Dudnik, K. Jermsittiparsert, and L. Rajabion, "Health care service delivery based on the Internet of things: a systematic and comprehensive study," *International Journal of Communication Systems*, vol. 33, no. 2, Article ID e4179, 2020.

[5] H. Z. Almarzouki, H. Alsulami, A. Rizwan, M. S. Basingab, H. Bukhari, and M. Shabaz, "An internet of medical things-based model for real-time monitoring and averting stroke sensors," *Journal of Healthcare Engineering*, vol. 2021, pp. 1–9, 2021.

[6] S. Suhail, R. Hussain, A. Khan, and C. S. Hong, "On the role of hash-based signatures in quantum-safe internet of things: current solutions and future directions," *IEEE Internet of Things Journal*, vol. 8, no. 1, pp. 1–17, 2021.

[7] R. Krishnamoorthi, S. Joshi, H. Z. Almarzouki et al., "A novel diabetes healthcare disease prediction framework using machine learning techniques," *Journal of Healthcare Engineering*, vol. 2022, Article ID 1684017, 10 pages, 2022.

[8] M. Al-Ghamdi, M. Al-Ghamdi, and A. Gutub, "Security enhancement of shares generation process for multimedia counting-based secret-sharing technique," *Multimedia Tools and Applications*, vol. 78, no. 12, pp. 16283–16310, 2019.

[9] M. Saravanan and A. Priya, "An algorithm for security enhancement in image transmission using steganography," *Journal of the Institute of Electronics and Computer*, vol. 1, no. 1, pp. 1–8, 2019.

[10] F. F. Alruwaili, "Artificial intelligence and multi agent based distributed ledger system for better privacy and security of electronic healthcare records," *PeerJ Computer Science*, vol. 6, p. e323, 2020.

[11] G. I. Ahmad, J. Singla, and K. J. Giri, "Security and privacy of E-health data," in *Multimedia Security*, pp. 199–214, Springer, Berlin, Germany, 2021.

[12] M. A. Almaiah, F. Hajjej, A. Ali, M. F. Pasha, and O. Almomani, "A novel hybrid trustworthy decentralized authentication and data preservation model for digital healthcare IoT based CPS," *Sensors*, vol. 22, no. 4, p. 1448, 2022.

[13] M. T. De Oliveira, L. H. Reis, R. C. Carrano et al., "Towards a blockchain-based secure electronic medical record for healthcare applications," in *Proceedings of the ICC 2019-2019 IEEE International Conference on Communications (ICC)*, pp. 1–6, IEEE, Shanghai, China, May 2019.

[14] M. A. Azad, J. Arshad, S. Mahmoud, K. Salah, and M. Imran, "A privacy-preserving framework for smart context-aware healthcare applications," *Transactions on Emerging Telecommunications Technologies*, Article ID e3634, 2019.

[15] S. Chenthara, K. Ahmed, H. Wang, and F. Whittaker, "Security and privacy-preserving challenges of e-health solutions in cloud computing," *IEEE Access*, vol. 7, pp. 74361–74382, 2019.

[16] M. A. Rahman, M. S. Hossain, M. S. Islam, N. A. Alrajeh, and G. Muhammad, "Secure and provenance enhanced internet of health things framework: a blockchain managed federated learning approach," *IEEE Access*, vol. 8, pp. 205071–205087, 2020.

[17] W. Y. Ng, T. E. Tan, P. V. H. Movva et al., "Blockchain applications in health care for COVID-19 and beyond: a systematic review," *The Lancet Digital Health*, vol. 3, no. 12, pp. e819–e829, 2021.

[18] J. Iqbal, M. Adnan, Y. Khan et al., "Designing a healthcare-enabled software-defined wireless body area network architecture for secure medical data and efficient diagnosis," *Journal of Healthcare Engineering*, vol. 2022, pp. 1–19, 2022.

[19] S. M. Karunarathne, N. Saxena, and M. K. Khan, "Security and privacy in IoT smart healthcare," *IEEE Internet Computing*, vol. 25, no. 4, pp. 37–48, 2021.

[20] A. Singh and K. Chatterjee, "ITrust: identity and trust based access control model for healthcare system security," *Multimedia Tools and Applications*, vol. 78, no. 19, pp. 28309–28330, 2019.

[21] J. J. Hathaliya and S. Tanwar, "An exhaustive survey on security and privacy issues in Healthcare 4.0," *Computer Communications*, vol. 153, pp. 311–335, 2020.

[22] M. Mehrtak, S. SeyedAlinaghi, M. MohsseniPour et al., "Security challenges and solutions using healthcare cloud computing," *Journal of Medicine and Life*, vol. 14, no. 4, pp. 448–461, 2021.

[23] F. Ali, S. El-Sappagh, S. R. Islam et al., "A smart healthcare monitoring system for heart disease prediction based on ensemble deep learning and feature fusion," *Information Fusion*, vol. 63, pp. 208–222, 2020.

[24] J. A. Alzubi, "Blockchain-based Lamport Merkle digital signature: authentication tool in IoT healthcare," *Computer Communications*, vol. 170, pp. 200–208, 2021.

Hindawi
Mathematical Problems in Engineering
Volume 2022, Article ID 7769951, 20 pages
https://doi.org/10.1155/2022/7769951

Research Article

Evaluation of Using Genetic Algorithm and ArcGIS for Determining the Optimal-Time Path in the Optimization of Vehicle Routing Applications

Da'ad Ahmad Albalawneh and Mohamad Afendee Mohamed

Computer Science Department, Faculty of Informatics and Computing, Universiti Sultan Zainal Abidin, Kuala Terengganu, Malaysia

Correspondence should be addressed to Da'ad Ahmad Albalawneh; si2784@putra.unisza.edu.my

Received 20 June 2022; Revised 25 July 2022; Accepted 22 August 2022; Published 27 September 2022

Academic Editor: Amandeep Kaur

Transportation is regarded as one of the most important issues currently being researched; this issue needs the search for approaches or processes that might lessen many contemporary traffic concerns. Congestion, pollution, and accidents have escalated lately, negatively impacting urban environments, economic development, and citizens' lifestyles. The rise of illnesses and epidemics throughout the world, such as COVID-19, has created an urgent need to find the best way to save people's lives. The vehicle routing problem (VRP) is a well-known moniker for improving transportation systems and is regarded as one of the ancient and contemporary difficulties in route planning applications. One of the main tasks of VRP is serving many customers by determining the optimal route from an initial point to a destination on a real-time road map. The best route is not necessarily the shortest-distance route, but, in emergency cases, it is the route that takes the least fitness cost (time) and the fastest way to arrive. This paper aims to provide an adaptive genetic algorithm (GA) to determine the optimal time route, taking into account the factors that influence the vehicle arrival time and cause delays. In addition, the Network Analyst tool in ArcGIS is used to determine the optimal route using real-time map based on the user's preferences and suggest the best one. Experimental results indicate that the performance of GA is mainly determined by an efficient representation, evaluation of fitness function, and other factors such as population size and selection method.

1. Introduction

Transportation problems, which many countries have faced, have been considered vitally significant in the last few decades; these problems necessitate a search for new techniques or alternatives that could determine the shortest time routes between any two locations. The vehicle routing problem (VRP) appeared for the first time in 1959 [1] to reduce the total route cost on continuously updated road maps. Several situations, particularly emergencies, require developing such techniques because the shortest-distance path sometimes is insufficient to save valuable human lives; the shortest-time route is optimum.

Two distinct types of VRP have been extensively explored individually, while appearing to be the same or overlapping at times due to mutual interests in network-based optimization models and techniques. First, a dynamic VRP that deals with dynamic road networks is a well-known and extensively studied class. Several dynamic and changeable characteristics, including traffic flow level, unanticipated occurrences, and weather conditions, impact such networks. The second type of VRP is the timetabled or scheduled VRP, which is concerned with public transportation and services involving the conveyance of passengers, such as buses, and operates primarily on regular timetables and trip schedules for public use.

This paper proposes a newly developed GA applied on a weighted directed graph representing a real-time road network of the study area, Al-Salt city in Jordan. An integrated ArcGIS Network Analyst tool has been used to

visually establish the optimal time route from a source point to the destination and suggest potential routes based on user preferences.

GA consists of consecutive procedures that attempt to find the best solutions to problems when it is possible to define the criteria used to evaluate and estimate the best solutions.

The proposed GA finds the shortest-time route with fitness function, which calculates the time influenced by different factors. The fitness function uses static and dynamic parameters to calculate each path's fitness value. The fixed parameters tend to be almost constant through time as follows:

(1) Route distance: the distance is the essential criterion for the shortest path problem; GA uses the road length as weight in the directed graph for obtaining the best route.

(2) Easiness of driving: the safer and more comfortable route is also a driver preference criterion. The proposed GA should find a vehicle route that achieves the driver requests based on this criterion; furthermore, the determined solution should avoid influencing factors like traffic signals.

(3) Streets conditions: these include street type, width, street topology, and street regulations (e.g., allowed velocity limit); the street conditions can be collected using cameras, sensors, car navigation system, and geodatabase of the real-time map. The proposed technique obtains the above parameters from the geodatabase of Al-Salt downtown map.

The dynamic factors, such as residential density, are relatively variable throughout time (low, medium, and high density). Travel time reflects the time spent travelling by automobile, such as rush hour in the morning from 6 a.m. to 10 a.m. The residential density in a given region may be calculated using real-time map data and then updated on a regular basis utilizing cameras and sensors, particularly during peak hours.

2. Related Work

Several researchers have made a considerable effort to optimize transportation systems by improving and developing various algorithms to solve VRP problems in route planning systems. Figure 1 shows the most popular algorithms for determining the optimal route in VRP, and they are classified as follows.

2.1. Exact Algorithms. A comparative study has been conducted for different VRP algorithms to evaluate their effectiveness in real-time routing applications and simulate the performance of Dijkstra's algorithm (DA) among them [2]. Position parameter [3, 4] was added to DA using the global positioning system (GPS). Once GPS retrieves the current position, DA calculates the distance from the source to every node in the graph [5, 6].

The researchers in [7] improved the DA; moreover, they have examined the weaknesses of other shortest path algorithms. Dijkstra algorithm was also applied in public transport planning system for Bangkok Metropolitan Area for Buses as in [8], intelligent bus transportation system in Philippines [9], shortest-distance bus routes in Yangon city [10], and parking system in Malaysia [11]. Other research works [12, 13] used breadth-first traversal (BFT) to improve the efficiency of DA in the searching process for the best solution for VRP.

2.2. Heuristic Algorithms. A* search algorithm has been studied and used to find the point-to-point shortest route using a weighted directed graph [14]. Another research [15] shows that the execution time of DA is lower than the A* search algorithm when a large number of nodes are selected. A public transportation system of Yangon's downtown area applied the A* approach in finding the shortest route [16]. The research in [17] has applied the branch-and-bound algorithm on the cost function $f(x)$, while the branch-and-cut algorithm was used in [18, 19] to solve the vehicle assignment problem and the two-echelon vehicle routing problem, respectively.

2.3. Metaheuristic Algorithms. GA is an evolutionary technique developed for the first time by Holland et al. in 1975 [20]. GA always begins with an initial population of randomly selected chromosomes; each chromosome represents a potential solution containing a combination of genes [21].

GA commonly uses one crossover and one mutation operator to solve the problem and determine a new optimal solution, but researchers in [11] defined one crossover and three mutation operators to find the optimal path. Depending on the experimental results, the algorithm was quick, prosperous, and stable and had a good convergence with high efficiency in determining the shortest emergency route [22]. Variable-length chromosomes with string type are proposed in [23].

When compared to other recent metaheuristics, GA offers a wide range of applications, including a vehicle routing problem (VRP) combining time frames [24–30] and a school bus routing issue [31–33]. A route guiding system used GA in a mobile application to determine the quickest driving time for Ankara's traffic network [34].

Several metaheuristic algorithms are also applied to solve VRP problem like Ant Colony Optimization (ACO) as in [35–38], Tabu Search in [39–43], and Particle Swarm Optimization (PSO) in [44]. Figure 1 summarizes the main three approaches, exact, heuristic, and metaheuristic algorithms, applied in VRP using real-time maps.

Many studies have demonstrated the effectiveness and importance of GIS in optimizing transportation systems and determining the most fitting routes for vehicles.

The ArcGIS Network Analyst tool has recently been used to optimize several route planning applications. The researchers in [45, 46] have used GIS Network Analyst to optimize the solid waste management field. In [47], the authors planned to provide information about tourist

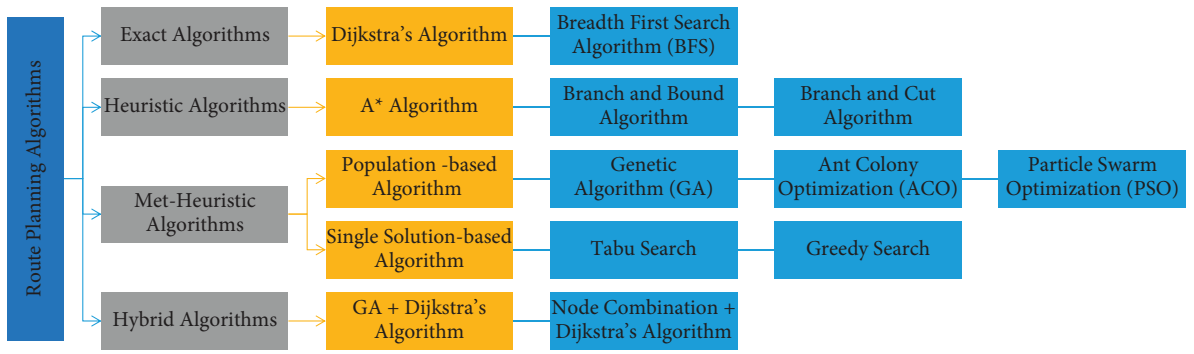

Figure 1: Classification of route planning algorithms.

attractions in Bandung and create a tourism-specific mass transit route. Based on a network-based spatial analysis of a GIS-based map, the study in [48] uses Dijkstra's algorithm to identify the shortest-distance route.

This study uses an integrated Network Analyst tool with a GA approach for vehicle routing optimization to determine a multiobjective optimal route based on user preferences. Generally, GA works well in problems with a huge solution space, long search times, and complex fitness functions. Furthermore, it performs well and gives better results when the function is discontinuous and noisy or has many local optimums. According to this study, GA becomes more complex when there are a considerable number of nodes in the real-time road network because unlimited-length chromosomes are created.

3. Study Area

Al-Salt city is one of the ancient and densely populated cities in Jordan. The city is located about 30 kilometers northwest of Amman, the capital city of Jordan, between longitude (35° 43′ 30″) east and latitude (32° 02′ 30″) north, at the height of 795 to 1,110 meters above sea level.

The study area represents road networks in the downtown of Al-Salt city; the greater municipality of Al-Salt provided the study with real-time maps and the road networks for the study area in cooperation with Al-Balqa' Applied University, which provided the study with the required equipment and tools used for data collection.

The streets in the city of Al-Salt represent 4% of Jordan's total streets, including secondary and main streets. According to the road classification law at the Ministry of Public Works, Table 1 shows the types and lengths of roads in Al-Salt city in 2018 [49].

The roads were classified according to the width of each road as follows:

(i) Main road: the width of the road is 8 m or more.

(ii) By road: the width of the road is 6 m up to less than 8 m.

(iii) Track road: the width of the road is 3 m up to 6 m.

Studying the road networks is one of the critical fields in transportation systems; it combines the spatial relation of the road networks with their characteristics then analyzes them according to space. Figures 2 and 3 show satellite images of the study area with the associated digitized road networks.

Table 1: Classification for the main types of roads in study area.

Type of road	Distance (km)	Percentage (%)
Main road	216.31	28.40
By road (secondary)	415.62	54.66
Asphalt (track)	128.51	16.94
Total	760.44	100

4. Methodology

Photogrammetry refers to the process of measuring and interpreting images in order to extract data needed for geospatial applications, which is often acquired by satellites and airplanes.

The key tool in this case study is ArcGIS. It is an ESRI-developed geographic information system (GIS) for dealing with maps and geographical information. It provides a framework for making maps, assembling geographic data, evaluating mapped data, and integrating maps with geospatial databases in a variety of applications [50]. Figure 4 depicts the methods for producing the study map to be combined and used with GA to discover the best-time route.

4.1. GPS Field Survey to Get the Ground Control Points (GCPs). The next step is to take the GPS data and postprocess it by importing raw data (the data from the GPS receivers) and exporting the final local grid coordinates and other coordinates. It is composed of the points BAU, reference, az, bs, seha, sew, hassan, hesba, salalem, and fatma. Only two receivers were used to measure the entire network.

The local grid coordinates of the points BAU, reference, az, bs, seha, sew, hassan, hesba, salalem, and fatma are derived and known as UTM ZONE 36 North projection and WGS84 Ellipsoid. Figure 5 displays the local grid coordinates for the previous selected points.

4.2. Process the GPS Field Data by Leica SKI-Pro Software to Get Values of GCPs. Leica's SKI-Pro software includes a comprehensive set of programs for GPS surveying with

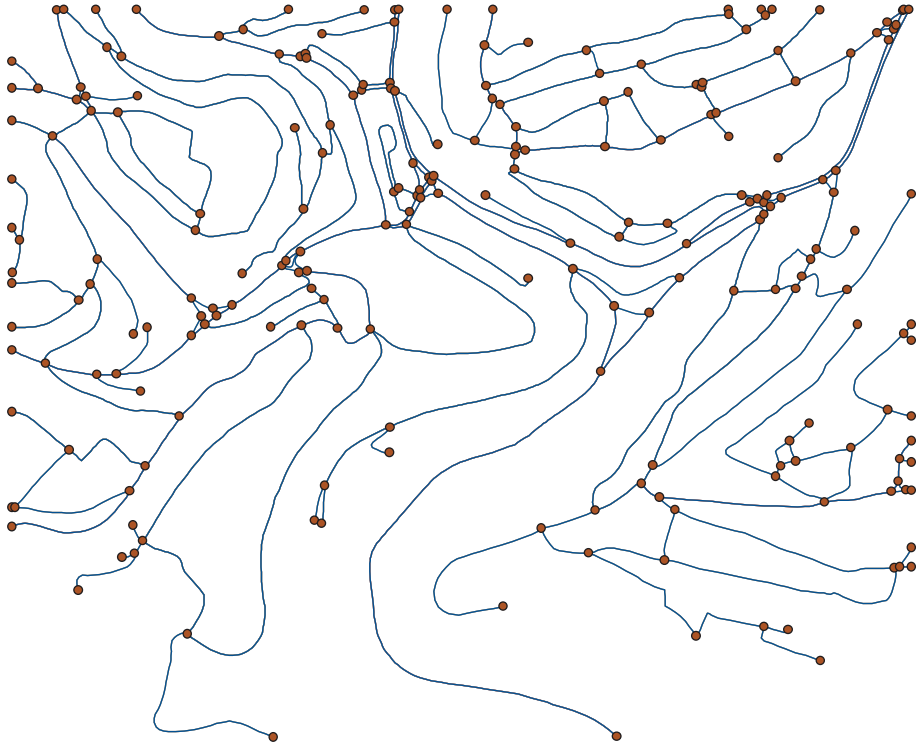

Figure 2: Real-time road networks of study area.

Figure 3: Satellite aerial photo of study area.

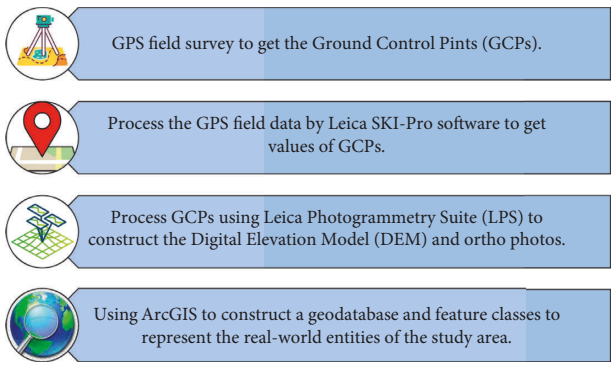

Figure 4: Procedures of georeferencing the study area.

Figure 5: Local grid coordinates of the study area.

postprocessing capabilities and real-time support. In SKI-Pro, GPS data that belong together can be collected and stored as shown in Figure 6.

4.3. Process GCPs Using Leica Photogrammetry Suite (LPS) to Construct the Digital Elevation Model (DEM) and Orthophotos. In this study, Leica Photogrammetry Suite (LPS) is applied to find the overlap area between two images, also known as triangulation, by rectifying images to determine orthophoto as well as extracting DTMs and contour maps for use in ArcGIS. Figures 7 and 8 display the locations of GCPs and determine their type and usage.

4.4. Using ArcGIS to Construct a Geodatabase and Feature Classes to Represent the Real-World Entities of the Study Area. The process of digitizing GIS data is to convert scanned images or hard copies of geographic data into vector maps by tracing their features. It is one of the ways to ensure that real-world spatial data is accessible. The digitization process involves capturing the underlying map features as coordinates, either as a point, line, or polygon. The task is accomplished by creating layers in ArcCatalog and then adding features to them in ArcMap. Several layers have been created in this stage for the study area in order to use them for retrieving the required spatial data by GA to calculate the optimal time route, as illustrated in Figure 9.

5. Proposed GA for Route Planning Systems

The most critical and challenging task for developing GA to this problem is how to encode a route in a weighted directed graph into a chromosome. This paper proposes a new GA for solving the shortest-time routing problem and determining the shortest-time route (optimal). Variable-length individuals (chromosomes) have been used; the genes in each chromosome represent nodes included in a path between a selected pair consisting of source (start) and destination (end) positions, and a priority-based encoding procedure is followed, which can probably represent all feasible routes in a graph.

5.1. Graph Design. In an implicit way, a road network can be represented as a directed graph $G = (V, E)$, where N is a set of vertices (nodes) and E is a set of edges (arcs). The ID of a node in the graph has given a unique positive integer value from $1,\ldots, N$, where N is the number of nodes as in Figure 10.

Each chromosome is created to represent a solution for the shortest-time routing problem, and it should not include duplicated nodes. Source and destination nodes are indicated by F and E, respectively, and each link (i, j) has associated with link connection indicator expressed by I_{ij}, which takes a part and plays an important role in chromosome production and encoding via providing connection information; this information describes whether the link from node i to node j is included in the routing path or not.

The connection information of the nodes with each other can be determined with an adjacency matrix as follows:

$$I_{ij} = \begin{cases} 1, & \text{if } i \text{ and } j \text{ are connected (adjacent),} \\ 0, & \text{otherwise.} \end{cases} \quad (1)$$

An adjacency matrix in Figure 11 is used to ensure the connectivity of the randomly selected pair of vertices; the length of the edge is considered as the weight of that edge in the graph. The adjacency matrix illustrates that all the diagonal elements of I_{ij} must equal zero, where the source and destination nodes are the same ($S = E$). The minimum potential value of the chromosome length is equal to the total number of nodes in the whole graph, because, in some worst cases, the shortest path may contain the total number of nodes. The gene length of a graph with N number of nodes is equal to N or more.

5.2. Chromosome Representation (Encoding). Chromosome length is variable, but it must not increase beyond the maximum feasible size, which, in the worst case,

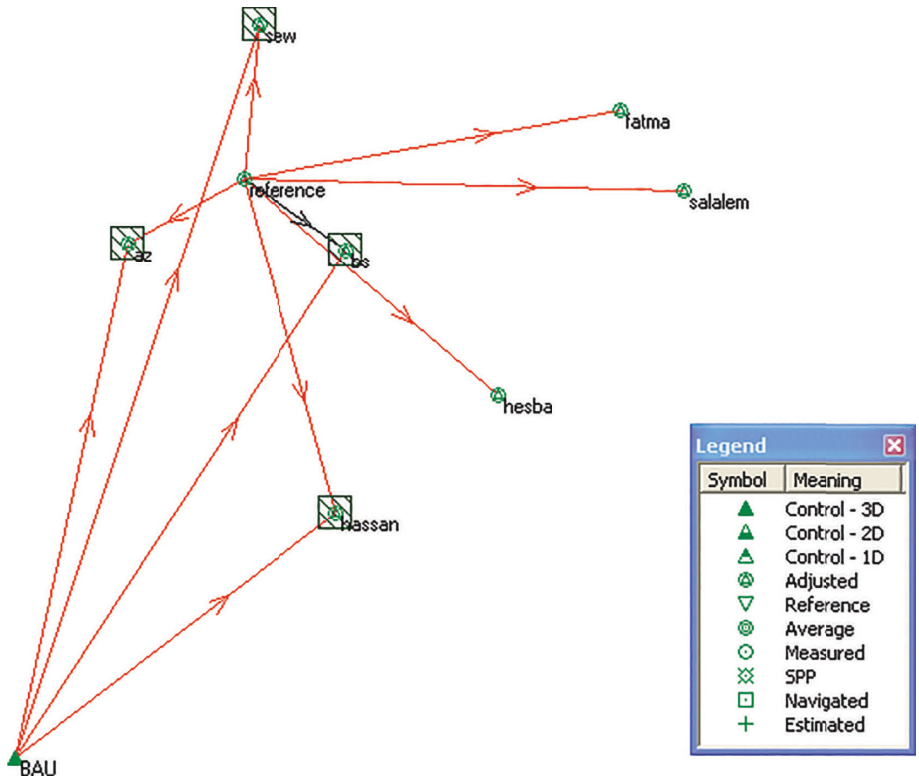

Figure 6: Distribution and adjustment of GCPs.

Figure 7: Location of GCPS on study map.

Point #	Point ID	>	Description	Type	Usage	Active	X Reference	Y Reference	Z Reference
1	1	>	az	Full	Control	X	757005.703	3547798.025	912.441
2	2		bs	Full	Control	X	757692.411	3547792.400	809.709
3	3		fatma	Full	Control	X	758540.116	3548253.885	920.186
4	4		hassan	Full	Control	X	757677.553	3546963.794	740.262
5	5		hesba	Full	Control	X	758178.094	3547347.288	767.178
6	6		reference	Full	Control	X	757362.178	3548008.234	839.290
7	8		salalem	Full	Control	X	758746.200	3548003.621	849.996
8	9		seha	Full	Control	X	757707.629	3548094.642	822.302

Figure 8: The type and usage of GCPs.

is the total number of nodes in the network since the chromosome length does not require more than the total number of nodes in order to create a routing path. Figure 12 shows the chromosome representation where the genes are selected randomly from source node 1 to destination node 4 based on the topological information database of the network; each chromosome should indicate a feasible route for the proposed GA.

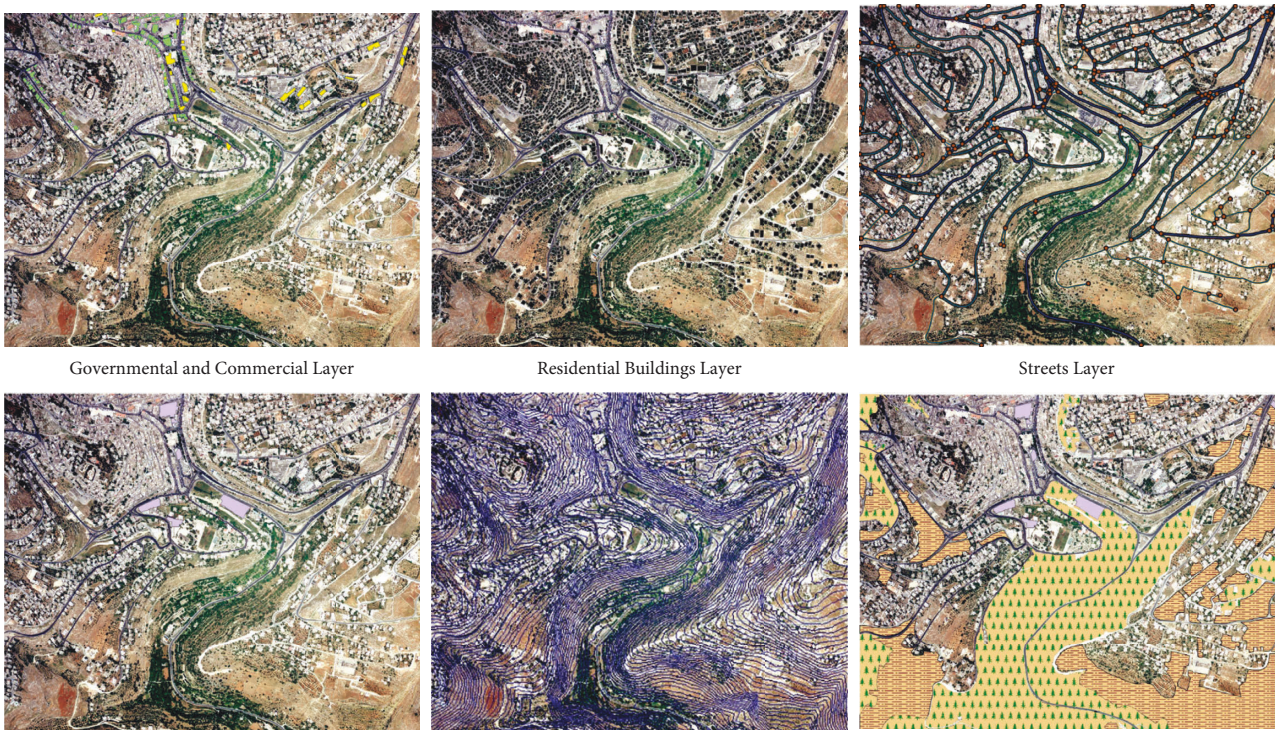

Figure 9: Digitized layers view concerning the rectified orthophoto.

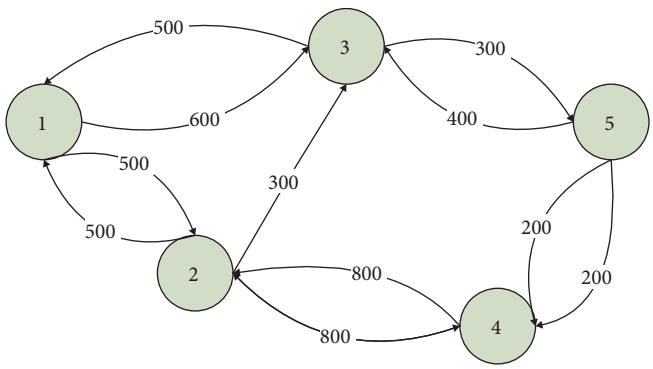

Figure 10: Directed graph for road network.

		N1	N2	N3	N4	N5
		1	2	3	4	5
N1	1	0	1	1	0	0
N2	2	1	0	1	1	0
N3	3	1	0	0	0	1
N4	4	0	1	0	0	1
N5	5	0	0	1	1	0

Figure 11: Adjacency matrix for road networks.

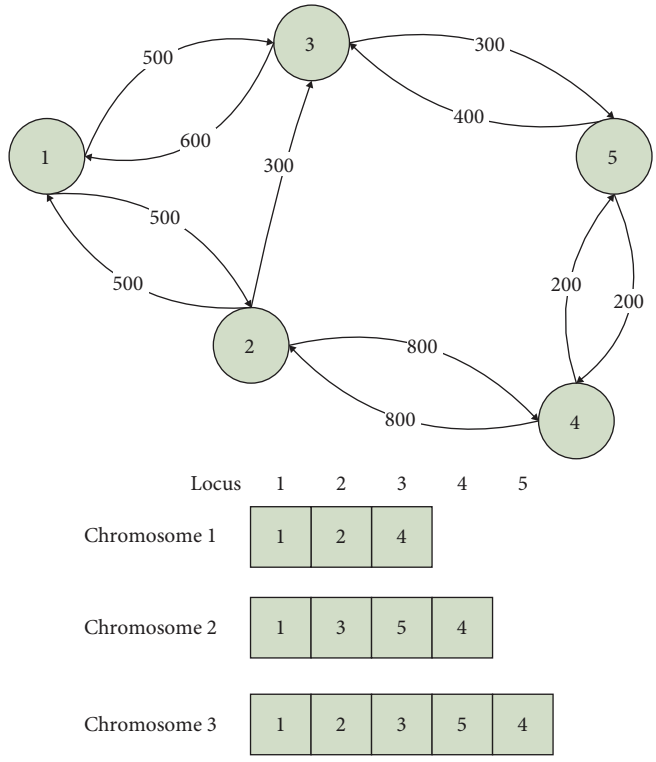

Figure 12: Chromosome representation procedure.

Table 2: Attributes table for road network segments.

Segment ID	Segment description (S, E)	Distance (m)	Allowable velocity limits (km/h)
$S1$	(1, 2)	500	60
$S2$	(2, 1)	500	60
$S3$	(1, 3)	500	60
$S4$	(3, 1)	600	60
$S5$	(3, 5)	300	40
$S6$	(5, 3)	400	40
$S7$	(4, 5)	200	40
$S8$	(5, 4)	200	40
$S9$	(2, 4)	800	40
$S10$	(4, 2)	800	40
$S11$	(2, 3)	300	60

5.3. Initial Population. The initial population consists of chromosomes (individuals), the lengths of which are variable. The first gene of each chromosome is the first node (S) and the last gene is the target node (E); if the path is between S, a new gene is produced; typically, all the chromosomes in the first generation are produced by this approach.

The large population is practically useful, but it requires unnecessary costs in both capacity and time. As expected, choosing a sufficient population size is critical for efficiency demands; for that reason, many researchers used the heuristic approaches for producing the chromosome for the initial population instead of the random method.

5.4. Fitness Function. Table 2 contains the cost attributes or parameters used in determining the fitness value for each segment of the road path and affects the result obtained.

Based on these criteria, the fitness cost for the candidate road pathways (chromosomes) from source node 1 to destination node 4 could be computed, and the optimum option with the least driving time would be chosen. Figure 13 depicts an actual value for each route in the research area's road network. Equations (2) to (7) define the fitness function of the GA while taking into account all of the associated parameters as follows:

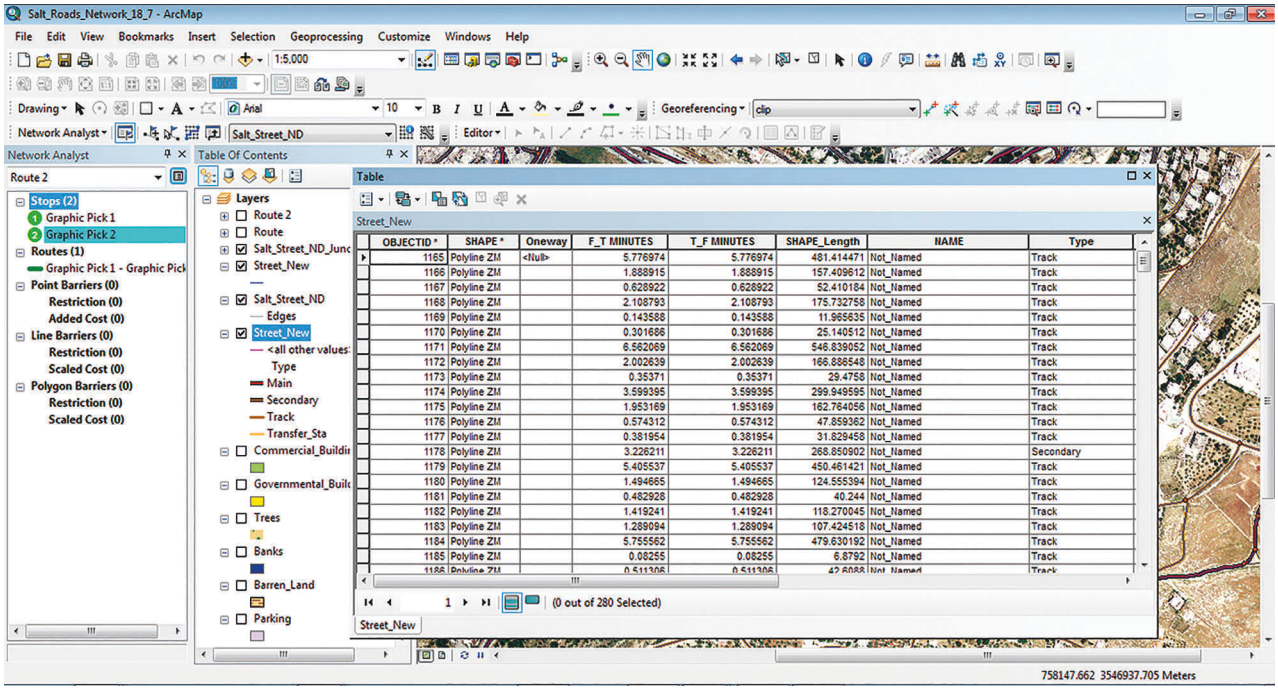

Figure 13: Attribute table of streets layer in ArcMap.

$$T1_{ij} = \sum_{n=i}^{j} \left(\frac{\mathrm{dis}_{ij}}{V_{ij}} \right). \tag{2}$$

Fij is the cost value from i to j, where $i \neq j$.

$$T1_{ij} = \sum_{n=i}^{j} \left(\frac{2\mathrm{dis}_{ij}}{V_{ij} - VRij} \right) \text{in rush hours}, \tag{3}$$

where dis_{ij} is the length of segment between i and j and V_{ij} represents the allowable velocity limits between i and j.

Then,

$$Dy = \frac{\sum L}{A} \times 100, \tag{4}$$

$$T2_{ij} = \sum_{n=i}^{j} \left(\frac{Dy}{V_{ij}} \right), \tag{5}$$

$$T3_{ij} = T1_{ij\_}T2_{ij}, \tag{6}$$

where

$$T4_{ij} = T3_{ij} - (NOTL * 0.5)\,(\text{minimum}), \tag{7}$$

$$F_{ij} = \sum_{n=i}^{j} T_{ij}. \tag{8}$$

T_{ij} is the time required to travel between i and j. Dy is the density of the roads network. $\sum L$ is the total length of the network roads. A is the area of the study region (square kilometer). NOTL is the number of traffic light signals. VR_{ij} is the estimated vehicle's speed in rush hours.

5.5. Selection and Crossover Procedures. The tournament selection method is the type of selection used for the proposed GA, two individuals are selected, and the more appropriate individual is chosen compared to the fitness of the other chromosomes in the population, but the corresponding individual should not be selected twice as a parent in the population.

In 1983, Birndlerproposed a tournament selection technique in which individuals, in pairs, were selected according to their fitness values from a stochastic roulette wheel. Selection of the individuals with the highest fitness values leads to the next generation.

The crossover between the two most fitting parents chosen by the selection increases the probability of generating offspring having robust characteristics [51]. The arithmetic crossover is used in this case as follows:

$$X_i = \delta.X_i^1 + (1 - \delta).X_i^2, \tag{9}$$

where $\delta\varepsilon(0, 1)$.

According to the previous equation, the new offspring generated by the arithmetic crossover are

$$\begin{aligned} P_i &= \delta.X_{i+(1-\delta)Y_i}, \\ q_i &= \delta.X_{i+(1-\delta)Y_i}. \end{aligned} \tag{10}$$

Figure 14 shows an illustrative example of the proposed crossover procedure.

5.6. Mutation Procedure. Mutation procedure leads to a bit of increment in the probability of producing the infeasible chromosomes; it keeps the diversity in the population

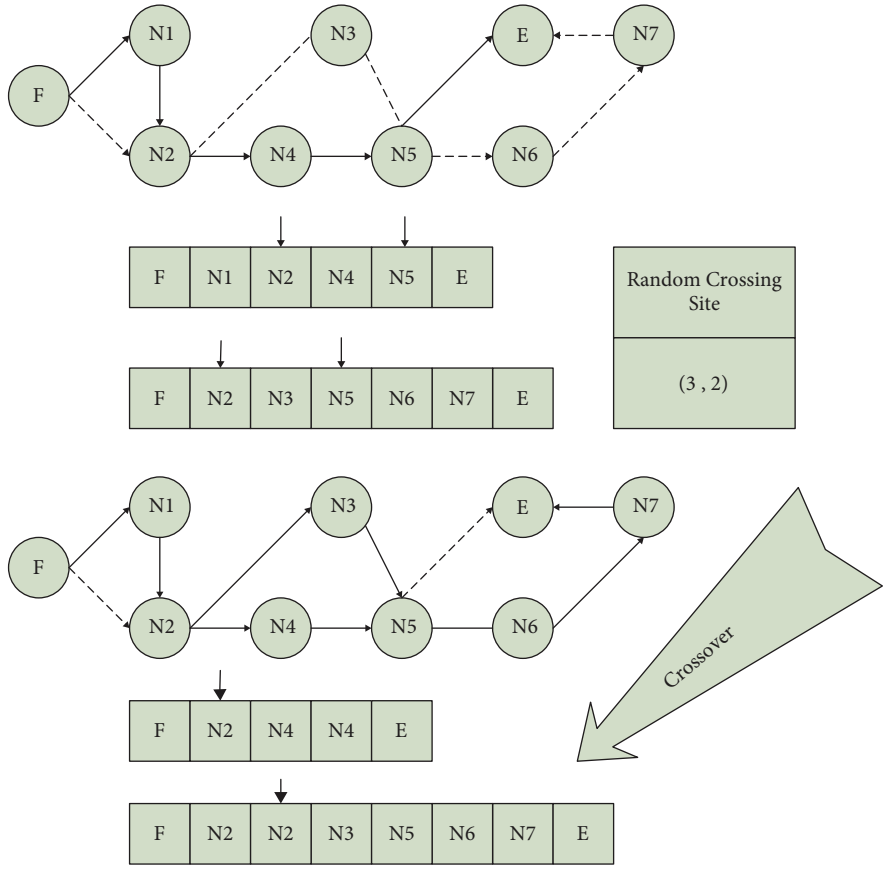

Figure 14: Crossover procedure.

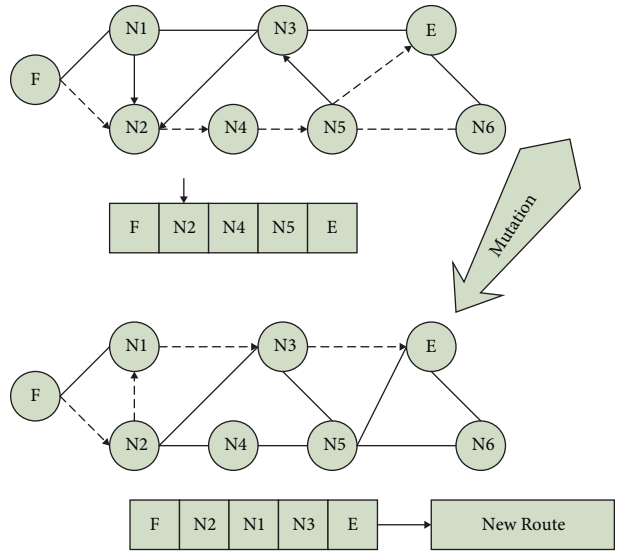

Figure 15: Mutation procedure.

solutions. Figure 15 illustrates a comprehensive description for the proposed mutation procedure in GA.

5.7. Reorganizing (Repairing) Function. GA is developed based on ideas inspired by evolutionary mechanisms, where successive generations of solutions become more and more efficient until an optimal or nearly optimal set of alternatives are reached.

Loops in the shortest-time route routing issue can be produced during the crossover and mutation procedures, resulting in infeasible chromosomes. There are two primary approaches to dealing with infeasible chromosomes. The first is to eliminate them, and the second is to

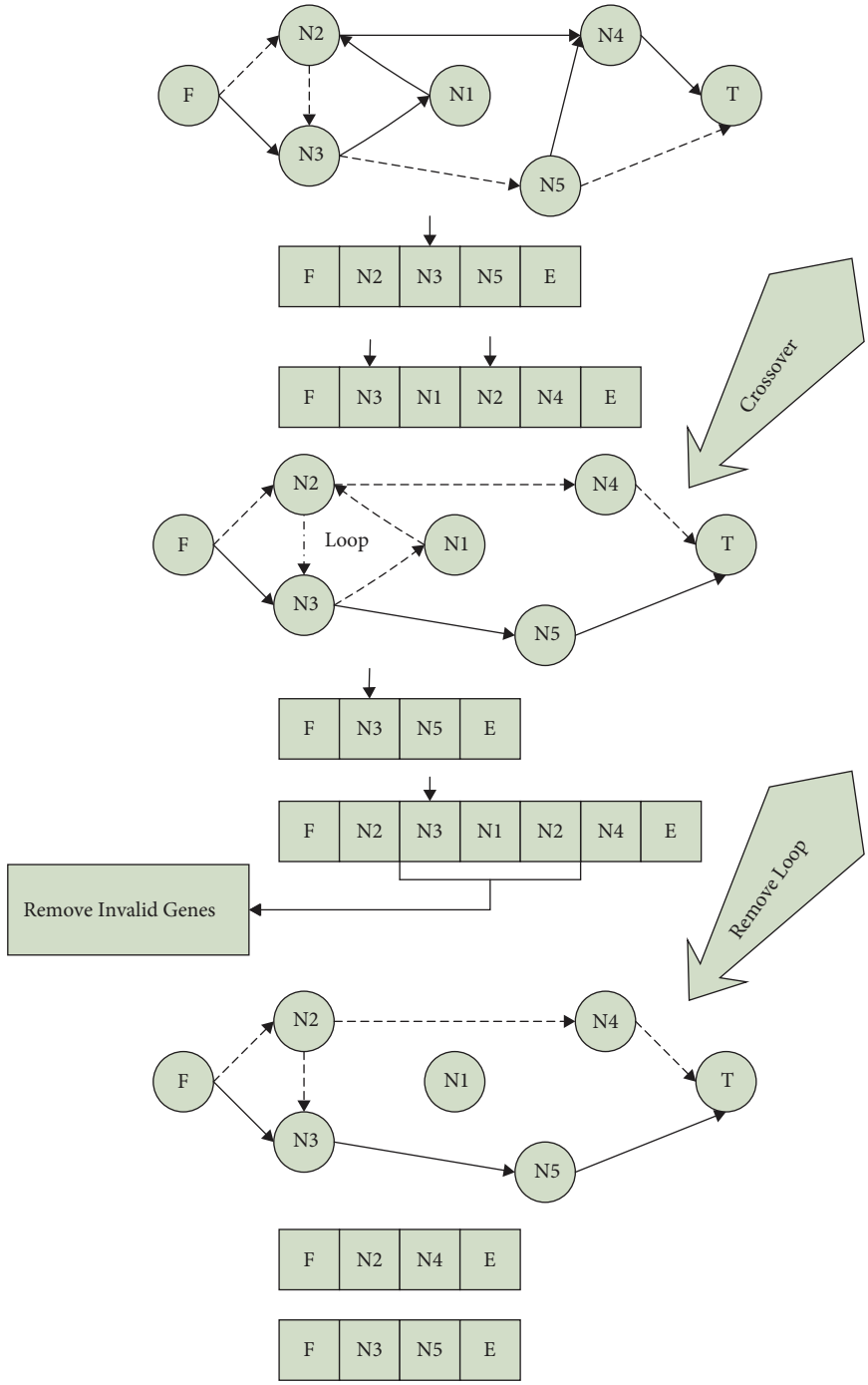

Figure 16: Repair procedure.

reorganize a chromosome with a repair function. The first is to apply a penalty, and the second is to reorganize a chromosome by removing and deleting the loop; in this work, the rearranging function is utilized to detect and eliminate the loops without incurring any additional capacity or time expenses. Figure 16 shows a description of the proposed reorganizing function with an example.

Algorithm 1 displays a pseudocode showing how the algorithm finds the minimum travel time route for the provided graph from start node to the end node.

6. Results and Findings

The road network in this study consists of 226 nodes (junctions) and 280 edges (segments), and each route has several interconnected edges. Determining the size of the initial population is crucial and influential in the effectiveness of the algorithm's performance. The initial population size tends to increase exponentially with the size of the road network due to an increase in chromosome length.

The quality of each chromosome in the population must be calculated accurately using efficient fitness

```
(1)  ►Input: Graph (V, E)
(2)    fNode/ ∗ initial node in the route */
(3)        dNode/ ∗ destination node */
(4)      ►Output: Ch[]/*array of Genes represents the optimal time route */
(5)      Define: Adj [][]/* 0, 1 Check nodes adjacency in the graph */
(6)      Ch [0] ← fNode
(7)        Pz ← Population size
(8)        Cr ← Crossover rate
(9)        Mr ← Mutatino rate
(10)         for each i, j where j = PZ
(11)       Create_Chromosome (fNode, dNode)
(12)       F ← Calculate Fitness Value for each chromosome
(13)         End for
(14)     Count ← 0
(15)     Gen ← 1
(16)       While Count ≤ 10 do
(17)     Ch1, Ch2 ← RouletteWheel _Selection ()
(18)     Ch1*,Ch2* ← Crossover (Ch1, Ch2)
(19)       Ch3 ← Mutation (Ch1*)
(20)       Ch4 ← Mutation (Ch2*)
(21)       F1 ← Fitness Value for the first chromosome
(22)       F2 ← Fitness Value for the second chromosome
(23)       Fm ← Minimum Value of fitness function
(24)         If Gen > 1 && Fm (Gen-1) = = Fm (Gen-2)
(25)       Count ++
(26)     if count > 10
(27)       Break
(28)     else
(29)     count = 0
(30)     End If
(31)     End while
(32)     Gen ++
(33)     Go to 17
```

Algorithm 1: Pseudocode for GA implementation.

Table 3: The calculated fitness value with allowable velocity limit for three chromosomes (routes).

Route	Segment (S, E)	Length (m)	Vehicle speed			
			40 km/h	60 km/h	90 km/h	120 km/h
Route 1	(1, 2)	500	0.750	0.50	0.333	0.250
	(2, 3)	300	0.450	0.30	0.200	0.150
	(3, 5)	300	0.450	0.30	0.200	0.150
	(5, 4)	200	0.300	0.20	0.133	0.100
Total (minutes)			1.950	1.30	0.867	0.650
Route 2	(1, 2)	500	0.750	0.50	0.333	0.250
	(2, 4)	800	1.200	0.80	0.533	0.400
Total (minutes)			1.950	1.30	0.867	0.650
Route 3	(1, 3)	500	0.750	0.50	0.333	0.250
	(3, 5)	300	0.450	0.30	0.200	0.150
	(5, 4)	200	0.300	0.20	0.133	0.100
Total (minutes)			1.500	1.00	0.667	0.500

function. Based on a geodatabase of the study area map, a multiobjective fitness function was used in GA to estimate the minimum vehicle arrival time. In this section, the fitness value is calculated for each factor separately in order to illustrate their influence on the estimated time.

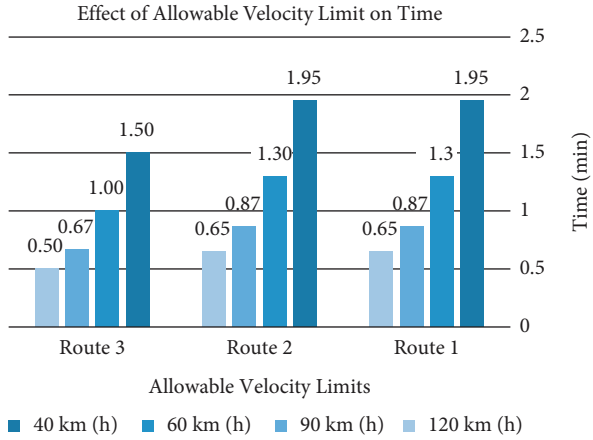

Figure 17: The effect of the vehicle speed on the expected arrival time.

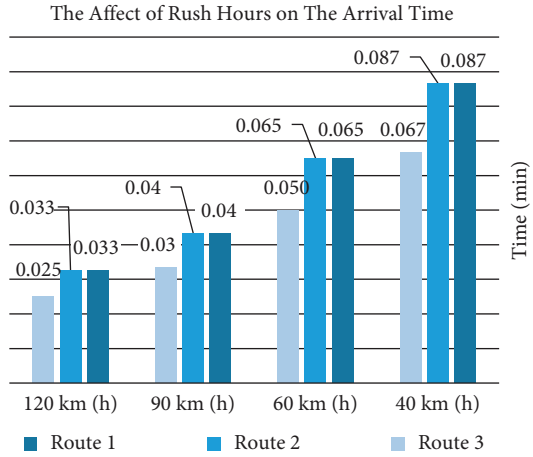

Figure 18: The effect of the rush hours on the expected arrival time.

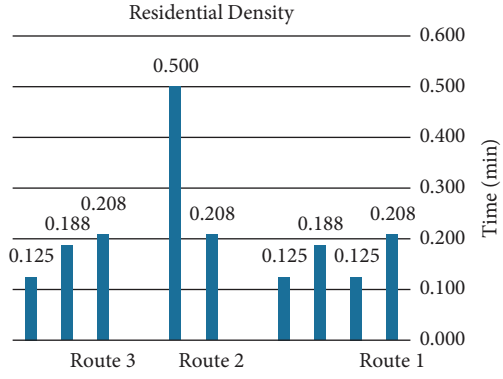

Figure 19: The effect of residential density of study area on the expected arrival time.

Table 3 shows the calculated fitness value for three chromosomes for the route from node 1 to node 4, considering the allowable velocity limit in measuring the value.

Figure 17 illustrates the effect of allowable velocity limits on the arrival time from node 1 to node 4 for three separate routes. As a result, the shortest-time route is not necessarily the shortest-distance one. The vehicle speed on the road, which is determined according to street condition (e.g., street type), has a significant effect on the time needed to arrive.

During peak hours, traffic congestion causes the creation of automobile lines, which decreases the speed of cars and delays their arrival at their destinations. Despite the fact that vehicle deceleration in real-world conditions is not exactly uniform, the delay for a specific vehicle may be estimated

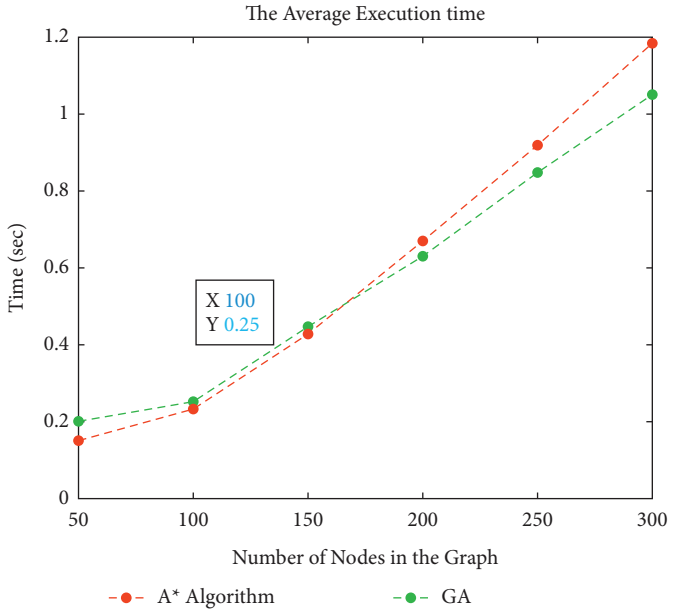

Figure 20: Execution time for A* algorithm and proposed GA.

Table 4: The calculated fitness value in rush hours for three chromosomes (routes).

Route	Segment description (*S*, *E*)	Segment length (m)	Allowable velocity limit	Res. density	Time in rush hours (km/h)			
					40	60	90	120
Route 1	(1, 2)	500	60	0.208	0.033	0.025	0.017	0.013
	(2, 3)	300	60	0.125	0.020	0.015	0.010	0.008
	(3, 5)	300	40	0.188	0.020	0.015	0.010	0.008
	(5, 4)	200	40	0.125	0.013	0.010	0.007	0.005
Total (minutes)				0.646	0.087	0.065	0.04	0.033
Route 2	(1, 2)	500	60	0.208	0.033	0.025	0.017	0.013
	(2, 4)	800	40	0.500	0.053	0.040	0.027	0.020
Total (minutes)				0.708	0.087	0.065	0.04	0.033
Route 3	(1, 3)	500	60	0.208	0.033	0.025	0.017	0.013
	(3, 5)	300	40	0.188	0.020	0.015	0.010	0.008
	(5, 4)	200	40	0.125	0.013	0.010	0.007	0.005
Total (minutes)				0.521	0.067	0.050	0.03	0.025

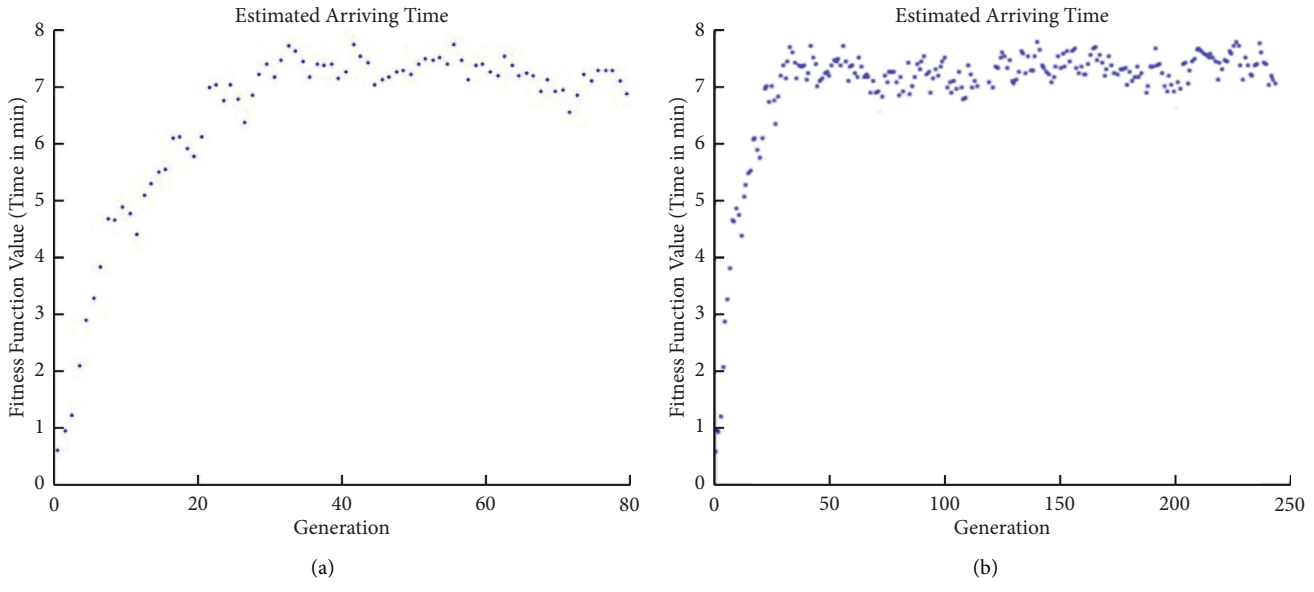

Figure 21: (a): Estimated time over 80 generations. (b) Estimated optimal time over 250 generations.

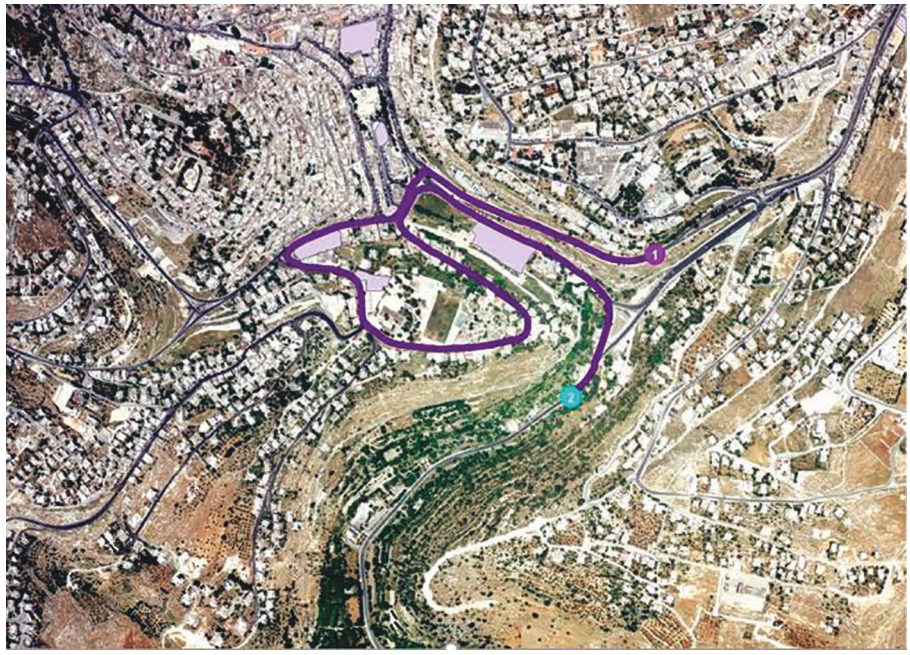

Figure 22: The first route from source to destination.

Figure 23: The first route from source to destination.

using fundamental dynamics equations. Because cars gradually slow down, this assumption should result in a somewhat realistic estimate of the time delay. Figure 11 depicts the effect of driving during rush hour on arrival time.

Figures 18 and 19 illustrate how deceleration of the vehicle during rush hours and the residential density affect the time needed to arrive, which are considered as important parameters in calculating each chromosome's fitness value in the proposed GA.

In order to emphasize the effectiveness of the genetic algorithm compared to heuristic algorithms such as the A* algorithm, a comparison was conducted according to the execution time required to determine the optimal solution as shown in Figure 20. Python is used to implement the algorithm, and the GA solver evaluates GA using MATLAB.

Figure 24: The shortest-time route for multiple locations.

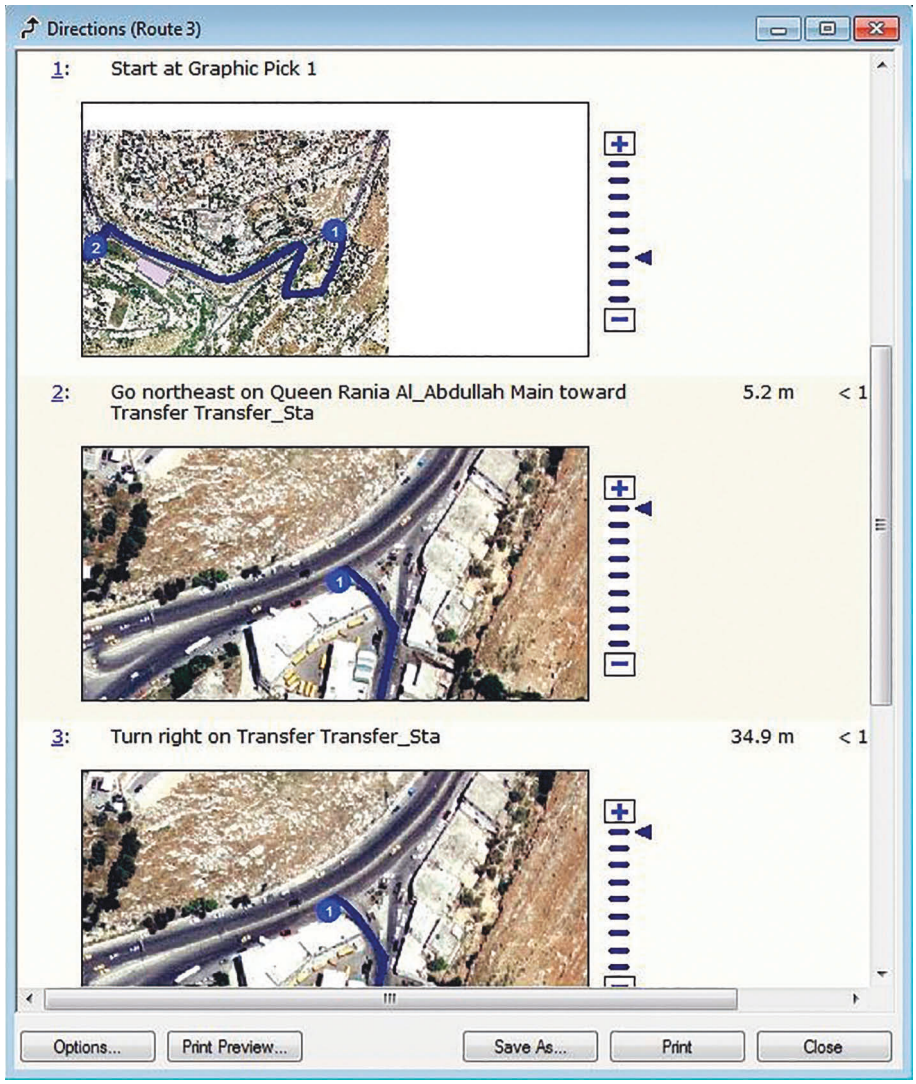

(a)

Figure 25: Continued.

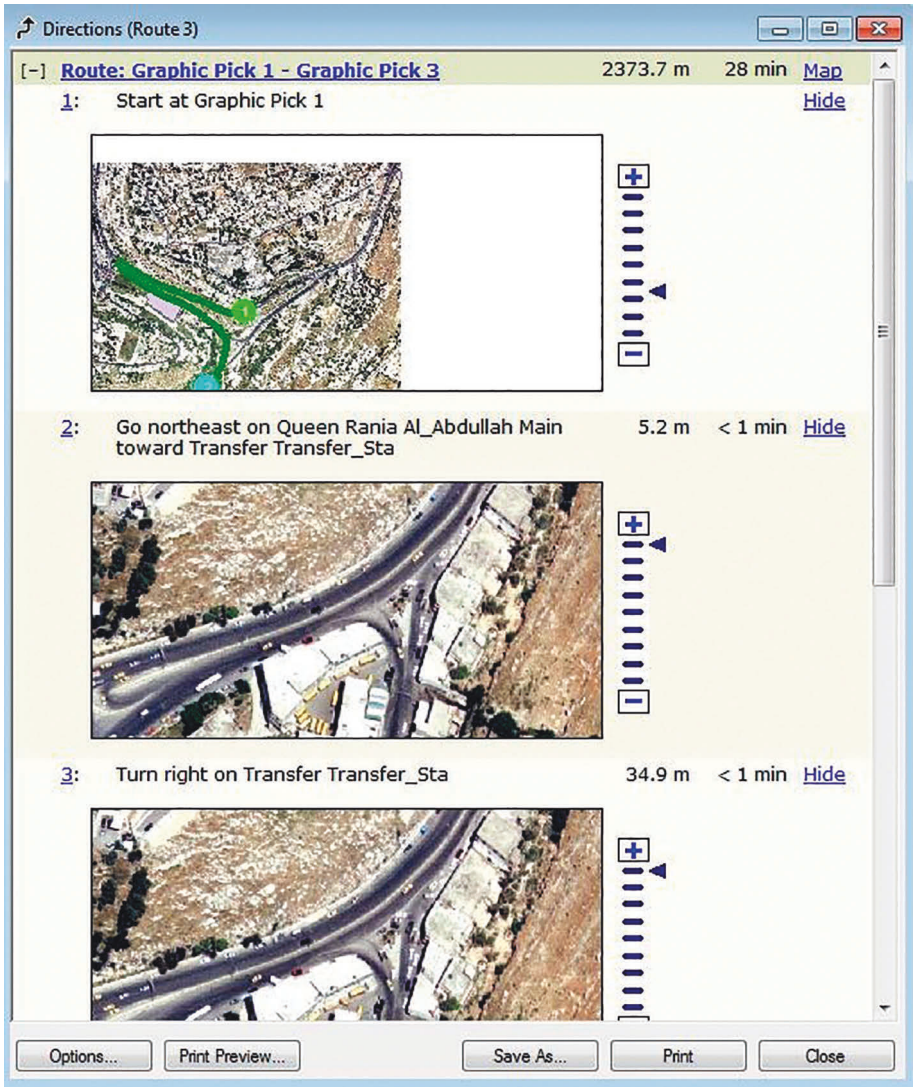

(b)

Figure 25: Route directions window.

Table 4 shows the calculated time for three routes during rush hour, along with the residential density for each segment of the route.

The simulation results of GA using GA solver indicate that the proposed GA determines the optimal time route starting from 30 generations and performs effectively over more than 200 generations up to 250, as illustrated in Figures 21(a) and 21(b).

Based on various factors that affect the arrival time, the experimental results show multiple routes from the source to the destination. Figures 22 and 23 illustrate the shortest-time path obtained with multiobjective calculated time between two locations using GA. The results indicate that GA can be used effectively to design the route planning system that computes the optimal arriving time based on spatial database within dynamic traffic information.

The Network Analyst tool can also obtain the optimal route for multiple locations. It can estimate the best route between the source and destination, passing through specific locations, as shown in Figure 24.

Using ArcGIS integrated with GA, the Network Analyst tool can also provide the driver with other services besides obtaining the optimal-time route and selecting a specific route based on the driver's preferences. Furthermore, the application displays turn-by-turn directions for the preferred route with details that include the estimated distance and time for that route, as shown in Figures 25 and 26, respectively.

Figure 26: Estimated time and calculated distance.

7. Conclusion

When the problem space includes a huge number of solutions and searching takes a long time, GA might be a useful alternative. To find the optimal route, a modified GA with population initialization, crossover, mutation, and repair functions is used. GA effectively obtained the shortest-time route with variable-length chromosomes based on several criteria (e.g., distance, speed limit, residential density, traffic signals, and rush hour) over 30 generations and remained near the optimum for 200 generations. By comparing the A* algorithm with the adaptive GA, it was found that, under increasing node density in spatial road networks, the proposed GA took the least execution time to find the optimal solution. Using ArcGIS to develop the Network Analyst tool helps users determine the shortest-distance route and simultaneously the shortest-time routes based on the user's impedance. GA will eventually be able to work perfectly with other heuristic algorithms, such as A* and Dijkstra's algorithm, in a wide range of multiobjective optimization techniques in order to maximize its effectiveness in determining the best or near optimum solution.

Data Availability

The data used to support the findings of this study are available from the author upon request (si2784@putra.unisza.edu.my).

Conflicts of Interest

The authors declare that they have no conflicts of interest.

Acknowledgments

There is no funding statement of this work.

References

[1] G. B. Dantzig and J. H. Ramser, "The truck dispatching problem," *Management Science*, vol. 6, no. 1, pp. 80–91, 1959.

[2] V. T. N. Nha, S. Djahel, and J. Murphy, "A comparative study of vehicles' routing algorithms for route planning in smart cities," in *Proceedings of the 2012 First international workshop on vehicular traffic management for smart cities (VTM)*, pp. 1–6, IEEE, Dublin, Ireland, 2012, November.

[3] P. Singal and R. RSChhillar, "Dijkstra shortest path algorithm using Global position system," *International Journal of Computer Applications*, vol. 101, no. 6, pp. 12–18, 2014.

[4] M. T. Winn, "A Road Network Shortest Path Analysis: Applying Time-Varying Travel-Time Costs for Emergency Response Vehicle Routing, davis County," *Utah: A Thesis Presented to the Department of Humanities and Social Sciences in Candidacy for the Degree of Master of Science*, Doctoral dissertation, Northwest Missouri State University, 2014.

[5] J. Shen and Y. Ban, "Route choice of the shortest travel time based on floating car data," *Journal of Sensors*, vol. 2016, pp. 1–11, 2016.

[6] S. Panahi and M. R. Delavar, "A GIS-based dynamic shortest path determination in emergency vehicles," *World Applied Sciences Journal*, vol. 3, no. 1, pp. 88–94, 2008.

[7] X. Xu, Y. Yin, and L. Liu, "Improved Dijkstra's algorithm and its application in intelligent transportation system," *Journal of Residuals Science & Technology*, vol. 13, no. 7, 2016.

[8] P. Tirastittam and P. Waiyawuththanapoom, "Public transport planning system by dijkstra algorithm: case study bangkok metropolitan area," *World Academy of Science, Engineering and Technology International Journal of Social, Behavioral, Educational, Economic, Business and Industrial Engineering*, vol. 8, no. 1, pp. 54–59, 2014.

[9] A. M. Lacorte and E. P. Chavez, "Analysis on the use of A ∗ and Dijkstra's algorithms for intelligent school transport route optimization system," in *Proceedings of the 4th International Conference on Human-Computer Interaction and User Experience in Indonesia*, pp. 12–17, CHIuXiD'18, 2018, March.

[10] O. Khaing, D. H. H. Wai, and D. E. E. Myat, "Using Dijkstra's algorithm for public transportation system in yangon based on GIS," *International Journal of Science and Engineering Applications*, vol. 7, no. 11, pp. 442–447, 2018.

[11] H. Jaafar, M. H. Zabidi, A. C. Soh, T. P. Hoong, S. Shafie, and S. A. Ahmad, "Intelligent guidance parking system using modified Dijkstra's algorithm," *Journal of Engineering Science & Technology*, vol. 9, pp. 132–141, 2014.

[12] C. H. Uy, N. Charoenlarpkul, T. Sarttra, and S. Rajsiri, "An efficient algorithm applied to capacitated vehicle routing problem with Consideration of time windows by using Ranking-based Concept and dynamic Programming," in *Proceedings of the 2019 International Conference on Management Science and Industrial Engineering*, pp. 267–274, 2019, May.

[13] S. Raagapriya, A. Ain, and P. Dasgupta, "Route optimization for an electric vehicle with priority destinations," in *Proceedings of the 2017 International Conference On Smart Technologies For Smart Nation (SmartTechCon)*, pp. 1244–1249, IEEE, Bengaluru, India, 2017, August.

[14] A. V. Goldberg and C. Harrelson, "Computing the shortest path: a search meets graph theory," in *Proceedings of the SODA '05: Proceedings of the sixteenth annual ACM-SIAM symposium on Discrete algorithms*, pp. 156–165, 2005, January.

[15] F. Engineer, "Fast shortest path algorithms for large road networks," in *Proceedings of the 36th annual ORSNZ conference*, 2001, December.

[16] M. T. Zar and M. M. Sein, "Using A ∗ algorithm for public transportation system in yangon region," in *Proceedings of the International Conference on Science, Technology, Engineering and Management (ICSTEM, 2015)*, Singapore, 2015, February.

[17] I. Kucukoglu and D. Cattrysse, "A branch-and-bound integrated simulated annealing algorithm for the electric vehicle routing problem with time windows," in *Proceedings of the International Conference on Computers & Industrial Engineering*, Lisbon, Portugal, October 2017.

[18] K. Dalmeijer and R. Spliet, "A branch-and-cut algorithm for the time window assignment vehicle routing problem," *Computers & Operations Research*, vol. 89, pp. 140–152, 2018.

[19] M. Jepsen, S. Spoorendonk, and S. Ropke, "A branch-and-cut algorithm for the symmetric two-echelon capacitated vehicle routing problem," *Transportation Science*, vol. 47, no. 1, pp. 23–37, 2013.

[20] J. H. Holland, M. Mahajan, S. Kumar, and R. Porwal, "Adaptation in natural and artificial systems," in *Applying Genetic Algorithm to Increase the Efficiency of a Data Flow-Based Test Data Generation Approach*, pp. 1–5, MIT Press, Ann Arbor, MI, 1975.

[21] N. J. Nilsson, *Principles of Artificial Intelligence*, Burlington, MA, 2014.

[22] W. T. Hu, K. D. Watts, P. Tailor et al., "CSF complement 3 and factor H are staging biomarkers in Alzheimer's disease," *Acta neuropathologica communications*, vol. 4, no. 5, pp. 14–21, 2016.

[23] C. W. Ahn and R. S. Ramakrishna, "A genetic algorithm for shortest path routing problem and the sizing of populations," *IEEE Transactions on Evolutionary Computation*, vol. 6, no. 6, pp. 566–579, 2002.

[24] S. R. Thangiah, K. E. Nygard, and P. L. Juell, "Gideon: a genetic algorithm system for vehicle routing with time windows," in *Proceedings of the The Seventh IEEE Conference on Artificial Intelligence Application*, pp. 322-323, IEEE Computer Society, Miami Beach, FL, USA, 1991, January.

[25] S. R. Thangiah and A. V. Gubbi, "Effect of genetic sectoring on vehicle routing problems with time windows," in *Proceedings of the IEEE International Conference on Developing and Managing Intelligent System Projects*, pp. 146–153, IEEE, Washington, DC, USA, 1993, March.

[26] S. R. Thangiah, R. Vinayagamoorty, and A. V. Gubbi, "Vehicle routing and time deadlines using genetic and local algorithms," in *Proceedings of the 5th international Conference on Genetic Algorithms*, pp. 506–515, 1993, June.

[27] S. R. Thangiah, "Vehicle routing with time windows using genetic algorithms," *Artificial Intelligence Lab*, 1993.

[28] S. R. Thangiah, "An adaptive clustering method using a geometric shape for vehicle routing problems with time windows," in *Proceedings of the 6th International Conference on Genetic Algorithms*, pp. 536–545, ACM, 1995, July.

[29] J. Y. Potvin and S. Bengio, "The vehicle routing problem with time windows part II: genetic search," *INFORMS Journal on Computing*, vol. 8, no. 2, pp. 165–172, 1996.

[30] S. J. Louis, X. Yin, and Z. Y. Yuan, "Multiple vehicle routing with time windows using genetic algorithms," in *Proceedings of the 1999 Congress on Evolutionary Computation-CEC99 (Cat. No. 99TH8406)*, pp. 1804–1808, IEEE, Washington, DC, USA, 1999, July.

[31] S. R. Thangiah and K. E. Nygard, "School bus routing using genetic algorithms," in *Proceedings of the Applications of artificial intelligence X: Knowledge-based systems*, pp. 387–398, International Society for Optics and Photonics, 1992, March.

[32] M. Kang, S. K. Kim, J. T. Felan, H. R. Choi, and M. Cho, "Development of a genetic algorithm for the school bus routing problem," *International Journal of Software Engineering and Its Applications*, vol. 9, no. 5, pp. 107–126, 2015.

[33] S. B. Sghaier, N. B. Guedria, and R. Mraihi, "Solving school bus routing problem with genetic algorithm," in *Proceedings*

of the 2013 International Conference on Advanced Logistics and Transport, pp. 7–12, IEEE, Sousse, Tunisia, 2013, May.

[34] U. Atila, I. R. Karas, C. Gologlu, B. Yaman, and I. M. Orak, "Design of a route guidance system with shortest driving time based on genetic algorithm," in *Proceedings of the World Scientific and Engineering Academy and Society (WSEAS)*, pp. 61–66, 2011, March.

[35] J. E. Bell and P. R. McMullen, "Ant colony optimization techniques for the vehicle routing problem," *Advanced Engineering Informatics*, vol. 18, no. 1, pp. 41–48, 2004.

[36] B. Bullnheimer, R. F. Hartl, and C. Strauss, "Applying the ant system to the vehicle routing problem," in *Meta-heuristics*, pp. 285–296, Springer, Boston, MA, 1999.

[37] B. Bullnheimer, R. F. Hartl, and C. Strauss, "An improved ant System algorithm for thevehicle Routing Problem," *Annals of Operations Research*, vol. 89, pp. 319–328, 1999.

[38] N. Christofides and S. Eilon, "An algorithm for the vehicle-dispatching problem," *Journal of the Operational Research Society*, vol. 20, no. 3, pp. 309–318, 1969.

[39] J. Jemai and K. Mellouli, "A neural-tabu search heuristic for the real time vehicle routing problem," *Journal of Mathematical Modelling and Algorithms*, vol. 7, no. 2, pp. 161–176, 2008.

[40] M. Gendreau and J. Y. Potvin, "Tabu search," in *Search Methodologies*, pp. 165–186, Springer, Boston, MA, 2005.

[41] J. P. Kelly and J. Xu, "A set-partitioning-based heuristic for the vehicle routing problem," *INFORMS Journal on Computing*, vol. 11, no. 2, pp. 161–172, 1999.

[42] J. J. Santa Chávez, J. W. Escobar, M. G. Echeverri, and C. A. P. Meneses, "A heuristic algorithm based on tabu search for vehicle routing problems with backhauls," *Decision Science Letters*, vol. 7, no. 2, pp. 171–180, 2018.

[43] Y. Xia and Z. Fu, "Improved tabu search algorithm for the open vehicle routing problem with soft time windows and satisfaction rate," *Cluster Computing*, vol. 22, no. 4, pp. 8725–8733, 2019.

[44] Y. Marinakis, M. Marinaki, and A. Migdalas, "A multi-adaptive particle swarm optimization for the vehicle routing problem with time windows," *Information Sciences*, vol. 481, pp. 311–329, 2019.

[45] D. Jaisankar, S. N. Behera, M. Yadav, and H. Upreti, "Current Trends and future Challenges for solid waste management: generation, characteristics, and application of GIS in mapping and optimizing transportation routes," in *Urban Mining for Waste Management and Resource Recovery*, pp. 17–41, CRC Press, 2021.

[46] C. V. Mai, S. H. Nguyen, C. D. Dao, T. V. Le, and H. A. Phan, "A GIS application in optimizing the collection and transportation route of Domestic solid waste in Hue city, Vietnam," in *Global Changes and Sustainable Development in Asian Emerging Market Economies*, pp. 599–609, Springer, Cham, 2022.

[47] Y. Astor, A. Purwandhari, and K. R. Aprian, "Determination of effective routes for tourism mass transportation in Bandung city using network analyst and GIS," in *Proceedings of the International Seminar of Science and Applied Technology (ISSAT 2020)*, pp. 265–269, Atlantis Press, 2020, December.

[48] M. B. Sushma and V. Reddy, "Finding an optimal path with hospital information system using GIS-based Network analysis," *WSEAS Transactions on Information Science and Applications*, vol. 18, pp. 1–6, 2021.

[49] D. Qtiashat, Z. Makhmreh, H. A. Taleb, and A. Khlaifat, "Urban land use pattern and road network characteristics using GIS in Al Salt City, Jordan," *Modern Applied Science*, vol. 12, no. 4, pp. 128–142, 2018.

[50] Esri, "Esri," www.esri.com, 2022.

[51] Y. Jiang, "Estimation of traffic delays and vehicle queues at freeway work zones," in *Proceedings of the 80th Annual Meeting of the Transportation Research Board*, Washington, DC, 2001, January.

Hindawi
Mathematical Problems in Engineering
Volume 2022, Article ID 6853196, 11 pages
https://doi.org/10.1155/2022/6853196

Research Article

Learning-Based Virtual Machine Selection in Cloud Server Consolidation

Huixi Li,[1,2] **Yinhao Xiao**,[1,2] **and YongLuo Shen**[1,2]

[1]*School of Information Science, Guangdong University of Finance and Economics, Guangzhou 510320, China*
[2]*Guangdong Intelligent Business Engineering Technology Research Center, Guangdong University of Finance and Economics, Guangzhou 510320, China*

Correspondence should be addressed to YongLuo Shen; sylkyo@126.com

Received 10 June 2022; Accepted 29 July 2022; Published 22 September 2022

Academic Editor: Amandeep Kaur

In cloud data center (CDC), reducing energy consumption while maintaining performance has always been a hot issue. In server consolidation, the traditional solution is to divide the problem into multiple small problems such as host overloading detection, virtual machine (VM) selection, and VM placement and solve them step by step. However, the design of host overloading detection strategies and VM selection strategies cannot be directly linked to the ultimate goal of reducing energy consumption and ensuring performance. This paper proposes a learning-based VM selection strategy that selects appropriate VMs for migration without direct host overloading detection, thereby reducing the generation of SLAV, ensuring the performance, and reducing the energy consumption of CDC. Simulations driven by real VM workload traces show that our method outperforms the existing methods in reducing SLAV generation and CDC energy consumption.

1. Introduction

The COVID-19 outbreak has spurred an accelerated embrace of cloud computing over the past two years [1]. In order to maintain social distance and cut off the transmission of the virus, our work and life have moved online. Thanks to the help of cloud computing, the world economy under the shadow of the epidemic has remained basically normal [2]. On the other hand, this has also led to the development of cloud computing accelerating again.

The influx of various enterprises and individual users makes cloud service providers (CSPs) face severe challenges in allocating computing resources[3]. Cloud users hope to obtain satisfactory services, and cloud service providers also hope to convert computing power into services with minimal operating costs. Therefore, the CSP needs to consider the following complex relationship when configuring and scheduling various computing resources of the cloud data center (CDC): seeking a balance between maximization the user performance and minimization the energy consumption of the CDC [4]. Pursuing the trade-off between energy consumption and performance has always been one of the key research issues in the field of CDC computing resource management.

1.1. Background. The quality of the service experienced by the users is a subjective feeling, but it can be measured by the computing power provided by the CSP. The relevant experience is quantified into a number of metrics described in the service-level agreement (SLA) for a direct assessment of service quality. SLA violation (SLAV) occurs when the metrics in the SLA cannot be met. Then, the CSP should give the user a certain amount of compensation, which is factored into the cost calculation. On the other hand, energy consumption accounts for a large part of the cost of keeping a CDC running [5]. Generally speaking, the energy consumption of a CDC consists of two parts, which are the energy consumption of maintaining the operation of hardware devices (such as hosts) and the energy consumption of cooling equipment [6]. In this paper, we mainly

consider the former. Because the CSP can directly reduce this part of energy consumption by optimizing task scheduling. For instance, a virtual machine (VM) packing algorithm is employed to save energy by packing virtualized devices (such as VMs and containers) into a smaller number of hosts, and then shutting down or switching additional empty hosts to power-saving modes [4]. In this server consolidation process, CSPs need to avoid a large-scale occurrence of SLAVs and a significant degradation of user experience caused by malicious competition for resources generated by excessively centralized VMs.

1.2. Motivation. In the study of server consolidation, a variety of overloading detection strategies, VM selection strategies, and VM placement strategies are proposed and implemented through combined execution [5]. The ultimate goal of server consolidation is to optimize the energy consumption or resource utilization efficiency of the CDC, but each strategy in the combination has a different purpose. When determining whether a host is overloading, there are strategies based on fixed thresholds and dynamic threshold strategies based on statistical methods. Due to the variety of criteria for determining whether a host is overloading, when SLAV occurs, there must be excessive competition for resources among VMs, and when the overloading state occurs, this competition does not necessarily occur at the same time. In other words, overloading is not necessarily accompanied by SLAV, but there must be overloading when SLAV occurs. The purpose of filtering out overloading hosts is to migrate some VMs in advance to prevent the generation of SLAV or to bring VMs out of SLAV state. Therefore, the goal of VM migration can be set as to avoid the occurrence of SLAV rather than the hosts overloading. When selecting VMs to be migrated, there are MMT that considers the migration time of VMs, random strategies, strategies that consider the minimum number of migrations, and MC strategy that considers the correlation between VMs and resources. The VM placement problem has always been a research hotspot in the field of cloud computing, and various algorithms have been proposed to solve this problem.

In solving the server consolidation problem, the above-mentioned combinations ignore the organic connection between various strategies. For instance, different CDCs, or even within the same CDC, need to deploy different VM placement algorithms to deal with different situations. In addition, the reason why overloading detection should be performed first in the server consolidation process is because the dynamic changes of VM workload make the emergence of SLAV uncertain. The host overloading threshold provides an early warning space for this uncertainty. In order to adapt to different placement algorithms and dynamic workloads, we use reinforcement learning to eliminate the host overload detection operation. In each time slot, our proposed method determines which hosts may be overloaded in the future, and also selects the VMs to be migrated, so as to achieve the goal of optimizing energy consumption and reducing SLAV.

2. Related Works

2.1. Non-Machine-Learning Methods in Server Consolidation

2.1.1. Host Overloading Detection Strategies. Hieu et al. [7] proposed a host overloading detection strategy based on a multiple linear regression forecasting method. When the resource utilization of the host in the current and future specified time exceeds a preset fixed threshold, it is considered to be overloading. Yadav et al. [8] proposed regression-based algorithms called Gdr and MCP to set a dynamic upper CPU utilization threshold for detecting overloading hosts. Yadav et al. [9] also proposed an overloading host detection strategy based on robust regression, called LmsReg, which can dynamically adjust the upper CPU utilization threshold. Zhou et al. [10] proposed a KMI (K-Means clustering algorithm-Midrange-Interquartile range) strategy to distinguish underloading, normally loading and overloading hosts in a cluster. Zahedi Fard et al. [11] proposed a host overloading detection strategy based on host CPU usage and temperature, both of which are fixed thresholds.

2.1.2. VM Selection Strategies. Hieu et al. [7] proposed a VM selection strategy called minimum resource temperature (MRT), which selects those VMs that cause the most workloads to migrate. Yadav et al. [8] proposed Bandwidth-Aware Dynamic VM selection policy (Bw), which selects VMs with the smallest migration time to migrate. Yadav et al. [12] also proposed the MuMs VM selection strategy, which selects VMs with a smaller ratio of CPU usage to RAM usage on overloading hosts to migrate. Yadav et al. [11] proposed minimum utilization prediction VM selection policy (MuP). This strategy uses statistical methods to analyze the CPU usage history of each VM to determine whether it should be migrated. Zhou et al. [10] divided the causes of host overloading into those caused by the use of CPU and those caused by the use of I/O. For the former, a strategy named MRCU (maximum ratio of CPU utilization to memory utilization) is proposed. For the latter, a strategy named MPCU (minimum product of CPU utilization and memory utilization) is proposed. The maximum fit (MF) strategy was proposed by Zahedi Fard et al. [11]. The strategy first calculates the deviation between utilization of overloading server and its threshold, and then picks the VM in which VM utilization is close to the deviation.

2.1.3. VM Placement Algorithms. Hieu et al. [7] used PABFD. Zhou et al. [10] took SLAV into consideration and proposed a VM placement strategy with maximizing energy efficiency (VPME). Zahedi Fard et al. [11] proposed a heuristic VM placement strategy to avoid SLAV. The core idea of this strategy is to classify hosts. A host with lower resource usage is less likely to experience SLAV in the future.

2.2. Reinforcement Learning-Based Methods in Cloud. Rjoub et al. [13] proposed a reinforcement learning-based method to improve the utilization of cloud resources and

shorten the waiting time of tasks. Energy consumption and SLA are not considered. Qu et al. [14] proposed DMRO, which utilizes reinforcement learning to offloading tasks from IoT devices to edge-cloud servers. Considering the complex network structure between users and resources, Karthiban and Raj [15] used reinforcement learning to achieve load balancing in the CDC. Sun et al. [16] proposed a reinforcement learning method to offload a computing mission from edge cloud to the vehicular cloud. Ma and Ding [17] proposed a reinforcement learning-based model to evaluate which specific variables in the system are related to the energy consumption in a CDC. Joseph et al. [18] proposed to use RL methods to solve the problem of mapping a given set of microservice containers to resources, aiming to reduce SLAV and energy consumption. Bitsakos et al. [19] proposed DERP, a reinforcement learning-based method that automatically scales various computing resources according to user needs, thereby achieving cloud elasticity. Cheng et al. [20] proposed DRL-cloud, which uses the RL method to distribute a large amount of jobs to different servers, reducing energy consumption while ensuring that jobs can be completed before the deadline. In DRL-cloud, electricity price fluctuations are also set as constraints so that energy costs are comprehensively considered. Tuli et al. [21] proposed a scheduling algorithm based on reinforcement learning and RNN to achieve seamless scheduling of application tasks between edge servers and cloud servers to reduce energy consumption and SLAV.

The above works did not focus on server consolidation, server load, and VM migration in CDC.

3. Problem Description and Proposed Methodology

In this section, we first describe the energy consumption model, then model VM migration and consolidation as a Markov decision process (MDP) and formulate the consolidation objective as the minimization of expected energy consumption increment.

3.1. Environment Model. The lifetime of the cloud cluster system is divided into multiple time slots, which can be denoted as a sequence $[0, 1, 2, \ldots, t, t+1, \ldots, \text{END}]$. The length of time in a time slot is T.

There are N VMs and M hosts in the cluster. The i-th VMs are denoted as vm_i, and the j-th host is denoted as host_j.

$h_{j,t}$ is the allocation of VMs (or the set of running VMs) on the host_j in t. $p_t = \{h_{1,t}, h_{2,t}, \ldots, h_{M,t}\}$ is the allocation of all VMs to the hosts.

The max amount of computing resource that host_j can provide is its capacity C_j. To describe whether $host_j$ is in idle state or not in t, a binary indicator $\chi_{j,t} \in (0, 1)$ is used. If $\chi_{j,t} = 1$, host_j is not in idle state, and there is at least one VM running on it in time slot t. If $\chi_{j,t} = 0$, host_j is in idle state, and it should be switched to energy-saving mode or shut down in time slot t.

3.2. Energy Consumption Model. Our energy consumption model is based on CPU utilization [5].

For vm_i, its energy consumption in t is calculated as

$$ec_{vm_{i,t}} = \int_{t \cdot T}^{(t+1) \cdot T} u_{vm_i}(x), \tag{1}$$

where $u_{vm_i}(x)$ is vm_i's CPU utilization at time x.

For host_j, its energy consumption, $ec_{\text{host}_{j,t}}$, in t consists of two parts. The first part, $\text{base}_{\text{host}_j}$, is the basic energy consumption when host_j is running and in idle state. $\text{base}_{\text{host}_j}$ is constant. The second part is the energy that consumed by all the VMs running on it, which can be calculated as $\sum_{vm_i \in h_{j,t}} ec_{vm_{i,t}}$. Hence, we obtain the energy consumption of all hosts in time slot t:

$$\text{EC}_{\text{host}_t} = \sum_{j=1}^{M} \chi_{j,t} \times \left(\text{base}_{\text{host}_j} + \sum_{vm_i \in h_{j,t}} ec_{vm_{i,t}} \right). \tag{2}$$

It should be noted that host_j does not consume any energy if $\chi_{j,t} = 0$.

Migration cost in time slot t should be considered. To migrate a VM, the cost is an extra 10% CPU usage of that VM at the source host. Hence, the total cost of VM migration is,

$$\text{MC}_t = 10\% \times \sum_{vm_i \in MIG_t} ec_{vm_{i,t}}. \tag{3}$$

SLAV compensation of a VM in time slot t is considered and is an important part of our optimization goal. If $host_j$ is experiencing 100% CPU utilization in t, it is overloaded and SLAV occurs. All VMs in $h_{j,t}$ should receive SLAV compensations at this time. A binary indicator $\Upsilon_{j,t}$ is used to tag whether $host_j$ is overloading and causes SLAV in t or not:

$$\Upsilon_{j,t} = \begin{cases} 0, & \text{if } \sum_{vm_i \in h_{j,t}} ec_{vm_{i,t}} < C_j, \\ 1, & \text{if } \sum_{vm_i \in h_{j,t}} ec_{vm_{i,t}} \geq C_j. \end{cases} \tag{4}$$

In this study, we map the SLAV compensation, which is denoted as $SLAVC_t$, to the energy consumption of related VMs

$$\text{SLAVC}_t = c_{slav} \times \left(\sum_{j=1}^{M} \Upsilon_{j,t} \times \int_{t \cdot T}^{(t+1) \cdot T} \sum_{vm_i \in h_{j,t}} d_{vm_i} \right), \tag{5}$$

where d_{vm_i} is vm_i's initial CPU demand and $c_{slav} \in [0, 1]$ is the SLAV penalty ratio. Since d_{vm_i} is the user requirement and is a fixed value, we obtain

$$\mathrm{SLAVC}_t = c_{slav} \times \left[\sum_{j=1}^{M} \Upsilon_{j,t} \times \left(T \times \sum_{vm_i \in h_{j,t}} d_{vm_i} \right) \right]. \quad (6)$$

According to Equations (2), (3) and (6), we obtain total energy consumption EC_t of the cluster in time t:

$$\mathrm{EC}_t = \mathrm{EC}_{\mathrm{host}_t} + \mathrm{MC}_t + \mathrm{SLAVC}_t. \quad (7)$$

3.3. Markov Decision Process (MDP). In the following, we model the MPD of our problem.

(i) State in time slot t: $s_t = p_t = \{h_{1,t}, h_{2,t}, \ldots, h_{j,t}, \ldots, h_{M,t}\}$.

(ii) The action a: the migration actions over all VMS, which is combined by two steps.

Step 1: select VMs to migrate from each host. At time t, the set of selected VMs on $host_j$ is denoted as $\mathrm{MIG}_{j,t}$. The set of all selected VMs is denoted as $\mathrm{MIG}_t = \cup_{j=1}^{M} \mathrm{MIG}_{j,t}$.

Step 2: implement a given VM placement algorithm P. Hence, $s_{t+1} = P(\mathrm{MIG}_t, s_t)$.

It should be noted here that our action is not a multilevel hierarchy model. Since our purpose is to train the decision-making policy in Step 1, which can fit the given VM placement algorithm.

The action space is denoted as $A(s)$.

(i) Reward $r(s, a, s')$: the direct reward of taking action a at state s and then arriving to certain new state s'.

(ii) Policy $\pi(s)$: the strategy at state s, which is the probability distribution of actions at state s.

(iii) Q-value $Q_\pi(s, a)$: the expected reward of taking action a at state s according to π.

3.4. VM Selection and Placement Constraints. The action is combined by two steps, and in each step, there are corresponding constraints.

Regarding VM selection policy, it must obey the following constraint:

VM selection constraint: for each host_j, $\mathrm{MIG}_{j,t} \subset h_{j,t}$, which means that the policy selects and only can select the VMs running on $h_{j,t}$ to be migrated.

Regarding VM placement policy, it must obey the following constraints:

VM placement constraint 1: every VM in MIG_t must be assigned to a certain host.

VM placement constraint 2: the source host and the destination host of a migrating host cannot be the same.

VM placement constraint 3: After the migration is complete, none of the VMs should be in the SLAV state.

In this study, we use a modified PABFD algorithm [5] to allocate VMs to the appropriate hosts. The pesudocode is presented in Algorithm 1. Comparing to the original PABFD, our algorithm modified the VM placement constraints and the core framework of the algorithm remains unchanged. Hence, the modified algorithm is also called PABFD.

3.5. Energy Minimization as Migration Goal. We define the reward function as the energy consumption decrement as action a is taken at state s and arriving at new state s'. It should be noted that the energy consumption is actually decreased at the new state if $r(s_t, a_t, s_{t+1}) > 0$. The goal is to design a VM selection strategy that minimizes the increment energy consumption:

$$r(s_t, a_t, s_{t+1}) = \mathrm{EC}_t - \mathrm{EC}_{t+1}. \quad (8)$$

The model is initialized as follows. p_0 is set to the VM allocation at time slot 0, and $p_o = \{h_{1,0}, h_{2,0}, \ldots, h_{M,0}\}$. $Q_\pi(s, a)$ is 0, and $\pi(s)$ is uniformly distributed among all actions for each state. Then, $Q_\pi(s_t, a_t)$ is updated by interacting with the cluster and server consolidation environment. The optimal strategy is given by the Bellman equation such that the expected reward of taking action a_t at state s_t is the sum of $r(s_t, a_t, s_{t+1})$ and the future reward of s_{s+1}. Hence, we obtain

$$Q_\pi(s_t, a_t) = \mathbb{E}_{s_{t+1}} \left[r(s_t, a_t, s_{t+1}) + \gamma \mathbb{E}_{a_{t+1} \sim \pi(s_{t+1})} \left[Q_\pi(s_{t+1}, a_{t+1}) \right] \right], \quad (9)$$

where $\gamma \in (0, 1)$ is the discounted factor of the future rewards.

The goal is to design a VM selection-based migration strategy that maximizes the cumulative of energy consumption decrement value $r(s_t, a_t, s_{t+1})$ in the dynamic consolidation progress. We leverage the deep reinforcement learning method to solve the problem.

We use actor-critic-based algorithm Proximal Policy Optimization (PPO) [22] to implement the VM selection-based migration agent. We assume the probability ratio between old and new policies as

$$r_t(\theta) = \frac{\pi_{\theta_{\mathrm{new}}}(a_t | s_t)}{\pi \theta_{\mathrm{old}}(a_t | s_t)}. \quad (10)$$

The clipped surrogate objective function is as follows:

$$J^{\mathrm{CLIP}}(\theta) = \hat{\mathbb{E}}_t(\theta) \left[\min \left(r_t(\theta) \hat{A}(s_t, a_t), \mathrm{clip}\left(r_t(\theta), 1 - \epsilon, 1 + \epsilon \right) \hat{A}(s_t, a_t) \right) \right], \quad (11)$$

where $r_t(\theta) \hat{A}(s_t, a_t)$ is the normal policy gradient objective, and $\hat{A}(s_t, a_t)$ is the estimated advantage function. $\mathrm{clip}(r_t(\theta), 1 - \epsilon, 1 + \epsilon)$ clips $r_t(\theta)$ to be in $[1 - \epsilon, 1 + \epsilon]$. The objective function of PPO is the minimum of the clipped and normal objective.

PPO restricts the range of large policy change as the incentive for the probability ratio to move outside of the interval is removed []. Hence, the stability of the policy networks is improved in PPO by restricting the policy update at each training step. Another reason of leveraging PPO for VM selection-based migration is that it is simpler to tune.

Input: hostlist, vmList (MIG_t)
Output: allocation of the VMs
(1) **for** each VM *in* vmList **do**
(2) minPower ← MAX
(3) allocatedHost ← NULL
(4) **for** host *in* hostList **do**
(5) **if** *no SLAV on this host and not the source host for* VM **then**
(6) power ← estimatePower (host, VM)
(7) **if** power < minPower **then**
(8) allocatedHost ← host
(9) manpower ← power
(10) **end if**
(11) **end if**
(12) **end for**
(13) **if** allocatedHost ≠ NULL **then**
(14) allocation.add (VM, allocatedHost)
(15) **end if**
(16) **end for return** allocation

Algorithm 1: PABFD.

4. Performance Evaluation

4.1. Experimental Setup. We use OpenAI [23] to simulate the CDC environment and the entire server consolidation process. PPO is one of the default reinforcement learning algorithms that comes with OpenAI [24].

We use real workload trace dataset, Bitbrains [25], collected from VMs in production data centers to drive our simulations. By sampling every 5 minutes (a time stamp), Bitbrains recorded the usage of different resources by more than 4,000 VMs over a month. Table 1 shows a sampling of resources used by a Bitbrains VM in a time stamp. In addition, Bitbrains also recorded the initial request for computing resources from these VMs.

We used Bitbrains trace to generate three sets of requests with different sizes. Request 1 consists of 250 VMs, request 2 consists of 500 VMs, and request 3 consists of 100 VMs. We selected the resource usage records of related VMs within a random day (24 hours) to generate each request. Therefore, each request contains 288 time stamps, which can be used for 288 consecutive time slots in server consolidation. Based on these three requests, we measure the performance of the algorithm on different scale tasks.

4.2. Evaluation Metrics. Our goal is to reduce energy consumption and also to reduce the generation of SLAV, and the corresponding indicators for evaluating the performance of the algorithm are EC and SLAV.

SLAV is calculated as follows. SLAV is related to (1) the SLAV time per active host (SLATAH): the percentage of time, during which active hosts have occupied the CPU utilization of 100% [5]; (2) the performance degradation due to the migration (PDM).

$$\text{SLATAH} = \frac{1}{M}\sum_{j=1}^{M}\frac{T_{s_j}}{T_{a_j}}, \tag{12}$$

where M is the number of hosts, T_{s_j} is the SLAV time on host_j, and T_{a_j} is the active time of host_j [5].

$$\text{PDM} = \frac{1}{N}\sum_{i=1}^{N}\frac{C_{d_i}}{C_{r_i}}, \tag{13}$$

where N is the number of VMs and C_{d_i} is the estimation of performance degradation (can be estimated by an extra 10% of CPU utilization [26]) of the vm_i caused by the migrations, and C_{r_i} is the total CPU capacity demanded by vm_i [5].

$$\text{SLAV} = \text{SLATAH} \cdot \text{PDM}. \tag{14}$$

EC is calculated in 7. In addition, since VM migrations consume additional resources and degrade performance to some extent, the number of VM migrations is also used as one of the evaluation metrics.

4.3. Baseline Algorithms. The study by Li et al. [4, 5] shows that the VM placement algorithm can show better results when the VM selection policy is MMT and the host overloading detection policy is LR. Therefore, in this paper, the combination of these two strategies is used to compare with our proposed method.

(i) MMT: the migration time is calculated by dividing the memory used by the VM by the available bandwidth. The MMT strategy selects the VM with the shortest migration time and adds it to the VM migration list.

(ii) LR: the local regression method is used to count the history of CPU resource usage by the specified host, and then, the strategy determines whether the host is overloading.

In addition, we also used two VM placement algorithms as the baselines, namely,

Table 1: An example record of the Bitbrains VM workload trace.

Time stamp (ms)	CPU cores	CPU capacity provisioned [MHZ]	CPU usage (%)	CPU usage [MHZ]	Memory capacity provisioned (KB)	Memory usage (KB)	Disk read throughput (KB/s)	Disk write throughput (KB/s)	Network received throughput (KB/s)	Network transmitted throughput (KB/s)
1376322046	4	11703.99824	64.37199032	0.55	6.71088647	0.0	0.0	1.4	0.0	1.0

(i) Random placement (Random): for the current VM to be migrated, an available host is randomly selected in the host list as the destination.

(ii) First fit placement (FF): for the current VM to be migrated, FF selects the first available host in the host list as the destination.

We adopt LR-MMT-Random, LR-MMT-FF, and LR-MMT-PABFD to compare with RL-PABFD, which is our proposed method, to evaluate its performance. The meaning of "LR-MMT-Random" is to use the combination of LR, MMT, and Random successively as the strategy for performing server consolidation.

4.4. Analysis of Results

4.4.1. EC. Figure 1 demonstrates the total energy consumption after processing three sets of requests by various methods. It is shown in Figure 1 that RL-PAABFD outperforms LR-MMT-Random, LR-MMT-FF, and LR-MMT-PABFD regarding energy consumption. When the number of requested VMs is small, such as request 1 and request 2, the differences between the energy consumption generated by LR-MMT-PABFD and RL-PABFD are also small. When processing request 3, RL-PABFD is significantly better than LR-MMT-PABFD. Under the same VM placement algorithm, RL does not show a sufficiently noticeable advantage over LR-MMT. The gap between RL-PABFD and LR-MMT-PABFD is far smaller than the gap between RL-PABFD and LR-MMT-Random. We believe that RL methods are not sufficiently convergent to deal with such problems. In addition, LR-MMT-Random, LR-MMT-FF, and LR-MMT-PABFD all adopt the same VM selection policy and host overloading detection policy. Therefore, the disparity in energy consumption between the three is mainly caused by the performance of different VM placement algorithms.

Figures 2–4 demonstrate the energy consumption in each time slot of the four methods when processing request 1, request 2, and request 3. There are two main reasons for the fluctuation of energy consumption in different time slots: (1) dynamic changes in many MV workloads lead to changes in energy consumption, and (2) changes in the number of hosts used lead to an increase or decrease in energy consumption. Among them, the drastic changes in the workload of the VMs are the main reason for this fluctuation. Therefore, when processing a given request, although the energy consumptions of the CDC generated by the four methods are constantly changing, some are more and some are less, but in most time slots, their overall trends are relatively close. For instance, in certain time periods, if the resource demands for resources of a large number of VMs increase significantly, the energy consumption of VMs will also inevitably increase. In order to reduce SLAV, more hosts must be used to load these VMs; thereby, energy consumption is further increased. This inevitable increase in energy consumption cannot be substantially reduced by algorithms. The underlying algorithms cannot influence the resource demands of higher-level users or tasks.

4.4.2. SLAV. Figure 5 demonstrate the SLAV generated by various methods after processing three sets of requests. It can be seen from Figure 5 that when processing requests of various sizes, the SLAV generated by RL-PABFD is significantly less than that of other methods. This is because part of the objective function, as shown in 8, consists of the SLAV penalty when we design the solution. Therefore, the policy will actively reduce the generation of SLAV during learning, thereby avoiding the increase of energy consumption. LR-MMT can only passively and indirectly reduce the possibility of SLAV generation, and their purpose is not directly reflected in the final optimization goal. As can be seen from Figure 5, comparing LR-MMT-Random and LR-MMT-FF, and LR-MMT-PABFD and RL-PABFD is more capable of reducing SLAV than reducing overall energy consumption.

Figure 5 also shows that the SLAV gaps among LR-MMT-Random, LR-MMT-FF, and LR-MMT-PABFD are smaller than that among RL-PABFD and them. This is because the three use the same combination of strategies, LR-MMT, to prevent the host from entering the overloading state or staying in this state for a long time. The generation of SLAV is mainly related to the host overloading detection strategy and VM selection strategy. The primary responsible goal of the VM placement algorithm is to select the appropriate host for each VM to be migrated. The constraints or optimization objectives related to SLAV are not considered by the Random, FF, and PABFD algorithms.

During the server consolidation process, multiple VMs were in the SLAV state in multiple consecutive time slots, so we will not show and compare the SLAV generated by the four methods in every time slots here.

4.4.3. Number of VM Migrations. Figure 6 shows the total number of VM migrations trigged by various methods after processing three sets of requests. As can be seen from Figure 6, RL-PABFD results in the smallest number of total VM migrations when processing requests of various sizes. However, compared with the other three methods, RL-PABFD does not show an absolute advantage. Although VM migrations will generate additional energy consumption, its purpose is the load balancing of the cluster, thereby better reducing SLAV. There is a trade-off between the two, but the focus is on reducing SLAV. Comparing Figure 6 with Figure 5, it can be seen that RL-PABFD reduces SLAV more than the other three methods when the difference in the total number of virtual machine migrations induced is small. This also means that, compared with the other three methods, RL-PABFD can select a more suitable VMs for migration, which can lead to SLAV generation when resources are fiercely contested. Observed from this perspective, RL is more efficient than LR-MMT.

Figures 7–9 demonstrate the number of VM migrations trigged by the four methods in each time slot when processing the three requests. From these figures, it can be seen that the number of VM migrations induced by the four methods tends to the same trend in multiple consecutive time slots. However, within a single time slot, the

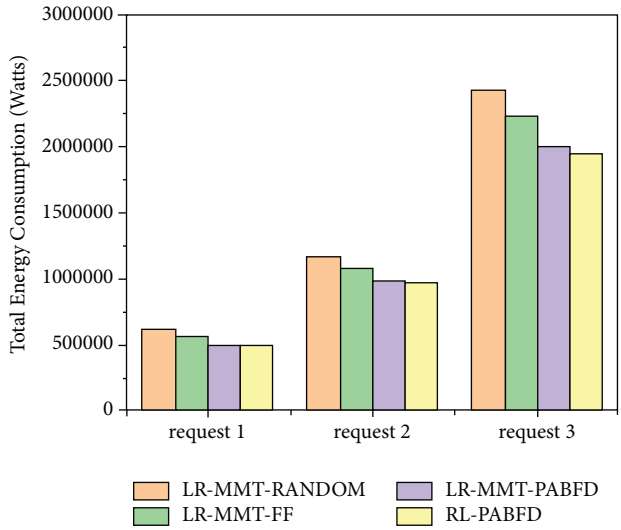

Figure 1: Comparing the total EC of four methods regarding requests 1, 2, and 3.

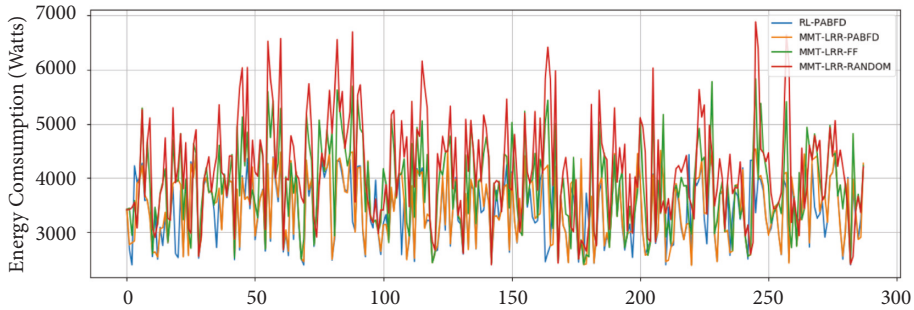

Figure 2: Comparing EC in every time slot of four methods regarding request 1.

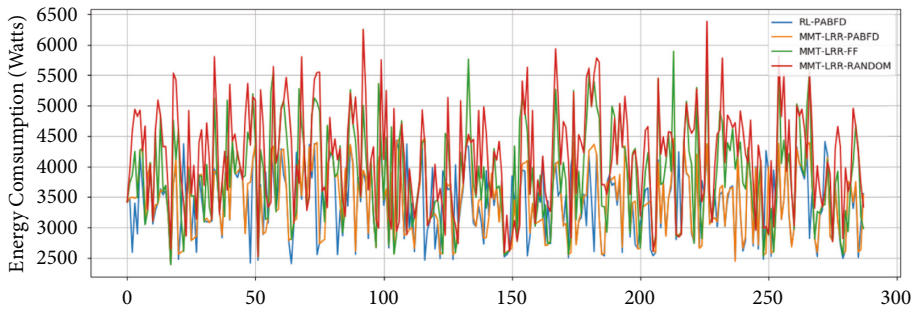

Figure 3: Comparing EC in every time slot of four methods regarding request 2.

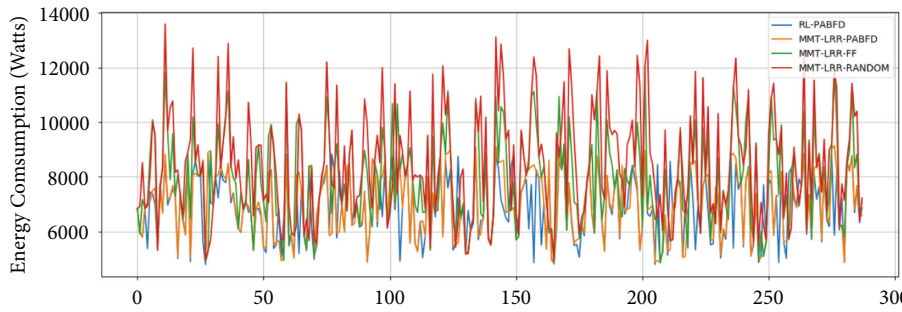

Figure 4: Comparing EC in every time slot of four methods regarding request 3.

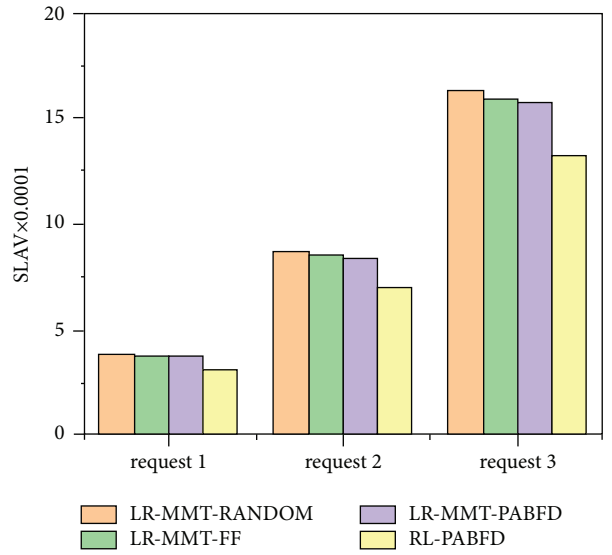

Figure 5: Comparing SLAV of four methods regarding requests 1, 2, and 3.

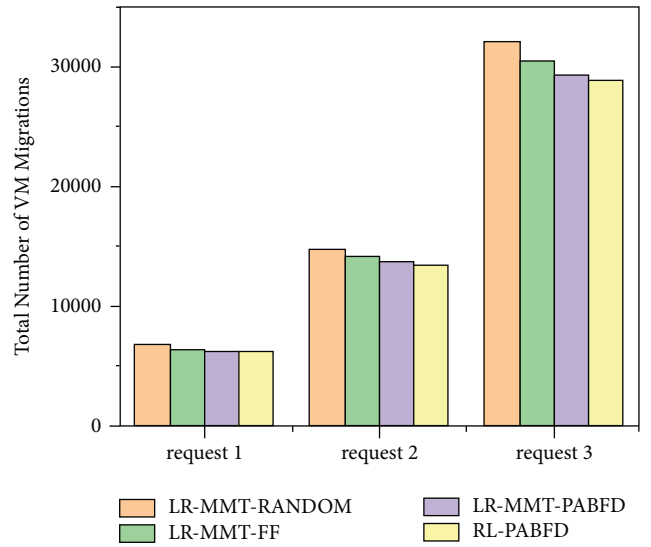

Figure 6: Comparing the number of VM migrations of four methods regarding requests 1, 2, and 3.

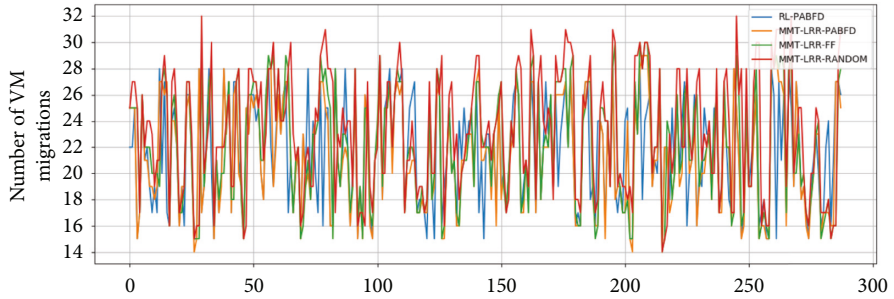

Figure 7: Comparing the number of VM migrations in every time slot of four methods regarding request 1.

fluctuations in the number of virtual machine migrations caused by the four methods are different. This phenomenon is similar to the EC fluctuation phenomenon shown in Figures 2–4. The reason for this phenomenon is still that the fluctuation of a large number of VM workloads leads to fluctuations in the demand for computing resources. When

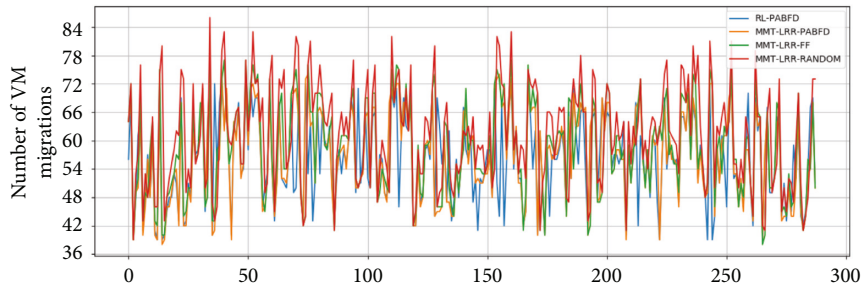

Figure 8: Comparing the number of VM migrations in every time slot of four methods regarding request 2.

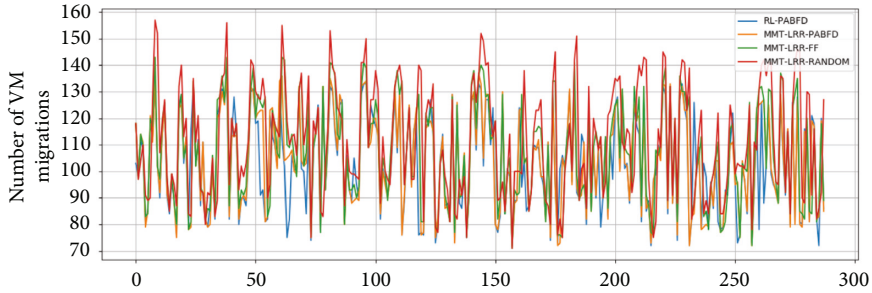

Figure 9: Comparing the number of VM migrations in every time slot of four methods regarding request 3.

most of the VMs are about to enter or are already in the peak business period, the centralized demand for computing resources will trigger the generation of SLAV and a large amount of energy consumption. Unlike reducing energy consumption, SLAV can only be eliminated by VM migrations.

5. Conclusions

This study proposes a reinforcement learning-based VM selection strategy, which selects appropriate VMs for migration from hosts that may be in or have been overloaded, so as to avoid the occurrence of SLAV and reduce the total energy consumption of CDC. Our proposed method combines the two steps of host overloading detection and VM selection during server consolidation, and unifies the two with the ultimate goal of reducing energy consumption. Simulations driven by real VM workload traces demonstrate that our method is slightly better than the existing methods in reducing the energy consumption of SLAV generation of CDC, showing a certain feasibility.

In future work, we will further improve the convergence performance of the proposed method and also incorporate VM placement into the consideration of using RL-based ideas to solve the server consolidation problem holistically.

Data Availability

No Data Statement here.

Conflicts of Interest

The authors declare that they have no conflicts of interest.

Authors' Contributions

Li Huixi, Xiao Yinhao, and Shen Yongluo conceptualized the data and contributed to funding acquisition; Li Huixi and Xiao Yinhao performed methodology; Li Huixi performed software, formally analyzed the study, investigated the study, performed resources and data curation, wrote original draft preparation, and involved in visualization; Li Huixi and Shen Yongluo validated the study; Xiao Yinhao and Shen Yongluo reviewed and edited the document; Shen Yongluo supervised the study and performed project administration. All authors have read and agreed to the published version of the manuscript.

Acknowledgments

This research was funded by the National Natural Science Foundation of China (no. 62002067), Guangzhou Youth Talent Program (QT20220101174), Department of Education of Guangdong Province (no. 2020KTSCX039), and SRP of Guangdong Education Dept (2019KZDZX1031).

References

[1] S. Agrawal, "A survey on recent applications of Cloud computing in education: COVID-19 perspective," *Journal of Physics: Conference Series*, vol. 1828, no. 1, Article ID 012076, 2021.

[2] I. J. Akpan, E. A. P. Udoh, and B. Adebisi, "Small business awareness and adoption of state-of-the-art technologies in emerging and developing markets, and lessons from the COVID-19 pandemic," *Journal of Small Business and Entrepreneurship*, vol. 34, no. 2, pp. 123–140, 2022.

[3] H. Li, W. Li, S. Zhang, H. Wang, Y. Pan, and J. Wang, "Page-sharing-based virtual machine packing with multi-resource

constraints to reduce network traffic in migration for clouds," *Future Generation Computer Systems*, vol. 96, pp. 462–471, 2019.

[4] H. Li, W. Li, H. Wang, and J. Wang, "An optimization of virtual machine selection and placement by using memory content similarity for server consolidation in cloud," *Future Generation Computer Systems*, vol. 84, pp. 98–107, 2018.

[5] A. Beloglazov and R. Buyya, "Optimal online deterministic algorithms and adaptive heuristics for energy and performance efficient dynamic consolidation of virtual machines in cloud data centers," *Concurrency and Computation: Practice and Experience*, vol. 24, no. 13, pp. 1397–1420, 2012.

[6] D. Mukherjee, S. Chakraborty, I. Sarkar, A. Ghosh, and S. Roy, "A detailed study on data centre energy efficiency and efficient cooling techniques," *International Journal*, vol. 9, 2020.

[7] N. T. Hieu, M. D. Francesco, and A. Ylä-Jääski, "Virtual machine consolidation with multiple usage prediction for energy-efficient cloud data centers," *IEEE Transactions On Services Computing*, vol. 13, no. 1, pp. 186–199, 2020.

[8] R. Yadav, W. Zhang, O. Kaiwartya, P. R. Singh, I. A. Elgendy, and Y. C. Tian, "Adaptive energy-aware algorithms for minimizing energy consumption and SLA violation in cloud computing," *IEEE Access*, vol. 6, pp. 55923–55936, 2018.

[9] R. Yadav, W. Zhang, K. Li, C. Liu, M. Shafiq, and N. K. Karn, "An adaptive heuristic for managing energy consumption and overloaded hosts in a cloud data center," *Wireless Networks*, vol. 26, no. 3, pp. 1905–1919, 2020.

[10] Z. Zhou, J. Abawajy, M. Chowdhury et al., "Minimizing SLA violation and power consumption in Cloud data centers using adaptive energy-aware algorithms," *Future Generation Computer Systems*, vol. 86, pp. 836–850, 2018.

[11] S. Y. Zahedi Fard, M. R. Ahmadi, and S. Adabi, "A dynamic VM consolidation technique for QoS and energy consumption in cloud environment," *The Journal of Supercomputing*, vol. 73, no. 10, pp. 4347–4368, 2017.

[12] R. Yadav, W. Zhang, H. Chen, and T. Guo, "Mums: Energy-aware vm selection scheme for cloud data center," in *Proceedings of the 2017 28th International Workshop on Database and Expert Systems Applications (DEXA)*, pp. 132–136, Lyon, France, August 2017.

[13] G. Rjoub, J. Bentahar, O. Abdel Wahab, and A. Saleh Bataineh, "Deep and reinforcement learning for automated task scheduling in large-scale cloud computing systems," *Concurrency and Computation: Practice and Experience*, vol. 33, no. 23, p. e5919, 2021.

[14] G. Qu, H. Wu, R. Li, and P. Jiao, "DMRO: a deep meta reinforcement learning-based task offloading framework for edge-cloud computing," *IEEE Transactions On Network And Service Management*, vol. 18, no. 3, pp. 3448–3459, 2021.

[15] K. Karthiban and J. S. Raj, "An efficient green computing fair resource allocation in cloud computing using modified deep reinforcement learning algorithm," *Soft Computing*, vol. 24, no. 19, pp. 14933–14942, 2020.

[16] F. Sun, N. Cheng, S. Zhang, H. Zhou, L. Gui, and X. Shen, "Reinforcement learning based computation migration for vehicular cloud computing," in *Proceedings of the 2018 IEEE Global Communications Conference (GLOBECOM)*, pp. 1–6, Abu Dhabi, UAE, December 2018.

[17] H. Ma and A. Ding, "Method for evaluation on energy consumption of cloud computing data center based on deep reinforcement learning," *Electric Power Systems Research*, vol. 208, Article ID 107899, 2022.

[18] C. Joseph, J. Martin, K. Chandrasekaran, and A. Kandasamy, "Fuzzy reinforcement learning based microservice allocation in cloud computing environments," in *Proceedings of the TENCON 2019-2019 IEEE Region 10 Conference (TENCON)*, pp. 1559–1563, Kochi, India, October 2019.

[19] C. Bitsakos, I. Konstantinou, and N. Koziris, "DERP: a deep reinforcement learning cloud system for elastic resource provisioning," in *Proceedings of the 2018 IEEE International Conference On Cloud Computing Technology And Science (CloudCom)*, pp. 21–29, Nicosia, Cyprus, December 2018.

[20] M. Cheng, J. Li, and S. Nazarian, "DRL-cloud: deep reinforcement learning-based resource provisioning and task scheduling for cloud service providers," in *Proceedings of the 2018 23rd Asia And South Pacific Design Automation Conference (ASP-DAC)*, pp. 129–134, Jeju, Korea (South), January 2018.

[21] S. Tuli, S. Ilager, K. Ramamohanarao, and R. Buyya, "Dynamic scheduling for stochastic edge-cloud computing environments using a3c learning and residual recurrent neural networks," *IEEE Transactions on Mobile Computing*, vol. 21, no. 3, pp. 940–954, 2022.

[22] J. Schulman, F. Wolski, P. Dhariwal, A. Radford, and O. Klimov, "Proximal policy optimization algorithms," 2017, https://arxiv.org/abs/1707.06347.

[23] G. Brockman, V. Cheung, L. Pettersson et al., *Openai Gym*, https://arxiv.org/abs/1606.01540, 2016.

[24] Github Project, "Openai/baselines," 2022, https://github.com/openai/baselines.

[25] S. Shen, V. Van Beek, and A. Iosup, "Statistical characterization of business-critical workloads hosted in cloud datacenters," in *Proceedings of the 2015 15th IEEE/ACM International Symposium On Cluster, Cloud And Grid Computing*, pp. 465–474, Shenzhen, China, May 2015.

[26] Y. Song, H. Wang, Y. Li, B. Feng, and Y. Sun, "Multi-tiered on-demand resource scheduling for VM-based data center," in *Proceedings of the 2009 9th IEEE/ACM International Symposium On Cluster Computing And The Grid*, pp. 148–155, Shanghai, China, May 2009.

Hindawi
Mathematical Problems in Engineering
Volume 2022, Article ID 5692350, 13 pages
https://doi.org/10.1155/2022/5692350

Research Article

Research on Path Planning of Mobile Robot with a Novel Improved Artificial Potential Field Algorithm

Tiezheng Guo,[1] **Jie Wang**,[1] **Zhiming Wang**,[2] **Wei Chen**,[1] **Guojun Chen**,[1] **and Shishi Zhang**[1]

[1]*Industrial Center, Nanjing Institute of Technology, Nanjing 211167, Jiangsu, China*
[2]*Key Laboratory of Crop Harvesting Equipment Technology of Zhejiang Province, Jinhua 321007, Zhejiang, China*

Correspondence should be addressed to Tiezheng Guo; gtz1988@outlook.com

Received 27 May 2022; Revised 6 July 2022; Accepted 19 July 2022; Published 9 September 2022

Academic Editor: Amandeep Kaur

For the path planning and obstacle avoidance problem of mobile robots in unknown surroundings, a novel improved artificial potential field (IAPF) model was proposed in this study. In order to overcome the shortages of low efficiency, local optimization trap, and unreachable target in the classical artificial potential field (APF) method, the new adaptive step length adjustment strategy was proposed in IAPF, which improved the path planning and obstacle avoidance efficiency. A new triangular navigation method was designed to solve the local optimization trap in joint force zero condition for a variety of path planning. In order to solve the target unreachable problem, a new target attraction model was established based on the distance of obstacle to improve convergence rate, and the new method was designed such as adding the aim factor to optimize the rejection force function and so on. The two methods of IAPF and APF are compared using MATLAB simulation, the average path planning efficiency of IAPF is increased by 42.8% compared with APF, the average path length is reduced by 8.6%, and the average target convergence rate is increased by 26.1%. Finally, the physical test of the mobile robot verified the effectiveness and accuracy of IAPF.

1. Introduction

Due to the rapid development of industrial automation and intelligence, as well as the constant improvement of human living conditions, the use of robots has become more and more extensive and has gradually become an indispensable part of human production and life. Motion planning technology has received widespread attention as a necessary link in the robot's intelligent autonomous operation [1].

In recent years, a large number of research results have been achieved in the path planning of mobile robots. The conventional methods have been widely used such as the grid method [2], $A*$ algorithm [3], and artificial potential field method [4]. In order to adapt mobile robots to different application fields and complex and changing industrial environments, various intelligent algorithms have emerged to provide new solutions for mobile robot path planning. The commonly used intelligent algorithms include genetic algorithm [5, 6], particle swarm algorithm [7], and neural network algorithm [8], as well as the proposed fusion and improvement based on the above algorithms. Among them, compared with other algorithms that have met some problems of the long computing time, poor real-time obstacle avoidance, and many iterations under some special circumstances, the artificial potential field method has a simple structure, small computation, fast response time, low hardware platform requirements, and easy underlying real-time control, and is widely used in real-time obstacle avoidance and smooth trajectory control.

Although it has many advantages, the classical APF method also has some defects, such as inaccessible target and easy to fall into local optimum [9]. Scholars have conducted several research in effort to address this issue. For example, a novel repulsive potential function was presented by Azzabi and Nouri [10]. When a robot is locked in a local minimum, the escape force is activated to assist the robot in breaking free from the stalemate position and turning gradually away from the obstacles in order to solve the local minimum problem. Rostami et al. [11] proposed a virtual target point, which creates a pulling force to assist the robot in escaping

when the robot falls into a local optimal state. Batista et al. [12] proposed a virtual obstacle model and modified the repulsion function to solve target unreachable problems in the planning algorithm. However, the algorithm used the equal-step path method and the overall planning efficiency was not high. Jung and Kim [13] used the tangent method to solve the local minimum problem formed by multiple obstacles and introduced a target factor to overcome the problem of the unreachable target. However, when there are multiple obstacles in front of the target point, the convergence speed of the robot is slow. Pashna et al. [14] improved the target unreachable and local minimum defects in the classical APF method, introduced a target distance factor, modified the repulsive force function in potential field, and solved the target unreachable problem. The deflection angle method was used to construct the traction force for solving the local minimum problem, but when escaping from the local minimum point of multiple obstacles, the planned path appears jagged and the path curve was not smooth obviously enough.

Based on the existing research and problems met, the novel improved artificial potential field (IAPF) path planning model in multiobstacles complex environment was proposed in this study. A new triangle navigation method was designed to establish a planning guide point when the mobile robot fell into a local optimal situation and used the additional attraction force of the guide point to get away from the local minimum value and solve the local optimal problem; An adaptive step length adjustment strategy was proposed to dynamically adjust step length according to the number of obstacles, so as to improve the planning efficiency of the system. A new target attraction model based on obstacle distance was built to improve the target convergence speed, and the target distance factor was added to optimize the repulsion function to address the problem of a nonreachable goal.

The structure of this study is organized as follows: Section 2 is mainly about the existing problems in the classical APF model. In Section 3, the corresponding improvement measures are proposed and a novel IAPF model is established. Demonstration of the effectiveness and superiority of the IAPF algorithm through simulation and algorithm comparison is illustrated in Section 4. Physical tests verifying the effectiveness and accuracy of the IAPF are introduced in Section 5. Finally, the conclusions are presented in Section 6.

The main contributions of this study are as follows:

(i) Aiming at the optimal path planning problem of mobile robots in unknown surroundings, a unique IAPF model was proposed, which overcomes the problems of the classical APF method, such as low efficiency in algorithm planning, easy to trap local optimum, and unreachable target.

(ii) A novel triangular navigation method was designed to solve the local optimization trap in joint force zero condition for a variety of path planning. The new adaptive step length adjustment strategy was designed to improve the efficiency of path planning and obstacle avoidance.

(iii) The target attraction model based on the distance of obstacles was built to improve the algorithm convergence speed, and the repulsion function was optimized by adding the target factor to solve the target unreachable problem.

2. Classical Artificial Potential Field Method

The basic idea of the APF method [15] is similar to the "electromagnetic field," which regards obstacles as repulsive points and targets as attractive points to construct repulsive and attractive potential fields. Obstacles and targets respectively generate repulsive force F_{rep} and attractive force F_{att} on the mobile robot. The mobile robot's movement, path planning, and real-time collision avoidance are all guided by the joint force F. The working principle is shown in Figure 1.

In order to calculate the attractive and repulsive forces received by the mobile robot, first, the attractive field function and repulsive field function are defined [16]. By taking the negative gradient of the two potential field functions, the attractive and repulsive functions are obtained. The classical functions of attractive field U_{att} and repulsion field U_{rep} are as follows:

$$U_{\text{att}} = \frac{1}{2}\mu q g^2 \overrightarrow{q_g}, \tag{1}$$

$$U_{\text{rep}} = \begin{cases} \dfrac{1}{2}\sigma\left(\dfrac{1}{q_{obs}} - \dfrac{1}{d_{obs}}\right)^2 \overrightarrow{q_{obs}}, & 0 \le q_{obs} \le d_{obs}, \\ 0, & q_{obs} > d_{obs}, \end{cases} \tag{2}$$

where μ is the attractive gain coefficient, σ is the repulsion gain coefficient, q_g is the distance between the current position of the robot and the target point, $\overrightarrow{q_g}$ is the unit vector of the current position of the robot pointing to the target point, q_{obs} is the distance between the current position of the robot to the obstacle, $\overrightarrow{q_{obs}}$ is the unit vector of the robot's current position pointing to the obstacle, and d_{obs} is the action distance of repulsive field of obstacle.

The corresponding attractive function F_{att} and repulsive function F_{rep} are as follows:

$$F_{att} = -\nabla U_{att} = -\mu q_g \overrightarrow{q_g}, \tag{3}$$

$$F_{\text{rep}} = -\nabla U_{rep} = \begin{cases} \sigma\left(\dfrac{1}{q_{obs}} - \dfrac{1}{d_{obs}}\right)\dfrac{1}{q_{obs}2}\overrightarrow{q_{obs}}, & 0 \le q_{obs} \le d_{obs}, \\ 0, & q_{obs} > d_{obs}. \end{cases} \tag{4}$$

The formula of the joint force on the robot is as follows:

$$F = F_{\text{att}} + \sum_{1}^{n} F_{\text{rep}}, \tag{5}$$

where n is the number of obstacles.

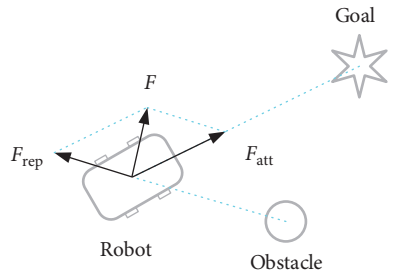

Figure 1: Schematic diagram of potential field.

In robot route planning and obstacle avoidance, the traditional APF approach is commonly employed. However, when it is tested in a complex unknown environment, the following problems are encountered: (i) APF adopts an equal step planning method, which cannot be fully applied in multiple obstacles environment, and the algorithm efficiency needs to be improved. (ii) When the joint force of the mobile robot is zero, the planning algorithm loses the next forward direction and the system falls into a local optimal state. (iii) When there are obstacles near the target point, the repulsion force is greater than the attractive force when the mobile robot reaches the target point, which causes the mobile robot to oscillate near the target point, the convergence speed is slow, and even cannot reach the target point.

3. Improved Artificial Potential Field Model

In the study, to solve the problems of the classical APF method in the path planning of mobile robot applicable to the complex unknown environments, the corresponding improvement methods are proposed and novel models are established from the following three aspects.

3.1. Adaptive Step Length Adjustment Method. The classical APF method adopts the equal step length in the path planning method, which has the problems of low efficiency and long operation time and cannot be fully applied in a complex unknown environment. The actual test shows that in the simple environment with a small number of obstacles, the step length can be appropriately enlarged so as to reduce the path points to be calculated and accelerate the robot moving speed, which leads to improve the efficiency of path planning and reduce the system operation time. In the complex environment with multiple obstacles, the robot moving speed can be decelerated by appropriately reducing the step length, so as to reduce the collision probability.

Based on the number of obstacles, the distance between robot and obstacle, and iteration times, an adaptive step length adjustment method is proposed and expressed as follows:

$$\text{step} = \rho \frac{1}{n} * 2^{\sqrt{q_{obs}/d_{obs}}} * e^{\left(c/c_{\max}\right)^2}, \tag{6}$$

where ρ is the step gain coefficient, c is the current iteration time, and c_{max} is the upper limit of iterations.

According to formula (6), step length is inversely proportional to the number of obstacles, so the more obstacles there are, the smaller step length is. Step length is proportional to the distance that from robot to obstacle, the closer the robot is to the obstacle, the smaller the step length and the lower the collision risk. Step length is proportional to the number of iterations, the more iterations, the larger the step length and the faster the target convergence rate.

3.2. Triangular Navigation. In the operation process of mobile robot, there are mainly two cases for the local optimal problem: (i) due to the scope of the obstacles potential field, it may happen that only one single obstacle potential field produces repulsion, and its direction is collinear with the attractive direction, which leads to the mobile robot wandering in the current position. When the joint force is zero, the robot stops moving. (ii) When the mobile robot encounters multiple obstacles, the repulsion force and attractive force are collinear, which leads to the mobile robot wandering in the current position. When the joint force is zero, it stops moving. The two cases are shown in Figure 2.

In view of the above two cases, the triangle navigation method is proposed to solve the local optimal problem in this study. The following two cases are discussed respectively.

3.2.1. Single Obstacle. The move direction of the mobile robot is provided by the joint force in the path planning. When the repulsion force and attractive force are collinear, the mobile robot oscillates back and forth or stops moving in the current position, so the extra force is needed to make the mobile robot escape from the local optimum. The solution is to use the triangle navigation method to determine the guidance point, which provides an attractive force to guide the robot escape from the local area. Figure 3 shows the triangle navigation method in a single obstacle condition.

As shown in Figure 3, $O(x, y)$ is the obstacle coordinate, $G(x, y)$ is the guidance point coordinate, and $P(x, y)$ is the current position coordinate of the robot. With the obstacle as the center of the circle and the safe distance d as the radius of the circle, the line perpendicular to straight line of connecting the obstacle and the robot that intersects the circle at point G is made, and guiding point G provides additional attraction F'_{att} to help the robot escape from the local optimum.

The guide point calculation formula is as follows:

$$\begin{cases} \sqrt{(G_x - O_x)^2 + (G_y - O_y)^2} = d, \\ \dfrac{G_y - O_y}{G_x - O_x} \dfrac{O_y - P_y}{O_x - P_x} = -1. \end{cases} \tag{7}$$

According to the known obstacle coordinates $O(x, y)$ and the robot's current position coordinates $P(x, y)$, the guiding point $G(x, y)$ can be obtained by formula (7).

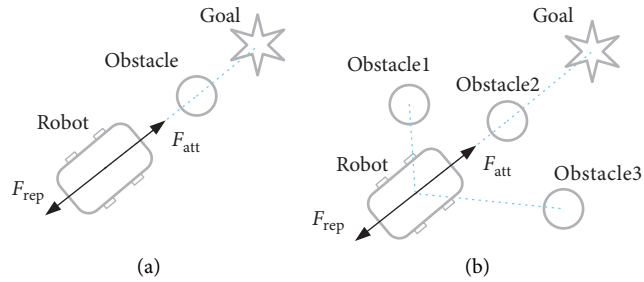

Figure 2: Local optimization trap. (a) Single obstacle. (b) Multiple obstacles.

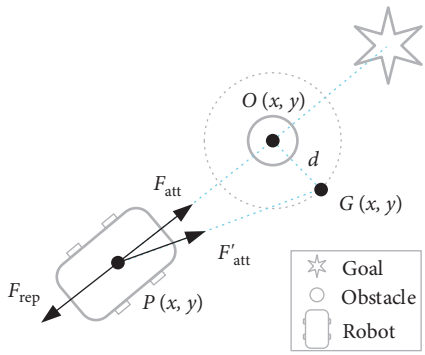

Figure 3: Triangle navigation method in single obstacle.

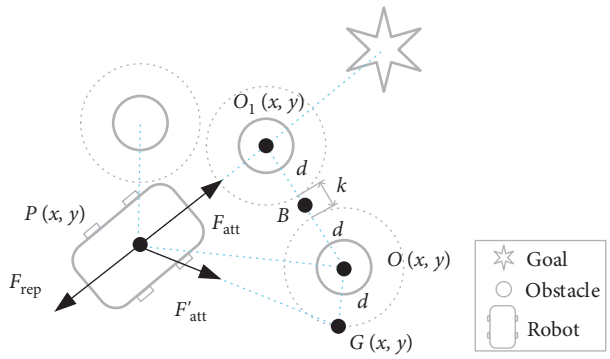

Figure 4: Triangle navigation method in multiple obstacles.

3.2.2. Multiple Obstacles. When the mobile robot encounters multiple obstacles and the joint force is zero, the robot falls into the local optimum and oscillates back and forth or stops. It needs to provide extra force to make the mobile robot escape from the local optimum. There are two solutions: the first is to pass through point B in the middle of multiple obstacles, and the second is to pass through G point, the outermost point of multiple obstacles, Figure 4 shows a schematic diagram of the two methods.

As shown in Figure 4, $O\ (x, y)$ and $O_1\ (x, y)$ are the coordinates of obstacles, and B is the midpoint of O and O_1. The first method is to determine whether the length of k is greater than the width of the vehicle body to judge whether the mobile robot can pass through safely. If the condition is true, the guidance point B is calculated, and the local optimum is escaped through the additional attraction of point B. If the first method is not feasible, the second method is adopted, namely, the triangulation method. The guide point G is determined at the outermost periphery of the multiple obstacles, and the local optimum is escaped through the attraction force generated by the G point. According to the known obstacle coordinates $O\ (x, y)$ and the robot's current position coordinates $P\ (x, y)$, the coordinates of the guiding point $G\ (x, y)$ can be obtained by formula (7).

3.3. Improved Repulsion Force Function. According to the attraction force and repulsion force of classic APF formulas (3) and (4), the closer the mobile robot to the target point is, the less attractive force it receives. The closer the robot to an obstacle is, the greater repulsion force it receives. Figure 5 shows the force analysis diagram of the target unreachable of the mobile robot.

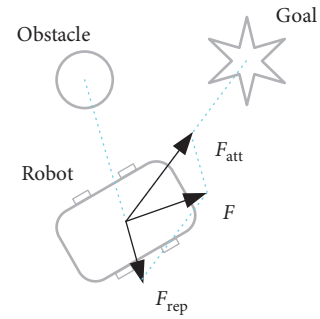

Figure 5: Schematic diagram of target unreachable.

Figure 5 shows how the mobile robot approaches the goal position when there is an impediment nearby, and the repulsive force F_{rep} it receives is substantially bigger than the attracting force F_{att}. It is unable to reach the goal location and oscillates near it.

The repulsion function is optimized, and the distance q_g between the mobile robot and the target point is incorporated as an adjustment factor, in order to tackle the problem of unreachable targets in the classical APF. The attractive force model F_{att1} is established to enhance the attractiveness of the target and ensure the attractive force received by the mobile robot near the target point is much greater than the repulsive force, so that the robot moves to the target point.

The optimized repulsion force function is as follows:

$$F_{\text{rep}} = \begin{cases} F_{rep1} + F_{rep2}, & 0 \le q_{obs} \le d_{obs}, \\ 0, & q_{obs} > d_{obs}, \end{cases} \tag{8}$$

where F_{rep1} is the repulsion force component, direction from the obstacle to the mobile robot, and F_{att1} is the attractive force component, direction from the mobile robot to the target point.

F_{rep1} and F_{att1} specific expressions are as follows:

$$\begin{cases} F_{\text{rep1}} = \sigma\left(\dfrac{1}{q_{obs}} - \dfrac{1}{d_{obs}}\right)\dfrac{q_g}{q_{obs}2} \cdot \overrightarrow{q_{obs}}, \\ F_{\text{att1}} = k \cdot \sigma\left(\dfrac{1}{q_{obs}} - \dfrac{1}{d_{obs}}\right)^2 q_{obs} \cdot \overrightarrow{q_g}, \end{cases} \tag{9}$$

where k is the scale factor.

After optimizing the repulsion function, the received force of the mobile robot near the target point is shown in Figure 6.

In the repulsion force function (8), the repulsion force F_{rep} is composed of two components F_{rep1} and F_{att1}. The target distance factor q_{g} is introduced, so that when the mobile robot approaches the target point, the repulsive force F_{rep1} component gradually decreases, and the attractive force F_{att1} component gradually increases, so that the mobile robot moves quickly to the target point. When the mobile robot reaches the target position, q_{g} becomes zero, and the joint force F acting on the mobile robot becomes zero as well, ensuring that the mobile robot reaches the target point stably and solving the problem of an unreachable target.

4. Simulations

In order to verify the effectiveness of the proposed IAPF model, MATLAB 2018b was used to simulate and analyse the path planning of the classic APF method and the IAPF method. The size of the simulation plane is 13 m × 13 m, and the system simulation parameter settings are listed in Table 1.

4.1. Simulation Analysis of Adaptive Step Length Adjustment. The classical APF method adopts the equal step path planning strategy, which is not suitable for the complex unknown environment and has met the problems of long system operation time and low path planning efficiency. The adaptive step length adjustment strategy is established and adopted in the improved algorithm, which gets the number and position of obstacles around the robot from the real-time scanning data of radar and automatically adjusts the forward step length of the mobile robot, as shown in Figure 7.

Figure 7(a) shows the classical path planning, which throughout adopts the equal-step path planning. Figure 7(b) shows an improved algorithm for path planning, and the density degree of the red dots in the curve depends on the step length of the path planning points. When there are many obstacles nearby, the robot planning step length decreases; that is, the moving speed decelerates, which reduces the probability of robot collision. Conversely, when there are fewer obstacles nearby, the robot planning step length increases, that is, to accelerate the moving speed, reduce the number of planning points, and improve the efficiency of path planning.

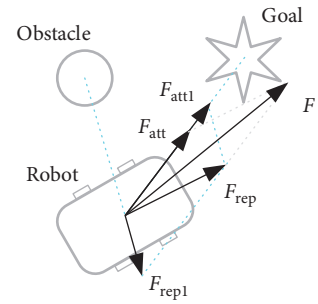

Figure 6: Optimized repulsion force function.

Table 1: Parameter setting.

Name	Symbol	Value
Attractive coefficient	μ	11
Repulsion coefficient 1	σ	3
Repulsion coefficient 2	k	2
Obstacle influence distance (m)	d_{obs}	1.5
Vehicle width (m)	*width*	0.8
Vehicle length (m)	*length*	1
Step length (m)	*T_step*	0.1
Number of cycles	$c_{\max}$	1000
Starting position (m)	P_0	(0, 0)
Target location (m)	P_g	(12, 12)

The specific algorithm comparison data are listed in Table 2. The IAPF algorithm has greatly improved the performance of the classical APF algorithm, the system planning efficiency has increased by 44.1%, the target convergence speed has increased by 26.3%, and the data calculated are listed in Table 2.

4.2. Local Optimal Simulation Analysis

4.2.1. Single Obstacle Situation. For the classic APF method, when the joint force of a single obstacle is zero, the robot loses the force of the potential field and loses the next planning path, so the robot stops moving. The simulation result is shown in Figure 8. Figure 8(a) depicts the robot being stuck at a local optimum. Under the potential field distribution, the robot is imprisoned in a local minimum, as shown in Figure 8(b). The coordinates of the minimum point are (5.62, 5.62). At this time, the mobile robot has a potential energy of 115.2 J.

For the IAPF method, when the robot falls into the local optimal state, the triangulation navigation method is started to generate a guide point. The guide point provides the attractive direction to help the mobile robot escape the local optimal state. The simulation result is shown in Figure 9. The improved model enables the mobile robot to overcome the local minimum and plan the destination path successfully.

Table 3 lists the simulation results for a single obstacle. The classical APF method falls into the local optimum, the robot stops moving, and the number of iterations is infinite.

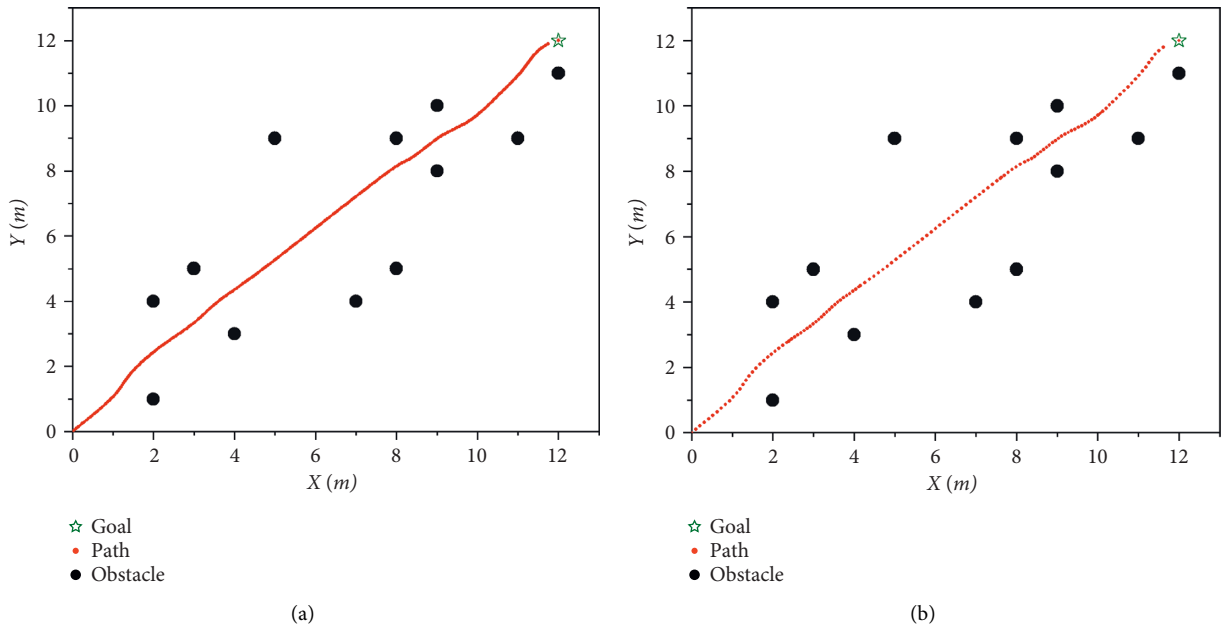

Figure 7: Simulation analysis of adaptive step length adjustment. (a) Classical APF algorithm. (b) IAPF algorithm.

Table 2: Algorithm comparison simulation data.

	Simulation time (s)	Number of iteration (s)	Planning efficiency*1 (improved)	Target convergence speed*2 (improved)
Classical APF method	0.1367	186	44.1%	26.3%
IAPF method	0.0765	137		

Note: *1 planning efficiency = | (simulation time of the IAPF method – imulation time of the classical APF method) | /simulation time of the classical APF method. *2 target convergence speed = | (number of iterations of the IAPF method – number of iterations of the classical APF method) | /number of iterations of the classical APF method.

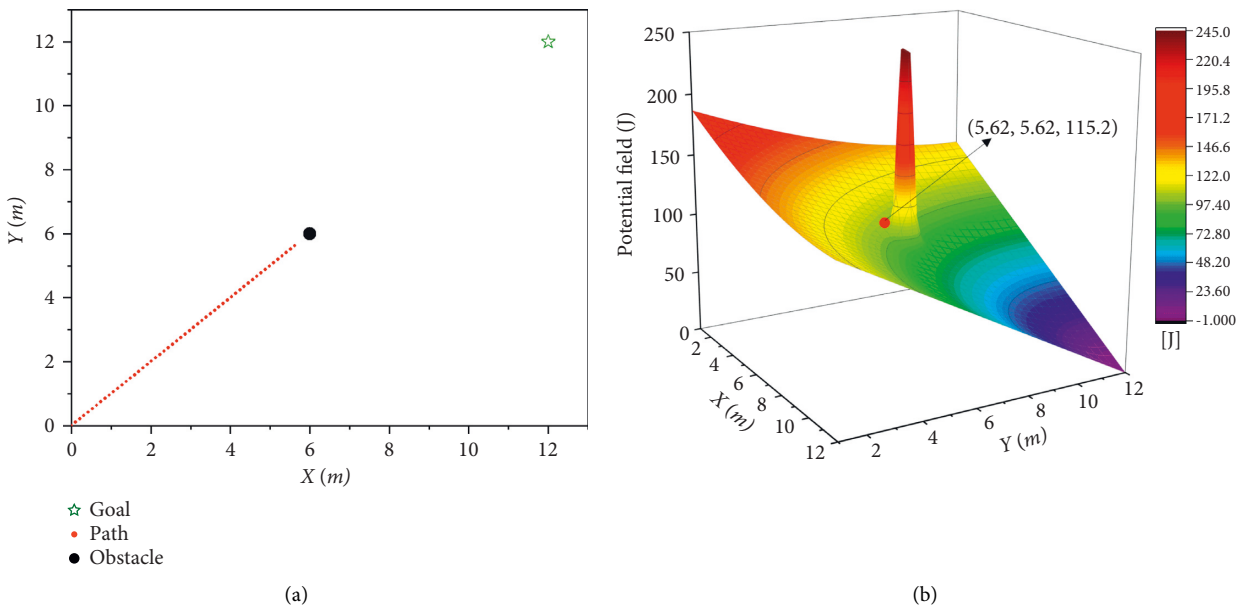

Figure 8: Simulation results of classical APF on single obstacle. (a) Trapped in local optimum. (b) Local most dominant field distribution.

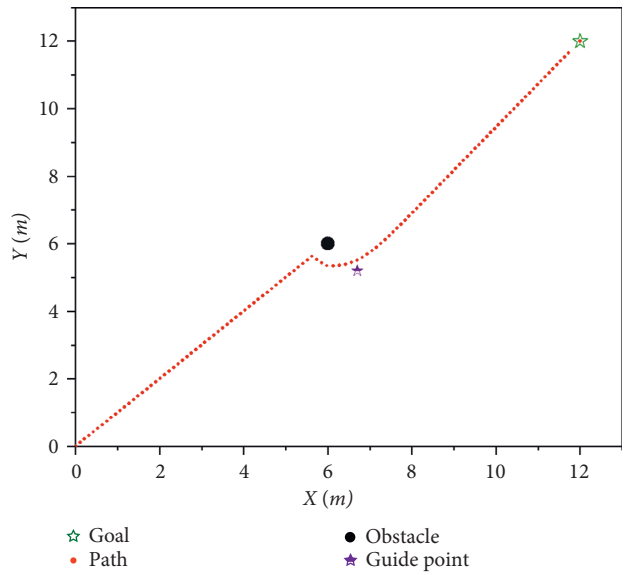

Figure 9: Simulation results of IAPF on single obstacle.

Table 3: Local optimal simulation results of a single obstacle.

Algorithm	Obstacle	Local optimum	Guidance point	Number of iterations
Classical APF method	(6, 6)	(5.62, 5.62)	Nothing	∞
IAPF method	(6, 6)	(5.62, 5.62)	(6.7, 5.2)	112

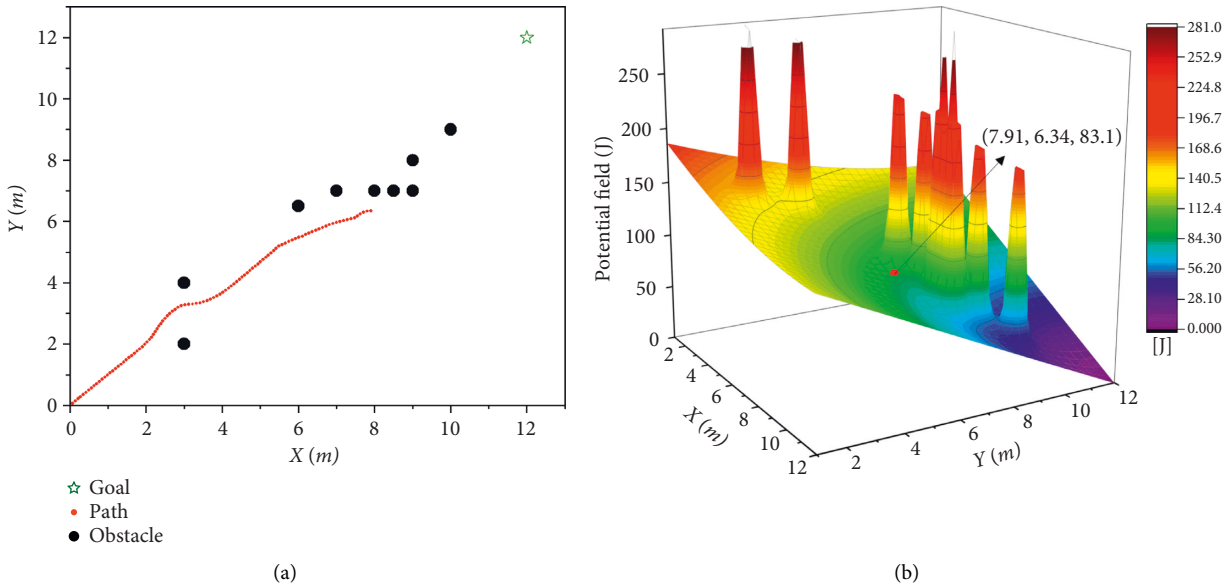

Figure 10: Simulation results of APF method on multiobstacles. (a) Trapped in local optimum. (b) Potential field distribution in local optimum.

The IAPF method solves the local optimal problem and reaches the target point smoothly. The whole process is iterated 112 times, with high efficiency and high speed.

4.2.2. Multiple Obstacles Situation. In the case of multiple obstacles and complex unknown environments, the mobile robot is easy to fall into the local optimal state, as shown in Figure 10. The robot is caught in local optimization, as shown in Figure 10(a). In Figure 10(b), it can be seen that the robot is at the local minimum point (7.91, 6.34). At this time, the potential energy of the mobile robot is 83.1 J.

When the mobile robot is in the local optimal state, the triangle navigation method of the IAPF model is used to establish the guidance point, which helps the robot

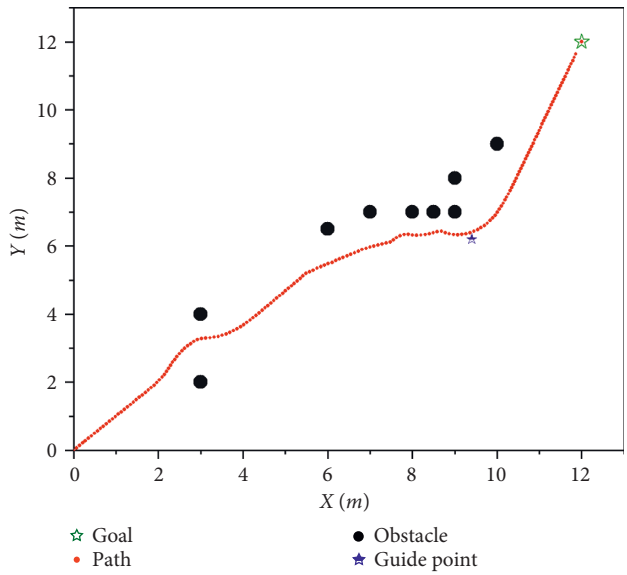

Figure 11: Simulation results of IAPF method with multiple obstacles.

Table 4: Local optimal simulation results of multiple obstacles.

Algorithm	Obstacles	Local optimum	Guidance point	Number of iterations
APF	(3, 2), (3, 4), (6, 6.5), (7, 7), (8, 7), (8.5, 7), (9, 7), (9, 8), (10, 9)	(7.91, 6.34)	Nothing	∞
IAPF	Dittos	(7.91, 6.34)	(9.4, 6.2)	180

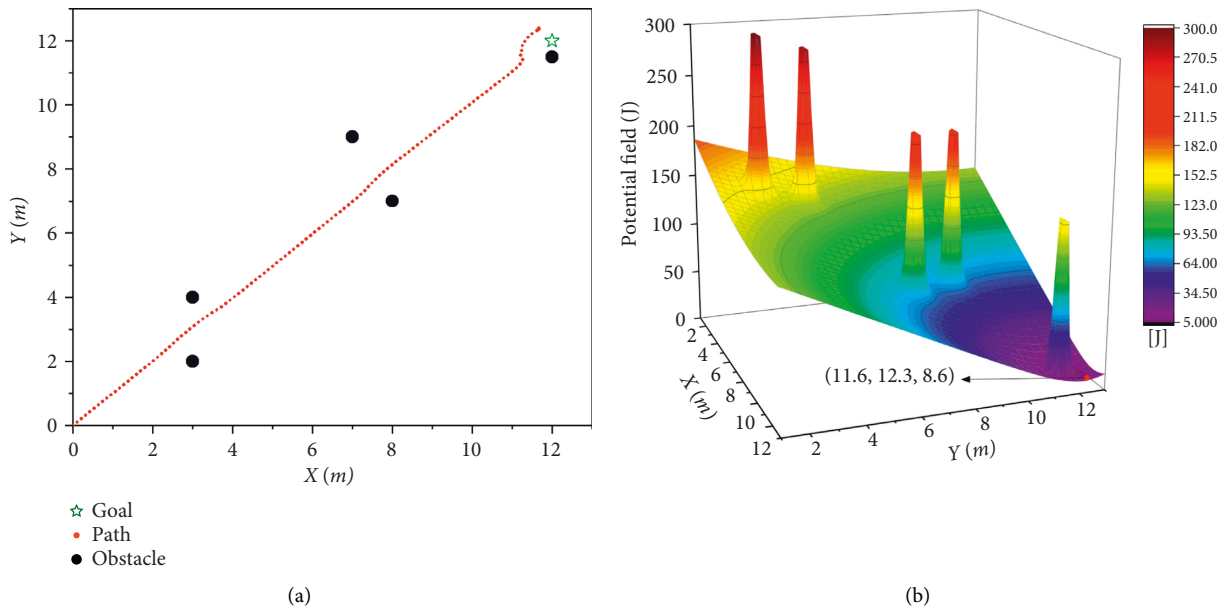

Figure 12: Simulation results of the classic APF method. (a) Target unreachable. (b) Potential field distribution condition of target unreachable.

successfully plan the path to the destination, and the path is smooth, as shown in Figure 11.

The simulation results of multiple obstacles are listed in Table 4. The APF method falls into the local optimum, the robot stops moving, and the number of iterations is infinite. The IAPF method solves the local optimal problem, and the whole process is iterated by 180 times, achieving fast convergence.

4.3. Target Unreachable Simulation Analysis. When obstacles are encountered near the target, the problem of target

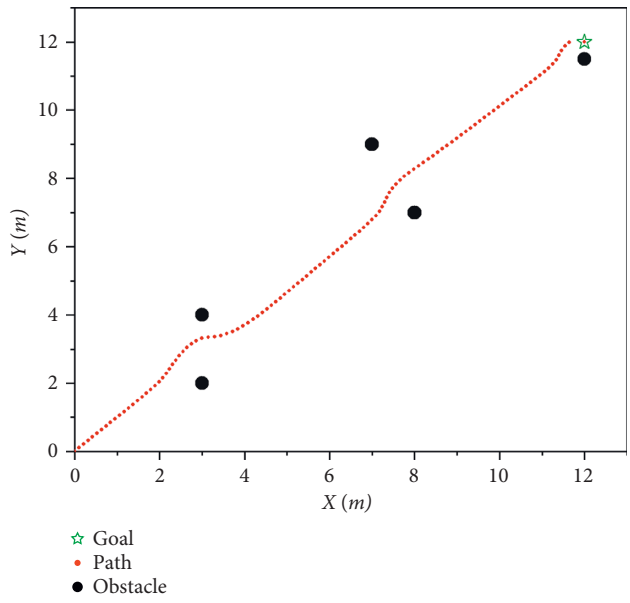

Figure 13: Simulation results of IAPF method.

Table 5: Simulation results of target unreachable.

Algorithm	Obstacles	Stop point	Number of iterations
APF	(3, 2), (3, 4), (7, 9), (8, 7) (12, 11.5)	(11.6, 12.3)	∞
IAPF	Dittos	(12, 12)	118

unreachable will occur by the APF method, as shown in Figure 12. Figure 12(a) shows the robot coming to a halt near the target spot. The repulsive force is seen near the target point in Figure 12(b), and the robot is unable to approach the target point directly, stopping at the coordinates (11.6, 12.3). At this time, the mobile robot has a potential energy of 8.6 J.

By improving the repulsion force model and optimizing the distance between the mobile robot and the target object into the repulsion function, the problem can be solved successfully. As shown in Figure 13, the robot overcomes the influence of repulsion and successfully reaches the endpoint.

The parameters of the simulation results of the target unreachable problem are listed in Table 5. The APF method cannot reach the target point, and the iteration times are infinite. The IAPF method reaches the target point after 118 iterations.

4.4. Comparative Simulation Analysis. According to the improved algorithm and the classical algorithm, several simulation experiments have been carried out, and the simulation is shown in Figure 14. Compared with the classical algorithm, the improved algorithm has a smoother path, shorter planned path, and faster convergence speed. Table 6 lists that the modified algorithm's average path planning efficiency has increased by 42.8%, while the average path length has decreased by 8.6%. The target's average convergence speed has improved by 26.1%.

5. Experiments

To test the viability of the suggested real-time planning algorithm, it is used to plan the paths of mobile robots in unknown surroundings in order to obtain the defined target information without colliding. The host is a Jetbot mobile robot equipped with XR-Lidar S1 radar, and the slave is a notebook computer with a processor Intel Core i5-6300 and running memory of 16 GB. In the ROS Kinetic system of Ubuntu16.04, the surrounding environment information is obtained through the corresponding sensors for two-dimensional map construction and feasible path planning. According to the size of the prototype, a $6 * 8$ m ground environment was selected for verification, and several cardboard boxes were placed as obstacles in the environment. The specific scenario is shown in Figure 15.

The Jetbot mobile robot is started, the Linux is opened on the computer, and the ROS system is loaded to enable the mobile robot to communicate with the computer. The mobile platform collects surrounding obstacle data through radar and odometer and transmits the collected data to the computer. The computer calls the gmapping function package to model the actual environment map. The mobile

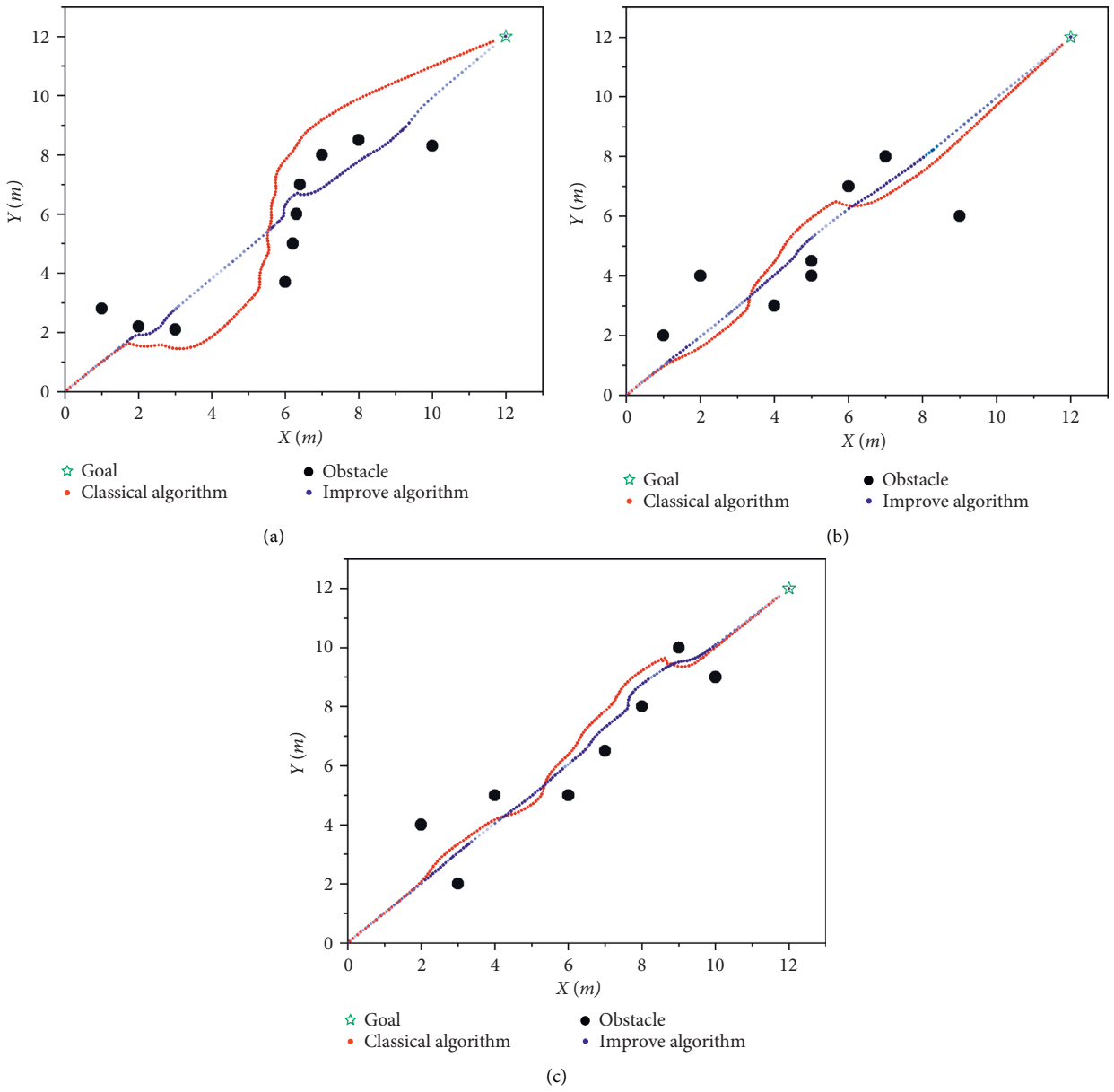

Figure 14: Algorithm simulation comparison. (a) Simulation one. (b) Simulation two. (c) Simulation three.

Table 6: Algorithm comparison on simulation data.

		Simulation time (s)	Path length (m)	Number of iterations	Planning efficiency (improved)	Path length*1 (decreased) (%)	Target convergence speed (improved)
Simulation one	APF	0.1234	19.2	186	44.6	10.4	29.1
	IAPF	0.0683	17.2	132			
Simulation two	APF	0.1354	18.7	174	37.2	8.5	27.0
	IAPF	0.0853	17.1	127			
Simulation three	APF	0.1172	18.6	183	46.8	6.9	22.4
	IAPF	0.0723	17.3	142			
Average planning efficiency (increased)						42.8%	
Average path length (decreased)						8.6%	
Average convergence speed (increased)						26.1%	

Note:*1 path length: | (path length of IAPF − path length of APF) | /path length of APF.

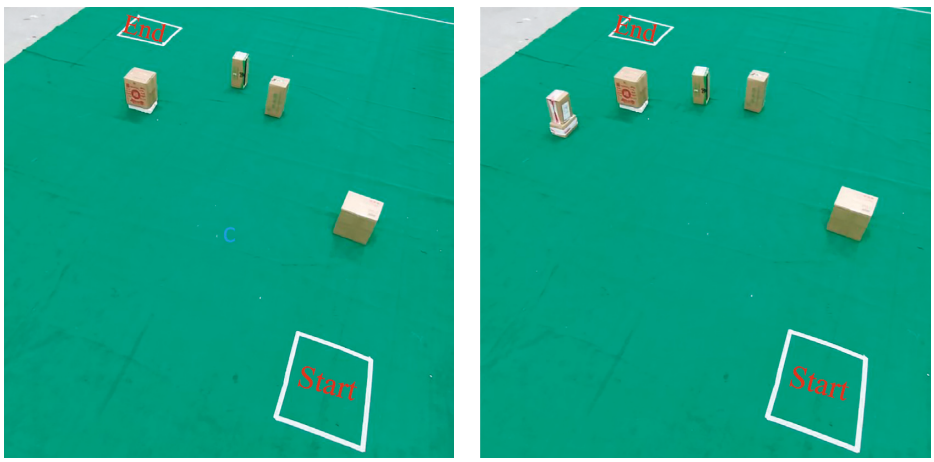

(a) (b)

Figure 15: Test site. (a) Scene 1. (b) Scene 2.

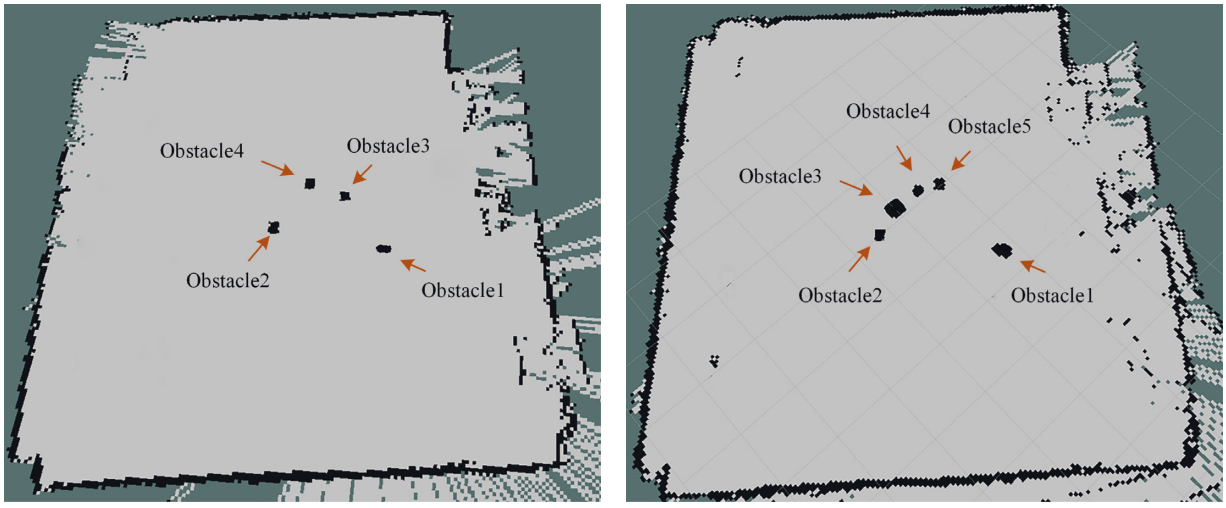

(a) (b)

Figure 16: Raster map. (a) Scene 1 mapping. (b) Scene 2 mapping.

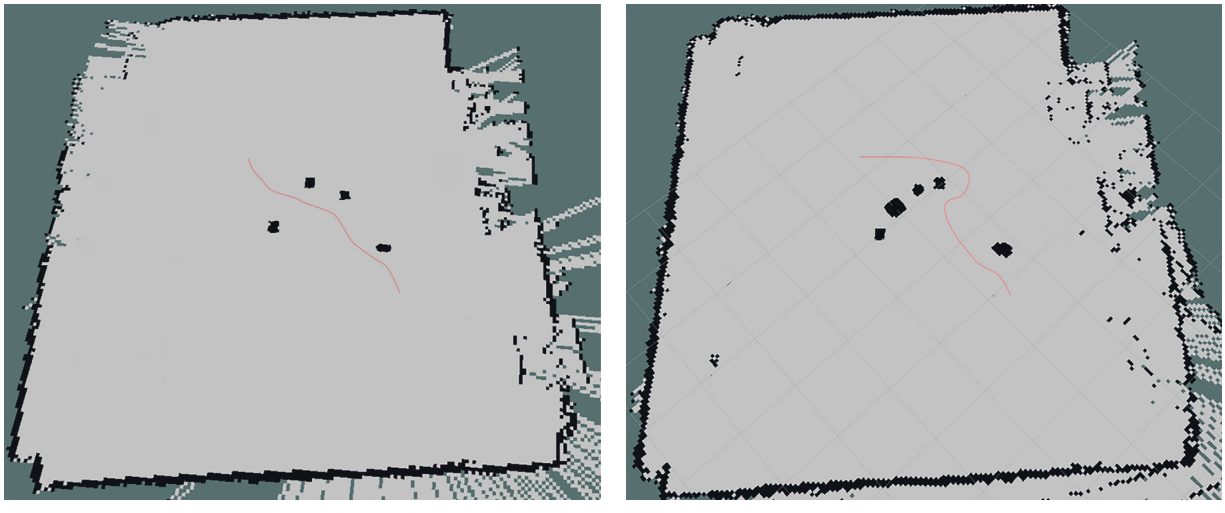

(a) (b)

Figure 17: Improved algorithm navigation path map. (a) Scene 1 path planning. (b) Scene 2 path planning.

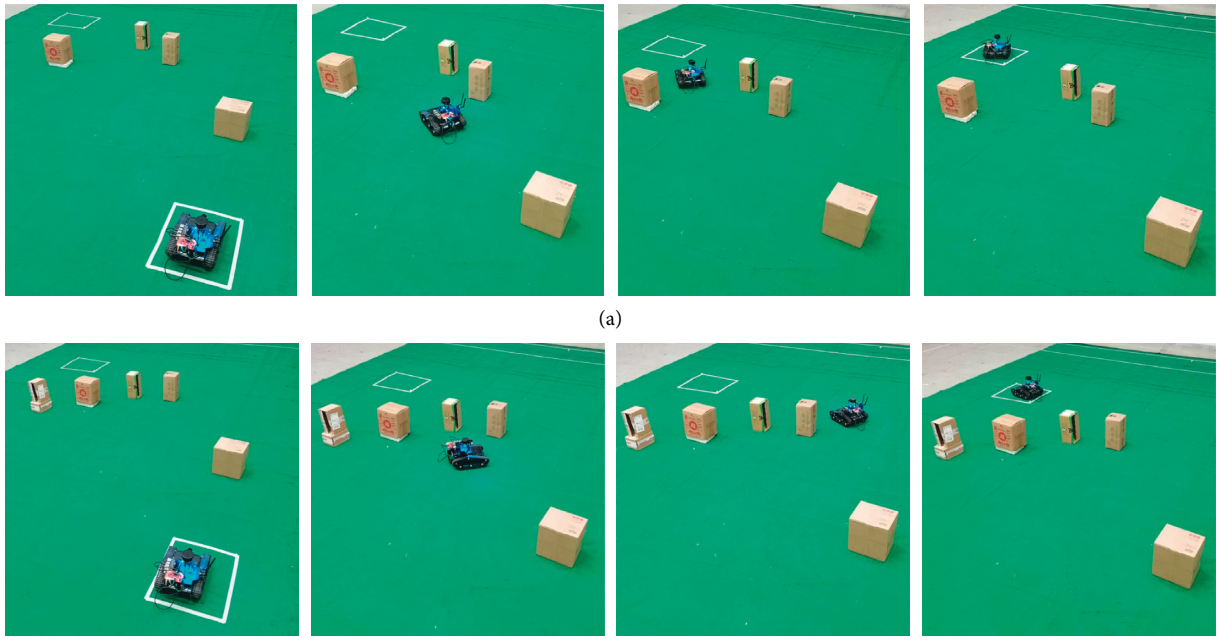

(a)

(b)

Figure 18: Physical test. (a) Scene 1 test. (b) Scene 2 test.

robot scans the actual environment to obtain a grid map, as shown in Figure 16.

The improved algorithm is used as a global planner in the ROS system in the form of a plug-in, and the parameters of the experimental platform are adjusted to write the launch file. The yaml file is loaded through rosparam to configure the platform parameters, the starting pose and target pose are set on the rviz visualization interface, and a global path is planned in the grid map. The path is shown in Figure 17. It can be seen from the path planning in the grid map that the improved algorithm successfully planned a feasible path with a smoother trajectory, which verified the feasibility of the improved artificial potential field algorithm.

The actual operation result of the ROS mobile platform in the ground environment is shown in Figure 18.

6. Conclusions and Future Work

Aiming at the problems existing in the application of classical APF method for mobile robots, a path planning model based on IAPF is designed. The simulation results show that the average path planning efficiency of the improved model increases by 42.8%, the average path length decreases by 8.6%, and the average target convergence speed increases by 26.1%, which verifies the effectiveness and accuracy of the IAPF.

A novel triangle navigation method is designed, and the guiding point is established to solve the problem that the mobile robot falls into local optimum. Adaptive step length adjustment strategy is designed, and step length is reasonably planned according to the number of obstacles, so as to improve the operation efficiency of the algorithm. A new target attractive force model based on obstacle distance is built to improve the convergence speed of the target, and a target factor is added to optimize the repulsion function, which solves the problem of unreachable targets.

The research described in the study was completed in a static environment with certain limitations and did not consider the presence of dynamic obstacles. Therefore, the dynamic obstacle environment will be studied in the future to realize the real-time obstacle avoidance function of the mobile robot. In addition, several aspects of the works in this study remain to be further investigated: first, the paths are deredundantly processed to get shorter paths. Second, the B spline curve strategy is introduced to smooth the paths.

Data Availability

The data used to support the findings of this study are available from the corresponding author upon request.

Conflicts of Interest

The authors declare that they have no conflicts of interest.

Authors' Contributions

Conceptualization, methodology, software, and data analysis are performed by Tiezheng Guo; formal analysis, investigation, validation, and writing—original draft preparation are performed by Jie Wang; project administration and funding acquisition are performed by Zhiming Wang; technical guidance, review, and editing are performed by Wei Chen and Guojun Chen; experimental platform construction and data collection are performed by Shishi Zhang. All authors have read and agreed to the published version of the manuscript.

Acknowledgments

This research work was supported by the Jiangsu Provincial Agricultural Science and Technology Independent Innovation Fund Project (grant number: CX(21)1007), the Open Project of the Zhejiang Provincial Key Laboratory of Crop Harvesting Equipment and Technology (grant numbers: 2021KY03 and 2021KY04), the Jiangsu Provincial Key Research and Development Project (grant number: BE2021016-5) and the Jiangsu Province Postgraduate Research and Practice Innovation Program (grant numbers: SJCX21_0933 and SJCX21_0940).

References

[1] K. Li, Q. Hu, and J. Liu, "Path planning of mobile robot based on improved multi-objective genetic algorithm," *Wireless Communications and Mobile Computing*, vol. 2021, Article ID 8836615, 2021.

[2] Z. Hong, W. Du, and H. Wang, "Design and implementation of path planning for wheel-track hybrid mobile robot[J]," *Mobile Information Systems*, vol. 2022, Article ID 6418706, 2022.

[3] X. Lai, J. H. Li, and J. Chambers, "Enhanced center constraint weighted a ∗ algorithm for path planning of petrochemical inspection robot[J]," *Journal of Intelligent and Robotic Systems*, vol. 102, no. 4, pp. 1–15, 2021.

[4] J. F. Duhé, S. Victor, and P. Melchior, "ContribUtions on artificial potential field method for effective obstacle avoidance," *Fractional Calculus and Applied Analysis*, vol. 24, no. 2, pp. 421–446, 2021.

[5] Y. V. Pehlivanoglu and P. Pehlivanoglu, "An enhanced genetic algorithm for path planning of autonomous UAV in target coverage problems," *Applied Soft Computing*, vol. 112, Article ID 107796, 2021.

[6] Y. Pan, Y. Yang, and W. Li, "A deep learning trained by genetic algorithm to improve the efficiency of path planning for data collection with multi-UAV," *IEEE Access*, vol. 9, pp. 7994–8005, 2021.

[7] M. D. Phung and Q. P. Ha, "Safety-enhanced UAV path planning with spherical vector-based particle swarm optimization," *Applied Soft Computing*, vol. 107, Article ID 107376, 2021.

[8] X. h Liu, D. Zhang, J. Zhang, T. Zhang, and H. Zhu, "A path planning method based on the particle swarm optimization trained fuzzy neural network algorithm," *Cluster Computing*, vol. 24, no. 3, pp. 1901–1915, 2021.

[9] U. Orozco-Rosas, O. Montiel, and R. Sepúlveda, "Mobile robot path planning using membrane evolutionary artificial potential field," *Applied Soft Computing*, vol. 77, pp. 236–251, 2019.

[10] A. Azzabi and K. Nouri, "An advanced potential field method proposed for mobile robot path planning," *Transactions of the Institute of Measurement and Control*, vol. 41, no. 11, pp. 3132–3144, 2019.

[11] S. M. H. Rostami, A. K. Sangaiah, J. Wang, and X. Liu, "Obstacle avoidance of mobile robots using modified artificial potential field algorithm," *EURASIP Journal on Wireless Communications and Networking*, vol. 1, pp. 70–19, 2019.

[12] J. Batista, D. Souza, J. Silva et al., "Trajectory planning using artificial potential fields with metaheuristics," *IEEE Latin America Transactions*, vol. 18, no. 05, pp. 914–922, 2020.

[13] J. H. Jung and D. H. Kim, "Local path planning of a mobile robot using a novel grid-based potential method," *International Journal of Fuzzy Logic and Intelligent Systems*, vol. 20, no. 1, pp. 26–34, 2020.

[14] M. Pashna, R. Yusof, Z. H. Ismail, T. Namerikawa, and S. Yazdani, "Autonomous multi-robot tracking system for oil spills on sea surface based on hybrid fuzzy distribution and potential field approach," *Ocean Engineering*, vol. 207, Article ID 107238, 2020.

[15] Y. Chen, G. Bai, Y. Zhan, X. Hu, and J. Liu, "Path planning and obstacle avoiding of the USV based on improved ACO-APF hybrid algorithm with adaptive early-warning," *IEEE Access*, vol. 9, pp. 40728–40742, 2021.

[16] Y. Shin and E. Kim, "Hybrid path planning using positioning risk and artificial potential fields," *Aerospace Science and Technology*, vol. 112, Article ID 106640, 2021.

Hindawi
Mathematical Problems in Engineering
Volume 2022, Article ID 3245251, 11 pages
https://doi.org/10.1155/2022/3245251

Research Article

Multiobjective Optimization of Vehicle Handling and Stability Based on ADAMS

Genge Zhang,[1] Yi Wei,[1] Chengwei Ju,[2] and Shuilong He[3]

[1]*Nanning University, Nanning 530000, China*
[2]*Guangxi Zhuang Autonomous Region Special Equipment Inspection Research Institute, Nanning 530000, China*
[3]*Guilin University of Electronic & Technology, Guilin 541004, China*

Correspondence should be addressed to Yi Wei; 1723872199@qq.com

Received 13 May 2022; Revised 5 July 2022; Accepted 15 July 2022; Published 30 August 2022

Academic Editor: Amandeep Kaur

In order to improve the steering characteristics, roll characteristics, and lateral characteristics of heavy commercial vehicles, a multiobjective handling stability comprehensive score optimization model (MHSCS optimization model) was proposed in this study. In this study, the main factors affecting the steering characteristics, roll characteristics, and lateral characteristics are determined by combining the road test method and ADAMS software simulation analysis method. Based on the above road tests and ADAMS software simulation analysis, the MHSCS optimization model was proposed with "understeering degree," "vehicle roll angle", and "rearward amplification (RWA)" as evaluation indexes, and the response surface method combined with genetic algorithm was used to carry out multiobjective optimization of heavy commercial vehicle. ADAMS simulation results show that the comprehensive improvement degree of steering characteristics, roll characteristics, and lateral characteristics of a heavy commercial vehicle after optimization is 15.26%. Finally, the field road test results show that the scoring error between the comprehensive scoring optimization model and the real vehicle test was controlled at 0.4%, which proves the accuracy of the optimization model established in this study and effectively improves the handling stability of heavy commercial vehicles.

1. Introduction

Handling and stability is very important for vehicle safety, and many vehicle structures and parameters will affect the operating stability [1]. In order to improve the vehicle handling stability, the vehicle handling stability optimization method based on d-Optimal experimental design, which established a response surface model based on D-Optimal experimental design was proposed by Li et al. [2]. This method is only better effective in improving the steering performance of the vehicle, but the ability to improve the roll characteristics and lateral characteristics of the vehicle is not too obvious effect. An improved genetic particle swarm optimization algorithm was used to optimize the vehicle handling stability. In view of the requirements of a four-wheel steering system on vehicle stability control and the existence of uncertainties, the hybrid H2/H∞ robust control method of a four-wheel steering system improves the handling stability of 4WS vehicles, which was proposed by Xu et al. [3]. This method has a good effect in improving the stability and robustness of four-wheel steering, but this method also has no way to improve the handling stability of the vehicle with multiple objectives. To solve the problem of poor handling stability of a car, Zhang et al. used the response surface method combined with a unified objective method to carry out multiobjective optimization of the handling stability of the car, so as to improve the handling stability of the car [4]. However, this method only provides multiobjective optimization in the roll characteristics and steering performance of the vehicle and does not take into account the roll characteristics and ability optimization of the vehicle. Deng et al. conducted simulation optimization on handling stability of FSAE racing Car based on ADAMS/Car and carried out multi-objective optimization design for the optimization objectives of front wheel positioning parameters and roll center height, which improved the steady-state response characteristics of the vehicle [5].

Because heavy commercial vehicles have the characteristics of high centroid and large inertia, the steering characteristics, roll characteristics, and lateral characteristics are particularly important to the steering performance and rollover resistance of heavy commercial vehicles. Therefore, it is necessary to optimize the steering, roll, and lateral characteristics of heavy commercial vehicles.

The purpose of this study is to establish a multiobjective handling stability comprehensive score optimization model. This model is an optimization model of the multiobjective manipulation stability comprehensive score with "understeering degree," "vehicle roll angle," and "rearward amplification (RWA)" as the evaluation indicators. Meanwhile, using the optimization model established, ADAMS simulation and road real vehicle test were used to optimize the steering characteristics, roll characteristics, and lateral characteristics of heavy commercial vehicles, which has high engineering practical value for improving the control stability of heavy commercial vehicles.

2. Validation of the Multibody Dynamics Model

2.1. Vehicle Multibody Dynamic Model Construction. Using ADAMS/Car software and combined with the dimension parameters and mechanical parameters of a heavy commercial vehicle, each vehicle subsystem was established and completed the assembly of the vehicle [6, 7]. The front suspension of the heavy commercial vehicle adopts a leaf-spring rigid axle suspension, the steering bridge adopts an integral structure, and the steering system adopts a recirculating ball type steering system. In order to make the multibody dynamic model established in this study more close to the real vehicle state and make the calculation result more accurate, the flexible body is adopted in this study [8]. Hyperwork software was used to generate MNF neutral files. The component modal synthesis method was used to deal with the problem that the finite element model has too many degrees of freedom.

Figure 1 shows the overall modal diagram of the frame, and its modal value is close to that of the real frame. Finally, the generated flexible body frame was imported into Adams/Car module to build the vehicle model, as shown in Figure 2.

2.2. Load Verification. To ensure that the built vehicle model can truly reflect the real vehicle system, the virtual prototype simulation model should be verified before the vehicle simulation analysis [4, 5]. The accuracy of each axle load is the basic of the vehicle multibody dynamic model, so it is necessary to verify the load. The axle load test platform of the real vehicle and model simulation is shown in Figure 3.

It can be seen from Table 1 that the multibody dynamic model established in this study is similar to the test results of the real vehicle. The loading error of tractor 1 axle is 0.02%, and that of tractor 2 + 3 axle is 0.1%. The 1-axis load error of a full load with a trailer is 0.3%, 2 + 3 axle load error is 0.2%, and 4 + 5+6 axle load error is 0.1%. The error of the vehicle model is controlled within 0.3%, which proves that the multibody dynamic model established in this study is very accurate in loading.

2.3. Handling Stability Working Condition Verification. In order to prove the multiobjective comprehensive score optimization model (MHSCS optimization model) proposed in this study has an optimization effect on the handling stability of heavy commercial vehicles, it is necessary to verify the multibody dynamics model established in this study. In this study, real vehicle and multibody dynamic models are compared under the same conditions of steady-state rotation test and single-lane transformation test to verify the accuracy of the model. Installation position of control stability test equipment is shown in Figure 4.

In order to more truly reflect the performance of steering characteristics, roll characteristics, and transverse characteristics of heavy commercial vehicles, this study selects classic understeering degree, vehicle roll angle, and rearward amplification (RWA) as evaluation indexes according to the standard GB/T 623–2014 [9]. Therefore, the steady-state rotation test and single-lane change test were carried out according to the current national standard vehicle handling and stability test method, and the experimental results were compared with the simulation results of the multibody dynamics model under the same working conditions. The comparative analysis results are shown in Figure 5.

Considering the complexity of the vehicle system and the uncertainty of actual test conditions, the consistency of the two outputs was defined as: the fluctuation trend of output curves is roughly the same, and the magnitude of peak values is the same. Local relative error according to different working conditions, the absolute error of simulation value, and corresponding test value should be less than 10% [10]. The error values were calculated by the following formula:

$$E = \frac{100 \times |(\mathrm{SV} - \mathrm{TV})|}{\mathrm{TV}} < 10\%, \tag{1}$$

where E is the error rate (%). SV is the simulated value. TV is the test result value.

According to formula (1) and the calculation of simulation and test results, the error value B of real vehicle test and multibody dynamics model simulation is sorted out as shown in Table 2.

As can be seen from Table 2 and Figure 5, the multibody dynamics model established in this study can truly reflect the state of the real vehicle under steady-state rotation and single-lane transformation test conditions. In the evaluation index of steering characteristics, the error of understeering degree U is 4.8%, the error of roll characteristics evaluation index of body roll degree K_{φ} is 0.8%, and the error of RWA of lateral characteristics evaluation index is 2.61%. The error of each evaluation index is controlled within 10%. It is proved that the multibody dynamic model established in this study is very accurate in handling stability.

3. Validation of the Multibody Dynamics Model

3.1. Optimization Goal. The evaluation method of handling stability is the main method to study the performance of vehicle handling stability [11]. In this study, an optimization model of a multiobjective handling stability comprehensive score optimization model (MHSCS optimization model) is established according to the handling stability evaluation

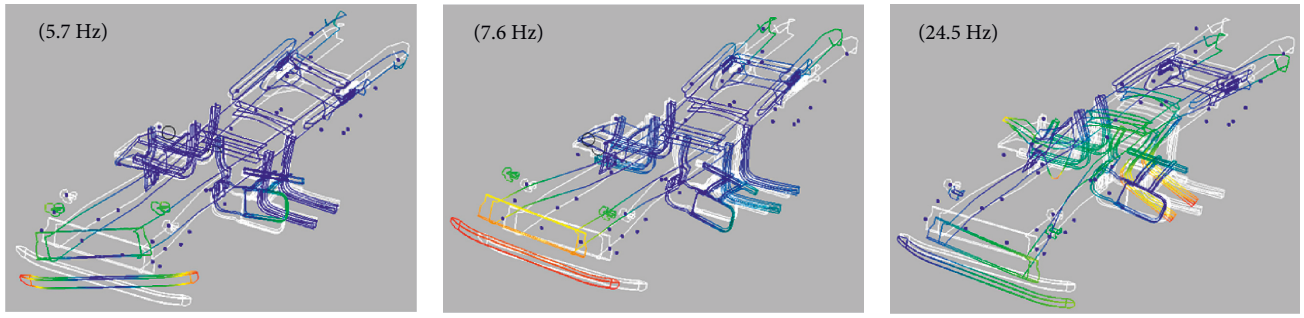

Figure 1: (a) Order 1 torsion mode of the flexible body frame. (b) Order 1 transverse bending mode of the flexible body frame. (c) Order 1 vertical bending mode of the flexible body frame.

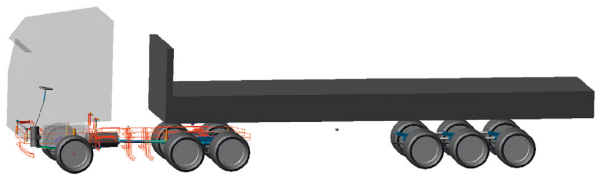

Figure 2: Vehicle multibody dynamics model.

Figure 3: Load test and verification of each axle of the vehicle.

method given by standard QC/T 480–1999 [12]. According to the handling stability evaluation method given by QC/T 480–1999, the scoring model of the item of vehicle roll angle K_φ is as follows:

$$N_\phi = 60 + \frac{40}{K_{\phi 60} - K_{\phi 100}} \times \left(K_{\phi 60} - K_\phi\right), \tag{2}$$

where N_φ is the score value of vehicle roll angle. $K_{\varphi 60}$ is the upper limit of the vehicle roll angle ($K_{\varphi 60} = 1.2^\circ/(\mathrm{m/s^2})$). $K_{\varphi 100}$ is the lower limit of the vehicle roll angle ($K_{\varphi 60} = 0.7^\circ/(\mathrm{m/s^2})$).

Due to QC/T 480–1999, there is no evaluation method for rear amplification factor. Therefore, based on the single score model of rearward amplification H_δ proposed in the literature [13], this study determines:

$$N_\delta = 60 + \frac{40}{H_{\delta\max} - H_{\delta\min}} \times \left(H_{\delta\max} - H_\delta\right), \tag{3}$$

where N_δ is the score value of rearward amplification (RWA). $H_{\delta max}$ is the maximum value of the index in the test design sample ($H_{\delta max} = 1.932$). $H_{\delta min}$ is the minimum value of the index in the test design sample ($H_{\delta min} = 0.812$).

According to the handling stability evaluation method given by QC/T 480–1999, the scoring model of the item of understeering degree U is as follows:

$$N_u = 60 + \frac{40}{\left(U_{100} - U_{60}\right)} \times \left(U_{100} - U\right), \tag{4}$$

where N_U is the score value of understeering degree. U_{60} is the maximum value of the index in the test design sample ($U_{60} = 0.731^\circ/(\mathrm{m/s^2})$). U_{100} is the minimum value of the index in the test design sample ($U_{100} = 0.072^\circ/(\mathrm{m/s^2})$).

Each index has a different influence on vehicle handling stability, that is, different contribution rates. In this study, the contribution rate of each objective evaluation index calculated in reference to [14] was used to determine the weight of each index. Finally, the comprehensive evaluation score model of heavy commercial vehicle handling stability optimization is as follows:

$$\begin{aligned} N_E &= 0.429N_U + 0.232N_\phi + 0.339N_\delta \\ &= 124.69 - 26.04U - 18.56K_\varphi - 12.12H_\delta, \end{aligned} \tag{5}$$

where N_E is the comprehensive score of heavy commercial vehicle handling stability optimization.

The objective of this study is to maximize the comprehensive optimization score of heavy commercial vehicle handling stability.

3.2. Optimize Variables and Constraints. The optimization variables of the optimization model of heavy commercial vehicles refer to the variable parameters that affect the optimization design results, and the general principle of selection should be the parameters that affect the handling stability of heavy commercial vehicles [15]. According to the above test and simulation results, front suspension

Table 1: Comparison of real vehicle test axle load and simulated axle load.

	1 axis of the tractor (kg)		2 + 3 axis of the tractor (kg)		4 + 5 + 6 axis of the trailer (kg)	
	Simulation	Test	Simulation	Test	Simulation	Test
Tractor	4889	4890	3786	3790		
Full load with trailer	5621	5640	14751	14720	24928	24960

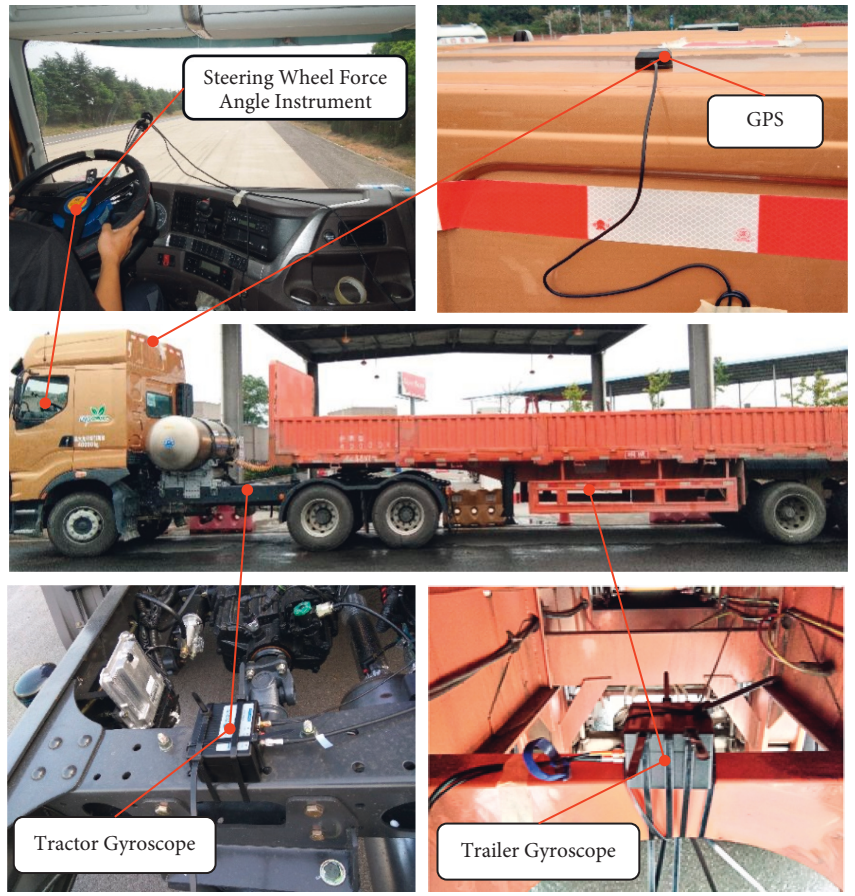

Figure 4: The installation position of test equipment.

spring stiffness K_f, tire lateral stiffness K_t, and front wheel toe angle β_T were selected as the design variables of this optimization.

According to the optimization mathematical model, the design variables in this study can be expressed as:

$$x = \left(K_f, K_t, \beta_T\right)^T. \tag{6}$$

In order to ensure the accuracy of the optimization result, the value range of the optimization variable should not be set too large, because too large or too small range will cause the distortion of the fitting model, and the accuracy of the optimization result cannot be guaranteed. This study makes constraints on optimization variables as shown in Table 3. At the same time, in order to facilitate the calculation and processing in the optimization design, the tire lateral stiffness K_t and the front suspension spring stiffness K_f, were multiplied by the scale factor λ, and the initial value of λ was set as 1.

3.3. Optimize Variables and Constraints. The advantage of the response surface model is that the experimental random error is taken into account and the calculation is relatively simple [1]. Therefore, the optimization process in this study adopts the response surface method, and the quadratic polynomial mathematical model of the response surface is as follows:

$$y = \beta_0 + \sum_{i=1}^{n} \beta_i x_i + \sum_{i=1}^{n} \sum_{j=1}^{n} \beta_{ij} x_i x_j + \sum_{j=1}^{n} \beta_j x_j^2, \tag{7}$$

where y is the response value. x_1, x_2, ..., x_n is the variable factor. β_0 is the constant term. β_i are polynomial coefficients respectively.

It is a key step to use the response surface method to select test design in the optimization process, and sample points and response values need to be established in the process of test design. In this study, response values are

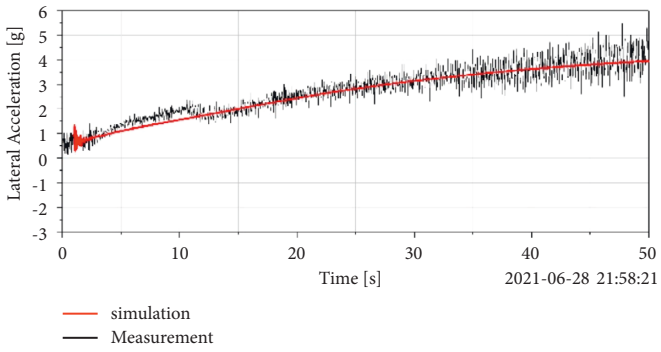

(a)

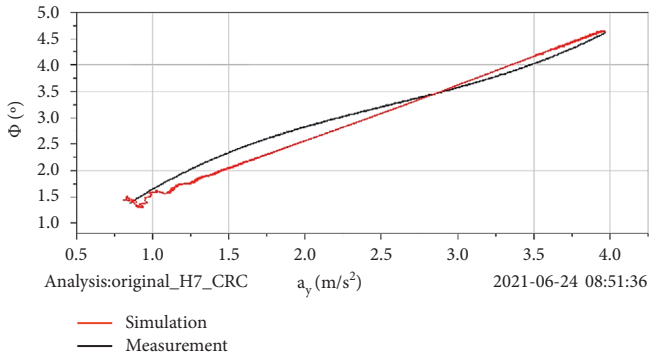

(b)

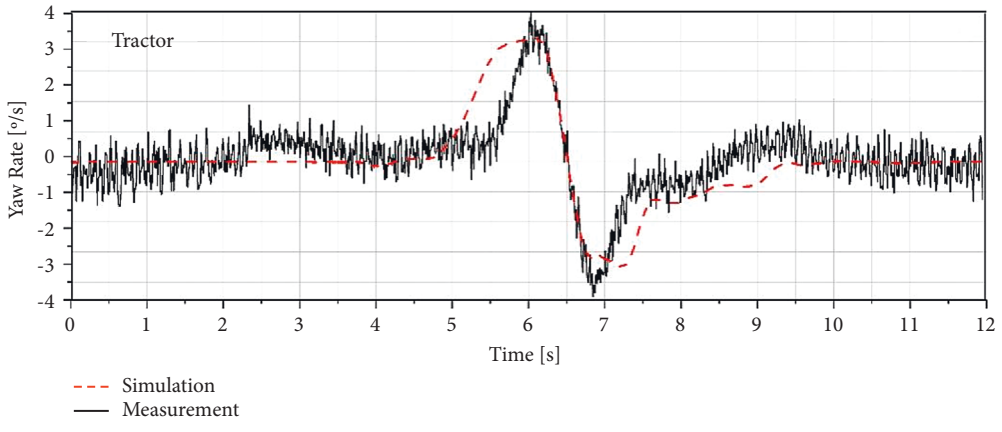

(c)

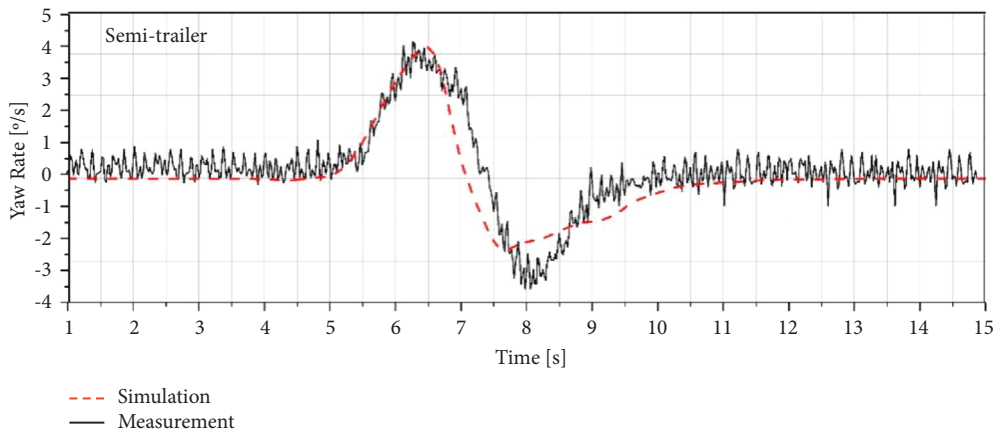

(d)

Figure 5: (a) Comparison of lateral acceleration test and simulation results. (b) Comparison of roll Angle test and simulation results. (c) Comparison between yaw of tractor test and simulation results. (d) Comparison between yaw of semi-trailer test and simulation results.

Table 2: Error values of real vehicle test and multibody dynamics model simulation.

Evaluation index	Test value	The simulation value	Error rate (%)
Understeer U	0.42	0.40	4.80
Vehicle roll angle K_φ	1.26	1.25	0.80
RWA	1.15	1.12	2.61

Table 3: Range of values of the variable factors.

Variable factors	Variable name	Initial value	Value range
λ_{Kf}	Front suspension spring stiffness	1	0.8~1.2
λ_{Kt}	Tire lateral stiffness	1	0.8~1.2
$\lambda_{\beta T}$	Front wheel toe angle	0	−1.0~1.0

obtained through the multibody dynamics model established above based on ADAMS simulation. For experimental design, Latin Hypercube Design (LHD), which has better uniformity, was used for each level of design variables and has the same number of tests for each design variable, is used in this study. Then use ISIGHT software to extract 30 sample points, and conduct simulation based on ADAMS in order, and then export the simulation data in the simulation analysis post-processing module. The corresponding objective function values of each sample point are shown in Table 4.

Finally, MATLAB program is used to further process the simulation test data. Call up the Rstool toolbox in MATLAB, and use the Quadratic Full model to fit the scale coefficients and target values of variable factors in Table 4. The fitting agent model is as follows:

$$\begin{aligned} U = {} & 1.13588 + 1.01807\lambda_{K_F} + 1.566884\lambda_{K_T} - 0.05679\beta_T \\ & - 0.95761\lambda_{K_F}^2 - 0.22346\lambda_{K_T}^2 - 0.05608\beta_T^2 \\ & - 0.54364\lambda_{K_F}\lambda_{K_T} - 0.32057\lambda_{K_F}\beta_T + 0.02659\lambda_{K_T}\beta_T, \end{aligned} \tag{8}$$

$$\begin{aligned} K_\varphi = {} & 0.81347 + 0.32165\lambda_{K_F} - 0.26756\lambda_{K_T} - 0.05679\beta_T \\ & + 0.03954\lambda_{K_F}^2 + 0.05689\lambda_{K_T}^2 - 0.02341\beta_T^2 \\ & - 0.26541\lambda_{K_F}\lambda_{K_T} - 0.32057\lambda_{K_F}\beta_T - 0.00569\lambda_{K_T}\beta_T, \end{aligned} \tag{9}$$

$$\begin{aligned} H_\delta = {} & 0.79567 + 0.39865\lambda_{K_F} - 0.76531\lambda_{K_T} - 0.06895\beta_T \\ & + 0.02637\lambda_{K_F}^2 + 0.08943\lambda_{K_T}^2 - 0.03016\beta_T^2 \\ & - 0.41026\lambda_{K_F}\lambda_{K_T} - 0.26734\lambda_{K_F}\beta_T - 0.00801\lambda_{K_T}\beta_T. \end{aligned} \tag{10}$$

The residual errors of the above fitting equations were 0.0234, 0.0452, and 0.0185, respectively. Therefore, the fitted G_U, G_K, and G_β are reliable. Formulas (8)–(10) above were substituted into formula (5) to obtain the final optimization model of multiobjective operational stability comprehensive score:

$$\begin{aligned} N_E = {} & 70.37016 - 37.312\lambda_{K_F} - 26.56019\lambda_{K_T} + 3.36851\beta_T \\ & + 23.8827\lambda_{K_F}^2 + 3.67913\lambda_{K_T}^2 + 2.26035\beta_T^2 \\ & + 24.05475\lambda_{K_F}\lambda_{K_T} + 17.53758\lambda_{K_F}\beta_T - 0.48972\lambda_{K_T}\beta_T. \end{aligned} \tag{11}$$

3.4. Optimal Solution. Genetic Algorithm (GA) has the advantages of strong global search ability and is widely used in complex problems such as planning. Therefore, this study uses the genetic algorithm GA to optimize the solution. Table 3 is taken as the value range of the design variables; formula (11) is taken as the optimization objective function. MATLAB is used to write the corresponding genetic algorithm optimization program to solve the optimal value of NE, that is, the maximum value, and obtain the optimal value of K_f, K_t, and β_T values. Finally, the optimal value is solved as shown in Table 5.

The optimized variable factor was converted into the actual value to obtain the front suspension spring stiffness, tire sideslip Angle stiffness, and front wheel beam Angle, as shown in Table 6.

4. Simulation Comparison before and after Optimization

According to the values in Table 6, the multibody dynamic model established in this study is used for steady-state rotary test simulation and single-lane transformation test simulation. The results of comparison between the difference of front and rear axle sideshow angles (δ_1-δ_2) and the lateral acceleration characteristic curves before and after optimization under steady-state rotary test conditions were obtained, as shown in Figure 6, and the vehicle roll Angle and the lateral acceleration characteristic curves, as shown in Figure 7. Comparison results of yaw velocity time domain curves of tractor and semi-trailer before and after optimization under single-lane changing conditions are shown in Figure 8.

According to the standard QC/T 480–1999, the curves in Figures 6–8 were processed and the scores of evaluation indexes before and after optimization were obtained, as shown in Table 7.

As can be seen from Tables 5 and 7, the optimization results of the multiobjective comprehensive stability scoring optimization model established in this study are very consistent with the results of the multibody dynamics simulation analysis, and the error was controlled within 0.97%, which proves the accuracy of the multiobjective comprehensive stability scoring optimization model established in this study. It is of practical engineering significance to improve the steering characteristics, roll characteristics, and transverse characteristics of heavy commercial vehicles. However, a large number of test samples are needed in the process of establishing the optimization model, which is also the limitation of the MHSCS optimization model.

Table 4: Target function values corresponding to each sample point.

Simulation serial number	λ_{Kf}	λ_{Kt}	$\lambda_{\beta T}$	RAW H_δ	Vehicle roll angle K_φ	Understeer degree U
1	0.997	1.180	0.116	1.071	1.289	0.463
2	0.990	0.827	−0.748	1.082	1.234	0.18
3	1.010	1.112	0.510	1.162	1.298	0.418
4	1.064	0.963	0.538	1.043	1.266	0.413
5	0.868	1.159	−0.775	1.16	1.281	0.243
6	1.186	0.990	0.749	1.106	1.295	0.553
7	1.044	0.936	0.478	1.158	1.276	0.322
8	0.983	1.092	0.914	1.063	1.273	0.388
9	1.017	1.017	−0.429	1.067	1.265	0.381
•	•	•	•	•	•	•
•	•	•	•	•	•	•
•	•	•	•	•	•	•
26	1.125	0.997	0.653	1.108	1.289	0.479
27	0.807	1.071	0.302	1.101	1.245	0.075
28	0.814	1.105	−0.691	1.137	1.257	0.109
29	1.089	0.942	−0.649	1.071	1.269	0.425
30	0.888	0.895	0.478	1.09	1.224	0.072

Table 5: Optimized design variable and target values.

Variable/target function	Initial value	Optimize value
Front suspension spring stiffness K_f	1	1.16
Tire lateral stiffness K_t	1	0.83
Front wheel toe angle β_T	0	1
Composite score N_E	77.50	88.47

Table 6: Actual value of the optimized design variables.

Variable/target function	Initial value	Optimize value
Front suspension spring stiffness K_f (N/mm)	220	255.2
Tire lateral stiffness K_t (N/mm)	4000	3340
Front wheel toe angle β_T (deg)	0	1

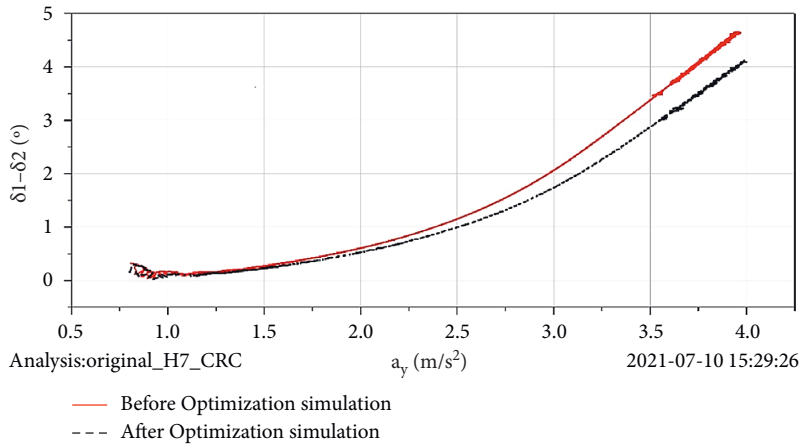

Figure 6: Comparison of the relationship curves between a_y and (δ_1-δ_2) before and after optimization simulation.

5. Real Vehicle Experiment Comparison before and after Optimization

In order to verify the optimization effect of the established multiobjective operation stability comprehensive scoring optimization model, a real vehicle verification was carried out in this study. According to Table 6, replace the front suspension spring of a heavy commercial vehicle with a leaf spring with 255.2 N/mm stiffness, replace the tire with tire with 3340 N/mm lateral stiffness, and adjust the front wheel beam Angle to 1. Steady-state rotation and single lane change test items were carried out on the adjusted real

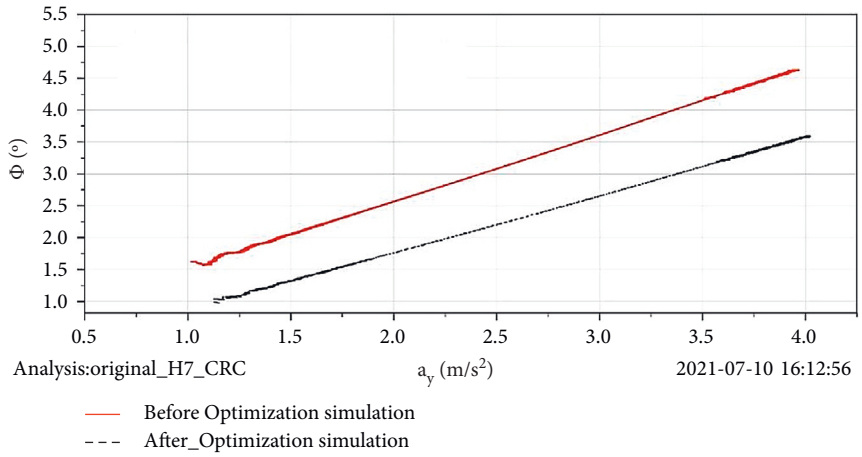

Figure 7: Comparison of the relationship curves between a_y and φ before and after optimization simulation.

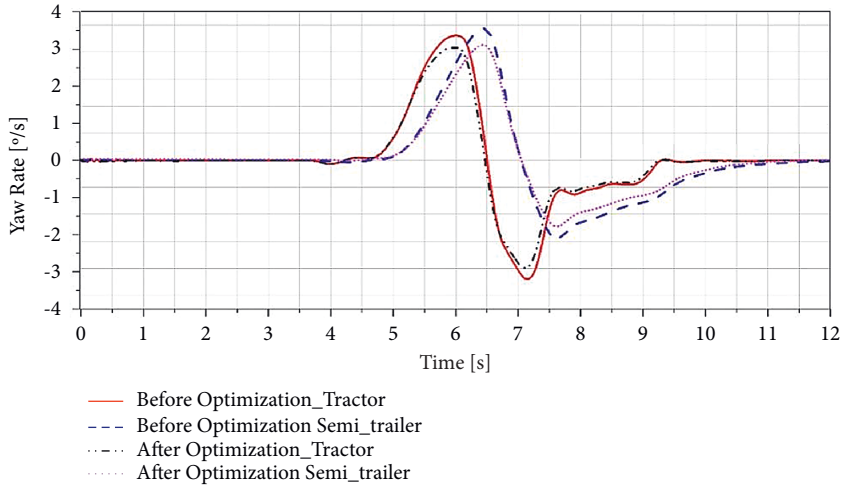

Figure 8: Comparison of the time domain curve of yaw velocity of tractor and semi-trailer before and after optimization simulation.

Table 7: Score values of the evaluation indicators before and after the optimization.

Evaluation index	After optimization (points)	Before optimization (points)	Improvement rate (%)
Understeer score N_U	84.34	87.85	4.16
Body roll angle score N_φ	56.00	88.51	58.05
RWA score N_δ	88.99	91.75	3.10
Composite score N_E	79.34	89.33	15.26

(a) (b)

Figure 9: (a) Steady turn test site. (b) Single lane change test site.

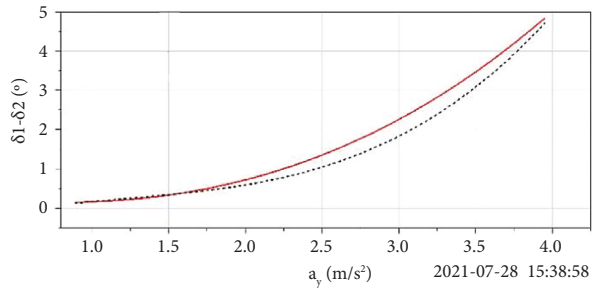

Test_Before_Optimization
Test_After_Optimization

(a)

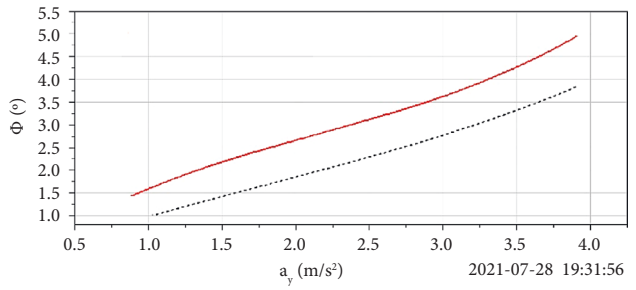

Test_Before_Optimization
Test_After_Optimization

(b)

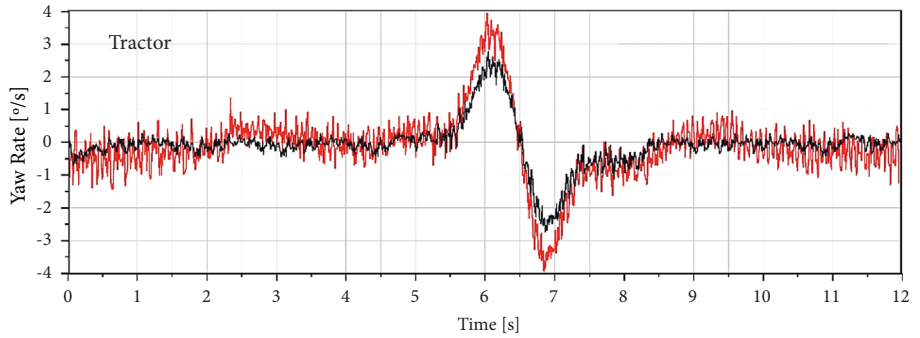

Test_Before_Optimization
Test_After_Optimization

(c)

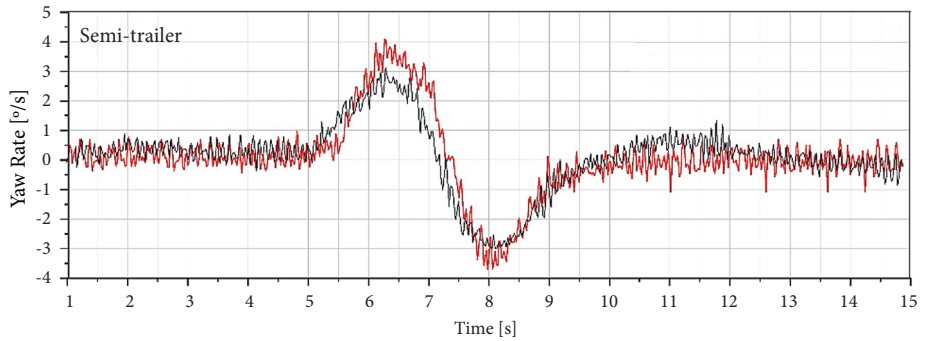

Test_Before_Optimization
Test_After_Optimization

(d)

Figure 10: (a) Comparison of the relationship curves between a_y and (δ_1-δ_2) before and after optimization test. (b) Comparison of the relationship curves between a_y and φ before and after optimization test. (c) Comparison of the time domain curve of yaw velocity of tractor before and after optimization test. (d) Comparison of the time domain curve of yaw velocity of semi-trailer before and after optimization test.

Table 8: Optimize the evaluation index score value before and after the real vehicle test.

Evaluation index	MHSCS optimization model	Multi-body kinetic model	Real vehicle tests
Understeer score N_U (points)	87.85	87.85	86.32
Body roll angle score N_φ (points)	86.97	88.51	87.72
RWA score N_δ (points)	90.30	91.75	90.54
Composite score N_E (points)	88.48	89.33	88.10

vehicle to verify the optimization effect. The experimental site is shown in Figure 9.

The comparison of real vehicle test data before and after optimization is shown in Figure 10, and the comprehensive score comparison results of each model after sorting are shown in Table 8.

It can be seen from Table 8 that the comprehensive scoring error between the MHSCS optimization model established in this study and the real vehicle after optimization is only 0.4%, which verifies the accuracy of the optimization effect of the MHSCS optimization model established in this study. At the same time, after the optimization of the MHSCS optimization model established in this study, the improvement degree of steering characteristics of the heavy commercial vehicle is 2.3%, the improvement degree of roll characteristics is 36.2%, and the improvement degree of lateral characteristics is 1.7%. The comprehensive score of heavy commercial vehicle operation stability was improved by 12.0%, and the vehicle handling stability of the heavy commercial vehicle is effectively improved.

6. Conclusions

This study summarizes the current methods of commercial heavy duty handling stability optimization, and proposes a multiobjective handling stability comprehensive score optimization model (MHSCS optimization model), which takes "understeering degree," "vehicle roll angle", and "rearward amplification (RWA)" as evaluation indexes.

(1) The accuracy of the multibody dynamic model was verified by comparing the simulation data with the experimental data of various axial load tests, steady-state turning tests, and single lane changing tests.

(2) Latin Hypercube Design (LHD) and ADAMS multibody dynamics model were used to obtain the response values. Finally, the Quadratic Full module in MATLAB was used to fit the proportional coefficient of the variable factor and the target value, and the MHSCS optimization model was obtained.

(3) The MHSCS optimization model was used to optimize the handling stability of heavy commercial vehicles. After optimization, the improvement degree of steering characteristics, roll characteristics, and lateral characteristics of heavy commercial vehicle is 2.3%, 36.2%, and 1.7%, respectively, and the comprehensive score improvement degree is 12.0%. Finally, the MHSCS optimization model established in this study is verified to have a comprehensive scoring error of only 0.4% by a real vehicle experiment, which proves the accuracy of the MHSCS optimization model established in this study and the effectiveness of the optimization results.

(4) The MHSCS optimization model proposed in this study is of practical engineering significance in improving the steering characteristics, roll characteristics, and lateral characteristics of heavy commercial vehicles. However, a large number of test samples are needed in the process of establishing the optimization model, and the initial test cost is relatively high. This is also the limitation of the optimization model.

Data Availability

The data used to support the findings of this study are available from the corresponding author upon request.

Conflicts of Interest

The authors declare that there are no conflicts of interest regarding the publication of this paper.

Acknowledgments

This paper was supported by Sub-Project of Construction of China-ASEAN International Joint Laboratory for Comprehensive Transportation (Phase I) (no. GuiKeAA21077011-7).

References

[1] L. Zhang, J. Liu, F. Pan, S. Wang, and X. Ge, "Multi-objective optimization study of vehicle suspension based on minimum time handling and stability," *Proceedings of the Institution of Mechanical Engineers - Part D: Journal of Automobile Engineering*, vol. 234, no. 9, pp. 2355–2363, 2020.

[2] B. Li, W. Ge, D. Liu, C. Tan, and B. Sun, "Optimization method of vehicle handling stability based on response surface model with D-optimal test design," *Journal of Mechanical Science and Technology*, vol. 34, no. 6, pp. 2267–2276, 2020.

[3] F. X. Xu, X. H. Liu, W. Chen, C. Zhou, and B. W. Cao, "Improving handling stability performance of four-wheel steering vehicle based on the H2/Hꝏ robust control," *Applied Sciences*, vol. 9, no. 5, p. 857, 2019.

[4] L. F. Zhang, Y. Fan, C. L. Xie, and M. J. Jin, "Multi-objective optimization of vehicle handling and stability based on response surface methodology," *Machinery Design & Manufacture*, vol. 38, no. 09, pp. 87–92, 2021.

[5] Z. W. Deng, S. J. Yu, L. Gao, and X. X. Kong, "Analysis on handling stability of racing cars based on the virtual

prototype," *Journal of Machine Design*, vol. 38, no. 09, pp. 87–92, 2021.

[6] P. Shi, Q. Zhao, and K. Wang, "Simulation and verification analysis of the ride comfort of an in-wheel motor-driven electric vehicle based on a combination of ADAMS and MATLAB," *International Journal of Modeling, Simulation, and Scientific Computing*, p. 2250002, 2021.

[7] G. Wang and C. Xie, "Simulation analysis on ride comfort of hybrid heavy truck based on ADAMS[C]//Journal of physics: conference series," *Journal of Physics: Conference Series*, vol. 1865, no. 4, p. 042128, 2021.

[8] L. Cheng and H. Haiyan, "Dynamic modeling and computation for flexible multibody systems based on the local frame of Lie group," *Chinese Journal of Theoretical and Applied Mechanics*, vol. 53, no. 1, pp. 213–233, 2021.

[9] Gb/T. 6233-2014, *Vehicle Handling and Stability Test Method*, Standardization Administration of China, Beijing, 2014.

[10] Y. Li, S. Wang, X. Duan, S. Liu, J. Liu, and S. Hu, "Multi-objective energy management for Atkinson cycle engine and series hybrid electric vehicle based on evolutionary NSGA-II algorithm using digital twins," *Energy Conversion and Management*, vol. 230, Article ID 113788, 2021.

[11] M. F. Soong, R. Ramli, A. A. Saifizul, and A. Mamat, "Handling performance criteria evaluation for vehicle suspension system with semi-active control strategies," *International Journal of Advanced Mechatronic Systems*, vol. 9, no. 1, p. 11, 2021.

[12] QC/T 480-1999, *Vehicle Handling and Stability index Limits and Evaluation Methods*, Automobile Industry Standard of the People's Republic of China, Beijing, 1999.

[13] Y. H. Zhang, H. G. Xu, H. F. Liu, and S. S. Qi, "Research on the evaluation index of handling stability of tractor and double trailer combination," *China Journal of Highway and Transport*, vol. 30, no. 05, pp. 145–151, 2017.

[14] K. H. Guo, L. G. Jin, Y. Cao, F. Bai, and C. B. Cui, "Dimensional reduction of objective evaluation criteria of vehicle handling behavior," *Automobile Technology*, vol. 2010, no. 02, pp. 1–4, 2020.

[15] M. Peng, J. Lin, and X. Liu, "Optimizing design of powertrain transmission ratio of heavy duty truck," *IFAC-PapersOnLine*, vol. 51, no. 31, pp. 892–897, 2018.

Hindawi
Mathematical Problems in Engineering
Volume 2022, Article ID 7459455, 8 pages
https://doi.org/10.1155/2022/7459455

Research Article

A Supervised Learning Identification System for Prognosis of Breast Cancer

Vandana Rawat,[1] Kamal Gulati,[2] Upinder Kaur,[3] Jitendra Kumar Seth,[4] Vikas Solanki,[5] A. Narasima Venkatesh,[6] Devesh Pratap Singh,[7] Neelam Singh,[7] and Muralidaran Loganathan[8]

[1]*Department of Computer Science & Engineering, Graphic Era Deemed to be University, Dehradun, Uttarakhand, India*
[2]*Amity School of Insurance, Banking and Actuarial Science, Amity University, Noida, Uttar Pradesh 201 304, India*
[3]*Department of Computer Science & Engineering, Akal University, Bathinda, Punjab, India*
[4]*Department of IT, KIET Group of Institutions, Ghaziabad, India*
[5]*Institute of Engineering and Technology, Chitkara University, Punjab, Chandigarh, India*
[6]*Professor and Head of The Department, HRM and General Management, ISBR Business School, Bangalore 560 100, India*
[7]*Department of Computer Science & Engineering, Graphic Era Deemed to be University, Dehradun, Uttarakhand, India*
[8]*St. Joseph University, Dar es Salaam, Tanzania*

Correspondence should be addressed to Muralidaran Loganathan; muralinew1986@gmail.com

Received 14 June 2022; Accepted 15 July 2022; Published 28 August 2022

Academic Editor: Amandeep Kaur

Breast cancer is one of the most dangerous cancers, accounting for a large number of fatalities each year. It is the leading cause of mortality among women globally. It is getting a lot of interest in the scientific community because of its possible life-threatening danger. As a consequence, many machine learning methods (MLMs) have been modified to provide the best results for early diagnosis of this malignancy. Machine learning methods (MLMs) offer several beneficial implications in breast cancer, including early prognosis, detection, and diagnosis. Compared to traditional statistical analysis, machine learning methods (MLMs) have the capacity to improve the analysis of various health data, such as unstructured, complicated, and noisy data. With the demanding prevalence of breast cancer and the arrival of "data reformation," it is thus imperative to mention the ethical consequences of machine learning (ML) on society and cancer care. It offers conclusively strong tools, smart methods, and efficient algorithms that can help in the prognosis of breast cancer. The focus of this review is on supervised techniques such as classification and regression that may be implemented and used for breast cancer data analysis. Some supervised learning methods like Naive Bayes, AdaBoost, and support vector machine are presented in this work in the early identification of breast cancer. These algorithms have been analyzed for their accuracy and efficiency using various assessment metrics and methods.

1. Introduction

Breast cancer is among the most significant threats to women worldwide. Among females, this is the second biggest cause of death [1]. Breast cancer is the second largest cause of death, according to the World Health Organization (WHO) [2]. Breast cancer claimed the lives of 70,218 Indian women in 2012. It is a stepwise procedure offering a range of cell types, but prevention remains a significant challenge for it, all over the world [2]. Huge methodological revolutions have occurred in this sector throughout the years; however, there are a variety of challenges.

In timely identification, several image processing methodologies have been applied to minimize the probability of death per year. As a result, a variety of machine learning techniques are applied to boost precision in the detection of breast cancer. In recent decades, various machine learning techniques have been developed and they are

divided into 3 stages: (a) preprocessing; (b) feature extraction; and (c) classification.

Preprocessing mammography pictures improves visibility of outlying regions and brightness, making data interpretation easier. Breast cancer survivors in certain industrialized nations have an overall 5-year survival rate of more than 80% due to early identification and care. Breast cancer stem cells have shown the genesis and methods of tumor-resistant strains, and various breast cancer genes have been found. People now have a plethora of pharmaceutical options for breast cancer prevention and treatment, and biological prevention has since been created to provide even greater advantages in terms of living standards [3–5].

2. Breast Cancer

Breast cancer has been defined as abnormal tissue development in the breast that results in malignant tumors. Noninvasive breast cancer refers to malignant cells that remain in the breast. Invasive malignancies cannot heal quickly and might spread to other regions of the body. These are deadly malignancies that can sprawl to other organs of the human body which results in metastatic cancer [6–9].

2.1. Categories of Breast Cancer. There are 2 categories of breast cancer: intrusive and non-intrusive. Ductal carcinoma in situ is a non-intrusive variety, whereas the rest are intrusive [10–13].

In Figure 1, various types of breast cancer are given, and they are defined in Table 1.

2.2. Breast Cancer Diagnosis. Multiple investigations are required for the diagnosis of breast cancer, such as a clinical examination, which is probing of the breast to discover cancer indicators, indicating the initial stage. Following the clinical examination, the next stage is medical imaging, which allows for the identification of tumor masses as well as the collection of data from the clinical examination. Many kinds of test include mammography, ultrasonography, and magnetic resonance imaging (MRI) [14–17]. One of these strategies is chosen based on the patient's circumstances as shown in Figure 2.

Machine learning is now in such high demand that it is being offered as a service. Machine learning is a high-barrier area that frequently necessitates specialist knowledge. A set of abilities and knowledge is required to design an efficient machine learning model, which includes the steps of preprocessing, feature selection, and classification processes. So, in Figure 2, some steps of breast cancer diagnosis are depicted.

3. Materials and Methods

In machine learning [18], there are various types of automatic models that are proposed to build from previous records in this type of learning. The machine learning model assesses and may generate future predictions based on that training model [19].

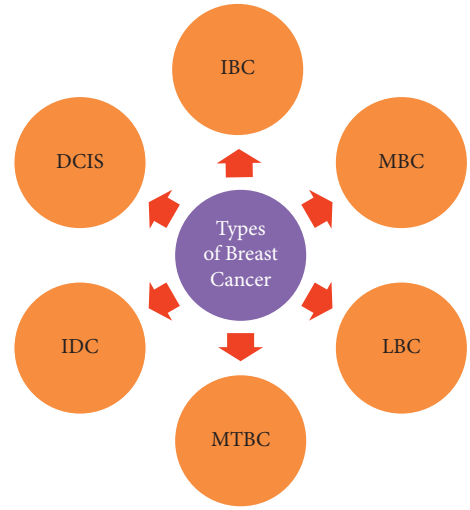

Figure 1: Multiple sorts of breast cancer.

To begin this investigation, the Wisconsin Breast Cancer Dataset was obtained from the UCI Machine Learning Repository. The datasets are classified into two types: malignant and benign. The points are derived from needle sputum imaging data from a breast tumor and describe the nucleus of the present picture. The WDBC database has been utilized to detect 212 cancer and 357 benign cases among 569 Wisconsin hospital patients [20–22].

The following subcategories will outline the process flow:

(i) Dataset definition

(ii) Dataset assessment

(iii) Training and testing

3.1. Dataset Definition. The Wisconsin Breast Cancer Dataset (WBCD) is shown in this work with separation of benign and malignant status in Figure 3. This dataset contains 357 benign and 212 malignant breast cancer patients, respectively.

All the breast cancer attributes are listed in Figure 3 and Table 2 with real-value characteristics.

3.2. Dataset Assessment. The entire dataset has been examined for the data patterns. The mean radius feature of the dataset is counter-plotted and found that expected cancer-free patients have a mean radius of 1, whereas probable cancer-bearing patients have a mean radius greater than 1.

3.3. Training and Testing. The dataset numbers are examined based on their properties before being used in the following stage. The dataset was then divided into two halves at random: training and testing, 75 and 25, respectively.

Patients are confronted with a variety of interventions on a regular basis, including ultrasound, biopsy, and mammography, depending on the severity of their breast cancer signs. The most common of these operations is biopsy, which entails the removal of a piece of tissue or cell for

Table 1: Types of breast cancer.

Type	Summary
Ductal carcinoma in situ	It comes under the non-intrusive cancer category, which is created inside the breast lactation, as the name implies.
Ductal carcinoma	Caused by cancerous cells penetrating the lactation ducts and through canal wall.
Lobular carcinoma	Cancerous cells grow in the lobules, which are gathered in the lobes, in this type of cancer. They subsequently cross the lobules' walls and disseminate throughout the surrounding tissues.
Inflammatory carcinoma	It manifests as a non-healing tiny nipple wound.
Paget's disease	It manifests as a non-healing tiny nipple wound.
Other carcinomas	Rarest type.

Figure 2: The steps of breast cancer diagnosis.

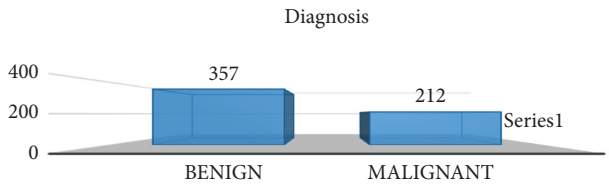

Figure 3: Breast cancer diagnosis.

investigation. A fine-needle aspiration (FNA) operation is used to remove a tissue sample from a breast and transmit it to a pathology laboratory for analysis under microscopy. Numerical qualities can be ascertained through an investigation of tissues at a microscopic level. The evidence received from fine-needle aspiration is evaluated in conjunction with other imaging analyses to find the possibility of the patient having a cancerous lump.

Six classification models are supposed to implement including ANN, logistic regression, AdaBoost, Naive Bayes, support vector machine, and K-nearest neighbor. The findings obtained are then assessed by the algorithms in order to find an efficient model. The workflow for the given dataset is illustrated in Figure 4.

4. Machine Learning Algorithms for Breast Cancer Prediction

4.1. K-Nearest Neighbor (KNN). KNN [23] (K-nearest neighbor) is a supervised method that categorizes data depending on how its neighbors are categorized. KNN maintains track of all existing instances and classifies new ones using a matching score. The KNN method looks through a database for data that are similar to what are already available. These newly found data are known as the current data's nearest neighbors. With the test station in this article, KNN is used to choose generally relevant adjacent stations. Assume the road network has a M station [24, 25].

In this algorithm, a random sample size dataset has been taken with various data fields. It is the m^{th} station's historic traffic flow data, which differ from the substation. The Euclidean distance is used to determine the degree of correlation between the substation and other locations.

4.2. Support Vector Machine (SVM). Vapnik was the first one to discover the support vector machine in 1979 [26]. Vapnik suggested it for classification and regression problems again in 1995 [27]. Support vectors with multilayer perceptron and radial-basis function networks can be utilized for pattern classification. The SVM is a cutting-edge technique that incorporates maximum classification algorithms into statistical learning [28]. Linear and non-linear data are categorized using SVM techniques. It involves converting training dimensional space using non-linear projection. The classification task is carried out by SVM, which maximizes the margin and classifies both classes while reducing classification errors. Although the SVM is used to solve a range of problems, such as regression, data categorization is the most popular one. Figure 2 depicts the main concept. The goal is to identify a hyperplane that separates them by the greatest possible margin with the categorization of positive and negative data points.

4.3. Artificial Neural Network (ANN). This algorithm is capable of performing a variety of tasks like prediction, curve fitting, and regression. It formulates the output using a transfer function [29, 30]. Each intake is multiplied by a weight, which acts as a link between the input, the neuron, and its layers. To acquire the result, the neuron uses a transfer function in the last stage. ANN approaches offer the advantage of having no prior understanding of mathematical computations across attributes, although they do demand less processing work and can handle multivariable problems [31].

4.4. Logistic Regression (LR). The only machine learning method that is not a black-box approach is logistic regression. In general, black-box techniques are difficult to comprehend, but logistic regression demonstrates how they work. Logistic regressions are classified into three types: binary, multinomial, and ordinal [32]. Logistic regression originated as a classification technique rather than a linear regression. Scikit-learn solves multiclass classification issues with a more appropriate logistic regression implementation technique [33–35].

Table 2: Dataset attributes of breast cancer patients.

Attribute no.	Attribute description
Radius	The average of both the distances between the center and circumferential endpoints
Texture	Gray-scale rating standard error of the mean (SD)
Perimeter	The length between the snake's endpoints
Area	The whole pixels on the snake's inside, along with one-half of the pixels around its perimeter
Smoothness	Diameter length varies locally
Compactness	Perimeter^2/area
Concavity	The amplitude of the contour's sloping sections
Concave points	The frequency of concavities from the inside of the contour
Symmetry	The length disparity in both ways to the cell edge between lines perpendicular to the major axis
Fractal dimension	Output of large value is less regular contour

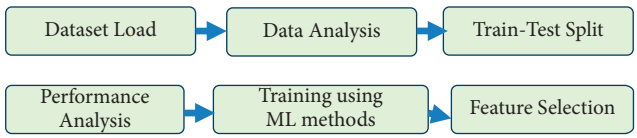

Figure 4: Data mechanism/workflow.

4.5. Naive Bayes. A probabilistic learner is called a Naive Bayes classifier. It is most commonly utilized in clinical conditions. Some of the significant benefits of this classifier are that it just requires a minimal scale of training dataset for computation. According to the Naive Bayes method, the occurrence of a particular feature in a class has no bearing on the inclusion or exclusion of any other feature [36]. Only the semantic content of the messages is classified by the Naive Bayes classifier. Operational filters take into account details like the existence of suspicious header, which provides extra properties to the message interpretation [37, 38].

Consider a set of experiments in which each statement is eventually represented as a vector $VY_1, VY_2, \ldots, VY_n$, where $Y_1, Y_2, \ldots, Y_n$ are given properties. Each characteristic contains information about a single message token. In the simple case, all the attributes are from Boolean [39]:

$$X_i = 1 \text{ (if the token is in the message);} \quad \text{otherwise, } X_i = 0. \tag{1}$$

Bayes' theorem represents the likelihood that a message with vector $(Y) = Y_1, Y_2, \ldots, Y_n$ belongs to the following category c:

$$P(C|\overrightarrow{Y}) = \frac{P(C) \cdot P(\overrightarrow{Y}|C)}{P(Y)}. \tag{2}$$

4.6. AdaBoost. AdaBoost is a sort of classification boosting technique. It focuses on data points, and this technique combines the prognosis efficiency of numerous weak classifiers into a single strong classifier [40–44]. This method focuses on classifier "training" and "weighting." It applies iteration to the provided method after assigning a weight value to every occurrence in the training dataset. Iteration raises the number of incorrect instances while lowering the number of correct ones. This iteration is carried out in order to improve the weak classifiers' accuracy [45–47]. The AdaBoost algorithm reduces the exponential loss as follows.

Step 1: Let us check an example as follows:

$$(x_1, y_1), \ldots, (x_n, y_n): x_i \in X,\ y_i \in (-1, +1). \tag{3}$$

Step 2: Assign the weight as $(W_1(i) = 1/N, i = 1 \ldots\ldots \ldots\ldots N$, for $n = 1, \ldots, N$.

Train the weak learner.

Step 3: Examine weak hypothesis h_n: $X \longrightarrow R$ with its inaccuracy:

$$\varepsilon n = \sum_{i=h_{m(xi)\neq y_i}} W_{n(i)}. \tag{4}$$

Step 4: Find

$$\varepsilon_{m=R}. \tag{5}$$

Step 5: Update

$$K_{m+1}(\mathrm{i}) = \frac{K_{m(i)\exp\left(-x_{my_m}M_m(x_m)\right)}}{c_m}. \tag{6}$$

D_{m+1} means distribution.

Step 6: Final hypothesis will be

$$H_{(a)} = \operatorname{sign}\left(\sum_{m=1}^{M} \alpha_m h_m(a)\right). \tag{7}$$

5. Measurement and Experimental Result

5.1. Confusion Matrix for Different ML Algorithms. In the given breast cancer dataset, various machine learning methods [48, 49] are used in the given breast cancer dataset. The performance of a classification technique is shown and summarized using a confusion matrix [50]. The anticipated and actual classification are shown in a confusion matrix of dimension $n \times n$ connected with a classifier, where n is the

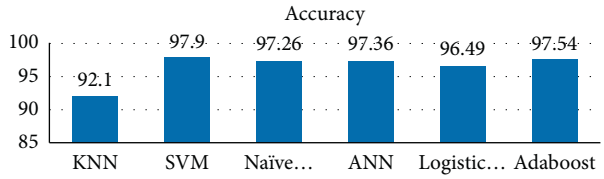

Figure 5: Accuracy.

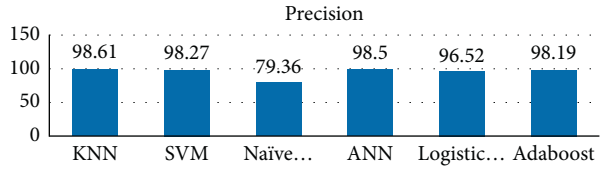

Figure 6: Precision.

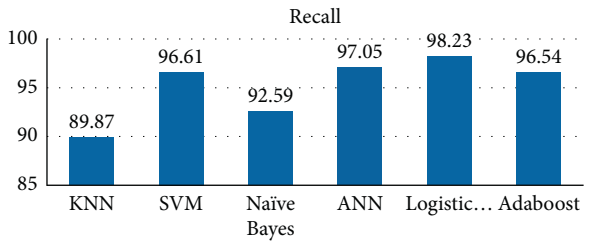

Figure 7: Recall.

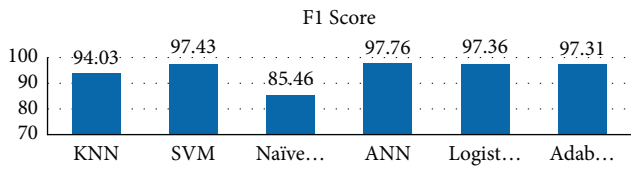

Figure 8: F1 score.

number of possible classes. A confusion matrix is used in this work [51] with the following interpretations for the entries.

A confusion matrix is frequently used to show the performance of a classifier based on the four values listed as TP, FP, TN, and FN [52–54]. The prediction accuracy and classification error [55] can be obtained from confusion matrix.

5.2. Results. The confusion matrix is used to assess method performance in classification. The results are then compared in the confusion matrix. In this matrix, 4 terms are used for evaluating performance, i.e., TP (true positive), FP (false positive), TN (true negative), and FN (false negative) [56–59].

Accuracy [60, 61]denotes correct figure of malignant patients whether it is positive or negative.

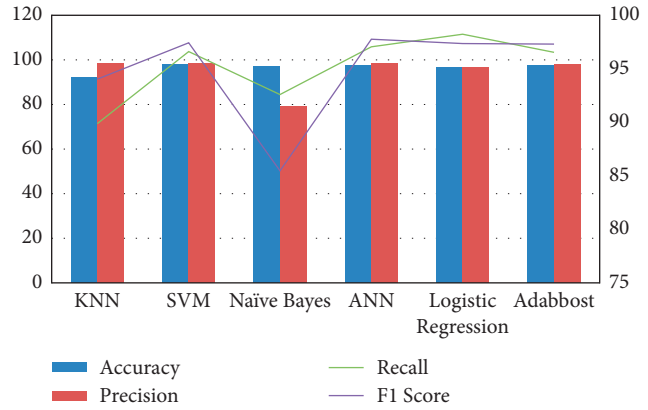

Figure 9: Comparative graph for breast cancer using supervised learning methods.

$$\text{Accuracy} = \frac{(\text{TP} + \text{TN})}{(\text{TP} + \text{TN} + \text{FP} + \text{FN})}. \tag{8}$$

Precision is a metric used to determine how many of the positive forecasts are correct (true positives) [62, 63]. The formula is as follows.

$$\text{Precision} = \frac{\text{TP}}{(\text{TP} + \text{FP})}. \tag{9}$$

Among all the positive examples in the data, recall means the positive cases, which the classifier correctly predicted [64]. Sensitivity is a term that is occasionally used to describe it [65]. The formula is as follows.

$$\text{Recall} = \frac{\text{TP}}{(\text{TP} + \text{FN})}. \tag{10}$$

The F1 score [66] is a statistic that incorporates precision and recall. The harmonic mean of the two is a term used frequently [67]. The harmonic mean is a method of determining "average" of integers that is supposed to be superior than the arithmetic mean for ratios (such as precision and recall) [68]. In this situation, the F1 score [69] formula is as follows.

$$F1 \text{ score} = 2 * \left(\frac{(\text{precision} * \text{recall})}{(\text{precision} + \text{recall})} \right). \tag{11}$$

Six supervised learning algorithms were examined for their prognosis and detection capacities in the diagnosis of breast cancer [70, 71]. In this dataset, a maximum of 569 instances were utilized [72]. There are eight input parameters and one output parameter for each item. Figures 5–9 and Table 3 show the anticipated outcomes for the six suggested supervised learning algorithms (KNN, SVM, Naive Bayes, ANN, logistic regression, and AdaBoost) based on the confusion matrix. Figure shows how the various approaches compare and depict all of the expected findings [73–75]. The anticipated results clearly show that, as compared to other algorithms, the bagging algorithm predicts breast cancer with the highest degree of accuracy. [56, 76].

Table 3: Comparison among various supervised learning methods.

ML method	Accuracy	Precision	Recall	F1 score
KNN	92.10	98.61	89.87	94.03
SVM	97.90	98.27	96.61	97.43
Naive Bayes	97.26	79.36	92.59	85.46
ANN	97.36	98.50	97.05	97.76
Logistic regression	96.49	96.52	98.23	97.36
AdaBoost	97.54	98.19	96.54	97.31

The support vector machine (SVM) gives the highest accuracy on the test dataset, which is 97.9%, as seen in this comparison table and graph. SVM has a higher accuracy percentage than other supervised learning algorithms. Support vector machine is the optimal algorithm for prediction, according to this research.

6. Conclusion

Breast cancer patients with a good prognosis and early discovery have a better chance of being cured. Finally, in the current study, several of the most prominent machine learning methods were utilized to classify "breast cancer" based on ten criteria. Some of the machine learning methods which are applied on this dataset are KNN, SVM, Naive Bayes, ANN, logistic regression, and AdaBoost with respective accuracy of 92.10%, 97.90%, 97.26%, 97.36%, 96.49%, and 97.54%. The defined methods have been applied on the prognosis of breast cancer. As a result, support vector machine (SVM) has been the most proficient algorithm among all supervised learning methods.

In future, some models can be implemented for supervised learning methods with some other techniques like genetic algorithm, ACO (ant colony optimization), PSO (particle swarm optimization), and so on so that early detection can be performed with efficient accuracy.

Data Availability

The data used to support the findings of this study are available from the author Vandana Rawat upon request (vandanarawat@geu.ac.in).

Conflicts of Interest

The authors declare that they have no conflicts of interest.

References

[1] T. V. Swathi, S. Krishna, and M. V. Ramesh, "A survey on breast cancer diagnosis methods and modalities," In *Proceedings of the 2019 International Conference on Wireless Communications Signal Processing And Networking (WiSPNET)*, pp. 287–292, IEEE, Chennai, India, March 2019.

[2] H. Dhahri, E. Al Maghayreh, A. Mahmood, W. Elkilani, and M. Faisal Nagi, "Automated breast cancer diagnosis based on machine learning algorithms," *Journal of healthcare engineering*, pp. 1–11, 2019.

[3] A. Bhoi, R. C. Balabantaray, D. Sahoo et al., "Mining Social media Text for Disaster Resource Management Using a Feature Selection Based on forest Optimization," *Computers & Industrial Engineering*, vol. 169, Article ID 108280, 2022.

[4] M. S. Mekala, G. Dhiman, G. Srivastava et al., "A DRL-based service offloading approach using DAG for edge computational orchestration," *IEEE Transactions on Computational Social Systems*, pp. 1–9, 2022.

[5] K. Yadav, A. Jain, N. M. Osman Sid Ahmed, S. A. Saad Hamad, G. Dhiman, and S. D. Alotaibi, "Internet of thing based koch fractal curve fractal antennas for wireless applications," *IETE Journal of Research*, pp. 1–10, 2022.

[6] T. Thomas, N. Pradhan, and V. S. Dhaka, "Comparative analysis to predict breast cancer using machine learning algorithms: a survey," In *Proceedings of the 2020 International Conference on Inventive Computation Technologies (ICICT)*, pp. 192–196, IEEE, Coimbatore, India, February 2020.

[7] B. Sumathy, A. Chakrabarty, S. Gupta et al., "Prediction of diabetic retinopathy using health records with machine learning classifiers and data science," *International Journal of Reliable and Quality E-Healthcare*, vol. 11, no. 2, pp. 1–16, 2022.

[8] R. Nair, M. Soni, B. Bajpai, G. Dhiman, and K. M. Sagayam, "Predicting the death rate around the world due to COVID-19 using regression analysis," *International Journal of Swarm Intelligence Research*, vol. 13, no. 2, pp. 1–13, 2022.

[9] A. Alferaidi, Y. Kusum, Y. Alharbi et al., "Distributed deep CNN-lstm model for intrusion detection method in IoT-based vehicles," *Mathematical Problems in Engineering*, vol. 2022, p. 8, Article ID 3424819, 2022.

[10] P. W. Dalrymple, "Data, information, knowledge: the emerging field of health informatics," *Bulletin of the American Society for Information Science and Technology*, vol. 37, no. 5, pp. 41–44, 2011.

[11] H. Ding, X. Cao, Z. Wang et al., "Velocity clamping-assisted adaptive salp swarm algorithm: balance analysis and case studies," *Mathematical Biosciences and Engineering*, vol. 19, no. 8, pp. 7756–7804, 2022.

[12] M. S. Mekala, G. Srivastava, J. C. W. Lin, G. Dhiman, J. H. Park, and H. Y. Jung, "An Efficient Quantum Based D2D Computation and Communication Approach for the Internet of Things," *Opt Quant Electron*, vol. 54, 2021.

[13] S. Swain, B. Bhushan, G. Dhiman, and W. Viriyasitavat, "Appositeness of optimized and reliable machine learning for healthcare: a survey," *Archives of Computational Methods in Engineering: State of the Art Reviews*, pp. 1–23, 2022.

[14] P.. M. Griffin and H. B. Nembhard, *Health Data and Informatics*, John Wiley & Sons, Hoboken, NJ, USA, 2016.

[15] W. Viriyasitavat, L. Da Xu, G. Dhiman, A. Sapsomboon, V. Pungpapong, and Z. Bi, "Service Workflow: State-Of-The-Art and Future Trends," *IEEE Transactions on Services Computing*, 2021, In press.

[16] G. Dhiman and A. R. Yildiz, "Nature-inspired algorithms for real-life complex engineering problems," *Recent Advances in Electrical & Electronic Engineering (Formerly Recent Patents on Electrical & Electronic Engineering)*, vol. 14, no. 3, p. 251, 2021.

[17] K. K. Singamaneni, K. Ramana, G. Dhiman, S. Singh, and B. Yoon, "A novel blockchain and Bi-linear polynomial-based QCP-ABE framework for privacy and security over the complex cloud data," *Sensors*, vol. 21, no. 21, p. 7300, 2021.

[18] D. Hanahan and R. A. Weinberg, "The hallmarks of cancer," *Cell*, vol. 100, no. 1, pp. 57–70, 2000.

[19] V. R. Brus, L. I. Voronova, and V. I. Voronov, "Neural network classification of cardiac activity based on cardiogram data for driver support system," In *Proceedings of the 2020*

Systems of Signals Generating and Processing in the Field of on Board Communications, pp. 1–5, Moscow, Russia, 2020.

[20] R. Kumar, V. Joshi, G. Dhiman, and W. Viriyasitavat, "An improved exponential metric space approach for C-mean clustering analysing," *Expert Systems*, Article ID e12896, 2021.

[21] S. P. Singh, G. Dhiman, P. Tiwari, and R. H. Jhaveri, "A soft computing based multi-objective optimization approach for automatic prediction of software cost models," *Applied Soft Computing*, vol. 113, Article ID 107981, 2021.

[22] M. Soni, G. Dhiman, B. S. Rajput, and K. N. Tejra, "Energy-Effective and Secure Data Transfer Scheme for Mobile Nodes in Smart City Applications," *Wireless Persedictive analytics for chronic kidney disease using machine learning technique Commun*, 2021.

[23] A. Holzinger, "Machine learning for health informatics," in *Machine Learning for Health Informatics*Springer, New York, NY, USA, 2016.

[24] A. Charleonnan, T. Fufaung, T. Niyomwong, W. Chokchueypattanakit, S. Suwannawach, and N. Ninchawee, "Predictive analytics for chronic kidney disease using machine learning techniques," In *Proceedings of the 2016 Management and Innovation Technology International Conference (MITicon)*, Bang-San, Thailand, 2016.

[25] E. Boonchieng and K. Duangchaemkarn, "Digital disease detection: application of machine learning in community health informatics," In *Proceedings of the 2016 13th International Joint Conference on Computer Science and Software Engineering (JCSSE)*, pp. 1–5, Khon Kaen, Thailand, July 2016.

[26] R. Bhardwaj, A. R. Nambiar, and D. Dutta, "A study of machine learning in healthcare," In *Proceedings of the 2017 IEEE 41st Annual Computer Software and Applications Conference (COMPSAC)*, pp. 236–241, Turin, Italy, 2017.

[27] A. P. Tafti, E. Larose, J. C. Badger, R. Kleiman, and P. Peissig, "Machine learning-as-a- service and its application to medical informatics," in *Machine Learning and Data Mining in Pattern Recognition*, Springer, Cham, Berlin, Germany, 2017.

[28] B. Nithya and V. Ilango, "Predictive analytics in health care using machine learning tools and techniques," In *Proceedings of the 2017 International Conference on Intelligent Computing and Control Systems (ICICCS)*, pp. 492–499, Madurai, Tamilnadu, 2017.

[29] H. Sharma, C. Mao, Y. Zhang, and H. Vatani, "Portable Phenotyping system: A Portable Machine-Learning Approach to i2b2 Obesity Challenge," In *Proceedings of the 2018 IEEE International Conference on Healthcare Informatics Workshop (ICHI-W)*, pp. 86-87, New York, NY, USA, 2018.

[30] F. Ahamed and F. Farid, "Applying internet of things and machine-learning for personalized healthcare: issues and challenges," In *Proceedings of the 2018 International Conference on Machine Learning and Data Engineering (iCMLDE)*, pp. 19–21, Sydney, Australia, 2018.

[31] R. Sivakani and G. A. Ansari, "Machine learning framework for implementing alzheimer's disease," In *Proceedings of the 2020 International Conference on Communication and Signal Processing (ICCSP)*, pp. 0588–0592, Chennai, India, 2020.

[32] M. Moreb, T. A. Mohammed, and O. Bayat, "A novel software engineering approach toward using machine learning for improving the efficiency of health systems," *IEEE Access*, vol. 8, Article ID 23169, 2020.

[33] R. Katarya and P. Srinivas, "Predicting Heart Disease At Early Stages Using Machine Learning: A Survey," In *Proceedings of the 2020 International Conference on Electronics and Sustainable Communication Systems (ICESC)*, pp. 302–305, Coimbatore, India, 2020.

[34] C. H. Pan and G. Dhiman, "Study on automatic tracking method of marking points in sports image sequence," *Recent Advances in Electrical & Electronic Engineering (Formerly Recent Patents on Electrical & Electronic Engineering)*, vol. 14, no. 7, pp. 708–717, 2021.

[35] M. S. Mekala, G. Dhiman, R. Patan et al., "Deep learning-influenced joint vehicle-to-infrastructure and vehicle-to-vehicle communication approach for internet of vehicles," *Expert Systems*, vol. 39, no. 5, Article ID e12815, 2021.

[36] H. O. Alanazi, A. H. Abdullah, and K. N. Qureshi, "A critical review for developing accurate and dynamic predictive models using machine learning methods in medicine and health care," *Journal of Medical Systems*, vol. 41, no. 4, p. 69, 2017.

[37] R. Kumar and G. Dhiman, "A comparative study of fuzzy optimization through fuzzy number," *International Journal of Modern Research*, vol. 1, no. 1, pp. 1–14, 2021.

[38] P. K. Vaishnav, S. Sharma, and P. Sharma, "Analytical review analysis for screening COVID-19 disease," *International Journal of Modern Research*, vol. 1, no. 1, pp. 22–29, 2021.

[39] F. Ahamed and F. Farid, "Applying Internet of Things and machine-Learning for personalized healthcare: Issues and challenges," In *Proceedings of the 2018 International Conference on Machine Learning and Data Engineering (iCMLDE)*, p. 19, Sydney, Australia, December 2018.

[40] K. Govindan, H. Mina, and B. Alavi, "A Decision Support System for Demand Management in Healthcare Supply Chains Considering the Epidemic Outbreaks: A Case Study of Coronavirus Disease 2019(COVID-19)," *Transp Res E Logist Transp Rev*, vol. 138, 2019.

[41] Z. Rayan, M. Alfonse, and A.-B. M. Salem, "Machine learning approaches in smart health," *Procedia Computer Science*, vol. 154, pp. 361–368, 2019.

[42] V. K. Gupta, S. K. Shukla, and R. S. Rawat, "Crime tracking system and people's safety in India using machine learning approaches," *International Journal of Modern Research*, vol. 2, no. 1, pp. 1–7, 2022.

[43] T. Sharma, R. Nair, and S. Gomathi, "Breast cancer image classification using transfer learning and convolutional neural network," *International Journal of Modern Research*, vol. 2, no. 1, pp. 8–16, 2022.

[44] S. K. Shukla, V. K. Gupta, K. Joshi, A. Gupta, and M. K. Singh, "Self-aware execution environment model (SAE2) for the performance improvement of multicore systems," *International Journal of Modern Research*, vol. 2, no. 1, pp. 17–27, 2022.

[45] K. G. Sheela and R. V. Anu, "MachineLearningbasedHealthMonitoringSystem," *Materials Today Proceedings*, vol. 24, pp. 1788–1794, 2020.

[46] K. Munir, H. Elahi, A. Ayub, F. Frezza, and A. Rizzi, "Cancer diagnosis using deep learning: a bibliographic review"," *Cancers*, vol. 11, no. 9, p. 1235, 2019.

[47] R. X. Zhang, G. B. Huang, N. Sundararajan, and P. Saratchandran, "Multicategory classification using extreme learning machine for microarray gene expression cancer diagnosis," *IEEE/ACM Transactions on Computational Biology and Bioinformatics*, vol. 4, pp. 485–495, 2007.

[48] J. A. Cruz and D. S. Wishart, "Applications of Machine Learning in Cancer Prediction and Prognosis," *Cancer Informatics*, vol. 2, pp. 59–77, 2006.

[49] W. L. Bi, A. Hosny, M. B. Schabath et al., "Artificial intelligence in cancer imaging: clinical challenges and applications," *CA: A Cancer Journal for Clinicians*, vol. 69, no. 2, pp. 127–157, 2019.

[50] S. S. Mahdavi, M. Moradi, W. J. Morris, S. L. Goldenberg, and S. E. Salcudean, "Fusion of ultrasound B-mode and vibro-elastography images for automatic 3-D segmentation of the prostate," *IEEE Transactions on Medical Imaging*, vol. 31, no. 11, pp. 2073–2082, 2012.

[51] L. Wang, F. Chu, and W. Xie, "Accurate cancer classification using expressions of very few genes," *IEEE/ACM Transactions on Computational Biology and Bioinformatics*, vol. 4, no. 1, pp. 40–53, 2007.

[52] M. Liang, Z. Li, T. Chen, and J. Zeng, "Integrative data analysis of multi-platform cancer data with a multimodal deep learning approach," *IEEE/ACM Transactions on Computational Biology and Bioinformatics*, vol. 12, no. 4, pp. 928–937, 2015.

[53] A. P. Athreya, A. J. Gaglio, J. Cairns et al., "Machine learning helps identify new drug mechanisms in triple-negative breast cancer," *IEEE Transactions on NanoBioscience*, vol. 17, no. 3, pp. 251–259, 2018.

[54] S. Hussein, P. Kandel, C. W. Bolan, M. B. Wallace, and U. Bagci, "Lung and pancreatic tumor characterization in the deep learning Era: novel supervised and unsupervised learning approaches," *IEEE Transactions on Medical Imaging*, vol. 38, no. 8, pp. 1777–1787, 2019.

[55] A. A. R. Magna, H. Allende-Cid, C. Taramasco, C. Becerra, and R. L. Figueroa, "Application of machine learning and word embeddings in the classification of cancer diagnosis using patient Anamnesis," *IEEE Access*, vol. 8, Article ID 106198, 2020.

[56] N. Fatima, L. Liu, S. Hong, and H. Ahmed, "Prediction of breast cancer comparative review of machine learning techniques and their analysis," *IEEE Access*, vol. 8, pp. 150 360–150 376, 2020.

[57] S. Iqbal, G. F. Siddiqui, A. Rehman et al., "Prostate cancer detection using deep Learning and traditional techniques," *IEEE Access*, vol. 9, Article ID 27085, 2021.

[58] M. Marsden and B. Weyers, "Intraoperative margin assessment in head and neck cancer using label-free fluorescence lifetime imaging, machine learning and visualization," *Advanced Biomedical and Clinical Diagnostic and Surgical Guidance Systems*, vol. 11631, Article ID 116310, N, D.G, 2021.

[59] G. Xu, N. Yin, and Q. Yang, "Study on the feasibility to detect cancer tumors by combining nanotechnology with SQUID" applied superconductivity," *IEEE Transactions on*, vol. 20, no. 3, pp. 1956–1959, 2010.

[60] D. C. Nguyen and F. Azadivar, "Application of computer simulation and genetic algorithms to gene interactive rules for early detection and prevention of cancer," *IEEE Systems Journal*, vol. 8, no. 3, pp. 1005–1013, 2014.

[61] M. Al Ahmad, A. Najar, A. El Moutaouakil et al., "Label-free cancer cells detection using optical sensors," *IEEE Access*, vol. 6, Article ID 55807, 2018.

[62] M. H. Waseem, M. S. A. Nadeem, A. Abbas et al., "On the feature selection methods and reject option classifiers for robust cancer prediction," *IEEE Access*, vol. 7, Article ID 141072, 2019.

[63] C. Liu, Y. Huang, J. A. Ozolek, M. G. Hanna, R. Singh, and G. K. Rohde, "SetSVM: an approach to set classification in nuclei-based cancer detection," *IEEE Journal of Biomedical and Health Informatics*, vol. 23, no. 1, pp. 351–361, 2019.

[64] Q. Zhou, B. Yong, Q. Lv, J. Shen, and X. Wang, "Deep autoencoder for mass spectrometry feature learning and cancer detection," *IEEE Access*, vol. 8, Article ID 45156, 2020.

[65] T. K. BamunuMudiyanselage, X. Xiao, Y. Zhang, and Y. Pan, "Deep fuzzy neural networks for biomarker selection for accurate cancer detection," *IEEE Transactions on Fuzzy Systems*, vol. 28, no. 12, pp. 3219–3228, 2020.

[66] Y. Rejani and S. T. Selvi, "Early Detection of Breast Cancer Using SVM Classifier Technique," 2009, https://arxiv.org/ftp/arxiv/papers/0912/0912.2314.pdf#:%7E:text=In%20the%20field%20of%20medical,fit%20in%20a%20feature%20space.

[67] B. Y. Sun, Z. H. Zhu, J. Li, and B. Linghu, "Combined feature selection and cancer prognosis using support vector machine regression," *IEEE/ACM Transactions on Computational Biology and Bioinformatics*, vol. 8, no. 6, pp. 1671–1677, 2011.

[68] M. Varjonen, "Three-dimensional digital breast tomosynthesis in the early diagnosis and detection of breast cancer," in *International Workshop on Digital Mammography*Springer, Berlin, Germeny, 2006.

[69] H. Saoud, A. Ghadi, and M. Ghailani, "Proposed approach for breast cancer diagnosis using machine learning," In *Proceedings of the 4th International Conference On Smart City Applications*, pp. 1–5, Casablanca, Morocco, October 2019.

[70] A. F. M. Agarap, "On breast cancer detection: an application of machine learning algorithms on the Wisconsin diagnostic dataset," In *Proceedings of the 2nd International Conference on Machine Learning and Soft Computing*, pp. 5–9, New York, NY, USA, February 2018.

[71] B. Al-Shargabi and F. A. Al-Shami, "An experimental study for breast cancer prediction algorithms," In *Proceedings of the Second International Conference on Data Science*, pp. 1–6, E-Learning And Information Systems, Dubai, UAE, December 2019.

[72] N. Eyal, M. Last, and E. Rubin, "Comparison of three classifiers for breast cancer outcome prediction," In *Proceedings of the 16th International Conference on Engineering Applications of Neural Networks (INNS)*, pp. 1–6, September 2015.

[73] R. Shen, Y. Yang, and F. Shao, "Intelligent breast cancer prediction model using data mining techniques," In *Proceedings of the 2014 Sixth International Conference on Intelligent Human-Machine Systems and Cybernetics*, vol. 1, pp. 384–387, IEEE, August 2014.

[74] S. Ara, A. Das, and A. Dey, "Malignant and benign breast Cancer Classification using Machine Learning Algorithms," In *Proceedings of the 2021 International Conference on Artificial Intelligence (ICAI)*, pp. 97–101, IEEE, Slamabad, Pakistan, April 2021.

[75] P. H. Abreu, M. S. Santos, M. H. Abreu, B. Andrade, and D. C. Silva, "Predicting breast cancer recurrence using machine learning techniques: a systematic review," *ACM Computing Surveys*, vol. 49, no. 3, pp. 1–40, 2016.

[76] J. T. Wassan, H. Wang, F. Browne, and H. Zheng, "A comprehensive study on predicting functional role of metagenomes using machine learning methods," *IEEE/ACM Transactions on Computational Biology and Bioinformatics*, vol. 16, no. 3, pp. 751–763, 2019.

Hindawi
Mathematical Problems in Engineering
Volume 2022, Article ID 9222636, 18 pages
https://doi.org/10.1155/2022/9222636

Research Article

Multi-Objective Stochastic Synchronous Timetable Optimization Model Based on a Chance-Constrained Programming Method Combined with Augmented Epsilon Constraint Algorithm

Yu Yuan,[1] Pengcheng Wang,[1] and Minghui Wang[2]

[1]*Information Engineering School, Nanchang University, Nanchang, China*
[2]*School of Economics and Management, Beijing University of Posts and Telecommunications, Beijing, China*

Correspondence should be addressed to Minghui Wang; wminghui@bupt.edu.cn

Received 11 May 2022; Revised 6 June 2022; Accepted 17 June 2022; Published 28 August 2022

Academic Editor: Amandeep Kaur

The design of the timetable is essential to improve the service quality of the public transport system. A lot of random factors in the actual operation environment will affect the implementation of the synchronous timetable, and adjusting timetables to improve synchronization will break the order of normal service and increase the cost of operation. A multi-objective bus timetable optimization problem is characterized by considering the randomness of vehicle travel time and passenger transfer demand. A multi-objective optimization model is proposed, aiming at minimizing the total waiting time of passengers in the whole bus network and the inconsistency between the timetable after synchronous optimization and the original timetable. Through large sample analysis, it is found that the random variables in the model obey normal distribution, so the stochastic programming problem is transformed into the traditional deterministic programming problem by the chance-constrained programming method. A model solving method based on the augmented epsilon-constraint algorithm is designed. Examples show that when the random variables are considered, the proposed algorithm can obtain multiple high-quality Pareto optimal solutions in a short time, which can provide more practical benefits for decisionmakers. Ignoring the random influence will reduce the effectiveness of the schedule optimization scheme. Finally, sensitivity analysis of random variables and constraint confidence in the model is made.

1. Introduction

With the acceleration of social and economic development and urban construction, the travel demand of citizens increases. In order to adapt to this change, the number of routes and stops in the public transport systems is increasing, and the optimization of the public transport network is becoming more and more complicated. Therefore, effectively improving the public transport system's service quality and operational efficiency has become a key measure. In the public transport network planning problem, the bus timetable is used to determine the departure time of each line. The relevance of generating a timetable relies on the fact that inadequate and/or inaccurate timetables confuse the passengers and reinforce the bad image of public transit as a whole [1]. At the same time, the design scheme of bus timetables also affects the operation planning of vehicle scheduling and crew arrangement. Hence, the design of timetables is essential for maximizing the quality of service of the bus system.

In the bus network of large cities, passengers often have to transfer between different routes because they cannot get to the destination directly, making it inevitable to spend time waiting for the bus at the transfer station. For commuters who choose to take the bus daily, on the premise that the transfer station can catch up with the following bus line in time, reducing their transfer waiting time to the maximum extent is of positive significance to save commuting time and improve the commuting experience. In order to minimize the transfer waiting time, it is necessary to cooperate

between different bus lines so that the bus network has good connectivity and the buses on different lines can complete a seamless connection at the transfer station. However, the public transport system is different from the railway transport system. There is no definite arrival schedule for each bus. Only the first departure time of each bus and the departure interval time of each bus can be known. The randomness of the arrival time of the bus may lead to a long waiting time for passengers and even miss the opportunity of transfer. A synchronized timetable, with good coordination between buses at transfer nodes, enables passengers to enjoy a smooth transfer service, which is a very important and attractive bus transportation service [2].

The public transit planning process is usually divided into a sequence of five steps: (1) the design of routes, (2) the setting of frequencies, (3) the timetabling, (4) the vehicle scheduling, and (5) the crew scheduling and rostering [3]. The optimization of bus timetables is essential because it is a link between the preceding and the following. As far as the existing research on bus timetable optimization is concerned, most of them are based on the assumption of the operating environment, and there are few studies on the actual operation problems. However, in the actual operating environment, there are a large number of random factors in the public transport system, such as vehicle travel time, stop time, bad weather, and passenger demand, which will affect the implementation of the synchronous timetable (Yu et al. [4]; Yao et al. [5]; Wu et al. [6]; Wu et al. [7]). Although some studies consider the uncertainty of vehicle driving in the design of the timetable, some do not consider the impact of this on operational planning. In the collaborative optimization of bus timetables, most researchers set up the condition of fixed headways without considering the effect of nonfixed headways, and most synchronous optimization methods are only a single objective. Few scholars have carried out multi-objective schedule optimization research. Recently, Tang et al. [8] proposed a robust scheduling strategy for the electric bus given the randomness of bus operating conditions. At the same time, they considered the limitation of the timetable and battery mileage and constructed an optimization model of static and dynamic combinations. The static model introduced the buffer distance strategy to solve the adverse effects caused by randomness. In contrast, the dynamic model used the real-time changing urban road traffic conditions to re-plan the bus schedule in operation within a day.

Besides the stochastic effect of operation conditions, the dynamic change of passengers' demand also increases the difficulty of vehicle synchronized optimization. In order to realize passengers' continuous transfer, bus companies often make buses between different routes arrive at the transfer point synchronously by adjusting the existing timetable. But suppose there is a big deviation between the revised timetable and the original timetable. In that case, it will not only destroy the normal service order of the bus timetable but also significantly increase the operation cost of the bus companies due to the adjustment of the next operation plan. The primary tradeoff faced in the planning and operating tasks is between the level of service faced by the user and the operating costs for agencies [9]. There is a conflict of interest between synchronizing bus timetables between different routes to minimize passengers' waiting time to transfer and minimize the deviation from the original timetables, which requires a difficult tradeoff between improving synchronization and operating costs.

Based on the above factors, we consider the influence of various random factors and take them as the research focus. At the same time, we consider the balance between passenger convenience and operation cost. In order to minimize the total waiting time of passengers in the whole road network and minimize the inconsistency between the synchronized optimized timetable and the original timetable, a multi-objective optimization method is proposed to solve the problem. This study optimizes the original timetable to improve the synchronization of vehicles arriving at transfer stations on different routes so that more passengers can reduce the waiting time and improve the service experience. In order to achieve this goal, we propose a multi-objective optimization model, which fully considers the randomicity of vehicle travel time in public transport routes as a random variable and finds that the stochastic programming model obeys normal distribution through large sample analysis. Therefore, the stochastic programming model is transformed into a new deterministic model using chance-constrained programming. In this study, we design a model-solving algorithm based on the augmented epsilon-constraint algorithm, which can obtain several Pareto optimal solutions reasonably. Finally, the sensitivity analysis of the random variables and the confidence of constraints in the model are carried out to verify the robustness of the model.

The rest of this study is as follows: Section 2 reviews the past work. Section 3 describes the multi-objective model. Section 4 analyzes the solution algorithm. Section 5 validates the model's effectiveness and makes a sensitivity analysis. Section 6 gives the conclusion.

2. Literature Review

The collaborative design and optimization of bus timetable are to optimize the departure time and arrival time from the planning layer and the operation layer, so as to reduce the waiting time of passengers and the operation cost of the bus company, and thus provide the service quality of the whole bus system.

From the point of view of transfer optimization, Cevallos and Zhao [10] proposed a systematic approach based on a genetic algorithm to optimize transfer time by adjusting existing timetables to find the best feasible solution for the optimization of transfer time, taking into account the randomness of bus arrivals. Shafahi and Khani [11] constructed a mixed-integer programming model intending to minimize the waiting time for passengers to transfer between different lines. The model considered the fixed headways, necessary vehicle stop time, and transfer time. The author also extended the model with other buses arriving as new variables. Parbo et al. [12] developed a heuristic algorithm, which used a tabu search algorithm to reduce the offset from the original timetable to minimize passengers' waiting time.

Abdolmaleki et al. [13] assumed that the bus on each line had fixed headways and proposed a model with the same departure constraint to minimize the vehicle travel time in the bus network. Based on the proof that the local search for the generalized problem is equivalent to the maximum-directed cut problem, the authors proposed an approximate algorithm for solving the problem of maximum-directed cut to solve the timetable synchronization problem. At last, the authors relaxed the assumption of the fixed headways and the endless number of transfer passengers between any two lines and designed a recursive quasi-linear time algorithm to solve the problem. To solve the operation problem of the BRT system with two-way lanes, Seman et al. [14] proposed a B-IHCPS strategy based on the simultaneous integrated control of the headway and sequencing of the directional bipartitions, which aims to minimize the total time for passengers to travel and wait. Based on a bimodal network composed of pedestrian and bus modes, De-Los-Santos et al. [15] constructed a mixed integer linear programming model to minimize the total travel time of users and considered service operator objectives. Finally, two new models of line network design and line planning are proposed.

While reducing waiting time for passengers, it is also necessary to reduce the operating costs of bus companies. Castelli et al. [16] proposed a heuristic algorithm for traffic network scheduling based on the Lagrange relaxation method to minimize the weighted sum of the time spent by passengers in the public transportation system and the cost of vehicles used by operators. Moreover, the model proposed by the authors is more suitable for the local network where passenger demand changes significantly within a day. Wu et al. [17] proposed a new coordination design model of stochastic bus timetables. Passengers can readjust their routes when they missed the bus transfer and established a two-level programming model. In the experiment, the authors found that the combination of vehicle scheduling coordination and dynamic diversion can reduce the vehicle size to save the cost of operation and reduce the loss caused by passengers' missed transfers. Considering that the traditional timetable adjustment is restricted by the dynamic traffic jam on the road, Zhang and Liu [18] adopted the dual dynamic method and used the Macroscopic Fundamental Diagram framework to model the traffic dynamics, thereby helping the operator reduce bus operating costs and net benefit while maintaining costs for passengers.

The above work is based on minimizing the waiting time of passengers or minimizing the operation cost. However, the collaborative design of the bus timetable can also be optimized by avoiding bus congestion at common stops and maximizing the number of synchronizations.

Considering the importance of designing the maximum synchronism timetable, Ceder et al. [19] defined synchronization as the simultaneous arrival of vehicles on different routes at the transfer station and then set up a mixed-integer linear programming model to maximize the number of vehicles arriving at the transfer station simultaneously. Based on the constraint of headways, they designed a heuristic algorithm that can solve this problem in polynomial time. Then, Ibarra-Rojas and Rios-Solis [20] loosened the definition of Ceder et al. [19], considering that the intervals between two routes are all synchronized in a small time window, and established a mixed-integer programming model considering the uneven headways. The flexible, collaborative design of the public transport network was adopted to maximize the number of vehicles arriving at the transfer station simultaneously and avoid bus congestion. After proving that the bus network timetable collaborative design problem is an NP-hard problem, the authors designed a multi-start iterative local search algorithm that efficiently finds high-quality solutions. In order to effectively combine global coordination and long-term operation, Wang and Sun [21] proposed a multi-agent deep reinforcement learning framework to develop a dynamic and flexible bus route retention control strategy to solve the bus bunching problem. To better explore the best strategy, the authors developed an effective headway-based reward function in the framework and used a joint action tracker. In order to train each bus within the framework, the authors also designed an efficient learning algorithm using approximate strategy optimization. In order to reduce the occurrence of bus congestion, Ma et al. [22] proposed a nonlinear optimal control model considering driving disturbance and passenger demand uncertainty. Considering the uncertainty of the bus system and the real-time control requirement of bus regulation, a robust optimal predictive control algorithm is proposed.

Collaborative optimization of bus timetables often involves multiple objectives, and the conflict of interests among them is unavoidable. Therefore, it is necessary to design a multi-objective optimization method to find the balance of interests.

Kwan and Chang [23] studied the synchronization of multi-objective metro timetables, aimed at minimizing the total passenger dissatisfaction index related to transfer waiting time and the total deviation index deviating from the original timetable. The Pareto frontier between these two indexes was searched by the nondominated solution sorting genetic algorithm-II (NSGA-II), and it was improved by the differential evolution of NSGA-II. In order to improve the service quality of the bus network, Hassold and Ceder [24] studied the dual-objective timetable design problem to minimize the expected waiting time of passengers and minimize the deviation from the deviation expected vehicle seating rate. By increasing the condition of using multiple vehicle types on the same line to avoid the constraints of uniform headways and passenger load. Assuming that the possible departure time is known, they designed a multi-objective label correction algorithm to solve the multi-objective problem. Wu et al. [25] studied the multi-objective public transport network design and frequency setting problem to minimize the cost of passengers and operators and proposed an alternate objective genetic algorithm to solve the problem with large search space and multiple constraints. Liu et al. [26] developed a dual-objective integer programming model, which aims at maximizing the number of vehicles arriving at the transfer station and minimizing the required vehicle size, and designed a sequential search method solving model based on the two-stage deficit

function. Fonseca et al. [27] proposed a mathematical method to solve the two-objective mixed integer programming problem of timetable coordination and vehicle scheduling. This method allows the timetable to be modified within the departure distance limit to minimize the weighted sum of passenger transfer time cost and bus operation cos. The timetable can be coordinated by modifying the departure time and prolonging the vehicle stay time at the transit station. Tang et al. [28] constructed a bi-objective bus timetable optimization model based on a data-driven method to minimize the total waiting time of passengers and the departure time of bus companies and designed an improved nondominated sorting genetic algorithm-II (NSGA-II) with the special coding scheme, which can search the Pareto optimal solution quickly. Wu et al. [29] proposed a mixed integer linear programming model to optimize the bus schedule and bus matching scheme, which aims at minimizing passenger waiting time, passenger travel time, and operating cost. In order to solve the model, the author designs an algorithm based on improved Lagrangian relaxation and proposes a rolling level scheme for dynamic algorithm implementation. Tian et al. [30] proposed a new three-level programming model to solve the problem of public transport network design with congestion, which minimizes the total operating cost and passenger transfer cost. In order to solve this problem, two methods are proposed to transform the nonlinear nonconvex problem into mixed integer linear programming and surrogate optimization.

There are many uncertain factors in the actual environment of bus operation, such as the random travel time of vehicles, the dynamic demand of passengers, and so on. In an uncertain environment, the above bus schedule optimization model based on the deterministic operation environment is challenging to solve such problems. In order to solve the problem of uncertainty, researchers consider adding random variables to the construction of a model.

Ting and Schonfeld [31] studied the problem of minimizing the total operating costs of multi-hub transportation networks and designed a heuristic algorithm to simultaneously optimize the headways and timetable relaxation time of transfer lines. The results show that the relaxation delay costs of vehicles and passengers increase with the relaxation time, while the costs of passenger missed transfer and vehicle scheduling delay decrease. Considering the stochastic disturbance caused by the change in passenger demand, Yan et al. [32] set up a stochastic demand scheduling model and developed two heuristic algorithms to solve the model using simulation technology and routing strategy-based online network and designed a performance evaluation method. Zhao and Zeng [33] defined a passenger cost function based on the random arrival time of passengers, line network, vehicle spacing, and timetable. They proposed a meta-heuristic optimization method of bus line network combined with simulated annealing, taboo, and greedy search to determine a bus line network that minimizes the passenger cost function. Yan et al. [34] proposed a bus network design problem considering the randomness of vehicle driving time, constructed a robust optimization model aiming at minimizing the weighted sum of operator cost, and designed a heuristic algorithm based on the k-shortest path algorithm, simulated annealing algorithm, Monte Carlo simulation, and probabilistic discrete selection model to solve the model. Wu et al. [6] constructed a random integer programming model for the three types of passengers, namely, transfer passengers, passenger passengers, and direct passengers, to minimize the total waiting time. The relaxation time was added to the timetable to reduce the randomness of bus travel time, and a genetic algorithm with local search was designed to solve the model. Berrebi et al. [35] regarded the bus scheduling problem as a random decision-making process. Assuming that there are random operating conditions and unstable driving distances, they proposed a strategy for scheduling buses using real-time information so that passengers can minimize the waiting time at the transfer station and maximize the bus frequency on the route. Li et al. [36] took the bus travel time as a fuzzy variable, constructed a bi-objective optimization model to minimize the total vehicle travel time and the total passenger waiting time in the bus network, and designed a genetic algorithm with variable chromosome length to solve the model. To cope with the impact of randomness, Morales et al. [37] proposed a bus injection bus operation strategy, namely the bus scheduling strategy for the situation of extremely long headway. The authors established a random model based on the second moment of interval distribution to determine whether the bus is worth injecting and developed a complete service model to determine when the bus should be injected. Based on the above literature research, a multi-objective optimization model is constructed in this study.

3. Model Formulation

3.1. Assumptions and Notations

3.1.1. Assumptions. The bus schedule optimization problem studied in this study is to find a reasonable and relatively optimal set of departure times for a certain route in a certain period from the point of view of the transfer station. Let the line set be X, and both line M and line N belong to the line set X. In order to simplify the problem, assuming that line M is the mainline and line N is another line, and line M to line N has transfer demand, it is necessary to optimize the bus departure schedule of line N. To simplify the problem, this study only considers the one-way transfer demand. For a large public transport network in real life, no matter whether the number of bus transfer lines is increased or the request for two-way transfer is considered, we only need to consider the problem by extending the model. Due to data confidentiality reasons, the GPS location information of Shenzhen bus cards is missing. It is no longer feasible to build a model considering the transfer of a single passenger in the traditional model building method. Therefore, we designed an innovative method that considered from the overall perspective, ignoring the heterogeneity of stations and stations, and considering the full sample planning problem.

(a) Passenger transfer demand: considering the same bus IC card, based on the analysis of large sample

data, for line M and line N, if the bus IC card has an adjacent swiping record of line M and line N and the bus IC card has to swipe record of line N after line M, the number of transfer passengers from line M to line N is assumed to be plus 1. We count the number of bus IC cards with these two properties to determine the number of interchange passengers from line M to line N and record them as P_M^N to represent passenger transfer demand.

(b) The total drop-off time of transfer passengers online M: assuming the boarding time of the transfer passenger who holds the ith IC card is t_i. All IC cards, namely all transfer passengers, are anonymously processed to avoid losing generality. Considering the statistical analysis of large samples, it is assumed that the total travel time of line M is T_M. And the passenger travel time online M can be approximately equal to the mean value of T_M, which is approximately substituted by $(1/2)T_M$ and recorded as H_M. Since the passenger's time to get off is equal to the sum of the passenger's boarding time and the ride time, the total drop-off time of transfer passengers online M can be calculated by the following formula:

$$\begin{cases} l_i = t_i + H_M, \\ L_M = \sum_{i=1}^{P_M^N} l_i, \end{cases} \tag{1}$$

where l_i is the drop-off time of the transfer passenger who holds the ith IC card in line M and L_M is the total drop-off time of all transfer passengers online M.

(c) The total boarding time of transfer passengers online N: assuming the number of trips corresponding to the record of the ith IC card online N is a (i). In general, the number of all trips in line N is counted, and it is assumed that there are A trips in total. Considering the statistical analysis of large samples, we can find out the earliest card swiping time of all card swiping times of each train in the data set, and set $Q_{\min}^N = \{q_1, q_2, \ldots, q_a, \ldots, q_A\}$, and set q_A and q_1 as the minimum and maximum card swiping time in the set, then we can calculate the original departure time of different trains approximately by the following formula:

$$\begin{cases} t = \dfrac{q_A - q_1}{A - 1}, \\ f_N^{a(i)} = q_1 + (a-1)t, \end{cases} \tag{2}$$

where $f_N^{a(i)}$ represents the departure time of the a (i)th bus online N in the existing timetable.

Similarly, based on the consideration of a large sample, it is assumed that the total travel time of line N is T_N. And the travel time of line N is approximately equal to the mean of T_N, which is approximately substituted by $(1/2)T_N$ and recorded as H_N. The boarding time of transfer passengers online N is the arrival time of the bus online N, which can be expressed by the sum of the departure time and travel time of the bus number. We can calculate the total boarding time of the transfer passengers online N according to the following formula:

$$\begin{cases} s_i = f_N^{a(i)} + H_N, \\ S_N = \sum_{i=1}^{P_M^N} s_i, \end{cases} \tag{3}$$

where s_i is the boarding time of the transfer passenger who holds the ith IC card in line N, and S_N is the total boarding time of all transfer passengers in line N.

(d) The total waiting time of passengers transferring from line M to line N: from (2) and (3), we can get the passengers' total drop-off time online M and total boarding time online N, respectively. The total waiting time of transfer passengers from line M to line N can be obtained by the difference calculation of the formula:

$$\begin{aligned} T_M^N &= S_N - L_M \\ &= \sum_{i=1}^{P_M^N} \left(f_N^{a(i)} + H_N \right)] - \left[\sum_{i=1}^{P_M^N} (t_i + H_M) \right], \end{aligned} \tag{4}$$

where T_M^N represents the total waiting time of passengers transferring from line M to line N.

3.1.2. Notations. The following terms have been defined and used in our model (Table 1).

3.2. Model Analysis

3.2.1. Objective Function Analysis. The objective function of bus departure schedule optimization is composed of two parts: the total waiting time of transfer passengers and the total adjustment time of the bus timetable. Passenger cost is determined by the total waiting time from line M to line N. The total bus departure adjustment time is equal to the deviation value between the optimized timetable and the original timetable of each bus. Thus, the total departure adjustment time of line M to line N of the bus company during the research period can be calculated based on the following formula:

$$B = \min \sum_{i=1}^{P_M^N} \left| x_N^{a(i)} - f_N^{a(i)} \right|, \tag{5}$$

where B represents the total departure adjustment time of line M to line N.

Table 1: Compliance description of notations used in this study.

Set	
X	Routes set, $N \in X$
$Q_{\min}^{N}$	The earliest card-brush time set of all vehicles in line N, $q_i \in Q_{\min}^{N}$
$C_N^{a(i)}$	All card-brush time of the $a(i)$th bus in line N, $c_i \in C_N^{a(i)}$
Parameters	
A	Total number of cars in route n
P_M^N	Passenger transfer demand
L_M	Total drop-off time of all transfer passengers in line M
T_M	Total vehicle travel time for line M
T_N	Total vehicle travel time for line N
H_M	Mean of total vehicle travel time for line M
H_N	Mean of total vehicle travel time for line N
t_i	Boarding time of the transfer passenger who holds the ith IC card
l_i	Drop-off time of the transfer passenger who holds the ith IC card in line M
s_i	Boarding time of the transfer passenger who holds the ith IC card in line N
a (i)	Number of trips corresponding to the record of the ith IC card in line N
q_i	The earliest card swiping time of the ith IC bus in line N
S_N	Total boarding time of all transfer passengers in line N
$f_N^{a(i)}$	Departure time of the a (i)th bus online N in the existing timetable, $\forall a(i) \in \{1, 2, \ldots, A\}$
T_M^N	Total waiting time of passengers transferring from line M to line N
B	Total departure adjustment time of line M to line N
H_N'	Optimized bus travel time online N
$G_{\max}$	Maximum departure time interval
$G_{\min}$	Minimum departure time interval
K	Adjustable range of departure timetable
J	Floating range of a vehicle's travel time
D_{early}	The earliest departure times of a bus line
D_{late}	The latest departure times of a bus line
$c_{\max}$	Maximum card swiping time of the a (i)th bus online N
$\overline{F_1}$	Optimal value of F_1 derived from deterministic programming
$\overline{F_2}$	Optimal value of F_2 derived from deterministic programming
$\widetilde{H_N'}$	Random travel time of vehicles online N
α_N	Confidence level of constraint satisfaction for stochastic programming
u_N	Mean of random travel time in line N
σ_N	Variance of random travel time in line N
λ_1	Probability that the random planning transfer time after considering the random variable is less than the deterministic planning transfer time
Decision variables	
D	$1 - \lambda_1$
$x_N^{a(i)}$	Departure time of the a (i)-th bus online N in the optimized timetable

According to the research contents of this study, the objective of the optimization is to minimize both the waiting time for transfer passengers and the total bus departure adjustment time as much as possible. The objective of the optimization is to minimize both the objective function F_1 and F_2, defined as follows:

$$\begin{cases} \min F_1 = \sum_{i=1}^{P_M^N} \left(x_N^{a(i)} + H_N'\right)] - \left[\sum_{i=1}^{P_M^N} \left(t_i + H_M\right)\right], \\ \min F_2 = \min \sum_{i=1}^{P_M^N} \left|x_N^{a(i)} - f_N^{a(i)}\right|, \end{cases} \tag{6}$$

where $x_N^{a(i)}$ is the departure time of the a (i)th bus online N in the optimized timetable and H_N' represents optimized bus travel time.

3.2.2. Model Constraint Analysis

(a) Vehicle Headway Constraint. After a large sample analysis and in light of actual needs, assuming that the maximum departure time interval is $G_{\max}$ and the minimum is $G_{\min}$, the vehicle headway constraint can be obtained as follows:

$$G_{\min} \le x_N^{a(i)+1} - x_N^{a(i)} \le G_{\max}, \quad \forall a(i) \in \{1, 2, \ldots, A\}, N \in X. \tag{7}$$

(b) Timetable Adjustment Range Constraint. From 3.1.1 (3), we can see that the departure time of the a (i)th bus online N in the existing timetable is $f_N^{a(i)}$. Assuming that based on the existing timetable, the departure time of each vehicle can be fluctuated up and down K ranges. Therefore, the adjustable departure time constraints are defined as follows:

$$f_N^{a(i)} - K \le x_N^{a(i)} \le f_N^{a(i)} + K, \quad \forall a(i) \in \{1, 2, \ldots, A\},\ N \in X. \tag{8}$$

(c) Departure Time Sequence Constraint. Since the departure time of the next bus must be later than that of the previous bus, the departure time sequence constraints are defined as follows:

$$x_N^{a(i)} \le x_N^{a(i)+1}, \quad \forall a(i) \in \{1, 2, \ldots, A\},\ N \in X. \tag{9}$$

(d) Reasonable Departure Time Constraint. Assume that D_{early} and D_{late} represent the earliest and latest departure times of a bus line, respectively, and that the departure times of each bus cannot be earlier than D_{early} and not later than D_{late}. The reasonable departure time constraint can be obtained as follows:

$$D_{\text{early}} \le x_N^{a(i)} \le D_{\text{late}}, \quad \forall a(i) \in \{1, 2, \ldots, A\},\ N \in X. \tag{10}$$

(e) Constraint of Relationship between Maximum Swipe Time and Departure Time. For line N, it is necessary to ensure at least that the sum of the maximum departure time in the timetable and the travel time is greater than the maximum card swiping time for transfer passengers. Assuming that all card swiping times of the a(i)th bus online N is set to $C_N^{a(i)} = \{c_1, c_2, \ldots\}$, and $c_{\max}$ is the maximum card swiping time in the set. The constraint of the relationship between the maximum card swiping time and the departure time is set out in (11) as follows:

$$x_N^{a(i)} + 2H_N \ge c_{\max}, \quad \forall a(i) \in \{1, 2, \ldots, A\},\ N \in X. \tag{11}$$

(f) Route N Bus Travel Time Floating Upper and Lower Bound. For line N, assuming that the travel time of the bus is a floating J based on the original data, the upper and lower limits of the travel time of the line N bus can be obtained as shown in:

$$H_N - J \le H_N' \le H_N + J, \quad \forall N \in X. \tag{12}$$

(g) Constraint of Relationship between the Total Drop-Off Time and the Total Boarding Time. Obviously, given that the total drop-off time of all transfer passengers online M is $\sum_{i=1}^{P_M^N} (t_i + H_M)$ and the total optimized boarding time is $\sum_{i=1}^{P_M^N} (x_N^{a(i)} + H_N')$, the constraint of the relationship between the total drop-off time and the total boarding time is defined as follows:

$$\sum_{i=1}^{P_M^N} \left(x_N^{a(i)} + H_N'\right) \ge \sum_{i=1}^{P_M^N} (t_i + H_M), \quad \forall a(i) \in \{1, 2, \ldots, A\}, M, N \in \text{X}. \tag{13}$$

3.3. Establishment and Optimization of the Model

3.3.1. Consideration and Selection of Random Variables. The three branches of stochastic programming are the expected value model, chance-constrained programming, and related chance programming. Chance-Constrained programming, which A. Charnes and W. W. Cooper proposed in 1959, is an optimal theory in a certain sense of probability. Considering randomness is more practical and can bring higher solution effect and precision. Therefore, we consider the travel time of line N as a random variable, defined as $\widetilde{H_N'}$. Then, the objective function and the corresponding constraint conditions are simplified by chance-constrained programming.

3.3.2. Objective Function Optimization. First, we define $\overline{F_1}$ and $\overline{F_2}$ as the optimal values of the two objective functions obtained by solving the deterministic programming through the above modeling process without considering random variables. $\overline{F_1}$ and $\overline{F_2}$ are the minimum of F_1 and the maximum of F_2 respectively. By counting the travel times of buses on route N from route M to route N on different days, it is clear that $\widetilde{H_N'}$ follows a normal distribution, thus converting it from random variables to deterministic equivalents $u_N + \sigma_N \cdot \Phi^{-1}(\lambda_1)$. Since we consider the general situation and ignore the extreme situation, here we calculate based on the existing data that the random variable obeys the normal distribution, which is consistent with the general reality and is directly simplified to consider the normal distribution. For extreme situations that may exist in reality, such as holidays, etc., passenger transfer needs will change greatly. Based on 3.2 (6), the optimized objective function can be expressed in a joint expression:

$$\begin{cases} P_r\left\{\min\left[\sum_{i=1}^{P_M^N}\left(x_N^{a(i)} + \widetilde{H_N'}\right)\right] - \left[\sum_{i=1}^{P_M^N}(t_i + H_M)\right] \le \overline{F_1}\right\} = \lambda_1, \\ \min F_2 = \min \sum_{i=1}^{P_M^N}\left|x_N^{a(i)} - f_N^{a(i)}\right|, \end{cases} \tag{14}$$

$$\begin{cases} \max \lambda_1, \\ \min F_2 = \min \sum_{i=1}^{P_M^N}\left|x_N^{a(i)} - f_N^{a(i)}\right|. \end{cases} \tag{15}$$

Let $D = 1 - \lambda_1$, convert the above union expression to the formula:

$$\begin{cases} \min D = 1 - \lambda_1, \\ \min F_2 = \min \sum_{i=1}^{P_M^N}\left|x_N^{a(i)} - f_N^{a(i)}\right|. \end{cases} \tag{16}$$

3.3.3. Model Constraint Optimization

(a) Constraint of Relationship between Maximum Swipe Time and Departure Time. Considering that the travel time of the buses online N is a random variable $\widetilde{H_N'}$, we change the model constraint equation (11) to the following equation (17), where α_N is the confidence level of constraint satisfaction.

$$P_r\left\{c_{\max} - x_N^{a(i)} \le 2\widetilde{H_N'}\right\} \ge \alpha_N, \quad \forall a(i) \in \{1, 2, \ldots, A\}, \mathrm{N} \in \mathrm{X}. \tag{17}$$

Let $(N) = c_{\max} - x_N^{a(i)} - 2\widetilde{H_N'}$, then it satisfies the following:

$$E[z(N)] = c_{\max} - x_N^{a(i)} - 2u_N, \tag{18}$$

$$\begin{aligned} D[z(N)] &= 4\left(\sigma_N\right)^2 \\ &= \left(2\sigma_N\right)^2. \end{aligned} \tag{19}$$

There is a constraint $c_{\max} - x_N^{a(i)} \le 2\widetilde{H_N'}$ equivalent to $c_{\max} - x_N^{a(i)} - 2\widetilde{H_N'} \le 0$ that satisfies equation (20) and can also be expressed as equation (21):

$$\frac{\left[\left(c_{\max} - x_N^{a(i)} - 2\widetilde{H_N'}\right) - \left(c_{\max} - x_N^{a(i)} - 2u_N\right) + \left(c_{\max} - x_N^{a(i)} - 2u_N\right)\right]}{2\sigma_N} \le 0, \tag{20}$$

$$\frac{c_{\max} - x_N^{a(i)} - \widetilde{H_N'} - \left(c_{\max} - x_N^{a(i)} - u_N\right)}{2\sigma_N} \le -\frac{c_{\max} - x_N^{a(i)} - u_N}{2\sigma_N}. \tag{21}$$

Let the inverse of the left equation of (20) be η, then η is expressed as equation (22), so n satisfies the standard normal distribution $\Phi(0, 1)$, and its probability density is expressed as equation (23):

$$\eta = \frac{\widetilde{H_N'} - 2u_N}{2\sigma_N}, \tag{22}$$

$$\Phi(\eta) = \frac{1}{\sqrt{2\pi}} \int_{-\infty}^{\eta} e^{-\left(t^2/2\right)} \mathrm{d}t. \tag{23}$$

Therefore, equation (21) can be transformed in form as shown in the following:

$$\frac{c_{\max} - x_N^{a(i)} - 2\widetilde{H_N'} - \left(c_{\max} - x_N^{a(i)} - 2u_N\right)}{2\sigma_N} \ge \frac{c_{\max} - x_N^{a(i)} - 2u_N}{2\sigma_N}, \tag{24}$$

$$\eta \ge \frac{c_{\max} - x_N^{a(i)} - 2u_N}{2\sigma_N}. \tag{25}$$

According to probability theory, there must be a number K_a for the confidence level α_N, which makes the following formula (26) true. So the derivation can be done as shown in equations (27)–(30):

$$P_r\{K_a \le \eta\} = \alpha_N \tag{26}$$

$$K_a = \Phi^{-1}\left(1 - \alpha_N\right) \tag{27}$$

$$P_r\left\{\frac{c_{\max} - x_N^{a(i)} - 2u_N}{2\sigma_N} \le \eta\right\} \ge \alpha_N \tag{28}$$

$$\frac{c_{\max} - x_N^{a(i)} - 2u_N}{2\sigma_N} \le K_a \tag{29}$$

$$\frac{c_{\max} - x_N^{a(i)} - 2u_N}{2\sigma_N} \le \Phi^{-1}\left(1 - \alpha_N\right). \tag{30}$$

Then, the constraint $x_N^a + \widetilde{H_N'} \ge c_{\max}$ is equivalent to equation (31), where $\Phi^{-1}(\alpha_N)$ is an inverse function of α_N. Further merging and simplification lead to equation (32).

$$c_{\max} - x_N^{a(i)} \le 2u_N + 2\sigma_N \cdot \Phi^{-1}\left(1 - \alpha_N\right), \tag{31}$$

$$c_{\max} - x_N^{a(i)} \le 2\left(u_N + \sigma_N \cdot \Phi^{-1}\left(1 - \alpha_N\right)\right). \tag{32}$$

(b) Variable Constraint. Standardize the range of values of ordinary parameters in the model, the specific meaning of which has been stated in the notation, and therefore is not repeated here but expressed in the formula as follows:

$$D \in [0, 1]. \tag{33}$$

3.3.4. Optimized Model. After considering random variables and changing the objective function and constraint condition, ns, as shown above, the final multi-objective chance-constrained model is proposed as follows:

$$
\begin{aligned}
&\min D \\
&\min \quad F_2 = \min \sum_{i=1}^{P_M^N} \left| x_N^{a(i)} - f_N^{a(i)} \right| \\
&\sum_{i=1}^{P_M^N} \left(x_N^{a(i)} + \left(u_N + \sigma_N \cdot \Phi^{-1}(\lambda_1) \right) \right)] - \left[\sum_{i=1}^{P_M^N} (t_i + H_M) \right] \le \overline{F_1} \\
&x_N^{a(i)} + 2\left(u_N + \sigma_N \cdot \Phi^{-1}(1 - \alpha_N) \right) \ge c_{\max} \quad \forall a(i) \in \{1, 2, \ldots, A\},\ \mathrm{N} \in \mathrm{X} \\
&G_{\min} \le x_N^{a(i)+1} - x_N^{a(i)} \le G_{\max}, \quad \forall a(i) \in \{1, 2, \ldots, A\},\ \mathrm{N} \in \mathrm{X} \\
&f_N^{a(i)} - K \le x_N^{a(i)} \le f_N^{a(i)} + K, \quad \forall a(i) \in \{1, 2, \ldots, A\},\ \mathrm{N} \in \mathrm{X} \\
\text{subject.to} \quad &x_N^{a(i)} \le x_N^{a(i)+1}, \quad \forall a(i) \in \{1, 2, \ldots, A\},\ \mathrm{N} \in \mathrm{X} \\
&D_{\text{early}} \le x_N^{a(i)} \le D_{\text{late}}, \quad \forall a(i) \in \{1, 2, \ldots, A\},\ \mathrm{N} \in \mathrm{X} \\
&\sum_{i=1}^{P_M^N} \left(x_N^{a(i)} + u_N + \sigma_N \cdot \Phi^{-1}(\lambda_1) \right) \ge \sum_{i=1}^{P_M^N} (t_i + H_M), \quad \forall a(i) \in \{1, 2, \ldots, A\},\ M, \mathrm{N} \in \mathrm{X} \\
&D = 1 - \lambda_1 \\
&D \in [0, 1].
\end{aligned}
\tag{34}
$$

4. Algorithm Design

The constrained programming model in this study belongs to the category of multi-objective optimization problems. Because multiple goals often conflict, tradeoffs can only be made between multiple goals, and different tradeoffs can be combined into a set of Pareto optimal solutions.

The Pareto solution is defined as if there are any two solutions S_1 and S_2, S_1 is superior to S_2 for all objectives, we call S_1 dominates S_2. And if the solution of S_1 is not dominated by other solutions, S_1 is called a nondominated solution, also known as the Pareto solution. And the definition of the weak dominating solution is as follows: if any two solutions S_1 and S_2 have $f(S_1) < f(S_2)$ for all targets, but at least one objective function has $g(S_1) < g(S_2)$, S_1 is called weak dominating S_2, that is, S_1 is the weak dominating solution.

In order to effectively find the Pareto solution to the multi-objective optimization problem, scholars have made a long effort. Epsilon-constraint is a representative constraint processing technique proposed by Takahama and Sakai [38], which can relax the constraint to a certain extent so that the algorithm can get a good solution at the edge of the feasible region. Later, on the basis of the original epsilon-constraint method, Mavrotas, and Florios [39] proposed an augmented epsilon-constraint method to improve the original algorithm, which solves the problem that when some constrained targets are not well constrained by inequalities, the original epsilon-constraint method may match to the weak dominated solution. Therefore, the augmented epsilon-constraint method can be well applied to our proposed two-objective optimization model.

4.1. Augmented Epsilon-Constraint Algorithm. Epsilon-Constraint is one of the multi-objective integer programming algorithms with both theoretical and computational attractions. It can loosen the constraint and get a feasible solution with low constraint violation and small objective function. Its basic principle is to retain only one objective in the multi-objective problem and add the remaining objective constraint values to the constraints to obtain the Pareto solution of the selected single objective by adjusting the values of the restricted objective.

To facilitate the algorithm description, we simplify the original problem to $\min z(x) = \{z_1(x), z_2(x)\},\ x \in X$.

Here, $z_1(x)$ represents the objective function D (the probability that the stochastic programming transfer time is less than the deterministic programming transfer time), and $z_2(x)$ represents the objective function F_2 (the variance between the optimized timetable and the original timetable), and the feasible region X includes all constraints of the optimization model proposed in Section 3.3.3.

For the optimization problem in this study, the model focuses on optimizing the total passenger transfer time and improving the passenger service experience, while minimizing changes in the timetable is less important than the former. Therefore, the priority of $z_1(x)$ is greater than that of

$z_2(x)$. Thus, by minimizing $z_1(x)$, constraining $z_2(x)$, and setting σ_2 as the constraint value of $z_2(x)$, the standard epsilon-constraint model of the original problem is

$$\begin{aligned} &\min \overline{z}(x) = z_1(x), \\ &\text{subject. to.} \begin{cases} z_2(x) \le \sigma_2, \\ x \in X. \end{cases} \end{aligned} \tag{35}$$

The Pareto solution of the original problem can be obtained by solving the above model. When all the inequality constraints of the constrained target are in effect, the original epsilon-constrained algorithm can correctly identify the nondominated solution when all the inequality constraints of the constrained target are in effect. However, it is possible to output the weak-dominated solution when the inequality constraints of the partially constrained target are not in effect [40]. The dominant solution has not reached the optimization effect of the Pareto solution, so we should avoid the weak dominant solution as far as possible. Therefore, we need to improve the original epsilon-constraint algorithm.

4.2. Customized Augmented Epsilon-Constraint Algorithm. The augmented epsilon-constraint algorithm is an improved multi-objective analytic class optimization algorithm aiming at the problem that the traditional epsilon-constraint algorithm may not get a practical Pareto solution set. By introducing relaxation variables, the inequality constraints corresponding to each constrained object are normalized as equality constraints. The range of values of the constrained object is divided into equidistant meshes and multiplied by a sufficiently small weight $\rho > 0$, which is then extended to the original objective function. The augmented epsilon-constraint algorithm ensures that only valid Pareto solutions are searched. Here are the steps of the augmented epsilon-constraint algorithm to solve this scenario in this study.

*Step 1.*Get the range of values of $z_1(x)$ and $z_2(x)$ as $[z_1^{\min}, z_1^{\max}]$ and $[z_2^{\min}, z_2^{\max}]$, where $z_i^{\min}$ and $z_i^{\max}$ are the minimum and maximum values of the objective function $z_i(x)$, respectively. When $z_1(x)$ obtains the minimum value $z_1^{\min}$, let x_1 be the optimal solution at this time, $z_2(x)$ will get the maximum value $z_2^{\max} = z_2(x_1)$ in the feasible region. Similarly, when $z_2(x)$ obtains the minimum value $z_2^{\min}$, let x_2 be the optimal solution at this time, $z_1(x)$ will get the maximum value $z_2^{\max} = z_2(x_1)$ in the feasible region. The two objective functions are optimized for lexicographic order as follows:

$$\begin{cases} z_1^{\max} = \min z_1(x), & \text{s.t.} z_2(x) = z_2^{\min}, \quad x \in X, \\ z_2^{\max} = \min z_2(x), & \text{s.} z_1(x) = z_1^{\min}, \quad x \in X. \end{cases} \tag{36}$$

Step 2. Mesh the range of values of $z_2(x)$. If we want to get $g_2 + 1$ Parato solutions, there will be $g_2 + 1$ grid points (including the grid points corresponding to the minimum and maximum of $z_2(x)$). Then, the range of values will be meshed into g_2 grids, with each grid having an interval size of $(z_2^{\max} - z_2^{\min})/g_2$.

Step 3. Determine the constraint level for each $z_2(x)$ in each grid interval. To facilitate the presentation of the algorithm, we set k_2 as the index of the grid points, numbering from 0, so that the grid points $k_2 = 0, 1, \ldots,$ g_2 correspond to the constraint level X12.

*Step 4.*By introducing the relaxation variable u2, the inequality constraint of constrained targets is changed into an equality constraint. The ratio of u2 to z1 is calculated to eliminate the dimensional effect. Then multiplied by the sufficiently small weight p, and extended to the objective function 1, the augmented epsilon-constraint method model is constructed. The final model is as follows:

$$\begin{aligned} &\min\left(\overline{z}_1(x) - \left(\frac{\rho\mu_2}{\nu_2}\right)\right), \\ &\text{s.t.} \begin{cases} \overline{z}_2(x) + \mu_2 = \sigma_2; \\ \mu_2 \ge 0; \\ x \in X; \\ k_2 = 0, 1, \ldots, g_2. \end{cases} \end{aligned} \tag{37}$$

For each lattice k_2, a corresponding Pareto solution $(\overline{z}_1(x^*), \overline{z}_2(x^*))$ and the current optimal solution $\{x^*, \mu_2^*\}$ will be obtained for the above model. If $\mu_2^* \ge (z_2^{\max} - z_2^{\min})/g_2$, that is, the value of the relaxation variable is greater than the size of the grid interval, then the next few grid intervals will not be optimized and the same Pareto solution will still be obtained. The Pareto solution can be searched directly by skipping these covered grid intervals. We make ξ_2 is the jump coefficient of the total risk objective and take $\xi_2 = [\mu_2 g_2/6500]$. If $\xi_2 \ge 1$, then let $k_2 = k_2 + \xi_2$, the algorithm continues. If the desired number of Pareto solutions is not reached, increase the value of G. Each Pareto solution is the optimal solution of a multi-objective function under various tradeoffs and can be used as a candidate solution. In different situations, decisionmakers can make decisions based on demand.

The algorithm flow chart is shown in Figure 1.

5. Example Analysis

5.1. Overview and Visualization Analysis of Examples. This study selects bus route 338 and bus route 615 in Shenzhen, China, as examples to verify the feasibility and effectiveness of the multi-objective optimization model of a bus timetable. In the actual operation of public transport, generally speaking, vehicles driving up and down independently do not affect each other, and the vehicle routes are used respectively according to the upward and downward directions. Bus route 338 has 40 stops, 95 minutes for the whole upward direction of the line, 101 minutes for the entire downward direction of the line, and Bus route 615 has 62 stops, 168 minutes for the whole upward direction of the line and 153 minutes for the whole downward direction of the line. This study chooses a downward direction bus to study to simplify the problem.

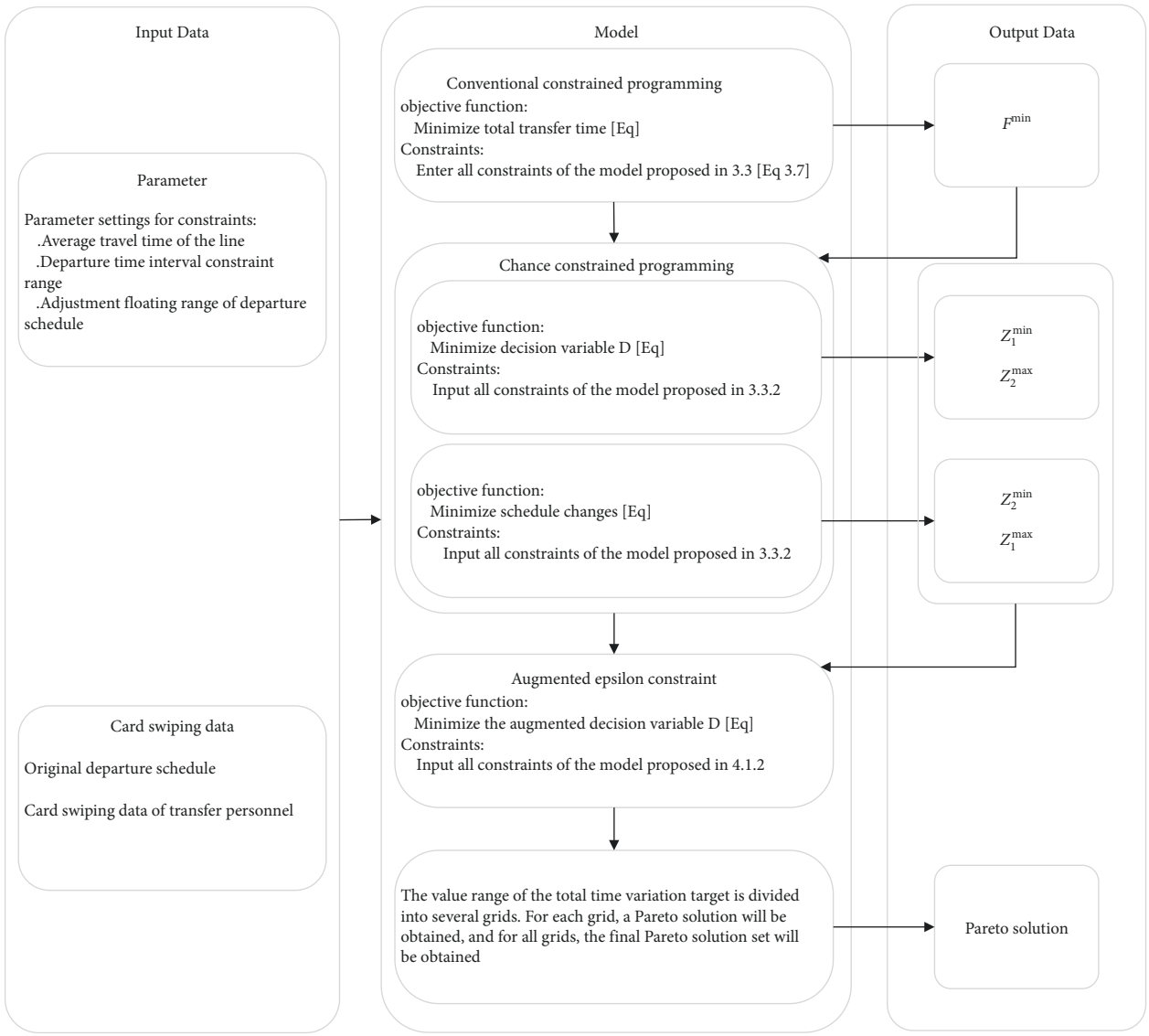

Figure 1: Algorithm flow chart of input data, model, algorithm, and output.

Figure 2 shows the route of 338 and 615 buses and the location of each station in the real environment. It can be clearly seen that the two bus routes have a section of overlapping paths. The route's two endpoints are Fuyong Seafood Market Station and Hedong Station. According to Section 3.3.1, we use the mean of the total travel time in one direction of the vehicles in different routes to approximate the passenger travel time. To prove the reasonableness of the assumption, we selected 338 and 615 roads with multiple identical sites and all sites evenly distributed on both sides of the line midpoint. As shown in Figure 2, passengers' transfer at any station in the overlap path can be equivalent to transferring at the path's endpoints (namely, Fuyong Seafood Market Station and Hedong Station). Therefore, for the convenience of the study, the selected bus network is simplified. The simplified diagram is shown in Figure 3. The arrows on each line in the diagram indicate the direction in which the bus will run.

In this study, the data include: passenger's IC card number, passenger's card transaction date and time, passenger's bus route, and vehicle's plate number. In the research period selected in this study, there are 23838 data on Bus route 338 and 6798 data on Bus route 615, where 65 pieces of data are generated by passengers swiping their cards from Bus route 338 to Bus route 615. Some of which are shown in Table 2. For passengers who take Bus route 338 but transfer to another route, use the same optimization method. Each passenger has a separate IC card number, so the IC card number can represent an independent passenger. The same IC card number record can be used to determine whether a passenger has a transfer demand. For the data shown in date and time of transaction, the first eight digits represent the specific transaction date, and the last six digits represent the specific transaction time (in 24-hour format). Each bus has a unique license plate number, through the license

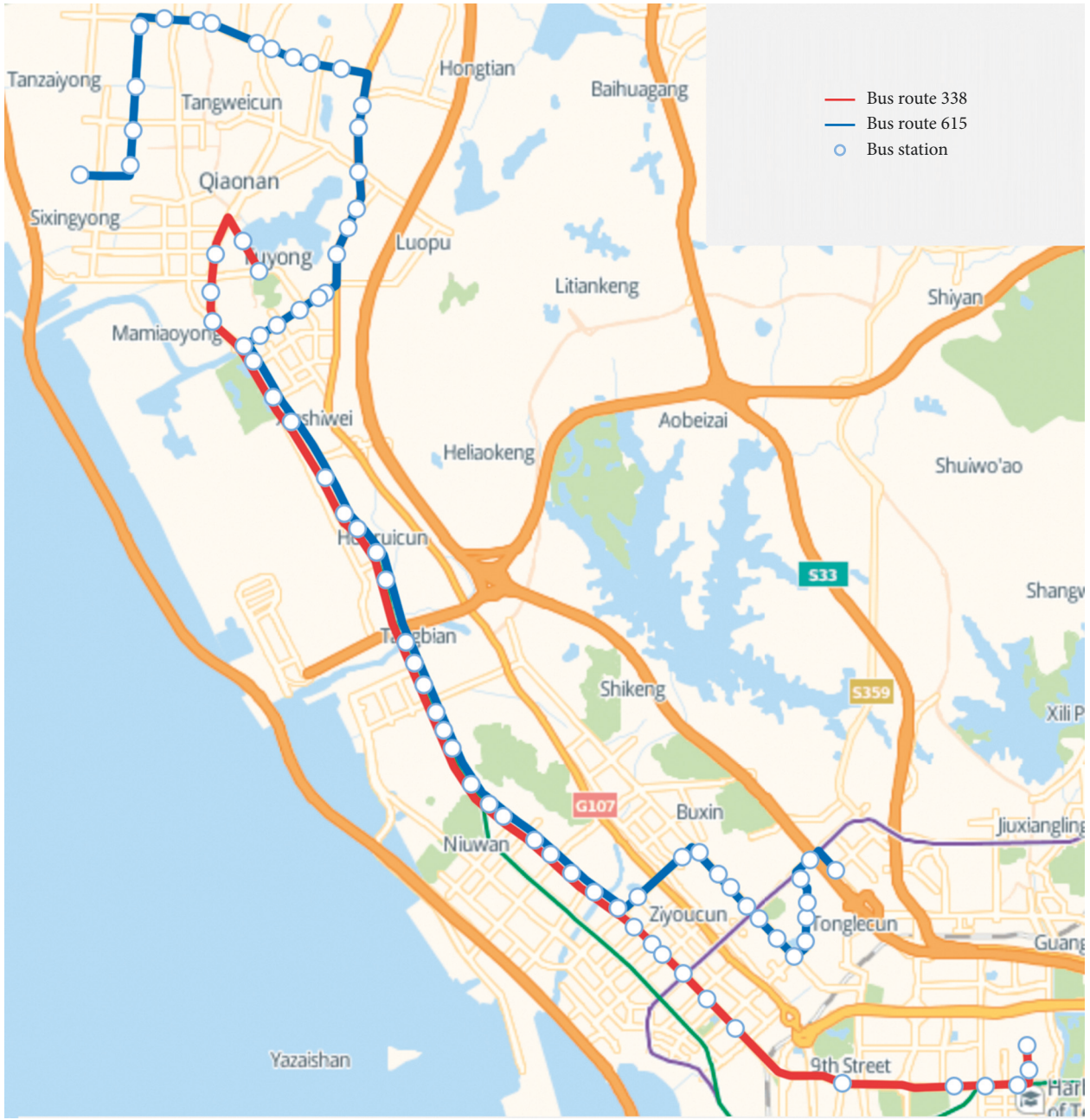

Figure 2: A real-world bus network in Shenzhen, China.

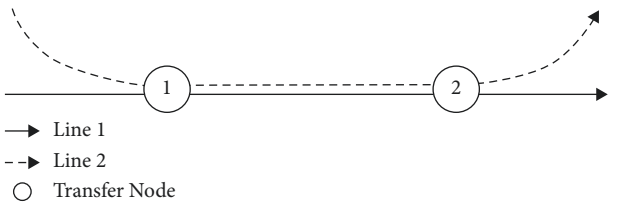

Figure 3: A simplified diagrammatic illustration of bus network.

plate number can be obtained in the number of bus routes, and each bus in the study period of the number of vehicles.

5.2. Summary and Presentation of Calculation Results. This model is nonconvex optimization. The augmented epsilon-constraint algorithm designed for solving the model is programmed by Python 3.7, and the optimization model is solved by calling Gurobi 9.12. All calculations pass on PCs with CPU Intel Core i5-9300H 2.40 GHz and RAM 8.00 GB, with all parameters being the default, except setting the Time Limit to a maximum of 300 seconds.

In the above initial optimization model, vehicle travel time is stochastic, so this study takes bus travel time as a random variable, introduces the chance constraint based on the scene, and deals with the uncertainty of the random variable by adjusting the confidence level. We transform the

Table 2: Passenger data samples of bus lines.

IC card number	Date and time of transaction	Route	License plate number
665483448	20161223071249	Bus route 338	YUE B93772
329219947	20161223084405	Bus route 338	YUE B93753
020816509	20161223063450	Bus route 338	YUE BBB439
684335961	20161223081852	Bus route 338	YUE BL7180
666734618	20161223072423	Bus route 338	YUE B87393
684060460	20161223071933	Bus route 338	YUE BL8287
665483448	20161223082307	Bus route 615	YUE BH0972
329219947	20161223093908	Bus route 615	YUE BBA947
020816509	20161223071808	Bus route 615	YUE B86900
684335961	20161223090336	Bus route 615	YUE BBB702
666734618	20161223073903	Bus route 615	YUE BBB743
684060460	20161223074057	Bus route 615	YUE BBB479

stochastic programming problem into a deterministic programming problem using chance-constrained programming. This study assumes that the travel time of each bus obeys the normal distribution $N(u_N, \sigma_N^2)$, where (u_N, σ_N) are the mean and variance of the travel time of each bus. We transform the objective F_1 of the initial model from solving the minimum passenger transfer waiting time without considering the random variable to solving the probability λ_1 that the random planning transfer time after considering the random variable is less than the deterministic planning transfer time. For ease of presentation, we make D the new deterministic programming objective function, where $D = 1 - \lambda_1$, which means that D is the complementary probability of λ_1. In addition, for the convenience of calculation, we transform the objective F_2 of the initial model from the sum of the absolute values of the optimized timetable and the original timetable offset to the sum of the squares of the timetable offset, which can be effectively substituted.

In this calculation example, Bus No.615 is selected as the route for passengers to take after transfer, and the departure timetable of 25 trains on this route during the study period (i.e., 6: 00 to 21: 30 during the operation period of the route on December 23, 2016) is optimized. The Pareto approximate optimal solution of the multi-objective optimization problem is obtained by test example. The target values of Pareto nondominated front and Pareto solutions are shown in Figure 4 and Table 3, respectively.

It can be seen from Figure 4 that the complementarity probability of the transfer time of stochastic programming less than that of deterministic programming is negatively correlated with the offset between the optimized timetable and the original timetable. It can be concluded that minimizing passenger transfer waiting time and minimizing timetable adjustment offset are two conflicting objectives when vehicle travel time is considered as a random variable. This is in line with the basic requirement that the Pareto optimal solution can be obtained only when the interests of each objective are conflicting in the multi-objective optimization problem. Therefore, the optimization objectives selected in this study are reasonable.

From Table 3, we get 10 Pareto approximate optimal solutions by the designed algorithm. Among them, the

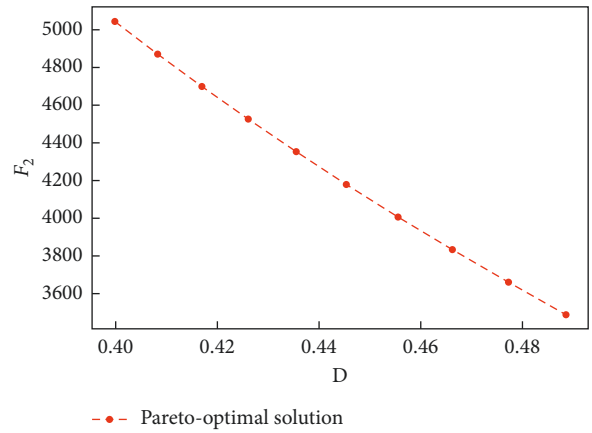

Figure 4: Pareto optimal front for the network example shown in Figure 2.

Table 3: Target values of Pareto optimal solutions.

Pareto optimal solution no.	D	F_2
1	0.400	5043.694
2	0.408	4871.264
3	0.417	4698.833
4	0.426	4526.402
5	0.435	4353.972
6	0.445	4181.541
7	0.456	4009.111
8	0.466	3836.680
9	0.477	3664.250
10	0.488	3491.819

nondominant solution one and the nondominant solution 10 represent the two preferences, respectively: the minimum total waiting time for passenger transfer and the minimum total offset from the original timetable when considering random variables. These two Pareto solutions correspond to the optimal adjustment range of the timetable and the optimized departure timetable, as shown in Tables 4 and 5, where different shades of color represent different timetable offsets. The larger the color depth offset, the smaller the color light offset.

By taking bus travel time as a random variable, the Pareto solution set of D is obtained between 0.40 and 0.49

Table 4: Adjustment time and optimized timetable of Pareto solution no.1.

Original	Adjust	Optimized	Original	Adjust	Optimized	Original	Adjust	Optimized
6:02:23	−45 s	6:01:38						
6:19:34	−7 min45 s	6:11:49	8:37:04	−4 min45 s	8:32:19	10:54:34	−7 min45 s	10:46:49
6:36:45	−7 min45 s	6:29:01	8:54:16	−10 min0 s	8:44:16	11:11:46	−10 min0 s	11:01:46
6:53:57	−9 min45 s	6:44:12	9:11:27	−7 min45 s	9:03:42	11:28:57	−10 min0 s	11:18:57
7:11:08	−7 min45 s	7:03:23	9:28:38	−10 min0 s	9:18:38	11:46:08	−8 min45 s	11:37:23
7:28:19	−9 min45 s	7:18:34	9:45:49	−7 min45 s	9:38:04	12:03:19	−8 min45 s	11:54:34
7:45:31	−7 min45 s	7:37:46	10:03:01	−7 min45 s	9:55:16	12:20:31	−10 min0 s	12:10:31
8:02:42	−10 min0 s	7:52:42	10:20:12	−10 min0 s	10:10:12	12:37:42	−8 min45 s	12:28:57
8:19:53	−7 min45 s	8:12:08	10:37:23	−9 min45 s	10:27:38	12:54:53	−9 min45 s	12:45:08

Table 5: Adjustment time and optimized timetable of Pareto solution no.10.

Original	Adjust	Optimized	Original	Adjust	Optimized	Original	Adjust	Optimized
6:02:23	−45 s	6:01:38						
6:19:34	−7 min21 s	6:12:13	8:37:04	−4 min20 s	8:32:44	10:54:34	−7 min18 s	10:47:16
6:36:45	−7 min24 s	6:29:22	8:54:16	−7 min19 s	8:46:57	11:11:46	−7 min19 s	11:04:27
6:53:57	−7 min16 s	6:46:41	9:11:27	−7 min20 s	9:04:07	11:28:57	−7 min21 s	11:21:36
7:11:08	−7 min21 s	7:03:47	9:28:38	−7 min20 s	9:21:18	11:46:08	−7 min29 s	11:38:39
7:28:19	−7 min19 s	7:21:00	9:45:49	−7 min18 s	9:38:31	12:03:19	−7 min18 s	11:56:01
7:45:31	−7 min20 s	7:38:11	10:03:01	−7 min20 s	9:55:41	12:20:31	−7 min19 s	12:13:12
8:02:42	−7 min22 s	7:55:20	10:20:12	−7 min21 s	10:12:51	12:37:42	−7 min18 s	12:30:24
8:19:53	−7 min20 s	8:12:33	10:37:23	−7 min20 s	10:30:03	12:54:53	−7 min20 s	12:47:33

approximately. When the complementarity probability of the transfer time of stochastic programming less than that of deterministic programming is the largest among all the Pareto solutions, the offset of the optimized timetable is the minimum of 173 min 48 s. With the decrease of complementary probability, the offset of the timetable increases gradually until the complementary probability is the smallest of all Pareto solutions. The offset of timetable reaches the maximum value of 210 min 30 s. When the complementary likelihood is less than the minimum Pareto solution, the offset of the optimized timetable is no longer in the range of the Pareto optimal solution set. Increasing the offset of the timetable will only increase the operation cost of the bus company, but not reduce the complementary probability, and reduce the total waiting time for passengers to transfer. It means that the service quality of the bus system cannot be improved, and the resource of transportation energy may be wasted.

Therefore, the bus operation department can choose one of the Pareto solutions as the final bus schedule according to operation and management needs. If the bus operation department prefers the minimum waiting time for passenger transfer, it is necessary to make the buses from different routes arrive at the transfer station as soon as possible. At this time, Pareto solution No.1 can be selected as the departure schedule. But more and irregular changes to the original timetable will affect the normal order of public transport services, make the subsequent vehicle scheduling and personnel arrangement more complicated, and lead to an increase in operation cost. If the public transport operation department prefers the minimum operation cost of the enterprise, it is necessary to maintain the original service order as far as possible and adjust the original timetable to the smallest extent or approximately the same extent. At this time, Pareto solution No.10 can be selected as the departure schedule. However, it will increase the waiting time of passengers and reduce the passenger's service experience. If the bus operation department needs to consider both the enterprise operating cost and the passenger's travel experience, it can choose the appropriate result from Pareto solution No.2–No.9 to make the bus timetable.

In addition, it can be seen from Table 4 that for the first vehicle departure time, Pareto solution one and Pareto solution ten both make smaller optimization adjustments at the same time. We find that in the other 8 Pareto solutions, the departure time of the first vehicle is the same as that of Pareto solutions 1 and 10, both of which are 45 s earlier. It can be explained that the change of timetable optimization

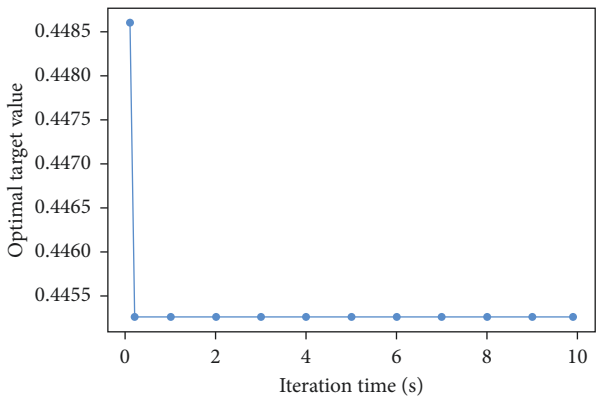

Figure 5: Algorithm iteration diagram.

goal will not have an obvious influence on the optimization of the departure time of the first vehicle. Similarly, for the bus departing at 8:37:04, all Pareto solutions have an optimized adjustment time range of 4 to 5 minutes (that is, the adjustment time range of the timetable is significantly smaller than that of other calculation results except for the first vehicle), and the corresponding optimization results are all in the time range of 8:32 to 8:33. Different optimization objectives will adjust this bus to the same time range. It shows that the bus operation department can get a smaller passenger transfer waiting time through a smaller timetable adjustment during this period.

Figure 5 shows that during the maximum solution period, the iterative solution process of the multi-objective function reduces with the iteration time, and the optimal target value does not change obviously after the 0.2 s iteration time. This shows that the convergence of the augmented epsilon-constraint algorithm is good, and the algorithm can find the approximate optimal solution more stably. This solution can be regarded as a practical solution process.

5.3. Analysis and Discussion of Calculation Results. Then, sensitivity analysis method is used to evaluate the effect of parameter K and confidence α on the objective function. According to the preliminary calculation experiment, the parameter K is taken 30 min as the base, 5 min each time as the step length, the maximum increase 10 min upward and the maximum decrease 20 min downward. The parameter α is taken 0.25 as the base, with each step of 0.01. The maximum increase is 0.05 upward, and the maximum decrease is 0.04 downward. The sensitivity analysis results of minimizing only the objective function D and minimizing only the sum of the departure time adjustments F_2 are shown in Tables 6 and 7 respectively.

As can be seen from Figure 6(a), the parameter K has a significant effect on the target function D. The value of the target D decreases monotonously and tends to be stable with the increase of the value of the parameter K. When the value of the parameter K reaches 15 minutes, the change amplitude of the target D caused by the rise of the value of the parameter K becomes slower. At the same time, the total adjustment time F_2 increases monotonously and tends to be stable with the increase of the value of the parameter K. The reason is that the adjustable range of the constraint becomes larger, the constraint becomes more relaxed, the allowable range of fluctuations becomes larger, and the total adjustment time F_2 is correspondingly larger.

As shown in Figure 6(b), parameter K has a significant effect on the total value of departure time adjustment F_2. The total value of departure time adjustment F_2 increases first and then stabilizes with the increase of parameter K, fluctuates slightly in a very small range, and achieves the minimum value when parameter K is 10 min. At the same time, the value of target value D decreases first and then stabilizes with the increase of parameter K, fluctuates slightly in a very small range, and maximizes when parameter K is 10 min.

To sum up, we can consider taking a better value of K between $K = 10$ min and $K = 15$ min to meet the balance of the minimum waiting time for passengers and the minimum total adjustment of departure time.

Empathy analysis: as shown in Figure 7(a), the confidence α has a significant effect on the target function D, the value of the target D increases monotonously with the increase of the confidence α, and the sum of the minimum departure time adjustment F_2 decreases monotonously with the rise of the confidence α. From Figure 7(b), it can be seen that confidence α has a significant effect on the sum of departure time adjustment values F_2, and the sum of departure time adjustment values F_2 decreases monotonously with the increase of confidence α values. In contrast, the value of the target D increases monotonously with the increase of confidence α values. To sum up, the confidence α of the compromise size can be taken into account to achieve the balance of minimizing the values of the two objective functions.

The 10 nondominated solutions solved show different application scenarios and meanings. Considering the meaning of the value of the objective function, the value of the objective function F_1, that is, the value of D, means the complementary probability that the sum of the waiting time of the transfer of passengers is smaller than that of the sum of the waiting time of the original deterministic programming model. In other words, it is a measure of the sum of waiting time for the transfer of passengers. The smaller the value of D, the greater the probability that passengers needless waiting time. For objective function F_2, that is, the sum of the adjustment of departure time, in order to avoid the consumption of human and material resources, the adjustment of time deviation should be as small as possible. Thus, the two objective functions are considered from the passenger's point of view and the bus company's point of view. In real life, if the number of passengers is huge, we can consider the nondominated solution which is in the front of the 10 nondominated solutions; If the network of public transport routes is especially complex, we can consider the nondominated solution which is in the back of the 10 nondominated solutions; if the number of passengers or the network of public transport routes is neither large nor complex, we can consider the non-dominated solution

Table 6: Sensitivity analysis of parameter K.

K	10	15	20	25	30	35	40
min$D$	0.400	0.383	0.383	0.383	0.383	0.383	0.383
F_2	5043.694	5447.369	5447.369	5447.369	5447.369	5447.369	5447.369
minF_2	3491.819	3532.187	3532.187	3532.187	3532.187	3532.187	3532.187
D	0.488	0.486	0.486	0.486	0.486	0.486	0.486

Table 7: Sensitivity analysis of parameter α.

α	0.21	0.22	0.23	0.24	0.25	0.26	0.27	0.28	0.29	0.30
min$D$	0.326	0.332	0.344	0.356	0.369	0.383	0.400	0.419	0.438	0.459
F_2	6500.000	6357.561	6107.638	5866.480	5601.604	5353.901	5043.694	4710.996	4398.832	4055.678
minF_2	3637.450	3623.206	3598.213	3574.098	3547.610	3522.840	3491.819	3458.549	3428.475	3407.052
D	0.479	0.480	0.482	0.483	0.485	0.486	0.488	0.491	0.493	0.495

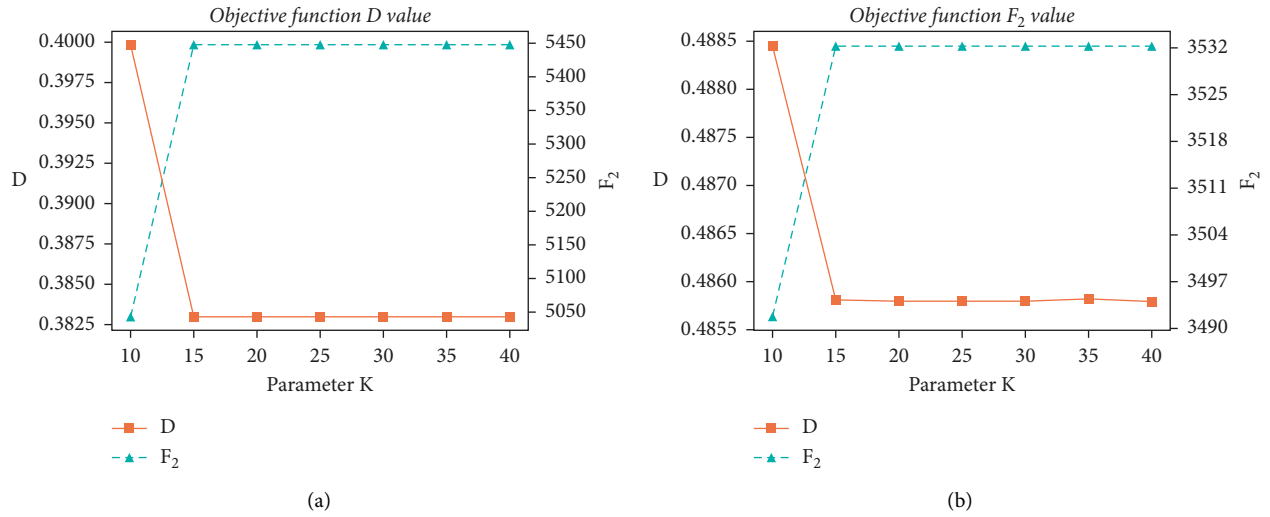

Figure 6: Sensitivity analysis of parameter K. (a) D takes the minimum. (b) F_2 takes the minimum.

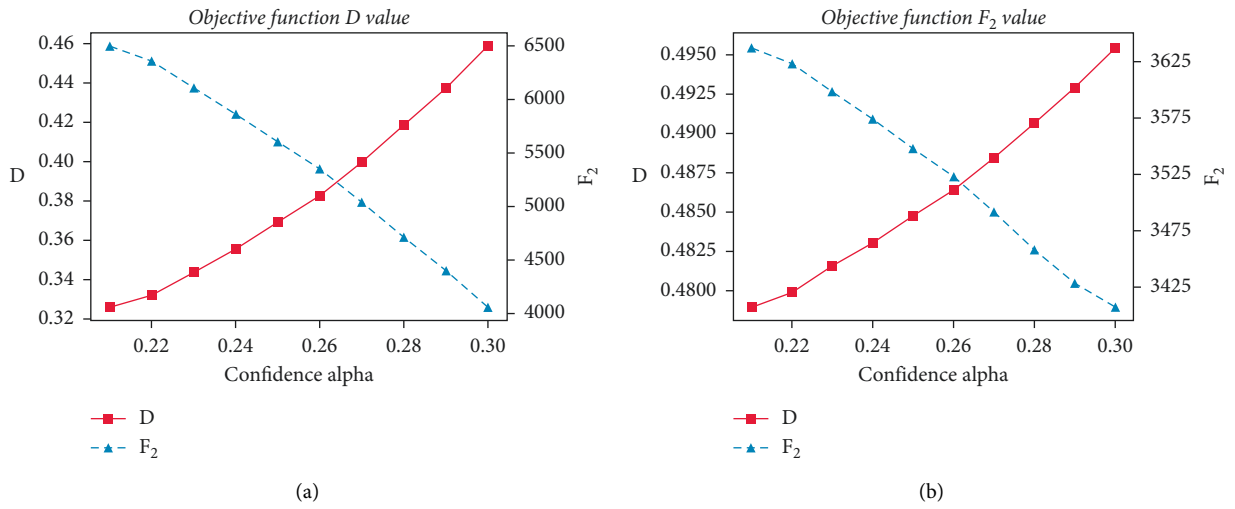

Figure 7: Sensitivity analysis of confidence α. (a) D takes the minimum. (b) F_2 takes the minimum.

which is in the middle of the 10 nondominated solutions, so that we can get the equilibrium state of two objective functions.

6. Conclusion

The optimization of the bus departure timetable is one of the key problems in traffic planning. Based on this, this study studies the cooperative optimization of multi-objective public transport network timetables. A deterministic multi-objective programming model is proposed considering the total waiting time and the total departure time, and the randomicity of bus travel time is fully taken into account. We optimize the preliminary proposed deterministic multi-objective programming model and simplify the model using the normal distribution property of travel time random variables. Thus, the chance-constrained programming method transforms random variables into deterministic variables. Finally, stochastic programming is transformed into a new deterministic multi-objective programming problem.

This study designs a model-solving algorithm based on the augmented epsilon-constraint algorithm. Numerical results show that the algorithm can obtain a high-quality Pareto solution in a short time. For the bus operation system, the bus operation plan is crucial, which not only controls the basic operation of all buses but also directly determines the efficiency and service level of the whole bus operation system. The main objective of this study is to minimize the waiting time of transfer passengers. Using the model established in this study, we can use the cumulative method to solve the problem of considering reverse bus routes and more bus routes in real life. Moreover, reducing the waiting time of passengers can optimize the passengers' experience and improve the passengers' satisfaction, thus increasing the passengers' willingness to take the bus and improving the revenue of bus companies. On the other hand, in the algorithm proposed in this study, another objective function is constrained so that the adjustment range of the timetable is not too large, which reduces the impact of the timetable adjustment on the bus operation to a certain extent. At the same time, the support guarantee of Pareto makes the model more in line with the actual situation in real life. In addition to using the cumulative method to expand the model, we can optimize the timetable of the entire bus network, the model proposed in this study can have many other applications in real life. In real life, the problems of connecting buses to subways, buses to trains, and buses to planes can be solved using our proposed model. Furthermore, the problem of transfer between subways, the problem of transfer between trains, etc. can also be solved using the model proposed in this study.

In the following work, we will analyze the performance of the augmented epsilon algorithm and the multi-objective programming model using a real large-scale example. We consider the stochastic characteristics of road section intervals congestion planning. However, due to computing power and data limitation, we ignore the heterogeneity between stations and simplify it to consider the stochastic programming with full samples. Due to the complexity of regional bus scheduling and the limitations of research conditions, we will introduce the actual bus GPS data and propose a more accurate model. In the future, we will also combine advanced artificial intelligence algorithms such as machine learning. Using the approximate optimal solution solved by it, the solution solved in this study can be further optimized, so that a more excellent optimization effect can be obtained.

Data Availability

All data, models, and code generated or used during the study appear in the submitted article.

Conflicts of Interest

The authors declare that they have no conflicts of interest.

References

[1] A. Ceder, *Public Transit Planning and Operation: Theory Modeling and Practice*, Elsevier, Butterworth-Heinemann, 2007.

[2] W. Wu, R. Liu, W. Jin, and M. Changxi, "Stochastic bus schedule coordination considering demand assignment and rerouting of passengers," *Transportation Research Part B: Methodological*, vol. 121, pp. 275–303, 2019.

[3] V. Guihaire and J. K. Hao, "Transit network design and scheduling: a global review," *Transportation Research Part A: Policy and Practice*, vol. 42, no. 10, pp. 1251–1273, 2008.

[4] B. Yu, S. Wu, B. Yao, Z. Yang, and J. Sun, "Dynamic vehicle dispatching at a transfer station in public transportation system," *Journal of Transportation Engineering*, vol. 138, no. 2, pp. 191–201, 2012.

[5] B. Yao, P. Hu, X. Lu, J. Gao, and M. Zhang, "Transit network design based on travel time reliability," *Transportation Research Part C: Emerging Technologies*, vol. 43, pp. 233–248, 2014.

[6] Y. Wu, J. Tang, Y. Yu, and Z. Pan, "A stochastic optimization model for transit network timetable design to mitigate the randomness of traveling time by adding slack time," *Transportation Research Part C: Emerging Technologies*, vol. 52, pp. 15–31, 2015.

[7] W. Wu, R. Liu, and W. Jin, "Designing robust schedule coordination scheme for transit networks with safety control margins," *Transportation Research Part B: Methodological*, vol. 93, pp. 495–519, 2016.

[8] X. Tang, X. Lin, and F. He, "Robust scheduling strategies of electric buses under stochastic traffic conditions," *Transportation Research Part C: Emerging Technologies*, vol. 105, pp. 163–182, 2019.

[9] O. J. Ibarra-Rojas, F. Delgado, R. Giesen, and J. Munoz, "Planning, operation, and control of bus transport systems: a literature review," *Transportation Research Part B: Methodological*, vol. 77, pp. 38–75, 2015.

[10] F. Cevallos and F. Zhao, "Minimizing transfer times in public transit network with genetic algorithm," *Transportation Research Record*, vol. 1971, no. 1, pp. 74–79, 2006.

[11] Y. Shafahi and A. Khani, "A practical model for transfer optimization in a transit network: model formulations and solutions," *Transportation Research Part A: Policy and Practice*, vol. 44, no. 6, pp. 377–389, 2010.

[12] J. Parbo, O. A. Nielsen, and C. G. Prato, "User perspectives in public transport timetable optimisation," *Transportation Research Part C: Emerging Technologies*, vol. 48, pp. 269–284, 2014.

[13] M. Abdolmaleki, N. Masoud, and Y. Yin, "Transit timetable synchronization for transfer time minimization," *Transportation Research Part B: Methodological*, vol. 131, pp. 143–159, 2020.

[14] L. O. Seman, L. A. Koehler, E. Camponogara, and W. Kraus Jr, "Integrated headway and bus priority control in transit corridors with bidirectional lane segments," *Transportation Research Part C: Emerging Technologies*, vol. 111, pp. 114–134, 2020.

[15] A. De-Los-Santos, D. Canca, and E. Barrena, "Mathematical formulations for the bimodal bus-pedestrian social welfare network design problem," *Transportation Research Part B: Methodological*, vol. 145, pp. 302–323, 2021.

[16] L. Castelli, R. Pesenti, and W. Ukovich, "Scheduling multimodal transportation systems," *European Journal of Operational Research*, vol. 155, no. 3, pp. 603–615, 2004.

[17] W. Wu, R. Liu, W. Jin, and C. Ma, "Stochastic bus schedule coordination considering demand assignment and rerouting of passengers," *Transportation Research Part B: Methodological*, vol. 121, pp. 275–303, 2019.

[18] F. Zhang and W. Liu, "Responsive bus dispatching strategy in a multi-modal and multi-directional transportation system: a doubly dynamical approach," *Transportation Research Part C: Emerging Technologies*, vol. 113, pp. 21–37, 2020.

[19] A. Ceder, B. Golany, and O. Tal, "Creating bus timetables with maximal synchronization," *Transportation Research Part A: Policy and Practice*, vol. 35, no. 10, pp. 913–928, 2001.

[20] O. J. Ibarra-Rojas and Y. A. Rios-Solis, "Synchronization of bus timetabling," *Transportation Research Part B: Methodological*, vol. 46, no. 5, pp. 599–614, 2012.

[21] J. Wang and L. Sun, "Dynamic holding control to avoid bus bunching: a multi-agent deep reinforcement learning framework," *Transportation Research Part C: Emerging Technologies*, vol. 116, Article ID 102661, 2020.

[22] Q. Ma, S. Li, H. Zhang, Y. Yuan, and L. Yang, "Robust optimal predictive control for real-time bus regulation strategy with passenger demand uncertainties in urban rapid transit," *Transportation Research Part C: Emerging Technologies*, vol. 127, Article ID 103086, 2021.

[23] C. M. Kwan and C. S. Chang, "Timetable synchronization of mass rapid transit system using multiobjective evolutionary approach," *IEEE Transactions on Systems, Man, and Cybernetics, Part C (Applications and Reviews)*, vol. 38, no. 5, pp. 636–648, 2008.

[24] S. Hassold and A. A. Ceder, "Multiobjective approach to creating bus timetables with multiple vehicle types," *Transportation Research Record*, vol. 2276, no. 1, pp. 56–62, 2012.

[25] Y. Wu, H. Yang, J. Tang, and Y. Yu, "Multi-objective re-synchronizing of bus timetable: model, complexity and solution," *Transportation Research Part C: Emerging Technologies*, vol. 67, pp. 149–168, 2016.

[26] T. Liu, A. A. Ceder, and S. Chowdhury, "Integrated public transport timetable synchronization with vehicle scheduling," *Transportmetrica: Transport Science*, vol. 13, no. 10, pp. 932–954, 2017.

[27] J. P. Fonseca, E. van der Hurk, R. Roberti, and A. Larsen, "A matheuristic for transfer synchronization through integrated timetabling and vehicle scheduling," *Transportation Research Part B: Methodological*, vol. 109, pp. 128–149, 2018.

[28] J. Tang, Y. Yang, W. Hao, F. Liu, and Y. Wang, "A data-driven timetable optimization of urban bus line based on multi-objective genetic algorithm," *IEEE Transactions on Intelligent Transportation Systems*, vol. 22, no. 4, pp. 2417–2429, 2021.

[29] M. Wu, C. Yu, W. Ma, K. An, and Z. Zhong, "Joint optimization of timetabling, vehicle scheduling, and ride-matching in a flexible multi-type shuttle bus system," *Transportation Research Part C: Emerging Technologies*, vol. 139, Article ID 103657, 2022.

[30] Q. Tian, D. Z. W. Wang, and Y. H. Lin, "Service operation design in a transit network with congested common lines," *Transportation Research Part B: Methodological*, vol. 144, pp. 81–102, 2021.

[31] C. J. Ting and P. Schonfeld, "Schedule coordination in a multiple hub transit network," *Journal of Urban Planning and Development*, vol. 131, no. 2, pp. 112–124, 2005.

[32] S. Yan, C. J. Chi, and C. H. Tang, "Inter-city bus routing and timetable setting under stochastic demands," *Transportation Research Part A: Policy and Practice*, vol. 40, no. 7, pp. 572–586, 2006.

[33] F. Zhao and X. Zeng, "Optimization of transit route network, vehicle headways and timetables for large-scale transit networks," *European Journal of Operational Research*, vol. 186, no. 2, pp. 841–855, 2008.

[34] Y. Yan, Z. Liu, Q. Meng, and Y. Jiang, "Robust optimization model of bus transit network design with stochastic travel time," *Journal of Transportation Engineering*, vol. 139, no. 6, pp. 625–634, 2013.

[35] S. J. Berrebi, K. E. Watkins, and J. A. Laval, "A real-time bus dispatching policy to minimize passenger wait on a high frequency route," *Transportation Research Part B: Methodological*, vol. 81, pp. 377–389, 2015.

[36] X. Li, H. Du, H. Ma, and C. Shang, "Timetable optimization for single bus line involving fuzzy travel time," *Soft Computing*, vol. 22, no. 21, pp. 6981–6994, 2018.

[37] D. Morales, J. C. Muñoz, and P. Gazmuri, "A stochastic model for bus injection in an unscheduled public transport service," *Transportation Research Part C: Emerging Technologies*, vol. 113, pp. 277–292, 2020.

[38] T. Takahama and S. Sakai, "Constrained optimization by the ε constrained differential evolution with an archive and gradient-based mutation," *IEEE*, in *Proceedings of the IEEE congress on evolutionary computation*, pp. 1–9, Barcelona, Spain, July 2010.

[39] G. Mavrotas and K. Florios, "An improved version of the augmented ε-constraint method (AUGMECON2) for finding the exact Pareto set in multi-objective integer programming problems," *Applied Mathematics and Computation*, vol. 219, no. 18, pp. 9652–9669, 2013.

[40] L. X. Huang and J. Zhao, "Multi-objective optimization for transfer station location problem in rail-road intermodal transportation of hazardous materials," *Computer Integrated Manufacturing Systems*, vol. 25, no. 1, pp. 235–246, 2019.

Hindawi
Mathematical Problems in Engineering
Volume 2022, Article ID 2886312, 14 pages
https://doi.org/10.1155/2022/2886312

Research Article

Soft Landing Parameter Measurements for Candidate Navigation Trajectories Using Deep Learning and AI-Enabled Planetary Descent

Janhavi H. Borse,[1] **Dipti D. Patil**,[2] **Vinod Kumar**,[3] **and Sudhir Kumar**[4]

[1]*Department of Computer Engineering, SKNCOE, Savitribai Phule Pune University, Pune, India*
[2]*Department of Information Technology, MKSSS's Cummins College of Engineering for Women, Savitribai Phule Pune University, Pune, India*
[3]*U. R. Rao Satellite Centre, Indian Space Research Organization, Bangalore, India*
[4]*PCPS College, Lalitpur, Nepal*

Correspondence should be addressed to Sudhir Kumar; sudhir.kumar@patancollege.org

Received 16 May 2022; Accepted 28 July 2022; Published 27 August 2022

Academic Editor: Amandeep Kaur

Smart instruments, sensors, and AI technologies are playing an important role in many fields such as medical science, Earth science, astronomy physics, and space study. This article attempts to study the role of sensors, instruments, and AI (artificial intelligence) based smart technologies in lunar missions during navigation of trajectories. Lunar landing missions usually divide the power descent phase into three to four sub-phases. Each sub-phase has its own set of initial and final constraints for the desired system state. The landing systems depend on human competencies for making the most crucial landing decisions. Trajectory planning and designing are very significant in lunar missions, and it requires inputs with precision. The manual systems may be prone to errors. In contrast, AI and smart sensor-based measurements give an accurate idea about the trajectory paths and make appropriate decisions where manual systems may turn into disasters. The manual systems are either pre-fed or have manual controls to guide the trajectory. For autonomous landing problems, trajectory design is a very crucial task. The automated trajectories play a vital role in the measurement and prediction of landing state parameters of the space rocket. Nowadays, sensors, intelligent instruments, and the latest technologies go hand in hand to devise measurement methods for accurate calculations and make appropriate decisions during landing space rockets at the designated destination. Space missions are very expensive and require huge efforts to design smart systems for navigation trajectories. This paper attempts to design all possible candidates of reference navigation trajectories for autonomous lunar descent by employing 3D non-linear system dynamics with randomly chosen initial state conditions. The generated candidates do not rely on multiple hops and thus exhibit an ability to serve autonomous missions. This research work makes use of smart sensors and AI federated techniques for smartly training the system to serve the ultimate purpose. The trajectories are simulated in an automated simulating environment to perform exhaustive analyses. The results accurately approximate the trajectories analogous to their numerical counterparts and converge to their measured final state estimates. The generation rate of feasible trajectories measures the accuracy of the algorithm. The algorithm's accuracy is near 0.87 for 100 sec flight time, which is reasonable.

1. Introduction

1.1. Background Details. Nowadays, the bulk of data is available through various space missions. Technological advancements are also taking place in domains like artificial intelligence and machine learning. These new technologies can be leveraged to find autonomous solutions to the safe planetary landing problem. AI-ML systems may use this mission data for performing numerous tasks specific to Guidance, Navigation, and control of space vehicles. Out of the recent technological advancements [1, 2], terrain relative navigation of NASA [3], and CE'4 [4] landing mission of

China showed flawless descent using AI-ML techniques and previous mission DEM data. It proves the capability of ML models to guide a spacecraft for navigation through space without the help of a GPS-like facility.

Along with the DEM data, analytical trajectory data are another powerful resource for the efficient training of such systems. Plenty of robust and qualitative trajectory data for autonomous systems must be available. Current lunar descent systems follow multi-hop pre-fed trajectory paths. But for self-driven systems, such data are not suitable. To solve this problem, we present an approach that takes care of terminal zero velocity constraints before touchdown and generates a single-hop trajectory from any randomized starting state. This attempt generates analytical reference trajectory data valid for the lunar power descent module. A complete 3-dimensional non-linear system dynamics and randomized initial system state parameters are used. Zero touchdown velocity is guaranteed by posing terminal velocity constraints on the guidance law.

A handful of literature is studied to understand trajectory estimation techniques, and experiments are done based on the knowledge gained. Research [4] shows that machine learning techniques are used to solve non-linear system problems. Few rely on this vast data and are called data-driven designs out of these systems. These typical supervised systems try to find a correlation between input and output. Such data-driven system designs need input and past trajectory information for efficient system training.

Few literature pieces also use non-linear system dynamics [5, 6] with few design variations. Researchers in [7] have solved dynamic system problems using physics laws through embedded programming solutions. Few researchers used a more straightforward 2D [8] system dynamics. At the same time, few dealt with the complete 3D system dynamics to solve non-linear state estimation problems. Few research studies concentrated on the optimization part of the non-linear dynamics. Ramanan and Lal [9] analyzed different trajectory optimization techniques and provided a clear overview. The hybrid optimization concept in trajectory analysis is introduced by [10]. Zhang and Barczyk focused on collision-free trajectory design using Non-linear Model Predictive Control (NMPC) for drone dynamics. Zhang, Xiaoxue et al. used a variant of Gaussian Mixture Models for trajectory generation to predict the uncertainty in moving obstacles. Barczyk and Martin employed a closed feedback loop for real-time trajectory prediction in the non-linear MPC system. Many valuable works [11, 12] describe guidance laws for lunar landing missions. The work in [13, 14] introduced guidance law for planetary missions, which tends to find the optimal path from the current position by solving a 2-point boundary problem. Research in [15] defines a crew-initiated explicit lunar descent guidance based on ground-based implicit law. The work in [16, 17] describes the guidance methods for hazard-free landing and analyses implicit video navigation requirements for autonomous missions. Reference [18] describes the hybrid propulsion design of the lunar lander and analyses its effect on the descent system as a whole. Few pieces of research converted optimal control problem to minimum fuel problem and accordingly posed constraints on guidance law. Research [19] demonstrates a trajectory generation algorithm for crewless missions with the help of simulation studies. Few researchers solved quadcopter dynamics in 3-dimensional state space for hazard avoidance in a cluttered environment, while few used non-linear dynamics for multi-robot trajectory generation and planning. 3-dimensional trajectory planning for terrain hazard avoidance and optimal control of a spacecraft is demonstrated in work [20].

1.2. Related Works. Survey [21] in the literature provides complete information about the working of AI-ML algorithms and their dependencies right from the data inception to the model existence. This work is a comprehensive survey of autonomous guidance methods analyzing planetary power descent constraints. Few works describe existing vision-based deep learning navigation techniques for orbital and landing missions. The analysis in [22, 23] discusses state-of-the-art feature extraction methods for deep learning applications. Depending on data availability, AI-based autonomous landing systems use deep learning approaches or deep reinforcement learning [24]. AI-ML approaches may use control software like General Pseudo-spectral OPtimal control Software (GPOPS) for generating trajectories for spacecraft guidance and control applications. A deep learning approach like [25] uses trajectory data for carrying out further investigation. The approach [26] discusses feasibility criteria for generating optimal fuel trajectories using deep learning techniques. Research [27] introduces dual-constrained guidance for hypersonic vehicles using a deep learning network. A deep reinforcement learning approach like [28] also depends on trajectory data. MATLAB tools like DIDO [29] and extended pseudo-spectral tools like GPOPS [30] are registered for commercial availability. These are not freely available to all. Certain open-source tools like Pyomo [31] are used to design research-specific frameworks for solving optimal control problems. A few of these tools and their applicability to the current problem are discussed below.

1.2.1. GPOPS. GPOPS is initially designed to solve non-linear, multi-phase optimal control problems using pseudo-spectral methods. Later on, GPOPS II used a Gaussian variant of pseudo-spectral methods. Basically, both the versions are written in MATLAB and possess leveled structure to allow user-defined specifications to be fed for each phase. It uses non-linear problem-solvers like SNOPT or IOPT to solve differential equations. The collocation method allows a user-defined number of nodes to incorporate multiple phases into the system, and the cost function can also be defined at the user level. Many researchers use this tool to generate trajectory data by manually providing initial guesses about the system's initial state.

1.2.2. DIDO. DIDO has been a part of NASA's first actual flight demonstration for solving optimal control problems since 2006. It provides a minimalist approach that uses

Pontryagin's principle as a baseline analytical tool. An early version of DIDO works on initial guesses. Still, later versions do not have that constraint as they contain multifaceted algorithms. These algorithms focus on spectral acceleration and provide feasible, robust, and optimal solutions. It is designed to meet the challenges of global space maneuvers. DIDO has fewer memory requirements and can be directly embedded into the mission hardware. It is not suitable for generating a complete dataset for training purposes as we need to train AI-ML systems.

1.2.3. Pyomo. Pyomo is a modeling language used by an open-source framework for dynamic optimization using pseudo-spectral methods. Although it is an open-source framework, it works on the same principles as GPOPS.

Almost all of these tools are not open-source, and their focus is on solving multi-phase control problems. The initial guess requirement is mandatory for generating a single optimal trajectory in many available tools. It introduces a subjective bias in each generated solution, although it produces one of the best optimal solutions. Human efforts are also required to generate many trajectories, which imposes hard constraints on the system. The data generated through this method misses the realistic random behavior of the trajectories. The ML models so trained may also involve subjective bias.

The existing approaches introduce subjectiveness in the generated trajectories, which is not desired for real-time applications. For autonomous missions, huge amounts of data must be produced with lower costs. These solutions are costly enough for researchers to generate such a large quantity of data. It motivates us to propose an autonomous trajectory generation solution by removing subjective bias with a zero-cost programmatic approach. The proposed algorithm works with randomized inputs adjusted automatically to address this drawback. The algorithm removes any subjective bias by incorporating all possible solutions that might not be optimal but are feasible in their respective ranges. When AI-ML models are trained on possible solutions, they perform well for favorable pre-known and unfavorable unknown inputs.

1.3. Research Contributions. The literature covered so far talks about how non-linear system dynamics are taken care of and how exactly physics-informed systems work. Existing physical systems use mathematical formulations and provide analytical solutions to planetary landing problems. With the advent of AI-ML technologies, new approaches to solving non-linear system dynamics for accurate planetary landing have come up. Intelligent techniques need more and more data to work. For instance, for supervised landing problems, accurate mission data with system state information must be available to make accurate predictions in real-time. This trajectory data has every piece of information about the physical system's past, current, and future state. It is not just landing problems for which an AI-ML solution would need trajectory data. All kinds of orbital and interplanetary missions also need such data. This data is not directly available to the researchers who work on such problems. Although few software solutions are available, they are licensed versions and hence not affordable to all. These solutions are detailed in Section 1.1 under the label of the related works.

The trajectory data requirement for implementing different AI-based systems is different. For example, missions like interplanetary, planetary landing, and orbital maneuvering follow different trajectories with varying constraints to reach their destinations. In essence, each problem carries its own challenges. Hence, the change in initial and final state parameters for each problem domain drifts the solution in different directions. Hence, an effort is made to limit our scope to the lunar landing problem, which would help AI-ML algorithms to be trained to make accurate state predictions. Before proceeding further, let us examine the challenges of the existing AI-ML solutions to the lunar landing problem as follows:

(i) Supervised learning techniques like deep neural networks need a foundation of accurate data to build an accurate model for state prediction.

(ii) Need for trajectory data with accurate past, current, and future state information comparable with natural physical systems.

(iii) Trajectories should be realistic. It means that, in case of any adverse event, a spacecraft following those trajectories should land softly on the ground.

(iv) Unexpected trajectory behavior should not end up in infeasible solutions.

(v) Unavailability of system state tracking system like GPS (Global Positioning System).

This paper attempts to meet those challenges through a programmatic approach. It generates accurate and feasible trajectory database solutions, which can be used to train AI-ML algorithms and help build predictive models for real-time applications. This database can also render the image data for providing real-time context information for the vision-based solutions. This is useful for creating a valid and labeled dataset, which further can be employed to train a neural network. One of the significant contributions of this work is that it tries to remove the subjective bias in training the AI-ML systems. All the trajectories are randomly generated and do not require any initial guesses. The focus is not on generating the optimal trajectories because such data trains the system only for favorable inputs. The data generated has all possible candidate trajectories, and at the same time, they are all feasible within acceptable ranges. When an AI-ML system comes across such a mixing of all possibilities, it makes the models more robust to unexpected environments. To be specific, the major contributions of this research work are as follows:

(i) The data generation removes the subjective bias and is hence more suitable for AI-ML tasks.

(ii) The generated trajectories are helpful for state prediction tasks.

(iii) The proposed takes into account 3-dimensional system dynamics as in real-time systems for generating data.

(iv) Existing work considers the multiple phases of the dynamic physical system. It hence needs initial guesses of landing parameters for every phase. The proposed design removes this multi-phase barrier, and thus possible system initialization delays are reduced through randomization.

(v) The proposed design considers only the final touchdown velocity constraint, eliminating all other constraints that are present in existing guidance laws, which guarantee soft landing trajectory computation.

1.4. Paper Organization. The entire paper is organized as follows. Section 1.1 introduces the topic with an overview of the background. Section 1.2 discusses prior AI-related works that need trajectories as the basis for training AI algorithms. Section 1.3 discusses the research contribution of this work and its benefits over existing techniques. Section 2.1 details the prerequisites needed to understand the mathematical formulation of the system better. A complete mathematical formulation and design of the proposed algorithm for autonomous trajectory generation is described in Section 2.2. Section 3 discusses results and simulations concerning the lunar power descent. Section 4 concludes the paper by describing the most significant achievements of this work.

2. Dynamic System Identification

Before formulating the system, it is necessary to understand a few concepts related to the 3-dimensional dynamics of any moving object. Every moving object possesses 3D motion dynamics about some stationary reference frame. This frame is often called the inertial frame of reference. In this case, the object is a Lunar Lander, and it is assumed to have the Moon as a stationary frame of reference. For each position, velocity parameters are calculated for this reference frame. Apart from the 3D frame of reference, once a lander starts descending, the objective is to track its decreasing altitude on the X-Y plane as it approaches the Moon's surface. This frame seems to have only 2 dimensions and is called the local vertical and local horizon frame of reference. Both these reference frames are explained in the following subsections. The following Section 2.1 is intended to make the reader understand the background and feel more comfortable reading upcoming sections.

2.1. Prerequisites

2.1.1. Inertial Frame of Reference. Newton's First Law of motion governs an inertial frame of reference. It states: "An object at rest remains at rest, and an object that is moving will continue to move straight and with constant velocity, if and only if there is no net external force acting on that object."

It means if $F_{\text{net}} = 0$ implies $v = 0$ or $\mathrm{d}v/\mathrm{d}t = 0$.

In particular, a spacecraft moving around a celestial body is assumed to move with constant velocity if no external forces are acting upon it. In the case of the Moon, there is no atmosphere, and hence there is no chance of external forces. The Moon's gravitational pull is the only force that keeps spacecraft tied to the Moon. Here the Moon is assumed to be stationary, and the spacecraft is in the inertial reference frame of the Moon.

For instance, in Figure 1, inertial reference frame M acts as a stationary observer for the spacecraft. The spacecraft with reference frame S moves at constant velocity unless other external forces acted. The spacecraft frame S is assumed to follow 3-dimensional motion dynamics and three axes (x', y', and z') of its inertial reference frame. In contrast, frame M's axes (x, y, and z) is assumed to be stationary. It is the 3D dynamics of the spacecraft and needs attention while computing trajectories.

2.1.2. Local Horizontal Local Vertical (LVLH) Frame. When a space vehicle starts descending toward the Moon, it is necessary to track its altitude and downward velocity components. This helps the vehicle control the final touchdown velocity and altitude. The assumption is to keep the X-Y plane as a constant Lunar surface to land on. The Z values keep on changing until the vehicle achieves its final altitude. The local vertical is a perpendicular axis for the Local Horizon as the lunar surface. For instance, Figure 2 shows such an LVLH frame where a vehicle is descending from altitude z_s to z_6. When it approaches the ground, it has traversed a downrange of $x_{\text{I}} + x_{\text{II}} + x_{\text{III}}$ km.

2.2. Mathematical Formulation. The lunar landing problem is solved in 3-dimensional state space governed by the physics laws. Each state parameter is a 3-dimensional vector along three axes of inertial reference frame according to the mean Earth coordinate system of the Moon. An autonomous lunar power descent phase exhibits dynamic behavior and is non-linear.

The governing motion equations for 3D non-linear system dynamics as given in [32] are given by equations as follows–:

$$\dot{r} = V, \tag{1}$$

$$\dot{\theta} = \frac{u}{r \cos \varnothing}, \tag{2}$$

$$\dot{\varnothing} = -\frac{w}{r}, \tag{3}$$

$$\dot{u} = -\frac{uv}{r} - \frac{vw}{r}\tan \varnothing + \frac{T}{m}\cos \alpha \cos \beta, \tag{4}$$

$$\dot{w} = \frac{u^2}{r}\tan \varnothing - \frac{vw}{r} + \frac{T}{m}\sin \alpha, \tag{5}$$

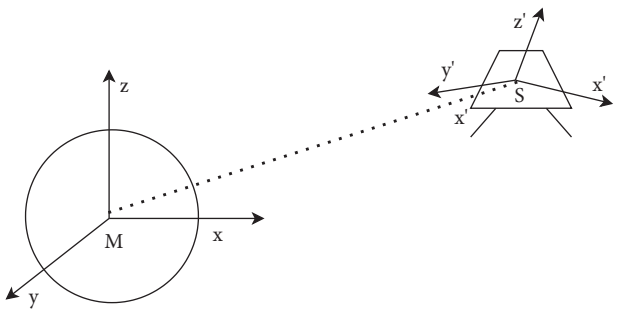

Figure 1: Inertial reference frame of spacecraft with respect to moon II.

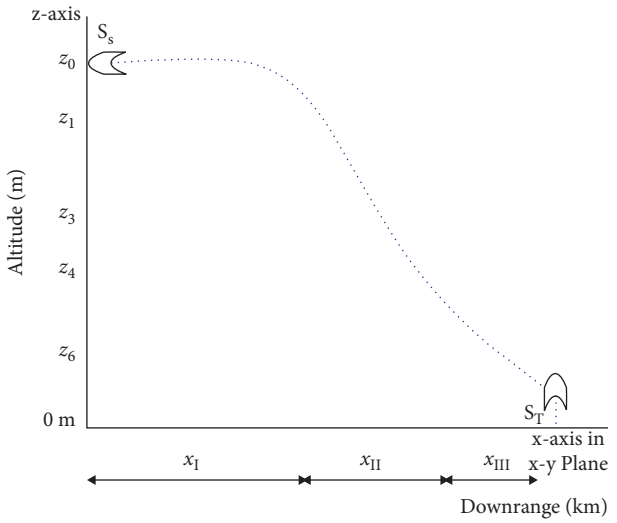

Figure 2: Local vertical local horizon (LVLH) frame.

$$\dot{v} = \frac{u^2}{r} + \frac{w^2}{r} - \frac{g_m}{r^2} - \frac{T}{m}\cos\,\alpha\,\sin\,\beta, \tag{6}$$

$$\dot{m} = -\frac{T}{I_{sp}g_0}. \tag{7}$$

The nomenclature followed with respect to the moon-centered reference frame for equations (1)–(7) is as follows:

$r = \left[\, x \;\; y \;\; z \,\right]^T$ is the distance between the current position of spacecraft and moon center (m).

θ, $\varnothing$ are the down range angle and cross range angle (degree).

$V = \left[\, u \;\; w \;\; v \,\right]^T$ are velocities along x, y, and z axes of 3D moon-centered reference frame (m/s).

$\dot{V} = \left[\, \dot{u} \;\; \dot{w} \;\; \dot{v} \,\right]^T$ is the net acceleration components along x, y, and z axes of 3D moon-centered reference frame (m/s^2).

$\dot{m}$ is the propellent mass flow rate (kg/s).

m is the mass of the spacecraft (kg).

T is the thrust magnitude (N).

α, β is the thrust Direction angles in LVLH frame.

At the start of the power descent phase, the spacecraft's altitude is less than 18 km. The gravitational acceleration is assumed to be constant, and the downrange angle is assumed to be very small in the range of 0.5 degrees. For the computation of trajectory state parameters, this simplified dynamics (equations (8)–(12)), as suggested in [33], is used.

$$\dot{r} = V, \tag{8}$$

$$\dot{V} = a - g_m, \tag{9}$$

$$a_x = \frac{T}{m}\cos\,\alpha\,\cos\,\beta, \tag{10}$$

$$a_y = \frac{T}{m}\sin\,\alpha, \tag{11}$$

$$a_z = \frac{T}{m}\cos\,\alpha\,\sin\,\beta, \tag{12}$$

where

$a = \left[\, a_x \;\; a_y \;\; a_z \,\right]^T$ is the acceleration vector.

$g_m = \left[\, 0 \;\; 0 \;\; 1.62 \,\right]^T$ is the acceleration due to the gravity of the Moon.

$\dot{r}$ is the time derivative of displacement = Velocity vector V.

$\dot{V}$ is the time derivative of velocity = Net Acceleration $(a - g_m)$.

The jerk is a time derivative of the acceleration vector as stated in

$$\begin{aligned} \dot{a} &= U, \\ U &= \left[\, u_x \;\; u_y \;\; u_z \,\right]^T. \end{aligned} \tag{13}$$

The minimum jerk guidance design [34] with constrained terminal velocity is employed to generate the acceleration command for the candidate trajectories. The minimum jerk guidance is used to minimize the following cost function as in the following equation:

$$\min_U \frac{1}{2}\int_0^{T_f} U^T U\,dt, \tag{14}$$

where T_f is the total time of flight.

2.3. Constrained System Design. Following initial values (equation (15)) are used to compute trajectories,

$$\begin{aligned} m &= 1000\,\text{kg}, \\ T &= 440\,\text{N}, \\ I_{sp} &= 310\,\text{s}, \\ g_m &= 1.62\,\text{m/s}^2, \end{aligned} \tag{15}$$

where I_{sp} is the specific impulse (s).

After solving the mass flow (16) we get mass flow rate, $\dot{m}$ = 0.1448 kg/s.

$$\dot{m} = -\frac{T}{I_{sp}g_0}. \tag{16}$$

For developing trajectories, we have randomly selected initial values of position, velocity, and final constraints are posed as given in Table 1.

Table 1: Initial position and initial velocity conditions and touchdown velocity constraints.

State parameter	Along axis	Initial condition range	Final condition range and velocity constraints
Position (m)	X	Random	Random
	Y	Random	Random
	Z	$Z < 15000$	$0 < Z < 1$
Velocity (m/s)	X	Random	0
	Y	Random	0
	Z	Random	0

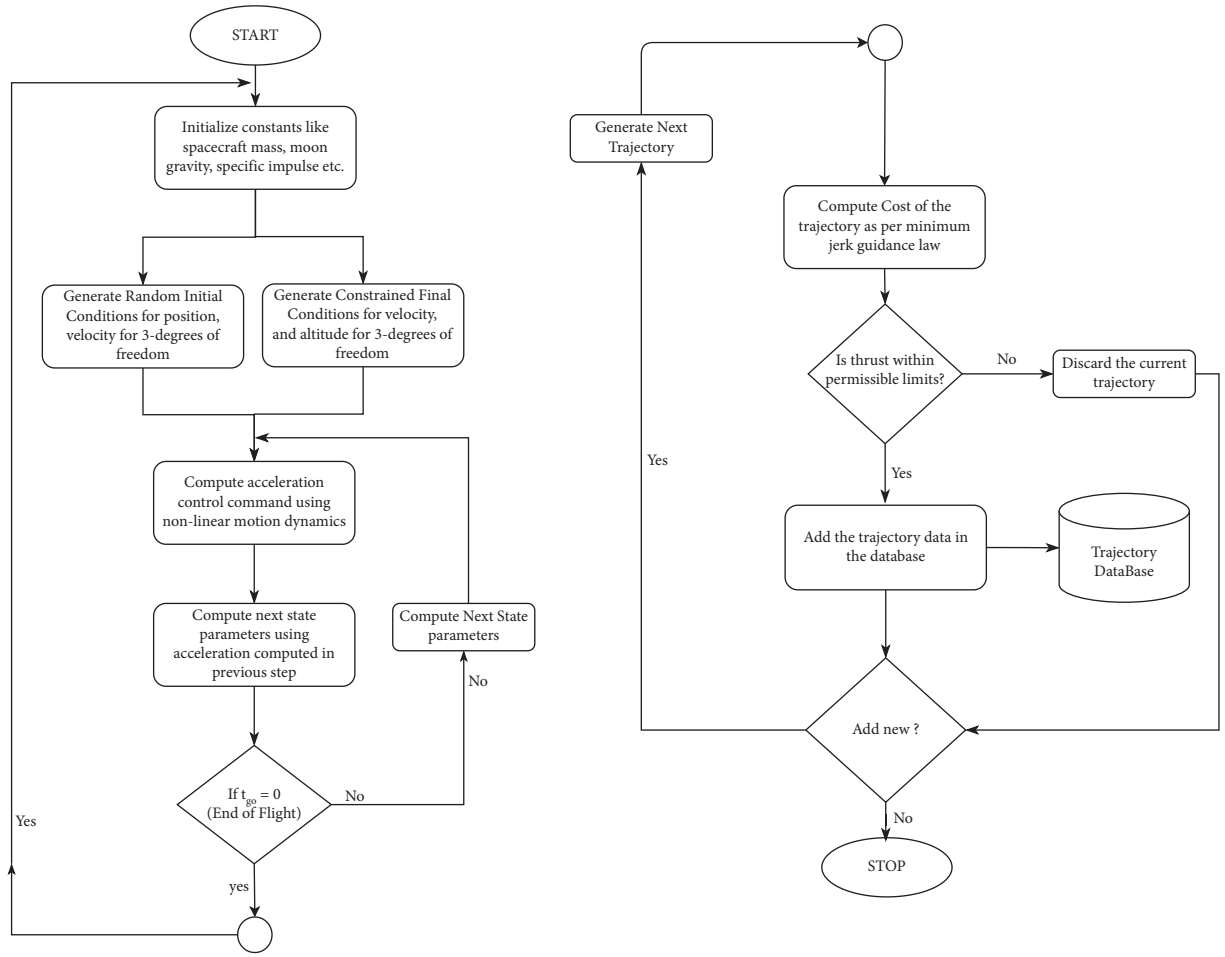

Figure 3: Trajectory generation flowchart.

The fundamental postulate regarding any physical landing system requires the final touchdown velocities to be as minimum as possible, near-zero, to minimize any hard landing possibility. This assumption forced us to put near-zero terminal velocities as a hard constraint while devising this algorithm. Along with that, a complete erect posture of the space vehicle is the one desired. It avoids the possibility of tumbling down due to imbalance. The perpendicular final thrust direction guarantees it such that the space vehicle lands softly on the landing surface. The feasibility of each generated trajectory is ascertained only after the validation of all these assumptions.

2.4. Autonomous Trajectory Generation Algorithm. Figure 3 shows a flow of the algorithm used for generating the trajectory database. This database is helpful for training machine learning models for autonomous lunar landing missions. It started with defining all constants mentioned in (15). The positions and velocities along x, y, and z directions are selected randomly from the range specified in Table 1. As the intention is to generate a hop-less trajectory, only starting and terminal constraints are known. The benefit of this algorithm is twofold: first, it is used to generate a one-shot trajectory; second, it can also be used to generate multi-hop trajectories using multiple hop-less trajectories depending on the mission demands.

Table 2: Position and velocity as a part of space vehicle state with randomized input and zero terminal velocity the constraint imposed by the algorithm for two samples.

Trajectory sample	State parameter	Along axis	Starting state parameters	Terminal state parameters
Sample[1]	Position (m)	X	14383	−29
		Y	350	−4
		Z	7799	0.26
	Velocity (m/s)	X	180	$4.5 \times e^{-12}$
		Y	9	0
		Z	−32	$0.4 \times e^{-12}$
Sample[2]	Position (m)	X	11946	−59
		Y	54	−7
		Z	3307	0.47
	Velocity (m/s)	X	208	0
		Y	7	0
		Z	−74	$0.3 \times e^{-12}$

After selecting the random positions and velocities, the next task is to compute the acceleration control command using non-linear simplified dynamics given by equations (8)–(12). Next-state parameters are computed using the previously computed acceleration. The whole process repeats till the total time of flight is reached. After the candidate trajectory is approximated, it passes through two checks: first, its thrust profile must be within the allowable non-inclusive limits i.e., $T_{\max} = 2000\,\mathrm{N}$ and $T_{\min} = 0\,\mathrm{N}$; second, the trajectory, which satisfies the minimum jerk command, is selected. Thus, a dataset with feasible reference trajectories is generated.

At each timestamp, the end of flight time is checked. For simplicity, only two values of total flight time are considered equal to 100 sec and 150 sec. The values for the total flight time are empirically chosen, giving more stable results and generating more feasible trajectories. If the end of flight time is reached, the vehicle has reached its destination. Accordingly, the current trajectory is assembled, and its cost is computed according to the minimum jerk guidance law. After computing the trajectory's cost, it has undergone a feasibility test to check if the thrusts are within permitted limits or not. Once the generated trajectory passes those two tests, it is stored in the database. Then, the initial and final constraints are initialized through the next trajectory's random function, and the procedure is repeated.

3. Results and Discussion

Experiments are performed to implement the proposed algorithm using a Python programming language. The generated trajectories are simulated to validate them analytically. A comprehensive analysis of sample trajectories is discussed in subsequent sections.

3.1. Single Trajectory Analysis. Table 2 enlists initial and final values of the position and velocity for two sample trajectories generated as an outcome of the trajectory generation algorithm. The initial and final position values are entirely random within the specified range as mentioned in Table 1. Velocity constraints are imposed while constructing these trajectories. This constraint results in the experimental touchdown velocities for samples, Sample[1] and Sample[2], almost approaching zero as demanded. The altitude of the space vehicle is also less than 1 m when the velocities approach zero. Hence, the decision can be made to allow the vehicle to free fall by switching off all engine thrusters. Thus, the generated analytical trajectories attain the best possible approximation of numerical constraints and are suitable for defining autonomous guidance law.

Further, to analyze the feasibility of the generated trajectories, simulation profiling of each state parameter is performed with respect to time. Figure 4 shows these simulations for Sample[1] trajectory from Table 2. Figure 4(a) shows position, velocity, and acceleration details along the x, y, and z axes of the moon-centered inertial reference frame. This sample trajectory exhibits the time of flight equal to 100 seconds. The convergence of all velocities and hence acceleration to numerical zero is apparent from the figure. Figure 4(b) shows the downrange profile with respect to the time axis. The altitude profile in the inertial reference frame is shown in Figure 4(c). Figure 4(c) says that the altitude is continuously decreasing and does not show an upper trend to decrease the horizontal velocity of the lander as in Figure 4(d). The altitude vs. downrange in the local vertical local horizontal (LVLH) frame is depicted in Figure 4(d). A local horizontal is an x-y plane, and the local vertical is perpendicular to this plane. Here, the space vehicle attitude is assumed along this perpendicular axis in the terminal descent phase. Figures 4(e) and 4(f) show profiles of horizontal and vertical velocity components. The velocities get reduced continuously and remain negative for the maximum period, which ascertains the decrease in altitude profile. Figures 4(g) and 4(h) are thrust and mass profiles that a trajectory follows throughout the time of the flight. The thrust profile shows thrust values along the time axis. Thrust is an external force applied to the lander that either accelerates or decelerates it to follow a specific trajectory.

3.2. Multiple Trajectory Analysis. Multiple trajectory analysis is performed to understand their state parameters' trends and compare them with other trajectory data as depicted in Figures 5–10. Figures 5–10 show altitude, downrange, angular velocity, thrust magnitude, horizontal velocity, and vertical velocity trends, respectively. 10 trajectories are randomly selected from the generated trajectory dataset, and trends are analyzed for each state parameter. Altitude and downrange profiles (Figures 5 and 6), starting with random input values, converge to their desired target values throughout the flight. The maximum change in angular velocity (Figure 7) is far less than 90 degrees and is proportional to the thrust magnitude (Figure 8) as the desired profile. A low rate of change in angular velocity guarantees less thrust application and lower fuel consumption. Horizontal velocity (Figure 9) reduces for the first few seconds as in the rough braking phase of power descent. In the end, it increases gradually to attain the zero touchdown

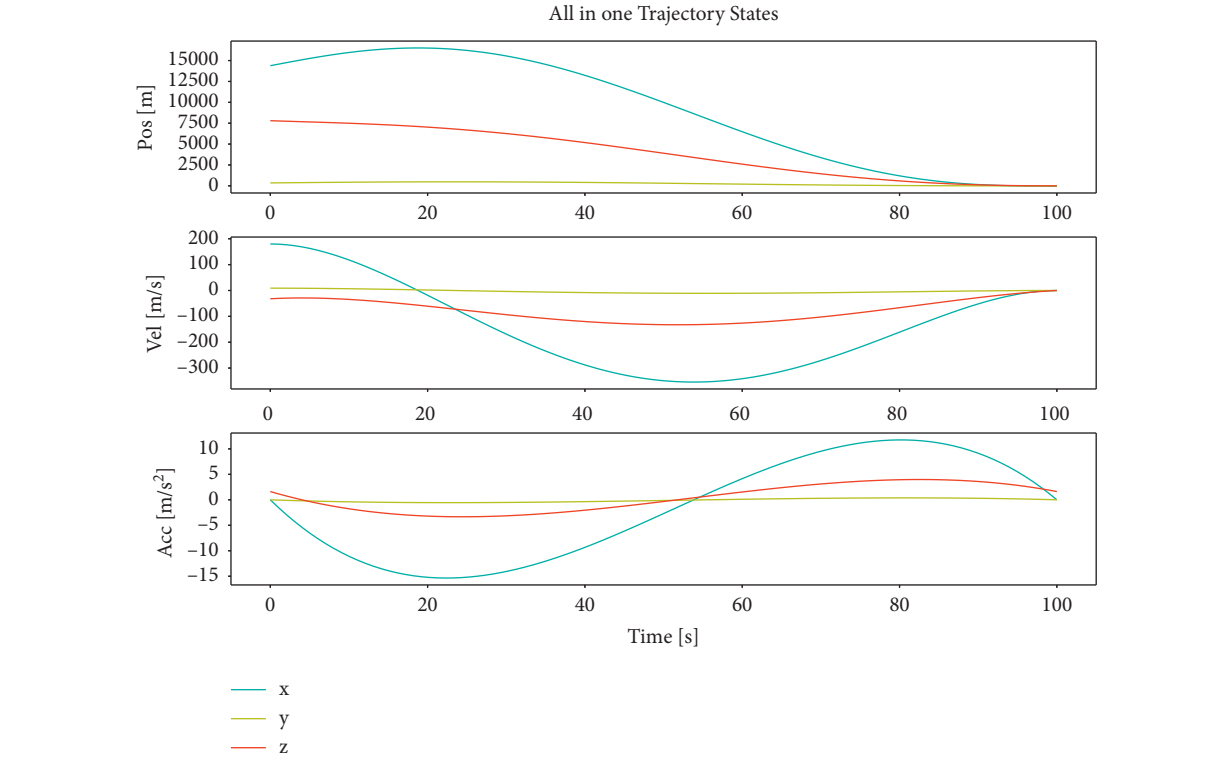

(a)

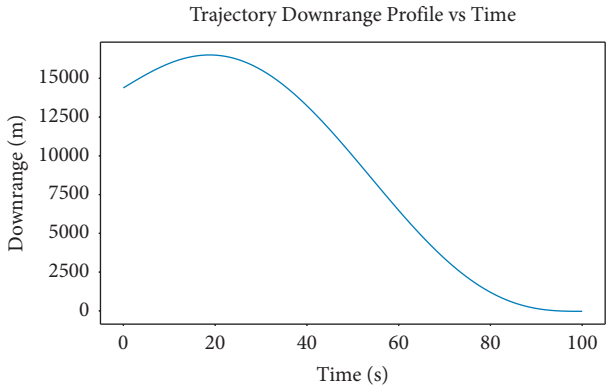

(b)

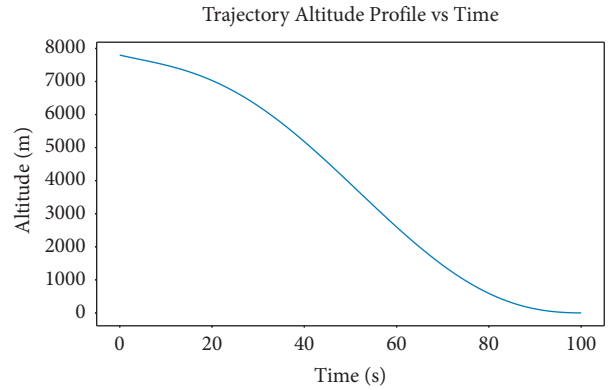

(c)

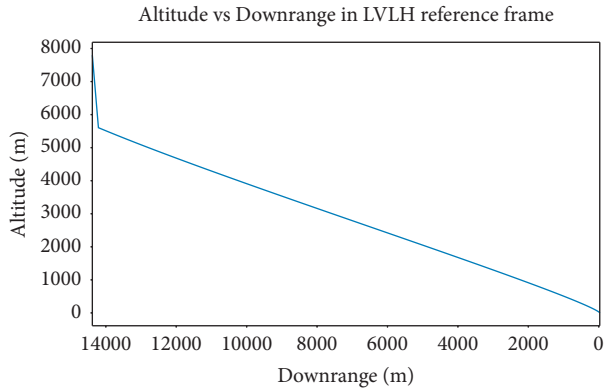

(d)

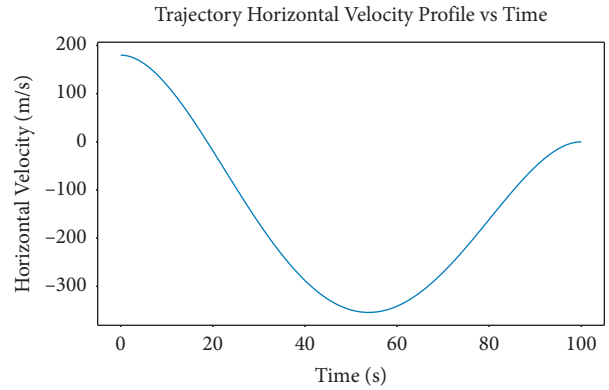

(e)

Figure 4: Continued.

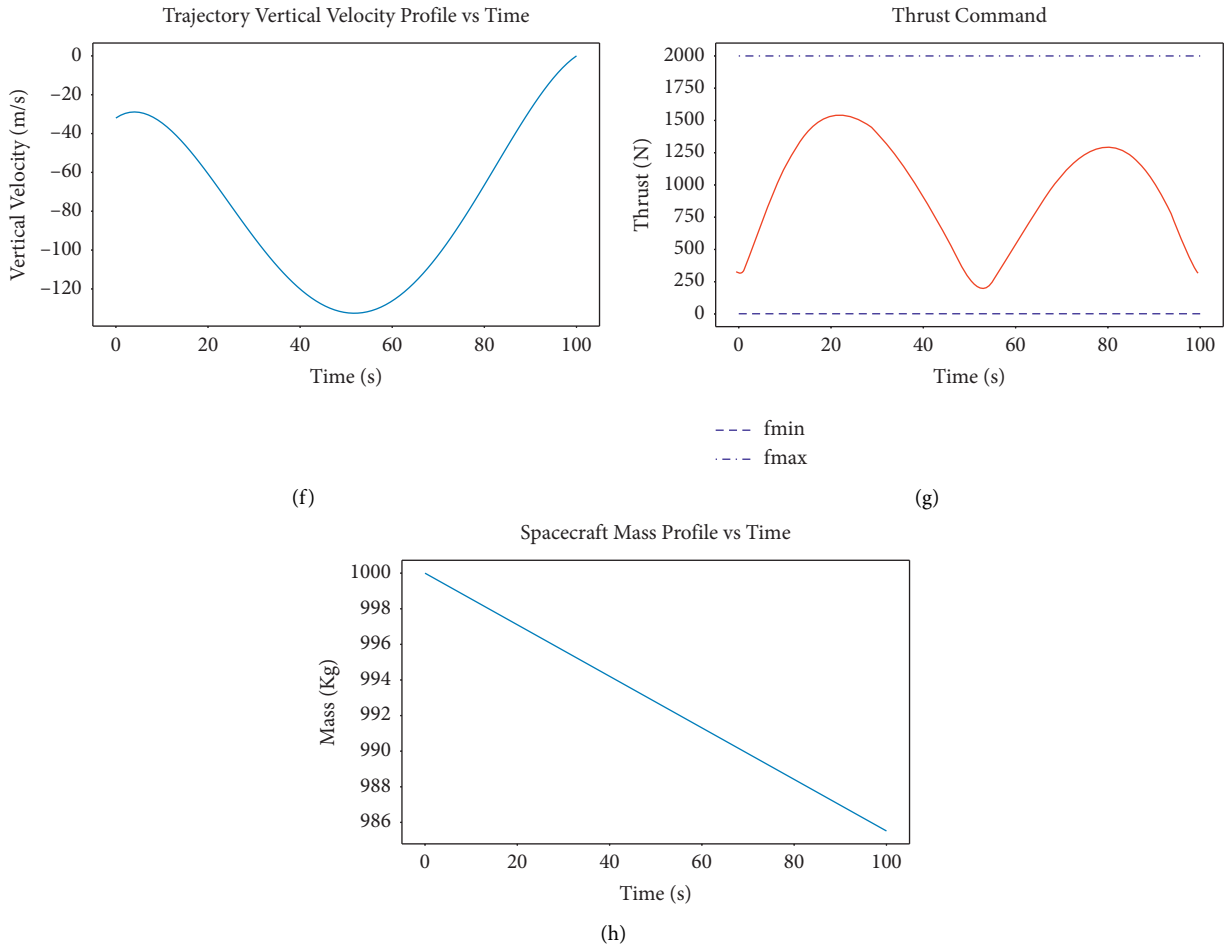

FIGURE 4: (a)–(h) Trajectory profiles for sample[1] (Table 2) at $T_f = 100$ sec. (a) Complete simulated trajectory. (b) Downrange profile. (c) Altitude profile. (d) Altitude in LVLH frame. (e) Horizontal velocity profile. (f) Vertical velocity profile. (g) Thrust profile. (h) Mass profile.

convergence. Vertical velocities (Figure 10) are changing as per hovering or maneuvering requirements of the lander but are obeying the zero touchdown constraint imposed.

3.3. Feasibility Measurement in Trajectory Computation. The algorithm tries to keep only the feasible trajectories by discarding the nonfeasible ones. We tried to measure the rate of generation of feasible trajectories in each algorithm run. The rate is defined by (17). As discussed in Section 2, the feasible candidates are found by applying two checks. The proposed algorithm is run for two values of time of flights $T_f = 100$ sec & $T_f = 150$ sec. For the first value, 4 times the algorithm is run, while 2 times it is run for the second value. The results of the feasibility rate are tabulated in Table 3 for each run. The feasible candidate generation rate of the algorithm for 100 sec flight time is 0.87, and for 150 sec flight time is 0.67. It means that the chance of getting feasible trajectories for greater flight time is the least. Regarding the power descent phase, flight time is also a tunable parameter. It needs more exhaustive experimentation to arrive at the optimal solution. It is again a new optimization problem, and it is beyond the scope of this research.

$$\text{rate}^{i}_{\text{feasible}} = \frac{\text{number of feasible candidates}^{i}}{\text{total candidates}^{i}}. \tag{17}$$

3.4. AI-ML Use Case for Usefulness of the Generated Data

3.4.1. State Prediction for Dynamic Systems. A typical AI-ML system for predicting the next state S_{i+1} of the system using the current state S_i is shown in Figure 11. The trajectory data generated through our proposed algorithm is fed to an AI-ML algorithm for training. The trajectory data contains information about all the system states S_i, where $i = T_0$ to T_f. In short, it contains all the training data with all the ground truth, which is what a supervised AI-ML system desires for training. This learning outcome is a state prediction model used to predict the next expected state of the system in real-time. An autonomous landing vehicle can use this state prediction model for making accurate maneuvering decisions.

The effectiveness of AI-ML technology is based on the quality of data used for training. This paper introduces an approach for generating such good quality data.

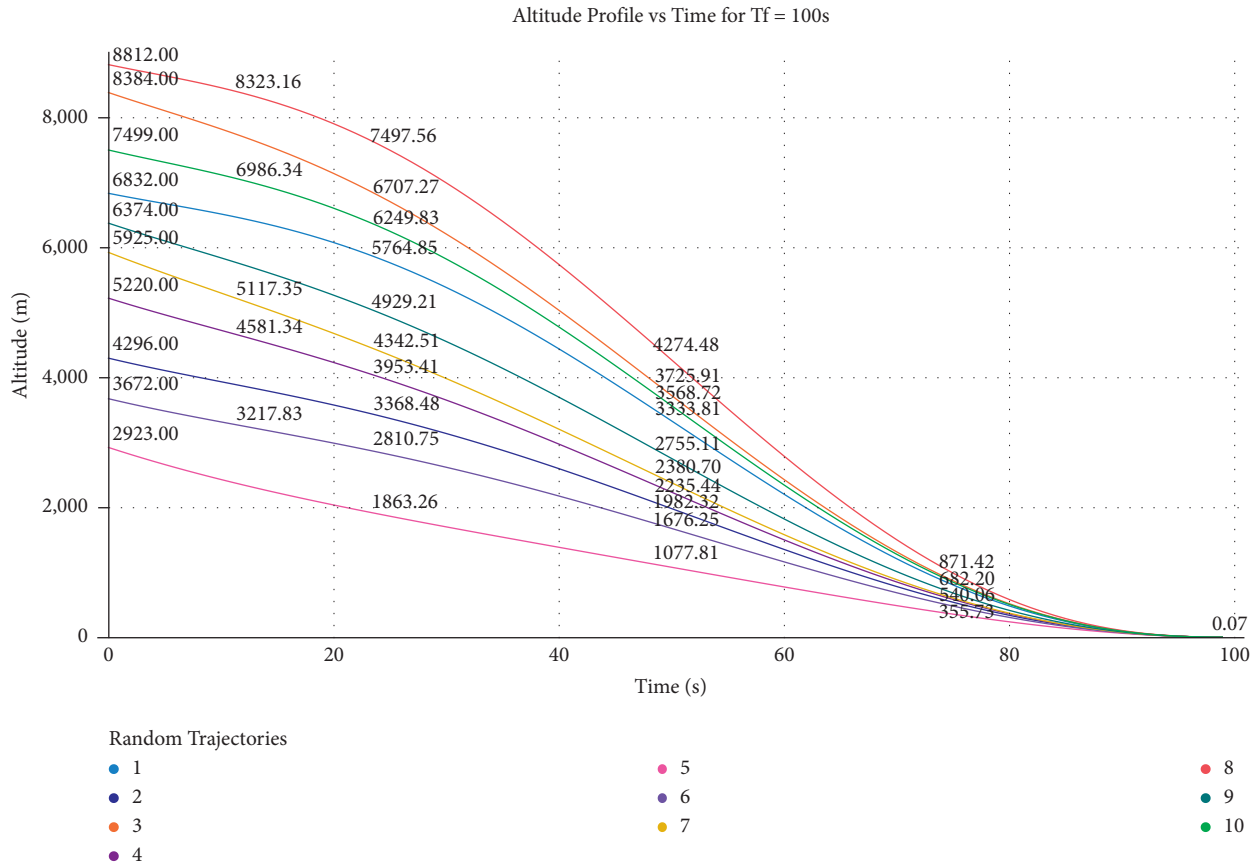

Figure 5: Trend analysis of altitude profiles for randomly selected 10 trajectories at $T_f = 100$ sec.

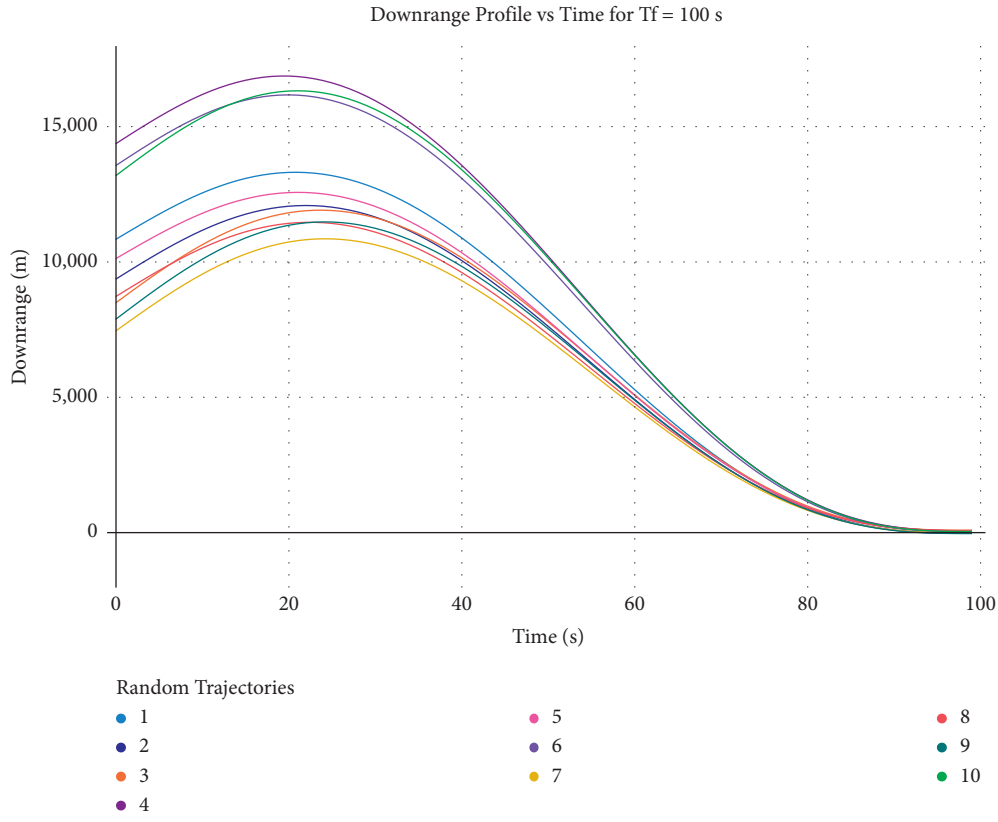

Figure 6: Trend analysis of downrange profile for randomly selected 10 trajectories at $T_f = 100$ sec.

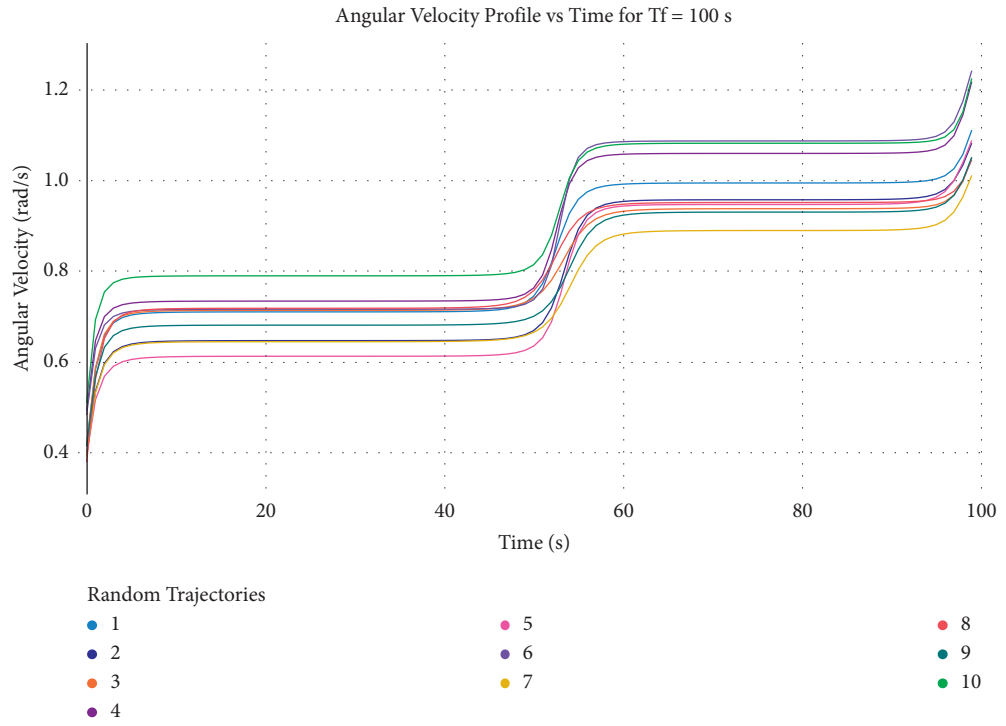

Figure 7: Trend analysis of angular velocity profile for randomly selected 10 trajectories at $T_f = 100$ sec.

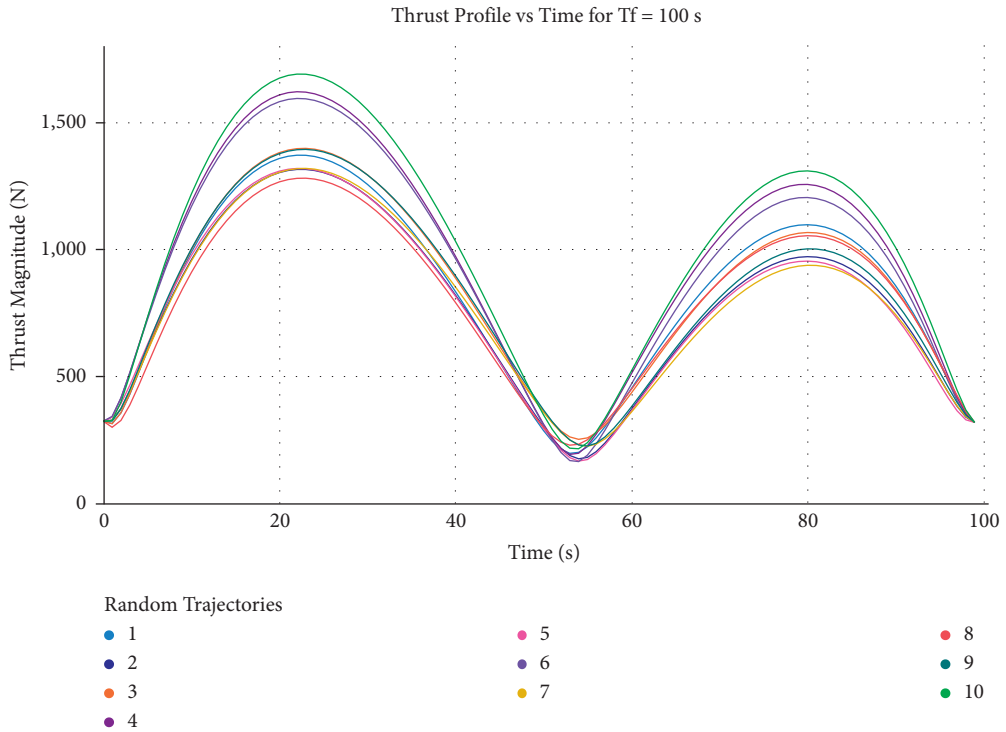

Figure 8: Trend analysis of thrust magnitude for randomly selected 10 trajectories at $T_f = 100$ sec.

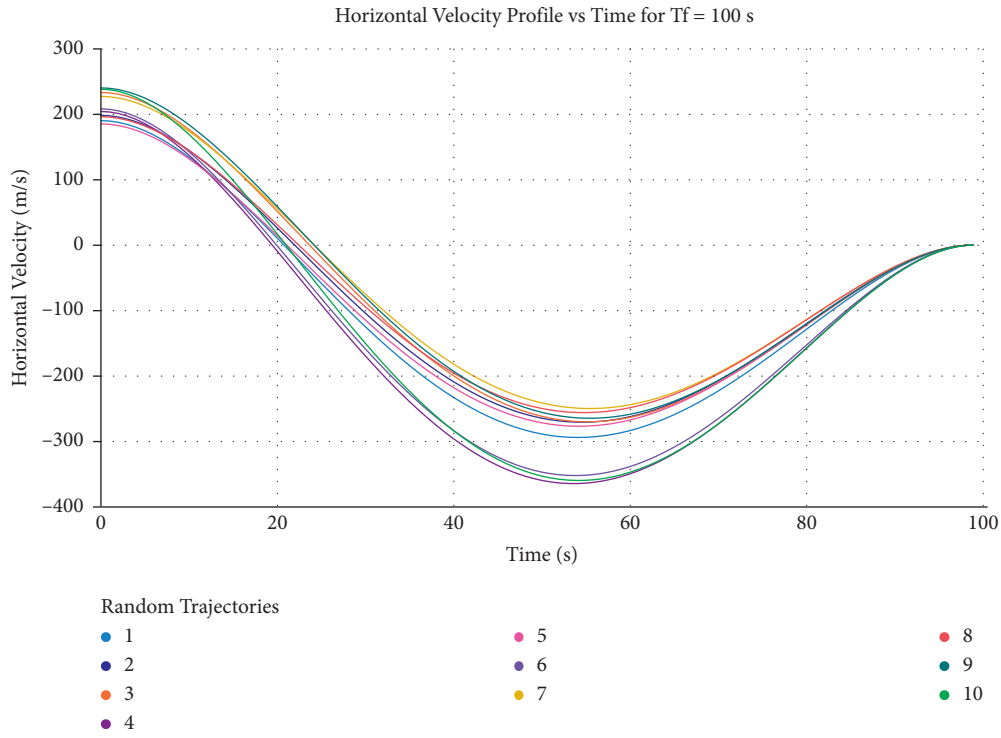

Figure 9: Trend analysis of horizontal velocity for randomly selected 10 trajectories at $T_f = 100$ sec.

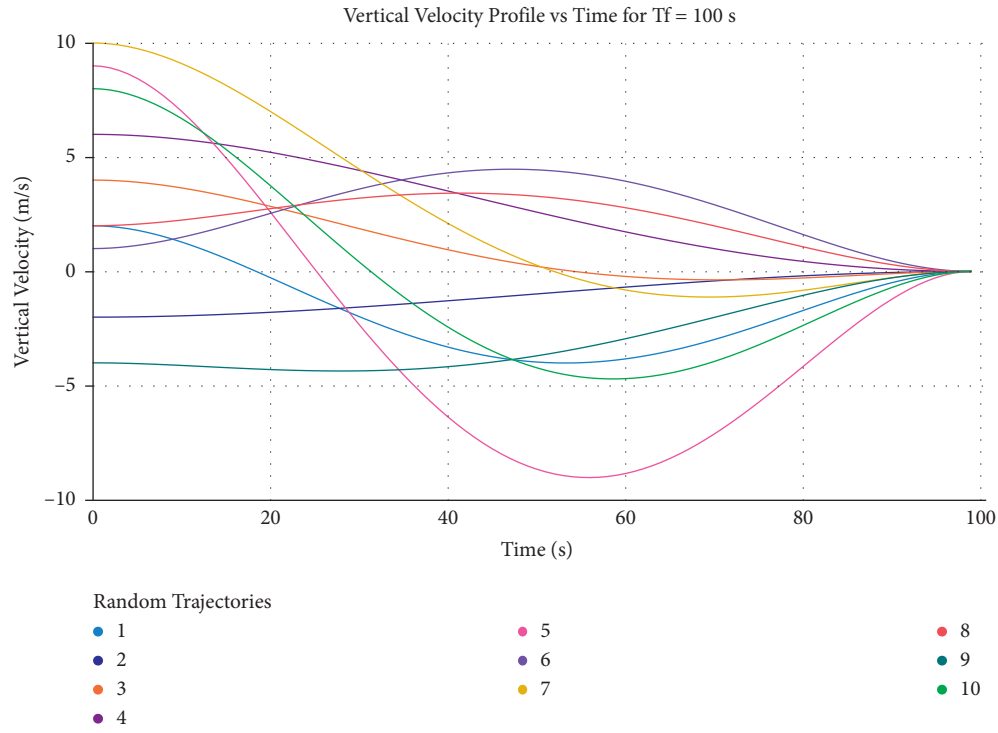

Figure 10: Trend analysis of vertical velocity for randomly selected 10 trajectories at $T_f = 100$ sec.

Table 3: Analysis of feasible trajectory generation rate of the proposed algorithm.

Time of flight	T_f = 100 sec				T_f = 150 sec	
i^{th} run	$i = 1$	$i = 2$	$i = 3$	$i = 4$	$i = 1$	$i = 2$
$rate^i_{feasible}$	0.89	0.86	0.87	0.86	0.70	0.65
Average	0.87				0.67	

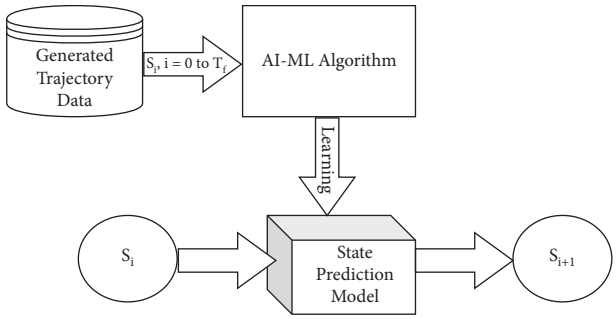

Figure 11: State prediction using AI-ML.

4. Conclusions and Future Scope

This paper presents an autonomous algorithm for generating possible candidates of feasible trajectory paths which a spacecraft would follow from a random initial state to a zero velocity end state. The algorithm is useful for training AI systems in autonomous landing missions. The presented study concentrated specifically on the lunar landing. However, the algorithm can be fine-tuned to generate trajectories for any autonomous mission. The algorithm uses 3-dimensional system dynamics with randomized inputs. It enforces a constrained terminal velocity guidance law to ensure a soft landing on the lunar surface. The actual engine design is taken into consideration while developing the proposed algorithm. Hence, the point-mass vehicle assumption of existing systems is discarded. A comprehensive analysis of generated trajectories is presented using simulation studies. It is found that the algorithm approximates the trajectories almost similar to their numerical counterparts and converges to their measured final state estimates. The generation rate of feasible trajectories measures the accuracy of the algorithm. The rate is near 0.87 for 100 sec flight time, which is reasonable accuracy. But it is also found that higher flight time significantly affects the accuracy. Flight time optimization is a further scope of research and can be targeted in future works. The overall impact of the trajectory generation algorithm is significant. It treats each state parameter with three degrees of freedom in the nonlinear sense that real-time missions require. These trajectories provide analytical measurements of dynamic state parameters and are further useful in future state predictions. It also removes the multi-hop barrier in the trajectory construction. The generated data consists of all possible solutions for proper training of AI-ML systems. The introduction of randomness in the trajectory computation minimizes the subjective bias in the training process. This research is a part of an autonomous landing project. It requires vast data to be prepared. The generated data can be used to generate prediction models for the spacecraft descent maneuver as a future task [6, 23, 24].

Data Availability

The data are available on request.

Conflicts of Interest

The authors do not have any conflicts of interest to declare.

Authors' Contributions

Janhavi H. Borse wrote the paper, Dipti D. Patil simulated the method, Vinod Kumar supervised the work, and Sudhir Kumar analyzed the method.

References

[1] M. Kaur, S. Kadam, and N. Hannoon, "Multi-level parallel scheduling of dependent-tasks using graph-partitioning and hybrid approaches over edge-cloud," *Soft Computing*, vol. 26, no. 11, pp. 5347–5362, 2022.

[2] J. H Borse, D. D Patil, and V. Kumar, "Tracking keypoints from consecutive video frames using CNN features for space applications," *Teh. Glas*, vol. 15, no. 1, pp. 11–17, 17, Mar. 2021.

[3] J. Song, D. Rondao, and N. Aouf, "Deep learning-based spacecraft relative navigation methods: a survey," *Acta Astronautica*, vol. 191, pp. 22–40.

[4] J. Liu, X. Ren, W. Yan et al., "Descent trajectory reconstruction and landing site positioning of Chang'E-4 on the lunar farside," *Nature Communications*, vol. 10, no. 1, pp. 1–10, 2019.

[5] D. Izzo and G. C. H. E. de Croon, "Nonlinear model predictive control applied to vision-based spacecraft landing," *EuroGNC*, pp. 1–17, 2013.

[6] X. Zhang, J. Ma, Z. Cheng, S. Huang, S. S. Ge, and T. H. Lee, "Trajectory generation by chance-constrained nonlinear MPC with probabilistic prediction," *IEEE Transactions on Cybernetics*, vol. 51, no. 7, pp. 3616–3629, 2021.

[7] Y. Al Younes and M. Barczyk, "Nonlinear model predictive horizon for optimal trajectory generation," *Robotics*, vol. 10, no. 3, p. 90, 2021.

[8] B. G. Park, J. S. Ahn, and M. J. Tahk, "Two-dimensional trajectory optimization for soft lunar landing considering a landing site," *International Journal of Aeronautical and Space Sciences*, vol. 12, no. 3, pp. 288–295, 2011.

[9] R. V. Ramanan and M. Lal, "Analysis of optimal strategies for soft landing on the moon from lunar parking orbits," *Journal of Earth System Science*, vol. 114, no. 6, pp. 807–813, 2005.

[10] Q. B. Peng, H. Y. Li, H. X. Shen, and G. J. Tang, "Hybrid optimization of powered descent trajectory for manned lunar mission," *Transactions of the Japan Society for Aeronautical and Space Sciences*, vol. 56, no. 3, pp. 113–120, 2013.

[11] J. Y. Zhou, K. L. Teo, D. Zhou, and G. H. Zhao, "Optimal guidance for lunar module soft landing," *Nonlinear Dynamics and Systems Theory*, vol. 10, no. 2, pp. 189–201, 2010.

[12] W. Zhang and M. Kaur, "A novel QACS automatic extraction algorithm for extracting information in blockchain-based systems," *IETE Journal of Research*, pp. 1–13, 2022.

[13] B. Mareschal, M. Kaur, V. Kharat, and S. S Sakhare, "Convergence of smart technologies for digital transformation," *Tehnički glasnik*, vol. 15, no. 1, 2021.

[14] C. N. D'Souza and C. D'Souza, "An optimal guidance law for planetary landing," *Guidance, Navigation, and Control Conference*, pp. 1376–1381, 1997.

[15] A. K. Automatica, *Apollo Lunar Descent Guidance,* Elsevier 1974, HYPERLINK ".https://www.sciencedirect.com/science/article/pii/0005109874900193."\o".https://www.sciencedirect.com/science/article/pii/0005109874900193".

[16] A. Jadhav, M. Kaur, and F. Akter, "Evolution of software development effort and cost estimation techniques: five decades study using automated text mining approach," *Mathematical Problems in Engineering*, vol. 2022, pp. 1–17, 2022, https://doi.org/10.1155/2022/5782587.

[17] J. Borse and V. K. Dipti Patil, *Deep Semantic Classification Of Visual Inputs For Hazard-Free Lunar Landing*, June, vol. 3, pp. 14–18, 2021.

[18] C. Schmierer, K. Tomilin, M. Kobald, J. Steelant, and S. Schlechtriem, "Analysis and Preliminary Design of a Hybrid Propulsion Lunar Lander," in *Proceedings of the Space Propulsion 2016Sp. Propuls*, Rome, Italy, May, 2016.

[19] M. S. Islam and I. M. Mehedi, "Landing trajectory generation and energy optimization for unmanned lunar mission," *Mathematical Problems in Engineering*, vol. 2021, pp. 2021–11.

[20] A. R. Babaei and H. Maghsoudi, "Aircraft three-dimensional hard-constrained trajectory planning using pseudospectral optimization method," *Journal of Aerospace Technology and Management*, vol. 13, p. 2021.

[21] D. Izzo, M. Märtens, and B. Pan, "A survey on artificial intelligence trends in spacecraft guidance dynamics and control," pp. 1–13, Astrodynamics, 2018.

[22] J. H. Borse and D. D. Patil, "Empirical analysis of feature points extraction techniques for space applications," *International Journal of Advanced Computer Science and Applications*, vol. 12, no. 9, pp. 81–87, 2021.

[23] R. Furfaro et al., "Deep learning for autonomous lunar landing," in *Proceedings of the 2018 AAS/AIAA Astrodynamics Specialist Conference*, pp. 1–22, Snowbird, Utah, U.S.A, Augest2018.

[24] R. Furfaro, I. Bloise, M. Orlandelli, P. Di, F. Topputo, and R. Linares, *A Recurrent Deep Architecture for Quasi-Optimal Feedback Guidance in Planetary Landing*, pp. 1–24.

[25] C. Sánchez-sánchez and D. Izzo, "Real-time Optimal Control via Deep Neural Networks," *Study on landing Problems*, pp. 1–35.

[26] Y. Song, X. Miao, L. Cheng, and S. Gong, "The feasibility criterion of fuel-optimal planetary landing using neural networks," *Aerospace Science and Technology*, vol. 116, p. 2021, Article ID 106860.

[27] L. Cheng, F. Jiang, Z. Wang, and J. Li, "Multiconstrained real-time entry guidance using deep neural networks," *IEEE Transactions on Aerospace and Electronic Systems*, vol. 57, no. 1, pp. 325–340, 2021.

[28] G. Ciabatti, S. Daftry, and R. Capobianco, "Autonomous planetary landing via deep reinforcement learning and transfer learning," in *Proceedings of the 2021 IEEE/CVF Conference on Computer Vision and Pattern Recognition Workshops (CVPRW)*, pp. 2031–2038, Nashville, TN, USA, June2021.

[29] M. Kaur, S. R. Sakhare, K. Wanjale, and F. Akter, "Early stroke prediction methods for prevention of strokes," *Behavioural Neurology*, pp. 1–9, 2022.

[30] S. L. Rexius, T. E. Rexius, T. R. Jorris, and A. V. Rao, "Advances in highly constrained multi-phase trajectory generation using the General Pseudospectral Optimization Software GPOPS," *AIAA Guidance, Navigation, and Control (GNC) Conference*, vol. 298, 2013.

[31] M. Kaur, A. Jadhav, and F. Akter, "Resource Selection from Edge-Cloud for IIoT and Blockchain-Based Applications in Industry 4.0/5.0," *Security and Communication Networks,Hindawi*, 2022.

[32] M. D. Li, M. MacDonald, C. R. McInnes, and W. X. Jing, "Analytical landing trajectories for embedded autonomy," *Proceedings of the Institution of Mechanical Engineers - Part G: Journal of Aerospace Engineering*, vol. 224, no. 11, pp. 1177–1191, 2010.

[33] D. H. Cho, D. Kim, and H. Leeghim, "Optimal lunar landing trajectory design for hybrid engine," *Mathematical Problems in Engineering*, vol. 2015, pp. 1–8, 2015.

[34] K. Uchiyama, Y. Shimada, and K. Ogawa, "Minimum-jerk guidance for lunar lander," *Transactions of the Japan Society for Aeronautical and Space Sciences*, vol. 48, no. 159, pp. 34–39, 2005.

Hindawi
Mathematical Problems in Engineering
Volume 2022, Article ID 8264359, 17 pages
https://doi.org/10.1155/2022/8264359

Research Article

Multisensor and Multitarget Tracking Based on Generalized Covariance Intersection Rule

Kuiwu Wang,[1,2] **Qin Zhang**,[1] **and Xiaolong Hu**[1]

[1]*School of Air Defense and Missile Defense, Air Force Engineering University, Xi'an 710051, China*
[2]*Graduate School of Air Force Engineering University, Xi'an 710051, China*

Correspondence should be addressed to Kuiwu Wang; wkw19971997@163.com

Received 21 March 2022; Revised 9 July 2022; Accepted 16 July 2022; Published 18 August 2022

Academic Editor: Ahmed Zeeshan

Distributed multitarget tracking (MTT) is suitable for sensors with limited field of view (FoV). Generalized covariance intersection (GCI) fusion is used to solve the MTT problem based on label probability hypothesis density (PHD) filtering in this paper. Because the traditional GCI fusion only has good fusion performance for the targets in the intersection of each sensor's FoV, and the targets outside the intersection range would be lost, this paper redivides the Gaussian components according to the FoV and distinguishes the Gaussian components of the targets inside and outside the intersection. GCI fusion is sensitive to label inconsistency between different sensors. For label fusion in the intersection region, the best match of labels is found by minimizing label inconsistency index, and then GCI fusion is performed. Finally, the feasibility and effectiveness of the proposed fusion method are verified by simulation, and its robustness is proved. The proposed method is obviously superior to local sensor and traditional GCI algorithm.

1. Introduction

MTT is a process of assigning the measurements to the targets, filtering them, and managing the tracks of multiple targets according to the time step [1, 2]. Traditional tracking algorithms, such as probabilistic data association (PDA), multiple hypothesis tracking (MHT), and others [3–6], transform the multitarget problem into a parallel single-target tracking problem by allocation of measurements. The core of its processing method is data correlation, but when there are many targets and a large number of false alarm clutter, correlation will bring combination explosion and make the calculation amount increase exponentially. Correlation error and state estimation error are coupled and influence each other, which results in large estimation error. The random finite set (RFS) provides a unified and clear framework for MTT. The first-order moment realization, that is, PHD filtering [7], avoids the complex data association problem in the process of state estimation, which can concentrate resources on tracking problems, and has good potential in solving target tracking problems under the conditions of insufficient prior knowledge and unknown number of targets. At present, it has been widely used in radar target tracking [8–10], computer vision [11], real-time positioning and map building [12], and group target tracking [13]. Among them, Gaussian mixture (GM) and sequential Monte Carlo (SMC) are two important methods of PHD operation, which are called GM-PHD [14] and SMC-PHD [15], respectively.

PHD filter has rigorous mathematical theoretical basis and can realize joint detection and tracking of targets. The structure is complete and clear, and the amount of calculation is small. However, PHD filter cannot identify the tracks of different targets in the tracking process. With the increase of targets or the approach of distances, the wrong judgment of tracks will lead to the inability of GM-PHD filter to track the targets that need attention. For PHD filter, accurate distinction of tracks is the key to ensure tracking performance [16–18]. In MTT, it is the premise of establishing the track on determining the identity of the target. The data association algorithm [19] proposed by Panta et al. provides a unique label for each target and obtains the track

of a single target through the state at each time and the association between the targets [20]. Vo et al. [21–23] also proposed label CBMeMBer filter and label multitarget Bayesian processing method, which effectively solved the track formation problem of RFS processing multitarget and belonged to the pioneering work of label RFS.

In many cases, combining the information collected by multiple sensors can improve the tracking performance. Distributed MTT algorithm has attracted a lot of attention recently because of its advantages of strong fault tolerance, high flexibility, and low computational burden compared with centralized fusion framework [24–28]. The latest method of distributed multisensor MTT is GCI [29, 30], also known as exponential mixed density (EMD) [31]. GCI fusion is equivalent to calculating and minimizing the density of Kullback-Leibler divergences [32, 33] (KLD) gains from local and avoids the problem of double calculation of common information [34]. In the past few years, many distributed RFS filters based on GCI fusion rules have been proposed [35–43], including PHD and CPHD filters [23], and the fusion density can be calculated in closed form. On the contrary, in the case of label-based RFS filter, the application of GCI fusion is not simple, because GCI fusion of label RFS density can only be calculated in a closed form under special circumstances [39]. Even if the fusion density can be calculated, its performance is very sensitive to the inevitable label inconsistency between different sensors [44].

Although GCI fusion rule has the advantage of avoiding double calculation, it has been observed that this fusion rule may be sensitive to high missed detection rate [45]. In fact, GCI fusion rules tend to keep only all tracks existing in local posterior. When the sensor has different FoV, this defect will be aggravated. Some new methods are proposed recently to deal with the target missing problem caused by different FoV in GCI fusion framework. For example, in [46], two possible solutions based on SMC-PHD filter were proposed to solve this problem. In the first method, particles from different sensors were combined only if they were considered to represent the same target. In the second method, particles corresponding to the same target were hierarchically clustered and used for state extraction. However, both methods were prone to estimation errors and underestimated the number of targets when adjacent targets appeared. In [47], a distributed fusion algorithm based on SMC-PHD filter was proposed, which abandoned the limitation of completely overlapping FoV and divided the received particles into ordinary particle set and external particle set. Based on GM-PHD filter, [48] proposed a solution to deal with different FoV under the background of simultaneous positioning and mapping. Specifically, the method of [49] was based on the idea of initializing all local PHD with uniform intensity in the whole area and modeled the uncertainty of target position in the unexplored area. A different solution was proposed in [49], which modified the traditional GCI fusion algorithm by considering the distance between Gaussian components. However, this method cannot solve the problem of false positives, and the cardinality is overestimated. Recently, some scholars have extended the labeled RFS filter to multisensors by using similar ideas [50–52], but it is more challenging to develop effective solutions under this filtering framework because possible label inconsistencies need to be considered.

In order to solve the target omission problem of distributed multisensor PHD filtering based on GCI fusion rules, a stable and effective fusion method is proposed in this paper, which makes the fusion results not affected by fusion mismatch in GCI-PHD fusion generated by multisensors with limited FoV. The method includes two parts: Firstly, by analyzing the GCI fusion mismatch caused by the limited field sensor, whether the Gaussian component falls into the field intersection area is divided and differentiated; secondly, the problem of label inconsistency in GCI fusion is analyzed. For the fusion of labels in the intersection area, the best match of labels is found by minimizing the label inconsistency index, and then GCI fusion is implemented. The targets not in the intersection area of FoV are directly added to the final multitarget state according to the state provided by each sensor and the labels.

The subsequent chapters are arranged as follows: the second section introduces the traditional PHD filtering and GCI fusion rules; the third section analyzes the problems in the GCI fusion process, including fusion mismatch analysis and label inconsistency analysis, and introduction, including the distinction of Gaussian components and the improvement of label fusion; Section 5 verifies the effectiveness of the algorithm through linear simulation experiments; Section 6 is the conclusion. Table 1 lists the acronyms in the text.

2. Background

For MTT, under the condition of missing detection and clutter, we focus on solving the problem of estimating the unknown number of target states through the measurement data provided by sensors. Assuming the location of the sensors is known, each sensor s has a finite FoV, defined as

$$FoV_s = \{x \in X:\ p_D^s(x) > 0\}. \tag{1}$$

Among them, p_D^s represents the detection probability of the sensor s in the limited field of view. And different sensors have different FoV (usually depending on sensor type, location, and orientation).

The detection range of the sensor s is denoted by FoV_s, and $R[\cdot]$ denotes the detection range that can be sensed by all sensors. Figure 1 below shows a sensing network consisting of two sensors; then the detection range of the first sensor is

$$FoV_1 = R[1] \cup R[3], \tag{2}$$

where $R[i]$ denotes the ith region, which satisfies $\forall i \neq j$, $R[i] \cap R[j] = \varnothing$. The whole detection region R can be expressed as

$$R = \bigcup_{i=1}^{3} R[i]. \tag{3}$$

2.1. PHD Filtering. Consider the following MTT scenario, where the target state set is $X_k = \{x_k^1, \cdots, x_k^{N_k}\}$ and the measurement set is $Z_k = \{z_k^1, \cdots, z_k^{M_k}\}$, where x_k^n and z_k^m

Table 1: List of notation.

MTT	Multitarget tracking
FoV	Field of view
GCI	Generalized covariance intersection
PHD	Probability hypothesis density
PDA	Probabilistic data association
MHT	Multiple hypothesis tracking
RFS	Random finite set
SMC	Sequential Monte Carlo
GM	Gaussian mixture
EMD	Exponential mixed density
KLD	Kullback-Leibler divergences

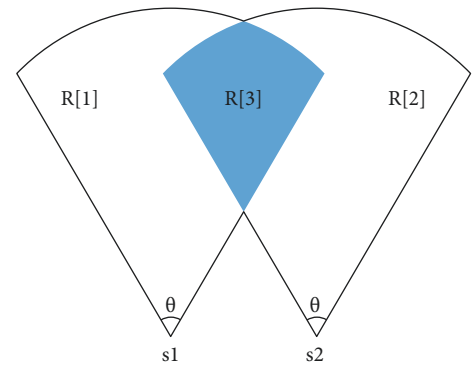

Figure 1: Distributed sensor network with limited field of view.

represent the nth target state and the mth measurement at time k, respectively. N_k and M_k are the number of targets and the number of measurements at time k, respectively. Assuming that the prior probability of multitarget approximately obeys Poisson distribution, with the help of random finite set statistics theory, the PHD recurrence equation [7] is

$$\begin{aligned} D_{k|k-1}(x) &= \int \left(p_{s,k|k-1} f_{k|k-1}(x|\zeta)\right) + \beta_{k|k-1}(x|\zeta) D_{k-1|k-1}(\zeta)\mathrm{d}\zeta + \gamma_k(x) \\ D_{k|k}(x) &= \left[1 - P_{D,k}\right] D_{k|k-1}(x) + \sum_{z_k \in Z_k} \frac{P_{D,k} g_k(z|x) D_{k|k-1}(x)}{\lambda c(z_k) + \int P_{D,k} g_k(z|\zeta) D_{k|k-1}(\zeta)\mathrm{d}\zeta}, \end{aligned} \tag{4}$$

$\gamma_k(x)$ and $\beta_{k|k-1}(x|\zeta)$ represent the target intensity of newborn and derived RFS, respectively [55], $p_{s,k|k-1}$ represent the survival probability of target at time $k-1$, and $p_{s,k|k-1} = p_{s,k-1}$, $P_{D,k}$ represent the detection probability of target at time k, $f_{k|k-1}(x|\zeta)$ represents the probability density function of state transition, $g_k(z|x)$ is the likelihood function of single target, λ is the average clutter number, and $c(z_k)$ obeys Poisson distribution. Poisson's RFS X multitarget density $\pi(X)$ takes the following form:

$$\pi(X) = \exp\left(-\int_X D(x)\mathrm{d}x\right) \prod_{x \in X} D(x). \tag{5}$$

Given a region $\chi \in X$, the number of prediction targets in the region can be calculated as $\int_{x \in \chi} D(x)\mathrm{d}x$, and the total number of prediction targets in the whole state space is $\int_X D(x)\mathrm{d}x$.

GM-PHD filter expresses the prior PHD and the posterior PHD of multiple targets as GM formation, and its iterative recursion can be expressed as a prediction update structure similar to Kalman filter (KF).

Assume that the multitarget posterior PHD at time $k-1$ can be expressed as GM, and the equation is as follows [53]:

$$D_{k-1}(x) = \sum_{i=1}^{J_{k-1}} w_{k-1}^i N\left(x; m_{k-1}^i, p_{k-1}^i\right), \tag{6}$$

where J_{k-1} is the number of Gaussian components at time $k-1$. w_{k-1}^i is the weight of the ith Gaussian component, and m_{k-1}^i and p_{k-1}^i present the mean and covariance of the ith Gaussian component.

The newborn and derived Gaussian components can be represented by a Gaussian mixture term [53]:

$$\begin{aligned} \gamma_k(x) &= \sum_{j=1}^{J_{\gamma,k}} w_{\gamma,k}^j N\left(x; m_{\gamma,k}^j, p_{\gamma,k}^j\right), \\ D_{\beta_{k|k-1}}(x) &= \sum_{j=1}^{J_{\beta,k}} w_{\beta,k}^j N\left(x; m_{\beta,k-1}^j, Q_{\beta,k-1}^j\right). \end{aligned} \tag{7}$$

Among them, $J_{\gamma,k}$ and $J_{\beta,k}$ represent the number of newborn and derived Gaussian components at time k, respectively. $w_{\gamma,k}^j$ and $w_{\beta,k}^j$ represent the weights of the newborn and derived j-th Gaussian components at time k, respectively. $m_{\gamma,k}^j$ and $p_{\gamma,k}^j$ are the mean and covariance of the j-th newborn Gaussian component, respectively. $m_{\beta,k-1}^j = F_{\beta,k-1}^j m_{k-1} + d_{\beta,k-1}^j$ and $Q_{\beta,k-1}^j$ are the mean and covariance of the j-th derived Gaussian component, respectively.

Then the multitarget prior PHD at time k can be expressed as [53]

$$D_{k|k-1}(x) = \gamma_k(x) + D_{\beta_{k|k-1}}(x) + D_{sv_{k|k-1}}(x), \tag{8}$$

where $D_{\beta_{k|k-1}}(x)$ and $D_{sv_{k|k-1}}(x)$ are the Gaussian mixture intensity functions of the derived and surviving targets, respectively, $J_{k|k-1}$ is the number of Gaussian components to predict PHD, w_{kk-1}^i, $m_{k|k-1}^i$, and $p_{k|k-1}^i$ are the weight, mean, and covariance of the ith Gaussian component in the predicted intensity function, respectively, w_k^j, m_k^j, and p_k^j are the update weights, mean, and covariance of the j-th component in the intensity function.

The derived Gaussian component intensity can be expressed as [53]

$$D_{\beta_{k|k-1}}(x) = \sum_{i=1}^{J_{k1|k-1}} \sum_{j=1}^{J_{\beta,k}} w_{k-1|k-1}^{i} w_{\beta,k}^{j} N\left(x; m_{\beta,k-1}^{i,j}, Q_{\beta,k-1}^{i,j}\right), \quad (9)$$

where

$$\begin{aligned} m_{\beta,k-1}^{i,j} &= F_{\beta,k-1}^{j} m_{k-1|k-1}^{i} + d_{\beta,k-1}^{j}, \\ Q_{\beta,k-1}^{i,j} &= F_{\beta,k-1}^{j} p_{k}^{i} \left(F_{\beta,k-1}^{j}\right)^{T} + Q_{\beta,k-1}^{j}. \end{aligned} \quad (10)$$

The surviving Gaussian component intensity can be expressed as [53]

$$D_{sv_{k|k-1}}(x) = p_{s,k|k-1} \sum_{i=1}^{J_{k-1|k-1}} w_{k-1|k-1}^{i} N\left(x; m_{sv,k|k-1}^{i}, p_{sv,k|k-1}^{i}\right), \quad (11)$$

where

$$\begin{aligned} m_{sv,k|k-1}^{i} &= F_{k-1} m_{k-1|k-1}^{i}, \\ p_{sv,k|k-1}^{i} &= F_{k-1} p_{k-1|k-1}^{i} F_{k-1}^{T} + Q_{k-1}, \end{aligned} \quad (12)$$

where F_{k-1} is the state transition matrix and Q_{k-1} is the process noise covariance. Then the k-time prior multitarget PHD can be expressed as a Gaussian mixture form [53].

$$D_{k|k-1}(x) = \sum_{i=1}^{J_{k|k-1}} w_{k|k-1}^{i} N\left(x; m_{k|k-1}^{i}, p_{k|k-1}^{i}\right). \quad (13)$$

Among them, $w_{k|k-1}^{i} = p_{s,k-1} w_{k-1|k-1}^{i}$ represents the prior weight from the posterior weight at time k-1. $J_{k|k-1} = J_{k-1|k-1}(1 + J_{\beta,k}) + J_{\gamma,k}$ represents the number of prior Gaussian components at time k.

Then, the posterior intensity at time k is as follows [53]:

$$\begin{aligned} D_{k}(x) &= \left[1 - P_{D,k}\right] D_{k|k-1}(x) \\ &\quad + \sum_{l=1}^{m_k} \sum_{i=1}^{J_{k|k-1}} w_{k|k}^{i}\left(z_{k}^{l}\right) N\left(x; m_{k|k}^{i,l}, p_{k|k}^{i,l}\right), \end{aligned} \quad (14)$$

where

$$w_{k|k}^{i}\left(z_{k}^{l}\right) = \frac{P_{D,k} w_{k|k-1}^{i} g_{k|k-1}\left(z|m_{k|k-1}^{i}, p_{k|k-1}^{i}\right)}{\lambda c\left(z_{k}^{l}\right) + P_{D,k} \sum_{j=1}^{J_{k|k-1}} w_{k|k-1}^{i} g_{k|k-1}\left(z|m_{k|k-1}^{j}, p_{k|k-1}^{i}\right)}, \quad (15)$$

$$K_{k}^{i} = \widehat{p}_{k|k-1}^{i} H_{k}^{T}\left[H_{k} \widehat{p}_{k|k-1}^{i} H_{k}^{T} + R_{k}\right]^{-1}, \quad (16)$$

$$\widehat{m}_{k}^{i} = \widehat{m}_{k|k-1}^{i} + K_{k}^{i}\left(z_{k}^{l} - H_{k} \widehat{m}_{k|k-1}^{i}\right), \quad (17)$$

$$\widehat{p}_{k|k}^{i} = \left[I - K_{k}^{i} H_{k}\right] \widehat{p}_{k|k-1}^{i}. \quad (18)$$

R_k is the measurement noise covariance matrix, and I is the identity matrix.

The number of predicted targets $\widehat{N}_{k|k-1}$ and $\widehat{N}_{k}$ associated with $D_{k|k-1}$ and D_k is obtained by the following equation [54]:

$$\begin{aligned} \widehat{N}_{k|k-1} &= \widehat{N}_{k-1}\left(p_{s,k} + \sum_{j=1}^{J_{\beta,k}} w_{\beta,k}^{j}\right) + \sum_{j=1}^{J_{\gamma,k}} w_{\gamma,k}^{j}, \\ \widehat{N}_{k} &= \widehat{N}_{k|k-1}\left(1 - p_{D,k}\right) + \sum_{z \in Z_k} \sum_{j=1}^{J_{k|k-1}} w_{k}^{j}(z), \end{aligned} \quad (19)$$

where $J_{\beta,k}$ and $J_{\gamma,k}$ represent the number of derived Gaussian components and newborn Gaussian components at time k, respectively. Therefore, at time k, the number of Gaussian components of D_k is $J_k = (J_{k-1}(1 + J_{\beta,k}) + J_{\gamma,k})(1 + |Z_k|)$.

2.2. GCI Fusion Rules. $\pi_k^1(X)$ and $\pi_k^2(X)$ of two multitarget posterior probability density functions are considered based on the measurement sets from two different sensors. When the correlation between two measurement sets is unknown, two multitarget posteriori can be fused by GCI fusion rule [29]. Under GCI fusion rule, two multitarget posterior probability density functions are fused to obtain

$$\pi_k^{1,2}(X) = \frac{\pi_k^1(X)^{\omega_1} \pi_k^2(X)^{\omega_2}}{\int \pi_k^1(X)^{\omega_1} \pi_k^2(X)^{\omega_2} \delta X}, \quad (20)$$

where ω_1 and ω_2 are the weights that determine the relative importance of each multitarget posteriori, satisfying $\omega_1 + \omega_2 = 1$. One method of weight selection is the Metropolis weight selection method [55]. It can guarantee fusion convergence. Another method is to select the cost function that minimizes the target weights according to the optimization process [56]. The fusion density provided by the fusion rule (20) is a minimization of the weighted sum of the KLD with respect to the density to be fused.

$$\pi_k^{1,2} = \arg\inf_{\pi}\left(\omega_1 D_{KL}\left(\pi \| \pi_k^1\right) + \omega_2 D_{KL}\left(\pi \| \pi_k^2\right)\right). \quad (21)$$

Among them

$$D_{KL}\left(\pi \| \pi_k^i\right) \triangleq \int \pi(X) \log \frac{\pi(X)}{\pi^i(X)} \delta X. \quad (22)$$

The density of N_s multitargets and their corresponding fusion weights are paired into a set; that is, $\prod = (\pi_s, \omega_s)_{s \in N_s}$; GCI divergence $G(\prod)$ is defined as [57]

$$G\left(\prod\right) = \min_{\pi} \sum_{s \in N} \omega_s D_{KL}(\pi \| \pi_s) = -\log c\left(\prod\right). \quad (23)$$

Among them

$$c\left(\prod\right) = \int \prod_{s \in N} \left[\pi_s(X)\right]^{\omega_s} \delta X, \quad (24)$$

where the GCI coefficient $c(\prod)$ satisfies $0 < c(\prod) < 1$.

For simplicity, only two sensors are considered.

According to GCI fusion rules, Poisson RFS with PHDs $D_k^1(x)$ and $D_k^2(x)$ are fused to produce a Poisson RFS fused with PHD

$$D_k^{1,2}(x) = \left[D_k^1(x)\right]^{\omega_1} \left[D_k^2(x)\right]^{\omega_2}. \quad (25)$$

When PHD is represented by GM, the above results cannot be calculated in closed form because the exponent of GM cannot be GM, so there is an approximation strategy to approximate each power $[D_k^l(x)]^{\omega_l}$ to a GM. For example,

$$\left[D_k^l(x)\right]^{\omega_l} = \sum_{i=1}^{N^l} \widetilde{\alpha}_{k,i}^l N\left(x; \widetilde{m}_{k,i}^l, \widetilde{p}_{k,i}^l\right), \tag{26}$$

where $\widetilde{m}_{k,i}^l$ is the mean of the ith Gaussian component of sensor l at time k, $\widetilde{p}_{k,i}^l$ is the covariance of the ith Gaussian component of sensor l at time k, and $\widetilde{\alpha}_{k,i}^l$ is the weight of the ith Gaussian component of sensor l at time k. Then, compute the fusion PHD

$$D_k^{1,2}(x) = \sum_{i=1}^{N^1} \sum_{j=1}^{N^2} \alpha_{k,i,j}^{1,2} N\left(x; m_{k,i,j}^{1,2}, p_{k,i,j}^{1,2}\right). \tag{27}$$

Among them

$$p_{k,i,j}^{1,2} = \left[\left(\widetilde{p}_{k,i}^1\right)^{-1} + \left(\widetilde{p}_{k,j}^2\right)^{-1}\right]^{-1}, \tag{28}$$

$$m_{k,i,j}^{1,2} = p_{k,i,j}^{1,2}\left[\left(\widetilde{p}_{k,i}^1\right)^{-1} \widetilde{m}_{k,i}^1 + \left(\widetilde{p}_{k,j}^2\right)^{-1} \widetilde{m}_{k,j}^2\right], \tag{29}$$

$$\alpha_{k,i,j}^{1,2} = \widetilde{\alpha}_{k,i}^1 \widetilde{\alpha}_{k,j}^2 N\left(\widetilde{m}_{k,i}^1 - \widetilde{m}_{k,j}^2; 0, \widetilde{p}_{k,i}^1 + \widetilde{p}_{k,j}^2\right). \tag{30}$$

$m_{k,i,j}^{1,2}$, $p_{k,i,j}^{1,2}$, and $\alpha_{k,i,j}^{1,2}$ are the mean, covariance, and weight of the fused Gaussian components, respectively.

3. Problem Analysis

3.1. GCI Fusion Mismatch Analysis. This paper analyzes the situation of GCI fusion when it is applied to different *FoV* sensors by actual scene and discusses the reasons why GCI fusion may fail in this case.

Considering a distributed sensor network with two sensors, GM-PHD filtering is used for tracking. The observation area is $[-2000, 2000] \times [0, 2000]\,(\mathrm{m}^2)$. For simplicity, the two targets move in a circle. The survival probability is $p_{s,k} = 0.99$, and the positions of the two sensors are $p_1 = [-1000, 0]^T$, $p_2 = [500, 0]^T$.

Each sensor has a limited *FoV*, which can only detect targets with relative angles in the interval $[-60^\circ, 60^\circ]$. Detect probability $p_{D,k} = 0.98$ in *FoV*; otherwise it is 0. The true trajectory is shown in Figure 2, and the cardinality estimation is shown in Figure 3.

As can be seen from Figure 2, Target 1 can only be detected by Sensor 1, and Target 2 can only be detected by Sensor 2. Therefore, the PHD of Sensor 1 does not contain a Gaussian component representing Target 2, whereas the PHD of Sensor 2 does not contain a Gaussian component representing Target 1, and the Gaussian component of Sensor 1 and the Gaussian component of the Sensor 2 are far apart. The result is that the tracking performance after fusion is obviously worse than that of a single sensor, and the number of targets after fusion is 0.

The essence of GCI fusion rule is the weighted multiplication between target densities. Only when both sensors detect the same target can the fusion process proceed normally. When a sensor does not detect a target, its PHD would approach zero in the corresponding region of the state space. Even if another sensor can detect the target and there are Gaussian components with nonnegligible weights in this region, the application of GCI fusion rules would significantly reduce such weights. Targets may be lost in the fused multitarget distribution, as happens in simulation. It can also be seen from GCI fusion, implemented based on the GM method (18), that large distances between Gaussian components result in small fusion weights because $N(\widetilde{m}_{k,i}^1 - \widetilde{m}_{k,j}^2; 0, \widetilde{p}_{k,i}^1 + \widetilde{p}_{k,j}^2)$ tends to zero as $\widetilde{m}_{k,i}^1 - \widetilde{m}_{k,j}^2$ increases.

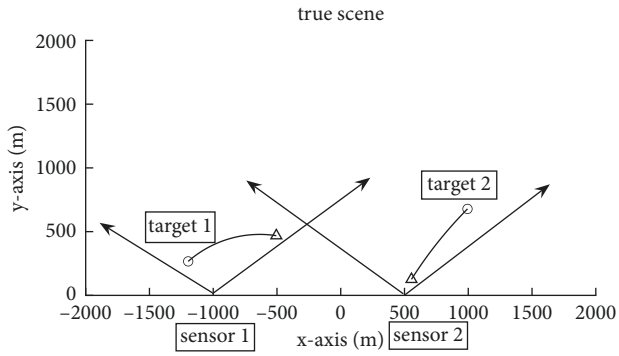

Figure 2: Real track.

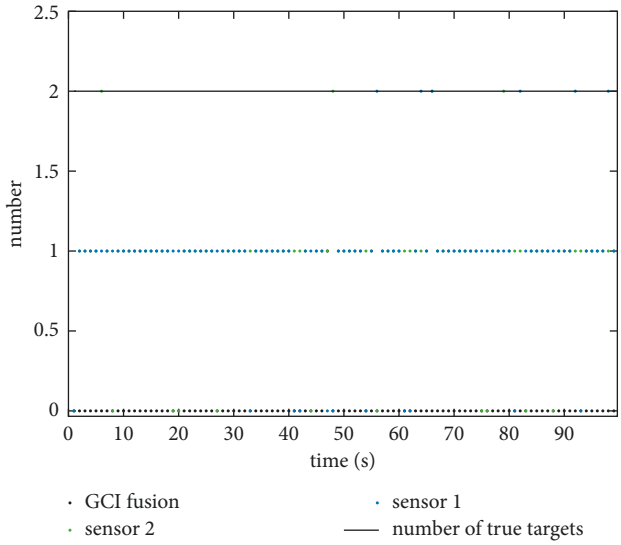

Figure 3: Estimated number of targets.

3.2. Label Inconsistency Analysis. In addition to PHD fusion, in order to form continuous tracks, Gaussian components also carry corresponding label information [57], so it is also necessary to fuse corresponding labels, and each Gaussian component is assigned a unique label

$$\Gamma_0 = \left\{\tau_0^1, \ldots, \tau_0^{J_k}\right\}, \tag{31}$$

τ_0^i represents the label of the ith Gaussian component.

Due to the inherent hypothesis of complete consistency between labels of different sensors, the parallelization of GCI

is actually realized. However, as pointed out in [57], it is precisely because of this inherent hypothesis that when labels are inconsistent, the performance of GCI fusion would drop sharply, which is called label inconsistency. Label inconsistency means that the same target is assigned different labels in different sensors.

In practice, even if the local filter works well, GCI fusion may not produce accurate results because the hypothesis of label consistency is difficult to guarantee. There are many reasons for label inconsistency, such as uncertainty in measurement, that is, noise, clutter, and low detection probability; take local pruning operation, etc.

Consider a set of multitarget densities and corresponding weights $\prod = \{(\pi_s, \omega_s)\}_{s\in N}$, where each π_s is defined in $F(X \times \tau_s)$ and supports $F(X \times \Gamma_s)$. Each π_s is an unlabeled version of π_s; given a set of unlabeled target states, and $x_1, \cdots, x_n$, the label information is described by the conditional joint probability distribution of its corresponding label $\tau_1, \cdots, \tau_n$.

$$\varpi(\{(\tau_1|x_1), \ldots, (\tau_n|x_n)\}) = \frac{\boldsymbol{\pi}(\{(\tau_1|x_1), \ldots, (\tau_n|x_n)\})}{\pi(\{x_1, \ldots, x_n\})}. \tag{32}$$

Among them, $\pi(\{x_1, \ldots, x_n\})$ accords the following marginal distribution [58].

$$\pi(\{x_1, \ldots, x_n\}) = \sum_{(\alpha_1,\ldots,\alpha_n)\in\Gamma^n} \boldsymbol{\pi}(\{(x_1|\alpha_1), \ldots, (x_n|\alpha_n)\}). \tag{33}$$

For n object states $x_1, \ldots, x_n$, they are labeled as Γ^n, and each marked mode can be expressed as a vector $(\alpha_1, \ldots, \alpha_n) \in \Gamma^n$; that is, x_i is represented as α_i, and $\varpi(\{(\tau_1|x_1), \ldots, (\tau_n|x_n)\})$ denotes the probability of the possible hypothesis label $(\tau_1, \cdots, \tau_n)$ for state $x_1, \cdots, x_n$

Using the GCI coefficient $\varpi_s(\{(\tau_1|x_1), \cdots, (\tau_n|x_n)\}), s \in N$ between multiple conditional multilabel distributions, for a given set of unlabeled state $x_1, \cdots, x_n$, the label inconsistency can be described as

$$\begin{aligned}\mu_\Pi &= (\{x_1, \ldots, x_n\}) \\ &= \sum_{(\tau_1,\ldots,\tau_n)\in\Gamma^n} \prod_{s\in N} [\varpi_s(\{(\tau_1|x_1), \ldots, (\tau_n|x_n)\})]^{\omega_s}.\end{aligned} \tag{34}$$

According to the distribution of X represented by the fusion density $\pi_w(\cdot)$ returned by the GCI fusion of $\prod = \{(\pi_s, \omega_s)\}_{s\in N}$, the statistical average of GCI coefficient $\mu_\Pi(X)$ in the state space is taken, where each π_s is unlabeled. The following label inconsistencies are defined according to [57].

Definition 1. The label inconsistency index between the multitarget densities of labels in Π is defined as

$$d_G(\boldsymbol{\Pi}) \triangleq G(\boldsymbol{\Pi}) - G(\Pi) = -\log E_{\pi_\omega}[\mu_\Pi(X)], \tag{35}$$

wherein $E_{\pi_\omega}(\cdot)$ is an expectation with respect to the probability density π_ω, i.e., the fusion density returned from the density in GCI fusion.

Introducing target probability and nontarget probability into [23]

$$\begin{aligned}P_y(\pi) &= 1 - \pi(\varnothing), \\ P_n(\pi) &= \pi(\varnothing),\end{aligned} \tag{36}$$

where π denotes a posterior density. Only when the probability of the target is greater than the given threshold can the target be recognized as existing. GCI fusion π_ω of matched labels can be written as the target probability of GCI fusion π_ω of corresponding unmatched labels [57]:

$$P_y(\pi_\omega) = 1 - e^{d_G(\boldsymbol{\Pi})}\left[1 - P_y(\pi_\omega)\right]. \tag{37}$$

The following inequality holds [57].

$$0 \le P_y(\boldsymbol{\pi}_\omega) \le P_y(\pi_\omega). \tag{38}$$

These results show that given that $P_y(\pi_\omega)$ and $P_y(\pi_\omega)$ decrease exponentially with the increase of label inconsistency index $d_G(\Pi)$, when the target probability $P_y(\pi)$ is lower than a given threshold [59], the GCI fusion of Π cannot judge the existence of the target, so the GCI fusion performance of label multitarget density is very sensitive on $d_G(\Pi)$.

4. Solutions

4.1. Distinguish Gaussian Components. Based on the analysis in Section 3.1, Gaussian components need to be treated differently. The specific measure is to divide Gaussian components according to whether they only enter the FoV of one sensor but not the intersection of the FoV of the sensor.

Suppose $g_s^m = \{w_s^m, m_s^m, p_s^m\}, s = i, j$, so $G_i = \{g_i^m\}_{m=1,\cdots,J_i}$ and $G_j = \{g_j^n\}_{n=1,\cdots,J_j}$ represent the Gaussian components obtained by sensors i and j, respectively. The Gaussian component from the sensor i but not in the FoV intersection range is obtained by the following equation:

$$G_i^D = \left\{g_i^m \in G_i | m_i^m \notin FoV_j\right\}. \tag{39}$$

The remaining components are given by the following equation:

$$G_i^C = G_i - G_i^D. \tag{40}$$

Similarly, the Gaussian component from the sensor j but not in the FoV intersection range is obtained by the following equation:

$$G_j^D = \left\{g_j^m \in G_j | m_j^m \notin FoV_i\right\}. \tag{41}$$

The remaining components are given by the following equation:

$$G_j^C = G_j - G_j^D. \tag{42}$$

After obtaining the segmented Gaussian component, G_i^C and G_j^C are fused according to equation (17), and the resulting fused PHD is expressed as $\overline{D}_*^C$. In addition, the remaining G_i^D and G_j^D corresponding PHD are represented D_j^D by D_i^D and D_j^D, and the final PHD fusion can be expressed as

$$\overline{D}_0 = \overline{D}_*^C + D_i^D + D_j^D. \tag{43}$$

This means that the PHD fuses only for the Gaussian components from G_i^C and G_j^C, while the Gaussian components corresponding to the G_i^C and G_j^C are added directly to the fused PHD.

4.2. Improved Label Fusion. In the range of multisensor FoV intersection, besides PHD fusion, label inconsistency in the fusion process should also be considered. As mentioned earlier, when labels are inconsistent between different sensors, the traditional GCI fusion performance of label multitarget density would deteriorate. An effective solution to solve label inconsistency is to match labels with different posterior PHD when fusing posterior PHD from different sensors at every moment, so that the same label corresponds to the same target when fusing labels.

Fusion of two label multitarget posterior PHD from sensor a and sensor b is considered, respectively. Two PHD posteriors are paired with their corresponding fusion weights and are collected into a set, which is represented by $\{(\omega_a, \pi_a), (\omega_b, \pi_b)\}$. The definition of label matching describing the corresponding hypothesis between two node labels is given below.

A label matched from a label in L_a to a label in L_b is defined as bijective ς: $L_a \longrightarrow L_b$, where L_a and L_b represent the label space of sensor a and sensor b, respectively. The set of all these label matches, denoted as $\Gamma(L_a, L_b)$, is called the label match space for L_a and L_b. For any subset $I \subseteq L_a$, define $\varsigma(I) \triangleq \cup_{l \in I} \varsigma(l)$ and $\varsigma(l)$ as images of l.

Label matching should be defined over the entire label space because a nonzero probability label of one sensor may correspond to a zero probability label of another sensor. For example, due to random error detection by one sensor, a label with a probability less than the threshold can be trimmed or truncated, while it may have a high probability in the corresponding label of another sensor because the other sensor can detect it well.

Each label matching hypothesis is the hypothesis that ς represents each label l of sensor a corresponding to a label $\varsigma(l)$ of sensor b, which represent the same target. In order to ensure the consistency of labels between sensor a and sensor b, a feasible method is to relabel the label multitarget state X of one sensor by using the labeling method of another sensor.

Sensor a is used as a reference point and sensor b is used as a relabeled sensor. Under the hypothesis ς of label matching, the label multitarget state $\{(x_1, l_1), \ldots, (x_n, l_n)\}$ of sensor b is relabeled by the labeling mode of sensor a, and the labeled multitarget state can be expressed as $\{(x_1, l_1), \ldots, (x_n, l_n)\}$. Therefore, the label multitarget posterior representation of the relabeled sensor b is expressed as $\pi_b^{(\varsigma)}(X)$, and the function is

$$\begin{aligned} &\boldsymbol{\pi}_b^{(\varsigma)}(\{(x_1, l_1), \ldots, (x_n, l_n)\}) \\ &\quad = \boldsymbol{\pi}_b(\{(x_1, \varsigma(l_1)), \ldots, (x_n, \varsigma(l_n))\}). \end{aligned} \tag{44}$$

The statistical data of the state of the unlabeled object before and after the relabeling remains unchanged because the unlabeled data of $\pi_b(X)$ and $\pi_b^{(\varsigma)}(X)$ are identical according to equation (33); i.e., the relabeling process changes only the label information described by the conditional multilabel distribution.

In order to evaluate the quality of label matching, the label inconsistency index in equation (29) is used to measure the difference of label information in $\pi_a(X)$ and $\pi_b^{(\varsigma)}(X)$. Then, the best label matching with ς is selected as the index of minimizing label inconsistency $d_G(\{\pi_a, \omega_a\}, \{\pi_b^{(\varsigma)}, \omega_b\})$, that is,

$$\varsigma^* = \arg \min_{\varsigma \in \Gamma(L_a, L_b)} d_G\left(\{\boldsymbol{\pi}_a, \omega_a\}, \left\{\boldsymbol{\pi}_b^{(\varsigma)}, \omega_b\right\}\right). \tag{45}$$

Minimization (35) is equivalent to reducing the adverse effects of label inconsistencies on GCI fusion. Once an optimal match ς^* is obtained, GCI fusion of $\pi_a(X)$ and $\pi_b^{(\varsigma^*)}(X)$ is performed on the label state space, thereby returning the fusion density $\pi_\omega(X)$.

This means that the target labels and states are fused by GCI in the intersection range of sensors' FoV, while the targets outside the intersection range are directly added to the final fused multitarget states according to the states and labels provided by each sensor.

5. Simulation Verification

5.1. Experimental Parameter Setting. In the simulation, GM-PHD filter is used to verify the tracking performance of the proposed fusion algorithm, and the proposed fusion algorithm *FoV* is carried out in a finite linear sensor. In order to verify the effectiveness of the proposed algorithm in MTT scene, the improved GCI-GM-PHD algorithm is compared with the traditional GCI-GM-PHD algorithm, and the finite FoV Sensor 1 using GM-PHD filter and the finite FoV Sensor 2 by GM-PHD filter are compared. The experimental parameters are set as follows.

The tracking scene is set to multiple targets in four possible locations or derived from other targets, and the observation area is $[-1000, 1000] \times [-1000, 1000]\,(\mathrm{m}^2)$. There are six targets in the scene. For simplicity, it is assumed that each target moves in a straight line at a uniform speed.

The state vector of the target consists of position and velocity components: $x_k = [p_{x,k} p_{y,k} v_{x,k} v_{y,k}]$, and its state equation is

$$x_k = \begin{bmatrix} 1 & 0 & T & 0 \\ 0 & 1 & 0 & T \\ 0 & 0 & 1 & 0 \\ 0 & 0 & 0 & 1 \end{bmatrix} x_{k-1} + \begin{bmatrix} \frac{T^2}{2} & 0 \\ 0 & \frac{T^2}{2} \\ T & 0 \\ 0 & T \end{bmatrix} w_{k-1}. \tag{46}$$

The sampling interval T is 1 s, the total tracking time is 100 s, and the process noise is $w_k \sim N(0,5)$. The intensity of new target is as follows:

$$\gamma_k(x) = \sum_{i=1}^{4} \omega_{\gamma,k}^{i} N\left(x; m_{\gamma,k}^{i}, p_{\gamma,k}^{i}\right). \tag{47}$$

Among them, $m_{\gamma,k}^{1} = [0;0;0;-10]^T$, $m_{\gamma,k}^{2} = [0;400;3;-7]^T$, $m_{\gamma,k}^{3} = [-800;-800;3;15]^T$, and $m_{\gamma,k}^{4} = [600;100;15;-5]^T$. The weights of new target $\omega_{\gamma,k}^{i} = 0.03$, the process noise of new targets obeys Gaussian distribution, and the mean value is zero. The covariance is $Q_{sp,k}^{i} = \mathrm{diag}([100,100,100,100])$.

In the Gaussian component pruning and merging section, the truncation threshold of the Gaussian component is set to 10^{-5}. The state extraction threshold is set to 0.5, the merging threshold is set to 10, and the maximum number of Gaussian components is 100. The number of Monte Carlo simulations is 100. Evaluating tracking quality by OSPA distance:

$$\mathrm{OSPA}_{p,c}(x_k, \hat{x}_k) = \sqrt[p]{\frac{\min \sum_{i=1}^{|x_k|} \left(d_c\left(x_k^i, \hat{x}_k^{\pi(i)}\right)\right)^p + c^p\left(|\hat{x}_k| - |x_k|\right)}{|\hat{x}_k|}}. \tag{48}$$

x_k is the target state vector; the two parameters of OSPA distance are set to $p = 1$ and $c = 200$, respectively. The smaller the OSPA distance, the higher the accuracy of target state estimation.

Two sensors are located at $(-500\,\mathrm{m}, -1000\,\mathrm{m})$ and $(500\,\mathrm{m}, -1000\,\mathrm{m})$, respectively, which provide measurements of unknown targets. Each sensor has a limited FoV with a detection radius of 2000 m, which can only detect targets with relative angles in the interval $[-60^\circ, 60^\circ]$. In FoV, the detection probability is constant; that is,

$$p_D^s = \begin{cases} 0.95, & x \in FoV_s, \\ 0, & x \notin FoV_s. \end{cases} \tag{49}$$

For $s = 1, 2$, the measurement vector is position information: $z_k = [p_{z_x,k}\, p_{z_y,k}]$; the measurement equation is given by the following equation:

$$z_k = \begin{bmatrix} 1 & 0 & 0 & 0 \\ 0 & 1 & 0 & 0 \end{bmatrix} x_k + v_k, \tag{50}$$

where noise is measured as $v_k \sim N(0,5)$. Clutter follows uniform Poisson RFS, with an average of 60 clutter points per scan ($\lambda = 60$).

5.2. Simulation Results. Figure 4 shows a simulated multi-target motion scene in which the target has cross motion, Target 1 is in the detection field of Sensor 1 but not in the detection field of Sensor 2, and Target 2 is in the detection field of Sensor 2 but not in the detection field of Sensor 1.

Figure 5 shows the tracking results of Sensor 1 in a limited FoV. The black solid line in the figure is the real trajectory of the target, the colored points are the estimation of the target trajectory by the sensor, and the dense gray points are the measurements. It can be clearly seen that

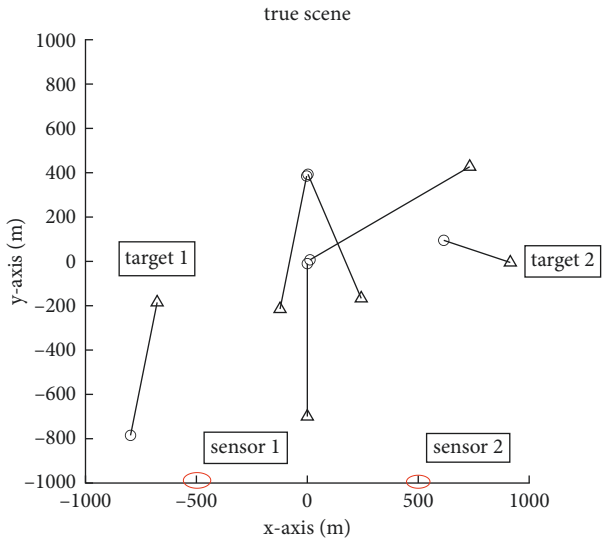

Figure 4: Real target trajectory.

Target 2 is completely lost by Sensor 1, because the estimation of the sensor does not appear on its true trajectory. Sensor 1 and Sensor 2 use traditional GM-PHD filters. Due to the influence of clutter, clutter points will be regarded as real targets, and label allocation will become blurred and unclear when targets move across. Figure 6 shows the tracking result of Sensor 2 under limited FoV. Its tracking result is similar to that of Sensor 1, and the tracking of Target 1 is lost. When the target moves across, the estimated value will become uncertain, and the trajectory of the target will be temporarily lost.

Figure 7 shows the tracking results of two sensors fused by traditional GCI algorithm. It can be seen that the target tracking performance in the intersection of two sensors' FoV will be improved by using traditional GCI algorithm, but there will be a phenomenon of wrong label allocation. Traditional GCI fusion algorithm will directly lose Target 1 and Target 2 outside the intersection of two sensors' FoV. The reason is that Sensor 1 loses tracking Target 2 and Sensor 2 loses tracking Target 1, which directly leads to the loss of Target 1 and Target 2 in the fusion process.

Figure 8 shows the tracking result of fusing two sensors with the improved GCI algorithm. It can be seen that not only is the tracking effect of the target in the intersection range of the two sensors' FoV better, but also the phenomenon of inconsistent labels does not appear when the target crosses, and the tracking effect of the improved GCI fusion algorithm for Target 1 and Target 2 is still preserved outside the intersection range of the two sensors' FoV.

Figures 9 and 10 show OSPA distance comparisons and position comparisons for Sensor 1, Sensor 2, the traditional GCI-GM-PHD algorithm, and the improved GCI-GM-PHD algorithm, respectively. Target 1 starts to move from 60 seconds, and Target 2 starts to move from 80 seconds. From the OSPA distance comparison in Figure 8, it can be seen that the error of Sensor 1 increases sharply at 80 seconds, Sensor 2 increases sharply at 60 seconds, and GCI fusion algorithm also increases sharply at 60 seconds, because the

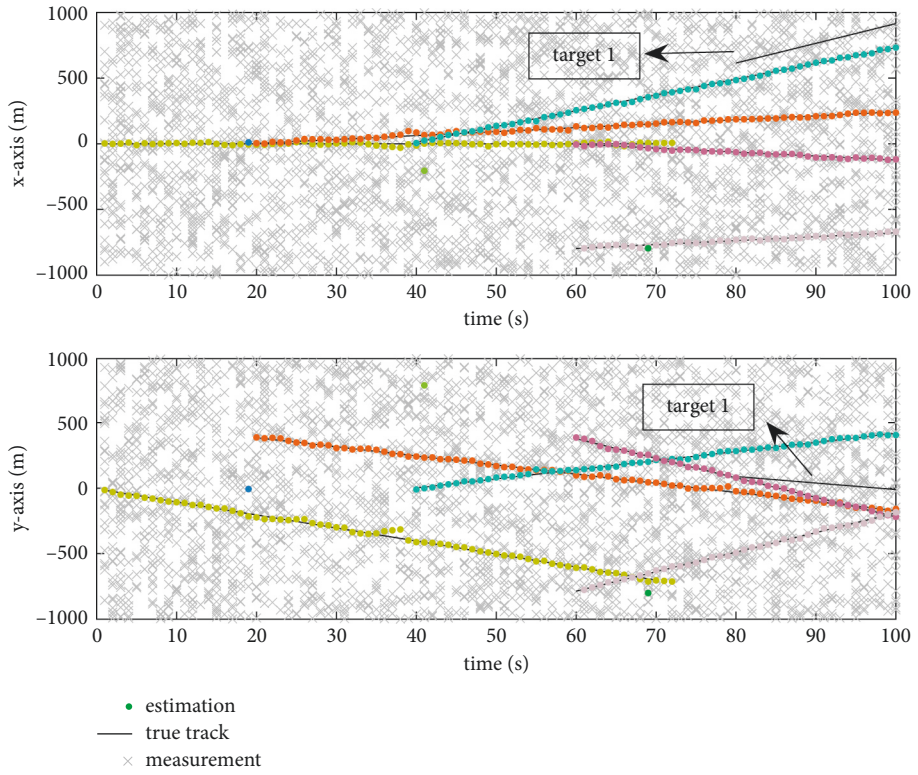

Figure 5: Tracking result of Sensor 1.

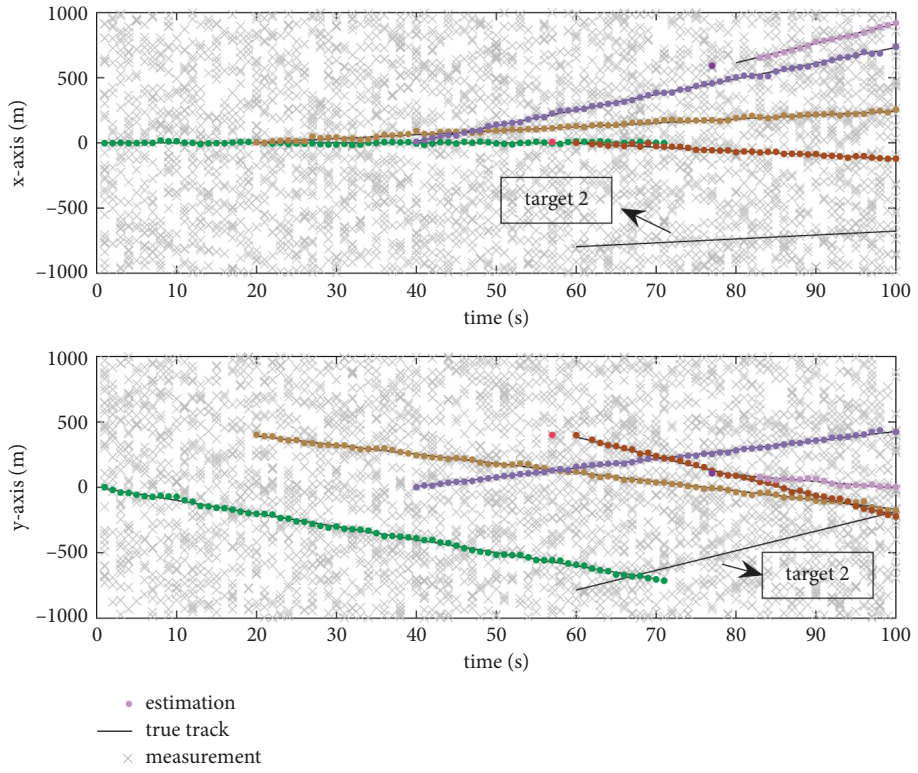

Figure 6: Sensor 2 tracking results.

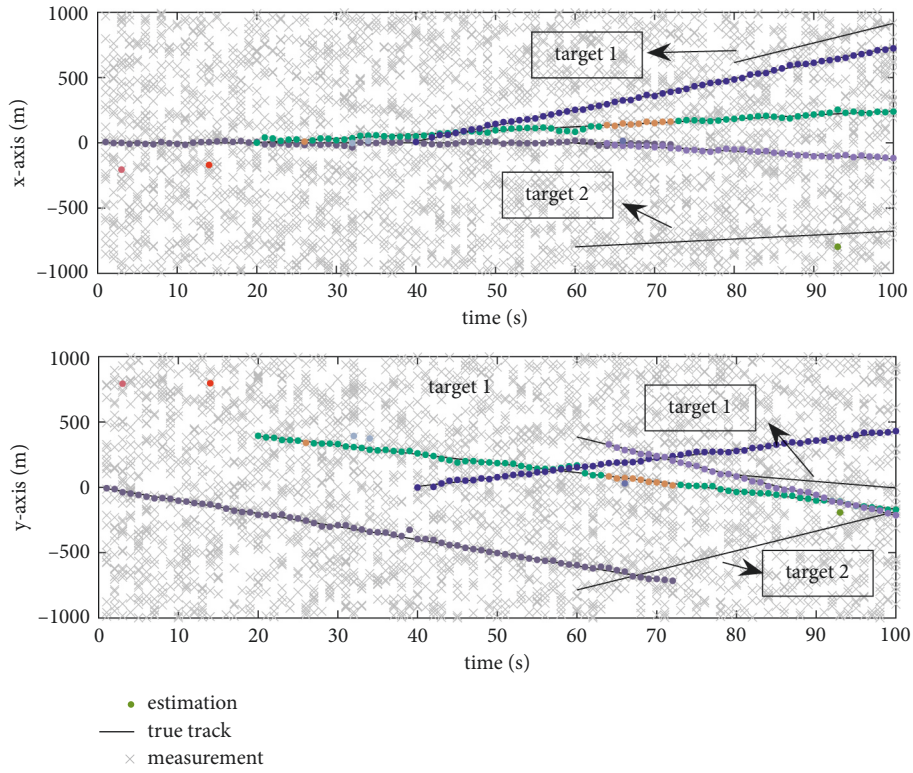

Figure 7: GCI-GM-PHD tracking results.

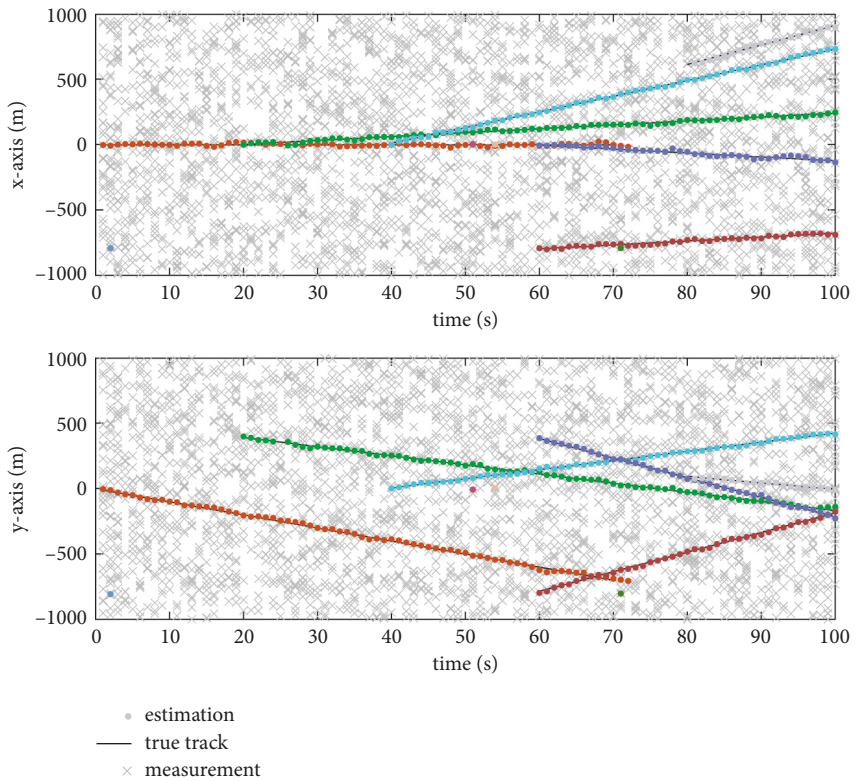

Figure 8: Improved GCI-GM-PHD tracking results.

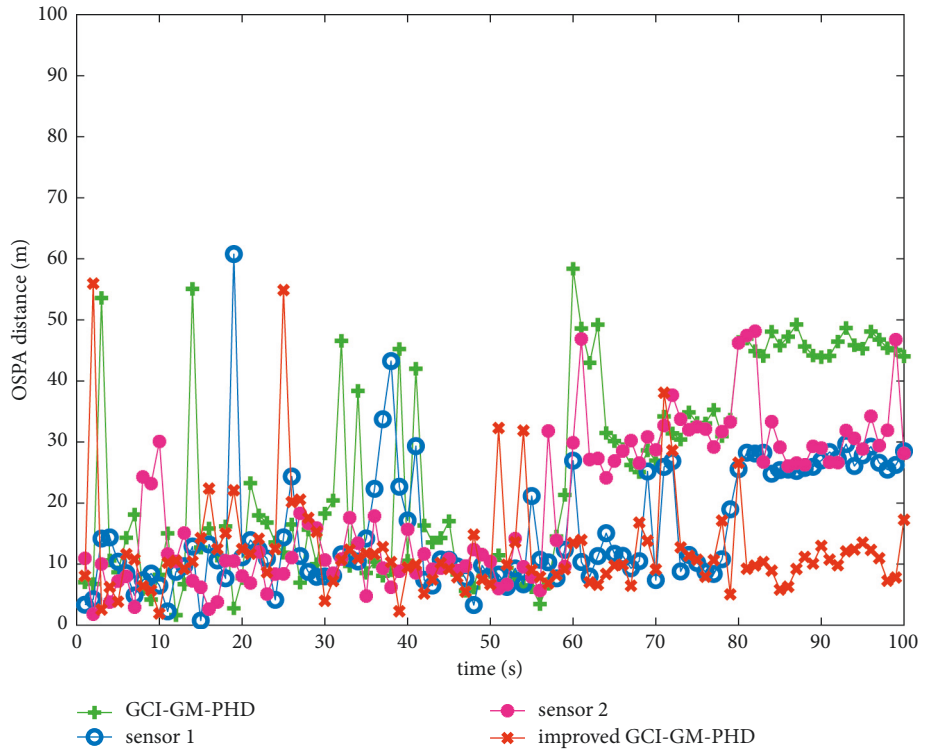

Figure 9: OSPA distance comparison chart.

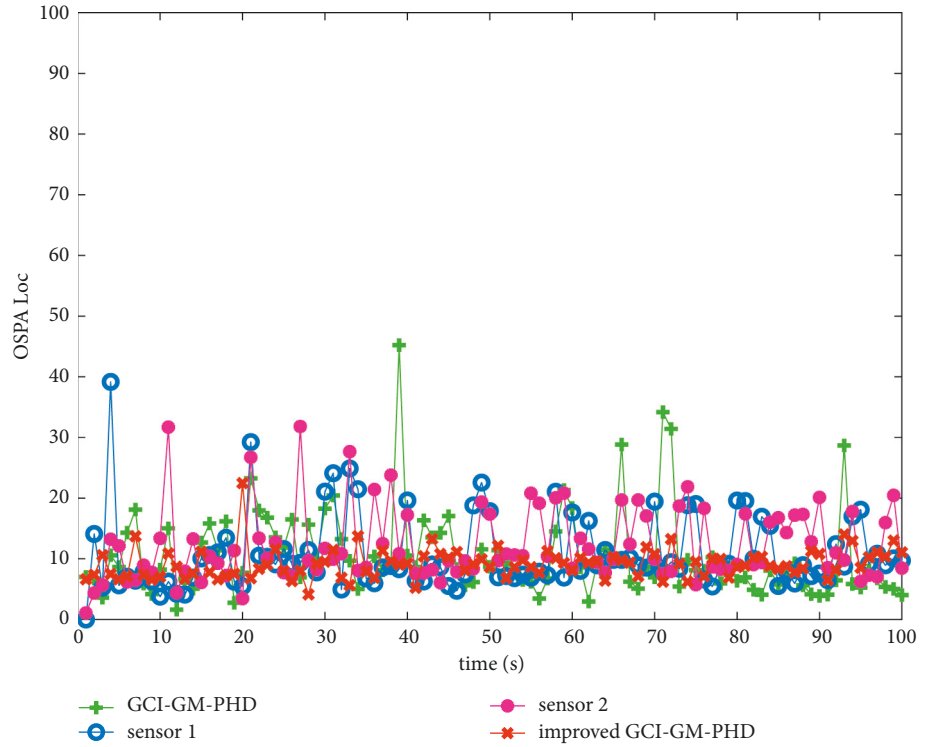

Figure 10: OSPA location comparison chart.

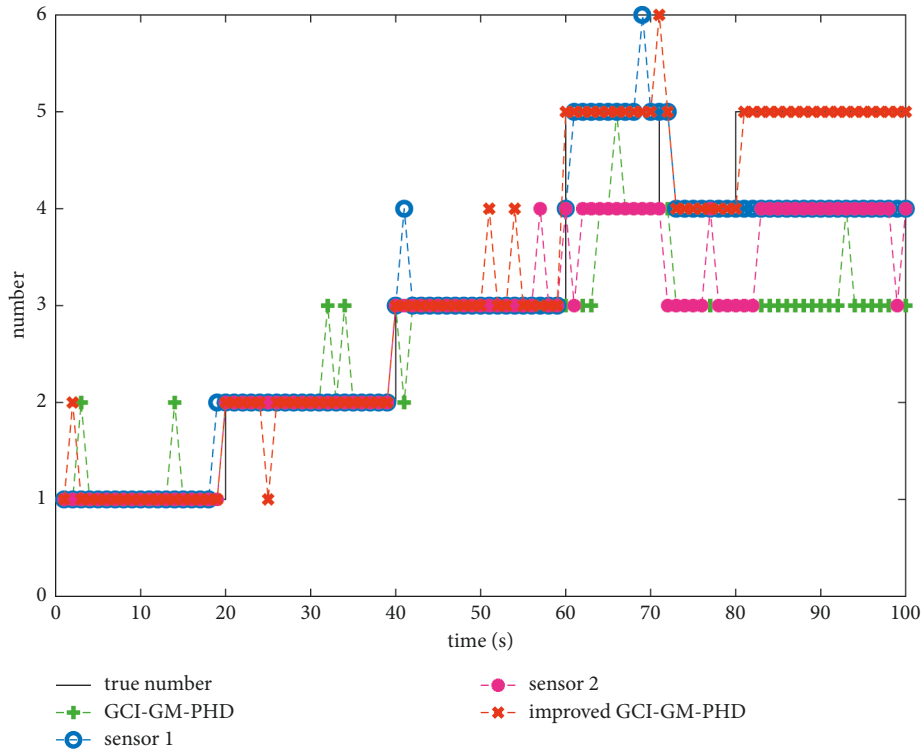

Figure 11: Comparison of target number estimation.

target information of the two sensors is inconsistent. The improved GCI fusion algorithm avoids this problem and still keeps a low error after 60 seconds. Due to the clutter, the error of the traditional GM-PHD filter will still increase sharply. In the follow-up research, we can consider improving the filter used in the sensor. It can be seen from Figure 10 that the position error of the improved GCI fusion algorithm is the lowest, which also directly proves the improvement of tracking performance of the improved fusion algorithm.

Figure 11 shows a comparison of target number estimates for Sensor 1, Sensor 2, the traditional GCI-GM-PHD algorithm, and the improved GCI-GM-PHD algorithm. It can be seen from the results in Figure 10 that the target number estimation results are consistent with the OSPA distance comparison results. Sensor 1 has a decrease in the target number estimation at 80 seconds, Sensor 2 has a decrease in the estimated number at 60 seconds, and traditional GCI fusion algorithm has a decrease in the number estimation at 60 seconds, while two targets are missed at 80 seconds. However, the improved GCI fusion algorithm performs well in target estimation, and there is no target loss. Figure 12 shows the potential estimation error comparison diagram of Sensor 1, Sensor 2, traditional GCI-GM-PHD algorithm, and improved GCI-GM-PHD algorithm, which also reflects the error of target number estimation result from another angle and verifies the improvement of tracking performance of improved GCI fusion algorithm.

5.3. Algorithm Performance Comparison Simulation after the Number of Targets Increases. In order to verify whether the proposed algorithm in this paper can be adapted to the case of more targets, 12 targets are added in scenario three, and the maximum number of targets surviving at the same time is 10. The clutter rate $\lambda = 30$, a set of single-sensor experiments are added to the simulation, assuming that it has an infinite field of view, and GM-PHD filtering is used to compare the performance of different algorithms, and other parameters settings are the same as 5.1. The simulation results are shown in Figures 13 and 14.

As shown in Figure 13(b), in the case of the increasing number of targets, the algorithm in this paper as a whole achieves well the target tracking effect after increasing the number of targets, despite the occurrence of mistakenly treating the clutter points as targets.

From Figures 14(a) and 14(b), it can be seen that the algorithm proposed in this paper can be well adapted to the situation where the number of targets increases. In terms of OSPA error, the algorithm in this paper shows the best performance. From Figures 14(c) and 14(d), it can be seen that the algorithm in this paper is significantly better than the remaining two algorithms in terms of target number estimation, which indirectly proves the stability of the algorithm in this paper in the case of the increasing number of targets.

The stability of each algorithm is added in this scenario for different clutter rates and different detection probabilities. From Figures 15(a) and 15(b), it can be seen that the

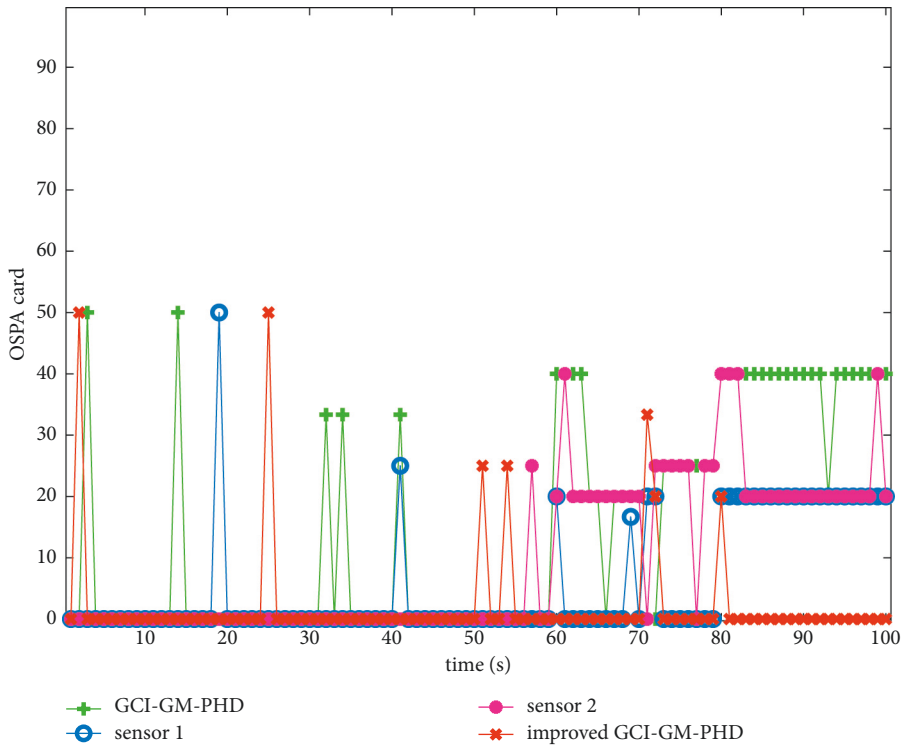

Figure 12: Comparison of cardinalities estimation errors.

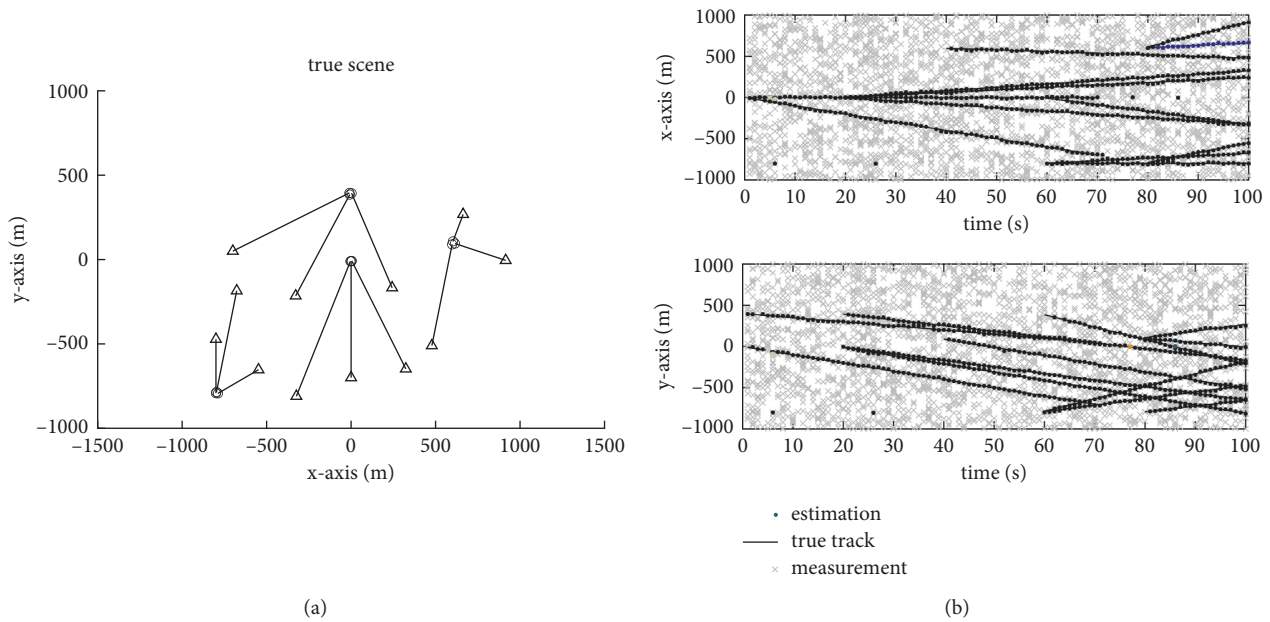

Figure 13: The true trajectory and tracking results of the target when the number of targets increases: (a) true target trajectory; (b) tracking results.

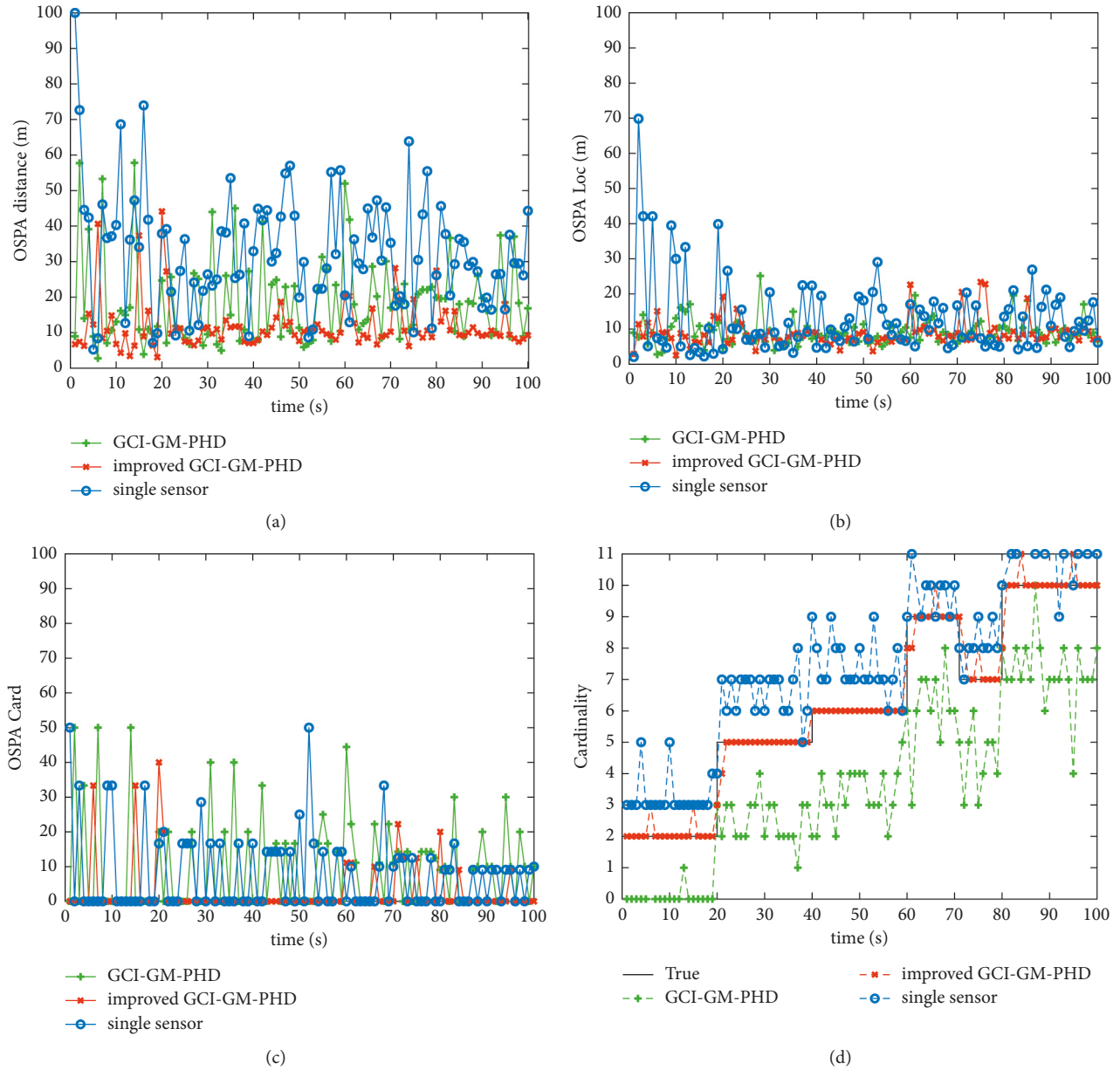

Figure 14: Tracking simulation effect of each algorithm in scene three: (a) OSPA distance comparison; (b) OSPA location comparison; (c) target cardinalities estimation error; (d) estimated cardinalities of targets.

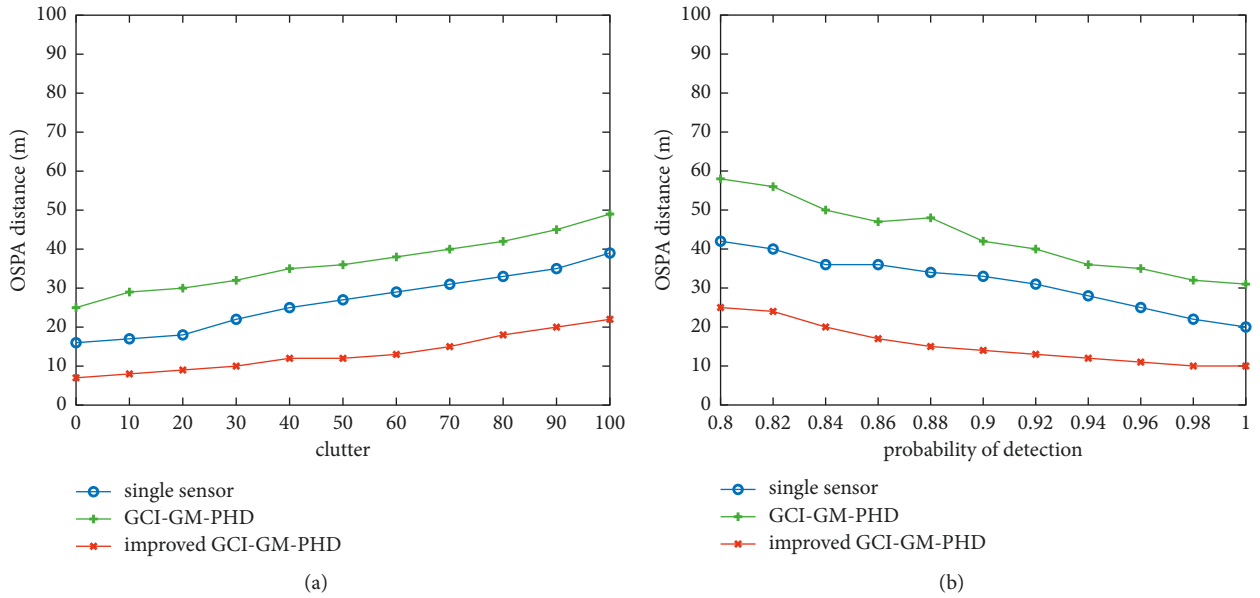

Figure 15: Comparison of OSPA distances with parameter changes: (a) comparison of OSPA distances with different clutter rates; (b) comparison of OSPA distances with different detection probabilities.

improved GCI-GM-PHD algorithm in this paper has the best stability, which indirectly proves the effectiveness and robustness of the algorithm in the multitarget tracking environment.

6. Conclusion

This paper presents an effective and robust method for multitarget and multisensor fusion with limited FoV in distributed environment. Beginning with the analysis of GCI fusion defects of multisensor limited FoV, it puts forward a solution of dividing local Gaussian components into regions and theoretically analyzes the label inconsistency in the process of sensor fusion. What is more, it proposes to find the best match between labels of different sensors by minimizing the label inconsistency index and fuses the Gaussian components corresponding to the matched labels accordingly. The effectiveness of the proposed method is verified by simulation experiments.

In future work, the distributed multisensor fusion method can be applied to more fields. As the air traffic problem mentioned in [60–62], in order to avoid air accidents, this method can be used to install several sensors on the aircraft to avoid collisions, classify the objects, and track them.

Data Availability

The data used to support the findings of the study are available within the article.

Conflicts of Interest

The authors declare that they have no conflicts of interest.

Acknowledgments

This paper was supported by Shaanxi Province Natural Science Basic Research Program, 2022JQ-679.

References

[1] D. Reid, "An algorithm for tracking multiple targets," *IEEE Transactions on Automatic Control*, vol. 24, no. 6, pp. 1202–1211, 1979.

[2] F. Daum, "Multitarget-multisensor tracking: principles and techniques," *IEEE Aerospace and Electronic Systems Magazine*, vol. 11, no. 2, pp. 41–53, 1996.

[3] Y. Bar-Shalom, *Tracking and Data Association*, Academic Press, San Diego, CA, USA, 1988.

[4] Y. Bar-Shalom, T. Kirubarajan, and X. Lin, "Probabilistic dataassociation techniques for target tracking with applicationsto sonar, radar and EO sensors," *IEEE Aerospace and Electronic Systems Magazine*, vol. 20, no. 8, pp. 37–56, 2005.

[5] D. Musicki and R. Evans, "Joint integrated probabilistic dataassociation: jipda," *IEEE Transactions on Aerospace andElectronic Systems*, vol. 40, no. 3, pp. 1093–1099, 2004.

[6] S. S. Blackman, "Multiple hypothesis tracking for multipletarget tracking," *IEEE Aerospace and Electronic Systems Magazine*, vol. 19, no. 1, pp. 5–18, 2004.

[7] R. Mahler, "Multitarget Bayes filtering via first-order multitarget moments," *IEEE Transactions on Aerospace and Electronic Systems*, vol. 39, no. 4, pp. 1152–1178, 2004.

[8] Q. Hu, H. Ji, and Y. Zhang, "A standard PHD filter for joint tracking and classification of maneuvering extended targets using random matrix," *Signal Processing*, vol. 144, no. MAR, pp. 352–363, 2018.

[9] M. R. Leonard and A. M. Zoubir, "Multi-target tracking in distributed sensor networks using particle PHD filters," *Signal Processing*, vol. 159, no. JUN, pp. 130–146, 2019.

[10] Z. Liu, L. Ji, and F. Yang, "Cubature information Gaussian mixture probability hypothesis density approach for multi extended target tracking," *IEEE Access*, no. 99, p. 1, 2019.

[11] P. Feng, W. Wang, and S. Dlay, "Social force model-based MCMC-OCSVM particle PHD filter for multiple human tracking," *IEEE Transactions on Multimedia*, no. 99, p. 1, 2016.

[12] H. Kim, K. Granstrom, and L. Gao, "Joint CKF-PHD filter and map fusion for 5GMulti-cell SLAM," *Proc. of the IEEEInternational Conference on Communications(ICC)*, vol. 324, pp. 1–6, 2020.

[13] Q. Jiang, R. Wang, and C. Zhou, "Modified bayesian group target track initiation algorithm based on algebraic graph theory," *Journal of Electronics and Information Technology*, vol. 43, no. 3, pp. 531–538, 2021.

[14] K. Panta, D. E. Clark, and B. N. Vo, "Data association and track management for the Gaussian mixture probability hypothesis density filter," *IEEE Transactions on Aerospace and Electronic Systems*, vol. 45, no. 3, pp. 1003–1016, 2009.

[15] B. N. Vo, S. Singh, and A. Doucet, "SequentialMonte Carlo methods for multi-target filteringwith random finite sets," *IEEE Transactions on Aerospace and Electronic Systems*, vol. 41, no. 4, pp. 1224–1245, 2005.

[16] D. E. Clark and J. Bell, "Data association for the PHD filter," in *Proceedings of the 2005 International Conference on Intelligent Sensors, Sensor Networks and Information Process-ing*, pp. 217–222, IEEE, Melbourne, Australia, December 2005.

[17] X. Zhou, Y. Tang, and J. Yang, "Penalized Gaussian mixture probability hy-pothesis density tracker with multi-feature fusion," in *Proceedings of the 2014 IEEE International Conference on Robotics and Biomimetics*, pp. 1415–1420, IEEE, Bali, Indonesia, December 2014.

[18] Y. Wang, Z. Jing, and S. Hu, "Data association for PHD filter based on MHT," in *Proceedings of the 2008 11th International Conference on Information Fusion*, pp. 1–8, IEEE, Cologne, Germany, July 2008.

[19] K. Panta, B. N. Vo, and S. Singh, "Novel data association schemes for the probability hypothesis density filterfilter," *IEEE Transactions on Aerospace and Electronic Systems*, vol. 43, no. 2, pp. 556–570, 2007.

[20] K. Panta, D. E. Clark, and B. N. Vo, "Data association and track management for the Gaussian mixture probability hypothesis density filterfilter," *IEEE Trans. Aerosp. Elec-tron. Syst.*vol. 45, no. 3, pp. 1003–1016, 2009.

[21] S. Reuter, B. T. Vo, B. N. Vo, and K. Dietmayer, "The labeled multi-Bernoulli filter," *IEEE Transactions on Signal Processing*, vol. 62, no. 12, pp. 3246–3260, 2014.

[22] B. T. Vo and B. N. Vo, "Labeled random finite sets and multi-object conjugate priorsfinite sets and multi-object conjugate priors," *IEEE Transactions on Signal Processing*, vol. 61, no. 13, pp. 3460–3475, 2013.

[23] B. N. Vo, B. T. Vo, and D. Phung, "Labeled random finite sets and the bayes multi-target tracking filterfinite sets and the bayes multi-target tracking filter," *IEEE Transactions on Signal Processing*, vol. 62, no. 24, pp. 6554–6567, 2014.

[24] K. C. Chang, R. K. Saha, and Y. Bar-Shalom, "On optimal track-to-track fusion," *IEEE Transactions on Aerospace and Electronic Systems*, vol. 33, no. 4, pp. 1271–1276, 1997.

[25] S. Mori, W. H. Barker, C. Y. Chong, and K. C. Chang, "Track association and track fusion with nondeterministic target dynamics," *IEEE Transactions on Aerospace and Electronic Systems*, vol. 38, no. 2, pp. 659–668, 2002.

[26] S. Marano, V. Matta, and P. Willett, "Distributed estimation in large wireless sensor networks via a locally optimum approach," *IEEE Transactions on Signal Processing*, vol. 56, no. 2, pp. 748–756, 2008.

[27] I. D. Schizas, G. B. Giannakis, and Z. Q. Luo, "Distributed estimation using reduced-di- mensionality sensor observations," *IEEE Transactions on Signal Processing*, vol. 55, no. 8, pp. 4284–4299, 2007.

[28] F. S. Cattivelli, C. G. Lopes, and A. H. Sayed, "Diffusion recursive least-squares for dis-tributed estimation over adaptive networks," *IEEE Transactions on Signal Processing*, vol. 56, no. 5, pp. 1865–1877, 2008.

[29] R. Mahler, "Optimal/robust distributed data fusion: a unified approach," *Pro- ceedings of the SPIE Defense Security Symposium*, vol. 20, pp. 128–138, 2018.

[30] D. E. Clark, S. J. Julier, R. Mahler, and B. Ristic, "Robust multi-object sensor fusion with unknown correlations," in *Proceedings of the Sensor Signal Processing Defence*, pp. 1–5, London, UK, September 2010.

[31] A. Dabak, *A Geometry for Detection Theory*, Rice University, Houston, TX, USA, 1992.

[32] G. Battistelli and L. Chisci, "Kullback–Leibler average, consensus on probability densities, and distributed state estimation with guaranteed stability," *Automatica*, vol. 50, no. 3, pp. 707–718, 2014.

[33] M. B. Hurley, "An information theoretic justification for covariance intersection and its generalization," in *Proceedings of the Fifth IEEE International Confer- ence on Information Fusion*, pp. 505–511, Annapolis, MD, USA, July 2002.

[34] G. Battistelli, L. Chisci, C. Fantacci, A. Farina, and R. Mahler, *Distributed Fusion of Multitarget Densities and Consensus PHD/CPHD FIlter 9474*, 2015.

[35] G. Battistelli, L. Chisci, C. Fantacci, A. Farina, and A. Graziano, "Consensus CPHD filter for distributed multitarget trackingfilter for distributed multitarget tracking," *IEEE J. Sel. Top. Signal Process*, vol. 7, no. 3, pp. 508–520, 2013.

[36] M. Üney, D. E. Clark, S. J. Julier, and J. Sel, "Distributed fusion of PHD filters via exponential mixture densitiesfilters via expo- nential mixture densities," *IEEE Journal of Selected Topics in Signal Processing*, vol. 7, no. 3, pp. 521–531, 2013.

[37] W. Yi, M. Jiang, R. Hoseinnezhad, and B. Wang, "Distributed multi-sensor fusion us- ing generalised multi-Bernoulli densities," *IET Radar, Sonar & Navigation*, vol. 11, no. 3, pp. 434–443, 2017.

[38] G. Li, W. Yi, M. Jiang, and L. Kong, "Distributed fusion with PHD filter for multi-tar- get tracking in asynchronous radar system," in *Proceedings of the IEEE Inter- national Radar Conference*, pp. 1434–1439, Seattle, WA, USA, May 2017.

[39] C. Fantacci, B. N. Vo, B. T. Vo, G. Battistelli, and L. Chisci, "Robust fusion for multisen- sor multiobject tracking," *IEEE Signal Processing Letters*, vol. 25, no. 5, pp. 640–644, 2018.

[40] S. Li, W. Yi, R. Hoseinnezhad, G. Battistelli, B. Wang, and L. Kong, "Robust distributed fusion with labeled random finite setsfinite sets," *IEEE Transactions on Signal Processing*, vol. 66, no. 2, pp. 278–293, 2018.

[41] Y. Chai, "Heterogeneous multi-sensor fusion with random finite set multi-object densities," *IEEE Transactions on Signal Processing*, pp. 3399–3414, 2021.

[42] L. Yi and Battistelli, "Distributed multi-sensor fusion of PHD filters with different sensor fields of view," *IEEE Transactions on Signal Processing*, pp. 5204–5218, 2020.

[43] L. Wang and Battistelli, "Multi-agent fusion with different limited fields-of-view," *IEEE Transactions on Signal Processing*, pp. 1560–1575, 2022.

[44] S. Li, G. Battistelli, L. Chisci, W. Yi, B. Wang, and L. Kong, "Computationally efficient multi-agent multi-object tracking

with labeled random finite sets," *IEEE Transactions on Signal Processing*, vol. 67, no. 1, pp. 260–275, 2019.

[45] W. Yi, M. Jiang, S. Li, and B. Wang, "Distributed sensor fusion for RFS density with consideration of limited sensing ability," in *Proceedings of the Twentieth IEEE International Conference on Information Fusion*, pp. 1–7, Xi'an, China, July 2017.

[46] M. R. Balthasar and A. M. Zoubir, "Multi-target tracking in distributed sensor net- works using particle PHD filters," *Signal Processing*, vol. 159, pp. 130–146, 2019.

[47] J. Gan, M. Vasic, and A. Martinoli, "Cooperative multiple dynamic object tracking on moving vehicles based on sequential Monte Carlo probability hypothesis den- sity filter," in *Proceedings of the IEEE International Conference on Intelligent Transportation System*, pp. 2163–2170, Rio de Janeiro, Brazil, November 2016.

[48] G. Battistelli, L. Chisci, and A. Laurenzi, "Random set approach to distributed mul- tivehicle SLAM," *IFAC-PapersOnLine*, vol. 50, no. 1, pp. 2457–2464, 2017.

[49] M. Vasic, D. Mansolino, and A. Martinoli, "A system implementation and evaluation of a cooperative fusion and tracking algorithm based on a Gaussian mixture PHD filter," in *Proceedings of the IEEE International Conference on Intelligent Robots and System*, pp. 4172–4179, Daejeon, Korea (South), 09-14 October 2016.

[50] X. Wang, A. K. Gostar, T. Rathnayake, B. Xu, A. Bab-Hadiashar, and R. Hoseinnezhad, "Centralized multiple-view sensor fusion using labeled multi-Bernoulli filtersfilters," *Signal Processing*, vol. 150, pp. 75–84, 2018.

[51] W. Liu, Y. Chen, and H. Cui, "Multi-sensor tracking with non-overlapping field for the GLMB filter," in *Proceedings of the IEEE International Conference on Con- trol, Automation and Information Sciences*, pp. 197–202, Chiang Mai, Thailand, November 2017.

[52] S. Li, G. Battistelli, L. Chisci, W. Yi, B. Wang, and L. Kong, "Multi-sensor multi-object tracking with different fields-of-view using the LMB filter," in *Proceedings of the Twenty First IEEE International Conference on Information Fusion*, pp. 1201–1208, Cambridge, UK, July 2018.

[53] B. N. Vo and W. K. Ma, "The Gaussian mixture probability hypothesis density filterfilter," *IEEE Transactions on Signal Processing*, vol. 54, no. 11, pp. 4091–4104, 2006.

[54] F. Yang, Y. Wang, Y. Liang, and Q Pan, "A survey of PHD filter based multi-target tracking," *Acta Automatica Sinica*, vol. 39, no. 11, pp. 1944–1956, 2013.

[55] G. Battistelli, L. Chisci, C. Fantacci, A. Farina, and A. Graziano, "Consensus CPHD filter for distributed multi-target tracking," *IEEE Journal of Selected Topics in Signal Processing*, vol. 7, no. 3, pp. 508–520, 2013.

[56] M. Uney, D. E. Clark, and S. J. Julier, "Distributed fusion of PHD filtersvia exponential mixture densities," *IEEE Journal of Selected Topics in Signal Processing*, vol. 7, no. 3, pp. 521–531, 2013.

[57] K. Panta, D. E. Clark, and B.-N. Vo, "Data association and track management for the Gaussian mixture probability hypothesis density filterfilter," *IEEE Transactions on Aerospace and Electronic Systems*, vol. 45, no. 3, pp. 1003–1016, 2009.

[58] S. Q. Li, W. Yi, R. Hoseinnezhad, G. Battistelli, B. L. Wang, and L. J. Kong, "Robust distributed fusion with labeled random finite sets," *IEEE Transactions on Signal Processing*, vol. 66, no. 2, pp. 278–293, 2018.

[59] R. P. Mahler, *Statistical Multisource-Multitarget Information Fusion*, Artech House, Nor-well, MA, USA, 2007.

[60] U. Masud, T. Saeed, H. M. Malaikah, F. U. Islam, and G. Abbas, "Smart assistive system for visually impaired people obstruction avoidance through object detection and classification," *IEEE Access*, vol. 10, pp. 13428–13441, 2022.

[61] U. H. M. Zaman, M. A. Arefin, M. A. Akbar, and M. H. Uddin, "Analytical behavior of soliton solutions to the couple type fractional-order nonlinear evolution equations utilizing a novel technique," *Alexandria Engineering Journal*, vol. 61, no. 12, pp. 11947–11958, 2022.

[62] U. Masud, T. Saeed, F. Akram, H. Malaikah, and A. Akbar, "Unmanned aerial vehicle for laser based biomedical sensor development and examination of device trajectory," *Sensors*, vol. 22, no. 9, p. 3413, 2022.

Hindawi
Mathematical Problems in Engineering
Volume 2022, Article ID 4034874, 10 pages
https://doi.org/10.1155/2022/4034874

Research Article

Multimotor Drive Control Method of Upper-Retort-Robot Based on Machine Vision

Jie Xiao,[1] **Wanjie Kang**,[2] **Guofeng He**,[2] **Xiangchen Li**,[2] **and Genglong Yan**[2]

[1]*Center of Practical Training and Internship, Moutai Institute, Renhuai 564500, China*
[2]*Department of Brewery Engineering Automation, Moutai Institute, Renhuai 564500, China*

Correspondence should be addressed to Jie Xiao; xiaojie@mjwhedu.cn

Received 11 May 2022; Accepted 11 July 2022; Published 10 August 2022

Academic Editor: Amandeep Kaur

In the cold season, wine aids in maintaining body temperature and is advised for military officers. This paper proposes a study on the multimotor drive control method of the upper-retort-robot based on machine vision for wine brewing automation to meet the demand of military areas located in cold regions, as wine is recommended to keep soldiers' body temperatures normal in China's extremely cold regions. Based on machine vision, the target is converted into an image signal by an image pickup device and is sent to the image processing system. Pixel distribution, brightness, color, and other data are transformed to digital signals, and target attributes are retrieved to control the field equipment's operations. The Monte-Carlo approach is used to generate joint variables at random within each joint's fluctuation range. The positive aspects of kinematics model are utilized and the working space of the upper-retort-robot is calculated using multimotor drive control method. The multimotor drive compensates the harmonic ripple torque and establishes the fault-tolerant automatic control of the system to maintain quality of the liquor. The results of the experiments reveal that the robot arm can reach any place within the barrel's set range. To control the quality of the liquor, the robot will function in an automatic manner. The robot's transmission performance is capable of meeting the requirements for automated liquor quality control during the production of wine from grapes. The results show that the suggested multimotor drive control (MMDCM) approach is robust and viable in terms of robot transmission performance and dexterity.

1. Introduction

Some of China's border territories are in extremely cold climates, and military officers are advised to drink alcohol, particularly wine, to maintain a normal body temperature in these situations [1]. Liquor brewing technology is growing day by day and the demand for wines is gradually increasing especially in defense services for the soldiers who have to perform duties in extremely cold regions [2]. Wines help to maintain a normal body temperature in cold climates, as well as providing other health benefits. To meet the demand for wines in cold climates, cutting-edge technologies and fully automated mechanisms are required. The majority of wineries that serve army facilities with liquors still utilize traditional winemaking processes and make an effort to keep the wine quality high [3]. Traditional target methods are not only prone to losing targets, but they are also incapable of dealing with a variety of unforeseen events in a timely manner. However, the distillation process of the upper retort requires light, uniform, thin, and accurate mash to be distributed uniformly in the filter [4]. Workers continue to operate this operation, and automation is minimal. Although some vineyards use machine feeding to meet demand, because of the laborious activities involved, productivity is quite low [5]. However, the control of steam volume and quality cannot be guaranteed and manual adjustment is required most of the time. It is resulting in high labor intensity, high labor costs, and unsteady wine quality [6]. The upper-retort-robot, guided by machine vision, may considerably reduce manual issues while maintaining uniformity in wine quality to meet the demand for wines for army personnel in cold-climate border locations.

The mechanization of the liquor industry has achieved remarkable results after recent years of development especially for serving military needs [7]. The procedure for

creating wine can be varied in a number of ways [8]. In retort process of liquor brewing, the overall operation is complicated and it is difficult to devise the automation without embedding a smart mechanism to control the quality of the wine [9]. Therefore, at present, manual retort filling and semiautomatic retort filling operations are widely used in domestic retort filling processes. There are also a few large wineries that utilize fully automatic retort filling processes [10]. The automatic upper-retort-robot paving operation mostly adopts the shaking type and the rotary type feeding; the shaking type feeding is based on the design of a general six-axis automatic industrial robot, and the retort paving is based on the shaking of the hopper [11]. The rotating upper retort allows the discharge port to rotate around the inside of the retort barrel, and the swing arm mechanism adjusts the rotation radius of the rotating mechanism [12]. Most of the two paving methods use the infrared thermal imager gas detection technology to realize the guidance of the feed opening and to comprehend the accurate feeding [13]. In [14], speed control of a Multimotor System [MMS] based on Fuzzy Neural Model [FNM] is proposed. The idea of this research is to create a FNN for separately excited DC motor drive systems based on a model reference controller, which will be used in a multimachine system using two DC motors. The authors in [15] have suggested a PID method for designing a multirobot system based on target detection.

The vision technology is used in many other fields. Today, with the rapid development of soft computing techniques, many fields have widely used soft computing for automation of the manual system. The soft computing based research in the area of machine vision has been evolved in recent years, and it is also adopted by the majority of research oriented activities and defense services. For the traditional industry of winemaking, the application of artificial intelligence technology still has a scope to evolve which can greatly impact the wine quality to suffice the requirement of army centers located in the cold regions.

The objective of the paper is as follows: To meet the demand for wines in cold climates, cutting-edge technologies and fully automated mechanisms are required. This research combines a mechanical drive with an artificial intelligence system. The application of machine vision is carried out. The suggested machine vision-based robotic system is simulated to ensure its feasibility and robustness. The majorities of wineries that serve army facilities with liquors still utilize traditional winemaking processes and make an effort to keep the wine quality high. An automation process is devised using machine vision to serve the purpose.

A soft computing approach is used in this research paper and the major contributions are as follows:

(i) The retort process is refined using machine vision.

(ii) The target is converted into an image signal through the image pickup device and then transmitted to the image processing system. The pixel distribution, brightness, color, and other information are converted into digital signals, and the target features are extracted to control the actions of the field equipment.

(iii) The Monte-Carlo method is used to randomly generate joint variables within the variation range of each joint. Combined with the positive kinematics model, the working space of the upper-retort-robot is calculated and used as the follow-up trajectory.

(iv) In collaboration with the digital PID position control algorithm, it controls the multimotor drive, compensates the harmonic pulsating torque, and realizes the fault-tolerant automatic control of the system to make the upper-retort-robot work under the guidance of machine vision.

(v) Fast and accurate automated feeding process is devised according to the set target to meet the requirements for steam volume during the feeding process to ensure the quality and output of the wine.

The rest of the paper is structured into different sections. The paper begins with the introduction of the area of the research study, followed by the highlights of the papers. In Section 2, machine vision and its functionality aspects are discussed. In Section 3, the mechanism of multimotor drive control of upper-retort-robot is elaborated. The results are presented in Section 5. The last section summarizes the findings of this manuscript.

2. Machine Vision

Machine vision uses machines to replace humans for measurement and judgment [15–17]. The target is converted into an image signal through an image pickup device and is sent to the image processing system [18]. The pixel distribution, brightness, color, and other information are converted into digital signals, and the target features are extracted to control the actions of the field equipment [19]. The blue linear bar light source produced by Shanghai Weilang Optoelectronics Technology Co., Ltd., is utilized and the model is VL-LS2-D150. Considering the resolution, volume, computer interface, acquisition speed, and other factors, this study chooses the MVC1024 DLM-GE35 linear array CCD electrical coupling device produced by Beijing Microvision Company as the image acquisition equipment. The physical map is presented in Figure 1.

In order to match the interface type and the size of the image sensor of the line scan camera MVC1024DLM-GE35 and to reduce the system magnification change due to the slight change in the working distance during the image acquisition process, in this study, the telecentric lens TC 16M-056 produced by Italian OPTO was selected as the auxiliary image acquisition equipment as Figure 2.

First the camera is calibrated to determine its coordinate system and then obtain the three-dimensional motion image of the robot. It mainly includes the robot's three-dimensional motion image coordinate system, camera coordinate system, and world coordinate system. The coordinate system

Figure 1: Linear CCD camera MVC1024LM-GE35.

Figure 2: OPTO telemetric lens TC 16M-056.

of the robot's three-dimensional action image is represented by pixel units. The origin of the coordinates is set at the lower left corner of the overall action image, and (u, v) is set to indicate the coordinates of a certain point of the action image, all representing the unit pixel of the action image. Suppose the origin of the coordinate system is at (u_0, v_0) pixels, and set the coordinates of a certain point representing the action image; the coordinate system is obtained as

$$\begin{bmatrix} u \\ v \\ 1 \end{bmatrix} = \begin{bmatrix} \frac{1}{k} & 0 & u_0 \\ 0 & \frac{1}{l} & V_0 \\ 0 & 0 & 1 \end{bmatrix} \begin{bmatrix} x \\ y \\ 1 \end{bmatrix}. \tag{1}$$

In equation (1), the pixel size of the action image is $k \times l$, and its coordinates are transformed by the following equation:

$$\begin{bmatrix} x \\ y \\ 1 \end{bmatrix} = \frac{1}{Z_C} \begin{bmatrix} f & -f\cot\theta & 0 & 0 \\ 0 & \frac{f}{\sin\theta} & 0 & 0 \\ 0 & 0 & 1 & 0 \end{bmatrix} \begin{bmatrix} X_C \\ Y_C \\ Z_C \\ 1 \end{bmatrix}. \tag{2}$$

In equation (2), f represents the focal length of the camera, and θ represents the skewness of the camera coordinate system.

On this basis, determine the relationship between the action image and the camera coordinate system, as shown in the following equation:

$$\begin{aligned} \begin{bmatrix} u \\ v \\ 1 \end{bmatrix} &= \frac{1}{Z_C} \begin{bmatrix} \frac{f}{k} \times \frac{-f\cot\theta}{k} u_0 0 \\ 0 \frac{f}{l\sin\theta} v_0, 0 \\ 0, 0, 1, 0 \end{bmatrix} \begin{bmatrix} X_C \\ Y_C \\ Z_C \end{bmatrix} \\ &= \frac{1}{Z_C} M \begin{bmatrix} X_C \\ Y_C \\ Z_C \\ 1 \end{bmatrix}. \end{aligned} \tag{3}$$

In equation (3), M represents the parameter matrix in the camera. The parameters $(k, l, u_0 v_0, f, \theta)$ represent the internal parameters of the camera. Through the world coordinate system, the three-dimensional motion image of the robot is acquired. The world coordinate system is a three-dimensional rectangular coordinate system established with any point in space as the origin [16]. The relationship between the camera coordinate system and the world coordinate system is as in the following equation:

$$\begin{bmatrix} X_C \\ Y_C \\ Z_C \\ 1 \end{bmatrix} = \begin{bmatrix} R_{3\times3} & t_{3\times1} \\ 0 & 1 \end{bmatrix} \begin{bmatrix} X_W \\ Y_W \\ Z_W \\ 1 \end{bmatrix}. \tag{4}$$

In equation (4), $R_{3\times3}$ represents the rotation matrix, $t_{3\times1}$ represents the translation vector, (X_C, Y_C, Z_C) represents the coordinates in the camera coordinate system, and (X_W, Y_W, Z_W) represents the world coordinate system. In the three-dimensional space, rotate the two-dimensional rotation of the x, y, z coordinate axis obtained above to determine the coordinate angle of the robot's three-dimensional motion image to complete the image acquisition as shown in the following equation:

$$\begin{bmatrix} x^1 \\ y^1 \end{bmatrix} = \begin{bmatrix} \cos\theta & \sin\theta \\ -\sin\theta & \cos\theta \end{bmatrix} \begin{bmatrix} x \\ y \end{bmatrix}. \tag{5}$$

3. Multimotor Drive Control of Upper-Retort-Robot

3.1. The Working Principle of Upper-Retort-Robot. In the field of industrial wine making, retort is the process of evenly spreading the fermented mash into a retort barrel with a diameter of 1.6 m and a depth of 0.8 m. The process flow of the upper retort is shown in Figure 3.

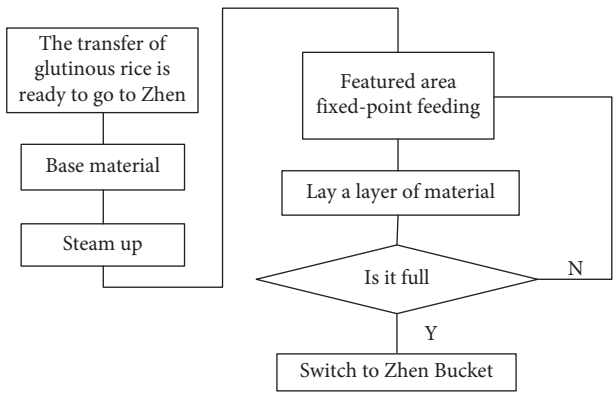

Figure 3: Process flowchart of the upper retort.

In combination with the actual retort process requirements of the winery, the preliminary drafting process of the retort-up by the robot is as follows: First, it is necessary to ensure that the wine can enter the feeding port of the retort-up robot in real time. Then the mash is transported by the robot's internal conveying mechanism to the discharge port of the paving head to prepare for the retort. Then 60–90 mm (3 layers) mash is evenly spread on the bottom of the retort barrel, and the wine is steamed at the bottom of the retort barrel. Then real-time monitoring of the temperature information on the surface of the material layer is obtained. When the temperature is too high (about to leak), it needs to be fixed-point replenishment. When the temperature is moderate, continue to spread a layer of material evenly. Repeat the operation until the retort bucket is full, and then switch to another retort bucket to perform the same operation.

A chassis, a column, two mechanical arms, a servo motor that controls the rotation of the chassis and the rotation of the mechanical arm, and an Jiaolong motor that detects the mixing action are the key components of the robot [19, 20]. The chassis not only supports the entire robot, but also can be driven by the servo motor 1 to establish the rotation on the horizontal plane. The robot arm 1 is connected with the base through the column; and the robot arm 1 and the column are connected by the ball screw. Driven by the servo motor 2, the robot arm is controlled to move up and down on the vertical plane. The two mechanical arms are connected by gear meshing, and the rotation of the mechanical arm 2 is established through the movement of the servo motor 3. The lifting plate and rotating arm motor adjust the mechanical arm according to the position of the barrel during operation to reach the relevant place in the barrel and wait for the material to be disseminated. Then start the feeding equipment to send the raw materials into the hopper, and the raw materials reach the sprinkler under the push of the screw. The spreading port automatically adjusts the spreading position according to the thickness of the material layer fed back by the vision system and the air leakage in the barrel to ensure that the raw materials are spread evenly and the thickness is consistent until the entire barrel is spread [21, 22]. The working principle of the feeding system is as shown in Figure 4.

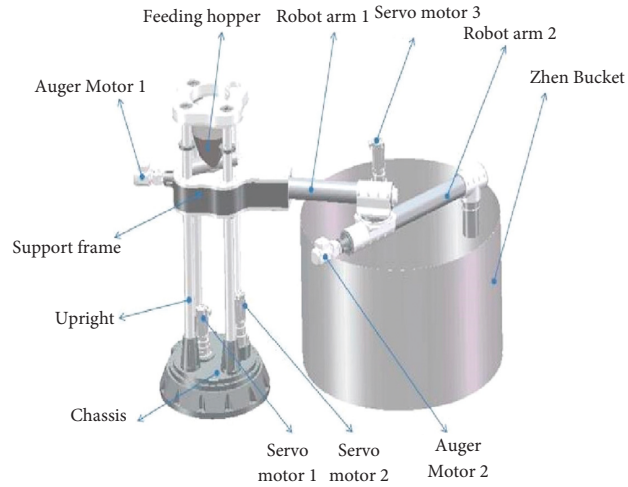

Figure 4: The working principle diagram of the upper retort system.

Clarifying the range of motion for the upper-retort-end robot's effectors, this will serve as a basis for the fermentation workshop's overall equipment architecture. When defining the above motion transformation, it is considered that the origin of the upper robot is located at the boom tilting mechanism, that is, the origin of the coordinate system {2}. In order to complete the model and analyze the working space, transform the base, transfer the origin of the robot to the lower end of the base connected to the ground, and replace the following expression p_z to improve the kinematics model:

$$\overline{p}_z = -a_2 s_2 - d_3 c_2 + 1875. \tag{6}$$

In equation (6), 1875 represents the distance between the origin of the coordinate system {2} and the lower end of the base in mm.

Equation (7), the kinematic equation of the upper robot, describes the position and posture of the fixed coordinate system {4} of Jiont4.

$$T = \begin{bmatrix} r_{11} & r_{12} & r_{13} & p_x \\ r_{21} & r_{22} & r_{23} & p_y \\ r_{31} & r_{32} & r_{33} & \overline{p}_z \\ 0 & 0 & 0 & 1 \end{bmatrix}. \tag{7}$$

For the upper robot, a tool transformation needs to be defined to reflect the transformation of the top of the cloth head device (and effectors) relative to the coordinate system {4}. The top of the cloth head device used extends 845 mm along the y-axis of the coordinate system {4}. The coordinate system model is revealed in Figure 5.

X_{tool} and Z_{tool} are the X-axis and Z-axis of the fixed cloth head coordinate system. Subsequently, the Monte-Carlo method is used to randomly generate joint variables within the variation range of each joint. Combined with the positive kinematics model, the working space of the upper-retort-robot is calculated and provides a reference for the subsequent trajectory generation. The working space projection is shown in Figure 6.

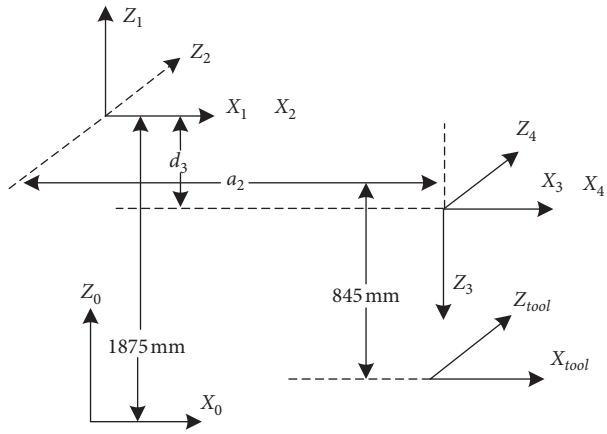

Figure 5: Coordinate system model.

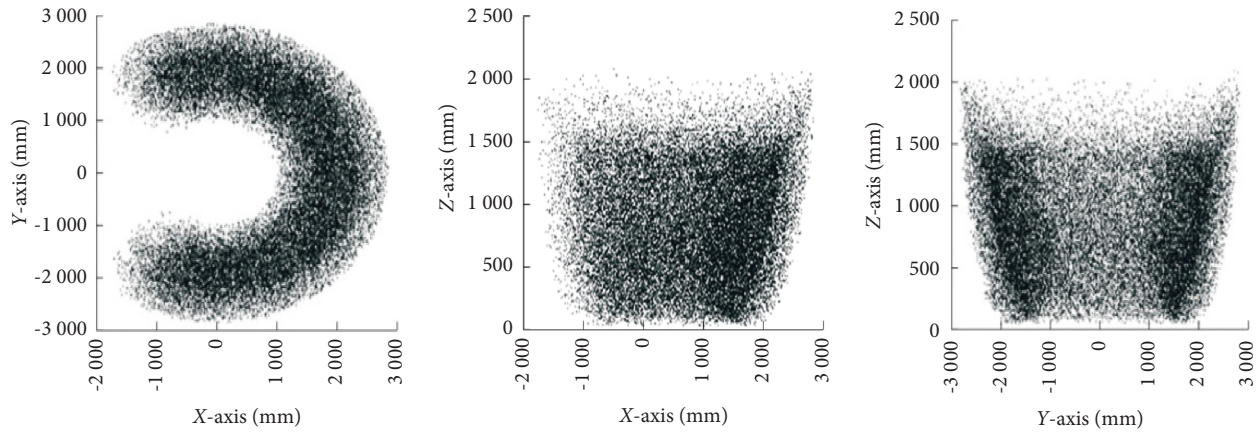

Figure 6: Workspace of the upper-retort-robot.

According to the projection of the feeding range of the three planes and the location relative to the upper-retort-robot, the upper-retort-robot may accomplish the full-coverage of the entire layer of paving duties for a retort drum with a radius of 1600 mm and a height of 2000 mm.

The upper-retort-robot needs to make a reciprocating circular motion around the barrel when spreading materials. The movement is complicated and the air leakage position is required to be accurately reached during the refilling phase. The weight of the robot arm is low when the robot is working, so it adopts an electric method. The control quantity for the electric control valve, which is employed in this system, corresponds to the opening of the electric control valve. At this time, the controller used in the system should as per the digital PID position control algorithm [12].

3.2. Tuning of Different PID Parameters. Determine the fuzzy relationship between the three parameters of PID (proportional parameter K_D , integral action parameter K_I , and derivative action parameter K_D) and the fuzzy relationship between the deviation derivative e_c and the control deviation e. During the operation of electrical equipment, continuity testing is performed on e_c and e. And based on the principle of fuzzy control, the three PID parameters are repeatedly modified to adapt to the different requirements of different deviation derivatives e_c and control deviation e for the three parameters, so that the dynamic and static performance of the controlled object is better [10]. e_c and e are the input items of the fuzzy controller, and the three parameters are the output items. The construction of fuzzy parameter self-tuning control structure is as shown in Figure 7.

In Figure 7, K_p represents the proportional coefficient; K_I represents the integral coefficient; K_D represents the differential coefficient. In the debugging process, firstly, make the integral coefficient adjustment and the differential coefficient adjustment invalid, so as to adjust the proportional coefficient [11]. If the output of the fuzzy parameter is volatile, the scale factor is enlarged until the fuzzy parameter changes have regularity. After setting the proportional coefficient P, set the integral coefficient I. The adjustment process of the integral coefficient is opposite to that of the proportional coefficient. After the integral coefficient I is set, the differential coefficient D is set in the same manner as the proportional coefficient.

The PID control deviation is obtained by subtracting the given parameter value $r(t)$ and the actual output value $c(t)$

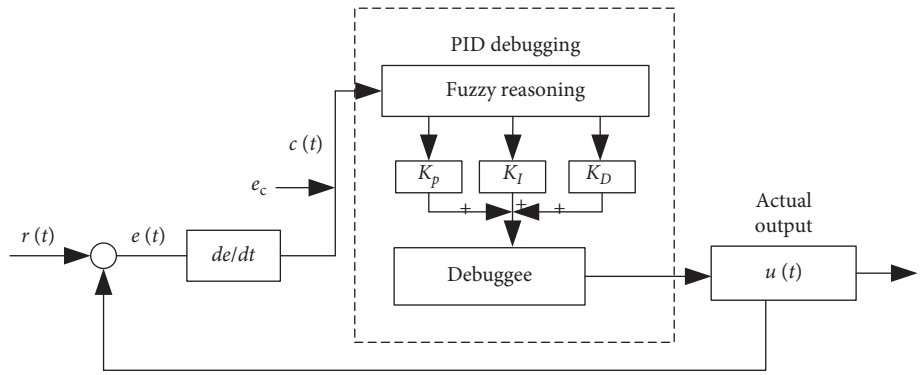

Figure 7: Fuzzy PID self-tuning debugging structure diagram.

of the electrical equipment to be debugged and is derived as given in the following equation:

$$e(t) = r(t) - c(t). \tag{8}$$

The proportional, derivative, and integral of the deviation obtained in equation (9) are linearly combined to form the control variable as follows:

$$u(t) = K_p\left[e(t) + \frac{1}{T_i}\int e(t)\mathrm{d}t + T_d\frac{\mathrm{d}e(t)}{\mathrm{d}t}\right]. \tag{9}$$

In equation (9), $u(t)$ represents the controller output; $e(t)$ represents the deviation signal; $(1/T_i)\int e(t)dt$ represents the integral control term; T_i represents the integral time constant; $T_d\mathrm{d}e(t)/\mathrm{d}t$ represents the integral control term, and T_d represents the derivative time constant. Then use the data approximation method to complete the realization of the PID control law in the computer [12]. If there are fewer test items T, use summation instead of integral, use difference quotient instead of derivative, and discretize the PID. The transformation expression is as follows:

$$\begin{aligned}\int_0^t e(t)dt &\approx T\sum_{j=0}^{k} e(jT) = T\sum_{j=0}^{k} e(j)\\ \frac{\mathrm{d}e(t)}{\mathrm{d}t} &\approx \frac{e(kT) - e[(k-1)T]}{T} = \frac{e(t) - e(k-1)}{T}.\end{aligned} \tag{10}$$

In equation (10), T represents the number of system startup debugging items, $k = 0, 1, 2, \cdots$.

In the process of discretization, if the value of e is too small, the controller will be greatly affected by external interference [13]. Therefore, in order to eliminate the influence of interference, the PID control process needs to be improved. The standard approach of obtaining the average value through numerous consecutive sampling can be used to filter out short-term and fast-changing interference, such as the sudden error of system A/D conversion [14]. However, because the difference term in the method is particularly sensitive to changes in value, when an error occurs, the error of the difference term is estimated and result will be greater. At this time, the four-point central difference calculation can be used to improve the difference term. The four-point central difference does not directly use $e(k)$ but takes the error average $\overline{e}(k)$ at four different moments as the benchmark. The expression is as given in

$$\overline{e}(k) = \frac{e(k) + e(k-1) + e(k-2) + e(k-3)}{4}. \tag{11}$$

After the weighted summation process is performed, the approximate differential is obtained as expressed in the following equation:

$$\frac{\overline{e}(k)}{T} = \frac{(e(k) - e/1.5T) + (e(k-1) - e/0.5T) + (e - e(k-2)/0.5T) + (e - e(k-3)/1.5T)}{4}. \tag{12}$$

After simplification equation (13) is obtained:

$$\frac{\overline{e}(k)}{T} = \frac{1}{6T}\left[e(k) + 3e(k-1) - 3e(k-2) - e(k-3)\right]. \tag{13}$$

Then the improved parameter self-tuning control based on fuzzy PID can be expressed as given in the following equation:

$$u(k) = k_p\left\{e(k) + \frac{T}{T_i}\sum_{i=0}^{k} e(i) + \frac{T_d}{6T}\left[e(k) + 3e(k-1) - 3e(k-2) - e(k-3)\right]\right\}. \tag{14}$$

Because the current is reset to 0 and no longer participates in energy conversion, torque ripple is created by phase torque loss, resulting in torque ripple [15]. As a result of the law of conservation of energy, the instantaneous electromagnetic torque can be estimated as shown in equation (15) when the permanent magnet synchronous motor is disconnected.

$$W_e(t) = \sum_{i\neq k}^{c} \frac{\eta K_m i}{2}\left(c - 1 - \cos\left(2\alpha - (i-1)\times\frac{4\pi}{c}\right)\right) = 4\eta K_m i + \sum_{i\neq k}^{c} \frac{\eta K_m i}{2}\left(\frac{\eta K_m i}{2}\cos\left(2\alpha - (i-1)\times\frac{4\pi}{c}\right)\right). \tag{15}$$

Equation (15) consists of a constant quantity and an alternating variable. In equation (15), e represents the capacity value; t represents the time; η represents the instantaneous electromagnetic torque; $W_e(t)$ indicates the instantaneous electromagnetic torque; K_m indicates the harmonic current injection value; i indicates the constant value of the fundamental torque current component of the motor before and after the fault; c indicates the phase of the permanent magnet synchronous motor; α indicates the current axis.

The constant value in equation (15) determines the average output torque and the alternating variable determines the output pulsating torque [12]. The motor is in phase asymmetric operation after the defect, and the fault-tolerant control method is the process of regulating the current of the normal phase. The fault-tolerant automatic control strategy formulated at this time utilizes the permanent magnet synchronous motor and its inherent n harmonic subspace to control the degree of freedom. The harmonic pulsing torque is compensated by dividing H types of harmonic current injection modes several times, resulting in fault-tolerant automatic control of the system. When the harmonic current injection times are set to 3 times, the expression obtained is as shown in the following equation:

$$i_{\beta 5} = i_{\gamma 5} = i_{\beta 7} = i_{\gamma 7} = 0. \tag{16}$$

When the harmonic current injection times are set to 3 or 5 times, the expression obtained is as shown in the following equation:

$$i_{\beta 7} = i_{\gamma 7} = 0. \tag{17}$$

When the harmonic current injection times are set to 3, 5, and 7, the expression obtained is as shown in the following equation:

$$i_3 \neq 0, \quad i_a \neq 0,\ i_7 \neq 0. \tag{18}$$

Among the above three sets of formulas, β and γ represent the axis of harmonic current; a represents a positive integer. Take the above formula as an example; delete the columns related to the 5th and 7th harmonic currents in the transformation matrix to obtain the transformation matrix as shown in matrix (19):

$$W = \begin{Bmatrix} 1 & 0 & 1 & 0 \\ \cos\theta & \sin\theta & \cos 3\theta & \sin 3\theta \\ \cos 2\theta & \sin 2\theta & \cos 6\theta & \sin 6\theta \\ \cos 3\theta & \sin 3\theta & \cos 9\theta & \sin 9\theta \\ \vdots & \vdots & \vdots & \vdots \\ \cos n\theta & \sin n\theta & \cos 3n\theta & \sin 3n\theta \end{Bmatrix}. \tag{19}$$

In equation (19), θ represents the current axis after transformation. After the harmonic current is injected, the output torque performance of the motor is improved, but the introduced harmonic current will increase the stator copper consumption and reduce the motor efficiency. Therefore, the minimum copper loss is taken as an additional condition, and the stator copper loss is set as shown in the following equation:

$$H = RI_i^w I_i. \tag{20}$$

In equation (20), I_i represents the phase current vector; R represents the resistance. Based on the results obtained above, a fault-tolerant automatic control strategy is formulated.

4. Experimental Analysis

4.1. Experimental Setup. The experimental environment selects the Geek Cloud server, which provides a variety of configurations of services and uses on-time billing. You can choose to occupy or share it alone, which has a very high cost performance. In order to ensure that the designed upper-retort-robot can meet the requirements in terms of speed and position accuracy, semiclosed loop AC servo control is used. The model gathered from the information that the VPL low inertia servo motor from the American A-B company (Rockwell Automation) has an optical encoder, and the accuracy and power can match the criteria of use. At the same time, it is matched with the K5500 series driver. The robot motor driver is shown in Figure 8.

The GPU model is Ge Force GTX1080Ti, 8 GB, GDDR5X, 1733 MHz. The deep learning framework is keras 2.1.2, and the ATT-LSTM network is built using the sequential model. Keras is a bundled Tensor Flow and Theano framework. It is a high-level neural network API that is completely edited by Python. It has the characteristics of modularity and scalability. It can quickly build a network and transform ideas into results. The configuration of the experimental environment is as shown in Table 1.

The methods used are mature, and the applicant is already proficient in relevant methods and is proficient in MATLAB simulation, programming, and motor drive related technical means and has the hardware and software conditions for each link of the test. The specific experimental program is as follows:

(1) Analyze current machine vision algorithms through reading and research of relevant literature; through analysis of existing algorithms, select appropriate

Figure 8: Part of the scene diagram of the automatic retort distillation production line and the robot motor driver.

Table 1: Experimental environment configuration.

Operating system	Ubuntu16.04
Memory	24 Core 64g
Processor	Intel(R)Core(TM)i7-8700k
Disk	200 GB SSD + 3 TB hard disk
Programing language	Python 3.6
Development environment	Pycharm community edition 2019
Others	Keras, Numpy, Pandas, Scikit-Learn

algorithms or improve existing algorithms based on the actual environment of the brewing retort.

(2) Data collection: On-site collection of images, temperature, humidity, and other data during the retort filling process.

(3) Import the collected data into the machine vision algorithm, and the simulation optimization algorithm makes the output control amount optimal.

(4) Import the vision algorithm into the microcontroller, and drive the simple automatic upper-retort-robot to automatically unload the material according to the set target.

4.2. Experimental Results. According to the above MATLAB program, the robot workspace is drawn, and the robot workspace is shown in Figure 9.

In Figure 9, the two barrels in the yellow area are completely in the working space of the robot, indicating that the robot arm can reach any position in the barrel within the defined range. The Jacobian matrix of the robot essentially contains some important information of the robot, such as position, direction, and joint limitations of the end effector. Therefore, the dexterity of the robot according to the Jacobian matrix can be ascertained and can be defined as a new variable as shown in the following equation:

$$\lambda = \sqrt{\det\left(JJ^T\right)}. \tag{21}$$

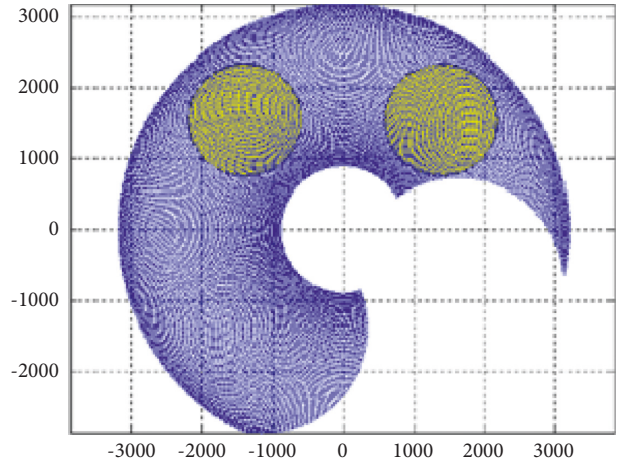

Figure 9: Schematic diagram of the robot workspace.

The robot Jacobian matrix is given in equation (21). The variable is simulated using the MATLAB programme for the motion space simulation stated before, and the equations are presented in equations (22) and (23):

$$J = [-1800\sin a, -1500\sin(a+b); 1800\cos a + 1500\cos(a+b), 1500\cos(a+b)], \tag{22}$$

$$\lambda = \det\left(\text{sqrt}\left(J. * J'.\right)\right). \tag{23}$$

The simulation image of the robot's dexterity is given in Figure 10.

As seen in Figure 10, the robot dexterity λ value range is above the x-y plane, indicating that λ will not be equal to zero, and there will be no singular configuration phenomenon when the robot is working.

In order to simulate the transmission performance of the robot, a transmission angle is defined. There is an angle θ_3 between the speed direction vector of the linear velocity V_B at the end of the rear arm and the joint axis of the forearm during robot movement. Therefore, we define this included angle as the transmission angle between the two arms of the robot and use the cosine value to indicate the excellent transmission performance, which is defined in the following equation:

$$k = \cos(\theta_3). \tag{24}$$

In equation (24), $k \in [0, 1]$, when $\theta_3 = 0$, $\cos(\theta_3) = 1$. The transmission performance between the two arms is the best at this time. When $\theta_3 = \pi/2$, $\cos(\theta_3) = 0$, the transmission performance at this time is the worst. At the same time, MATLAB is used to simulate the value of k, and the result of the robot transmission performance is as shown in Figure 11.

Figure 11 shows that k is predominantly concentrated in the areas of 1 and −1, where transmission performance is excellent, whereas the distribution near 0 is sparse, indicating that transmission performance is poor. It shows that the transmission performance of the robot can meet the needs of the work.

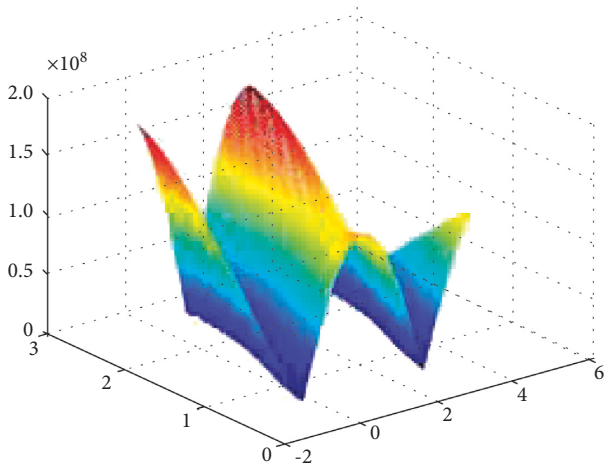

Figure 10: Robot dexterity.

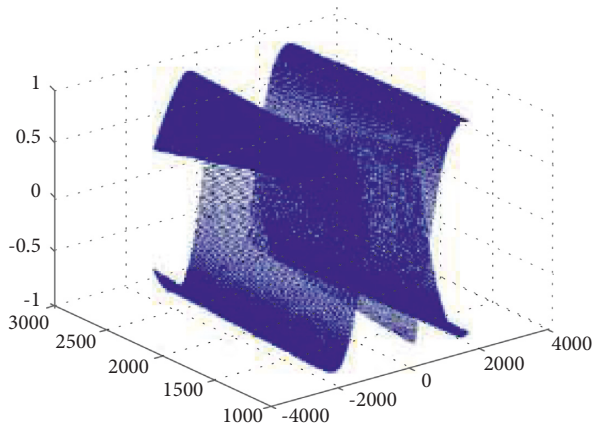

Figure 11: Robot transmission performances.

5. Summary

To meet the demand for wines in cold climates, cutting-edge technologies and fully automated mechanisms are required. This research combines a mechanical drive with an artificial intelligence system. The application of machine vision is carried out. The suggested machine vision-based robotic system is simulated to ensure its feasibility and robustness. The majorities of wineries that serve army facilities with liquors still utilize traditional winemaking processes and make an effort to keep the wine quality high. An automation process is devised using machine vision to serve the purpose. The algorithm parameters are fine-tuned according to the field measured data to deliver the best output. A simple and automatic retort loading robot is designed and developed to apprehend visual algorithm control to drive the robot to load materials automatically. The machine vision algorithm and driving algorithm are further optimized, so that the upper-retort-robot guided by machine vision can automatically unload materials quickly and accurately as per the predefined goals. The brewing retort is automated with the proposed machine vision-based mechanism. The results are calculated on the basis of accuracy in robot transmission and robot dexterity. It is proved that the proposed machine vision-based mechanism can improve the robotic performance by improving the transmission and dexterity. It also promotes automation to suffice the wine requirement in cold regions of army bases in China.

Data Availability

The data are available to researchers on request.

Disclosure

The article is available at Research Square as preprint and available online at https://assets.researchsquare.com/files/rs-1078165/v1_covered.pdf?c=1637001861.

Conflicts of Interest

The authors declare that they have no conflicts of interest.

Acknowledgments

The research was partially supported by the Zunyi Science and Technology Bureau, Moutai Institute Joint Science, and the Technology Research Fund Project: Research on Automatic Technology of Steamer-Filling under the guidance of machine vision.

References

[1] W. Dong, Q. Yang, Y. Liao et al., "Characterisation and comparison of the microflora of traditional and pure culture xiaoqu during the baijiu liquor brewing process: microflora of traditional and pure culture xiaoqu during the baijiu liquor brewing process," *Journal of the Institute of Brewing*, vol. 126, no. 2, pp. 213–220, 2020.

[2] T. Q. Khai, Y. J. Ryoo, W. R. Gill, and D. Y. Im, "Design of kinematic controller based on parameter tuning by fuzzy inference system for trajectory tracking of differential-drive mobile robot," *Int.l J. of Fuzzy Systems*, vol. 7, pp. 1–7, 2020.

[3] A. Zengin, G. Erdemir, T. C. Akinci, F. Selçuk, M. Erduran, and S. Seker, "ROSETLineBot: one-wheel-drive low-cost power line inspection robot design and ctrl," *J. of Electrical Systems*, vol. 15, pp. 626–634, 2019.

[4] Z. Yang, X. Yi, P. Meng, H. Geng, and L. Fu, "Sys. Design of autonomous following robot based on UWB," *Aut. and Instrumentation*, vol. 35, no. 3, pp. 37–40, 2020.

[5] K. Yamato, Y. Tanaka, H. Oku, K. Yasutomi, and S. Kawahito, "Quasi-simultaneous multi-focus imaging using a lock-in pixel image sensor and TAG lens," *Optics Express*, vol. 28, no. 13, Article ID 19152, 2020.

[6] E. M. Burghold, Y. Frekers, and R. Kneer, "Transient contact heat transfer measurements based on high -speed IRthermography," *International Journal of Thermal Sciences*, vol. 115, pp. 169–175, 2017.

[7] S. Gao, Z. Li, and W. Zhang, "Automatic modeling simulation and 3D navigation planning of motion trajectory for manipulator," *Computer Simulation*, vol. 37, no. 10, pp. 297–302, 2020.

[8] A. Mancisidor, A. Zubizarreta, I. Cabanes, P. Bengoa, A. Brull, and J. H. Jung, "Inclusive and seamless control framework for safe robot-mediated therapy for upper limbs rehabilitation," *Mechatronics*, vol. 58, pp. 70–79, 2019.

[9] Z. Qi, Q. Shi, and H. Zhang, "Tuning of digital PID controllers using particle swarm optimization algorithm for a CAN-based DC motor subject to stochastic delays," *IEEE Transactions on Industrial Electronics*, vol. 67, no. 7, pp. 5637–5646, 2020.

[10] M. N. Pham, P. Hamelin, B. Hazel, and Z. Liu, "A two-stage state feedback controller supported by disturbance-state observer for vibration control of a flexible-joint robot," *Robotica*, vol. 38, no. 6, pp. 1082–1104, 2019.

[11] E. Urenda-Cazares, A. Gallegos, and R. Jaimes-Reategui, "Effects of multiplicative noise on the Duffing oscillator with variable coefficients and its integral of motion," *International Journal of Modern Physics C*, vol. 31, no. 07, Article ID 2050095, 2020.

[12] J. Moaryn, J. Petryszyn, and S. Ozana, *PLC Based Fractional-Order PID Temperature Control in Pipeline: Design Procedure and Experimental Evaluation*, pp. 1–17, Meccanica, 2020.

[13] A. M. Dissanayake and N. C. Ekneligoda, "Multi-objective optimization of droop controlled distributed generators in DC microgrids," *IEEE Transactions on Industrial Informatics*, vol. 16, no. 4, pp. 2423–2435, 2020.

[14] W. I Breesam, A. L Saleh, K. A Mohamad et al., "Speed control of a multi-motor system based on fuzzy neural model reference method," *Actuators*, vol. 11, no. 5, 123 pages, 2022.

[15] D. Grzelczyk, O. Szymanowska, and J. Awrejcewicz, "Kinematic and dynamic simulation of an octopod robot controlled by different central pattern generators," *Proceedings of the Institution of Mechanical Engineers - Part I: Journal of Systems & Control Engineering*, vol. 233, no. 4, pp. 400–417, 2019.

[16] A. Jadhav, M. Kaur, and F. Akter, "Evolution of software development effort and cost estimation techniques: five decades study using automated text mining approach," *Mathematical Problems in Engineering*, vol. 2022, Article ID 5782587, 17 pages, 2022.

[17] M. Kaur, "FastPGA based scheduling of dependent tasks in grid computing to provide QoS to grid users," in *Proceedings of the 2016 International Conference on Internet of Things and Applications (IOTA)*, pp. 418–423, Pune, India, January 2016.

[18] N. K. Al-Shammari, "Dynamic simulation and design of a simple hexapod robot," *Indian Journal of Science and Technology*, vol. 13, no. 36, pp. 3801–3819, 2020.

[19] W. Suliman, C. Albitar, and L. Hassan, "Optimization of central pattern generator-based torque-stiffness-controlled dynamic bipedal walking," *Journal of Robotics*, vol. 2020, pp. 1–12, Article ID 1947061, 2020.

[20] L. Jiang, S. R. Sakhare, and M. Kaur, "Impact of industrial 4.0 on environment along with correlation between economic growth and carbon emissions," *Int J Syst Assur Eng Manag*, vol. 13, no. S1, pp. 415–423, 2021.

[21] M. Kaur and S. Kadam, "Bio-inspired workflow scheduling on HPC platforms," *Tehnički Glasnik*, vol. 15, no. 1, pp. 60–68, 2021.

[22] M. Kaur, A. Jadhav, and F. Akter, "Resource selection from edge-cloud for IIoT and blockchain-based applications in industry 4.0/5.0," *Security and Communication Networks*, vol. 2022, Article ID 9314052, 2022.

Hindawi
Mathematical Problems in Engineering
Volume 2022, Article ID 3146658, 9 pages
https://doi.org/10.1155/2022/3146658

Research Article

Performance Optimization of Helicopter Rotor in Hover Based on CFD Simulation

Chenglong Zhou,[1] Anan Xu,[2] Fang Wang,[3] Ming Chen,[3] Wei Li,[1] and Rui Yin[1]

[1]*Information Science Academy of China Electronics Technology Group Corporation, Building 4, Yard 30, Jinfu Road, Shijingshan District, Beijing 100041, China*
[2]*School of Aeronautic Science and Engineering, Beihang University, Xueyuan Road No. 37, Beijing 100191, China*
[3]*Institute of Unmanned System, Beihang University, Xueyuan Road No. 37, Beijing 100191, China*

Correspondence should be addressed to Fang Wang; buaaairforce@buaa.edu.cn

Received 7 June 2022; Accepted 13 July 2022; Published 10 August 2022

Academic Editor: Amandeep Kaur

An optimization method of helicopter rotor hovering performance is proposed, which is mainly carried out by means of CFD simulation. This method can be used to obtain the rotation speed of any blade model under the designed hovering tension through several iterations, and then, the tension, torque, power, and power load of the rotor under the rotation speed can be obtained. By comparing different blade pitch, radius, twist, and chord length, the blade parameters at the highest power load can be selected. A series of new rotor models are obtained by changing the model parameters on the basis of C-T rotor. NASA has carried out a lot of experiments on the C-T rotor model and published detailed experimental reports. The transient simulation is carried out by the embedded grid method.

1. Introduction

The aerodynamic performance of helicopter has a great impact on its overall performance, which is a key problem to be solved in engineering development. Hovering state is one of the most important flight states of a helicopter, which must be considered in the process of helicopter aerodynamic design [1].

In the past, the aerodynamic performance of the helicopter was mainly studied by experimental methods. Now, with the rapid development of computer technology, computational fluid dynamics has been paid more and more attention. The results of the experimental method are more reliable and more suitable for simple problems such as reducing fuselage resistance [2, 3]. However, the experimental method is difficult to observe the detailed characteristics of the helicopter flow field and is often time-consuming and expensive. CFD technology has been developing rapidly in the field of helicopter aerodynamic optimization due to its low cost, short time consumption, and high accuracy.

Nowadays, there are many CFD methods applied to helicopter rotor aerodynamic simulation [4, 5]. Among them, the embedded grid method [6] is the most widely used. This method is applicable to helicopter hovering, forward flight, vertical flight, near ground flight, and other complex flight states. Due to the difficulty in realizing the periodic change of pitch, the sliding grid method cannot be applied to the forward flight state of helicopter. However, it is suitable for calculating the hovering state of the helicopter and is widely used in this field. Steijl and Barakos [7] introduced the sliding mesh method and proved that this method has high precision through several examples. The adaptive mesh method [8, 9] can automatically encrypt the region with large gradient according to the preliminary calculation results, so as to improve the calculation accuracy. It is highly regarded in the field of helicopter aerodynamic simulation, and it can easily capture the wake of rotor vortex. Jameson and Mavriplis [10] adopted the multigrid method to effectively improve the computational efficiency of CFD simulation. Zhao et al. [11] developed the CLORNS code to

solve the unsteady aerodynamic flow field of helicopter rotors and achieved good results. Zhou and Chen [12] proposed a CFD balancing method for helicopter forward flight state, which has a high engineering practical value. Barakos et al. [13] used the method of Actuator Disks (AD) to calculate the rotor flow field in hovering and forward flight and captured the main vortex structure around the rotor disc well. Lyu et al. [14] put forward some improvement suggestions on the hybrid trim method based on CFD for helicopter rotor forward flight.

Generally, in order to determine the accuracy of numerical simulation results, it is necessary to compare the numerical solutions with the experimental values. Detailed test parameters of the C-T rotor selected in this paper at different pitch and rotation speed have been disclosed by NASA.

2. Rotor Aerodynamic Simulation Method

2.1. Solving Equations. The Reynolds average Navier–Stokes (N-S) equation [15, 16] is used for solving:

$$\frac{\partial}{\partial t}\iiint_V \vec{W}\,dV + \iint_S \left(\vec{F}_c - \vec{F}_v\right)\cdot\vec{n}\,dS = 0, \tag{1}$$

where $\vec{W} = [\rho, \rho u, \rho v, \rho w, \rho e]^T$ is the conservation variable, $\vec{F}_c = (f, g, h)$ is the convection flux, and $\vec{F}_v = (a, b, c)$ is the viscous flux. They can be expressed as follows:

$$f = \begin{bmatrix} \rho u \\ \rho u^2 + p \\ \rho uv \\ \rho uw \\ \rho ue + up \end{bmatrix},$$

$$g = \begin{bmatrix} \rho v \\ \rho uv \\ \rho v^2 + p \\ \rho vw \\ \rho ve + vp \end{bmatrix},$$

$$h = \begin{bmatrix} \rho w \\ \rho uw \\ \rho vw \\ \rho w^2 + p \\ \rho we + wp \end{bmatrix},$$

$$a = \begin{bmatrix} 0 \\ \tau_{xx} \\ \tau_{yx} \\ \tau_{zx} \\ u\tau_{xx} + v\tau_{yx} + w\tau_{zx} - q_x \end{bmatrix},$$

$$b = \begin{bmatrix} 0 \\ \tau_{xy} \\ \tau_{yy} \\ \tau_{zy} \\ u\tau_{xy} + v\tau_{yy} + w\tau_{zy} - q_y \end{bmatrix},$$

$$c = \begin{bmatrix} 0 \\ \tau_{xz} \\ \tau_{yz} \\ \tau_{zz} \\ u\tau_{xz} + v\tau_{yz} + w\tau_{zz} - q_z \end{bmatrix}, \tag{2}$$

where the stress is expressed by

$$\begin{aligned}
\tau_{xx} &= \frac{2}{3}\mu\left(2\frac{\partial u}{\partial x} - \frac{\partial v}{\partial y} - \frac{\partial w}{\partial z}\right),\\
\tau_{xy} &= \tau_{yx} = \mu\left(\frac{\partial v}{\partial x} + \frac{\partial u}{\partial y}\right),\\
q_x &= -\mathrm{K}\frac{\partial T}{\partial x},\\
\tau_{yy} &= \frac{2}{3}\mu\left(2\frac{\partial v}{\partial y} - \frac{\partial u}{\partial x} - \frac{\partial w}{\partial z}\right),\\
\tau_{yz} &= \tau_{zy} = \mu\left(\frac{\partial w}{\partial y} + \frac{\partial v}{\partial z}\right),\\
q_y &= -\mathrm{K}\frac{\partial T}{\partial y},\\
\tau_{zz} &= \frac{2}{3}\mu\left(2\frac{\partial w}{\partial z} - \frac{\partial u}{\partial x} - \frac{\partial v}{\partial y}\right),\\
\tau_{xz} &= \tau_{zx} = \mu\left(\frac{\partial w}{\partial x} + \frac{\partial u}{\partial z}\right),\\
q_z &= -\mathrm{K}\frac{\partial T}{\partial z}.
\end{aligned} \tag{3}$$

The correlation between pressure and temperature is expressed by the following formula:

$$\begin{aligned}
p &= \rho(\gamma - 1)\left[e - \frac{1}{2}\left(u^2 + v^2 + w^2\right)\right],\\
p &= \rho RT,
\end{aligned} \tag{4}$$

where ρ is the density, p is the pressure, e is the total energy of gas per unit mass, μ is the viscosity coefficient, K is the heat conduction coefficient, T is the temperature, q_x, q_y, and q_z are the components of the heat flow along three directions, γ is the specific heat capacity, for ideal gas, $\gamma = 1.4$, and $R = 287.3$.

This study adopts the Spalart–Allmaras (S-A) turbulence model proposed by Spalart and Allmaras [17] because this turbulence model is widely used in the field of aerodynamic simulation of aircraft and has been verified by many cases.

The flow field of rotor is discretized by the finite volume method. According to different discrete methods of inviscid flux, different interpolation schemes are formed. In this study, Roe format [18] is adopted, which is a relatively common type of upwind format.

In the transient simulation of this study, the time discretization method adopts the dual time stepping method. Jameson [19] explained the principle and advantages of this method in his article.

The outermost boundary of helicopter flow field is set as nonreflective boundary, and the surfaces of rotor blades are set as nonsliding wall.

2.2. Grid System. The rotor motion is modeled by the embedded grid method. This method divides the flow field into multiple subdomains and generates mesh blocks for each subdomain. Different mesh blocks can be overlapped, nested, or covered.

For the aerodynamic simulation of helicopter rotor in this study, a structured embedded grid method is adopted. It is mainly composed of two parts. The first is an H-O grid surrounding the blades. In order to make the calculation results more accurate, the grid points in the area with significant viscous effect are locally encrypted. The H-O grid moves with the blade. The second is a stationary background grid nested on the H-O grid, which is a cylindrical region with a radius of $5R$. Its upper boundary is $3R$ away from the paddle plane, and its lower boundary is $5R$ away from the paddle plane, where R is the radius of the blade. Figure 1 shows the embedded grid system of helicopter rotor aerodynamic simulation in this paper.

3. Optimization of Hover Performance

The power load of the helicopter rotor in hovering conditions is mainly affected by the rotation speed, total pitch, radius, torsion angle, chord length, and other factors of the blades. Meanwhile, different airfoils also have certain influences on the power load of the rotor.

The power load formula of the rotor is shown as

$$q = \frac{G}{N_e^{(0)}}, \tag{5}$$

where q represents the gravity that the engine can lift at the rated power under standard atmospheric conditions at sea level, and its unit is N/kW. The gravity of the helicopter in hover is close to the pulling force of the rotor ($T \approx G$), and the output shaft power of the engine at sea level is simplified to the available power of the rotor ($(N_e^{(0)} \approx M * \Omega)$). M represents the torque of the rotor around the spindle, and Ω represents the angular velocity of the rotor.

The main purpose of hover performance optimization is to increase the power load of the rotor as much as possible on the premise of satisfying the limitation factors such as material strength and space. The higher the power load is, the less power the rotor needs to provide the same pulling force and the longer the helicopter's endurance is.

In the process of blade design and optimization, in order to ensure that the pulling force provided by the rotor is not changed, with the change of blade radius, total pitch, torsion angle, chord length, etc., the rotation speed of the blade should also be changed accordingly, resulting in different power loads of different blade models.

In this study, a method to optimize the hovering performance of helicopter rotors is designed. The specific steps are as follows:

(1) Determine the pulling force of the helicopter rotor designed in hover, defined as T_{desire}.

(2) Design an initial blade with a fixed aspect ratio and no torsion, and determine the number of blades, so as to obtain the initial rotor.

(3) An assumed total distance φ was given to the blade. Meanwhile, a relatively large rotation speed n_1 and a relatively small rotation speed n_2 were set, respectively. CFD method was used to calculate the rotor's pulling force T_1, T_2, and torque M_1 and M_2, respectively, at the rotation speed n_1 and n_2, which met the requirements of $T_1 > T_{\text{desire}} > T_2$.

(4) According to the formula $n_3 = n_1 - (T_1 - T_{\text{desire}}/T_1 - T_2) * (n_1 - n_2)$, the new rotation speed n_3 can be obtained. The CFD method was used to calculate the pulling force T_3 and torque M_3 of the rotor at rotation speed n_3. If $|T_3 - T_{\text{desire}}| < \varepsilon$, it is considered that the requirement of design hover tension can be met at the rotation speed of n_3. If $|T_3 - T_{\text{desire}}| \geq \varepsilon$, the formula $n_4 = n_3 - (T_3 - T_{\text{desire}}/T_3 - T_2) * (n_3 - n_2)$ is used to get the new rotation speed of n_4, and the CFD method is used again to calculate the pulling force T_4 and torque M_4 of the rotor at the rotation speed of n_4. In this way, iterate i times until $|T_i - T_{\text{desire}}| < \varepsilon$ is satisfied, which means that the design hovering pulling force requirement is satisfied when the rotation speed is n_i. The CFD method is used to calculate the pulling force T_i and moment M_i of the rotor at the speed n_i, and the power load q of the rotor can be obtained according to the rotation speed n_i, pulling force T_i, and moment M_i. Here, ε represents a small value, which is taken as 10 N in this paper.

(5) Given different total pitch of the blades, repeat steps 3 and 4 in turn to get the power load of the rotor at different total pitch, select the maximum power load, and take the total pitch corresponding to the maximum value as the optimal total pitch.

(6) The blades with the optimal total pitch were enlarged or reduced in turn according to the specified multiple, and then, steps 3 and 4 were repeated to calculate the power load of the models with different amplification or reduction multiples. On the premise that the strength, space, and other factors of the blade meet the design requirements, the radius of maximum power load is selected as the optimal radius of the blades.

(7) The blades with the optimal total pitch and the optimal radius were used to repeat steps 3 and 4 with different torsion angle successively, and the power loads of the blade models with different torsion angle were calculated. The torsion angle corresponding to the maximum power load was taken as the optimal torsion angle of the blades. In this study, the torsion angle of the designed blades changes according to the linear law.

(8) The blade models with the optimal total pitch, optimal radius, and optimal torsion angle were scaled to change the chord length, and steps 3 and 4 were repeated to obtain the power load of the blade models with different chord lengths. The chord length with the maximum power load is selected as the optimal chord length of the blades.

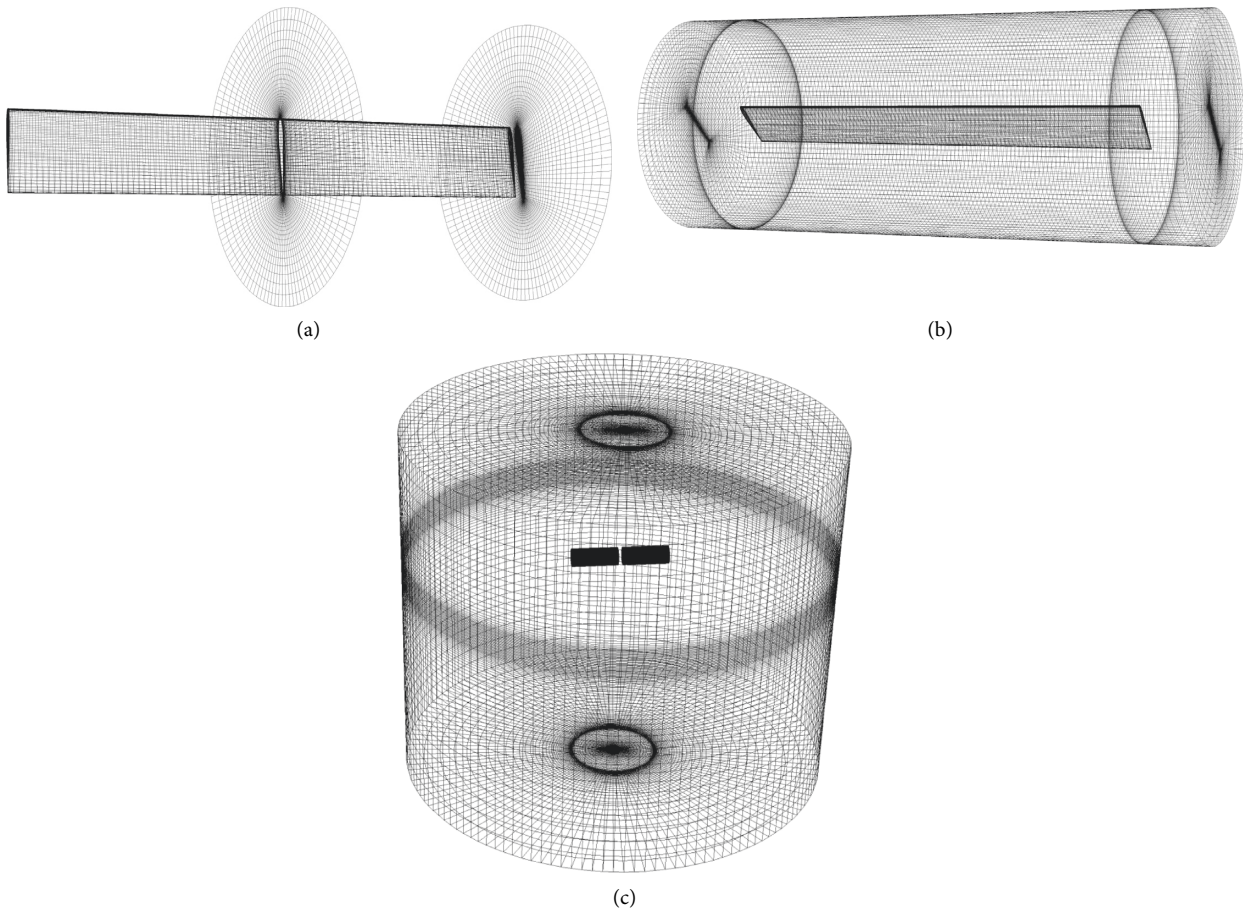

Figure 1: Embedded grid system of helicopter rotor aerodynamic simulation. (a) Profile of the blade grid. (b) An H-O grid around the blade. (c) Assembly of the embedded grid.

Table 1: Detailed design data of C-T rotor.

Number of blades (N)	2
Blade radius (R)	1.143 m
Plane shape of blade	Rectangle
Airfoil	NACA0012
Chord length (c)	0.1905 m
Undercut (R_{cut})	0.243R
Torsion angle	0°

By this method, the optimal parameters of the helicopter blade model can be obtained at a relatively low cost with only a few flight tests at the initial stage of blade design, thus greatly shortening the design cycle of the blade and saving a lot of research costs.

4. Examples and Discussion

In this study, taking the C-T [20] single rotor model as an example, the influence of blade radius, total pitch, torsion angle, and chord length on the power load of the rotor in hover is sequentially analyzed by the CFD method. Table 1 shows the detailed design data of C-T rotor.

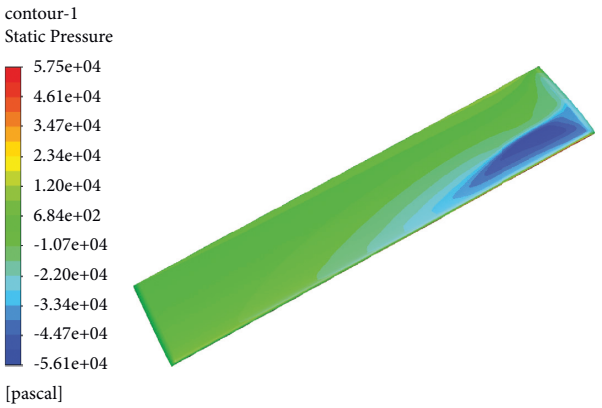

Figure 2: Pressure contours of C-T blade.

Four experimental states from NASA's experimental reports were selected to verify the credibility of the CFD method proposed in this paper. They are, respectively, (1) $M_{tip} = 0.433$, $\theta_c = 5^\circ$, $\Omega = 1250$ rpm, and $C_T = 0.00213$; (2) $M_{tip} = 0.612$, $\theta_c = 8^\circ$, $\Omega = 1750$ rpm, and $C_T = 0.00455$; (3) $M_{tip} = 0.877$, $\theta_c = 8^\circ$, $\Omega = 2500$ rpm, and $C_T = 0.00473$; (4) $M_{tip} = 0.612$, $\theta_c = 12^\circ$, $\Omega = 1750$ rpm, and $C_T = 0.00807$,

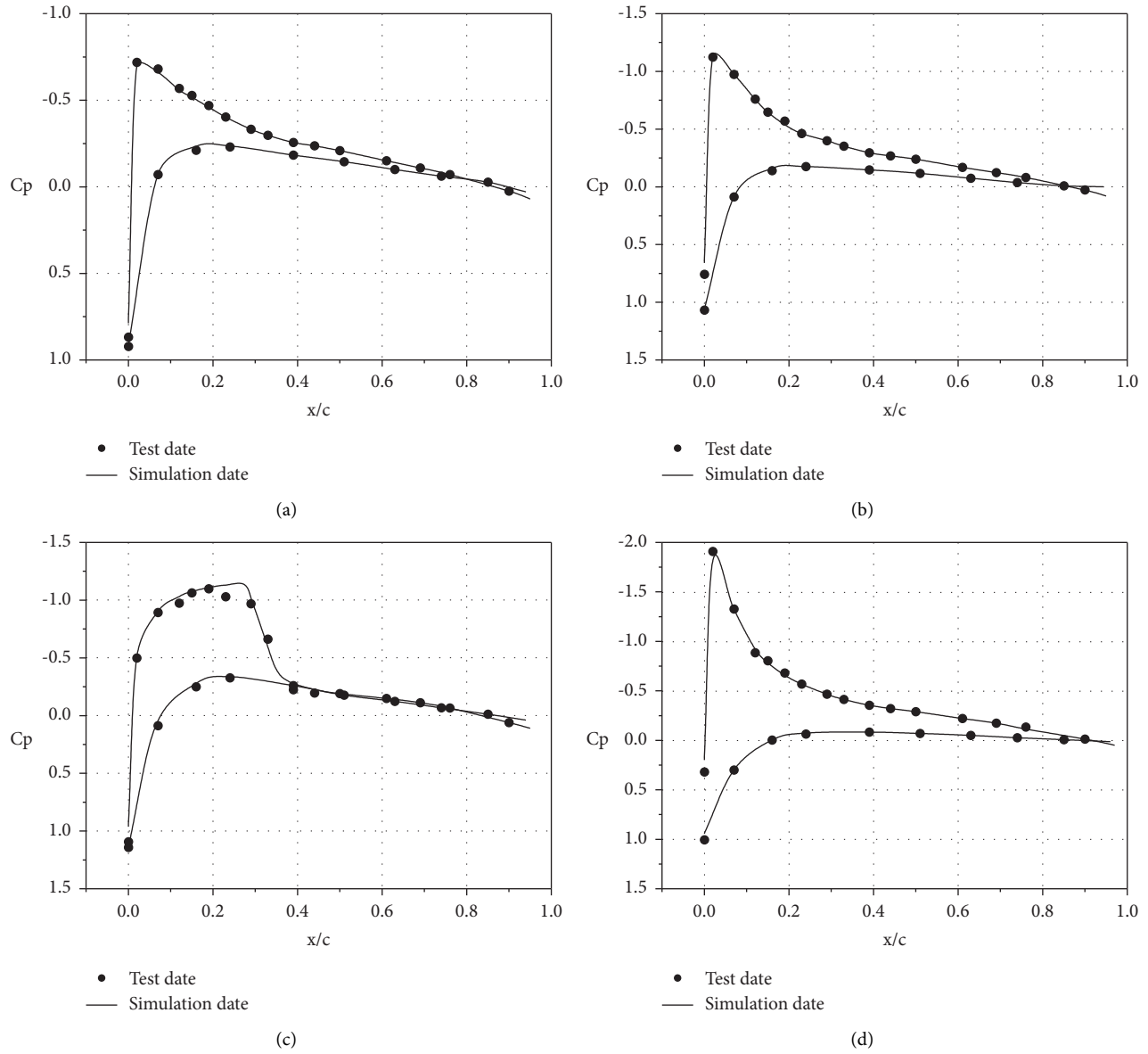

Figure 3: Surface pressure coefficients of C-T rotor at 0.96R profile in hover. (a) $M_{\text{tip}} = 0.433$ and $\theta_c = 5^\circ$. (b) $M_{\text{tip}} = 0.612$ and $\theta_c = 8^\circ$. (c) $M_{\text{tip}} = 0.877$ and $\theta_c = 8^\circ$. (d) $M_{\text{tip}} = 0.612$ and $\theta_c = 12^\circ$.

where M_{tip} is the Mach number at the blade tip, θ_c is the total pitch, Ω is the rotation speed, and C_T is the thrust coefficient of the rotor.

Figure 2 is the pressure contours of C-T rotor corresponding to test state 3. In this figure, obvious shock waves appear at the blade tip position of CT rotor.

Figure 3 compares the simulation date and the test date of the pressure coefficient at 0.96 R of the C-T rotor, from which it is not difficult to find that the simulation date and the test date are highly consistent.

Figure 4 shows the comparison between the simulation date and the test date of the thrust coefficient:

In Figure 4, SMA stands for simple moving average, which allows curves to appear in a smoother manner. The SMA formula is as follows:

$$\text{SMA} = \frac{x_M + x_{M-1} + x_{M-2} + \cdots + x_{M-(n-1)}}{n}. \tag{6}$$

Figure 4 shows that the simulation value of thrust coefficient is in good agreement with the experimental value.

In this study, working condition 3 is selected as the basic working condition before rotor performance optimization. Under this working condition, the thrust and torque of the rotor are 2218 N and 298.98 N $*$ m, respectively, by CFD calculation.

Firstly, the performance of the rotor was optimized by changing the total pitch of the blade. In the optimization process, the thrust value of the rotor calculated in working condition 3 was taken as the desired thrust T_{desire} of the rotor in hover. The thrust value calculated with a different total pitch should be almost equal, which is mainly realized by

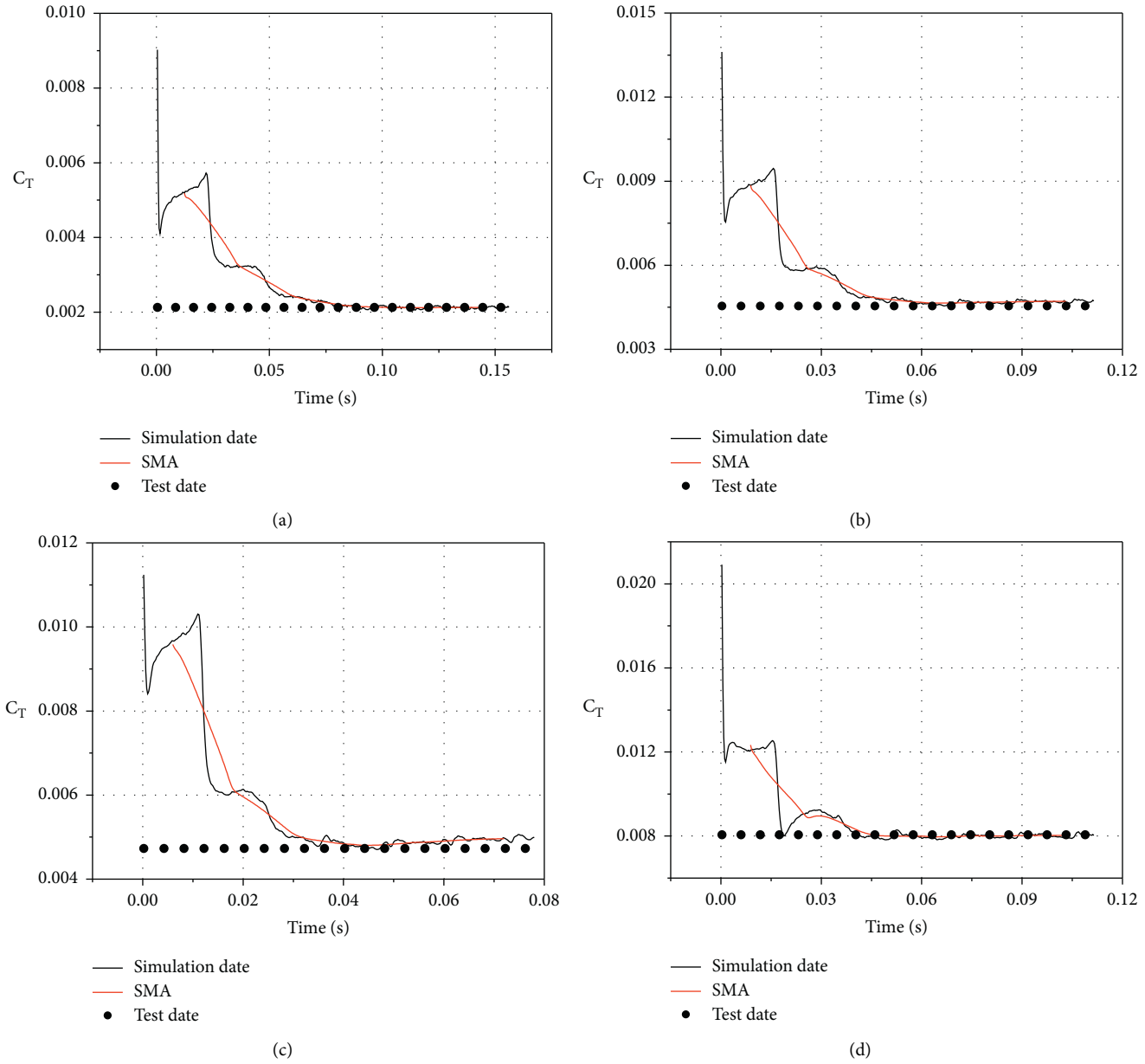

Figure 4: The comparison between simulation date and test date of thrust coefficient. (a) $M_{tip} = 0.433$ and $\theta_c = 5^\circ$. (b) $M_{tip} = 0.612$ and $\theta_c = 8^\circ$. (c) $M_{tip} = 0.877$ and $\theta_c = 8^\circ$. (d) $M_{tip} = 0.612$ and $\theta_c = 12^\circ$.

Table 2: CFD simulation results of rotors with a different total pitch.

Total pitch (°)	Rotation speed (rpm)	Thrust (N)	Torque (N ∗ m)	Power load (N/kW)
6	2975	2223	410.68	17.37
7	2730	2216	317.44	24.42
8	2500	2218	292.98	28.92
9	2320	2221	293.16	31.18
10	2180	2220	309.57	31.42
11	2060	2216	328.22	31.30
12	1962	2220	350.10	30.87
13	1890	2225	373.01	30.14
14	1825	2222	999.90	29.08

Table 3: CFD simulation results of rotors with different radius.

Radius (m)	Rotation speed (rpm)	Thrust (N)	Torque (N ∗ m)	Power load (N/kW)
0.8R	3310	2221	283.18	22.63
0.85R	2960	2219	281.82	25.40
0.9R	2660	2219	285.32	27.92
0.95R	2400	2212	294.58	29.88
R	2180	2220	309.57	31.42
1.05R	1977	2220	323.93	33.10
1.1R	1813	2220	336.44	34.75
1.15R	1660	2211	349.54	36.39
1.2R	1530	2212	367.92	37.52
1.25R	1415	2223	384.42	39.03
1.3R	1310	2222	400.71	40.43

Table 4: CFD simulation results of rotors with different torsion angles.

Torsion angle (°)	Rotation speed (rpm)	Thrust (N)	Torque (N ∗ m)	Power load (N/kW)
−2	1880	2226	323.24	34.97
−4	1890	2217	317.66	35.27
−6	1907	2218	314.88	35.28
−8	1920	2214	309.06	35.64
−10	1935	2221	306.05	35.82
−12	1950	2212	302.13	35.86
−14	1975	2219	302.86	35.42
−16	1995	2219	302.72	35.09

Table 5: CFD simulation results of rotors with different chord lengths.

Chord length (m)	Rotation speed (rpm)	Thrust (N)	Torque (N ∗ m)	Power load (N/kW)
0.8 ∗ 1.1c	2055	2216	292.57	35.20
0.9 ∗ 1.1c	2020	2228	297.09	35.45
1.0 ∗ 1.1c	1950	2221	302.13	36.00
1.1 ∗ 1.1c	1880	2222	310.82	36.31
1.2 ∗ 1.1c	1820	2215	317.32	36.62
1.3 ∗ 1.1c	1776	2219	318.47	37.46
1.4 ∗ 1.1c	1745	2220	320.28	37.93

changing the rotation speed of the rotor. Table 2 shows the results of CFD calculation:

It can be seen from Table 2 that when the total pitch is 10°, the C-T rotor has the maximum power load, that is, the optimal hovering performance. Therefore, the total pitch of 10° is selected as the optimal total distance of the blade.

The total pitch of the blades was maintained at 10°, and the airfoil, undercut, and aspect ratio remained unchanged. Then, the model of the blades was scaled up or down in equal proportion. Table 3 shows the results of the CFD simulation:

According to the analysis of Table 3, as the rotor radius increases, so does the power load of the rotor. Therefore, in theory, the blade radius should be as large as possible. However, due to the limitation of the blade material, if the radius of the blade is too large, it is easy to break. At the same time, the large-sized rotor is more likely to achieve large torque, which the engine cannot withstand. Considering comprehensively, 1.1R is temporarily selected as the optimal radius of the blade in this study, where R is 1.143 m. In the process of engineering design, the radius of the blade must be determined according to the rated parameters of the engine, so as to achieve a higher matching degree between the blade and the engine.

After the optimal size of the rotor radius is determined, the rotor blades are given different torsion angles, and the influence of torsion angle on the hovering performance of the rotor is analyzed through CFD simulation. The simulation results are shown in Table 4.

It can be seen from Table 4 that the rotor has the highest power load when the torsion angle is −12°, that is, the rotor has the optimal hovering performance. Therefore, −12° is chosen as the optimal torsion angle of the blades.

After the optimal values of the rotor's total pitch, radius, and torsion angle are selected, the power loads of the blades with different chord lengths are calculated to select the optimal chord length of blades. When determining the optimal radius of the blades, the proportion of the blades is enlarged by 1.1 times. Therefore, when selecting the blades with a radius of 1.1R as the basic model for the optimization analysis of chord length, the initial chord length should be 1.1c, and c is the chord length of the C-T rotor. The calculated results are shown in Table 5:

Table 5 shows that, for this design condition, the power load of the rotor increases gradually with the increase of chord length. However, bigger is not always better because too large a chord length can affect the forward flight performance of a rotor. In the process of engineering design, the determination of the chord length of the blades should also consider the requirements of working conditions such as forward flight of the helicopter.

Through the analysis in Tables 2 to 5, the optimal total pitch, optimal radius, optimal torsion angle, and optimal chord length of the rotor in hover can be determined in turn, thus obtaining an initial design scheme of the blade with excellent hovering performance.

5. Conclusion

This study proposes and verifies a CFD simulation method to optimize the hovering performance of helicopter rotors, from which some useful inspiration can be obtained:

(1) In this simulation, the Navier–Stokes equation is solved by the embedded grid method, and multiple working conditions of C-T rotor are calculated and verified, thus proving that the numerical method has high accuracy for rotor flow field in hovering state.

(2) Take the C-T rotor as an example to explain the optimization process in detail. This method avoids the shortcomings of traditional test methods, such as long research period and huge cost, and has high versatility. Therefore, it has the high engineering application value.

(3) There is still room for further improvement. In this study, the optimal value of each parameter is determined in order of total pitch, radius, torsion angle, and chord length. In the next step, we can try to exchange the order of each parameter to determine the optimal parameter order. In addition, the variation of chord length with radius should also be considered.

(4) The airfoil of the blade optimization example discussed in this study is NACA0012. In the engineering design stage, the blades of different airfoils should be optimized and compared, respectively.

(5) The CFD method does not consider the influence of blade deformation. In the next step, the coupling method of CFD/CSD can be adopted to fully consider the interaction between blade structure and flow field, so as to further improve the accuracy of simulation.

Data Availability

All data, models, and code generated or used during the study are included within the article.

Disclosure

Chenglong Zhou and Anan Xu are co-first author.

Conflicts of Interest

The authors declared no potential conflicts of interest with respect to the research, authorship, and/or publication of this article.

Acknowledgments

This study was funded by the National Key Research and Development Project of China (no. 2021YFC3002101).

References

[1] M. Costes, T. Renaud, and B. Rodriguez, "Rotorcraft simulations: a challenge for CFD," *International Journal of Computational Fluid Dynamics*, vol. 26, no. 6-8, pp. 383–405, 2012.

[2] C. L. Burley, T. F. Brooks, K. Y. Rozier et al., "Rotor wake vortex definition-evaluation of 3-C PIV results of the HART-II study," *International Journal of Aeroacoustics*, vol. 5, no. 1, pp. 1–38, 2006.

[3] N. M. Komerath, M. J. Smith, and C. Tung, "A review of rotor wake physics and modeling," *Journal of the American Helicopter Society*, vol. 56, no. 2, p. 22006, 2011.

[4] A. Brocklehurst and G. N. Barakos, "A review of helicopter rotor blade tip shapes," *Progress in Aerospace Sciences*, vol. 56, no. JAN, pp. 35–74, 2013.

[5] F. E. Tejero, P. Doerffer, and O. Szulc, "Numerical simula-tion of the tip aerodynamics and acoustics test," *Journal of Thermal Science*, no. 2, pp. 153–160, 2016.

[6] J. A. Benek, P. G. Buning, and J. L. Steger, "A 3-D chimera grid embedding technique," *7th Computational Physics Con-ference*, pp. 322–331, 1985.

[7] R. Steijl and G. Barakos, "Sliding mesh algorithm for CFD analysis of helicopter rotor-fuselage aerodynamics," *International Journal for Numerical Methods in Fluids*, vol. 58, no. 5, pp. 527–549, 2008.

[8] A. M. Wissink, M. Potsdam, V. Sankaran, and J. Sitaraman, "A coupled unstructured-adaptive Cartesian CFD approach for hover prediction," *66th Annual Forum Proceedings - AHS International*, pp. 1300–1317, 2010.

[9] J. Lim, A. M. Wissink, and B. Jayaraman, "Application of adaptive mesh refinement technique in Helios to blade-vortex interaction loading and rotor wakes," *67th American Helicopter Society International Annual Forum*, pp. 228–250, 2011.

[10] A. Jameson and D. Mavriplis, "Finite volume solution of the two-dimensional Euler equations on a regular triangular mesh," *AIAA Journal*, vol. 24, no. 4, pp. 611–618, 1986.

[11] Q. Zhao, G. Zhao, B. Wang, Q. Wang, Y. Shi, and G. Xu, "Robust Navier-Stokes method for predicting unsteady flowfield and aerodynamic characteristics of helicopter rotor," *Chinese Journal of Aeronautics*, vol. 31, no. 2, pp. 214–224, 2018.

[12] C. Zhou and M. Chen, "Computational fluid dynamics trimming of helicopter rotor in forward flight," *Advances in Mechanical Engineering*, vol. 12, no. 5, pp. 168781402092525–13, 2020.

[13] G. N. Barakos, T. Fitzgibbon, A. N. Kusyumov, and S. A. Jusyumov, "CFD simulation of helicopter rotor flow based on unsteady actuator disk model," *Chinese Journal of Aeronautics*, vol. 33, no. 09, pp. 37–52, 2020.

[14] W. Lyu, S. Wang, and A. Yang, "Some improvements of hybrid trim method for a helicopter rotor in forward flight,"

Aerospace Science and Technology, vol. 113, no. 9, p. 106709, 2021.

[15] G. X. Xiang, Y. C. Zhang, C. F. Zhang, and Y. Kou, "Study on initiation mechanism of oblique detonation induced by blunt bump on wedge surface," *Fuel*, vol. 323, p. 124314, 2022.

[16] G. X. Xiang, Y. Zhang, X. Gao, H. Li, and X. Huang, "Oblique detonation waves induced by two symmetrical wedges in hydrogen-air mixtures," *Fuel*, vol. 295, p. 120615, 2021.

[17] P. R. Spalart and S. R. Allmaras, "A one-equation turbulence model for aerodynamic flows," *Recherche Aerospatiale*, vol. 1, no. 1, pp. 5–21, 1994.

[18] P. L. Roe, "Approximate riemann solvers, parameter vectors, and difference schemes," *Journal of Computational Physics*, vol. 135, no. 2, pp. 250–258, 1997.

[19] A. Jameson, "Time dependent calculations using multigrid, with applications to unsteady flows past airfoils and wings," *10th Computational Fluid Dynamics Confer-ence*, vol. 1991, p. 87686, 1991.

[20] F. X. Caradonna and C. Tung, "Experimental and analytical studies of a model helicopter rotor in hover," *Vertica*, vol. 5, no. 2, pp. 149–161, 1981.

Hindawi
Mathematical Problems in Engineering
Volume 2022, Article ID 3013777, 8 pages
https://doi.org/10.1155/2022/3013777

Research Article

Applying Meta-Frontier Approaches to Profitability Estimation: In Case of the Effects of Official Independent Directors

Xiaozhi Xu[1], **Lichen Chou**[2], **Qing Lu**[3] and **Yaqi Tian**[4]

[1]*School of Finance and Trade, Wenzhou Business College, Wenzhou, China*
[2]*Business School, Shantou University, Shantou, China*
[3]*School of Economics and Trade Management, Wenzhou Vocational College of Science and Technology, Wenzhou, China*
[4]*Department of Diplomacy and Foreign Affairs Management, China Foreign Affairs University, Beijing, China*

Correspondence should be addressed to Qing Lu; luqing@wzvcst.edu.cn

Received 23 May 2022; Revised 19 June 2022; Accepted 14 July 2022; Published 8 August 2022

Academic Editor: Amandeep Kaur

The meta-frontier approach can mathematically understand the production dynamics. With the help of meta-frontier approach differences, the efficiency of income and earnings between companies with different structure can be estimated. Considering the great influence of independent directors on the economic market, this study estimated such effects from the perspective of production function models. It is found that the revenue efficiency results can be optimized without considering the technology heterogeneity for listed companies. When considering the common production boundary, there is an issue that the revenue efficiency of listed companies that own official independent directors is lower than other listed companies that without official independent directors, and the empirical results show that the withdrawal of official independent directors in the market has a positive impact on the profitability of the company.

1. Introduction

The board of directors is an important part in the company's investment decision-making and execution process, and independent directors play an important role in relieving agency conflicts and protecting the interests of small and medium investors [1, 2]. Previous literature suggested that the company's directorship mechanism could fully exert its functions such as supervisory, strengthening, and supporting operational resources [3, 4]. In the study of officials as independent directors, domestic literature pointed out that listed companies could establish good interoperability with the government by hiring government officials to enter the board of directors and obtain more resources, policy support, and projects. Lu et al. [5] pointed out that the appointments of government and university officials as independent directors are obviously different in terms of business operation violations. The violation of the former is significantly higher than the latter. The author believed that the relevant provisions of the central organization department were conducive to the maintenance and development of the market order [6–8].

The differences in the operating patterns of listed companies not only reflect the difference in management culture but also cause differences in the marketing targets required in the operation process; thus, the input structure of the company's revenue, manpower, or capital investment would be influenced [9–11]. However, previous literature on the operational efficiency of enterprises mostly used the stochastic boundary method of Battese and Coelli [12] or extended the data-envelope analysis method proposed by Charnes et al. [13] to explore the impact of different management types on operating efficiency. These researchers use different management patterns as exogenous environmental variables to explore their impact on operating efficiency or estimate a representative production boundary and calculate the operating (technical) efficiency of each sample hotel and make comparison between each group's different management patterns [14, 15]. However, both of these approaches ignore the issue of using

heterogeneous production technologies for different types of management. Different types of managers in the same industry may have different production behaviors and technologies due to differences in organizational structure, structure of operating directors, or input factor attributes [16, 17]. Under such circumstances, if the performance assessment is still conducted by using the homogeneous assumption of traditional production techniques, the estimation results may be biased or miscalculated. If companies consider the heterogeneity of production techniques in each group and individually estimate the production boundaries of each group, then they compare the performance of cross-group operations and would lose their economic significance due to differences in the baseline (production boundary).

This study therefore takes China's listed companies of the textile industry as a case and discusses the effect of official independent directors on the profitability of listed companies. Based on the perspective of production performance, the author uses the performance model to analyze the differences in the operating efficiency and income efficiency between companies with official independent directors and other companies. Since the regulation limiting official independent director was not actually implemented until 2015, the author therefore empirically collects the panel data of six years from 2010 to 2015 for research. The characteristics of this study are as follows: (1) under the requirements of the comparison of technical heterogeneity and efficiency, the author uses the meta-frontier model proposed by Battese et al. [18] and O'Donnell et al. [19] to divide the samples into groups such as companies with official independent directors and companies without official independent directors according to different management patterns. The meta-frontier model is adopted because this study was inspired by the work of Walheer et al. [20] in European Journal of Operational Research. The methodological reflections will be explained in the next section. Based on the baseline of the overall industry, the differences in the operating efficiency and profit earning efficiency of different directors' structure types are compared. (2) This study also quotes a stochastic boundary model proposed by Battese and Coelli [12], which includes location (such as whether the enterprise is located in the municipality), market characteristics (market competition degree), individual enterprise characteristics (operating year), and the effect of exogenous environment variables on operation and earnings efficiency.

2. Reflections on Estimation Methodologies

The concept of co-production boundary was first proposed by Hayami [21] and Hayami and Ruttan [22]. Hayami and Ruttan [22] thought that the common production function could be regarded as the envelope of the classical production function. Ruttan et al. [23] defined the common production function as the envelope formed by the most efficient production sites among the groups. This innovative concept provided a more appropriate basis for further analysis and reduced the misgivings of comparative analysis errors between groups [24–26]. Then, Lau and Yotopoulos [27], and Kim and Lau [28] applied and conducted empirical analysis of cross-country data. Besides, Gunaratne and Leung [28] and their followers such as Kovalevsky and Máñez-Costa [30] added random concepts to common production functions.

Battese and Rao [31] proposed the random co-production boundary model and used the SFA method to estimate the technical efficiency of cross-group comparisons and no longer used the methods proposed in the previous literature [27]. He first converted the factors of each group into a certain proportion, then deleted the individual differences between the conversion factors of each group by means of differentials, and concluded that the conversion factor could not be estimated. Battese et al. [18] modified the model of Battese and Rao [31], assuming that there was only one data-generation process, and proposed a two-stage method for estimating common boundary parameters. In the first stage, the SFA method was used to estimate the production boundary and technical efficiency for each group. In the second stage, the parameters obtained from the first stage were estimated and the data of each group were merged. The linear programming (LP) and the quadratic programming (QP) were used to estimate the common production boundary and technology. The technology gap ratio (TGR) could be used to solve the problem that the common production boundary could not envelop the production boundaries of all groups, and a cross group comparison could also be made.

O'Donnell et al. [19] used the concept of distance function to establish the theoretical framework of the joint production boundary, group boundary, and the relationship between the two more clearly. At the same time, the DEA method and the SFA method were used to estimate the common production boundary. Between 1986 and 1990, the agricultural production data of 97 countries were divided into four groups according to regions, and the technical efficiency of each group was compared. Since Battese et al. [18] and O'Donnell et al. [19] proposed a two-stage method for estimating common production functions, the development of the common production function has matured. At present, most scholars entitled such SFA also as "meta-frontier analysis." Recently, many scholars have paid attention to it and applied it to empirical research. For example, Shen et al. [32], Luo et al. [33], Nakaishi et al. [34], Chou et al. [35], and Chou and Zhang [39]havesuccessful applications. Similar to these literature, this study uses meta-frontier analysis as an exploratory tool for further estimation in case of the textile industry.

3. Methodology: Meta-Frontier Analysis

Assuming that there are J (>1) groups, the ith manufacturer of the jth group uses N kinds of inputs, $x = (x_1, \cdots, x_N)$, produces M kinds of outputs, $y = (y_1, \cdots, y_M)$, and the production technology is of strong disposability. The production technology of jth group could be expressed as follows:

$$T^j = \{(x, y):\ x \geq 0;\ y \geq 0;\ x \text{ can be used by firms in group } j \text{ to produce } y\} \tag{1}$$

According to the production technology T, the input requirement set of the jth group and the input surface distance function are, respectively, defined as follows:

$$L^j(y) = \left\{x:\ (x, y) \in T^j\right\},\ j = 1, 2, \cdots, J;\ \text{and,} \tag{2}$$

$$D_I^j(x, y) = \sup_{\lambda}\left\{\lambda > 0:\ \frac{x}{\lambda} \in L^j(y)\right\}\ j = 1, 2, \cdots, J. \tag{3}$$

According to Färe and Primont [37], the input surface distance function satisfies the normal conditions such as nondecreasing, convexity, and linear homogeneous for the factor input vector x. Therefore, the input distance function could be expressed as the reciprocal of the technical efficiency of the input surface defined by Farrell [38]. That is,

$$0 \leq \frac{1}{D_I^j(x, y)} = TE_I^j(x_t, y_t) \leq 1. \tag{4}$$

According to Battese et al. [18] and O'Donnell et al. [19], all the manufacturers with the basic concepts of the common production boundary have the potential opportunities to use the common boundary technology, but the manufacturers of the groups will be faced with different production environments, such as the production resources, the relative input price, and the overall economic environment. The function of selecting different production technologies for production and using the common boundary technology for production is a meta-frontier production function, which could be regarded as the envelope curve of the production function of each group. In other words, meta-technology could be considered as the convex hull of each group's technical boundary [19], which is defined as follows:

$$T^* \equiv \text{convex hull}\left\{T^1 \cup T^2 \cup \cdots \cup T^J\right\}. \tag{5}$$

Therefore, according to O'Donnell et al. [19], the meta-technology set can be expressed as follows:

$$T^* = (x, y):\ x \geq 0;\ y \geq 0;\ x \text{ can produce } y \text{ in at least one group's technology, } T^1 \cup T^2 \cup \cdots \cup T^J. \tag{6}$$

According to the common border production technology T^*, the input set of the common boundary and the input meta distance function can be defined as follows:

$$L^*(y) = \left\{x:\ (x, y) \in T^*\right\}, \tag{7}$$

$$D_I^*(x, y) = \sup_{\lambda}\left\{\lambda > 0:\ \frac{x}{\lambda} \in L^*(y)\right\}. \tag{8}$$

According to equations (1)–(8), it can be concluded that the common boundary is the boundary of the unrestricted technology set, and the group boundary is the boundary of the restricted technology set. The reason for the limitation is that different groups of vendors face the different production environment. The distance function between the input surface distance function and input surface of any group must satisfy the following relationship:

$$D_I^j(x, y) \leq D_I^*(x, y) \Rightarrow TE_I^*(x, y) \leq TE_I^j(x, y),\ j = 1, 2, \cdots, J. \tag{9}$$

Using formula (9), we can derive the technical gap ratio (TGR_I^j) for each group's input surface as follows:

$$0 \leq TGR_I^j(x, y) = \frac{D_I^j(x, y)}{D_I^*(x, y)} = \frac{TE_I^*(x, y)}{TE_I^j(x, y)} \leq 1. \tag{10}$$

The value should be between 0 and 1, which represents the ratio of the potential output of the jth group's production boundary output relative to the common production boundary. The larger the TGR_I^j value, the closer the production boundary of the jth group is to the common production boundary, and the smaller the value is, the further the jth group production boundary is from the common production boundary.

Finally, using formula (10), the input surface can be used to produce the boundary. The technical efficiency TE_I^* is decomposed as follows:

$$TE_I^*(x, y) = TE_I^j(x, y) \times TGR_I^j(x, y). \tag{11}$$

In this study, the two-stage common distance function estimation step is used. In the first stage, the stochastic boundary model of Battese and Coelli [12] is used to consider the influence of the exogenous environmental variables on the technical efficiency, and the most approximate method is used to estimate the parameter vector of the input surface distance function in each group and calculate each vendor's technical efficiency estimate (TE_{it}^j).

In the second stage, the author uses the linear programming (LP) and quadratic programming (QP) proposed by Battese et al. [18] to estimate the parameters of the common distance function parameters of the input surface. Special attention should be paid to the fact that both of the above estimation methods must be solved through mathematical programming methods. The estimated standard error of the parameter estimation formula is obtained by Battese et al. [18] by using the simulation or bootstrap method. Estimation of the TE_{it}^* value from the parameter estimates is obtained in the second stage, together with the estimate TE_{it}^j obtained in the first stage, and an estimate of TE_{it}^j could be obtained by using equation (11).

According to Chen et al. [39], the detail description is as follows:

Table 1: Variable definitions.

Variable attribute	Variate	Definition
Output variable	Y	Annual operating income of listed textile enterprises (RMB million)
Input variable	L	Total input labor force (thousand people)
	K	Total investment in fixed assets, intangible assets and other long-term assets (RMB million)
Director	GOV	Official independent director employed by listed company in current year = 1
Environment variables	HHI	Market concentration
	AGE	Business year (year)
	CITY	Company located in a municipality = 1
	COASTAL	Company located in a coastal province = 1

(1) Minimum sum of absolute deviations, which is also known as linear programming (LP), is used to solve the optimization problem:

$$\text{Min}L \equiv \sum_{i=1}^{N}\sum_{t=1}^{T}\left|\ln f\left(X_{it},\beta^{*}\right)-\ln f\left(X_{it},\widehat{\beta}_{(j)}\right)\right|. \quad (12)$$

$$s.t.\ \ln f\left(X_{\text{it}},\beta^{*}\right)\geq \ln f\left(X_{\text{it}},\widehat{\beta}_{(j)}\right). \quad (13)$$

If the production function is log linear, then the target function can be simplified as follows:

$$\text{Min}L \equiv \sum_{i=1}^{N}\sum_{t=1}^{T}\left(X_{\text{it}}\beta^{*}-X_{\text{it}}\widehat{\beta}_{(j)}\right),\qquad s.t.X_{it}\beta^{*}\geq X_{\text{it}}\widehat{\beta}_{(j)}. \quad (14)$$

Since each individual group's estimated parameter value is $\widehat{\beta}_{(j)}$, $j=1,\ldots,R$, in the minimization process which is assumed to have a fixed value, this LP problem is equivalent to the minimized target function $L^{*}\equiv\overline{X}\beta^{*}$, where $\overline{X}$ denotes the average vector of all variables.

(2) Minimum sum of squares of deviations, which also known as the quadratic programming method (QP), is used to solve the optimization problem as follows:

$$\text{Min}LL \equiv \sum_{i=1}^{N}\sum_{t=1}^{T}\left(X_{it}\beta^{*}-X_{it}\widehat{\beta}_{(j)}\right)^{2},\quad s.t.X_{it}\beta^{*}\geq X_{it}\widehat{\beta}_{(j)}. \quad (15)$$

This estimation method is equivalent to the restricted least squares method. The whole calculation process is carried out through STATA 17.

4. Results and Discussion

This study applies the CSMAR database and selects samples of private China's listed energy companies in textile industry from 2010 to 2015. The CSMAR database is currently the largest in China and contains comprehensive economic and financial research databases. The database includes China's corporate stocks, companies, funds, bonds, derivatives, economy, industry, currency markets, overseas, sectors, information and technology, finance, special topics, and many other economic indicators. It is important to note that Content and Format Standard of Company Information Disclosure of Public Offering Securities No. 2 "Annual Report Content and Format" announced by the China Securities Regulatory Commission (CSRC) in December 2007 explicitly requires companies listed in China, which should be published in 2007 and in the following years to disclose a summary report on the performance of the board of auditors set up by the board of directors. Therefore, we can check the changes of directors' structure in listed companies in subsequent years. In the study sample selection, after excluding the missing data and nonaccounting firm independent executive sample, we get a total of 254 calculations. In terms of variable setting, we consider whether the official director (GOV) is employed in that year, business income of the current year (Y), total input labor (L), total investment (K) in purchasing and building fixed assets, intangible assets, and other long-term assets. In addition, environmental variables such as location variables (whether the company is located in a municipality or a coastal province), market concentration (HHI), and business operating time (AGE) are considered. The specific variables are listed in Table 1. Among them, the author uses the variable GOV director status as a group of companies to analyze and compare whether there is a clear difference in the efficiency of the common border between listed companies with official independent directors and those companies without official independent directors.

The empirical model is set as follows:

$$\ln 1 = \ln D_{I}\left(y_{\text{it}},x_{\text{it}},t;\beta\right)+v_{\text{it}}-u_{\text{it}}. \quad (16)$$

Among them, y_{it} is the tth operating income of the ith company, x_{it} is the tth factor input variable of the ith enterprise (total investment labor and total asset investment), β is the vector to be estimated, v_{it} is the random interference item, which is the same and independent normal random variable, u_{it} represents the technical inefficiency term, a nonnegative random variable, and v_{it} and u_{it} are assumed to be statistically independent. Table 2 summarizes the results of the first-stage random boundary estimation. The empirical results show that all variables except the variable AGE (business year) have a statistically significant level. Among them, the empirical results show that the input variables of the company's production process have a significant positive impact on its revenue. In the estimation of environmental variables, the results show that the variables HHI, CITY, and COASTAL all have positive effects and have statistically significant effects, indicating that the higher the market concentration, the higher the company's revenue. In addition, when the company is located in a municipality directly

Table 2: Random boundary estimation of the first stage.

Variable	Company with official independent director (GOV) operating income logarithm ln (Y)		Company with no official independent director (GOV) operating income logarithm ln (Y)	
	Coefficient value	Standard error	Coefficient value	Standard error
Constant term	2.534***	0.306	−2.548***	0.288
$\ln(L)$	0.406*	0.061	1.662***	0.345
$\ln(K)$	1.884**	0.950	2.545***	0.603
$\ln(L)\times\ln(K)$	−2.571***	0.551	0.450	0.961
Environment variables				
Constant term	3.567***	1.554	5.202***	1.325
HHI	1.555***	0.566	2.551***	0.614
AGE	0.021	0.088	0.028	0.045
CITY	2.423***	0.457	2.811***	0.181
COASTAL	0.450**	0.230	0.451**	0.200
$\sigma_u^2+\sigma_v^2$	0.088***	0.022***	0.022***	0.008
$\sigma_u^2/(\sigma_u^2+\sigma_v^2)$	0.819***	0.022	0.988***	0.028
Log-likelihood	273.800		364.340	
n	117		137	

Data source: CSMAR database. Note: ***, **, * indicates statistical significance at the level of confidence of 1%, 5%, and 10%, respectively.

Table 3: Estimation for pool-SFA and QP methods.

Variable	Pool-SFA		QP model	
	Estimated value	Standard error	Estimated value	Standard error
Constant term	2.516	0.791	7.340	5.376
$\ln(L)$	3.789	1.473	3.330	1.912
$\ln(K)$	0.005	0.519	-2.272	0.866
$\ln(L)\times\ln(K)$	2.516	0.791	7.340	5.376

Note. (1) Estimated standard errors of QP are estimated by using bootstrapping. (2) The pool-SFA model does not list the estimated value of σ_u^2 and σ_v^2.

under the central government or in a coastal province, it indicates that companies in the relatively developed regions with economic development also have a positive impact on their revenue.

Based on the quadratic programming (QP) method proposed by Battese et al. [17], Table 3 shows the estimation results. To be more specific, we applied the random boundary distance function shown in formula (12). It could be found that there are some differences between the traditional random boundary model (pool-SFA, in which pool means multiple cross-sectional data were merged) and the QR estimation results, but the basic effect of input variables on output variables is consistent with the results in Table 2. The main reason for the differences between the two is that the pool-SFA method combines the group data of different boards of directors together and directly estimates the random boundary distance function while neglecting the different management and the heterogeneity of the production technology. The two-order programming rule applies the mathematical programming to estimate the common production function relationship. In addition, the use of the QP model system assumes that there are differences in the operating revenue performance of a listed food company with an official independent director and a company without official independent director. The author uses the likelihood-ratio (LR) test and the null hypothesis to assume that the production boundaries of the two types of firms are the same, and the LR verification statistic $\lambda = -2\{\ln(H_0) - \ln(H_1)\}$ is used for estimation. Among them, $\ln(H_0)$ is the log-likelihood function value obtained by merging and accumulating the estimated values of all the group samples, and $\ln(H_1)$ is the sum of the values of the individual random boundary logarithm probabilistic functions for each group. The LR test statistic is 181.080. It rejects the null hypothesis. It means that there is indeed heterogeneity among the independent directors and nonexistent officials of the listed food companies. It is appropriate to use the common boundary function to analyze and compare the production efficiency and profit performance of different groups.

Table 4 lists the related technical efficiency estimated value under the common production boundary of the group. The size of the TGR reflects the difference in the manufacturer's level of production technology. The greater the TGR value, the closer the technical level used by the manufacturer is to the common boundary technology. Bos et al. [40] analyzed the banking industry competition and pointed out that the TGR value and the market competition presented a U-shaped curve. It represented that as the degree of competition increases, manufacturers' production behavior would gradually shift to the production of high-quality and specialized products. From this table, it can be found that without considering the technical heterogeneity, there is an efficiency gain (the average efficiency is 0.865) for the listed company with official independent directors over the other companies (the average efficiency is 0.831).

Table 4: Profitability of listed companies.

	QP model			
	Mean	Variance	Min	Max
Listed company with official independent director (GOV)				
Technological gap (TGR)	0.786	0.116	0.499	1.000
Random boundaries of the first stage (TE)	0.865	0.078	0.599	0.945
TE*	0.714	0.118	0.372	0.942
Listed company with no official independent director (NO-GOV)				
Technological gap (TGR)	0.844	0.081	0.519	1.000
Random boundaries of the first stage (TE)	0.831	0.090	0.552	0.943
Common border efficiency (TE*)	0.739	0.106	0.410	0.927
Whole sample				
Technological gap (TGR)	0.800	0.102	0.405	0.950
Random boundaries of the first stage (TE)	0.834	0.082	0.552	0.945
Common border efficiency (TE*)	0.703	0.112	0.351	0.942

Table 5: Average common boundary efficiency and technical gap for each group.

Year	Listed company with official independent director (GOV)			Listed company without official independent director (NO-GOV)		
	TE	TGR	TE*	TE	TGR	TE*
2010	0.791	0.700	0.604	0.834	0.765	0.670
2011	0.851	0.945	0.793	0.822	0.884	0.766
2012	0.806	0.899	0.831	0.849	0.783	0.735
2013	0.842	0.819	0.700	0.819	0.848	0.748
2014	0.894	0.815	0.694	0.820	0.859	0.748
2015	0.857	0.699	0.652	0.775	0.869	0.725

However, when considering the common production boundary, the TGR value of listed company with official independent director is less than other companies, and the production activity level of listed company with official independent director is farther from the common technology boundary than the other. When considering the common production boundary, the earnings performance (the average efficiency is 0.714) of listed company with official independent director is lower than listed company without official independent director (the average efficiency is 0.739).

Table 5 further lists the average common boundary efficiency and technical gaps for different groups over the years. It can be found that when considering the common border efficiency and technical gap, the earnings performance (TE*) of listed company with official independent director (GOV) is lower than that of listed company without official independent director (except for the year of 2009 and 2010). As for the reasons for the differences in earnings performance among groups, Ye et al. [41] and Lu and Yang [5] believed that in a transitional economy such as China with weak property rights protection and high government intervention, listed companies that appointed government officials to enter the board of directors and established a good relationship with the government could obtain more critical resources and policy support, and this might also induce listed companies to seek rent-seeking space. This situation shows that companies that hire official independent directors may invest other capital in the business process in the nonproduction investment and nontechnical upgrading. That may indirectly cause waste of input resources and bring about negative influence on the company's own production efficiency and profitability.

5. Conclusion

This study uses the CSMAR database to examine the operating data of listed companies in textile industry from 2010 to 2015 and analyzes the effect of official independent directors on the profitability of listed companies. By using the empirical model, this study uses the common boundary performance model to analyze the differences in the operating efficiency and income efficiency between companies with official independent director and the others. The empirical evidence shows that under the condition of not considering technological heterogeneity, there is a higher efficiency of the earnings of listed companies with official independent directors than other companies. However, when considering the common production boundary, there is an issue that the earnings performance of listed companies with official independent directors is lower than other companies; the research results show that the withdrawal of the official independent directors in the market has a positive impact on the profitability of the company. This article believes that the poor performance of earnings of listed companies with official independent directors may be caused by the fact that other capitals in the business process are invested in nonproduction and nontechnical upgrading,

indirectly leading to waste of input resources, and negatively affecting the company's own production efficiency and profitability.

To sum up, the announcement of the Chinese government's Opinions on Further Stipulating the Issue of Party and Government Cadres Working in Enterprises and Notice of the General Office of the Ministry of Education on Conducting a Special Inspection of Party and Government Leading Cadres Part-time in the Enterprise has cut off companies' channels of building political relations with governments by hiring government officials to serve as independent directors, reducing the potential for capital to invest in nonproduction inputs and nontechnical upgrades. This not only helps maintain the market order but also has a substantial positive impact on the development of industrial competition. Looking at the changing trend of China's economy and industry, the professionalization and specialization of independent directors and the professional competence of independent directors should be regarded as the current major development goals. In addition, this study focuses more on using meta frontier to show the regulatory changes in China, but there are still many limitations in this research. First of all, due to the lack of data, we cannot discuss the situation 10 years ago, so we did not cover it. In addition, we are looking at one industry and therefore may need to compare with other industries simultaneously in the future. Meanwhile, future research directions of our work may include cases from other developing countries.

Data Availability

The datasets used during the current study are available from the corresponding author upon reasonable request.

Conflicts of Interest

The authors declare that they have no conflicts of interest.

Authors' Contributions

Xiaozhi Xu and Lichen Chou performed conceptualization and formal analysis and developed the methodology and wrote the original draft. Qing Lu performed conceptualization, wrote the final draft, and performed the supervision. Yaqi Tian collected data and performed the final draft editing.

References

[1] E. F. Fama and M. C. Jensen, "Separation of ownership and control," *The Journal of Law and Economics*, vol. 26, no. 2, pp. 301–325, 1983.

[2] R. B. Adams, B. E. Hermalin, and M. S. Weisbach, "The role of boards of directors in corporate governance: a conceptual framework and survey," *Journal of Economic Literature*, vol. 48, no. 1, pp. 58–107, 2010.

[3] D. L. Delano and J. D. Knottnerus, "The Khmer Rouge, ritual and control," *Asian Journal of Social Science*, vol. 46, no. 1-2, pp. 79–110, 2018.

[4] E. Gerharz and J. Pfaff-Czarnecka, "Spaces of violence in south asian democracies," *Asian Journal of Social Science*, vol. 45, no. 6, pp. 613–638, 2017.

[5] D. Lu and D. Yang, "Independent directors' official background and corporate fraud," *Accounting Research*, vol. 8, pp. 55–61, 2017.

[6] H. Fu and X. Liu, "Research on the phenomenon of Chinese residents' spiritual contagion for the reuse of recycled water based on SC-iat," *Water*, vol. 9, no. 11, p. 846, 2017.

[7] Z. Liu, "Teaching reform of business statistics in college and university," *Eurasia Journal of Mathematics, Science and Technology Education*, vol. 13, no. 10, pp. 6901–6907, 2017.

[8] A. M. Yang, Y. Han, S. S. Li, H. W. Xing, Y. H. Pan, and W. X. Liu, "Synthesis and comparison of photocatalytic properties for bi2wo6 nanofibers and hierarchical microspheres," *Journal of Alloys and Compounds*, vol. 695, pp. 915–921, 2017.

[9] M. V. Achim, S. N. Borlea, and A. M. Anghelina, "The impact of fiscal policies on corruption: a panel analysis," *South African Journal of Economic and Management Sciences*, vol. 21, no. 1, pp. 1–9, 2018.

[10] M. Altwaiji, "History of Saudi folklore and factors that shaped it," *Trames. Journal of the Humanities and Social Sciences*, vol. 21, no. 2, p. 161, 2017.

[11] D. Fagan, "Activist archive: youth culture and the political past in Indonesia, written by doreen lee," *Asian Journal of Social Science*, vol. 46, no. 1-2, pp. 208–210, 2018.

[12] G. E. Battese and T. J. Coelli, "A model for technical inefficiency effects in a stochastic Frontier production function for panel data," *Empirical Economics*, vol. 20, no. 2, pp. 325–332, 1995.

[13] A. Charnes, W. W. Cooper, and E. Rhodes, "Measuring the efficiency of decision making units," *European Journal of Operational Research*, vol. 2, no. 6, pp. 429–444, 1978.

[14] A. Ahmed, "The philosophy of nuclear proliferation/nonproliferation: why states build or forgo nuclear weapons?" *Trames. Journal of the Humanities and Social Sciences*, vol. 21, no. 4, p. 371, 2017.

[15] K. Anniste, L. Pukkonen, and T. Paas, "Towards incomplete migration: Estonian migration to Finland," *Trames. Journal of the Humanities and Social Sciences*, vol. 21, no. 2, p. 97, 2017.

[16] J. Gans and M. D. Ryall, "Value capture theory: a strategic management review," *Strategic Management Journal*, vol. 38, no. 1, pp. 17–41, 2017.

[17] H. J. Kim and B. K. Kim, "Risk-based perspective on the choice of alliance governance in high-tech industries," *Journal of Management and Organization*, vol. 23, no. 5, pp. 671–688, 2017.

[18] G. E. Battese, D. S. P. Rao, and C. J. O'Donnell, "A metafrontier production function for estimation of technical efficiencies and technology gaps for firms operating under different technologies," *Journal of Productivity Analysis*, vol. 21, no. 1, pp. 91–103, 2004.

[19] C. J. O'Donnell, D. S. P. Rao, and G. E. Battese, "Metafrontier frameworks for the study of firm-level efficiencies and technology ratios," *Empirical Economics*, vol. 34, no. 2, pp. 231–255, 2008.

[20] B. Walheer, "Meta-frontier and technology switchers: a nonparametric approach," *European Journal of Operational Research*, 2022.

[21] Y. Hayami and V. W. Ruttan, *Agricultural Productivity Differences Among Countries*, pp. 895–911, The American economic review, United States, 1970.

[22] Y. Hayami and V. W. Ruttan, *Agricultural Development: An International Perspective*, The Johns Hopkins Press, Baltimore, Md/London, 1971.

[23] V. W. Ruttan, H. P. Binswanger, Y. Hayami, W. W. Wade, and A. Weber, "Factor Productivity and Growth: A Historical Interpretation," *Induced Innovation: Technology institution, and developments*, vol. 12, pp. 44–90, 1978.

[24] X. Zhao, X. Ma, Y. Shang, Z. Yang, and U. Shahzad, "Green economic growth and its inherent driving factors in Chinese cities: based on the Metafrontier-global-SBM super-efficiency DEA model," *Gondwana Research*, vol. 106, pp. 315–328, 2022.

[25] N. Shen, H. Liao, R. Deng, and Q. Wang, "Different types of environmental regulations and the heterogeneous influence on the environmental total factor productivity: empirical analysis of China's industry," *Journal of Cleaner Production*, vol. 211, pp. 171–184, 2019.

[26] G. Pu, Y. Zhang, and L. C. Chou, "Estimating financial information asymmetry in real estate transactions in China - an application of two-tier Frontier model," *Information Processing & Management*, vol. 59, no. 2, Article ID 102860, 2022.

[27] L. J. Lau and P. A. Yotopoulos, "The meta-production function approach to technological change in world agriculture," *Journal of Development Economics*, vol. 31, no. 2, pp. 241–269, 1989.

[28] J. I. Kim and L. J. Lau, "The sources of economic growth of the East Asian newly industrialized countries," *Journal of the Japanese and International Economies*, vol. 8, no. 3, pp. 235–271, 1994.

[29] L. H. P. Gunaratne, "Asian black tiger shrimp industry: a productivity analysis," in *Chapter 5 in Economics and Management of Shrimp and Carp Farming in Asia: A Collection of Research Papers Based on the ADB/NACA Farm Performance Survey*, P. S. Leung and K. R. Sharma, Eds., p. 240, Network of Aquaculture Centers in Asia-Pacific (NACA), Bangkok, 2001.

[30] D. V. Kovalevsky and M. Máñez-Costa, "Dynamics of water-constrained economies affected by climate change: nonlinear and stochastic effects," *Mathematical Topics on Modelling Complex Systems*, vol. 1, pp. 105–129, 2022.

[31] G. E. Battese and D. P. Rao, "Technology gap, efficiency, and a stochastic metafrontier function," *International Journal of Business and Economics*, vol. 1, no. 2, p. 87, 2002.

[32] Z. Shen, K. Bai, T. Hong, and T. Balezentis, "Evaluation of carbon shadow price within a non-parametric meta-frontier framework: the case of OECD, ASEAN and BRICS," *Applied Energy*, vol. 299, Article ID 117275, 2021.

[33] Y. Luo, Z. Lu, S. Muhammad, and H. Yang, "The heterogeneous effects of different technological innovations on eco-efficiency: evidence from 30 China's provinces," *Ecological Indicators*, vol. 127, Article ID 107802, 2021.

[34] T. Nakaishi, H. Takayabu, and S. Eguchi, "Environmental efficiency analysis of China's coal-fired power plants considering heterogeneity in power generation company groups," *Energy Economics*, vol. 102, Article ID 105511, 2021.

[35] L. C. Chou, W. H. Zhang, M. Y. Wang, and F. M. Yang, "The influence of democracy on emissions and energy efficiency in America: new evidence from quantile regression analysis," *Energy & Environment*, vol. 31, no. 8, pp. 1318–1334, 2020.

[36] L. C. Chou and W. H. Zhang, "The effect of democracy on energy efficiency in European countries," *Economic Research-Ekonomska Istraživanja*, vol. 33, no. 1, pp. 3476–3491, 2020.

[37] R. Färe and D. Primont, "Distance functions. In Multi-Output Production and Duality: Theory and Applications," pp. 7–41, Springer, Dordrecht, Netherlands, 1995.

[38] M. J. Farrell, "The measurement of productive efficiency," *Journal of the Royal Statistical Society: Series A (General)*, vol. 120, no. 3, pp. 253–281, 1957.

[39] C. Y. Chen, S. H. Lin, L. C. Chou, and K. D. Chen, "A comparative study of production efficiency in coastal region and non-coastal region in Mainland China: an application of Metafrontier model," *Journal of International Trade & Economic Development*, vol. 27, no. 8, pp. 901–916, 2018.

[40] J. W. Bos, J. W. Kolary, and R. V. Lamoen, *Competition and Innovation: Evidence from Financial Services*, Working paper, China, 2009.

[41] Q. Ye, L. Y. Zhao, and S. C. Liu, "A study of politician-to-firm revolving door of independent directors: evidence from a natural experiment," *Economic Research Journal*, vol. 6, pp. 98–113, 2016.

Hindawi
Mathematical Problems in Engineering
Volume 2022, Article ID 9697832, 10 pages
https://doi.org/10.1155/2022/9697832

Research Article

A Method of Selecting Optimal Control Nodes for WSNs Based on C-Means Clustering Algorithm

Na Fang[1] **and Xiaojing Wang**[2]

[1]*College of Software Engineering, Zhengzhou University of Light Industry, Zhengzhou 450001, China*
[2]*Mechanical and Electronic Engineering Department, Henan Light Industry Vocational College, Zhengzhou 450001, China*

Correspondence should be addressed to Xiaojing Wang; wxiaojing@zzuli.edu.cn

Received 16 April 2022; Accepted 16 June 2022; Published 8 August 2022

Academic Editor: Amandeep Kaur

The wireless sensor networks (WSNs) require an optimal selection of control nodes for improving the operational performance of the overall network. The data are increasing day by day, and it is difficult to a handle huge amount of data. For speedy transmission of data, it is mandatory to deploy sophisticated methods for improving the operations of WSNs. There are many methods proposed by the researchers to improve the operations of WSNs, but the data are increasing and more methods are needed to be explored to handle the operations of WSNs to smoothly handle a huge amount of data. To cater to this need, this research is proposing a method of selecting optimal control nodes for WSNs based on the C-means clustering algorithm (CCA). The CCA is improved by the weighting mechanism in the cluster, and the remaining energy of the node is taken into account. If the node energy is more as compared to the average energy in the cluster in each round, it will have the chance to serve as the cluster head node (CHN) and the adaptive assignment of CHN is made according to the generated cluster size by WSN. Every node possesses the probability of becoming a CHN to save the energy utilization of the node and to obtain the optimal control for node selection in WSN. The experimental results reveal that the coverage rate of WSN is improved after applying the proposed method. The network energy utilization is optimized, which effectively prolongs the lifetime of WSN and improves the overall network output including throughput, energy consumption rate, and data transmission rate.

1. Introduction

The WSN is the group of distributed and exclusively allocated sensors for keeping the record and examining the conditions around. The data that have been gathered are arranged and stored at the central repository. The WSN is a comprehensive intelligent information system, which is integrating information collection, information transmission, and information processing [1]. It has broad application prospects including organization and management of the network [2]. It is a new field in information network technology and an area of research for many aligned applications [3]. Data collection and quantification, processing, and transmission applications can be used in diverse fields like military reconnaissance for strategic planning, environmental observation, medical examination, space research, traffic control in the cities, and warehouse management [4–7]. The WSNs generally have the specific characteristics of encompassing large-scale networks, self-organization of data, random deployment, and spanning complex environment. The WSN also has challenges when it comes to the number of sensor node resources and frequently changing network nodes [8, 9]. Inappropriate selection of control node in WSNs leads to the problems such as (a) more power consumption during transmission or communication of data, (b) lifespan of the network will get compromised as a result of limited node energy, and (c) the wireless signal of each node in the network will cover a large number of other nodes, which will aggravate signal interference between nodes and affect communication quality, which will eventually reduce the network throughput [10–13]. There will be a large number of redundant edges in

the generated network nodes, resulting in a huge amount of repetitive information in the network nodes. It will enhance complex routing calculations and exhaust valuable computing resources [14, 15].

In [13], authors address the issue of distributed scheduling of MSNs. It enhances the region span and reduces the coverage holes with minimum energy loss. They also have stated various algorithms for multiple MSNs with their performance comparison. In [14], authors have focused on the control and optimization of WSNs' nodes. The problems with the design and management of WSNs have also been discussed. It also emphasizes on the importance of energy consumption consideration in the protocol design of each layer of the network. The establishment of node control mechanism for effective energy consumption has been proposed to optimize the energy utilization and the network lifespan. In [15], authors have proposed the QACS method for programmed mining of the encoded information in blockchain communications.

In [16], authors have proposed an optimal relay node (RN) selection method. The suggested methodology picks RN depending on the combined optimization of delay in data transmission and reliability of the network link. The Pareto frontier of this optimization is used to describe the balance between the two abovementioned parameters. The proposed node selection method identifies all possible RNs. It addresses the joint optimization problem; in each hop, the weight of the biobjective problem is updated and the best RN is selected among all possible RNs. This method has good operational reliability but poor efficiency. In [17], authors have proposed a combined selection of relay along with link rate assignment based on OHD selection. It saves energy, which analyzes the influence of the minimal hop distance in WSNs on the network life while considering the link service quality needs. The OHD measures the distance between the optimal relay position of a node and its next hop to the target node, and ORP finds the output of the energy-saving relay. For the given node pair, the minimum energy path can be obtained if the OHD comes out to be equal to that of the characteristic distance of the path. This method has better operating efficiency but poor reliability.

In [18], authors have proposed a two-phase solution. In phase I, the distributed algorithm is used to enhance the probability perception algorithm, and it is based on the probability model. In phase II, phase I is expanded to 3D space. The heuristic algorithm (greedy) is used. The simulation shows better performance of the algorithm as compared to the existing methods. In [19], authors have proposed a technique for node deployment. It uses the grey wolf-based technique for optimization. The study explores the wolf representation scheme and a new multiobjective fitness function. The efficiency of the proposed technique is proven with the help of simulation and statistical techniques. In [20], authors have proposed a novel approach for the simultaneous selection of control node in the complex network. The method focuses on an open-loop optimal control problem. An adaptive search method is used as a solution for the resulting mixed-integer optimization.

In the selection of optimal control nodes in WSN, four major performance factors need to be considered: (a) coverage, (b) energy consumption, (c) mobile node rate, and (d) lifetime. The existing work in the selection of optimal control nodes in WSN compromises one or more above factors. In this study, our aim is to have fair efficiency toward all the four factors.

The major highlights of the study are as follows.

This study offers a method for selecting optimal control nodes for WSNs based on CCA. The weight-based rough C-means algorithm is proposed to optimize and enhance the network performance by calculating the degree to which the node object deviates from the cluster center where each node object is assigned a different weight value. Different weights are dynamically assigned to each node object, which improves the performance of node clustering and makes the position of nodes evenly distributed. Based on this, the optimal control node selection model for WSNs is obtained and the CCA achieves the target of enhancing the performance of the network.

(i) This study is proposing a method of selecting optimal control nodes for WSNs based on weight-based rough CCA.

(ii) The CCA is improved by the weighting mechanism within the cluster, and the remaining energy of the node is taken into account.

(iii) If the node is greater than the average energy in the cluster in each round, it will have the opportunity to serve as the CHN and adaptive assignment of CHN is made according to the generated cluster size by WSN.

(iv) Each node has the probability of becoming a cluster CHN to save the energy consumption of the node and to obtain the optimal control for node selection in WSN.

(v) The experimental results reveal that the coverage rate of WSN is improved after applying the proposed method. The network energy consumption is optimized, which effectively prolongs the lifetime of WSN and improves the network parameters including throughput, energy consumption rate, and data transmission rate.

The next section elaborates on the proposed work in detail.

2. CCA Based on Intracluster Weighting

In WSNs, clustering is the process of dividing the nodes in the network into multiple clusters to extend the life cycle of the network. However, the nodes in the WSN are densely distributed in the monitoring area. How to use the clustering method to select the optimal control node and improve the scalability of the network is the current key research problem. The partition-based clustering algorithm divides the nodes in the network into multiple regions, and each region can independently perform tasks such as data

perception. The typical partition-based clustering algorithms such as the C-means algorithm can be used to enhance the output of the nodes. This study first summarizes the rough CCA and improves the shortcomings of the algorithm by weighting within the cluster.

2.1. CCA. The basic idea of the C-means algorithm is to set the initial parameters before updating the algorithm of each iteration, that is, given the input parameter X and the specified number of clusters C, we first select C sample points as the initial cluster centers; then calculate other samples that point the distance to the initial cluster center and assign the sample objects to the clusters closest to it; then update the cluster center formula to calculate C new cluster centers; and loop execution until a certain termination condition is met and the algorithm ends. In general, the *C*-means algorithm uses Euclidean distance as a similarity measurement method, and through iterative steps, the updated objective function is minimized, thereby obtaining the optimal clustering effect [17]. Rough CCA uses C-means clustering to partition a group of objects into the sets, which are nonoverlapping. Rough sets are more accommodating for real-time representation than classical sets. It uses fuzzy sets with hard partitioning along with subjective member function on the dataset. The proposed rough CCA encompasses the advantages of the abovementioned methods. There are limitations of the mean iterative function when the same weights have been assigned to all the data. The proposed hybrid model proves to be more suitable for real-life applications like selecting optimal control nodes for WSN [18]. In [21], authors consider various performance parameters to determine variations and similarities by using *C*-means. The proposed clustering function for validity proves to be more effective for clustering on different datasets. The results have been proven with the help of simulation.

This makes *C*-means algorithm the perfect choice for developing a method of selecting optimal control nodes for WSN.

The rough set is introduced into the *C*-means algorithm. The sample points are arbitrarily allocated to the nearest cluster, and the distance between the point and the center of the cluster is determined. If it is less than a certain threshold, the sample point belongs to the upper set of the cluster; otherwise, it is the next approximation set [18]. Finally, it is judged whether the objective function is less than a predetermined value, and the algorithm ends.

The step-by-step approach of the rough C-means is as follows.

A rough set $X \in U$, $\overline{a}U\,\underline{a}U$ is its upper approximation and lower approximation, respectively, and its attributes are as follows:

(1) Some object x_k, if $x_k \in \underline{a}U_i$, then $x_k \notin \underline{a}U_j$, and $i \neq j$.

(2) If the object is $x_k \notin \underline{a}U_i$, then $x_k \in \overline{a}U_i$.

(3) If the object is $x_k \in ab_i$, then $x_k \in \overline{a}U_i, \underline{a}U_i \ldots, i \neq j$.

The rough *C*-means algorithm iteratively divides the sample points into *C* clusters, which minimizes the objective function considering the remaining energy of the nodes. The cluster center update formula of each cluster is shown in equation (1).

$$\overrightarrow{m_k} = \left\{ w_l \sum_{\overrightarrow{x_n} \in C_k} \frac{\overrightarrow{x_n}}{C_k} \right. \tag{1}$$

The objective function formula is shown in equation (2).

$$J = \sum_{c=1}^{c} \left(\left| x_i - m_k \right|^2 \right). \tag{2}$$

The basic algorithm flow is shown below as follows:

Step 1: We initialize the parameters, set the number of clusters *C*, and arbitrarily select *C* sample center $C_i = (i = 1, 2, \ldots, c)$, distance threshold ε, and weight values w_l and w_u.

Step 2: We calculate the Euclidean distance d_{ik} from each object x_k to the cluster center $C_i = (i = 1, 2, \ldots, c)$, and d_{jk} is the Euclidean distance from x_k to the cluster center c_i, c_j.

Step 3: We choose d_{ik} as the minimum value and d_{jk} as the second minimum value.

If $d_{jk} - d_{ik} < \varepsilon$, then x_k cannot belong to the lower approximation of any cluster; otherwise, d_{ik} is the smallest value among C clusters.

Step 4: We update the cluster center formula m_k.

Step 5: We repeat steps 2 to 4 until the objective function *J* is the smallest.

2.2. Rough CCA Based on Intracluster Weighting. The rough C-means algorithm mentioned above uses a uniform weight value for the upper and lower approximations when calculating cluster centers, ignoring the differences within the sample objects. According to the difference in the degree of contribution of sample objects to their clusters, differentiated metrics should be used to measure the contribution of sample objects; otherwise, it will lead to the misclassification of certain points. Although some scholars are aware of the differences in the objects in the cluster, they mainly change the weight of the objects in the cluster by adding complex weight formulas, which increases the execution time of the algorithm during the operation of the algorithm [19].

2.2.1. Weighted Metrics within Clusters. By calculating the degree to which the sample objects in the cluster deviate from the cluster center, each object is assigned a different weight value. The closer the sample object to the cluster center is, the heaviest contribution to the cluster is, and the more weight should be assigned [20].

When the formula is iterated, the intracluster weight value of each sample object is set as shown in equation (3).

$$A_{ij} = \frac{1}{\sigma_{ij}^2 \sum_{j=1}^{m_i} \left(1/\sigma_{ij}^2 \right)}. \tag{3}$$

The constraints are as follows: $\sum_{j=1}^{m_i} A_{ij}$, where σ_{ij} is the standard deviation from the sample object to the cluster center, and m_i is the number of samples in i categories. It can be seen from the above formula that the closer the object within the class is to the cluster center, the smaller the value of σ_{ij}, which indicates that the greater its contribution to the class, the greater the weight value assigned. Conversely, if the offset is greater, the distance from the σ_{ij} sample object to the cluster center is farther, the contribution to its class is lower, and the weight value obtained by the corresponding sample object is lower.

The values of w_l and w_u are as follows. This section no longer uses the default parameter values, but refers to the number of upper and lower approximation objects in the sample. w_l and w_u are the number of approximation objects under (upper) sample compared to the number of samples as shown in equations (4) and (5).

$$w_l = \frac{\sum_{x_j \in \underline{a}U} 1}{\sum_{x_j \in \underline{a}U} 1 + \sum_{x_j \in \overline{a}U} 1}, \tag{4}$$

$$w_u = \frac{\sum_{x_j \in \overline{a}U} 1}{\sum_{x_j \in \underline{a}U} 1 + \sum_{x_j \in \overline{a}U} 1}. \tag{5}$$

2.2.2. In-Cluster Weighted Improved CCA Algorithm. The rough CCA based on intracluster weighting is improved on the basis of formula (1), where the weight of the sample object in the cluster is the reciprocal of the total number of all samples; ignoring the difference in the contribution of individual samples to the class, this study will introduce formula (2) into the cluster center iteration formula. At the same time, w_l and w_u in formula (1) are greatly affected by the initial parameters. Considering the number of objects of the upper and lower approximate samples, the specific process of the improved algorithm is as follows:

Step 1: We initialize the parameters, set the number of clusters C, and arbitrarily select C sample center $C_i = (i = 1, 2, \ldots, c)$ and distance threshold [13].

Step 2: We calculate the weight values w_l, w_u, and the Euclidean distance from each object x_k to the center of the sample $C_i = (i = 1, 2, \ldots, c)$. d_{ik} and d_{jk} are the Euclidean distance from x_k to the center of mass c_i, c_j.

Step 3: We choose d_{ik} as the minimum value and d_{jk} as the second minimum value.

Step 4: We update the cluster center formula shown in equation (6).

$$V_i = \begin{cases} w_l \sum\limits_{xj \in \underline{a}U_i} A_l s_j + w_u, \\ \sum\limits_{xj \in \underline{a}U_i} A_l s_j + \underline{a}U_i, \\ \sum\limits_{xj \in \overline{a}U_i - \underline{a}U_i} A_l s_j - \underline{a}U_i. \end{cases} \tag{6}$$

Step 5: We repeat steps 2 to 4 in a loop until the objective function value is less than the set threshold. In step 4, the weight values of the lower approximation and the boundary area are no longer fixed values in the traditional sense. In each iteration, the corrected cluster center is close to the center of the cluster and tends to be stable.

3. Selection Method of Optimal Control Node for WSN

In WSNs, energy constraints are strong, reducing energy consumption and promoting load balancing, which play a pivotal role in extending the life of WSNs. The WSNs have certain complexity. Due to different application scenarios, the requirements for network coverage will be different. Network coverage control optimization is to control network nodes and optimize the coverage structure in order to reduce node energy consumption and increase A network resource optimization method used for network coverage quality. However, in the network, often because of the difference in the task amount of each node, some nodes are exhausted due to the excessive task amount, while other nodes are rarely used [14, 15].

In order to improve the survival time of WSNs and balance the network load consumption, the intracluster weighted improved CCA is used to balance the network load; the node optimal control optimization selection algorithm is proposed; and the optimal control node selection method is studied to reduce the network medium energy consumption, optimize the configuration of node resources in the network, and extend the network lifetime.

3.1. Construction of WSN Cluster. The CHN is randomly selected with equal probability periodically, and the adjacent ordinary nodes dynamically join the CHN. The ordinary node only communicates with the CHN of the cluster, and the CHN integrates the data information of the cluster, which is processed by it. The data are forwarded to the base station in a single-hop or multihop fashion. Since the CHN needs to fuse and process the information of ordinary nodes, and transmit the result to the base station, the CHN consumes more energy in the communication process. A rotation system is adopted to balance the energy consumption of the network to each node so that the CHN in each round will not lose its working ability due to the exhaustion of battery energy.

The stage of cluster construction includes cluster head selection and cluster formation. The CHNs are randomly generated with equal probability during the cluster head selection stage. Whether each node becomes a CHN is related to the optimal number of cluster heads expected in the network and whether it has served as a CHN until this round. Whether it becomes the expected percentage of CHNs in the current round depends on the total number of nodes in the network, which is generally a given fixed value. The flowchart of the LEACH protocol in the cluster construction phase is shown in Figure 1.

In the initial state, each node randomly assigns a random number of [0, 1]. If the random number is less than the

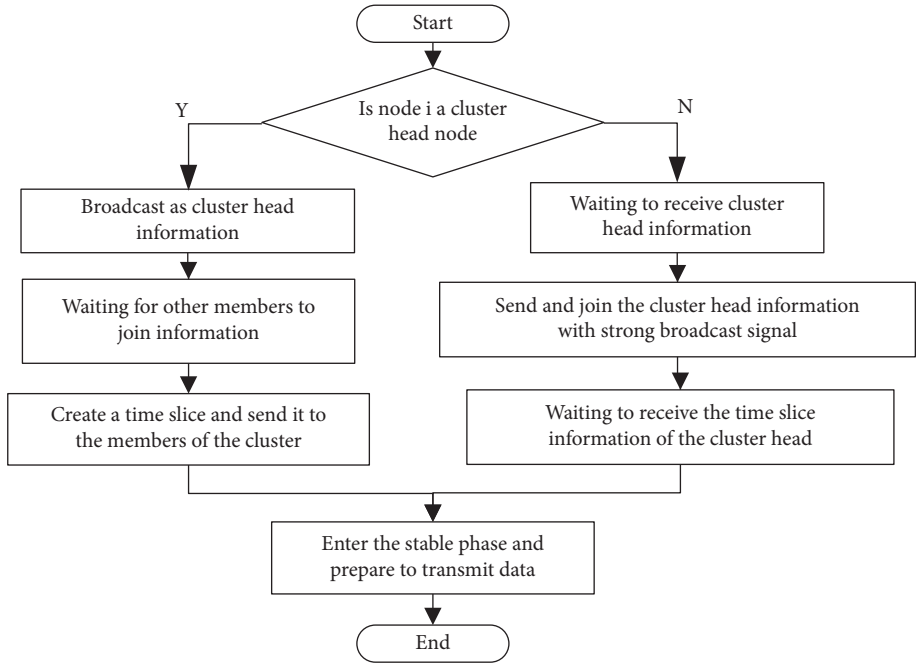

Figure 1: The construction phase of the LEACH protocol cluster.

threshold value $T(n)$ set in this round, then this node is determined as the CHN in this round of selection; otherwise, it becomes a normal node. The formula for threshold $T(n)$ is as shown in equation (7).

$$T(n) = \begin{cases} \dfrac{p}{1 - p * (\mathrm{rmod}(1/p))}, & n \in G, \\ 0, & \text{other.} \end{cases} \tag{7}$$

In formula (7), p represents the expected percentage of nodes becoming CHNs in a certain round, generally the ratio of the number of CHNs in the network to the number of all nodes; r represents the current number of rounds of cluster head selection; n represents each node in the WSN, and each has a unique ID; and G represents a collection of ordinary nodes that have not served as CHNs in the last $(1/p)$ rounds.

Once a node confirms that it has become a CHN, it immediately broadcasts the information that it has become a CHN to other nodes in the network and informs other ordinary nodes that a CHN has been generated, and other ordinary nodes rely on the CHN's received broadcast signal strength, join this CHN based on the principle of proximity, and notify the corresponding cluster head, so that all nodes in the network form numerous virtual clusters. When an ordinary node joins the CHN, the CHN will set a TDMA transmission time slice for each ordinary node to avoid cluster members sending information to the cluster head at the same time to cause network congestion and allow non-CHNs not to be in their working time slice, in a dormant state, thereby reducing node energy consumption. After the members of the cluster obtain the TDMA time slice designated by the CHN, the establishment of the cluster is completed and the stable data transmission phase is entered.

In the stable phase, cluster member nodes automatically adjust their own transmission power according to the broadcast signal strength of the received cluster head information to ensure that there is enough energy to transmit data to the CHN. At the same time, according to the time slot allocated in the TDMA table, the monitored data are time-shared and sent to the cluster head, and it stays in the dormant state at other times to save energy. The cluster head receives the data collected by all cluster members, first performs fusion processing on these data to reduce redundant data and noise interference, and then forwards the processed data to the base station. The round ends. Because the CHN has been processing the working state and needs to fuse data in the cluster, it needs to consume a lot of energy. In order to reduce the additional processing overhead, the general stabilization phase lasts longer than the construction phase. After the stabilization phase lasted for a while, the entire network began to enter a new cycle, re-entering the cluster construction phase, making each node take turns to serve as the CHN, balancing the energy consumption in the network to each node, and improving WSN node energy utilization.

3.2. Optimal Control CHN Selection Based on CCA. The rough C-means algorithm based on intracluster weighting is used to improve the optimal control CHN selection method. Through node positioning technology, the geographical coordinates of randomly deployed sensor nodes are obtained. According to their coordinate values, all nodes are divided into C subsets according to the distance from themselves to the cluster center by using the WCRCM algorithm. C represents the number of optimal clusters, namely, dividing the sensor nodes of the entire monitoring

area into C virtual subarea nodes, so as to ensure the even distribution of nodes in the geographical position. According to the nature of the rough set, the nodes in each area are classified into the upper approximation set or the lower approximation set of the area. The nodes in the lower approximation set must belong to the area, and the residual energy factor of the node is added to the objective function. Through the optimized objective function, the attribution of the sensor node is determined to achieve the purpose of automatic classification.

The proposed work has been compartmentalized into three phases as follows:

(a) Identifying the range of CHN;
(b) Calculating the probability of the node to become CHN;
(c) Selecting optimal control node for WSN using CCA.

3.2.1. The Range of CHN Selection. The WCRCM algorithm names the node as the upper node or the lower node. Since the upper node belongs to multiple areas, it may perceive information from multiple adjacent areas, and the upper node is generally at the boundary of the area, so the data fusion, processing, and transmission process will consume more energy, but the lower A node only exists in one area, and only the information in the area is monitored. Therefore, when selecting the CHN in this study, only the lower nodes in each area are considered.

3.2.2. Probability of Becoming a CHN. The calculation formula for the number of cluster heads is as follows:

$$k = \frac{\sqrt{N}}{\sqrt{2\pi}} * \frac{M}{d}. \tag{8}$$

In formula (8), the monitoring area is divided into k subareas. If each area has a CHN, then the probability that all nodes defined by the LEACH protocol become CHNs p is the reciprocal of the number of all nodes in each newly divided area. We add the remaining energy of the node and the average energy of the area where the node is located into the probability formula of becoming a CHN as shown in equation (9).

$$p = \frac{k}{C}. \tag{9}$$

3.2.3. Selection Method of Optimal Control Node for WSN. In the WSN coverage algorithm, it is necessary to consider optimizing the network energy consumption as much as possible while increasing the network coverage. At the same time, a balance between a single node and the total energy consumption of the network should also be considered. If the energy in the network is low, and if the node still performs the same task as other nodes, then the node will "die" early, affecting the transmission performance and reliability of the entire network. This study proposes a method for selecting optimal control nodes for WSNs based on CCA, analyzes the factors that affect the life cycle of WSN nodes, and establishes the dependency between the life cycles of WSN nodes and the quality of target tracking. The CCA and the CHN probability formula are introduced into the optimal control node selection method to obtain the optimal control node selection method.

If the error data probability of the abnormal dynamic node o in the high-dimensional data flow in the network is set to FA, $h(FA_o)$ represents the possibility of the false alarm rate of target tracking data of the abnormal node FA_o, when the optimal control node o is selected, the energy loss formula is as shown in equation (10).

$$C_{\mathrm{o}}^{c} = \begin{cases} h(\mathrm{FA}_o) \cdot (C_{\mathrm{o}}^{s} + C_{\mathrm{o}}^{a}), D_o = \varnothing, \\ h(\mathrm{FA}_o) \cdot (C_{\mathrm{o}}^{s} + C_{\mathrm{o}}^{a} + c^{*} C_{\mathrm{o}}^{r}), |D_o| = c. \end{cases} \tag{10}$$

In equation (10), when C_{o}^{r}, C_{o}^{a}, and C_{o}^{s} are sampling the target key sequence data, the energy consumed by dynamic nodes are r, a, and o in the whole cycle, s describes the number of target tracking nodes of dynamic node o, and D_o describes variables.

To set the optimal control node set $\ddot{N} = \{n_1, \ldots n_{|\ddot{N}|}\}$ of the WSN, it is necessary to obtain the element vector $(y_1, \ldots y_{|\ddot{N}|})$ of $|\ddot{N}|$ and the middle $y_o \in \{0, 1\}$. The following conditions must be met.

(1) Maximize the value of $\min_{o \in \ddot{N}} y_o l_o$.
(2) $\sum_{o \in \ddot{N}} y_o A_o \le \mathrm{FA}_T$.
(3) $\sum_{o \in \ddot{N}} y_o \ge k$.

Among them, the value of FA_T is set according to the actual target tracking requirements, and k is the minimum value of the target tracking node. According to the CCA, it is used to balance the network load and reduce the energy consumption in the network. The optimal control node selection model of the WSN is obtained through the selection range of the CHN as shown in equation (11).

$$x_i^{\kappa+1} = x_i^{(\kappa)} + \delta(P + V_i). \tag{11}$$

4. Experimental Analysis

In order to verify the effectiveness of the proposed method for selecting optimal control nodes for WSNs based on the CCA, the literature [3] method and the literature [4] method are used as experimental comparison methods. Through simulation experiments, the network coverage, analysis of network energy consumption, and network connectivity are determined.

4.1. Experimental Environment and Parameter Settings. The experiment was carried out in the MATLAB simulation software. The scene was set as follows: static sensor nodes and mobile nodes were set in the monitoring area $100 * 100\,\mathrm{m}^2$. The node sensing radius range was 5–20 m, and the simulation parameters are shown in Table 1.

During the research, the network is set to an ideal state without considering the phenomenon of interference

Table 1: Experimental environment simulation parameters.

Parameter	Value
Network size	100 ∗ 100
Node number *a*	200
Node number *a*	300
Sensing range	5–20
Min energy(J/battery)	0.01

Table 2: Simulation parameters of WSN model.

Parameter	Value	Unit
Number of nodes	100	A
Data packet length	4000	Bit
Control message length	32	bit

between nodes and packet loss in transmission. The network model of the wireless sensor assumed in this study has parameters as shown in Table 2.

The nodes used in this study are 100 nodes randomly generated by MATLAB2012, which are randomly distributed in a 100 ∗ 100 square row area, and the distribution is shown in Figure 2.

In the above experimental environment, the effectiveness of the proposed method is verified, and the experimental results are analyzed.

4.2. Analysis of Experimental Results

4.2.1. WSN Coverage Experiment. Network coverage can reflect the effective coverage of the entire network and is one of the effective indicators to measure the quality of network coverage. For most application scenarios, as long as the network coverage is controlled within a certain reasonable range, the network effectiveness will not be affected. Comparing the WSN coverage under the control of the three methods, the comparison result is shown in Figure 3.

The number and location of static node equipment in the network are the same. In the initial stage of network operation, the network coverage changes are not very different, but with the introduction of mobile nodes, the network coverage of the proposed method is beginning to be higher than that of the literature comparison method, and especially over time, this advantage becomes more apparent.

4.2.2. Energy Consumption of WSN. The limited energy of WSNs determines that network energy consumption is one of the key factors affecting the performance of the entire network. Nodes in the network perceive each other. Due to the difference in the amount of tasks each node undertakes, as the network time runs, the remaining energy and perception range of the nodes have a certain difference. Comparing the three methods of WSN energy consumption, the comparison result is shown in Figure 4.

It can be seen from the results in Figure 4 that the proposed method takes into account the remaining energy of the surrounding nodes when calculating the specific location of the mobile node to repair the network blind zone, effectively reducing the number of dead nodes in the

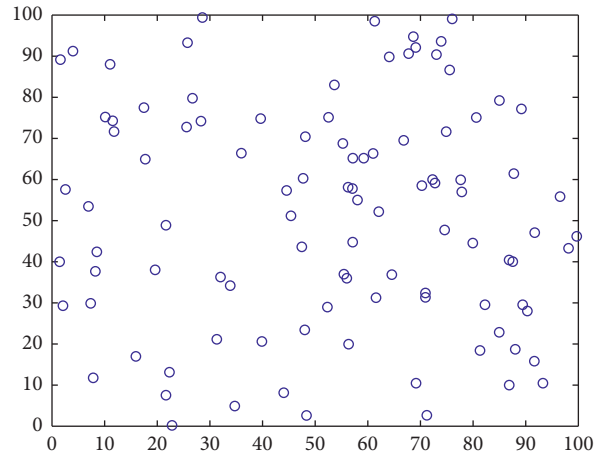

Figure 2: Distribution of 100 nodes.

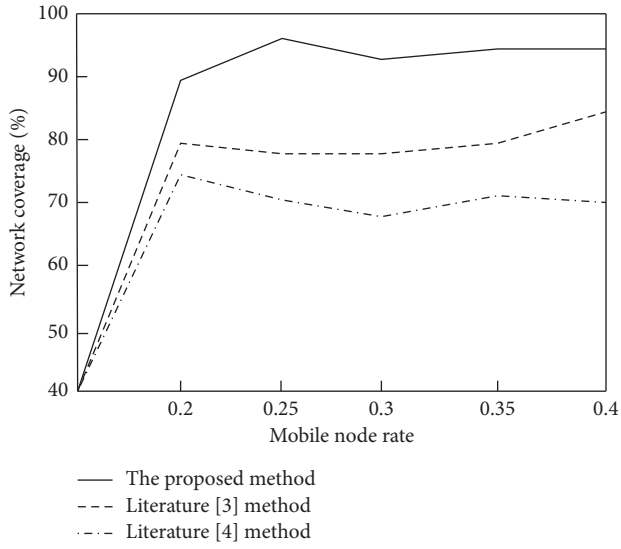

Figure 3: Comparison of results of network coverage.

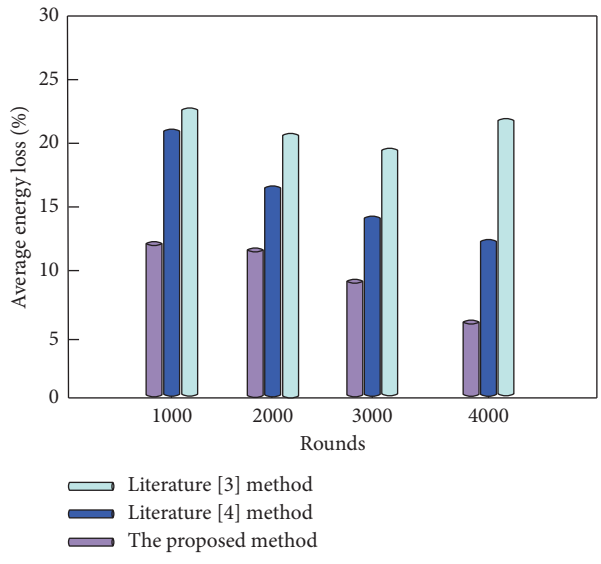

Figure 4: Comparison results of network energy consumption.

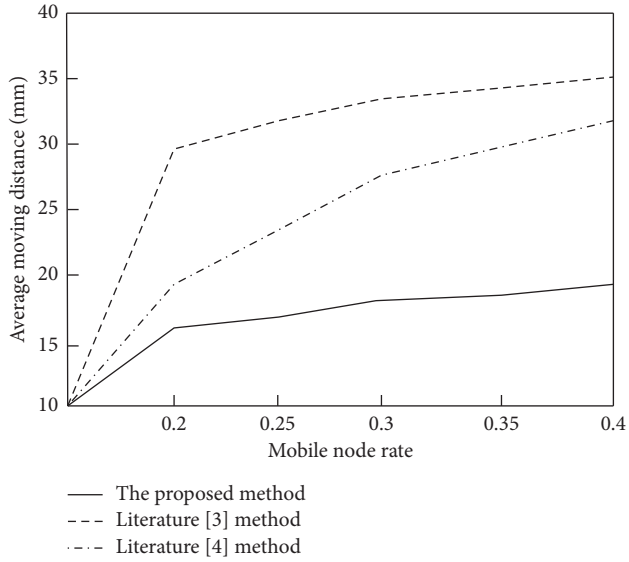

Figure 5: Comparison results of average mobile node distance.

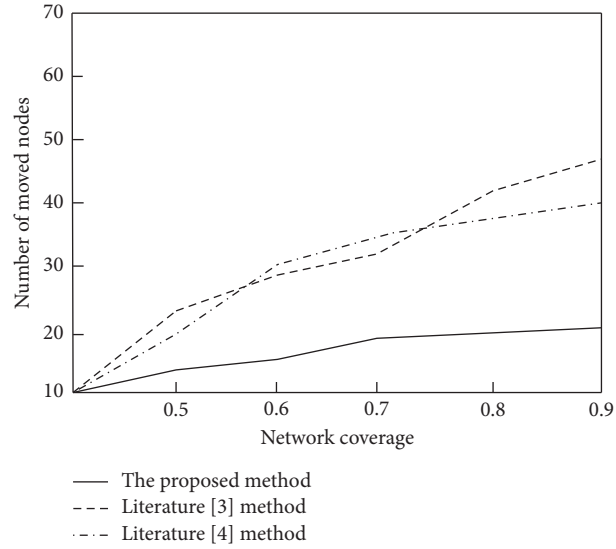

Figure 6: Comparison results of average mobile node distance.

network and reducing the number of new networks due to dead nodes. In terms of energy consumption of the entire network, the three algorithms show an upward trend, but the energy consumption of the proposed algorithm is lower.

4.2.3. Mobile Node Rate of WSN. The mobile node rate is the ratio of the number of mobile nodes working in the network to the total number of all working nodes in the network. In the case of the same network mobile node rate, the algorithm compares the average moving distance of the mobile node during the coverage area repair process. If the average moving distance is relatively short, it means that the mobile node has a shorter moving distance during the area repair process, which reduces the mobile nodes. For the energy consumption caused by mobility, the average mobile node distance of the three methods is shown in Figure 5.

Analyzing Figure 5, we can see that the average moving distance of the proposed method is relatively short, and it can be found that the average moving distance of the algorithm smoothly changes, indicating that the algorithm is superior to the literature comparison method in planning the moving path of mobile nodes.

Using mobile nodes to repair the network coverage area can improve the network coverage quality, but during the repair process, it is necessary to move as few nodes as possible, reduce the energy consumption of mobile nodes during the movement, and complete the network area coverage repair task. It can be seen from Figure 6 that after coverage restoration, the network coverage rate is constant. When the proposed method uses mobile nodes for coverage restoration, the number of mobile nodes used is relatively small, and the network restoration rate is better.

4.2.4. Lifetime of WSN. The network lifetime is a relatively intuitive performance indicator that reflects the operating conditions of network nodes. It can effectively measure the

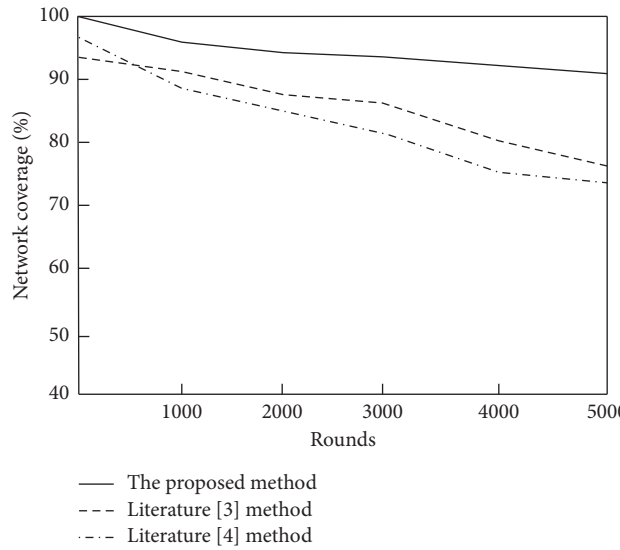

Figure 7: Comparison results of network lifetime.

length of the network's service life. When the network coverage reaches a certain critical value, the network performance will be reduced and the quality of service will be reduced. The specific network monitoring task means the end of the network lifetime at this time. Figure 7 shows the coverage changes.

It can be seen from the figure that the actual network service quality of the proposed method is slightly higher than the expected value, which is closer to the network coverage requirement than the literature comparison method, and makes the distribution of resources within the network more balanced. The proposed method determines the optimal location of mobile nodes, controls the number of network nodes based on the network coverage, repairs the network coverage area, improves network coverage and connectivity, and extends the network lifetime.

5. Conclusions

Due to the limited energy of the nodes in the WSNs, there is generally no power to supplement the equipment. At the same time, the nodes in the WSN are large in scale and randomly distributed where the communication radius of the nodes is limited. It makes the architecture of the new WSN more complex. The method and communication protocol are different from traditional networks. The main task of the traditional wireless network routing algorithm is to find the optimal path from the source node to the destination node by avoiding the network congestion and by improving the quality of service of the network. However, problems such as balancing network traffic and network energy consumption are beyond the scope of its design. In this study, a method for selecting optimal control nodes for WSNs based on CCA is proposed, and a rough C-means clustering based on intracluster weighting is proposed. By calculating the degree of deviation of the node object from the cluster center, it is determined for each node object. The closer the node to the cluster center, the greater the weight of the cluster where it is located, which indicates that the object contributes the most to the cluster where it is located. The sensor nodes in the entire wireless network area are divided into multiple subareas, and the number and location of the nodes in each area are roughly the same, thereby ensuring the uniformity of the CHNs in the geographic location. A rough C-means clustering is used to construct the optimal control node selection model for WSNs. The experimental results of the proposed work have been compared with the state-of-the-art methods for the parameters like network coverage, energy consumption, mobile node rate, and network lifetime. The simulation experiment on the proposed work shows outstanding performance in all the above-mentioned parameters. In the future, more performance parameters will be considered and more algorithms will be introduced to achieve better efficiency in the process of selecting optimal control nodes for WSNs.

Data Availability

The data are available on valid request.

Conflicts of Interest

The authors have no conflicts of interest to declare.

Acknowledgments

The work was supported in part by the Henan Province Science and Technology Research Project.

References

[1] P. Bhavathankar, S. Chatterjee, and S. Misra, "Link-quality aware path selection in the presence of proactive jamming in fallible wireless sensor networks," *IEEE Transactions on Communications*, vol. 66, no. 4, pp. 1689–1704, 2018.

[2] M. Kaur, "FastPGA based scheduling of dependent tasks in grid computing to provide QoS to grid users," in *Proceedings of the 2016 International Conference on Internet of Things and Applications (IOTA)*, pp. 418–423, Pune, India, September 2016.

[3] S. Redhu, M. Anupam, and R. M. Hegde, "Optimal relay node selection for robust data forwarding over time-varying IoT networks," *IEEE Transactions on Vehicular Technology*, vol. 68, no. 9, pp. 9178–9190, 2019.

[4] Z. Ding, S. Xing, and F. Yan, L. Shen, Impact of optimal hop distance on the network lifetime for wireless sensor networks with QoS requirements," *IEEE Communications Letters*, vol. 23, no. 3, pp. 534–537, 2019.

[5] S. Redhu and R. M. Hegde, "Optimal relay node selection in time-varying IoT networks using network contact pattern information"," *IEEE Transactions on Vehicular Technology*, vol. 98, Article ID 102065, 2020.

[6] M. Kaur and S. Kadam, "Bio-Inspired workflow scheduling on HPC platforms," *Tehnički Glasnik*, vol. 15, no. 1, pp. 60–68, 2021.

[7] K. Patil, K. De Turck, and D. Fiems, "A two-queue model for optimizing the value of information in energy-harvesting sensor networks," *Performance Evaluation*, vol. 119, no. 03, pp. 27–42, 2018.

[8] P. Rajpoot and P. Dwivedi, "Optimized and load balanced clustering for WSNs to increase the lifetime of WSN using MADM approaches," *Wireless Networks*, vol. 26, no. 1, pp. 215–251, 2020.

[9] G. Yogarajan and T. Revathi, "Nature inspired discrete firefly algorithm for optimal mobile data gathering in WSNs," *Wireless Networks*, vol. 24, no. 4, pp. 2993–3007, 2018.

[10] S. Basak and T. Acharya, "Spectrum-aware outage minimizing cooperative routing in cognitive radio sensor networks," *Wireless Networks*, vol. 26, no. 1, pp. 1069–1084, 2020.

[11] M. Kaur, S. Kadam, and N. Hannoon, "Multi-level parallel scheduling of dependent-tasks using graph-partitioning and hybrid approaches over edge-cloud," *Soft Computing*, vol. 26, no. 4, https://doi.org/10.1007/s00500-022-07048-1, 2022.

[12] A. Gumusalan, R. Simon, and H. A. Aydin, "Dynamic modulation scaling enabled multi-hop topology control for time critical WSNs," *Wireless Networks*, vol. 26, no. 3, pp. 35–49, 2020.

[13] A. Jadhav, M. Kaur, and F. Akter, "Evolution of software development effort and cost estimation techniques: five decades study using automated text mining approach," *Mathematical Problems in Engineering*, vol. 202211 pages, 2022, https://doi.org/10.1155/2022/5782587, Article ID 5782587.

[14] M. Kaur, A. Jadhav, and F. Akter, "Resource Selection from Edge-Cloud for IIoT and Blockchain-Based Applications in Industry 4.0/5.0," *Security and Communication Networks*, vol. 2022, Article ID 9314052, 13 pages, 2022, https://doi.org/10.1155/2022/9314052.

[15] W. Zhang and M. Kaur, "A novel QACS automatic extraction algorithm for extracting information in blockchain-based systems," *IETE Journal of Research*, 2022.

[16] R. Kumar and T. Amgoth, "Adaptive cluster-based relay-node placement for disjoint WSNs," *Wireless Networks*, vol. 26, pp. 651–666, 2020.

[17] J. Xu and C. Song, Y. D. Zhang, S. H. Wang, and S. Liu, Design and improvement of optimal control model for WSN nodes," in *Multimedia Technology and Enhanced Learning. ICMTEL 2020. Lect. Notes of the Inst. For Comp. Sci, Social Info. and*

*Telecom. Engineering*vol. 327, Berlin, Germany, Springer, 2020.

[18] K. Jaiswal and V. Anand, "A QoS aware optimal node deployment in WSN using Grey wolf optimization approach for IoT applications," *Telecommunication Systems*, vol. 78, no. 4, pp. 559–576, 2021.

[19] A. Haber, S. A. Nugroho, P. Torres, and A. F. Taha, "Control node selection algorithm for nonlinear dynamic networks," *IEEE Control Sys Letters*, vol. 5, no. 4, pp. 1195–1200, 2021.

[20] T. Zhang, L. Chen, and F. Ma, "A modified rough CCA based on hybrid imbalanced measure of distance and density," *International Journal of Approximate Reasoning*, vol. 55, no. 8, 2014.

[21] G. Wang, J. S. Wang, and H. Y. Wang, "Fuzzy C-mens clustering validity function based on multiple clustering performance evaluation components," *International Journal of Fuzzy Systems*, vol. 24, 2022, https://doi.org/10.1007/s40815-021-01243-2.

Hindawi
Mathematical Problems in Engineering
Volume 2022, Article ID 1639262, 12 pages
https://doi.org/10.1155/2022/1639262

Research Article

Performance Analysis of Two-Loop Interleaved Boost Converter Fed PMDC-Motor System Using FLC

C. T. Manikandan,[1] **G. T. Sundarrajan**,[1] **V. Gokula Krishnan**,[2] **and Isaac Ofori**[3]

[1]*Department of Electrical and Electronics Engineering, Sathyabama Institute of Science and Technology, Chennai, Tamil Nadu, India*
[2]*Department of Computer Science and Engineering, Saveetha School of Engineering, Saveetha Institute of Medical and Technical Sciences (SIMATS), Thandalam, Chennai 602105, Tamil Nadu, India*
[3]*Department of Environmental and Safety Engineering, University of Mines and Technology, Tarkwa, Ghana*

Correspondence should be addressed to C. T. Manikandan; manikandansathphd@gmail.com and Isaac Ofori; iofori@umat.edu.gh

Received 17 April 2022; Revised 21 May 2022; Accepted 25 May 2022; Published 1 August 2022

Academic Editor: Amandeep Kaur

Nowadays, the Permanent Magnet DC (PMDC) motors are intended to achieve the maneuver with elevated exactness and accurateness. To elevate the exactness and accurateness of the Permanent Magnet DC motors, the two-loop Interleaved Boost Converter (ILBC) is intended to control methods. The projected Converter is located between DC load and Permanent Magnet DC motor loads. The united construction of Permanent Magnet DC motors and Interleaved Boost Converter may be miscarried owing to steady state error, speed disparity, and slow response. To condense the difficulties, the Fuzzy Logic Controller is intended in the recommended Converter and Permanent Magnet DC motor. This exertion enlightened the modelling, simulation, and relevance of the Interleaved Boost Converter with Permanent Magnet DC motor (ILBC-PMDCM). The recommended technique chief objective aims at upholding the mandatory DC voltage from the input supply voltage with the assistance of Fuzzy Logic Controller. Current mode Fuzzy Logic Controller is proposed in the present work. The objective is to improve small-scale stability of ILBC-PMDCM system. The recommended controller is functioning based on closed-loop alignment. The projected FL controller is simulated and equated with the Proportional Integral (PI) controller in Permanent Magnet DC motor. From the investigation, the projected controller presents the finest outcomes than the Proportional Integral controller. The projected controller has altered benefits such as declined steady state error and enriched time domain response. The hardware outcomes of the projected controller are also presented, which are evaluated against the simulation outcomes.

1. Introduction

DC power supplies were usually adopted in abundant precincts swapping off of elementary electronic gadgets, for instance, notepad PCs, until pointedly more development relevance, for instance, electric vehicle and moreover the aviation relevance [1]. Subsequently, DC-DC Converter was normally utilized by altering the voltage of DC form to an alternate voltage of DC form subsequently to underwrite the DC voltage necessity of heat to the DC power flexibly; furthermore, DC-DC Converter was likewise a significant relevance for the force molding of the option electrical energy, for instance, PV, breeze generator, and energy unit framework. For each of these explanations, the DC-DC Converter relevance will make a beeline for the accompanying possible markets later on [2].

Predominantly, the DC-to-DC Converter incorporated of power semiconductor apparatus worked as electronic controllers and designated traded approach DC-DC Converters or constantly suggested as SMPS. To embrace the yield voltage consistent, the analysis control circle was used to, therefore, alter the commitment cycle, paying little regard to incorporate voltage assortment and weight changes [3]. Action of the trading contraptions caused the Boost Converter ordinarily nonlinear characteristics [4]. Due to these futile nonlinear appearances, the Converters require a controller with a

genuine degree of vibrant reaction [5]. Proportional Integral Derivative controllers go through kept regulation of their limits for disturbance conditions and altered weights [6]. Proportional Integral Derivative controller has a couple of burdens, for instance, slow reactions to the surprising change in the stack or exacerbation in the data voltage. Main design centers for electronic experts were to work on the feasibility of power change. For Pulse Width Modulation Converters, trading adversity was a large show measure [7]. The fake sharp control, for instance, Fuzzy Logic and brain framework, was completely capable for the distinctive verification, flexible, and control for nonlinear dynamical structures [8].

A clear Boost convertor changes over a low-level DC voltage to raised level DC voltage, which diminishes the wave factors in equal data and yield circuits. To procure higher viability, the yield current was separated into 2 ways which decline I^2R disasters and AC hardships. IBCS are used in a wide extent of purposes, for instance, PFC circuits, energy unit systems, and PV bunches [9–13]. In this, the construction approach of interleaved Boost Converter has been clarified. The computation of the inductance and the channel capacitance of the interleaved Boost Converter has been done. The construction of interleaved Boost Converter has been finished with a conclusive objective of diminishing the wave in the yield voltage and the data current. Fuzzy Logic is an etymological procedure which ascends to structure fundamental, bewildering, and introduced systems with control inputs. A Fuzzy Logic can be seen as a continuous expert system that uses Fuzzy Logic to control emotional elements [14].

In this topic, the present work is exposed to fuzzy logic control to improve the dynamic response of 2SILBC-DCM and is organized in six sections. Section 2 presents the 2SILBC and the block diagram of the proposed closed loop 2SILBC-DCM. The behavior of 2SILBC-DCM in closed loop is presented in Section 3. The control strategies for 2SILBC-DCM are evaluated in Section 4, and Section 5 gives the experimental results for 2SILBC-DCM. Conclusion is discussed in the last section.

The arrangement of a Fuzzy Logic-structure can be arranged as a request issue in high layered space, where each guide talks with a standard set, support limits, and contrasting systems directly. Semantic variables, portrayed as elements whose characteristics were sentences in a trademark language (for instance, close to nothing and large), may be addressed by fluffy sets. Fuzzy Logic controllers were an appealing choice when accurate mathematical plans are unreasonable. The Interleaved Boost Converters used 2 Boost Converters which work at 1800. The inductor expands, clearing out happens half in the commitment cycle. The capacitor yield was the total of 2diode current (I1 + I2) which was not enhanced by the yield DC, which hence reduces the wave current of the yield capacitor (IOUT). It also filled in as a part of the commitment cycle. Exactly when the commitment cycle watches out for 0%, half, and 100 percent, the whole of the two diode streams in the like manner watches out for dc yield. Under any effect of ideal working centers, the capacitor yield is expected to channel the inductor grow streams. Fundamental 2P-Interleaved Boost Converters are laid out in Figure 1.

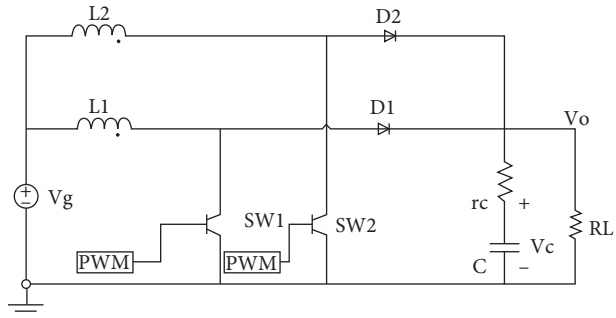

Figure 1: A basic 2P-Interleaved Boost Converter.

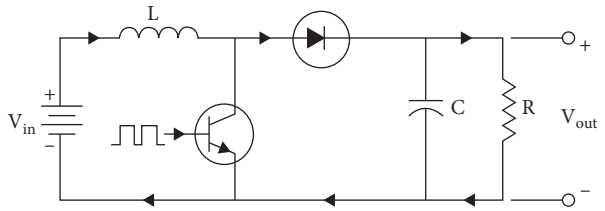

Figure 2: DC-DC-boost converter circuit.

The Interleaved Boost Converters, which encompass of 2 single stage Converters, are related in equal and afterward to a solitary yield capacitor [9–13, 15–18]. The 2-pulse width modulation sign distinction is 1800, and each switch is controlled by the interleaving strategy. Since every inductor current greatness is diminished by one for each stage, the inductor size and inductance can be diminished and furthermore the info current wave is diminished.

2. DC-to-DC Boost Converter

Boost Converter aptitude aims to fill in as venture up voltage starting on one level then to the next level. The DC-DC Boost Converter circuit is appeared in Figure 2.

BC equation in CCM can be inscribed as the following [17]. The input to yield voltage conversion-ratio is assimilated as follows:

$$V_o = \frac{V_i}{1 - D}. \tag{1}$$

The loss Boost Converter duty ratio is

$$D = 1 - \frac{\eta}{M_{\mathrm{DC}}} 1 - \frac{\eta V_i}{V_o}, \tag{2}$$

where "Converter efficiency" is η and "transferal function of voltage" is C. The minimum and maximum load resistances are

$$R_{\min} = \frac{V_o}{I_{o\min}},$$

$$R_{\max} = \frac{V_o}{I_{o\min}}, \tag{3}$$

$$M_{\mathrm{DCmin}} = \frac{V_o}{V_{i\max}}.$$

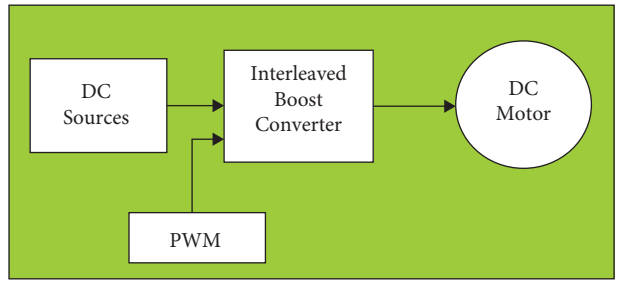

Figure 3: Block diagram of open loop Interleaved Boost Converter-DC Motor System.

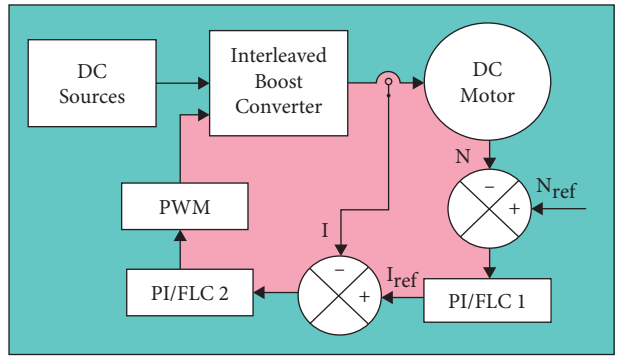

Figure 4: Block diagram of two Interleaved Boost Converter-DC Motor System with PI/Fuzzy logic controller.

2.1. Research Gap. The exceeding literature does not pact with DCM fed from 2-stage ILBC. This work proposes 2-stage ILBC for 2-stage ILBC-DCM. There is a prerequisite to augment the dynamic response of Interleaved Boost Converter-DC Motor System. The overhead writing does not talk about augmentation of the dynamic response using Proportional integral/fuzzy logic controlled two-loop ILBC-DCMS. This work suggests Fuzzy logic controller for Interleaved Boost Converter-DC Motor System as Interleaved Boost Converter and DC Motor characteristics are nonlinear.

2.2. System Description. Figure 3 outlines the block diagram of open-loop ILBC-DCMS. Figure 4 outlines the block diagram of two-loop Interleaved Boost Converter-DC Motor System with Proportional integral/Fuzzy logic controller. The speed of DC Motor is linked to a dimension speed. The F. Law is pragmatic to a speed Proportional integral controller. The yield of Proportional integral is equated with the actual current. The yield of the current Proportional integral is functional on a comparator. The comparator apprises the pulse size applied to Interleaved Boost Converters.

The equations of DC machine are as follows:

$$V_{i1b} = Ri + L\frac{\mathrm{d}i}{\mathrm{d}t} + e_b,$$
$$T = \mathrm{B}fw + Jm\frac{\mathrm{d}w}{\mathrm{d}t}. \tag{4}$$

The equations of PI-PI are as follows:

$$Iref = k1Ie + k4\dagger Ne,$$
$$Vpi2 = k3Ie + k4\dagger Ie. \tag{5}$$

3. Results and Discussion of ILBC-DCMS

3.1. Open-Loop ILBC-DCMS with Source Disturbance. Figure 5 delineates the circuit diagram of ILBC-DCMS with source disturbance. Figure 6 delineates the input voltage specified to the framework. The input voltage assessment is augmented from 48 V to 55 V. Figure 7 delineates the voltage across the motor load of ILBC-DCMS with source disturbance. The significance of voltage across the motor load initially upsurges and then declines to 410 V at $t = 2.5$ sec and it is stable. Figure 8 delineates the current through the motor load of ILBC-DCMS with source disturbance. The value of current through the motor load initially upsurges and then declines to 5 A and it is stable. Figure 9 delineates the motor speed of ILBC-DCMS with source disturbance. The value of motor speed initially upsurges and then diminishes to 1250 RPM and it is stable. Figure 10 delineates the motor torque of ILBC-DCMS with source disturbance, and the assessment attained is 5 N-m.

The voltage output and speed of open-loop interleaved Boost Converter-DC Motor System upsurges due to a disturbance at the input. Hence, it is projected to go for closed-loop ILBC-DCMS with Proportional Integral/Fuzzy Logic controller.

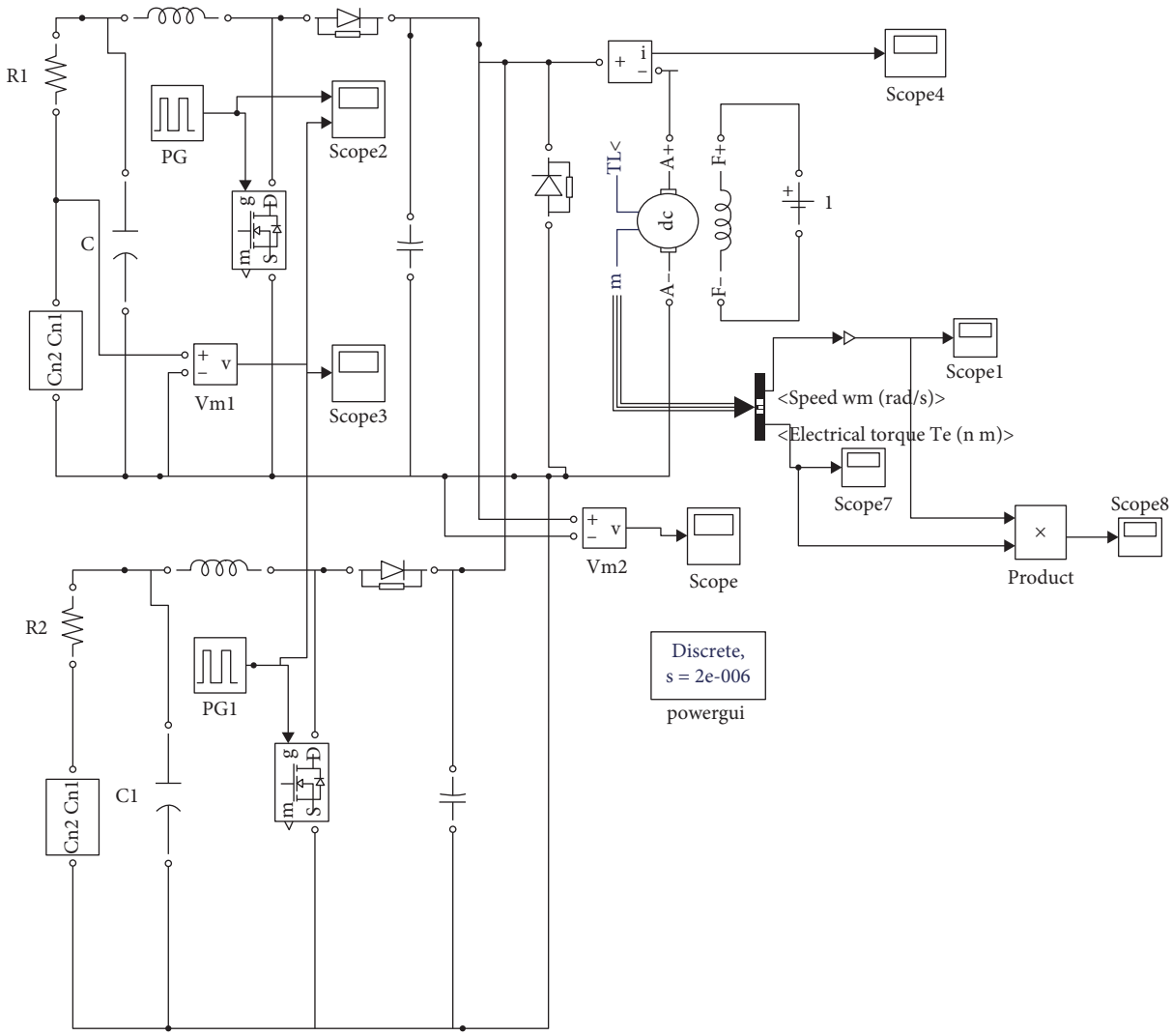

Figure 5: Circuit diagram of open-loop Interleaved Boost Converter-DC Motor System with source disturbance.

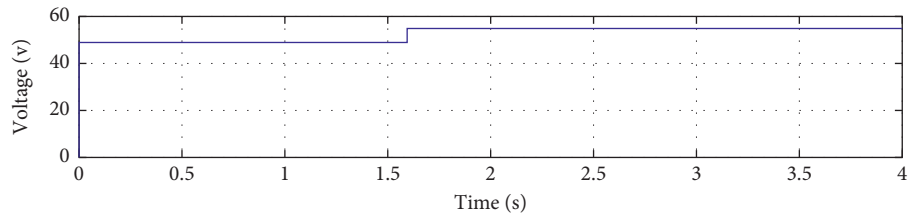

Figure 6: Input voltage of Interleaved Boost Converter-DC Motor System.

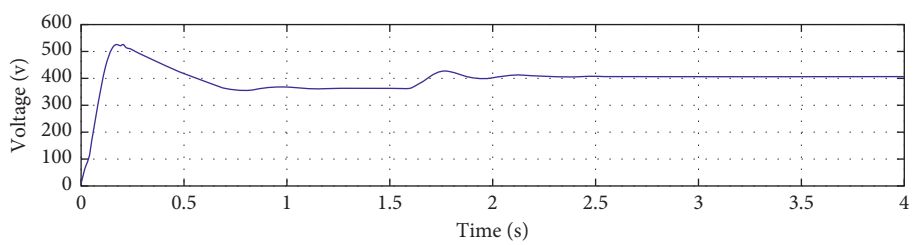

Figure 7: Voltage across motor load of Interleaved Boost Converter-DC Motor System.

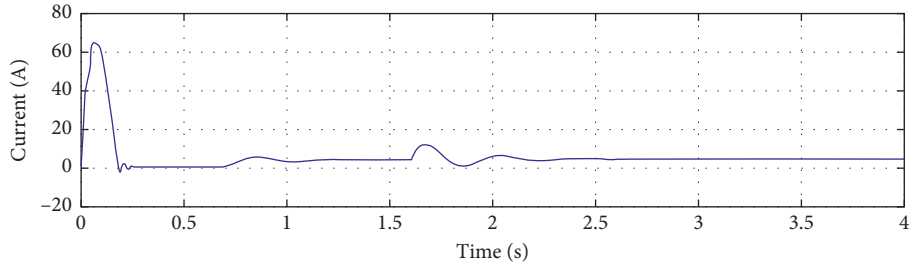

Figure 8: Current through the motor load of Interleaved Boost Converter-DC Motor System.

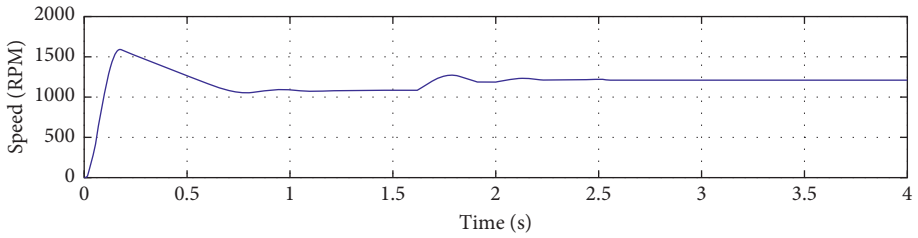

Figure 9: Motor speed of Interleaved Boost Converter-DC Motor System.

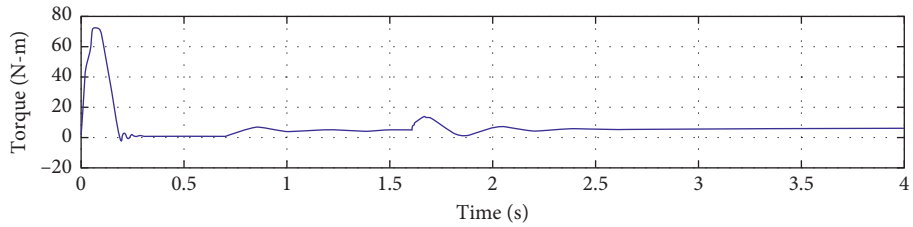

Figure 10: Motor Torque of Interleaved Boost Converter-DC Motor System.

3.2. Two-Loop ILBC-DCMS with and without P.I–P.I Controller and FLC-FLC. Figure 11 delineates the two-loop Interleaved Boost Converter-DC Motor System circuit diagram with P.I–P.Controller. Figure 12 delineates the two-loop Interleaved Boost Converter-DC Motor System circuit diagram with FLC-FLC. Figure 13 delineates the Voltage across the motor load of Interleaved Boost Converter-DC Motor System with and without P.I–P.Controller and FLC-FLC. The value of Voltage across the motor load without controller is 410 V. The Voltage across the motor load with PI-PI initially upsurges and then declines to 410 V at $t = 2.5$ sec and it is stable. Voltage across the motor load with FLC-FLC gradually upsurges and reaches 380 V. Figure 14 delineates the Current through the motor load of Interleaved Boost Converter-DC Motor System with and without p.I–P.Icontroller and FLC-FLC. The value of current through the motor load without controller initially upsurges and then declines to 8 A and it is stable. The value of current through motor load with PI-PI initially upsurges and then declines to 6 A and it is stable. The value of current through motor load with FLC-FLC initially upsurges and then declines to 4 A and it is stable. Figure 15 delineates the Motor speed of Interleaved Boost Converter-DC Motor System with and without P.I–P.I and FLC-FLC controller. The value of motor speed without controller initially enhances and then gradually declines to 1300 RPM. The value of motor speed for PI-PI initially declines and then gradually upsurges to 1000 RPM and it is stable. The value of motor speed for FLC-FLC initially declines and then gradually upsurges to 1000 RPM and it is stable. Figure 16 delineates Interleaved Boost Converter-DC Motor System's motor torque value without and with p.I–P.I and FLC-FLC controller. Motor torque of Interleaved Boost Converter-DC Motor System without controller is 10 N-m. Motor torque value of Interleaved Boost Converter-DC Motor System with PI-PI controller is 9 N-m.

Assessment of time domain parameters using P.I–P.I and F.LC-F.LC (NREF = 1000 RPM) is specified in Table 1. By using F.LC-F.LC, the rise time is moderated from 1.74 Sec to 0.33 Sec; greatest time is moderated from 2.10 Sec to 0.64 Sec; the settle down time is moderated from 2.15 Sec to 0.72 Sec; the steady state error is moderated from 1.6 V to 0.1 V; and ripple voltage is moderated from 0.9 N-m to 0.008 N-m.

Assessment of time domain parameters using P.I–P.I and F.LC-F.LC (NREF = 950 RPM) is specified in Table 2. By using F.LC-F.LC, the rise time is moderated from 1.77 Sec to 0.38 Sec; greatest time is moderated from 2.75 Sec to

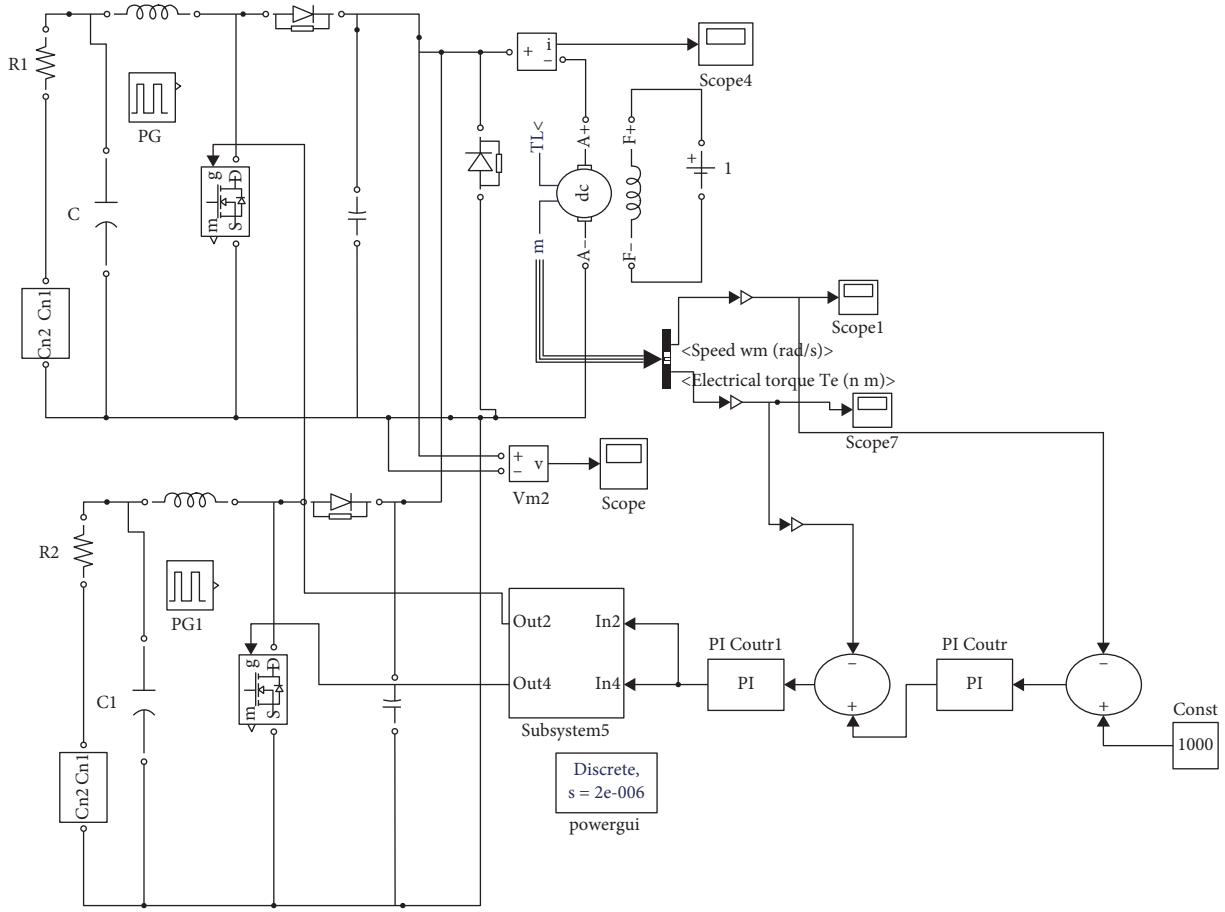

Figure 11: Two-loop Interleaved Boost Converter-DC Motor System with P.I–P.I controller.

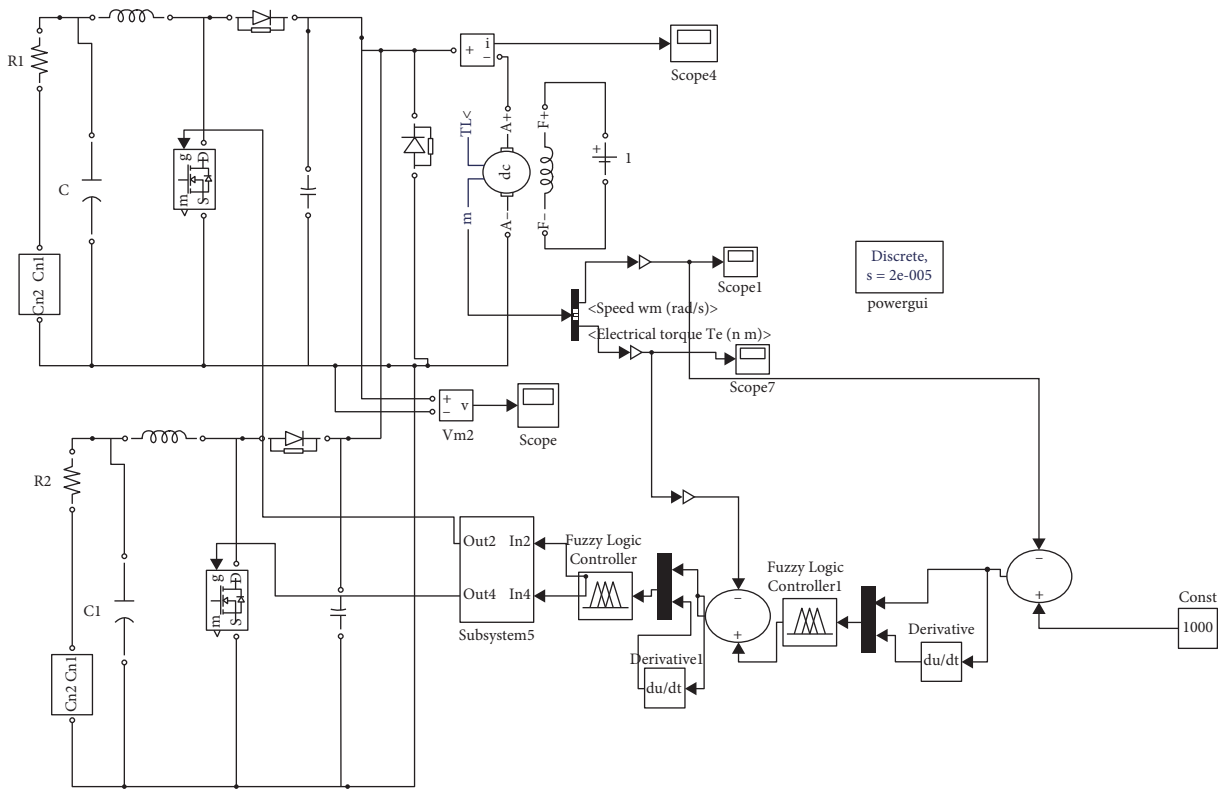

Figure 12: Two-loop Interleaved Boost Converter-DC Motor System with FLC-FLC.

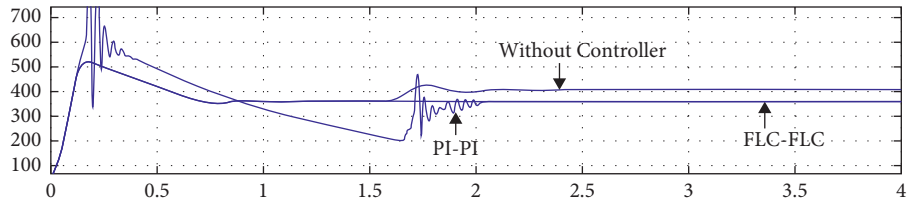

Figure 13: Voltage across motor load controller, PI-PI and FLC-FLC.

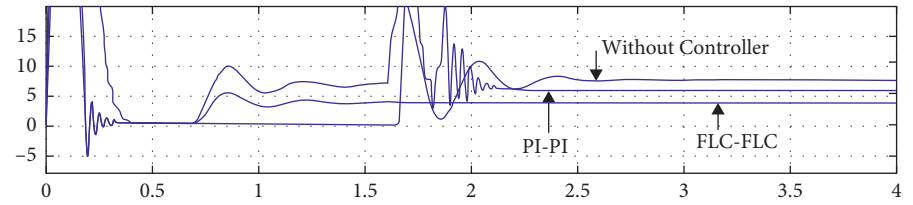

Figure 14: Current through motor load controller, PI-PI and FLC-FLC.

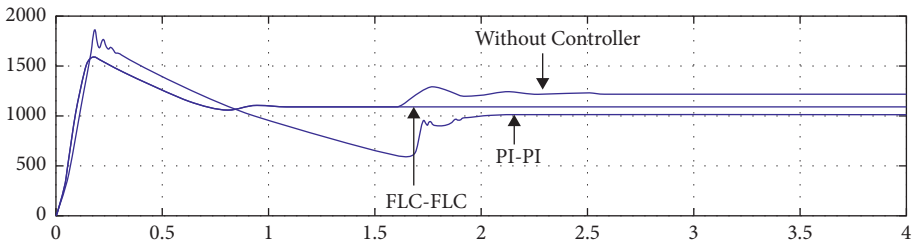

Figure 15: Motor speed controller, PI-PI and FLC-FLC.

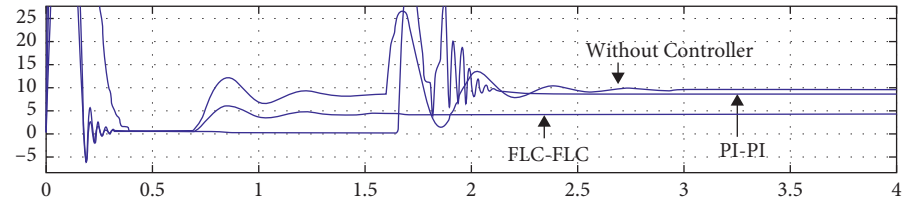

Figure 16: Motor Torque controller, PI-PI and FLC-FLC.

Table 1: Assessment of time domain parameters NREF = 1000 RPM.

Type of controller	Tr	Tp	Ts	Ess
PI–PI	1.74	2.10	2.15	1.6
FLC-FLC	0.33	0.64	0.72	0.1

Table 2: Assessment of time domain parameters Nref = 950 RPM.

Type of controller	Tr	Tp	Ts	Ess
PI–PI	1.77	2.30	2.75	1.8
FLC-FLC	0.38	0.70	0.79	0.3

Table 3: Comparison table of time domain parameters Nref = 900 rpm.

Type of controller	Tr	Tp	Ts	Ess
PI–PI	1.79	2.48	2.86	1.9
FLC-FLC	0.39	0.73	0.81	0.4

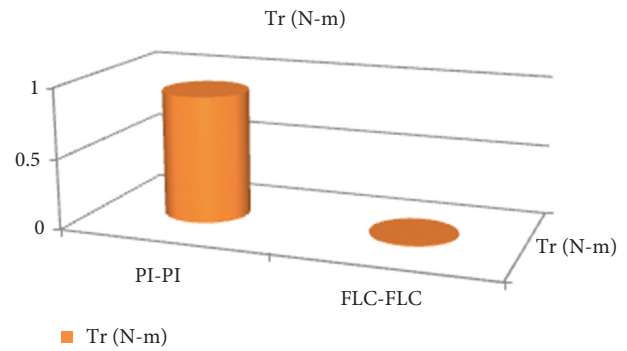

Figure 17: Bar chart representation of torque ripple using P.I–P.I and F.LC-F.LC.

Table 4: Comparison of Torque Ripple using P.I–P.I and F.LC-F.LC

Type of controller	Tr (N-m)
P.I –P.I	0.9
F.LC-F.LC	0.008

Table 5: Simulation parameters.

Vin	48 V
C1, C2	0.1 μF
L1, L2	10 mH
C3, C4	2000 μF
Frequency	50 Hz
Mosfet	IRF840
Diode	IN4007
N	1000 rpm
V0	360 V

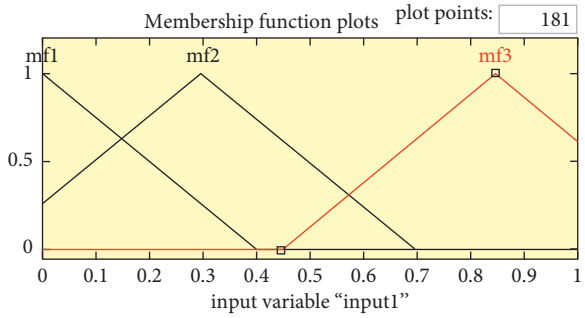

Figure 18: Plot for input1.

0.79 Sec; settle down time is moderated from 2.75 Sec to 0.79 Sec; the steady state error is moderated from 1.8 V to 0.3 V.

Assessment of time domain parameters using P.I–P.I and FLC-FLC (NREF = 900 RPM) is specified in Table 3. By using F.LC-F.LC, the rise time is moderated from 1.79 Sec to 0.39 Sec; greatest time is moderated from 2.48 Sec to 0.73 Sec; settle down time is moderated from 2.86 Sec to 0.81 Sec; the steady state error is moderated from 1.9 V to 0.4 V.

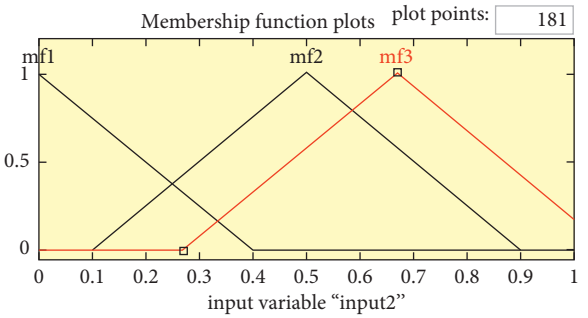

Figure 19: Plot for input2.

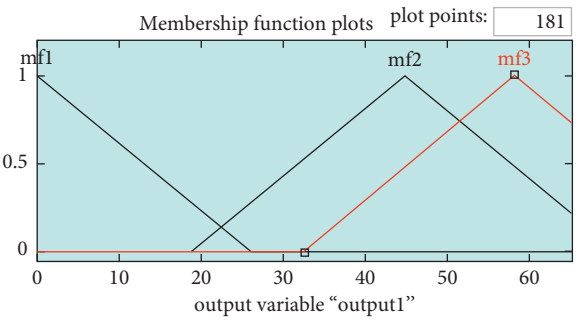

Figure 20: Plot for output.

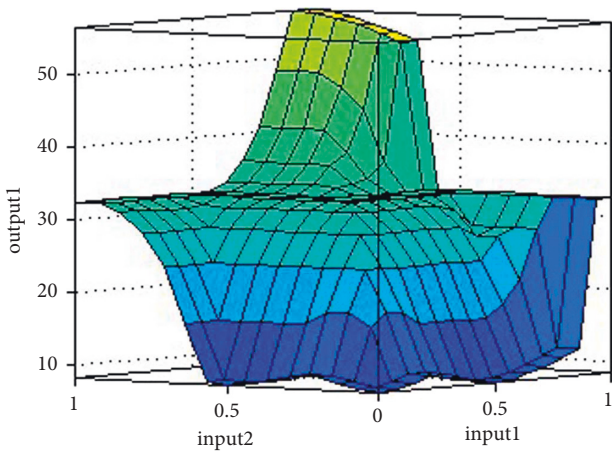

Figure 21: Surface viewer plot.

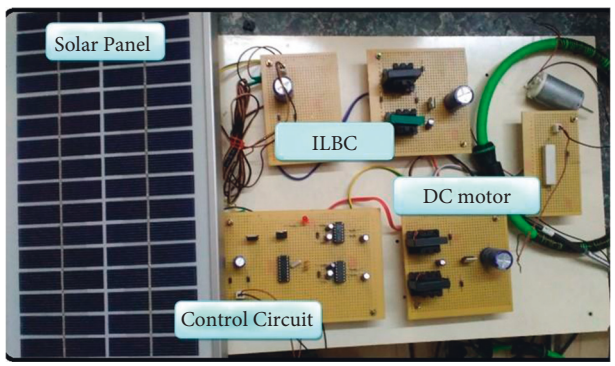

Figure 22: Hardware snap shot of Interleaved Boost Converter-DC Motor System.

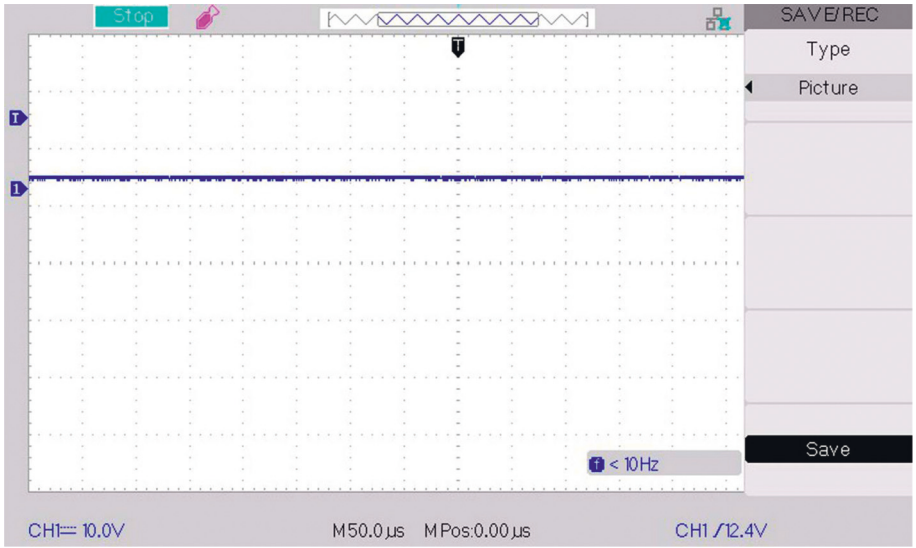

Figure 23: Voltage input of Interleaved Boost Converter-DC Motor System.

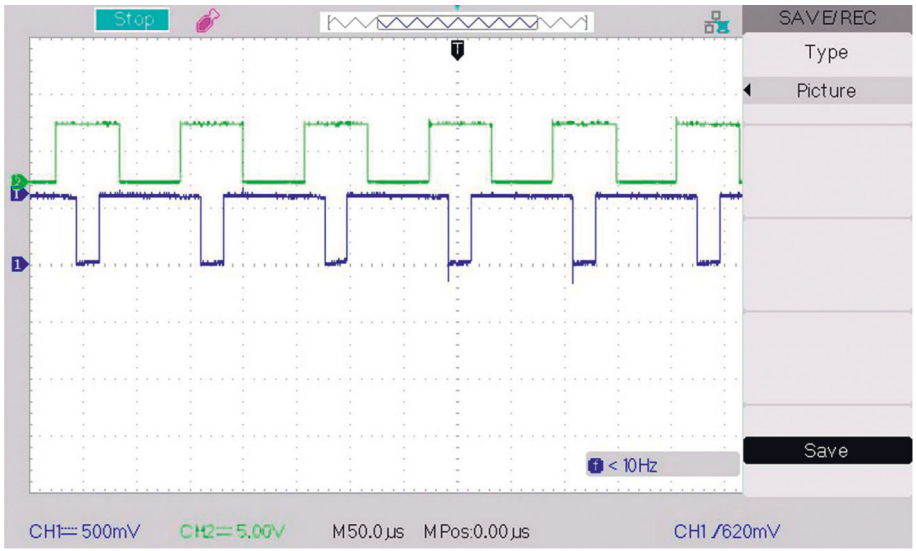

Figure 24: Switching pulses for M1 and M2.

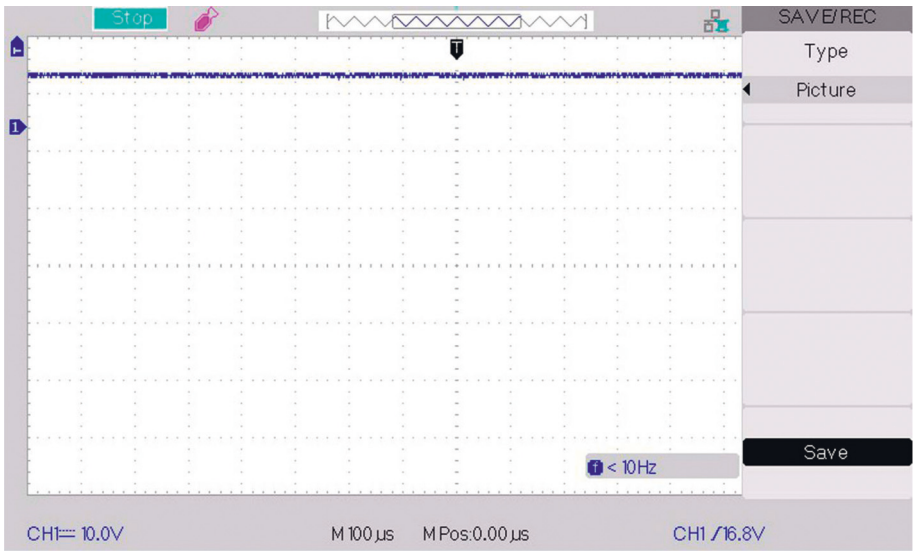

Figure 25: Voltage output of Interleaved Boost Converter-DC Motor System.

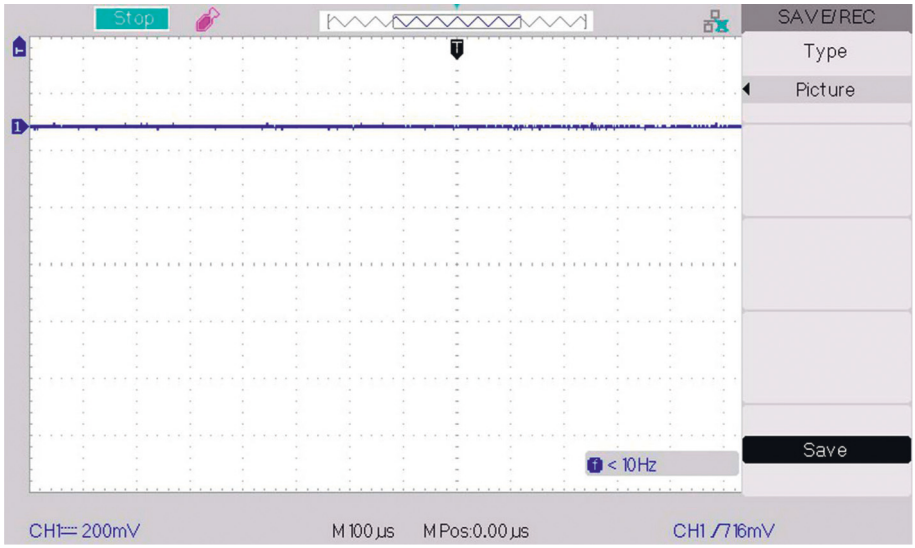

Figure 26: Motor current of Interleaved Boost Converter-DC Motor System.

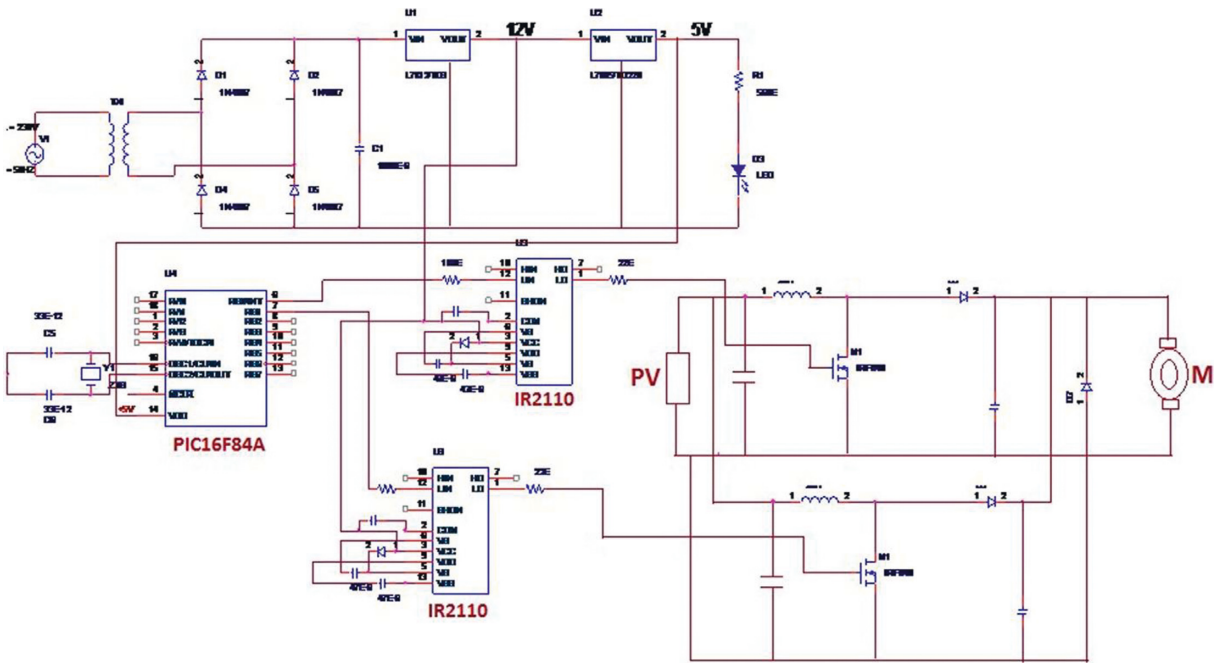

Figure 27: Hardware diagram of Interleaved Boost Converter-DC Motor System.

Figure 17 outlines the bar chart representation of ripple voltage. Comparison of torque ripple using P.I–P.I and F.LC-F.LC is specified in Table 4. Hence, the outcome represents that the F. LC-F.L-controlled two-loop Interleaved Boost DC-DC Converter is superior to P.I–P.I controlled two-loop Interleaved Boost DC-DC Converter. Torque ripple of Interleaved Boost Converter-DC Motor System with F.L-F.L controller is as minimum as 0.008 N-m.

Simulation parameters are presented in Table 5.

The input variable 1 is shown in Figure 18. The input variable 2 is shown in Figure 19. The output variable is shown in Figure 20. The surface viewer plot is shown in Figure 21.

4. Experimental Results of Interleaved Boost Converter-DC Motor System

To verify the routine and functionality of the Modified Interleaved, Boost Converter-DC Motor System has been carried out using mat lab/ ∗ Simulink and a prototype is established. An IRF840 MOSFET is cast-off as the switch. For the gate pulses, P.IC16F84 A microcontroller is utilized to generate a pulse of 10 kHz frequency. The hardware comprises of control circuit, rectifier circuit, I.L.B.C-board, and the load. The I.L.B.C hardware and snap shot are outlined in Figure 22. The PV panel powered by halogen lamp is utilized as a source, and by using a charge controller,

Table 6: List of components of Interleaved Boost Converter-DC Motor System.

S. No.	Name	Rating	Type
1	Capacitor	$1.00E-03$	Electrolytic
2	Capacitor	$4.70E-05$	Electrolytic
3	Capacitor	$3.30E-11$	Disc
4	Capacitor	$2.20E-03$	Electrolytic
5	Diode	1000 V, 3 A	PN junction
6	Inductance	10 uH	Ferrite coil
7	MOSFET (IR840)	600 V, 8 A	N-channel
8	Resistor	1 k	Quarter watts
9	Resistor	100 E	Watts
10	Resistor	22 E	Disc
11	Regulator	12 V	L7812/TO3
12	Regulator	5 V	L7805/TO220
13	IC	IR2110	Opto-coupler
14	PIC controller	P.IC16F84	Disc
15	PCB	V105	General

the input voltage is regulated to 12 V and is supplied to the Converter. Input voltage is outlined in Figure 23. Switching pulses for M1 and M2 are seemed in Figure 24. The Interleaved Boost Converter-DC Motor System's output voltage is seemed in Figure 25. Motor current of I.L.B.C-D.C.MS is outlined in Figure 26. Complete hardware circuit diagram of Interleaved Boost Converter-DC Motor System is delineated in Figure 27. Hardware component list for Interleaved Boost Converter-DC Motor System is given in Table 6.

5. Conclusion

This work deals with two-loop P.I–P.I and F.LC-Fuzzy logic controls two Interleaved Boost-Converter-DC Motor System. Interleaved Boost Converter speed is regulated using two-loop configurations. Two-loop P.I–P.I and F.LC-Fuzzy logic controlled Interleaved Boost DC-DC Converters are designed, analyzed, and simulated. The response of F.LC-F.LC Interleaved Boost Converter-DC Motor System is compared with Proportional Integral-controlled Interleaved Boost Converter-DC Motor System. F.LC-F.LC has minimum overshoot and produces a constant yield of D.C.M speed. From these data, it can be deduced that the settling time is reduced from the array of 2.15 seconds to 0.72 seconds, which would enhance the permanence of the framework with Fuzzy Logic Controller platform than a PIC-platform.

The proposed two-loop interleaved Boost Converter-DC Motor System has advantages like high power capability and improved time domain response. Interleaved Boost Converter-DC Motor System has a disadvantage like the requirement of two Boost Converters. The contribution of this work is to advance the dynamic report of the two-loop interleaved Boost Converter-DC Motor System with a feedback system. Current ripple is reduced using 2SILBC and a fast time response in ILBC-DCM is achieved using FLC. ILBC requires two controlled switches and DC motor has high inertia. The SMC-based two-loop interleaved Boost Converter-DC Motor system will be simulated in future. The hardware of ILBC-DCM is implemented using PIC16F84. The hardware of ILBC-DCM can be implemented using DSPIC to increase the switching frequency. High power ILBC-DCM -drive may be implemented using IGBTs.

Data Availability

The data shall be made available on request.

Conflicts of Interest

The authors declare that they have no conflicts of interest.

References

[1] L. Yin and C. Cheng, "DSP based control of parallel DC-DC Boost Converters by adaptive fuzzy sliding mode control scheme," in *Proceedings of the IEEE 4thInternational Conference on Genetic and Evolutionary Computing (IC-GEC)*, pp. 130–133, IEEE, Shenzhen, China, December 2010.

[2] J. D. Navamani, "Analysis of modified quadratic DC-DC Boost Converter," in *Proceedings of the IEEE International Conference on Inventive Systems and Control (ICI-SC)*, pp. 1–5, IEEE, Coimbatore, India, January 2017.

[3] O. Ibrahim, N. Z. Yahaya, and N. Saad, "PID Controller response to set point change in DC-DC converter control," *International Journal of Power Electronics and Drive Systems*, vol. 7, no. 2, 2016.

[4] A. Ali, "Implementation of simple moving voltage average technique with direct control incremental conductance method to optimize the efficiency of DC microgrid," in *Proceedings of the IEEE International Conference on Emerging Technology (ICET)*, vol. 1-5, December 2015.

[5] M. Khayamy, "Adaptive fuzzy logic control mixing strategy of dc/dc Converter in both discontinuous and continuous conduction mode," *Journal of Control, Automation and Electrical Systems*, vol. 27, no. 3, pp. 274–288, 2016.

[6] P. V. R. Kumar and M. S. Kalavathi, "Fractional order P.ID-Controlled interleaved boost Converter fed shunt active filter system," *International Journal of Power Electronics and Drive Systems*, vol. 9, no. 1, 2018.

[7] M. Zainuri, "Development of adaptive perturb and observe fuzzy control maximum power point tracking for photovoltaic Boost dc-dc Converter," *IET Renewable Power Generation*, vol. 8, no. 2, pp. 183–194, 2014.

[8] Saidah, "Control strategy for PWM voltage source converter using fuzzy logic for adjustable speed DC motor," *International Journal of Power Electronics and Drive Systems*, vol. 8, no. 1, 2017.

[9] R. Ahmed and M. F. Chouikha, *Design and Analysis of Fuzzy Controllers for Dc-Dc Converters*, pp. 479–482, Electrical & Computer Engineering Department, Howard University, Washington, WA, USA, 2004.

[10] W. C. So, C. K. Tse, and Y. S. Lee, "Development of A Fuzzy logic controller for DC-DC converters," *IEEE Trans.on Power Electronics*, vol. 11, no. 1, pp. 24–32, 1996.

[11] M. B. Camara, H. Gualous, F. Gustin, and Berthon, "Design and new control of DC/DC Converter to share energy between SCAP and battery in hybrid vehicle," *IEEE Transactions on Vehicular Technology*, vol. 57, no. 5, pp. 2721–2735, 2008.

[12] M. B. Camara, H. Gualous, B. Dakyo, C. Nichita, and P. Makany, "Buck boost Converters design for ultracapacitors and lithium battery mixing in hybrid vehicle applications," *IEEE Vehicle Power and Propulsion Conference(VEEEPPC)*, vol. 1-6, 2010.

[13] V. Maheswari, P. Elangovan, M. Baranidharan, S. Deepa, and L. Dhanesh, "Theoretical and simulation analysis of first generation dc-dc converters," *International journal of Advanced Science and Technology*, vol. 28, no. 19, pp. 72–78, 2019.

[14] R. Wai, "Design of adaptive control and fuzzy neural network control for single stage boost inverter," *IEEE Transactions on IEs*, vol. 62, no. 9, pp. 5434–5445, 2015.

[15] Budiyanto and R. Setiabudy, "Inverter development as A boost converter for DC-microgrid," *TELKOMNIKA-Telecommunication Computing Electronics and Control*, vol. 11, no. 2, 2013.

[16] LiP. IngGuo, J. Y. Hung, and R. M. Nelms, "Evaluation of dsp based P.ID and fuzzy-controller for dc Converters," *IEEE Transactions on Industrial Electronics*, vol. 56, 2009.

[17] V. S. C. Raviraj and P. C. Sen, "Comparative study of proportional-integral, sliding mode and fuzzy logic controllers for power converters," *IEEE Transactions on Industry Applications*, vol. 33, no. 2, 1997.

[18] L. Gao, Z. Jiang, and R. A. Dougal, "Evaluation of active hybrid fuel cell/battery power sources," *IEEE Trans.on Aeros Electron Systems*, vol. 41, no. 1, pp. 346–355, 2005.

Hindawi
Mathematical Problems in Engineering
Volume 2022, Article ID 9679050, 12 pages
https://doi.org/10.1155/2022/9679050

Research Article

An Internet of Things (IoT) Based Block Chain Technology to Enhance the Quality of Supply Chain Management (SCM)

Ali Rizwan,[1] **Dimitrios A. Karras**,[2] **Jitendra Kumar**,[3] **Manuel Sánchez-Chero**,[4] **Marlon Martín Mogollón Taboada**,[5] **and Gilder Cieza Altamirano**[6]

[1]*Department of Industrial Engineering, Faculty of Engineering, King Abdulaziz University, Jeddah 21589, Saudi Arabia*
[2]*School of Science, National and Kapodistrian, University of Athens (NKUA), Athens 34400, Greece*
[3]*Department of Electronics and Communication Engineering, GLA University, Mathura, Utter Pradesh, India*
[4]*Facultad de Ingeniería de Industrias Alimentarias y Biotecnología, Universidad Nacional de Frontera, Sullana, Peru*
[5]*Facultad de Ciencias Empresariales y Ambientales, Universidad Nacional de Frontera, Sullana, Peru*
[6]*Universidad Nacional Autónoma de Chota, Cajamarca, Peru*

Correspondence should be addressed to Ali Rizwan; arkhan71@kau.edu.sa

Received 18 May 2022; Revised 29 June 2022; Accepted 6 July 2022; Published 21 July 2022

Academic Editor: Amandeep Kaur

Recent technological developments indicate possible advancements in supply chain management (SCM). These innovations have attracted a lot of interest from industries including logistics, manufacturing, packaging, and transportation. The conventional systems, however, use centralised servers to control all operations, including the exchange of raw materials, making orders, dealing with buyers and sellers, and updating orders. The network's supply chain may thus be insecure as a result of every activity being routed via centralised servers. The danger is additionally increased by a number of difficulties, including scalability, data integrity, security, and availability. Block chain technology may be used in these circumstances to decentralise transaction processing and eliminate the need for a centralised controller. In this approach, the performance of the resource-constrained supply chain network is improved by the effective use of edge computing and priority data access. The Intelligent *K*-Means (IKM) clustering algorithm is suggested across the edge nodes in the current research to categorise the priority level of each piece of data. This classifier determines if the edge node has received data that is high priority or low priority. Low priority data is recorded in the log files for future data analysis. Then, to allow safe data flow in the open block chain while excluding outside parties, the High Priority Access based Smart Contract (HPASC) technique is deployed. The whole experiment was conducted in a Python environment, and variables including scalability, reaction time, throughput, and accuracy were studied. Current systems' constrained block sizes and fork creation lengthen the time transactions must wait before being processed. The suggested methodology is quicker and uses less storage space than current block chain systems. The results show that the suggested approach works better than current blockchain technology to raise the standard of supply chain management.

1. Introduction

Due to technology improvements over the previous several decades, outdated systems were replaced by smart devices. Similar to this, automated systems for monitoring, uploading food stockpiles, making orders, and handling financial transactions have replaced the conventional Excel systems used in supply chain operations. In a small-scale company, managing the supply chain process is considerably more difficult since it requires complete web access to the core component. SCM becomes more active in optimising customer value and dependability as a result of the development of smart solutions like enterprise resource planning, smart logistics, and online tracking. SCM reveals informational and physical fluxes. While the latter performs buyer-seller contact and live-stock monitoring from production to consumer, the former deals with vehicle mobility and storage management. The modern supply chain systems

have to deal with a number of difficulties, including asset tracking, scalability, resource constraints, and information hacking. To address these issues, a number of researchers have put forward several methods [1]. But there is still a problem with finding the best option for an effective SCM. One of the technologies used in conjunction with business logic to carry out smart contracts that deal with product licencing improved asset monitoring, and security transparency is blockchain. By using a public ledger system to continuously record shipping containers, monitor inventory, and manage tax bills and payments, block chain technology may also be used to logistics.

It also lays the way for a genuine, scalable solution for SCM procedures. According to a 2019 assessment, Zeto, Modum, Waltonchain, Ambrosus, and Devery are a few examples of blockchain SCM initiatives that have found success. Generally speaking, SCMs often rely on centralised servers for processing, which lower network throughput and processing power. As a result, depending only on cloud computing is not an ideal option. A developing technology called edge computing makes it possible for edge nodes to carry out computation. The main goal of edge computing is to distribute certain jobs from cloud servers to the participating edge nodes in order to lessen the strain on the central point. Block chain can provide secure and dependable SCMs because of its distributed environment. Although the edge-block chain has several benefits over current SCMs, there is still need for development in areas like scalability, privacy, energy use, and security. There have been several scalability measures implemented, and some of the shortcomings of such studies are given here.

(i) The large data processing in a resource-constrained setting is not addressed by the current scalable blockchain approaches.

(ii) Uploading a lot of data to the cloud servers could cause congestion and use up additional bandwidth.

(iii) Using greater processing resources to handle all types of data sent over the SCM network.

Furthermore, there is no precise answer that more closely meets the requirements of contemporary SCMs. In order to address these issues, this study proposes an intelligent automated method for scalable food traceability. Due to its effective work automation, machine learning (ML) technologies have made great strides in recent years, drawing interest from a variety of groups [2, 3]. In order to shorten the computation time across the edges, the present study divides the data into two groups, "prioritised" and "low-prioritized," using an intelligent clustering approach.

1.1. Contribution of the Study

(i) Edge nodes are presented to categorise the priority level of each data using the Intelligent *K*-Means (IKM) clustering approach.

(ii) Data transfer on the public blockchain is safeguarded via the High Priority Access Smart Contract (HPASC) approach.

(iii) Scalability, reaction time, throughput, and accuracy were all measured in this study, which was carried out entirely in a Python environment.

(iv) Compared to current block chain systems, the suggested approach is quicker and uses less storage space.

1.2. Motivation of the Study. Lack of technical know-how and understanding of blockchain technology's applications serve as a barrier to the supply chain's adoption of this new technology. Blockchain is gaining popularity in the technical community; however, there are not many applications or technical developers yet, which is a problem. Information technologies such as blockchain may be disruptive and call for the replacement or alteration of existing legacy systems.

Additionally, each edge stores the low priority data in log files for later analysis. Because the blocks only contain the priority data, the suggested system has great scalability. Additionally, by processing the data according to its priority, it works better in a setting with limited resources. The ML-based priority classification gives increased scalability and availability measures since it defines the classes of the training data among the edge nodes.

2. State-of-the-Art Analysis

The following explores the existing studies that prevailed in supply chain management using blockchain. Also, it presents recent state-of-art methodologies to overcome scalability issues in blockchain networks. Alzahrani and Bulusu [4] propose a technique to employ NFC tags to track and trace the products over the supply chain networks [4]. They highlight some of the key features such as security, storage efficiency, and location tracking using Unique ID (UID). Later, Kefalakis et al. [5] develop an object tracking using NFC tags comprising a list of tagged objects [5]. They develop a handheld device to pick up the list of intended objects in the goods. Furthermore, the research enforces blockchain to promote secure data transfer over the network. As advancement over the UID-based supply chain, the authors have developed an RFID-based strategy for monitoring transportation in the entire SCM network [6, 7]. Also, the article [8] ascertains for detecting the counterfeit product in the SCM process using RFID tags. Recent researchers suggested implementing blockchain functionalities in the SCM processes. In this context, an Agri-based traceability system proposed by authors highlights the importance of blockchain when combined with the RFID tags [9]. This study encapsulates food safety and traceability in food supply chain networks. Later, the authors propose a mechanism to achieve transparency throughout the SCM network. They adopt EPC global network for the effective use of RFID in the garment supply chain [10]. As an enhancement, Zhao et al. suggest an SCM using blockchain and distributed ledger for a globally connected supply chain framework [11]. Followed by Zhao et al. [11], researchers present a novel "Blockchain-as-a-Service" to provide insights for deploying blockchain in IoT networks [12, 13].

Also, blockchain in intelligent transportation systems has made remarkable achievements [14, 15]. In recent decades, blockchain increasingly combined with edge computing to overcome the problems such as response time, network pressure, and security. The security in edge computing is increasingly exposed due to data tampering, data destruction, and data leakage [16, 17]. As an innovation, blockchain stores the information and transactions over the peer-to-peer networks [18]. In some applications, machine learning algorithms are applied effectively to classify special device information to achieve scalability and security [19]. Many researchers have proposed many solutions for scalability enhancement in the blockchain. For instance, a chain-partitioned scalability mechanism is put forth in literature [20]. In this study, on-chain, off-chain, and side-chain structures are established to increase the throughput and transmission rate during reduced block size. Additionally, in DAG-based scalability, the authors design a graph-based blockchain where the vertices represent the contracts and edges represent the interactions [21]. Here, partitioning is performed where the partition is balanced by minimizing the edges in the blockchain network to achieve scalability. Furthermore, the sharing mechanism is practiced in many blockchain networks where the database splits horizontally to spread the nodes.

3. Theoretical Framework

In this section, we consider sea food supply chain management in which edge-based block chain scheme encompassing priority-based access scheme to achieve scalability. Figure 1 depicts the sea food supply chain management. Consider a supply chain environment comprising of following activities: (i) Raw material supply, (ii) Production encompassing accurate planning and inventory management, (iii) processing the sea food followed by packaging, (iv) Efficient storage, and (v) Distributing the sea foods to the end users (wholesale/retail).

If the aforementioned activities are not handled properly, the entire SCM will fail which in turn leads to the loss of faith on company and food quality. Meanwhile, the deployed IoT sensors collect operational data from each division and transfer the data over the network to perform real-time monitoring of sea foods. It often requires RFID to check whether the sea food products are counterfeit or not [22, 23]. The edge nodes collect and analyze the data received from diverse ends of the supply chain management.

Figure 2 depicts the system flow of the proposed SCM processes. While edge computing exclusively refers to compute at the ingress of the network, fog computing is inclusive of computing anywhere along the continuum, from cloud to the edge. Block chain coupled with edge computing can provide fairness in end-user experience and scalable infrastructure. The underlying decentralized and distributed edge platform perform simulation of block chain. Each edge node effectively does the storage and information exchange for reducing the burden of computing load and memory consumption while handling superfluous information. The primary objective of the proposed SCM is

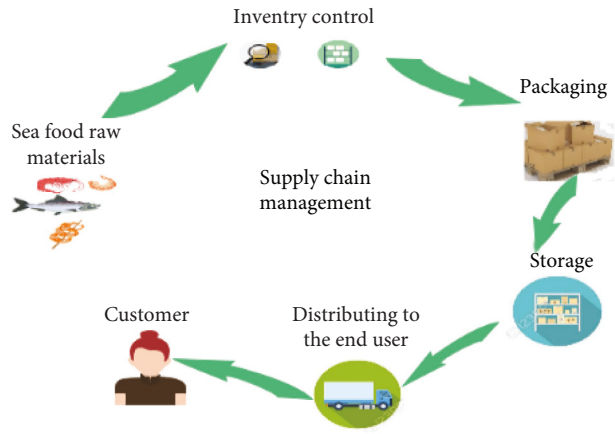

Figure 1: Sea food supply chain management.

to leverage the block chain's immutability in a scalable manner. The overall scheme introduces a distributed edge-based SCM network where the data is uploaded to the blockchain based on its priority. Table 1 shows the input data and their notations that were processed by edge nodes.

The architectural flow of the proposed scheme consists of an access network where each edge node is coupled with IoT sensors meant for tracing location, temperature, and humidity levels. The location information of the vehicles is traced using RFID tags in each vehicle, and the temperature and humidity levels are measured using temperature sensors. After connecting the devices at each edge node, IP addresses for each device are returned. Then, each edge node performs broadcasting of each information over the SCM network once it receives. Next, the sharing of information is accomplished through the blockchain consensus scheme. Each edge data detects for its priority score using intelligent fuzzy K-means classification. When the IoT sensors detect the high-priority data, they will upload the corresponding information to the edge node. When the smart contract recognizes the intended information, it will then stimulate the HPSAC for secure data transfer over the SCM network. The schematic flow of the suggested methodology is illustrated in Figure 3.

4. Result and Discussion

4.1. Basic Edge-Based Blockchain Structure. Due to the technological advances in blockchain, numerous applications have adopted blockchain as their business strategy. Some of the noteworthy footprints of blockchain are Bitcoin, Ethereum, and Hyperledger platforms. Bitcoin and Ethereum platforms generally adopt the Proof of Work Consensus mechanism with high-end security, but it needs more energy and computation power. On the other hand, Hyperledger uses the Byzantine fault tolerance to secure the blocks. It often relies on the number of failure nodes while securing the network. The number of failure nodes should not exceed one-third part of the available nodes. In Sybil attacks, the Hyperledger network is cumbersome as most of the nodes become compromised by the attackers, which damages the whole framework. Recent applications have adopted

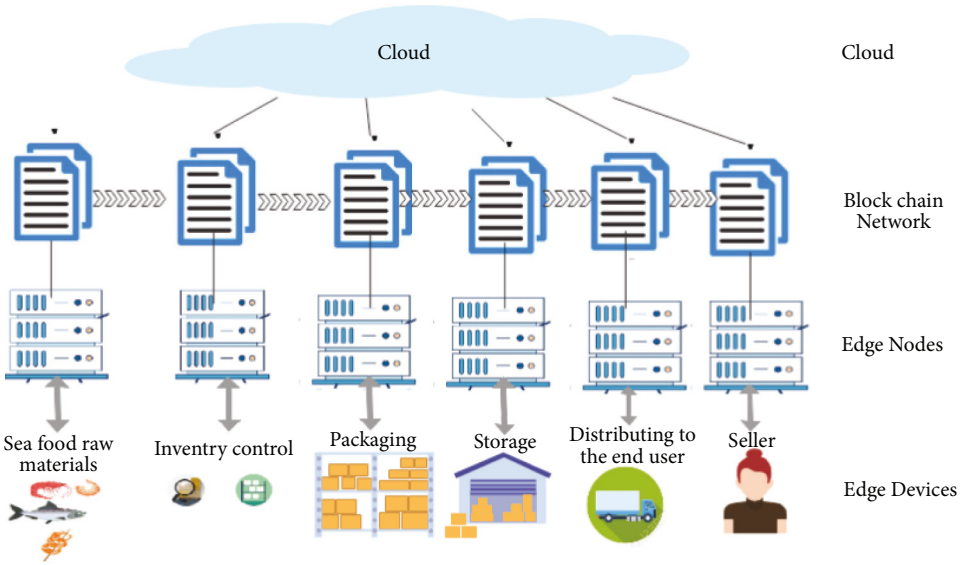

Figure 2: System architecture.

Table 1: List of inputs processed in edge nodes.

Input data	Notation
Name of the manufacturer	N_1
Name of the manufacturer company	C_1
Name of the manufacturer city	P_1
Manufacturer contact number	M_1
Name of the truck company	N_2
Name of the truck dealer	N_3
Name of the truck dealer city	P_2
Truck dealer contact number	M_2
Logistics company name	N_4
Name of the logistics dealer name	N_5
Logistics dealer contact number	M_3
Time and date of delivery of raw sea food to the manufacturer	TD_1
Temperature recorded at the time of arrival of sea foods in raw state	T_1
Time and date when the sea food taken by the distributors	TD_2
Temperature of the sea food recorded while reaching the distributors end	T_2
Time and date when the sea food loaded in the center	TD_3
Temperature of the food in the logistics section	T_3
Time and date when the sea food transported from the logistics section to the shipment truck	TD_4
Temperature recorded at the truck	T_4
Time and date when the sea food gets loaded to the retailer end	TD_5
Temperature of the food at the retailer section	T_5
Time and date when picked up by the consumer	TD_6
Temperature of the sea food at the time of arrival	T_6
Customer name	N_6
Customer contact number	M_4
Customer city	P_3

Ethereum for its feature of adopting Proof of Stack (PoS). It consumes less energy and resource and thereby increasing the scalability of the network. Moreover, Hyperledger possesses constraints such as configuring sandbox and uncertainty, directly affecting the system's security.

Henceforth, we decide to use Ethereum as the blockchain platform for its enhanced reliability and scalability. The proposed edge-based blockchain architecture is shown in Figure 4. The bottom layer consists of data that are gathered from the IoT devices connected across the SCM networks. As stated in Table 1, each edge node collects the information about the status of sea food at each instance. Next, the blockchain layer enables the key enabling features such as distributed networking, disseminating the data across the network, and verification of prioritized data among all the edge nodes. The PoS layer constitutes the sharing of data

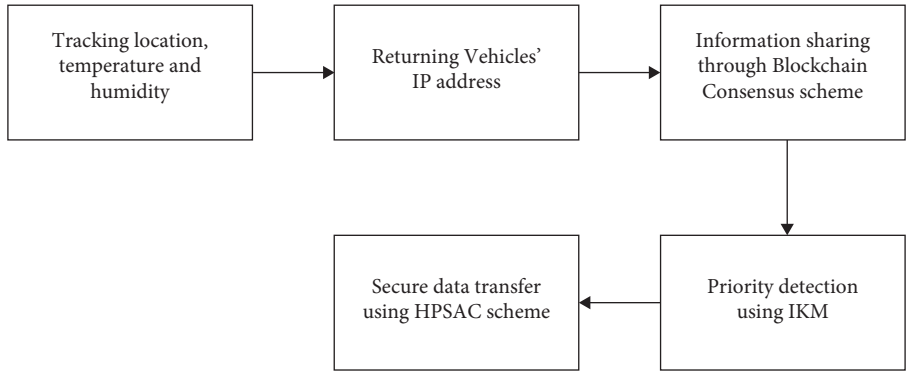

Figure 3: Overall process flow of the proposed system.

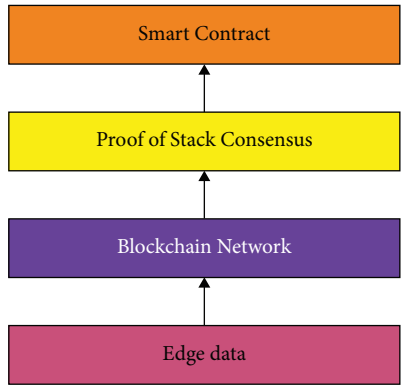

Figure 4: Structure of edge-based blockchain.

among the edge nodes by adopting PoS Consensus mechanism. The smart contract layer performs the HPASC scheme for real-time secure access of the SCM network.

4.2. Priority Detection Using Intelligent K-Means (IKM) Algorithm. Consider a scenario; the seafood is produced in the manufacturer factory, the IoT sensors and RFID measure the temperature and location information, and the corresponding data are stored in the manufacturer edge servers. Likewise, the sensors continuously transmit the data gathered at different instances such as inventory, packaging, storage, distribution, and the retailer section. The data are gathered in the edges manipulated for analyzing the priority of each data before uploading to the blockchain. An example of the sensor messages gathered at the manufacturer end is a 3-tuple data: <*Timestamp*, *Sensor ID*, *content*>.

Furthermore, RFID tracks the location of the food material transported across the path. The dataset consists of additional information stated in Table 1. In our proposed scheme, priority detection is the primary step. The detection mechanism includes the intelligent *k*-means algorithm for detecting the priority of the data. This section furnishes the principle of IKM and IKM process.

4.2.1. Principle of IKM. Clustering mainly leads to data partition into various clusters to find out the closest relationship between those data objects. In this context, we plan to propose a massive-scale prioritization using Intelligent *K*-Means (IKM) in which the number of clusters and attributes are massive. In this research, we perform clustering based on the stakeholders' requirements such as food condition tracked by IoT sensors and time and date at each instance from shipment to delivery. At the outset, the preferential requirements from stake holders are selected before implementation. Then, normalized weights for each attribute are calculated accordingly. In this scenario, the requirements set of all attributes are collected from 5 stack holders. The preferential requirements lie in the range (0, 10).

Upon collecting the preferential requirements from the stack holders, the relative weights for each attribute are being calculated for scaling the value between 0 and 1. The normalized weights are computed using the following equation:

Table 2: Attributes and weights.

Attribute	Relative preference weight
N_1	0.2
C_1	0.2
P_1	0
M_1	0.6
N_2	0
N_3	0.2
P_2	0.5
M_2	0.6
N_4	0.4
N_5	0.5
M_3	0.3
T_6	0.91
M_4	0.4
TD_1	0.96
T_1	0.98
TD_2	0.96
T_2	0.93
TD_3	0.91
T_3	0.93
TD_4	0.94
T_4	0.96
TD_5	0.94
T_5	0.92
TD_6	0.91
N_6	0.3
P_3	0.2

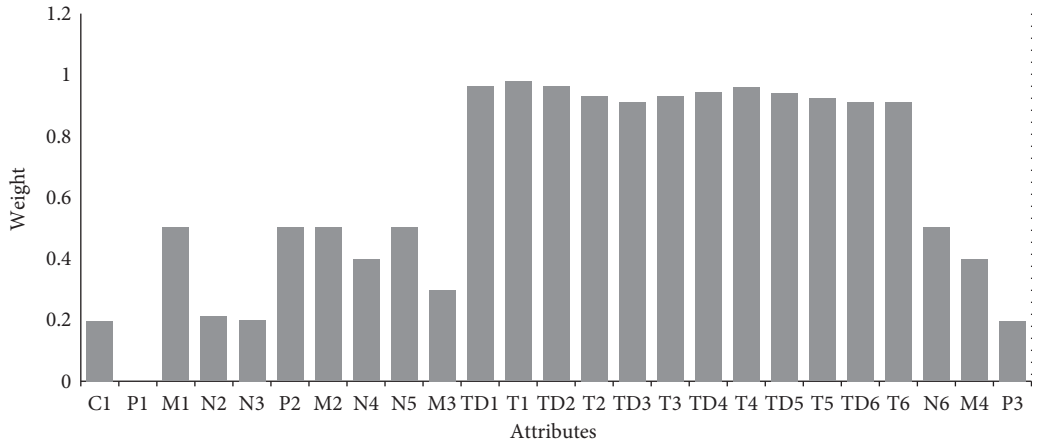

Figure 5: Illustration of weights and attributes.

$$X_{\text{normalized}} = \frac{X - X_{\min}}{X_{\max} - X_{\min}}. \quad (1)$$

For example, the average value of $N_1 = 1.2$, the minimum value of X is 1, and the maximum value of X is 2. Hence, by using (1), the normalized value of $N_1 = 0.2$.

Generally, the preference weights for temperature and time & date will be high when compared to other information stored in the edge servers. Hence the weights for each attribute are illustrated in Table 2. It clearly shows that the weight of attribute T_1 is higher when compared to other attributes.

In Figure 5 the bar graph shows the relative weights of the given attributes. *K*-means clustering is an unsupervised learning model that allows the realization of similar data in clusters. We adopted *k*-means to effectively segregate the attributes into two clusters ($K = 3$) based on the priority of each attribute. The primary objective of the *k*-means is to find similar groups or assign the preferential weights to the cluster based on the similitude among the attributes. Some of the basic terminologies involved in *K*-means are as follows.

Cluster: It is the grouping of identical data points having some similarities among each other and being accumulated.

Centroid: Random data point assumed as the center of the cluster made.

K- parameter: It refers to the target variable that denotes the number of centroids (clusters) in the corresponding dataset. Here, k denotes the number of clusters.

Mean: It refers to the average of data points for calculating the centroid in the cluster.

Euclidean distance: It is defined as the root-mean square of the addition of squared distances between the two points. Let $P(x_1, x_2)$ and $Q(y_1, y_2)$, then ED is given by

$$ED = \sqrt{(x_1 - y_1)^2 + (x_1 - y_1)^2}. \quad (2)$$

And the general form of (2) is given in the following equation:

$$ED = \sqrt{\sum_{i=1}^{n} (x_i - y_i)^2}. \quad (3)$$

4.2.2. IKM Process. This section clearly depicts the process flow of IKM. For efficient clustering of data, each edge node performs clustering of data with its relative weights. It consists of following steps.

Step 1: First, select the attributes and weights stored in each edge.

Step 2: Calculate the preferred relative weights for each attribute.

Step 3: Scale the weights for each attribute to the range 0 to 1.

Step 4: Scatter the points in the two-dimensional space to perform clustering.

Step 5: Select the '*k*' value. Consider in this case $k = 3$.

Step 6: Pick random points in the cluster and consider those points as the centroid.

Step 7: Distance from the first point to the chosen centroids has to be identified.

Step 8: Calculate the Euclidean distance (ED) using equation (2). If the measured ED from the first point to the first centroid is minimum, then consider the first point to be in the first cluster. If the measured ED from the first point to the second centroid is minimum, then the first point belongs to the centroid II. Likewise, the ED for first data point to the third centroid is measured and if this distance is minimum, then the first data point belongs to the third cluster.

Step 9: Updating centroids for every arrival of new data point has to be ascertained using equation (4). The vectorized value of the centroid has been calculated as

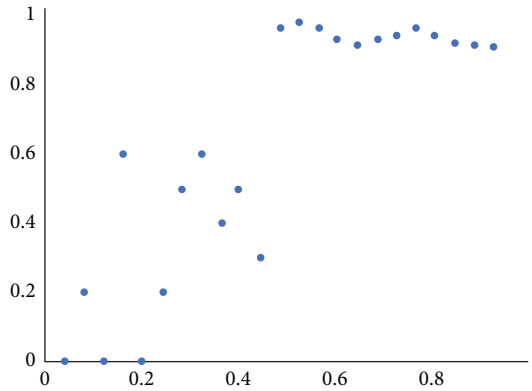

Figure 6: Scatterplot of the preferred relative weights.

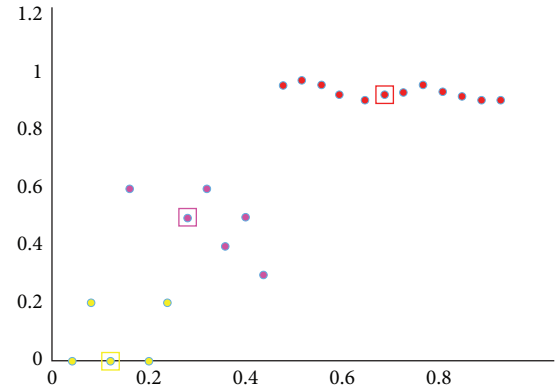

Figure 7: Clustering of data points after iterations with $k = 3$.

Table 3: Attributes with cluster value.

Attribute	Relative preference weight	Cluster
N_1	0.2	1
C_1	0.2	1
P_1	0	1
M_1	0.6	2
N_2	0	1
N_3	0.2	1
P_2	0.5	2
M_2	0.6	2
N_4	0.4	1
N_5	0.5	2
M_3	0.3	1
T_6	0.91	3
M_4	0.4	2
TD_1	0.96	3
T_1	0.98	3
TD_2	0.96	3
T_2	0.93	3
TD_3	0.91	3
T_3	0.93	3
TD_4	0.94	3
T_4	0.96	3
TD_5	0.94	3
T_5	0.92	3
TD_6	0.91	3
N_6	0.3	2
P_3	0.2	1

Table 4: Attributes with priority label.

Attribute	Priority Label
N_1	Low
C_1	Low
P_1	Low
M_1	Medium
N_2	Low
N_3	Low
P_2	Medium
M_2	Medium
N_4	Low
N_5	Medium
M_3	Low
T_6	High
M_4	Medium
TD_1	High
T_1	High
TD_2	High
T_2	High
TD_3	High
T_3	High
TD_4	High
T_4	High
TD_5	High
T_5	High
TD_6	High
N_6	Medium
P_3	Low

$$V_{\text{centriod}} = \frac{1}{|\text{centriod}_i|} \sum_{j=1}^{\text{centriod}_i} x_j. \tag{4}$$

Step 10: Repeat the step 7 to all the attributes with its preferred relative weights.

Figure 6 represents the scatterplot of the preferred relative weights and Table 3 illustrates the attributes and its corresponding clusters. Simply bringing the total beta weights for each person's judgement up to 100 yields the relative weights. As combined with beta weights, relative weights will always be positive.

Using Table 3, the raw values are plotted in the scattered plot, followed by choosing the number of clusters $k = 3$. Then, by assigning the random centroid and calculating the similarity, the centroids are getting updated and final clusters are ascertained. The process of clustering involves grouping the population or data points into a number of groups such that the data points within each group are more similar to one another than the data points within other groups. Simply said, the goal is to separate groups with similar characteristics and place them in clusters. Figure 7 depicts the clustering of data points with $k = 3$. The red square box indicates the centroid point of cluster 3, which normally holds the high-prioritized data. The purple box indicates the centroid point of cluster 2 having medium-prioritized data, and the yellow square indicates the centroid of cluster 1 having low-prioritized data. Finally, Table 4

illustrates the priority label as low, medium and high according to each attributes.

The proposed scheme encapsulates the high-prioritized data for further uploading to the blockchain by excluding the medium- and low-prioritized data. The low- and medium-prioritized data remain in the edge storage for further analysis. After exempting the low- and medium-priority data, the data set is reformed, in order to reduce the block size. Eventually, it enhances the scalability in the entire blockchain network.

4.3. High Priority-Access Based Smart Contract (HPASC). This section highlights the terminologies and processes used in the proposed HPASC scheme. It includes Blockchain and Consensus, PoS and Smart Contracts, and implementation of high-priority access-based smart contract. To achieve scalability in the blockchain SCM network, HPASC serves the purposes like reducing the block size with PoS consensus.

4.3.1. Blockchain and Consensus. Recent surveys have reported that blockchain databases store 10% of the global GDP per the world economic forum. Blockchain is a distributed ledger that can be operated by multiple nodes situated in different locations. Also, it is a decentralized system where each node can have the ability to create a block. Essentially, blockchain is a set of blocks that undergo a set of transactions, which creates a cryptographic hash; henceforth, if any intruder attempts to tamper with the content, the link to the previous block being lost due to the change in the hash value. In addition, there may be byzantine nodes that are malicious in some instances, trying to claim false consensus across the nodes in the blockchain. Consensus in the blockchain is the voting mechanism given for a new node to get accepted as a block in the network. It is a set of transactions that becomes a part of the ledger with a common notion, "the neutral nodes are voting all blocks in the network."

4.3.2. Proof of Stack (PoS) and Smart Contracts. In the proposed scheme, we took Ethereum blockchain to perform supply chain management. The consensus algorithm considered here is the Proof of Stake, which performs the consensus with a limited resource. Consensus is sometimes proof of stake in which a miner puts a stake by claiming itself as a voter with a certain percentage of voting rights. If a node votes for a malicious node, then it loses its stake. Before a node claims to become part of the blockchain, it allows putting a stake over the intended blockchain network. Henceforth, a node with the highest stack won the puzzle and become a part of the blockchain network. In the Ethereum network, trust is built by running smart contracts for every transaction. For instance, if the supplier needs to sell their product for $100, the buyer also accepts the product cost and accepts the order for payment with commission cost for the delivery company. The smart contract is an automated system that consists of a plan of codes working under **if-then rules**.

Figure 8 shows the smart contract in supply chain management. The figure illustrates that the manufacturer can gain the profit only if the end user receives the product and the supplier can receive the money if the buyer receives the product and the delivery company can receive the commission only if they successfully deliver the product.

4.3.3. Implementation of HPASC. Our proposed HPASC adopts a PoS consensus mechanism for sharing the information among the nodes. When the edge node E includes a new transaction consisting of attributes stated in Table 1, the adjacent edge node will obtain the transaction details. The edge node labels the attribute with its priority values and stores the data in the blockchain through the high-priority access-based smart contract. When the next edge nodes start receiving the recently added transaction, which was broadcasted by the edge node E, it then verifies the device IP addresses and data format of the transaction. After the completion of the verification process, the other edge nodes update the information through the high-priority access-based smart contract. The HPASC Algorithm 1 is illustrated below.

The prioritization of the attributes is realized by implementing the HPASC scheme over the edge servers without the intervention of untrusted third parties. Every HPASC includes the following activities.

(i) The HPASC scheme inquires the attribute information from the edge nodes and obtains the priority value of each attribute that are about to pass through the information of the prioritized attributes.

(ii) According to Algorithm 1, the priority information submitted by edge nodes is formulated by using the HPASC scheme. Henceforth, the HPASC scheme forecasts the prioritized information to the corresponding edge nodes. Once the edge nodes receive the information, it updates in its blocks for further processing.

In HPASC, the incoming attributes are trained using the improved K-means algorithm for classifying the attributes with its priority labels. IKM is used to detect each weight as discussed in Section 1.1. If the incoming attribute contains the prioritized attribute, the HPASC scheme gets triggered. According to Algorithm 1, the HPASC scheme sends the high-priority attributes to the edge nodes. After the edge nodes pass the information finely, the edge nodes upload the information to the block, and storing the remaining information in the local storage buffer.

The rise of blockchain technologies starts increasing in growing numbers but still, the scalability challenges the network's performance. The block size for storing the data is limited to 1 MB [24]. In recent scenarios, the reduced block size has become the biggest bottleneck. Nowadays, blockchain is facing raise in waiting time per transaction due to the limited block size and generation of forks for every

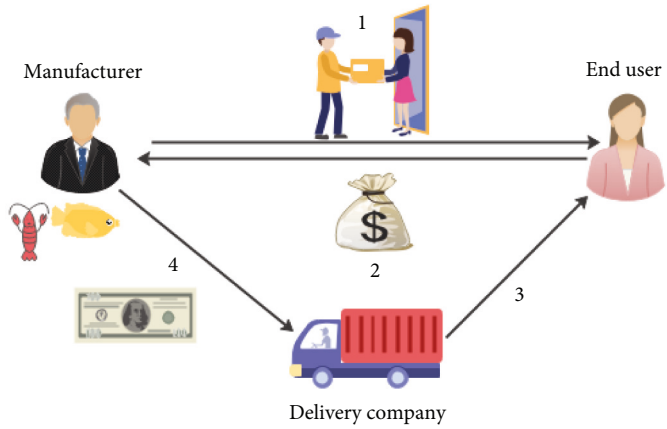

Figure 8: Smart contract in supply chain management.

Input: Attribute Information and Device ID
Output: High Prioritized Information in the blocks
Information_for_Sharing//Every edge node uploads the information to be stored in blockchain
Prioritized_attribute_dataset//data set having prioritized information
Edge_storagebuffer//data set having information for future analysis
Information_for_localstorage //Every edge node stores the information in local storage
P//Whether the attribute labelled with priority = 'high'
if **P** then
Prioritized_attributedataset.add (Information_for_sharing) //Upload theimportant information to the blockchain
else
Edge_storagebuffer.add (Information_for_local storage) //Stores the information in local storage buffer
endif
return Information_for_Sharing

Algorithm 1: High-priority based access based smart contract.

transaction. As a result, the time taken for block generation also increases exponentially with poor throughput.

Furthermore, the transaction constitutes transaction cost which becomes a great burden for micro-industries. Finally, the proliferation of blocks leads to high memory consumption. More generally, the scalability problems are classified into two main categories.

(i) Storage space
(ii) Waiting time

The major objective of performance evaluation is to validate how the proposed scheme provides scalability to the SCM blockchain users. Three existing schemes, such as Chain Partitioning [24], DAG scheme [21], and Horizontal Scalability mechanism [22], are taken into consideration and compared with the proposed HPASC scheme.

Consumed stores essentially refer to the use of consumables. Sports equipment, for instance, is consumable at a club. Magazines are a consumable in a library. The act of storing goods in warehouses and logistical facilities is known as storage. Its function is to keep the market supplied with products on a consistent basis to bridge the temporal gap between producers and consumers. From the implementation results, the comparison is made between the number of transactions and the scalability parameters, which is illustrated in Figures 9 and 10. First, a comparison is made between the number of transactions and block size to analyze the storage efficiency. Initially, we start investigating the effect of the Ethereum platform on applying the existing scalability solutions and HPASC.

For analysis, we gradually increase the transaction from 16 to 2048 transactions and analyze the impact on the count of successful transactions over the entire run of 90 transactions. The storage space occupied by every transaction is being recorded and tabulated in Table 5. The proposed scheme reports reduced storage consumption when compared to the existing mechanisms.

It is observed in Figure 9 that the consumption of storage by the blocks eventually is less in HPASC when compared to different transactions [20–22].

Furthermore, the average waiting time for every transaction is being recorded and tabulated in Table 6. In Ethereum Blockchain platforms, every transaction has to be verified before it is mined. Hence the increase in network

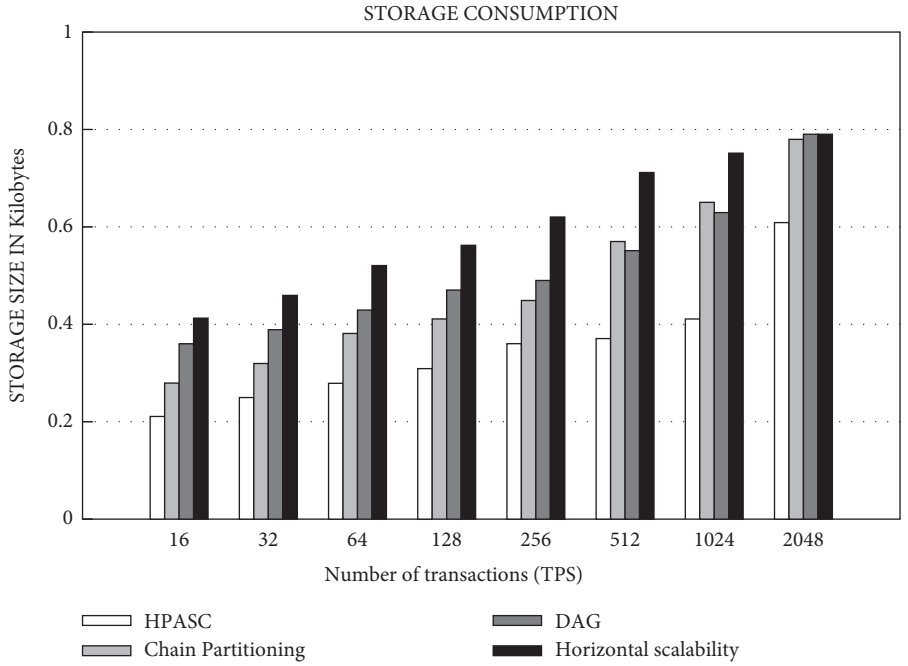

Figure 9: Storage consumption graph.

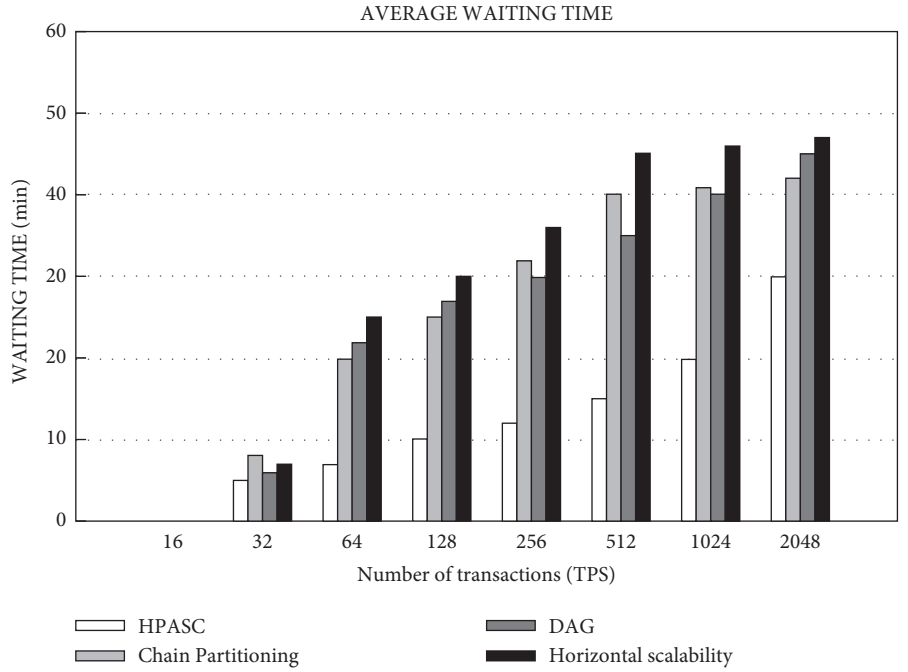

Figure 10: Average waiting time graph.

size may lead to an increase in verification time. Furthermore, it results in the elevation of waiting time due to the increase in queue size in the blocks.

From Figure 10, the average waiting time for handling the transactions found to be less in the HPASC scheme when compared to the other existing scalability solutions. Average Waiting Time is often known as A.W.T. The average amount of time a call spends in the queue before an agent responds is known as the Average Speed of Answer (ASA). Since this is the typical wait time that callers encounter, it is also referred to as the "Average Delay". The measure is accessible per ring group, per number, and for the global account. Hence, the proposed scheme effectively overcomes the scalability challenges by

Table 5: Storage size for every transaction.

Transactions (block size)	Storage space in KB			
	HPASC	CPM	DAG	HSM
16	0.21	0.28	0.36	0.41
32	0.25	0.32	0.39	0.46
64	0.28	0.38	0.43	0.52
128	0.31	0.41	0.47	0.56
256	0.36	0.45	0.49	0.62
512	0.37	0.57	0.55	0.71
1024	0.41	0.65	0.63	0.75
2048	0.61	0.78	0.79	0.79

Table 6: Waiting time for 2048 transactions.

Transactions (block size)	Average waiting time in mins			
	HPASC	CPM	DAG	HSM
16	0	0	0	0
32	5	8	6	7
64	7	20	22	25
128	10	25	27	30
256	12	32	30	36
512	15	40	35	45
1024	20	50	40	46
2048	30	55	45	47

Table 7: Simulation parameters.

Max transactions per block	10
Maximum block generation time	30 s
Consensus algorithm execution time	200 ms
Transaction generation rates	[10, 40, 100] txs/s
Transaction generation rates changing time	[2500, 4000] s

uploading high -prioritized information to the blocks. Table 7 depicts the simulation parameters.

5. Conclusion

An HPASC scheme is applied to achieve scalability in blockchain-based SCM networks. Experimental results report that the priority classification using intelligent k-means clustering over the supply chain datasets works effectively and feasibly. Later, Ethereum was taken as the underlying blockchain platform to carry out the consensus mechanism over the edge networks. Three existing methods are considered and compared to the proposed HPASC scheme, including Chain Partitioning, DAG scheme, and Horizontal Scalability Mechanism. By accurately identifying the properties in the data set, the proposed method primarily improves the scalability of the edge-based blockchain. Comparison results show that the selected scheme reports good scalability against some existing mechanisms. As further work, the real-time datasets can be used to perform relevant operations to achieve scalability in the supply chain networks.

There are new potential to improve supply chain integrity and operational effectiveness when blockchain technology is combined with IoT. As a result, new issues may arise as a result of the new technology. The immutability of a blockchain, for example, is viewed as a crucial property. Many factors have sparked increased interest in the creation of "mutable" blockchains, but immutability is one of them. As a result, more academic study is required to thoroughly investigate, explain, and forecast various application situations. It is vital to keep in mind that blockchain integration in an IoT setting has a number of restrictions and obstacles. As IoT infrastructure grows in complexity, the blockchain will be at the forefront of handling ever-increasing volumes of data that demand very high scalability. Permissioned blockchains, which are less resource-intensive, may help with privacy and scalability concerns, and the idea of "Blockchain pruning" has been floated as a potential solution. Although these alternatives feed the debate over Blockchain's immutability and the monopolistic attitude of consortium ledgers, which imposes obstacles to entry and inhibits innovation, these alternatives are still a viable option.

Data Availability

The data that support the findings of this study are available on request from the corresponding author.

Conflicts of Interest

The authors declare that they have no conflicts of interest.

References

[1] B. Lester, "Best Supply Chain Blockchain Projects, Rated and Reviewed for 2019," 2019, https://www.remedi.com/blog/best-supply-chain-blockchain-projects-rated-and-reviewed-for-2019.

[2] R. Krishnamoorthi, S. Joshi, H. Z. Almarzouki et al., "A novel diabetes healthcare disease prediction framework using machine learning techniques," *Journal of Healthcare Engineering*, vol. 2022, Article ID 1684017, 10 pages, 2022.

[3] A. Rizwan, P. Priyanga, E. H. Abualsauod, S. N. Zafrullah, S. H. Serbaya, and A. Halifa, "A Machine Learning Approach for the Detection of QRS Complexes in Electrocardiogram (ECG) Using Discrete Wavelet Transform (DWT) Algorithm," *Computational Intelligence and Neuroscience*, vol. 2022, Article ID 9023478, 8 pages, 2022.

[4] N. Alzahrani and N. Bulusu, "Block-supply chain: A new anticounterfeiting supply chain using NFC and blockchain," in *Proceedings of the CRYBLOCK 2018 - 1st Work. Cryptocurrencies Blockchains Distrib. Syst. Part MobiSys*, pp. 30–35, ACM, Munich, Germany, June 2018.

[5] N. Kefalakis, N. Leontiadis, J. Soldatos, K. Gama, and D. Donsez, "Supply chain management and NFC picking demonstrations using the AspireRfid middleware platform," in *Proceedings of the ACM/IFIP/USENIX Middlew. 2008 Conf. Companion*, pp. 66–69, ACM, Leuven, Belgium, December 2008.

[6] O. K. Ha, Y. S. Song, K. Y. Chung, K. D. Lee, and D. Park, "Relation model describing the effects of introducing RFID in the supply chain: Evidence from the food and beverage

industry in South Korea," *Personal and Ubiquitous Computing*, vol. 18, no. 3, pp. 553–561, 2014.

[7] Y. P. Tsang, K. L. Choy, C. H. Wu, G. T. S. Ho, and H. Y. Lam, "Blockchain-driven IoT for food traceability with an integrated consensus mechanism," *IEEE Access*, vol. 7, Article ID 129000, 2019.

[8] M. Q. Saeed, Z. Bilal, and C. D. Walter, "An NFC based consumer-level counterfeit detection framework," in *Proceedings of the 2013 11th Annu. Conf. Privacy, Secur. Trust. PST*, pp. 135–142, IEEE, Tarragona, Spain, July 2013.

[9] F. Tian, "Agri-foodchain traceability system using RFID and Blockchain," in *Proceedings of the 2016 13th International Conference on Service Systems and Service Management (ICSSSM)*, pp. 2161–1904, IEEE, Kunming, June 2016.

[10] Bo Yan and Bo Du, "Research on garment supply chain management system based on RFID," in *Proceedings of the 2009 ISECS International Colloquium on Computing, Communication, Control, and Management*, IEEE, Sanya, China, August 2009.

[11] J. L. Zhao, S. Fan, and J. Yan, "Overview of business innovations and research opportunities in blockchain and introduction to the special issue," *FinancInnov*, vol. 2, p. 28, 2016.

[12] A. Abeyratne and R. P. Monfared, "Blockchain ready manufacturing supply chain using distributed ledger," *International Journal of Renewable Energy Technology*, vol. 5, no. 9, pp. 1–10, 2016.

[13] V. Astarita, V. P. Giofrè, G. Mirabelli, and V. Solina, "A review of blockchain-based systems in transportation," *Information*, vol. 11, no. 1, 2019.

[14] A. Pradana, G. Ong, Y. Jaya, and A. A. Mohammed, "Blockchain traffic offence demerit points smart contracts: proof of work," *International Journal of Advanced Computer Science and Applications*, vol. 9, no. 11, pp. 375–382, 2018.

[15] M. A. Khan and K. Salah, "Iot security: Review, blockchain solutions, and open challenges," *Future Generation Computer Systems*, vol. 82, pp. 395–411, 2018.

[16] Y. Xiao, Y. Jia, C. Liu, X. Cheng, J. Yu, and W. Lv, "Edge computing security: state of the art and challenges," *Proceedings of the IEEE*, vol. 107, no. 8, pp. 1608–1631, 2019.

[17] S. Underwood, "Blockchain beyond bitcoin," *Communications of the ACM*, vol. 59, no. 11, pp. 15–17, 2016.

[18] I. Ahmad, S. H. Serbaya, A. Rizwan, and M. S. Mehmood, "Spectroscopic analysis for harnessing the quality and potential of gemstones for small and medium-sized enterprises (SMEs)," *Journal of Spectroscopy*, vol. 2021, pp. 1–12, 2021.

[19] H. T. Vo, Z. Wang, D. Karunamoorthy, J. Wagner, E. Abebe, and M. Mohania, "Internet of blockchains: techniques and challenges ahead," in *Proceedings of the IEEE Confs on Internet of Things, Green Computing and Communications, Cyber, Physical and Social Computing, Smart Data, Blockchain, Computer and Information Technology, Congress on Cybermatics*, IEEE, Halifax, NS, Canada, July 2018.

[20] K. Cong, Z. Ren, and J. Pouwelse, "A blockchain consensus protocol with horizontal scalability," in *Proceedings of the IFIP Networking Conference (IFIP Networking) and Workshops*, IFIP, Zurich, Switzerland, May 2018.

[21] M. Du, X. Ma, Z. Zhang, X. Wang, and Q. Chen, "A review on consensus algorithm of blockchain," in *Proceedings of the 2017 IEEE International Conference on Systems, Man, and Cybernetics (SMC)*, pp. 2567–2572, IEEE, Banff, AB, Canada, Oct. 2017.

[22] S. Mondal, K. P. Wijewardena, S. Karuppuswami, N. Kriti, D. Kumar, and P. Chahal, "Blockchain inspired RFID-based information architecture for food supply chain," *IEEE Internet of Things Journal*, vol. 6, no. 3, pp. 5803–5813, 2019.

[23] J. Tu and S. Piramuthu, "On Addressing RFID/NFC-based relay Attacks: An overview," *Decision Support Systems*, vol. 129, no. 2, Article ID 113194, 2019.

[24] Q. Zhou, H. Huang, Z. Zheng, and J. Bian, "Solutions to scalability of blockchain: A survey," *IEEE Access*, vol. 8, Article ID 16440, 2020.

Hindawi
Mathematical Problems in Engineering
Volume 2022, Article ID 1909851, 12 pages
https://doi.org/10.1155/2022/1909851

Research Article

Multi-Criteria Decision-Making Approach for Analyzing Competency Model of Technology Managers

Chunbo Lin,[1] **Hanyuan Liang**,[1] **Taiyu Su**,[1] **and Minyechil Alehegn Tefera**[2]

[1]*Zhanjiang University of Science and Technology, Zhanjiang 524094, China*
[2]*Department of Information Technology, Mizan-Tepi University, Tepi, Ethiopia*

Correspondence should be addressed to Hanyuan Liang; hanyuanliang@zjkju.edu.cn and Minyechil Alehegn Tefera; minyechil.alehegn@mtu.edu.et

Received 24 March 2022; Revised 20 May 2022; Accepted 30 May 2022; Published 15 July 2022

Academic Editor: Amandeep Kaur

The economies of all the countries are growing with the passage of time. In order to promote the businesses in the global markets, technology managers/technical brokers play a key role such as in the optimal allocation of scientific and technological resources. The industrialization of scientific and technological achievements is also possible due to optimal utilization of resources and a balance between exports and imports. The technology managers should be competent enough to bridge the gaps between the resource requirements and the availability of the resources required to run the businesses smoothly. This paper is using multi-criteria methods for analyzing the qualities in the technical managers which can assist the managers to run the businesses in an efficient manner to compete in the global markets. The interviews and questionnaire are used to collect the primary data. The opinion of experts is also considered. Then, SPSS 22.0 statistical analysis software is used to analyze the reliability and validity of the factors considered in the questionnaire. Then by using statistical techniques, a quantifiable competency model of technology managers is constructed. The multi-criteria AHP (analytical hierarchical process) method is used to compare the competency characteristic indexes of each level in pairs and quantitatively describe their importance of the criteria. It also assigns weights to judge the importance of each competency characteristic index. Since the evaluation of technical managers' competency will be affected by various factors as mentioned in the paper, the fuzzy comprehensive evaluation method is also used to transform the evaluation dimension to accurately evaluate the competency of the technical manager which assists to judge the effectiveness of model evaluation. The proposed method provides theoretical and practical basis for the selection, evaluation, and cultivation of technical managers. It provides accuracy in results by 94% by adopting the statistical techniques.

1. Introduction

In order to implement the innovation-driven development strategy, China has revised and promulgated a series of policies and regulations such as the law on the promotion of transformation of scientific and technological achievements for accelerating the pace of technology for the technical managers. The new policies are promoting the development of factor markets and supporting the transformation of economic development models along with the optimization of structures of the organizations. It can be seen that the transformation of scientific and technological achievements is an important breakthrough for any country in the world to improve its comprehensive strength and to achieve leapfrog development [1]. However, science and technology are not directly related to the commercial market, but they are present at every walk of industry globally where every manual effort is getting replaced by the technology these days [2]. In order to equip the business with the global markets, technical advancements in the business are important and this role can be played by the technical managers [3].

In 2016, the term "technical manager" was first put forward in the action plan for promoting the transformation of scientific and technological achievements issued by the general office of the State Council in China. Technical managers refer to practitioners who take the transformation of scientific and technological achievements as their own responsibility and apply professional knowledge and practical experience to promote the commercialization and

industrialization globally [4]. In ancient times, the technical managers were termed as technical brokers. Foreign research on technical managers started earlier, and foreign scholars mainly focus on the management policies and service work of technical managers. For example, the USA passed the "Bayh-Dole Act" in 1980 to establish a technology transformation mechanism and cultivate technology brokers. The "Technology Transfer Commercialization Act" enacted in 2000 provides legal protection for technology brokers to work as service intermediaries [5]. In Japan, companies use R&D (research and development) funds every year to provide a strong financial guarantee for the technical services of the technology brokers [5]. In China, scholars focus their research on the status and role of technical brokers, as well as the quality and training of technical brokers. The researchers believe that technical brokers should have professional ethics, scientific literacy, ability to capture and screen information, and ability to organize and coordinate [6].

A research group led by McClelland explored the reasons for excellent work performance in technical managers to allow technical advancements in industries [7, 8]. McClellan believes that individual job performance depends more on some potential factors which can better predict individual performance in a specific job. He calls the personal characteristic that can distinguish the performance level of a specific job in the organizational environment [9]. Since then, the competency theory has been widely concerned by scholars in psychology, management, and other disciplines [10]. In [11], the author has constructed a general model of competency which includes six competency feature groups such as target and action management, human resource management, guidance to subordinates, attention to others, and knowledge. In [12], the competency of technical managers is based on multiple factors such as motivation, attitude or values, self-image, characteristics, knowledge in a certain field, cognitive or behavioral ability, and other individual characteristics that can distinguish excellent performance from general performance [12]. In [13], the author has paid attention to the public service management competency model of public managers by suggesting a model which includes task competency, entity policy and administrative competency, political competency, and ethical competency [13]. In [14], the author has taken up the lead in research of managers' competency in Chinese enterprises. The data are collected to analyze the behavior of family business executives through interviews and studied the characteristics of corporate executives' competence by building an executive competency model [14]. To sum up, existing research has begun to include the quality of technical managers but has not yet formed a model which can help to evaluate the competency of technical managers. This has motivated us to prepare a model based on multiple criteria for analyzing the competency of technical managers which provides basis for the evaluation of managers for global assignments. In this paper, author builds a model for ascertaining the technical managers' competency on the basis of multiple factors.

1.1. Highlights of the Proposed Study

1.1.1. Study Focus. By analyzing the recruitment advertisements and in-depth interviews of technical managers, the key competency characteristics of technical managers are initially extracted and then SPSS13.0 is used to test the reliability and validity of the questionnaire scale of technical managers' competency. A competency model of technical managers is developed to provide evaluation indicators and basis for experts to evaluate the competency of technical managers.

1.1.2. Estimated Achievements. Multiple factors are considered to analyze the competency of technical managers on the basis of multi-criteria decision-making model. The model is capable for comprehensively describing and extracting the competency characteristics of technical managers. This model is making use of the analytic hierarchy process (AHP) and fuzzy comprehensive evaluation method to evaluate the competency of technical managers. The multi-criteria analysis technique is given preference over the multi-objective optimization in order to reduce the time and space complexity of the proposed model.

The study contributes in developing a model based on multiple criteria for evaluating the competency of technical managers.

2. Construction of Competency Analytical Model

2.1. Questionnaire Design. The authors have pointed out that the technology managers require a competency model [15]. First, a questionnaire survey has been designed. In order to ensure the reliability and validity of the questionnaire, 21 recruitment advertisements for technical managers are arranged, the key words are screened out, and preliminarily determinants are found out. The content of the questionnaire is combined with the connotation of competency model and with the existing research.

2.1.1. Index Design

(1) Literature Analysis. Collect and study the literature on competency model and technical manager quality research at home and abroad, consult the competency dictionary, clarify the connotation of general competency and the requirements of technical manager competency, and then determine that the content of the questionnaire will cover five aspects: motivation, characteristics, self-concept characteristics, knowledge, and skills [16, 17].

(2) In-Depth Interview. Five technical managers were interviewed to guide the interviewees to describe the most unsuccessful and successful key events in their work. Then analyze the key factors, refine the key qualities of technical managers, and provide basis for the contents of the questionnaire.

2.1.2. Questionnaire Preparation. The content of the questionnaire consists of the competency characteristics of technical managers, their explanations, and options. After comparison, selection, and combination, 35 high-frequency competency items were selected and the competency items were arranged in the questionnaire for given corresponding explanations. Then, Likert five-point scoring was used to design five scores. The scores from "1" to "5" correspond to "unimportant," "less important," "general," and "more important." The five options of "very important," from low to high, require the respondents to judge the importance of each item.

2.2. Investigation Implementation. In December 2020, with the assistance of Guangdong University Scientific and Technological Achievements Transformation Center, a questionnaire survey was conducted among technical managers of universities, scientific research institutes and enterprises, human resources experts, and relevant scholars. In this study, 109 questionnaires were actually filled in and 109 were recovered, with a recovery rate of 100% of which the effective questionnaire was 109 copies, and the effective rate was 100%.

2.3. Data Statistical Analysis

2.3.1. Reliability Analysis. Internal consistency reliability test is the most commonly used reliability analysis method using Cronbach's alpha conduct internal consistency test for each dimension. At the beginning, the author classifies 35 competency items into 7 dimensions as shown in Table 1.

Then, Cronbach's alpha can be calculated by formula (αCoefficientαValue) to illustrate the reliability of the questionnaire data. The calculation formula is as follows:

$$a = \frac{n}{n-1}\left(1 - \frac{\sum_{i=1}^{n} s_t^2}{S_T^2}\right), \quad (1)$$

where n represents the number of all test items, which is the variance of the score of the question "i" and the variance of the total score of all tests.

The data are analyzed with SPSS22.0 statistical software, and the reliability test results of seven dimensions are shown in Tables 2 to 8.

The higher the coefficient is, the higher the reliability of the questionnaire. The coefficient >0.60 is acceptable, the coefficient between 0.70–0.98 has high reliability, and <0.35 has a lower reliability. It can be seen that the reliability of the questionnaire is good and the measurement results are reliable.

In addition, in order to ensure the credibility of the overall scale, the overall scale value is significantly higher than the original value after deleting a question item. Secondly, it should be considered to delete the question item if the overall correlation coefficient between the question item and the scale is low or negative. If both conditions are met, it should be deleted. This study conducts internal consistency test between the competency of each dimension and the total

Table 1: Competency dimensions and characteristic items.

Serial number	Dimension	Competency items
1	Achievement motivation	Enterprise Initiative Sense of adventure Enterprising spirit Dedication
2	Personal traits	Self-confidence and charisma Tenacity Sincerity Flexibility
3	Self-concept	Conscientiousness Service consciousness Emotion control time management Professional ethics
4	Decision-making ability	Market insight Ability to deal with emergency innovation ability Planning ability Strategic thinking
5	Public relation ability	Social ability Information capture and screening capabilities Networking Negotiation ability
6	Organization and communication skills	Team work ability organization skills Expressive ability Coordination ability Horizontal knowledge
7	Knowledge learning and application ability	Subject knowledge Technical manager expertise Continuous learning Research ability Demonstration and evaluation capability Document writing ability

Table 2: Reliability test results of seven dimensions.

Serial number	Dimensions	α coefficient	N of items
1	Achievement motivation dimension	0.656	5
2	Personal trait reliability	0.730	5
3	Self-concept dimension	0.693	5
4	Decision-making ability dimension	0.854	5
5	Public relation ability dimension	0.840	4
6	Organization and communication ability dimension	0.814	4
7	Knowledge learning and application ability dimensions	0.803	7

Table 3: Reliability test results of competency items of achievement motivation dimension.

Competency items	Scale average after deleting items	Scale variance after deleting items	Correlation between corrected items and total scores	Value α after item deletion
Enterprise	12.230	14.481	0.479	0.573
Initiative	12.218	13.312	0.562	0.529
Sense of adventure	12.126	19.391	−0.011	0.776
Enterprising spirit	12.092	13.410	0.496	0.560
Dedication	12.115	13.173	0.606	0.509

Table 4: Reliability test results of competency items of personal trait dimension.

Competency items	Scale average after deleting items	Scale variance after deleting items	Correlation between corrected items and total scores	Value α after item deletion
Self-confidence	12.138	16.237	0.556	0.657
Charisma	12.287	21.812	0.066	0.824
Tenacity	12.264	15.848	0.556	0.656
Sincerity	12.023	14.930	0.684	0.603
Flexibility	12.207	15.050	0.654	0.615

Table 5: Reliability test results of competency items of self-concept dimension.

Competency items	Scale average after deleting items	Scale variance after deleting items	Correlation between corrected items and total scores	Value after item deletion
Conscientiousness	11.747	14.773	0.516	0.613
Service consciousness	11.805	13.229	0.685	0.531
Emotion control	11.736	20.522	0.019	0.801
Time management	11.598	14.941	0.546	0.602
Professional ethics	11.782	14.638	0.550	0.598

Table 6: Reliability test results of competency items of decision-making ability dimension.

Competency items	Scale average after deleting items	Scale variance after deleting items	Correlation between corrected items and total scores	Value after item deletion
Market insight	11.782	21.266	0.669	0.825
Ability to deal with emergencies	11.483	24.253	0.589	0.844
Innovation ability	11.897	21.605	0.687	0.819
Planning ability	11.667	21.202	0.678	0.822
Strategic thinking	11.563	22.156	0.728	0.810

Table 7: Reliability test results of competency items of public relation competency dimension.

Competency items	Scale average after deleting items	Scale variance after deleting items	Correlation between corrected items and total scores	Value after item deletion
Social ability	9.011	12.732	0.695	0.787
Information capture and screening capabilities	8.920	12.889	0.648	0.808
Networking	8.943	13.939	0.642	0.81
Negotiation ability	9.126	12.368	0.708	0.781

Table 8: Reliability test results of competency items in the dimension of organization and communication ability.

Competency items	Scale average after deleting items	Scale variance after deleting items	Correlation between corrected items and total scores	Value after item deletion
Team work ability	8.874	13.53	0.687	0.740
Organization skills	8.851	14.477	0.601	0.781
Expressive ability	8.885	13.498	0.65	0.757
Coordination ability	8.736	14.15	0.594	0.784

Table 9: Reliability test results of competency items of knowledge learning and application ability dimension.

Competency items	Scale average after deleting items	Scale variance after deleting items	Correlation between corrected items and total scores	Value after item deletion
Horizontal knowledge	18.483	33.927	0.697	0.747
Subject knowledge	18.368	33.282	0.727	0.741
Technical manager expertise	18.379	35.029	0.639	0.758
Continuous learning	18.287	34.533	0.642	0.757
Research ability	18.425	34.271	0.623	0.760
Demonstration and evaluation capability	18.322	34.825	0.628	0.760
Document writing ability	18.356	47.837	−0.107	0.877

table of this dimension. The test results are shown in Tables 3 to 9.

Value α of achievement motivation dimension is 0.656. After deleting the "risk awareness" indicator, the α value after deleting the item is 0.776 which is significantly improved and greater than the threshold value of 0.7. Therefore, this indicator is deleted. Table 4 shows reliability test results of competency items of personal trait dimension.

Value α of the personal trait dimension is 0.730. After deleting the "charisma" indicator, the value of the deleted item is 0.824 which is significantly improved and greater than the threshold value of 0.7. Therefore, this indicator is deleted. Table 5 shows reliability test results of competency items of self-concept dimension.

The value of self-concept dimension is 0.693. After deleting the "emotion control" indicator, the value after deleting the item is 0.801 which is significantly improved and greater than the threshold value of 0.7. Therefore, this indicator is also deleted. Table 6 shows reliability test results of competency items of decision-making ability dimension.

When the value of decision-making ability is 0.854, no significant increase is found in the deleted value. Therefore, all indicators are retained. Table 7 shows reliability test results of competency items of public relation competency dimension.

The value of the public relation capability dimension is 0.840, and no significant increase is found in the deleted value. Therefore, all indicators are retained. Table 8 shows reliability test results of competency items in the dimension of organization and communication ability.

The value of the organization and communication ability dimension is 0.814. After the item is deleted, no significant increase is found. Therefore, all indicators are retained. Table 9 shows reliability test results of competency items of knowledge learning and application ability dimension.

Table 10: KMO and Bartlett's spherical test results.

KMO sampling suitability quantity		0.859
Bartlett sphericity test	Chi-square value	1557.971
	Freedom	465
	Significance	000

The value of knowledge learning and application ability dimension is 0.803. After deleting the "official document writing ability" indicator, the value after deleting the item is 0.877 which is significantly improved and greater than the threshold value of 0.7. Therefore, this indicator is deleted.

2.3.2. Validity Analysis. Structural validity test is used to measure the degree of isomorphism between the actual evaluation results and the assumed evaluation characteristics [16]. Structural validity is generally determined through factor analysis; that is, the statistical method of extracting common factors from the variable group and dividing the variables with high correlation which is closely related to the same category [17, 18]. Each category of variables actually represents an essential factor, so that the original observation can be separated. The variables are expressed as a linear combination of new factors to present the basic structure of the scale [19, 20]. The analysis steps are as follows:

(1) Correlation Test. The validity of the questionnaire can be judged by the correlation between the KMO value and the Bartlett test. The test results are shown in Table 10.

KMO value is used to test the partial correlation between variables, and the value range is 0~1. When KMO value is

Table 11: Factor characteristic and variance interpretation rate.

Factor	Factor load before rotation			Factor load after rotation		
	Characteristic root	Variance solution release rate%	Cumulative variance interpretation rate%	Characteristic root	Variance solution release rate%	Cumulative variance interpretation rate%
1	12.186	39.308	39.308	3.412	11.005	11.005
2	1.967	6.346	45.654	3.383	10.912	21.917
3	1.753	5.655	51.309	3.049	9.836	31.753
4	1.531	4.939	56.249	2.975	9.597	41.351
5	1.307	4.216	60.464	2.860	9.226	50.577
6	1.228	3.961	64.425	2.764	8.915	59.492
7	1.089	3.513	67.938	2.618	8.446	67.938

Table 12: Project structure of essential factors of competency.

Competency items	Factor load						
	1	2	3	4	5	6	7
Enterprise							0.716
Initiative							0.655
Enterprising spirit							0.546
Dedication							0.618
Self-confidence							
Tenacity			0.694				
Sincerity			0.62				
Flexibility			0.718				
Conscientiousness			0.602				
Service consciousness							
Time management					0.713		
Professional ethics					0.761		
Market insight					0.591		
Ability to deal with emergencies		0.677			0.595		
Innovation ability		0.699					
Planning ability		0.636					
Strategic thinking		0.674					
Social ability		0.783		0.704			
Information capture and screening capabilities				0.623			
Networking				0.807			
Negotiation ability				0.711			
Team work ability							
Organization skills							
Expressive ability						0.680	
Coordination ability						0.547	
Horizontal knowledge						0.672	
Subject knowledge	0.651					0.727	
Technical manager	0.529						
Professional knowledge	0.568						
Continuous learning	0.648						
Research ability	0.778						
Demonstration and evaluation capability	0.648						

less than 0.5, it indicates that the observed variables are not suitable for factor analysis. When KMO value is closer to 1, it indicates that the correlation of each variable indicates that the reliability and validity are good and suitable for factor analysis. The results of KMO and Bartlett's test of sphericity show that the KMO value is 0.859, which is a high score. While the significance value of Bartlett's test of sphericity is 0.000, it indicates that there is a difference between the original variables. The data in the questionnaire are valid, and both methods as discussed above prove that factor analysis is suitable for the study.

(2) Principal Component Analysis (*PCA*). PCA is the most commonly used analysis method in factor analysis [2]. PCA is used to extract common factors with characteristic roots greater than 1. Then, in order to make the results easy to explain, the factor load matrix is rotated orthogonally with the maximum variance, and seven factors are extracted. The cumulative variance interpretation rate is 67.938%. Therefore, the structural validity of the questionnaire is good as shown in Table 11.

The essential factor structure of competency is shown in Table 12.

Table 13: Competency components of technical managers.

Competency dimension	Competency
Motivation	Dedication, initiative, enterprising spirit, and dedication
Personal traits	Confidence, tenacity, integrity, and flexibility
Self-concept	Sense of responsibility, sense of service, time management, and professional ethics
Decision-making ability	Market insight, ability to deal with emergencies, innovation ability, planning ability, and strategic thinking
Public relation ability	Social skills, information capture and screening skills, networking, and negotiation skills
Organizational and communication skills	Team work ability, organization ability, expression ability, and coordination ability

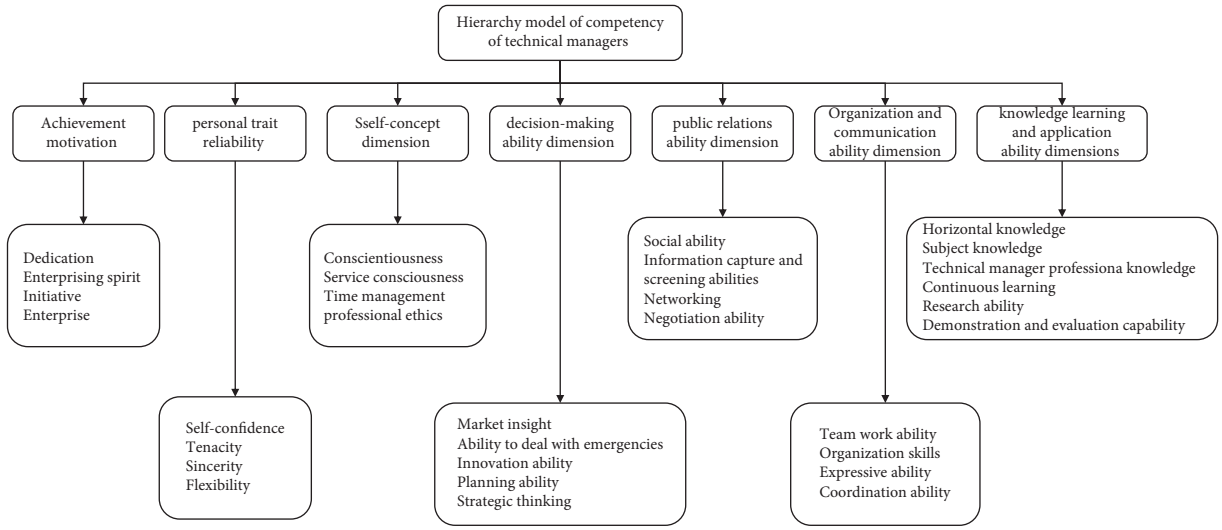

Figure 1: Hierarchy structure of competency of technical managers using AHP.

(3) Construction of Competency Model for Technical Managers. Through the above analysis, the technical manager competency model is finally obtained which includes 7 dimensions and 31 competency characteristics as shown in Table 13.

3. Application of Competency Model of Technical Managers

The first is to evaluate the model and then to determine the differences in competency requirements to solve the problem of unreasonable personal competency structure. Then use the model to evaluate the competency of a technical manager and show the practical application of the model [3].

3.1. Construction of Evaluation Index System. According to the results of the previous research, the seven dimensions of the technical manager competency model are taken as the primary indicators and the competency items of each dimension are taken as the secondary indicators to form the evaluation index system of the technical manager competency model.

3.2. Steps of Implementation Evaluation

3.2.1. Analytic Hierarchy Process (AHP). AHP combines qualitative analysis such as the experience judgment of experts and scholars with mathematical methods of quantitative calculation which not only highlights the advantages of stratification but also has both logic and rationality [3–6]. The main steps are as follows:

(1) Establish Hierarchical Model. Construct the hierarchical structure model of technical manager competency according to the evaluation index system as shown in Figure 1.

(2) Construct the Importance Judgment Matrix of Pairwise Comparison. The judgment matrix indicates starting from the second layer of the hierarchical structure model for the factors of the same layer subordinate to each factor of the upper layer. The paired comparison matrix is constructed by the paired comparison method and 1~9 scale method to the lowest layer. The structural form of the judgment matrix is shown in Table 14.

B_{ij} represents the quantitative judgment of the relative importance of B to B. Generally, the value of b_{ij} can take 1, 2,. . .,9 and their reciprocal as shown in Table 15.

Table 14: Structure of judgment matrix.

B	B	B	...	B
B	b	b	...	b
B	B	b	...	b
...	...	...	...	...
B	b	b		b

Table 15: Meaning of scale 1~9.

Importance level	B assignment
B is as important as B	1
B is slightly more important than B	3
B is more important than B	5
B is obviously more important than B	7
B is absolutely more important than B	9
B is more important than B between the above two levels	2,4,6,8
The importance of B over B is the reciprocal of the importance of B and B	1,1/2,. . .,1/9

(3) Consistency Test. The consistency index, random consistency index, and consistency ratio are used for consistency test. The calculation formula of consistency index is given in the following formula:

$$CI = \frac{(\lambda \max - n)}{(n-1)}, \tag{2}$$

where CI is the maximum eigenvalue of the judgment matrix.

For the average random consistency index, for the judgment matrix of order 1~12, the values are shown in Table 16.

By comparing the importance of seven dimensions, the first judgment matrix is constructed as shown in Table 17. The maximum eigenvalue and eigenvector values are calculated by using the numerical calculation software MATLAB. Table 17 shows judgment matrix of primary indicators.

The specific calculation steps are as follows:

(1) Steps for calculating eigenvalue and index weight:

$$\widetilde{w}_{ij} = \frac{b_{ij}}{\sum_{i=1}^{n} b_{ij}}, \tag{3}$$

$$\overrightarrow{B}\overrightarrow{w_{ij}} = \sum_{j=1}^{n} \widetilde{w}_{ij}, \tag{4}$$

$$\widetilde{w} = \left(\widetilde{w_1}, \widetilde{w_2}, \ldots, \widetilde{w_n}\right)^T. \tag{5}$$

$$W = [0.0810.0650.1280.1790.1900.1830.175]. \tag{6}$$

Step 1: Normalize each column vector of judgment matrix B as given below:

$\widetilde{w}_{ij}$ indicates the index weight.

Step 2: Add the normalized vectors of each row as shown in

Step 3: Normalize the vector to obtain the weight as shown in

By calculating weight matrices, W is calculated as shown in equation (6): eigenvalue : $\lambda_{\max} = 7.739$

(2) Calculate consistency index CI as shown in

$$\begin{aligned} CI &= \frac{\lambda_{\max} - n}{n-1} \\ &= \frac{7.739 - 7}{7-1} \\ &= 0.123. \end{aligned} \tag{7}$$

(3) Calculate consistency ratio as shown in equation (8):

Since n is 7, according to the above table, RI = 1.32,

$$\begin{aligned} CR &= \frac{CI}{RI} \\ &= \frac{0.123}{1.32} \\ &= 0.093. \end{aligned} \tag{8}$$

Similarly, the consistency test method of the secondary indicator judgment matrix of other dimensions is the same as that of the primary indicator, and the test results are as follows.

The weight of four secondary indicators of achievement motivation dimension = (0.338, 0.270, 0.237, 0.154), = 4.215, = 0.072, = 0.90, = 0.080 < 0.1.

The weight of four secondary indicators of personal trait dimension = (0.231, 0.148, 0.426, 0.195), = 4.046, = 0.015, = 0.90, = 0.017 < 0.1.

The weight of four secondary indicators of self-concept dimension = (0.283, 0.183, 0.163, 0.371), = 4.118, = 0.039, = 0.90, = 0.044 < 0.1.

The weight of five secondary indicators in the dimension of decision-making ability = (0.343, 0.122, 0.169, 0.124, 0.242), = 5.325, = 0.081, = 1.12, = 0.073 < 0.1.

The weights of four secondary indicators of public relation capability dimension = (0.146, 0.277, 0.373, 0.205), = 4.207, = 0.069, = 0.90, = 0.077 < 0.1.

The weight of four secondary indicators of the dimension of organizational communication ability = (0.239, 0.395, 0.198, 0.168), = 4.061, = 0.020, = 0.90, = 0.022 < 0.1.

The weights of six secondary indicators of knowledge learning and application dimension = (0.209, 0.110, 0.254, 0.196, 0.081, 0.149), = 7.739, = 0.123, = 1.24, = 0.093 < 0.1.

3.2.2. Fuzzy Comprehensive Evaluation Method. Select a technical manager a as the object of expert evaluation, and then use the fuzzy comprehensive evaluation method to evaluate his competency. The specific steps are as follows:

Table 16: Average random consistency index.

dimension	1	2	3	4	5	6	7	8	9	10	11	12
RI	0.00	0.00	0.58	0.90	1.12	1.24	1.32	1.41	1.45	1.49	1.51	1.53

Table 17: Judgment matrix of primary indicators.

B	B	B	B	B	B	B	B	Weight
Achievement motivation B	1	1	1/2	1/3	1	1/2	1/2	0.081
Personal characteristics B	1	1	1/3	1/3	1/2	1/2	1/2	0.065
Self-concept B	2	3	1	1	1/3	1	1/2	0.128
Decision-making ability B	3	3	3	1	1	1/3	2	0.179
Public relation capability B	1	2	3	1	1	2	1	0.190
Organizational and communication skills B	3	3	1	1/2	1/2	1	1/2	0.183
Knowledge learning and application ability B	2	2	2	1/2	1	2	1	0.175

Table 18: Evaluation of "achievement motivation" dimension of technical manager A.

Primary index	Secondary index	Evaluation grade				
		Excellent	Good	Commonly	Poor	Very bad
Achievement motivation	Enterprise	12	4	4	0	0
	Initiative	13	4	2	1	0
	Enterprising spirit	9	4	5	1	1
	Dedication	12	5	3	0	0

(1) Determining the fuzzy comprehensive evaluation factor (FCEF) set of technical manager competency == {achievement motivation, personal characteristics, self-concept, decision-making ability, public relation ability, organizational communication ability, knowledge learning and application ability} == {dedication, initiative, enterprising spirit and dedication} == {confidence, tenacity, integrity, flexibility} == {sense of responsibility, sense of service, time management, professional ethics} == {market insight; ability to deal with emergencies; innovation ability and planning ability; strategic thinking} == {social skills, information capture and screening skills, networking, negotiation skills} == {team work ability, organization ability, expression ability, coordination ability} == {horizontal knowledge, discipline knowledge, professional knowledge of technical managers, continuous learning, research ability, demonstration and evaluation ability}.

(2) Establish a comment set for comprehensive evaluation == {excellent, good, average, poor, very poor}.
V Indicates the evaluation level.

(3) Determine the weight of each evaluation index and construct a single factor fuzzy evaluation matrix.

The weight of each evaluation index has been obtained by using the AHP method. Here, only the single factor fuzzy evaluation matrix needs to be determined. 20 experts are invited to evaluate the secondary indicators of 7 dimensions of the competency of technical manager "A." The evaluation of experts on the "achievement motivation" dimension of technical manager "A" is shown in Table 18.

The distribution of the expert group evaluation on five levels constitutes a single factor evaluation matrix. When evaluating the "dedication" of technical manager a, 12 experts think that a is excellent, 4 think it is good, and 4 think it is average. Therefore, the fuzzy evaluation vector of the index of "dedication" = (0.6, 0.2, 0.2, 0, 0, 0). Using the same evaluation method, the fuzzy evaluation vectors of initiative, enterprising spirit, and dedication are obtained as follows: = (0.65, 0.2, 0.1, 0.05, 0) = (0.6, 0.25, 0.15, 0, 0) = (0.55, 0.25, 0.15, 0.05, 0).

The single factor fuzzy evaluation matrix of "achievement motivation" of technical manager "A" is as follows as shown in Matrix (9):

Achievement motivation:

$$= \begin{bmatrix} 0.6 & 0.2 & 0.2 & 0 & 0 \\ 0.65 & 0.2 & 0.1 & 0.05 & 0 \\ 0.6 & 0.25 & 0.15 & 0 & 0 \\ 0.55 & 0.25 & 0.15 & 0.05 & 0 \end{bmatrix}. \quad (9)$$

Similarly, it can be concluded that personal characteristics can be obtained by

$$= \begin{bmatrix} 0.5 & 0.3 & 0.1 & 0.1 & 0 \\ 0.4 & 0.3 & 0.2 & 0.05 & 0.05 \\ 0.5 & 0.3 & 0.15 & 0.05 & 0 \\ 0.4 & 0.2 & 0.15 & 0.15 & 0.1 \end{bmatrix}. \quad (10)$$

Self-concept is given by

$$= \begin{bmatrix} 0.5 & 0.25 & 0.25 & 0 & 0 \\ 0.5 & 0.2 & 0.2 & 0.1 & 0 \\ 0.45 & 0.25 & 0.15 & 0.1 & 0.05 \\ 0.55 & 0.25 & 0.2 & 0 & 0 \end{bmatrix}. \quad (11)$$

Decision-making ability is given by

$$= \begin{bmatrix} 0.45 & 0.3 & 0.2 & 0.05 & 0 \\ 0.4 & 0.25 & 0.2 & 0.1 & 0.05 \\ 0.4 & 0.3 & 0.2 & 0.05 & 0.05 \\ 0.45 & 0.25 & 0.25 & 0.05 & 0 \\ 0.35 & 0.2 & 0.25 & 0.1 & 0.1 \end{bmatrix}. \quad (12)$$

Public relation ability is given by

$$= \begin{bmatrix} 0.5 & 0.3 & 0.15 & 0.05 & 0 \\ 0.45 & 0.35 & 0.1 & 0.05 & 0.05 \\ 0.5 & 0.25 & 0.1 & 0.1 & 0.05 \\ 0.4 & 0.3 & 0.2 & 0.1 & 0 \end{bmatrix}. \quad (13)$$

Organizational and communication skills are given by

$$= \begin{bmatrix} 0.55 & 0.2 & 0.2 & 0.05 & 0 \\ 0.45 & 0.2 & 0.15 & 0.15 & 0.05 \\ 0.5 & 0.25 & 0.1 & 0.1 & 0.05 \\ 0.5 & 0.15 & 0.15 & 0.1 & 0.1 \end{bmatrix}. \quad (14)$$

Knowledge learning and application are given by

$$= \begin{bmatrix} 0.5 & 0.35 & 0.1 & 0.05 & 0 \\ 0.5 & 0.25 & 0.2 & 0.05 & 0 \\ 0.6 & 0.3 & 0.1 & 0 & 0 \\ 0.5 & 0.25 & 0.2 & 0.05 & 0 \\ 0.55 & 0.2 & 0.15 & 0.05 & 0.05 \\ 0.5 & 0.2 & 0.15 & 0.1 & 0.05 \end{bmatrix}. \quad (15)$$

(4) Carry Out Fuzzy Comprehensive Evaluation. Since there are many factors involved in the competency evaluation of technical managers, the evaluation results should be reasonable and should be able to comprehensively reflect the information of each single factor. The weighted average fuzzy synthesis algorithm is adopted to carry out the fuzzy comprehensive evaluation.

Table 19: Total evaluation of technical manager "*A*."

Evaluation grade	Excellent	Good	Average	Poor	Very poor
Percentage (%)	48.9	25.5	16.4	0.66	0.26

First-level comprehensive evaluation is given by

$$B_1 = W_1 \cdot U_1 \begin{bmatrix} 0.338 \\ 0.27 \\ 0.237 \\ 0.15 \end{bmatrix}' \cdot \begin{bmatrix} 0.6 & 0.2 & 0.2 & 0 & 0 \\ 0.65 & 0.2 & 0.1 & 0.05 & 0 \\ 0.6 & 0.25 & 0.15 & 0 & 0 \\ 0.55 & 0.25 & 0.15 & 0.05 & 0 \end{bmatrix} \quad (16)$$

$$= [\, 0.605 \;\; 0.219 \;\; 0.153 \;\; 0.021 \;\; 0.000 \,].$$

Similarly, the conclusion is obtained by

$$\begin{aligned} B_2 &= [\, 0.466 \;\; 0.281 \;\; 0.146 \;\; 0.081 \;\; 0.027 \,], \\ B_3 &= [\, 0.510 \;\; 0.241 \;\; 0.206 \;\; 0.035 \;\; 0.008 \,], \\ B_4 &= [\, 0.411 \;\; 0.264 \;\; 0.218 \;\; 0.068 \;\; 0.039 \,], \\ B_5 &= [\, 0.466 \;\; 0.296 \;\; 0.128 \;\; 0.079 \;\; 0.033 \,], \\ B_6 &= [\, 0.492 \;\; 0.202 \;\; 0.152 \;\; 0.108 \;\; 0.046 \,], \\ B_7 &= [\, 0.529 \;\; 0.272 \;\; 0.142 \;\; 0.045 \;\; 0.012 \,]. \end{aligned} \quad (17)$$

The above evaluation vectors form a comprehensive fuzzy evaluation matrix as given by Matrix (18) to obtain the secondary comprehensive evaluation of technical manager *A*:

$$B = W \cdot U$$

$$= \begin{bmatrix} 0.081 \\ 0.065 \\ 0.128 \\ 0.179 \\ 0.190 \\ 0.183 \\ 0.175 \end{bmatrix}' \cdot \begin{bmatrix} B_1 \\ B_2 \\ B_3 \\ B_4 \\ B_5 \\ B_6 \\ B_7 \end{bmatrix} \quad (18)$$

$$= [0.489 \;\; 0.255 \;\; 0.164 \;\; 0.066 \;\; 0.026].$$

(5) Analysis and Processing of Evaluation Results. The evaluation results show that in the evaluation of the comprehensive competence of technical manager "a," 48.9% of the experts think that the comprehensive quality of a is "excellent," 25.5% of the experts think that its comprehensive quality is "good," 16.4% of the experts think that its comprehensive

quality is "average," and 0.66% of the experts think that its comprehensive quality is "poor." The total evaluation of experts on technical manager "A" is shown in Table 19.

The above fuzzy comprehensive evaluation result is still a fuzzy vector, so it is difficult to determine the level of comprehensive evaluation. Therefore, it is necessary to make the vector accurate. Firstly, give corresponding scores [100 80 60 40 20] to the comment set {excellent, good, average, poor, and very poor} of the comprehensive evaluation and then calculate the comprehensive quality evaluation score of technical manager A as shown in

$$K = B \cdot \begin{bmatrix} 100 \\ 80 \\ 60 \\ 40 \\ 20 \end{bmatrix}^{T} = 82.30. \tag{19}$$

The results show that the comprehensive quality evaluation is close to the "good" level.

3.3. Discussion

(1) The competency model of technical managers constructed in this study covers 7 dimensions and 31 secondary competency indicators. At the same time, the judgment results of the importance of competency show that "public relation ability," "decision-making ability," and "organizational communication ability" are the most important competency dimensions of technical managers. The relevant departments can focus on three important dimensions to carry out targeted professional qualification certification and related training.

(2) The application research results of the competency model of technical managers show that the model is suitable for the effective evaluation of the competency of technical managers which will provide effective methods and ideas for the evaluation of the competency and performance of technical managers.

4. Conclusion

With the growing demands of development of the industry globally, the competency evaluation model for technical managers should be designed using multi-objective or multi-criteria decision analysis. The model should be continuously adjusted and improved, the design of indicators should be close to practice rather than theoretical concepts, and the methods of evaluation should be dynamic to adapt the changes with the time. Quality is a dynamic development process such as decision-making ability, public relation ability, organizational communication ability, and knowledge learning, and application ability will continue to improve with the growth of technical managers. Therefore, the evaluation model based on multiple criteria is designed and developed in this paper for evaluating the competency of technical managers. In order to ensure the accuracy and objectivity of the samples, questionnaires are used and the data are collected from Beijing, Shanghai, Chengdu, Nanjing, or developed cities in the eastern, central, and western regions. Then, statistical tests are performed to consider the factors that assist in judging the competency of technical managers. Then, multi-criteria techniques are applied such as AHP and fuzzy evaluation scheme (FCEF) and promising quantitative results are obtained as explained in the result section. In the future, more parameters will be studied and more multi-criteria methods will be applied to judge the competency level of technical managers based on multiple factors.

Data Availability

The data is available on request.

Conflicts of Interest

The authors have none to declare for conflicts of interest with respect to this article.

Acknowledgments

The work is supported by the research on "The policy synergy and its effectiveness of the scientific and technological achievements transformation of Guangdong-Hong Kong-Macao Greater Bay Area" (2021GXJK416) and the non-funded science and technology project of Zhanjiang namely "Reserch on the Coordination of S&T innovation policies of Guangdong-HongKong-Macao Greater Bay Area" (2021B01517).

References

[1] L. Tang and T. Zhang, "Study on the dynamic mechanism of technology transfer institutions in China," in *Proceedings of the 2021 International Conference on Diversified Education and Social Development (DESD 2021)*, pp. 244–247, Guiyang, China, June 2021.

[2] M. Kaur and S Kadam, "Discovery of resources over Cloud using MADM approaches," *International Journal for Engineering Modelling*, vol. 32, pp. 83–92, 2019.

[3] B. Mareschal, M. Kaur, V. Kharat, and S. Sakhare, "Convergence of smart technologies for digital transformation," *Tehnički Glasnik - Technical Journal*, vol. 15, p. 1, 2021.

[4] M. Kaur and S. S. Kadam, "Discovery of resources using MADM approaches for parallel and distributed computing," *Engg Sc. and Tech., an Int. J.*vol. 20, no. 3, pp. 1013–1024, 2017.

[5] M. Kaur, S. Kadam, and N. Hannoon, "Multi-level parallel scheduling of dependent-tasks using graph-partitioning and hybrid approaches over edge-cloud," *Soft Computing*, vol. 26, 2022.

[6] A. Jadhav, M. Kaur, and F. Akter, "Evolution of software development effort and cost estimation techniques: five decades study using automated text mining approach," *Mathematical Problems in Engineering*, vol. 2022, Article ID 5782587, 2022.

[7] M. Kaur, S. R. Sakhare, K. Wanjale, and F. Akter, "Early stroke prediction methods for prevention of strokes," *Behavioural Neurology, Hindawi*, vol. 2022, Article ID 7725597, 2022.

[8] T. Mandicak, P. Mesaros, M. Spisakova, and A. Kanalikova, "The knowledge competencies and digital competencies of project managers in life cycle cost management," in *Proceedings of the 2020 18th International Conference on Emerging eLearning Technologies and Applications (ICETA)*, pp. 438–443, Košice, Slovenia, November 2020.

[9] D. C. McClelland, "Testing for competence rather than for "intelligence"," *American Psychologist*, vol. 28, 1973.

[10] L. Jones and R. Moore, "Appropriating Competence: the competency movement, the New Right and the "culture change" project," *British Journal of Education and work*, vol. 8, no. 2, pp. 78–92, 1995.

[11] Y. Fajar Sitohang, "Competency evaluation of project manager performance in network construction projects," in *Proceedings of the 2020 Fifth International Conference on Informatics and Computing (ICIC)*, pp. 1–8, Gorontalo, Indonesia, November 2020.

[12] R. Dewi, W. Verina, and S. L. Rahayu, "Application of AHP Method Based on Competence for Determining the Best Graduate Students," in *Proceedings of the 2018 6th Int. Confe on Cyber and IT Service Mgmt (CITSM)*, pp. 1–5, Parapat, Indonesia, August 2018.

[13] T. Virtanen, "Changing competences of public managers: tensions in commitment," *Int. J.of Public Sector Mang.*vol. 13, no. 4, pp. 333–341, 2000.

[14] S. Ait Bahom, L. Sefiani, and N. Sefiani, "Identification of quality manager's competencies by the AHP method," in *Proceedings of the 2018 International Colloquium on Logistics and Supply Chain Management (LOGISTIQUA)*, pp. 133–139, Tangier, Morocco, April 2018.

[15] L. L. Luisito and M. P. Gary, "Competency-based mapping tool in personnel management system using analytical hierarchy process," in *Proceedings of the 2021 The 4th Int. Conf. on Machine Lear. and Machine Int.(MLMI'21)*, pp. 57–64, ACM, NY, USA, September 2021.

[16] V. Dulewicz and P. Herbert, "Predicting advancement to senior management from competencies and personality data: a seven-year follow-up study," *British Journal of Management*, vol. 10, no. 1, pp. 13–22, 1999.

[17] K. Zheng, "Analysis and research on professional quality and ability improvement for technology brokers," *Jiangsu Science & Tech. Info.*vol. 11, p. 41, 2019.

[18] L. Alencar and A. Almeida, "Supplier selection based on the PROMETHEE VI multicriteria method," in *Evolutionary Multi-Criterion Optimization. EMO 2011 Lecture Notes in Computer Science*vol. 6576, Berlin, Heidelberg, Springer, 2011.

[19] T. Wang and Y. Chen, "Applying fuzzy PROMETHEE method for evaluating IS outsourcing suppliers," in *Proceedings of the 2008 Fifth International Conference on Fuzzy Systems and Knowledge Discovery*, pp. 361–365, Jinan, China, October 2008.

[20] W.-C. Morais, A. T. de Almeida, L. H. Alencar, T. R. N. Clemente, and C. Z. B. Cavalcanti, "PROMETHEE-ROC model for assessing the readiness of technology for generating energy," *Mathematical Problems in Engineering*, vol. 2015, Article ID 530615, 11 pages, 2015.

Hindawi
Mathematical Problems in Engineering
Volume 2022, Article ID 8996629, 8 pages
https://doi.org/10.1155/2022/8996629

Research Article

Customizable Encryption Algorithms to Manage Data Assets Based on Blockchain Technology in Smart City

Kawther A. Al-Dhlan,[1] Hamad A. Alreshidi,[2] Shahbaz Pervez,[3] Zahida Paraveen,[1] Akram M. Zeki,[4] Nada M. O. Sid Ahmed,[5] Eid J. Alshammari,[6] and Velmurugan Lingamuthu[7]

[1]*College of Computer Science and Engineering, University of Ha'il, Ha'il, Saudi Arabia*
[2]*Instructional Technology Department, College of Education, University of Ha'il, Ha'il, Saudi Arabia*
[3]*ICT, WhiteCliffe Technology & Innovation, Christchurch, New Zealand*
[4]*Information System Department, Kulliyyah of Information and Communication Technology, Selangor, Malaysia*
[5]*Computer Engineering Department, College of Computer Science and Engineering, University of Ha'il, Ha'il, Saudi Arabia*
[6]*Department of Curricula Teaching, College of Education, University of Ha'il, Ha'il, Saudi Arabia*
[7]*Department of Computer Science, School of Informatics and Electrical Engineering, Ambo University, Ethiopia*

Correspondence should be addressed to Velmurugan Lingamuthu; velmurugan.lingamuthu@ambou.edu.et

Received 12 March 2022; Revised 15 June 2022; Accepted 28 June 2022; Published 13 July 2022

Academic Editor: Ardashir Mohammadzadeh

The adoption of blockchain technology can provide data asset management's high security, privacy, and traceability. After a comprehensive investigation of the present blockchain-based data asset management mechanism, it was determined that it is only relevant to a portion of the blockchain system design. To address this issue, a new model of data asset management based on blockchain technology is being developed, which incorporates applications at all levels of the blockchain system. This model implements a network layer node authority control mechanism, a consensus layer consensus mechanism with customizable attributes, improved data query efficiency at the data layer by optimizing the structure and building indexes, intelligent data management, and smart contract layer management. Furthermore, at the transaction layer, sharing information encryption using customizable encryption algorithms is introduced. The experimental results reveal that, when compared to the traditional paradigm, the new blockchain-based data asset management strategy enhances the efficiency of on-chain data queries by 2.33 times.

1. Introduction

Data asset refers to the data resources that are owned or controlled by an enterprise and can bring future benefits to the enterprise and are recorded in a physical or electronic way, such as documents and electronic data [1–3]. Now that we have entered the era of big data, the value of data assets is self-evident in the era of big data, so data asset management methods are particularly important. In 2012, the National Science Foundation and the National Institutes of Health jointly launched the "Developing Big Data Science and Engineering Core Technologies" project, which aims to extract, manage, and analyze useful information from massive data sets. The essence of this useful information is data assets. In 2016, Google relied on its company's unique advantages to collect a large number of users' information and used the data assets extracted from this information to promote the company's revenue growth. China has long realized the practical application value of data assets. At the "World's First Data Asset Evaluation Model Release and Zhongguancun Data Asset Double Innovation Platform Establishment Ceremony" in April 2016, Guizhou Oriental Century Technology Co., Ltd. used data assets for "mortgage" and received the first payment from the Bank of

Guiyang "Data lending". Lending has enabled major companies to fully feel the actual value of data assets. In June 2019, the "Data Asset Management Practice White Paper (Version 4.0)" released at the 2019 Big Data Industry Summit pointed out that although the concept of data as an asset has been fully recognized by the industry, the management and application of data assets is still in the exploratory stage. In response to this situation, the white paper introduces the key activity steps of data asset management, aiming to better guide enterprises [4, 5].

2. Data Asset Management

2.1. Data Asset Concept Traceability. The concept of data assets was first proposed by Richard E. Peters in 1974. Data assets include government bonds, corporate bonds, and physical bonds held by individuals, enterprises, or institutions [6]. At this time, the scope of data assets is still relatively limited. In 2009, the International Data Management Association (DAMA International) [7] pointed out in the "DAMA Data Management Knowledge System Guide" that in the information age, data is considered an essential corporate asset and every company needs to be effective on it. At this time, people have gradually realized the more connotations of the concept of data assets. Then in 2013, the United States Government US Army [8] pointed out that data assets include any entity composed of data as well as services provided by applications to read data; files, databases, documents or web pages output by systems or applications etc.; services that return a single record from the database; and websites that produce specific query data. People, systems, or applications can create data assets. Compared with the past, data assets have a broader definition. Unifying information assets, digital assets, data assets, etc., into data assets, clearly defines data assets as data in cyberspace that has data ownership, which is a valuable, measurable, and readable resource. Data assets have the characteristics of both intangible assets and tangible assets, current assets and long-term assets, and are a new asset class [9]. At present, this concept is generally accepted by the industry [10, 11].

2.2. Data Resource Management. With the advent of the significant data era, data management has received more and more attention. The current data management can be divided into three levels: data management, data resource management, and data asset management. Data is defined as symbols that record and identify objective occurrences, such as physical signs or combinations of these physical indicators that record the type, status, and connection of real objects. The effective and efficient storage, processing, and use of data using computer technology is referred to as data management [12, 13]. Traditional data management focuses on the physical management of data and pays more attention to the stored data structure and the correlation between data. This management level only regards data as the form and carrier of information, and the management of related links between data is only the management of the shallow information embodied by the data. The International Data Management Association defines data management as data resource management. The two concepts are similar, but data resource management focuses more on data application than just the data processing process like data management. Data resource management is carried out based on data management and is mainly used for decision support [14, 15]. Data asset management expands data management and data resource management. Data assets should first be owned and controlled by the enterprise. In addition, not all data are data assets, and only data resources that can bring future economic benefits to the enterprise can be called data assets [16].

Data asset management treats data resources as a particular form of assets and manages them by asset management standards.

Figure 1 shows the relationship between data management, data resource management, and data asset management. Data management only focuses on the storage layer, mainly focusing on data storage and data caching. Data resource management no longer only pays attention to the storage layer because data has been regarded as a resource in data resource management, so the data resource management process is more concerned with the application layer, that is, how to use data resources to help enterprises make decisions and optimize production process. As a result, the connotation of data asset management is richer. Data management has been transformed into asset management. Data is managed as a unique asset. Data can assist enterprises or institutions in internal optimization, and data can be traded to generate income. Therefore, in addition to focusing on the storage and application layers, data asset management should also consider how to manage and share data as a unique asset securely. One of the current methods is to use block chain technology to give data assets the characteristics of safe sharing, tamper resistance, and traceability [17, 18].

2.3. Data Sanitization Process. Not all data resources are data assets. The process of realizing data resources is called data resource capitalization. The specific method of data sanitization is shown in Figure 2. During the production process of an enterprise, product-related data resources will be generated. In the next step, the data resources can be converted into data assets in two ways. The first situation is that the data itself can generate value [19, 20]. For example, medical data can help doctors study the condition of the disease in depth, thereby bringing benefits to the hospital. Trading this type of data resources under the premise of reasonableness and lawfulness is the most direct realization of data resources. The second case is that the data itself does not produce value, but it can empower the current business. For example, each application uses data mining technology to analyze user behavior to understand users' needs in-depth. Data resources are explored to optimize production and operation methods and indirectly increase the income of existing products. This is an indirect way of realizing data resources.

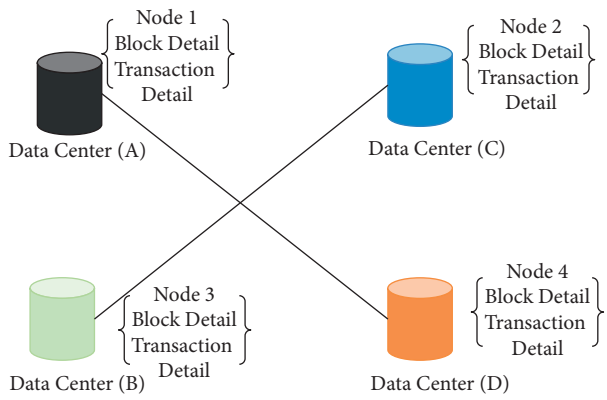

Figure 1: Block chain data management data center.

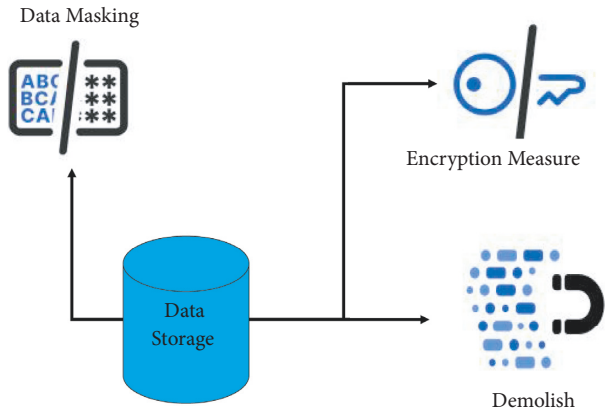

Figure 2: Data sanitization process.

3. Related Work

Blockchain is a new type of database in which multiple nodes that do not trust each other jointly maintain a global state. Blockchain [21–23] and references [24 and 25] has the advantages of data traceability, high data security, and data tamper resistance, which can solve the problem of secure data storage and multiparty noncompliance. Moreover, the issue of data sharing in the context of mutual trust is very applicable to data asset management [26–30].

3.1. Safe Sharing of Data Assets. The current blockchain is mainly used for data security sharing in data asset management. Ahmed et al. [23] proposed a method to confirm the rights of transferred economic data assets based on blockchain technology [31–33]. Allowing the sharing platform to disperse different services in different blocks of the blockchain [34 and 35] and empowering users of the sharing platform to dispose of data effectively, breaks the "data island" and solves the difficulties faced by shared data collection and shared data applications. The orderly and stable development of the sharing economy has provided solutions to many disputes in sharing economy. Aiming at the lack of adequate circulation of e-government data assets and hindering the sharing and efficient use of e-government data, Chen and Xue [24] proposed a series of measures to strengthen the application of blockchain technology in big government data, such as the use of blockchain technology creates big data collection channels for government affairs, combines blockchain technology with government services to protect data security, and uses blockchain technology to promote the progress of China's information system. Combining blockchain technology with big government data can effectively solve the dilemma of independent and uncorrelated data and "data islands" among e-government data and help government service platforms carry out informatization transformation better.

3.2. Tamper-Proofing of Data Assets. There are also many studies on blockchain technology in realizing tamper-proofing of data assets. Due to the particularity of the industry, the human resources and social security departments retain a large number of data assets and critical information involving citizens in the system. This requires that every link in the flow of information cannot be lost. In human resources and social security projects, some third-party system developers or internal staff of the department uses their positions to steal and tamper with information. Shahzad et al. [25] proposed the builder community blockchain system to realize the safe sharing and credible circulation of human and social asset project data. The combination of controllable blockchain technology, secure digital service, digital resource management platform and other elements, credible circulation of social security cards, personnel information, labour contracts, and the safe and barrier-free sharing of human and social information resources is realized. In addition, when ocean data assets are shared across departments, data sharing methods using traditional centralized systems face security risks such as data being easily tampered with and illegal copying and utilization. Ding et al. [26] developed a blockchain-based ocean data sharing platform based on the alliance chain, which realized data sharing between ocean departments and better protected the rights and interests of owners in the cross-departmental use of ocean data. It prevents data from being tampered with and copied in violation of regulations, and at the same time reduces the cost of data transactions caused by the existence of third parties, improves the motivation of various departments to share and open data on the data asset value network, and further forms a healthy development ecological environment [36, 37].

3.3. Traceability of Data Assets. At present, there are also some researches using the traceability characteristics of blockchain to optimize data asset management. For example, Wang et al. [27] designed a blockchain-based food traceability scheme, which uses radio frequency identification (RFID) technology to obtain food-related data and stores the acquired data assets in the blockchain.

3.4. Intelligence of Data Assets. Intelligent management of data assets focuses on the combination of blockchain technology and data asset management in the future. The verification, storage, and synchronization of medical data assets have always been a difficult point. Patients, doctors, and researchers are subject to strict restrictions when accessing and sharing medical data assets. In this process, a lot of resources and time are required for permission review and data verification. Zheng et al. [28] designed a medical data asset management model based on blockchain, using smart contracts to realize safe and reliable automatic sharing and management of medical data assets. In addition, Gao et al. [29] used blockchain smart contracts to implement a crowd sourcing system, which can effectively realize the distribution of task assets and significantly improve work efficiency.

3.5. Privacy Protection of Data Assets. The problem of data asset privacy protection can also be solved using blockchain technology. In response to the crisis of sensitive data such as power data being reproducible and easy to be abused in the traditional centralized data transaction system, Jain et al. [30] designed a method that is limited to sharing between power grid companies, power production companies, and scientific research entities, or a platform for the security, privacy, and mutual trust of power data transactions. The platform uses Hyperledger Fabric, combined with Golang-based microframework Gin, accesses the underlying blockchain services for system development, completes the back-end business logic of the power data association and transaction system, and users can easily register, recharge, and cancel accounts. Zheng et al. [31] used blockchain technology and distributed hash table (DHT) storage methods to build a user data asset authority management system to realize the privacy protection function of data assets.

4. Data Asset Management

The existing data asset management technique applies only to one layer of the blockchain system architecture and does not fully integrate the blockchain system and data asset management. As a result, this paper analyses the aforementioned procedures and suggests blockchain-based data assets. The new model of blockchain-based data asset management employs not only a single or a few levels of the blockchain system, but also the network layer, consensus layer, data layer, and intelligence layer. Furthermore, the contract layer and the application layer are combined and optimized separately. At the network layer and the consensus layer, data security sharing is achieved through node authority classification and a custom consensus mechanism. At the data layer, data query efficiency is improved by optimizing storage structure and query methods (such as establishing effective indexes), and data is guaranteed by logging data on the chain It is traceable and privacy is ensured by using encryption algorithms to encrypt data. At the smart contract layer, part of the data is automatically managed by using intelligent contract program segments. At the application layer, the security of user sensitive information is improved by encrypting transaction information.

The role of the network and consensus layers of the traditional blockchain is to ensure that each node in the blockchain network maintains the consistency of the complete copy through the consensus algorithm. Only when the computing power of the malicious node reaches more than half of the total computing power, it is possible to modify the storage of the data in the blockchain. Hence, the blockchain has the characteristics of data security sharing. In the traditional blockchain, the network layer uses a peer-to-peer (P2P) network. The authority of chain managers in the blockchain network is not the same. The blockchain manager is responsible for managing the entire blockchain and is suitable as a super node with the highest authority. The data asset owner and the data asset being shared only have access rights to the data assets they participate in, and they can control the access rights through information encryption. Therefore, the data asset owner and the shared data asset do not need to enjoy more information at the network layer.

The blockchain network participants belong to the nodes that have not yet taken any action in the blockchain network. Therefore, these three kinds of nodes can be regarded as ordinary nodes participating in the blockchain network. In the new model of blockchain-based data asset management, while setting up the P2P network, the network layer imitates the traditional database to classify the rights of nodes. It sets up two types of nodes: super nodes and ordinary nodes. The super node is controlled by the government and its responsible for managing the blockchain network to ensure the security and lawfulness of data asset sharing. Users who need to share data assets include data asset owners, data assets being transferred, and blockchain network participants. They can join the network as ordinary nodes, and normal nodes are managed by super nodes, and common nodes are equal. In traditional blockchains, public chains generally adopt consensus mechanisms based on proof of work or proof of equity, while private chains or consortium chains generally adopt consensus mechanisms such as practical Byzantine fault tolerance (PBFT). The essence is to ensure that all the consistency of the nodes also avoids damage to the blockchain network by malicious nodes to a certain extent. Although these consensus mechanisms safeguard the consistency of nodes, they largely sacrifice the efficiency of data on-chain and are not suitable for application scenarios of data asset management. Therefore, at the consensus layer in the new model of blockchain-based data asset management, the official can design a custom consensus mechanism in the initial stage of creating a blockchain platform to meet data asset management needs. For example, because the super node is controlled by the blockchain manager and can guarantee the security of its identity, the super node verifies the uploaded data during the data chaining process, and then packages the verified data

into blocks and broadcasts the notification. Every ordinary node, every normal node synchronizes to the local data copy after receiving the message.

In the data layer of the traditional blockchain, a linked list structure is used between the blocks to connect all blocks end to end. The Merkle tree structure is used to store data in the block, so the blockchain has the characteristics of data tamper-proof. In addition, the timestamp field in the data layer can ensure that the stored data is time-sequential, and all historical operations can be restored and traced based on nontamperable data. The data structure of the traditional blockchain is single, and the query method is simple, so the efficiency of data queries on the chain is not high. However, in data asset management scenarios, there are many situations of data interaction, and the efficiency of data queries on the chain is very high. Therefore, in the data layer of the new model of data asset management, blockchain technology is used to ensure that data assets are tamper-proof. Merkle-B tree is used to optimize the existing data structure, and structure such as skip table is used to establish effective query index and to improve the efficiency of data query on the chain. The Merkle tree structure in the block can be modified and combined with other balanced tree structures to improve query efficiency while ensuring that the data is difficult to tamer. In the case of a blockchain chain structure, query indexes such as skip tables can be established on the chain structure to improve query efficiency. In addition, uploading log-type data that is difficult to tamper with can be easily traced to the source of all historical operations, thereby making it easier to define responsibility for unexpected situations in the process of data asset management and circulation. The intelligent contract layer of the traditional blockchain can ensure reliable operations without human involvement. These operations are traceable and irreversible, thus guaranteeing the automation properties of the blockchain. In the new model of data asset management, officials can use intelligent contracts composed of automated script codes to formulate shared transaction rules, conduct identity reviews and data verification through super nodes in the network to ensure the legitimacy of data asset sharing transactions. Users can use smart contracts to automate data asset management through ordinary nodes, and they can also use smart contracts to realize automated data asset sharing with other users. In the traditional blockchain, the intelligent contract deployment method is used as a particular transaction on the chain. Similarly, in the new blockchain-based data asset management model, super nodes can package their released smart contracts into blocks and upload them to the blockchain for deployment. In contrast, the contracts of ordinary nodes need to pass through the super node's only after verification can they be deployed on the chain.

5. Experiment and Result Analysis

The experiment uses Python language to build a blockchain platform for a new model of data asset management. Through multithreading, a super node is generated, and 2, 4, 6, and 8 ordinary nodes are generated, respectively, and the nodes can communicate and interact with each other.

First, this experiment uses a self-defined encryption algorithm to manage data assets. It uses a hybrid encryption method of advanced encryption standards (AES) and RSA to encrypt data assets that interact between nodes. Among them, the AES algorithm has a fast encryption speed, which is responsible for encrypting the main part of the transmitted file and improving the transmission efficiency. The RSA algorithm is responsible for encrypting the AES key and improving transmission security. When data assets are exchanged between nodes, first, the data initiator creates an AES key through the AES algorithm, encrypts the interactive data, and generates an interactive data encryption file. Then, the data receiver uses the RSA algorithm to create an RSA key, an RSA public key and an RSA private key, and broadcasts the RSA public key to the entire network. After the data sender receives the RSA public key, the RSA public key is used to encrypt the AES key. After the encryption is completed, the data sender transmits the interactive encrypted file and the AES key to the receiver. Finally, the data receiver decrypts the AES key and it retains the RSA private key. The interactive data encrypted file is decrypted by the AES key to obtain the original interactive data. In this way, the risk of data leakage in the network is effectively reduced and data transmission efficiency is also improved.

Second, the experiment uses a custom consensus mechanism. The content of the consensus mechanism is that ordinary nodes can upload data to the blockchain network, and the super nodes collect scattered upload data in the blockchain network. After a certain amount of upload data is collected, the information is verified for credibility to ensure the data is true and effective and the data source is safe. After that, the super node will package the verified data to generate blocks and broadcast the block information across the network. After the ordinary nodes collect the blocks, they will copy the blocks to copy the blockchain [38] in the node to complete the data update. The specific experiment is as follows: upload data to the blockchain network within a certain period through 2, 4, 6, and 8 ordinary nodes, and each ordinary node uploads the same amount of data. The normal node upload command is issued as the upload starts, and the generated block is added to the blockchain copy of each normal node as the upload end. The time for uploading the data to the blockchain platform is shown in Figure 3.

It can be concluded from Figure 3 that with the constant increase in the number of nodes, the corresponding increase in data upload time is relatively stable and in line with expectations and the overall linear distribution. This proves that the new model of data asset management based on blockchain technology proposed in this paper is stable. Furthermore, through the data upload time of multiple nodes, it can be found that the data upload time of the new model of data asset management based on blockchain technology is shorter, which proves the high efficiency of this model.

Four nodes are chosen for the data throughput test based on local hardware and testing methods. On the server side,

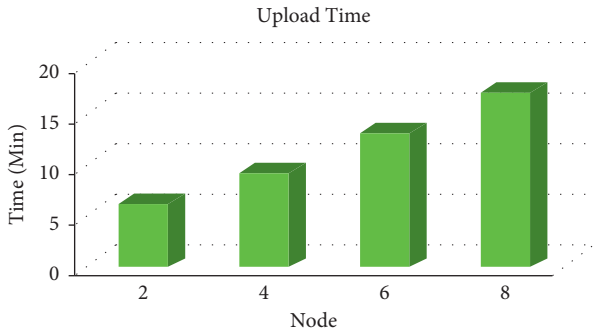

Figure 3: Upload data time on blockchain platform.

four terminals are enabled and four sets of experimental data are picked at random to form Figure 4.

Transaction latency is another important performance parameter. It reflects the period between transaction submission and blockchain writing. In the same network setting, the Merkle-B tree algorithm reduces the consensus process. Figure 5 shows the transaction latency comparison histogram for the Merkle-B tree algorithm, mix, and the skip list technique.

Finally, this paper designs a new optimized query algorithm that uses the Merkle-B tree to optimize the existing data structure. At the same time, it uses the skip table structure to establish an effective query index to improve the efficiency of the data queries on the blockchain.

To evaluate the query performance of the new method, a comparative experiment was designed. The investigation contains four ways: the first method uses the traditional blockchain method to query (origin method). The second method uses the technique of optimizing the existing data structure through the Merkle-B tree for query (Merkle-B tree method). The third method uses the method of a skip table structure for question (skip list method). The fourth method uses the optimized query algorithm of Merkle-B tree and forgettable system proposed in this paper for question (mix method). The data asset information of different capacities is queried separately through these four methods, and the query time is recorded.

The query time result is shown in Table 1 and Figure 6. By comparing the query time of the four methods, it can be found that, compared with the original method, the query speed of the three methods (Merkle-B tree method, skip list method, and mix method) using optimized structures has been improved. Among them, the query efficiency of the mixing method is the highest, the efficiency of the skip list method is the second, and the efficiency of the Merkle-B tree method is the lowest. The reason is that although the Merkle-B tree method optimizes the block data structure, the amount of data inside the block is small, so the speed is only slightly increased, only 17%. The skip list method builds an index between blocks, and the query speed is greatly improved, which is increased by 1.24 times, while the mixing method combines the advantages of the Merkle-B tree method and the skip list method, so the data query speed is the fastest, which is increased by 2.33 times.

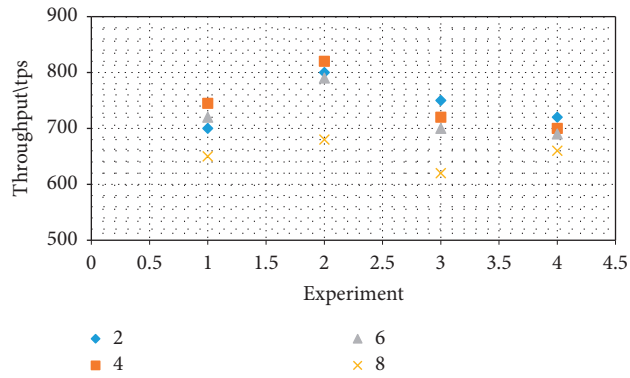

Figure 4: Data throughput over attack.

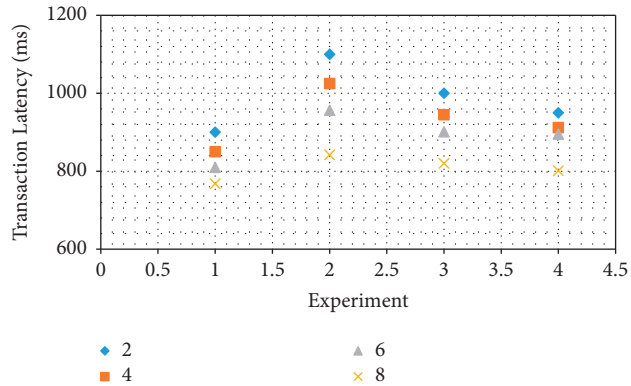

Figure 5: Transaction delay over attack.

Table 1: Data query time of different methods.

Nodes	Origin	Merkle -B Tree	Skip list	Mix
2	2	4	3	5
4	3.9	5.2	3.5	4.5
6	4.9	6.5	5.2	6
8	5.2	7	6	6.3

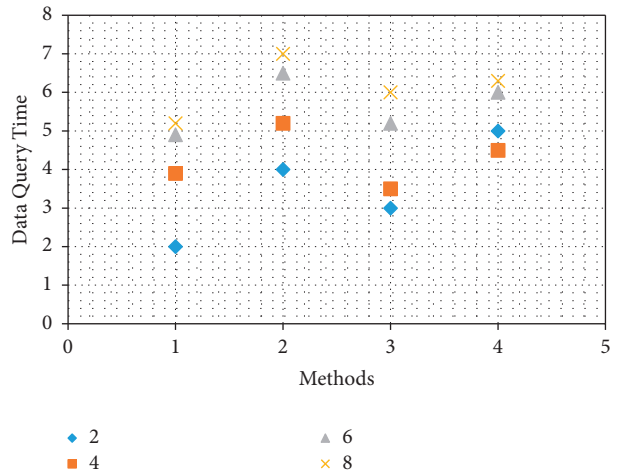

Figure 6: Comparison of data query time of different methods.

6. Conclusion

Data asset management is crucial in today's big data era. Emerging blockchain technology may be applied to data asset management to assure data asset security, privacy, and traceability. Many data asset management systems are based on blockchain technology, but each is tailored to a certain layer of the blockchain system architecture. This article provides a novel model of data asset management based on blockchain, which incorporates applications at all levels of the blockchain system, by summarising and analyzing these mechanisms. It employs them at the network, consensus, data, and smart contract layers. Furthermore, the layer and transaction layers have been optimized.

Data Availability

The data used to support the findings of this study are available from the author upon request (k.aldahlan@uoh.edu.sa).

Conflicts of Interest

The authors declare that they have no conflicts of interest.

Authors' Contributions

Kawther A. Al-Dhlan wrote the paper, Hamad A. Alreshidi simulated the work, Shahbaz Pervez proof read the paper, Zahida Paraveen validated the method, Akram M. Zeki and Nada M. O. Sid Ahmed added the results, and Eid J. Alshammari and Velmurugan Lingamuthu suggested the changes.

Acknowledgments

The authors would like to extend their sincere appreciation to the Deanship of Scientific Research at University of Ha'il for funding of this Research group Number (RG–191308).

References

[1] M. S. Mekala, G. Dhiman, G. Srivastava et al., "A DRL-based service offloading approach using DAG for edge computational orchestration," *IEEE Transactions on Computational Social Systems*, pp. 1–9, 2022, In press.

[2] S. Sharma, S. Gupta, D. Gupta et al., "Deep Learning Model for the Automatic Classification of White Blood Cells," *Computational Intelligence and Neuroscience*, vol. 2022, Article ID 7384131, 2022.

[3] F. Ahmadi Zeidabadi, M. Dehghani, P. Trojovský, Š. Hubálovský, V. Leiva, and G. Dhiman, "Archery algorithm: a novel stochastic optimization algorithm for solving optimization problems," *Computers, Materials & Continua*, vol. 72, no. 1, pp. 399–416, 2022.

[4] S. Swain, B. Bhushan, G. Dhiman, and W. Viriyasitavat, "Appositeness of optimized and reliable machine learning for healthcare: a survey," *Archives of Computational Methods in Engineering: State of the Art Reviews*, vol. 123 pages, 2022.

[5] K. K. Singamaneni, K. Ramana, G. Dhiman, S. Singh, and B. Yoon, "A novel blockchain and Bi-linear polynomial-based QCP-ABE framework for privacy and security over the complex cloud data," *Sensors*, vol. 21, no. 21, p. 7300, 2021.

[6] Z. Fan, X. Li, Y. Li et al., "Design of power grid data asset management system based on directory blockchain," in *Proceedings of the 2020 International Conference on Computer Science and Management Technology (ICCSMT)*, pp. 212–216, Shanghai, China, November 2020.

[7] S. Liang, H. Baozhong, L. Yang et al., "Blockchain-based power grid data asset management architecture," in *Proceedings of the 2020 International Conference on Computer Science and Management Technology (ICCSMT)*, pp. 207–211, Shanghai, China, November 2020.

[8] Z. Zhang, C. Cui, L. Tao et al., "Research on Consistency Tracing Technology of Dispatching Control Model Data Based on Blockchain," in *Proceedings of the 2021 IEEE 5th Advanced Information Technology, Electronic and Automation Control Conference (IAEAC)*, pp. 234–239, Chongqing, China, March 2021.

[9] D. Ding, K. Li, L. Jia, Z. Li, J. Li, and Y. Sun, "Privacy protection for blockchains with account and multi-asset model," *China Communications*, vol. 16, no. 6, pp. 69–79, June 2019.

[10] R. Kumar, V. Joshi, G. Dhiman, and W. Viriyasitavat, "An improved exponential metric space approach for C-mean clustering analysing," *Expert Systems*, Article ID e12896, 2021, In press.

[11] S. P. Singh, G. Dhiman, P. Tiwari, and R. H. Jhaveri, "A soft computing based multi-objective optimization approach for automatic prediction of software cost models," *Applied Soft Computing*, vol. 113, Article ID 107981, 2021.

[12] H. Singh, P. Kaushal, M. Garg, and G. Dhiman, "Deep learning in content-based medical image retrieval," in *Artificial Intelligence, Machine Learning, and Data Science Technologies*, pp. 73–92, CRC Press, Boca Raton, Florida, 2021.

[13] C. H. Pan and G. Dhiman, "Study on automatic tracking method of marking points in sports image sequence," *Recent Advances in Electrical & Electronic Engineering (Formerly Recent Patents on Electrical & Electronic Engineering)*, vol. 14, no. 7, pp. 708–717, 2021.

[14] W. Dai, C. Dai, K.-K. R. Choo, C. Cui, D. Zou, and H. Jin, "SDTE: a secure blockchain-based data trading ecosystem," *IEEE Transactions on Information Forensics and Security*, vol. 15, pp. 725–737, 2020.

[15] B. N. Biswas, S. D. Bhitkar, and S. N. Pundkar, "Secure login: a blockchain based web application for identity access management system," in *Proceedings of the 2021 2nd International Conference for Emerging Technology (INCET)*, pp. 1–5, Belagavi, India, May 2021.

[16] Z. Song, L. Yang, G. LI et al., "An improved data provenance framework integrating blockchain and PROV model," in *Proceedings of the 2020 International Conference on Computer Science and Management Technology (ICCSMT)*, pp. 323–327, Shanghai, China, November 2020.

[17] M. S. Mekala, G. Dhiman, R. Patan et al., "Deep learning-influenced joint vehicle-to-infrastructure and vehicle-to-vehicle communication approach for internet of vehicles," *Expert Systems*, vol. 39, no. 5, Article ID e12815, 2021.

[18] S. R. Das, A. K. Sahoo, G. Dhiman, K. K. Singh, and A. Singh, "Photo voltaic integrated multilevel inverter based hybrid filter using spotted hyena optimizer," *Computers & Electrical Engineering*, vol. 96, Article ID 107510, 2021.

[19] R. Kumar and G. Dhiman, "A comparative study of fuzzy optimization through fuzzy number," *International Journal of Modern Research*, vol. 1, no. 1, pp. 1–14, 2021.

[20] P. K. Vaishnav, S. Sharma, and P. Sharma, "Analytical review analysis for screening COVID-19 disease," *International Journal of Modern Research*, vol. 1, no. 1, pp. 22–29, 2021.

[21] S. Biswas, K. Sharif, F. Li, I. Alam, and S. Mohanty, "DAAC: digital asset access control in a unified blockchain based E-health system," *IEEE Transactions on Big Data*, p. 1, 2020, In press.

[22] J. Grabis, V. Stankovski, and R. Zariņš, "Blockchain enabled distributed storage and sharing of personal data assets," in *Proceedings of the 2020 IEEE 36th International Conference on Data Engineering Workshops (ICDEW)*, pp. 11–17, Dallas, TX, USA, April 2020.

[23] M. Ahmed, S. Reno, N. Akter, and F. Haque, "Securing Medical Forensic System Using Hyperledger Based Private Blockchain," in *Proceedings of the 2020 23rd International Conference on Computer and Information Technology (ICCIT)*, pp. 1–6, DHAKA, Bangladesh, December 2020.

[24] J. Chen and Y. Xue, "Bootstrapping a Blockchain Based Ecosystem for Big Data Exchange," in *Proceedings of the 2017 IEEE International Congress on Big Data (BigData Congress)*, pp. 460–463, Honolulu, HI, USA, June 2017.

[25] A. Shahzad, C. Wenyu, and R. Kumar, "Blockchain based monitoring on trustless supply chain processes," in *Proceedings of the 2021 IEEE 6th International Conference on Cloud Computing and Big Data Analytics (ICCCBDA)*, pp. 216–221, Chengdu, China, April 2021.

[26] Y. Ding, L. Feng, Y. Qin et al., "Blockchain-based access control mechanism of federated data sharing system," in *Proceedings of the 2020 IEEE Intl Conf on Parallel & Distributed Processing with Applications, Big Data & Cloud Computing, Sustainable Computing & Communications, Social Computing & Networking (ISPA/BDCloud/SocialCom/SustainCom)*, pp. 277–284, Exeter, United Kingdom, December 2020.

[27] Z. Wang, L. Yang, Q. Wang, D. Liu, Z. Xu, and S. Liu, "ArtChain: Blockchain-Enabled Platform for Art Marketplace," in *Proceedings of the 2019 IEEE International Conference on Blockchain (Blockchain)*, pp. 447–454, Atlanta, GA, USA, July 2019.

[28] X. Zheng, R. R. Mukkamala, R. Vatrapu, and J. M Ordieres, "Blockchain-based Personal Health Data Sharing System Using Cloud Storage," in *Proceedings of the 2018 IEEE 20th International Conference on e-Health Networking, Applications and Services (Healthcom)*, pp. 1–6, Ostrava, Czech Republic, September 2018.

[29] Z. Gao, H. Li, K. Xiao, and Q. Wang, "Cross-chain oracle based data migration mechanism in heterogeneous blockchains," in *Proceedings of the 2020 IEEE 40th International Conference on Distributed Computing Systems (ICDCS)*, pp. 1263–1268, Singapore, Singapore, November 2020.

[30] A. Jain, A. Kumar Tripathi, N. Chandra, and P. Chinnasamy, "Smart contract enabled online examination system based in blockchain network," in *Proceedings of the 2021 International Conference on Computer Communication and Informatics (ICCCI)*, pp. 1–7, Coimbatore, India, January 2021.

[31] S. Zheng, L. Pan, D. Hu, M. Li, and Y. Fan, "A blockchain-based trading platform for big data," in *Proceedings of the IEEE INFOCOM 2020 - IEEE Conference on Computer Communications Workshops (INFOCOM WKSHPS)*, pp. 991–996, Toronto, ON, Canada, July 2020.

[32] X. Li, X. Wu, X. Pei, and Z. Yao, "Tokenization: Open Asset Protocol on Blockchain," in *Proceedings of the 2019 IEEE 2nd International Conference on Information and Computer Technologies (ICICT)*, pp. 204–209, Kahului HI USA, March 2019.

[33] S. Sharmilan and C. Farook, "Blockchain & machine learning based secure personal medical record storage and sharing platform - DataBlock," in *Proceedings of the 2019 4th International Conference on Information Technology Research (ICITR)*, pp. 1–6, Moratuwa, Sri Lanka, December 2019.

[34] I. Chatterjee, "Artificial intelligence and patentability: review and discussions," *International Journal of Modern Research*, vol. 1, no. 1, pp. 15–21, 2021.

[35] V. K. Gupta, S. K. Shukla, and R. S. Rawat, "Crime tracking system and people's safety in India using machine learning approaches," *International Journal of Modern Research*, vol. 2, no. 1, pp. 1–7, 2022.

[36] T. Sharma, R. Nair, and S. Gomathi, "Breast cancer image classification using transfer learning and convolutional neural network," *International Journal of Modern Research*, vol. 2, no. 1, pp. 8–16, 2022.

[37] S. K. Shukla, V. K. Gupta, K. Joshi, A. Gupta, and M. K. Singh, "Self-aware execution environment model (SAE2) for the performance improvement of multicore systems," *International Journal of Modern Research*, vol. 2, no. 1, pp. 17–27, 2022.

[38] Z. H. A. O. Ming and D. O. N. G. Dazhi, "Study on data asset management mechanism based on blockchain technology," *Big Data Research*, vol. 7, no. 4, Article ID 2021038, 2021.

Hindawi
Mathematical Problems in Engineering
Volume 2022, Article ID 3222601, 6 pages
https://doi.org/10.1155/2022/3222601

Research Article

Industrial Demand and Innovation: An Application of Binomial Regression Model to Project Statistics of NSFC of China

Yan Tu,[1] **Jian Chu**,[2] **and Mohd Asif Shah**[3]

[1]*College of Art, Zhengzhou University of Science and Technology, China*
[2]*School of Arts and Media, Suqian University, Suqian, China*
[3]*Bakhtar University, Kabul, Afghanistan*

Correspondence should be addressed to Jian Chu; mrchujian@hotmail.com and Mohd Asif Shah; ohaasif@bakhtar.edu.af

Received 21 April 2022; Revised 6 June 2022; Accepted 17 June 2022; Published 30 June 2022

Academic Editor: Amandeep Kaur

The carbon emission reduction potential of photothermal utilization of solar energy is outstanding, but the breakthrough of technology is closely related to the management of innovation and research in higher educational institutions. What factors affect such relationship is discussed in this paper. Based on the photothermal technology project data released by the National Natural Science Foundation of China (NSFC) and China education yearbook, this paper analyzes the variable relationship between the output of solar thermal technology innovation and industrial demand. Specifically, the negative binomial regression was constructed based on the technological project approval data. The results show that the input of scientific research resources has a key influence on the development of solar thermal technology, the establishment of technological projects or the subsequent patent application derived from technological projects. The results also show that the demand for photothermal technology and green innovation complement each other.

1. Introduction

With the increasing shortage of global fossil energy supply and increasingly prominent environmental problems, solar energy, as typically clean and renewable energy, has attracted more and more attention [1]. The development and application of solar thermal utilization technology are gradually becoming a hot spot in the energy industry [2]. The main thermal energy of the earth comes from the sun, and the total energy of solar radiation received by the earth's surface every year is about 1018 kWh, which is about ten times the sum of the energy generated by all fossil fuels on the earth. Solar thermal power generation technology generates electricity by gathering solar energy and converting photoelectric energy by physical means, which does little harm to the environment. The CO_2 emission of a solar thermal power plant in the whole life cycle are only 13–19 g/kWh [3]. At the same time, the use of inexhaustible solar energy resources for power generation can effectively save fossil energy and alleviate the energy crisis. Due to its technical characteristics, solar thermal power generation can be equipped with heat storage devices, and fuels like natural gas can be used as an ancillary power generation system [4]. The solar photothermal power generation system with heat storage devices and an ancillary power generation system can solve the problem of unstable unit output caused by the intermittency of light resources, ensure the operational continuity of the power generation system, significantly smooth the output curve, and better match with the load. Compared with photovoltaic power generation, the solar photothermal power generation system can reduce the cost of ancillary services such as the operating reserve and has better grid friendliness [5]. Given these advantages of solar photothermal power generation technology, it is of great significance to promote the rapid development of the solar photothermal power generation industry for the environment, resources, and economy of all countries in the world. At present, the utilization of solar thermal resources is still in the form of photothermal power generation mainly based on the Rankine cycle principle, which makes it difficult to

further improve the cycle efficiency of the solar thermal power plant. At the same time, the power generation system based on this cycle mode will aggravate the pressure of water resources in areas with abundant solar energy resources but relatively short of water supply to a certain extent. Therefore, how to use this rich and pollution-free clean energy efficiently and safely is one of the main directions of current research.

Basic research is the source of the national innovation system and the most critical part to promote applications. The scientific research results of colleges and universities have a promoting effect on the development of the industry. Li et al. [6] pointed out that China's fund in basic research increased from USD 880 million in 2002 to USD 14.57 billion in 2017, with an average annual growth rate of 17.6%, but its investment intensity and proportion in total scientific research expenditure are still lower than those of developed countries. The support for the development of downstream industries is weak, and the scientific research fund the management system still needs to be further improved. This paper intends to discuss the relationship between scientific research and China's industrial demand and green sustainable innovation in the project approval from the perspective of university fund project information. To understand the basic research fund, by applying the binomial regression model, this paper evaluates the efficiency of the National Natural Science Foundation of China in the process of stimulating the basic knowledge innovation of universities (upstream innovation carriers) to promote the transformation of application achievements of enterprises (downstream innovation carriers) and makes a specific description of its transformation channels. As for data, the project data from the National Natural Science Foundation of China from 2018 to 2019, has been used as the research object, taking the number of projects in the photothermal industry as the explained variable, and education and scientific research in various provinces as explanatory variables to explore the impact of various variables.

Compared with the literature, this study provides empirical evidence for the dissemination and transformation of tacit knowledge among innovation entities. For tacit knowledge that is difficult to encode or record, industry-university-research cooperation has always been considered as the most effective channel for its dissemination from upstream to downstream. However, due to data limitations, relevant studies have stopped at qualitative analysis, and few works of literature have carried out quantitative mathematical analysis [7, 8]. The structure of this paper is as follows: the second section is the literature discussion; the third part is the data and empirical results; and finally comes the summary of this paper.

2. Literature Review

In recent years, with the continuous development and innovation of photothermal technology, policy research on promoting the development of photothermal technology has also been accumulating. For example, Zongxian et al. [9] believe that the rapid development of China's solar photothermal industry is mainly attributed to the fact that the price of solar photothermal, a new energy source, is lower than that of traditional energy sources such as electricity and natural gas, which can fully meet the needs of residents. It is further found that the rising price of traditional energy sources, the improvement of residents' living conditions and behavior, large-scale housing construction, and Chinese society's emphasizing on environmental protection will further promote the growth of the solar thermal industry [10, 11]. As for investment costs, like all emerging industries, the investment cost of photothermal technology is relatively high due to the lack of large-scale production in the early stage of development. The photothermal technology of the United States, Spain, and other countries is relatively mature, and the investment cost is lower than that in the early stage of industrial development [12]. References [13, 14] used the system advisor model (SAM) simulation software to estimate the current and future costs of trough power plants and molten salt tower power plants in the U.S. power market. The prediction results show that the levelized cost of energy (LCOE) of the two power generation technologies will be reduced to 11 cents/kWh, which makes the cost of photothermal power generation competitive compared with the benchmark electricity price of California. Li et al. [15] established a comprehensive indicator system of solar thermal power generation technology from five aspects: development conditions, power generation technology, the economics of power generation, grid connection requirements, and policy environment; and comprehensively evaluated the current situation of solar thermal power generation in China. The evaluation results show that solar thermal power generation has certain advantages in terms of grid connection requirements, power generation technology, and development conditions, but not in terms of advantages in the policy environment and the economics of power generation [16]. Given the development environment of China's solar thermal industry, Yu and Schwieter [17] pointed out that the development of China's solar thermal industry is more business-opportunity oriented than government-environment oriented. Similarly, Xu et al. [18] believe that the development of the solar photothermal industry requires a reasonable allocation of corresponding R & D funds and a favorable policy environment. The discussion on fund research in Europe and America started much earlier than in China. The national innovation system theory proposed by Freeman provides a classic analytical framework for people to understand the process of transforming basic research funding into application innovations [19]. The authors point out that government-promoting research funding involves the main entities of the government, universities, scientific research institutions, enterprises, etc. They divide work and cooperate to capitalize knowledge, with knowledge creation, dissemination, and transformation as the mainline. In this process, universities and scientific research institutions are upstream of the knowledge dissemination chain and mainly carry out basic research. Enterprises are located downstream of the knowledge dissemination chain to develop and utilize the research results generated upstream, and finally, transform

them into new products and technologies that meet the market demand [20]. In actual economic activities, due to the externality of knowledge, the scientific research achievements based on research investment will reduce the R & D costs and R & D investment returns of enterprises. Hence, the motivation of independent R & D of enterprises will decline [21]. At the same time, due to the reduction of market access cost and the increase in market competition, the profit margin of the enterprise fund in application R & D is reduced. Therefore, the final impact of basic research funding on enterprise innovation remains to be empirically studied and tested.

The frequent interaction between various main innovation entities in formal and informal ways can promote the dissemination and transformation of knowledge and improve the efficiency of the national innovation system [22]. In terms of the transmission channel of knowledge from upstream to downstream, the existing literature mostly conducts qualitative research, such as case analysis, to provide evidence. Explicit knowledge in the form of words or patents can be transferred to enterprises through learning or transfer [23]. In addition, a large amount of tacit knowledge depends heavily on forms such as the cooperation between schools and enterprises, face-to-face communication, and the flow of scientific researchers to disseminate and transform [24, 25].

Combing the above literature, it can be seen that the discussions on scientific research are more focused on path orientation, qualitative analysis, etc., and there are relatively few discussions on quantification. The relevant research literature on China is even more scarce. Based on this, the statistics of the National Natural Science Foundation of China from 2018 to 2019, are taken as the research object, the number of projects in the photothermal industry as the explained variable, education and scientific research, etc., in various provinces as explanatory variables to explore the impact of each variable.

3. Data and Empirical Results

As mentioned above, this paper considers the research on solar thermal in China's scientific research development as the object. Because the situation of scientific research in colleges and universities may be affected by the number of local schools, the applicant's achievement requirements at the time of project application, the number of scientific researchers in their region, the fund for scientific research, and intellectual investment, based on the project data of the National Natural Science Foundation of China from 2018 to 2019, this study analyzes the keywords or titles related to solar thermal in the project during the year. Based on the empirical data, the number of projects approved by the National Nature Fund and the data of China's education statistics yearbook are sorted out. From the 2018–2019 China's education statistics yearbook, we have sorted out the number of schools, the number of teaching staff with a Ph.D. degree or a Master's degree, the number of professors or associate professors, the number of graduates and undergraduates, and the school's teaching and scientific research assets; and listed their abbreviations into Table 1. In the statistics of the projects approved by the National Natural Science Foundation of China, the statistics of photothermal projects and projects approved in each province are compiled. Table 2 sorts out the descriptive statistics of basic variables. It can be seen from Table 2 that among the faculty members in China's current colleges and universities, the number of teaching staff with a master's degree is higher than that of a Ph.D. degree, and the overall faculty members are made up mostly of associate professors. In addition, the number of undergraduates is about 6-7 times that of graduates.

Table 3 shows the correlation coefficient matrix of each variable. The statistical results show that the correlation among the variables is mainly between −0.400 and 0.800. First, the positive correlation between the number of teaching staff with a Ph. D. degree, the number of graduate students in colleges and universities, and the total number of projects the highest, which is 0.945 and 0.947, respectively. The number of professors in colleges and universities also has an important impact, and the correlation coefficient is 0.907. Since scientific research institutions need to list the structure of scientific research teams when applying for projects, the requirements for professors and associate professors in scientific research teams are relatively important. The statistical results reflect the relationship between professors and project establishment.

Empirically, we adopt two methods: ordinary least square (OLS) and negative binominal regression. Since the explained variable is nonnegative count data (count data), we mainly take the ordinary least square method as the corresponding method and the negative binomial regression as the main research result. In previous literature, negative binomial regression has been considered as the main way to process count data.

The model is set as follows:

$$\ln(\lambda_i) = x_i'\beta + \varepsilon_i, \quad i = 1, 2, \ldots, n. \tag{1}$$

In the model, ε_i represents the unobservable part or the individual heterogeneity in conditional expectation, and formula (2) can be obtained through calculation:

$$\lambda_i = \exp(x_i'\beta)\exp(\varepsilon_i) = u_i v_i. \tag{2}$$

u_i is the deterministic function of the explanatory variables and v_i is still a random variable, which belongs to the unobservable part. Therefore, the empirical model still obeys the Poisson distribution:

$$P(Y_i = y_i \mid x_i, v_i) = \frac{\exp(-u_i v_i)(u_i v_i)^{y_i}}{y_i!} \tag{3}$$

Since v_i is usually greater than 0, it is assumed to obey the Gamma distribution, and it is assumed that $v_i \sim \text{Gamma}((1/a), a), a > 0$. Therefore, the expected value of v_i is 1 and the variance is a. The negative binomial distribution can be obtained by substituting its probability density into the equation, and MLB can be estimated to form a negative binomial regression.

Table 1: List of abbreviations.

Description	Symbols
The total number of approved projects in the province	N_i
The number of teaching staff with a Ph.D. degree	P_a
The number of teaching staff with a master's degree	P_b
The number of professors	P_c
The number of associate professors	P_d
The number of undergraduate students	P_e
The number of graduate students	P_f
The teaching and research asset of a school (10,000 RMB)	A_r
Logarithm of the number of people logarithm of	P_a
Logarithm of the numbers of professors and associate professors logarithm of	$P_h + P_d$
Logarithm of the number of graduate students logarithm of	P_g
Logarithm of the number of undergraduates logarithm of	P_m
Logarithm of the teaching, science and research asset of a school logarithm of	A_r

Table 2: The descriptive statistics of basic variables.

Variable name	Mean	Std. Deviation	Minimum	Maximum
N_i	30.17	20.532	1	72
P_a	17678	10757	312	38109
P_b	23323	8963	1052	36928
P_c	9420	4449	741	17534
P_d	20696	7661	1355	34764
P_e	773045	291920	42248	1236156
P_f	110176	87839	3035	299562
A_r	2018069	1265583	64211	4592204

Data Source: National Natural Science Foundation of China and China's education statistics yearbook.

Table 3: Correlation coefficient matrix of each variable.

		(1)	(2)	(3)	(4)	(5)	(6)	(7)	(8)
(1)	N_i	1.000							
(2)	P_a	0.945	1.000						
(3)	P_b	0.110	0.212	1.000					
(4)	P_h	0.907	0.965	0.360	1.000				
(5)	P_d	0.563	0.654	0.846	0.758	1.000			
(6)	P_m	0.177	0.290	0.982	0.429	0.893	1.000		
(7)	P_g	0.947	0.955	−0.025	0.902	0.451	0.041	1.000	
(8)	A_r	0.951	0.990	0.148	0.953	0.596	0.219	0.968	1.000

Data source: National Natural Science Foundation of China.

To further verify whether the empirical results under the negative binomial regression estimation are consistent with the Poisson regression results, Table 3 and 4 sort out the negative binomial regression estimation results. The coefficient estimates β consistent with each explanatory variable x_i can be deduced from equation (2). In the above formula, x is the explanatory variable. Empirically, the impact on the explained variable is discussed based on the number of doctoral teaching staff, the number of associate professors, the number of graduates and undergraduates, and the teaching and scientific research assets of schools in the province.

Table 4 first estimates regression and negative binomial regression, and the explained variable is the total number of approved projects. The estimation results show that the number of teaching staff, students, and teaching and scientific research assets has a significantly positive impact on the project approval in colleges, universities, and regions. Based on the consistency of OLS estimation and NBR estimation results, taking the sixth column of Table 4 as an example, the empirical results of the estimation combination show that the impact of teaching staff with a Ph. D. degree on the explained variable is 0.227, indicating that the increase in the number of teaching staff can positively drive the growth rate of the region. Secondly, the coefficient estimates of graduates and undergraduates are 0.737 and 0.747, respectively, indicating that there is a positive effect on the total number of project approval when the number of students increases.

Panel estimation is done in Table 5. First, the random effect empirically shows that the number of teaching staff with a Ph. D degree, the number of undergraduate students, and the scale of school teaching and scientific research assets in the province have a significantly positive impact on the number of photothermal projects. It shows that with the development of China's economy and industrial demands, human resources provided by colleges and universities and the use of teaching and scientific research resources have a significantly positive impact on whether the school is approved or not. In addition, the possible regional differences should be considered, for example, the industrial technology in north China is more intensive than that in south China, mainly due to the difference in the distribution of natural resources. Therefore, the fixed effect is also analyzed in Table 5. The empirical results show that the number of teaching staff with a Ph. D degree and the number of professors and associate professors in the province have a significantly positive impact on the explained variable. For example, in the fixed effect (2) in Table 5, all explanatory variables are significant, indicating that the increase in the number of teaching staff with a Ph. D degree in the province has a positive and significant impact on the number of projects. And the increase in the number of graduate and undergraduate students as planned also has a positive impact on the scientific research development of the university and the region. Both correlations reflect that in terms of the scientific research development, the approval of scientific research projects of solar thermal or the follow-up patent application derived from the scientific research projects, the investment in teaching and scientific research, and human

Table 4: Regression estimation.

	Explained variable: total number of approved projects					
	(1) OLS	(2) OLS	(3) OLS	(4) NBR	(5) NBR	(6) NBR
ln $(P_{a)}$		0.002 ***	0.003		0.505 ***	0.227 **
		(0.001)	(0.002)		(0.046)	(0.120)
ln $(P_{h+}P_{d)}$		0.004 *	0.014 ***		0.889 ***	0.603
		(0.003)	(0.003)		(0.114)	(0.849)
ln(P_g)	0.002 ***		−0.006	0.621 ***		0.737 **
	(0.0003)		(0.007)	(0.126)		(0.368)
ln $(P_{m)}$	0.973 ***		0.002 **	0.758 ***		0.747 ***
	(0.093)		(0.001)	(0.441)		(0.107)
ln $(A_{r)}$			0.077 ***			0.204 ***
			(0.018)			(0.047)
Constant term	−1.593 **	−0.790	−0.054	1.951 ***	2.256 ***	2.046 ***
	(0.831)	(0.852)	(0.876)	(0.044)	(0.039)	(0.048)
N	483	483	483	483	483	483
R^2	0.916	0.894	0.929			
Log likelihood				−1658.582	1675.872	−1625.618

Data source: National Natural Science Foundation of China.

Table 5: Panel estimation.

Explained variable:	The total number of approved projects			
The total number of approved projects	Random effect (1)	Random effect (2)	Fixed effect (1)	Fixed effect (2)
ln $(P_{a)}$	0.504 **	0.510 ***	0.776 **	0.410 *
	(0.326)	(0.127)	(0.398)	(0.189)
ln $(P_{h+}P_{d)}$	0.212	0.641	0.897 **	0.844 **
	(0.276)	(0.462)	(0.404)	(0.437)
ln(P_g)	0.008		0.554 ***	
	(0.290)		(0.132)	
ln $(P_{m)}$		0.550 ***		0.510 ***
		(0.204)		(0.221)
ln $(A_{r)}$	0.153 *	0.159 *	0.218 ***	0.322 ***
	(0.091)	(0.091)	(0.090)	(0.065)
Constant term	−8.922 ***	−4.261 **		
	(1.930)	(2.660)		
N	483	483	483	483

Data source: National Natural Science Foundation of China.

resources in colleges and universities have a key impact. The results also show that the development of scientific research projects, industrial demand, and green sustainable innovation complement each other.

4. Conclusion

This paper empirically analyzes the count data through regression and constructs a negative binomial regression empirical model through the project data of the National Natural Science Foundation of China on solar thermal and the China education statistics yearbook from 2018 to 2019. The results show that the human resources provided by colleges and universities and the use of teaching and scientific research resources have a significantly positive impact on whether the department of thermodynamics is approved or not. The empirical results show the importance of talent education and training. Talent training drives scientific research funding, which is extremely important for the development of environmental science and has a key impact on the correlation between China's industrial demand and green sustainable innovation.

Based on the national science fund, this paper analyzes the factors affecting scientific research in the education system. However, this paper also has many limitations. Due to the lack of centralized release of official data in China, the project data that can be made public can only be obtained by crawling, and the research year is lagging behind and short. At the same time, although quantitative methods can find correlation more directly, they cannot completely explain the meaning behind the data. In the follow-up research, it is proposed to further explore the issues of industry-university cooperation. Industry-university-research cooperation can effectively coordinate the innovation needs of various innovating entities, thereby significantly improving the transformation efficiency of basic research funding into the innovation of middle and downstream enterprises. A series of national science fund for cultivating innovative talents and teams can further promote the patent output of enterprises. How to effectively combine scientific research with

current and future environmental development is the focus of follow-up research.

Data Availability

Requests for access to the data used to support the findings of this study should be made to Jian Chu (mrchujian@hotmail.com).

Conflicts of Interest

The authors declare that they have no conflicts of interest.

Authors' Contributions

Tu Yan performed conceptualization and formal analysis, developed the methodology, and wrote the initial draft. Chu Jian collected data, wrote the original draft, and performed supervision. Mohd Asif Shah wrote the final draft and performed supervision.

Acknowledgments

This study was supported by the 2021 Talent Introduction Research Start-Up Fund Project of Suqian University.

References

[1] X. Yuan, C. W. Su, M. Umar, X. Shao, and O. R. Lobonţ, "The race to zero emissions: can renewable energy be the path to carbon neutrality?" *Journal of Environmental Management*, vol. 308, Article ID 114648, 2022.

[2] K. Ravi Kumar, N. Krishna Chaitanya, and N. Sendhil Kumar, "Solar thermal energy technologies and its applications for process heating and power generation–A review," *Journal of Cleaner Production*, vol. 282, Article ID 125296, 2021.

[3] H. Wei, J. Dai, I. Maharik, A. Ghasemi, A. Mouldi, and A. Brahmia, "Simultaneous synthesis of H2, O2, and N2 via an innovatory energy system in coronavirus pandemic time: design, techno-economic assessment, and optimization approaches," *International Journal of Hydrogen Energy*, 2021.

[4] P. A. Østergaard, N. Duic, Y. Noorollahi, H. Mikulcic, and S. Kalogirou, "Sustainable development using renewable energy technology," *Renewable Energy*, vol. 146, pp. 2430–2437, 2020.

[5] S. F. Rafique, P. Shen, Z. Wang et al., "Global power grid interconnection for sustainable growth: concept, project and research direction," *IET Generation, Transmission & Distribution*, vol. 12, no. 13, pp. 3114–3123, 2018.

[6] Z. Li, J. Zhang, S. Zhao, Q. Liu, Y. Wang, and C. Wang, "Joint funds of the national natural science foundation of China: a review of information sciences between 2011 and 2020," *Science China Information Sciences*, vol. 64, no. 12, p. 227101, 2021.

[7] Y. Zhang, J. Dai, B. Chen, and K. Chen, "Correlation between economic and industrial demand and scientific innovation: a case study of thermodynamics discipline statistics of National Natural Science Foundation of China," *Journal of Thermal Analysis and Calorimetry*, vol. 144, no. 6, pp. 2347–2355, 2021.

[8] G. Pu, X. Zhu, J. Dai, and X. Chen, "Understand technological innovation investment performance: evolution of industry-university-research cooperation for technological innovation of lithium-ion storage battery in China," *Journal of Energy Storage*, vol. 46, Article ID 103607, 2022.

[9] Z. Zongxian, W. Yang, S. Xiaofei, and Z. Ming, "Risk assessment of concentrating solar power based on fuzzy comprehensive evaluation," *Systems Engineering Procedia*, vol. 4, pp. 99–106, 2012.

[10] J. Huang, J. Fan, and S. Furbo, "Feasibility study on solar district heating in China," *Renewable and Sustainable Energy Reviews*, vol. 108, pp. 53–64, 2019.

[11] W. H. Zhang, L. C. Chou, and M. Chen, "Consumer perception and use intention for household distributed photovoltaic systems," *Sustainable Energy Technologies and Assessments*, vol. 51, Article ID 101895, 2022.

[12] O. May Tzuc, A. Bassam, F. Anguebes-Franseschi, L. J. Ricalde, M. Flota-Bañuelos, and M. Castillo Téllez, "Multivariate optimization applied for the economic competitiveness analysis of photothermal systems into industrial heat production: an approach based on artificial intelligence," *Journal of Renewable and Sustainable Energy*, vol. 12, no. 5, Article ID 055501, 2020.

[13] T. Lopes, T. Fasquelle, and H. G. Silva, "Pressure drops, heat transfer coefficient, costs and power block design for direct storage parabolic trough power plants running molten salts," *Renewable Energy*, vol. 163, pp. 530–543, 2021.

[14] S. Comello, S. Reichelstein, and A. Sahoo, "The road ahead for solar PV power," *Renewable and Sustainable Energy Reviews*, vol. 92, pp. 744–756, 2018.

[15] T. Li, A. Li, and X. Guo, "The sustainable development-oriented development and utilization of renewable energy industry——a comprehensive analysis of MCDM methods," *Energy*, vol. 212, Article ID 118694, 2020.

[16] M. H. Ahmadi, M. Ghazvini, M. Sadeghzadeh et al., "Solar power technology for electricity generation: a critical review," *Energy Science & Engineering*, vol. 6, no. 5, pp. 340–361, 2018.

[17] Z. Yu and J. W. Schwieter, "Recognizing the effects of language mode on the cognitive advantages of bilingualism," *Frontiers in Psychology*, vol. 9, p. 366, 2018.

[18] Y. Xu, J. Pei, J. Yuan, and G. Zhao, "Concentrated solar power: technology, economy analysis, and policy implications in China," *Environmental Science and Pollution Research*, vol. 29, no. 1, pp. 1324–1337, 2022.

[19] E. Souzanchi Kashani and S. Roshani, "Evolution of innovation system literature: intellectual bases and emerging trends," *Technological Forecasting and Social Change*, vol. 146, pp. 68–80, 2019.

[20] T. Clarke, J. Chelliah, and E. Pattinson, "National innovation systems in the Asia Pacific: a comparative analysis," in *Innovation in the Asia Pacific*, pp. 119–143, Springer, Singapore, 2018.

[21] O. Bertrand, "Effects of foreign acquisitions on R&D activity: evidence from firm-level data for France," *Research Policy*, vol. 38, no. 6, pp. 1021–1031, 2009.

[22] G. Schienstock, *Sustainable development and the regional dimension of the innovation system. In Towards Environmental Innovation Systems*, pp. 97–113, Springer, Berlin, Heidelberg, 2005.

[23] W. M. Cohen, R. R. Nelson, and J. P. Walsh, "Links and impacts: the influence of public research on industrial R&D," *Management Science*, vol. 48, no. 1, pp. 1–23, 2002.

[24] I. Cockburn and R. Henderson, "Public–private interaction in pharmaceutical research," *Proceedings of the National Academy of Sciences*, vol. 93, no. 23, pp. 12725–12730, 1996.

[25] L. G. Zucker, M. R. Darby, and J. S. Armstrong, "Commercializing knowledge: university science, knowledge capture, and firm performance in biotechnology," *Management Science*, vol. 48, no. 1, pp. 138–153, 2002.

Hindawi
Mathematical Problems in Engineering
Volume 2022, Article ID 6864015, 5 pages
https://doi.org/10.1155/2022/6864015

Research Article

Econometric Modelling Based on Dynamic Count Regression and China Power Supply Dataset

Yixin Yan,[1] **Jiliang Hu**,[1] **Xiding Chen**,[2] **and A. P. Senthil Kumar**[3]

[1]*School of Economics and Business Administration, Central China Normal University, Wuhan, China*
[2]*School of Finance and Trade, Wenzhou Business College, Wenzhou, China*
[3]*School of Social Work, Jigjiga University, Somali Regional State, Jigjiga, Ethiopia*

Correspondence should be addressed to Jiliang Hu; jilianghucentral@outlook.com and A. P. Senthil Kumar; senthilapsk@gmail.com

Received 18 March 2022; Revised 13 April 2022; Accepted 4 May 2022; Published 28 May 2022

Academic Editor: Amandeep Kaur

Traditionally, economic data of power supply is often analyzed through the count regression model due to the type of empirical data in the decision-making process. However, in reality, it is difficult to use count data model for data with autoregressive features. The main reason is that the time series features and autoregressive attributes cannot be controlled through the count regression model, which violates the assumptions set by the model. Therefore, there may be errors in the empirical analysis results. This letter firstly describes the characteristic of the count regression model and the problem, and then we refine the multiplicative autoregressive count model for dynamic count data. The model has desirable theoretical properties and is trivial to incorporate into existing models for the count data. In this study, the multiplicative autoregressive counting model for dynamic counting data is improved. The model has ideal theoretical properties and can be easily incorporated into existing economic models of counting data, especially for power supply policy analyses.

1. Introduction

In traditional economic modelling in energy problems, the traditional regression models are not suitable for analyzing nonnegative count data from an empirical dataset [1]. This is because traditional regression uses the ordinary least squares (OLS), which assumes that data are normally distributed, where count data do not follow a normal distribution [2]. Therefore, in terms of analyzing count data, three types of count regression models are often used, that is, Poisson Regression [3], Zero-Inflated Poisson Regression [4], and Negative Binominal Regression [5]. For example, Bai et al. [6] employed data from scientific research projects in China, where the research object is the number of thermodynamic research projects. Another example is that in the current COVID-19 outbreak, the number of infections among different people diagnosed is actually similar to a pattern of count data, but this pattern is more similar to a pattern with time series characteristics. The data are thus nonnegative statistical values, and it is more suitable to apply Poisson Regression for analysis. In recent years, with the progress of measurement methods and software technology, great progress has been made in measurement problems and carding model construction that could not be solved in the past [7–9].

In energy planning, power supply policy plays a vital role in the national economy and is important for people's livelihoods. Reference [10] pointed out that during the annual peak electricity consumption period, the coordination of energy supply in China becomes a challenge. The power consumption is directly determined by the size and load of the power generation capacity. Therefore, it is important for the power sector in China to accurately predict the development of power generation in China so that policies can be made accordingly based on the data. However, as the authors in [11] pointed out, power generation in China has shown the characteristics of being long term, seasonal, and periodical. In terms of the developing trend, as time goes by and with the improvement of people's living standards, the power generation fluctuates, with an

overall trend of increase in the total amount. As for periodicity, due to the influence of various factors such as seasons or demand, the power generation in China shows a repeated cyclic change every 12 months. Reference [12] found that this phenomenon led to a serious problem that the power generation of the power plant in each period actually has a certain degree of time series problem, which also results in the existence of time series in the data used for power supply economic planning and policy formulation.

The stability of the time series directly affects the validity of the constructed model [13]. The numerical characteristics of a stable time series, such as the mean, variance, and covariance, do not change with time, and the randomness of the time series at each time point follows a certain probability distribution [14]. That is, it can use the information from a previous time point in the time series to build a model to fit the past information and then make predictions [15]. However, for a nonstable time series, the numerical characteristics change with time, and thus, it is impossible to grasp the overall randomness of the time series through known information [13]. Hence, it is difficult to model and predict a nonstable series. When a regression model is built with two independent nonstable time series, a statistically significant regression function is more likely to occur, which is called a spurious regression. The commonly used method for testing the stability of time series is the unit root test [16]. However, the unit root test is often misused with an inappropriate method, leading to wrong tests and spurious regression. Therefore, when analyzing data with an econometric model, a specific model must be selected according to the characteristics of data [17, 18]. In the face of count data with nonnegative values, it is recommended to use the count regression model. However, in reality, the observation data sometimes have the nature of time series or autoregression. In this case, analyzing data with the count regression model will cause biases in estimation because it cannot deal with the problem of autoregression and possible heteroscedasticity. When it comes to data analysis in electric power research, data in this field often have a certain degree of timing problem in the power generation of power plants in each period. If this phenomenon cannot be effectively solved, other robust analyses may still be required for empirical analysis to ensure the correctness of the empirical results. Scholars have used generalized linear models and dynamic regression models to deal with the above problems. However, using a combination of the two has proven difficult, especially because of the difficulties in using lagged dependent variables in generalized linear models as means of modelling autoregressive dynamic processes. These problems exist in dynamic count models, including the problem that taking lagged dependent variables as a regression variable often leads to econometric difficulties [19]. For this reason, the literature has proposed different approximations, including some original approaches [20, 21]. But most of these models are difficult to implement and have unrealistic assumptions about the data-generating process of the dependent variable. To address this issue, we used the improved multiplicative autoregressive model for count data proposed by [22] and proposed a revised model for the count regression model. This paper is structured as follows: Section 2 constructs the count regression model used in traditional econometrics and explains related issues. In Section 3, a revised model incorporating the time series features and autoregressive properties is proposed. In Section 4, the paper concludes with a summary of the main findings and points out the potential application of the revised model.

2. Constructing Count Regression Models

Some statistical data follow a distribution skewed to the right and thus do not appear to be normally distributed. In this case, the classical regression model is usually not an optimal option for model estimation. In event analysis, for example, if the observed variable has a large number of values such as 0 or 1 in the data, Poisson regression is generally used for analysis [23]. This model is set as follows.

Suppose that the dependent variable representing the number of events $\mathbf{Y_i}, \mathbf{i} = 1, 2, \ldots, \mathbf{n}$ is a nonnegative random variable, with the observation $\mathbf{y_i}$ coming from the Poisson distribution $\mathbf{Poi}(\mathbf{u_i})$ of the parameter $\lambda_\mathbf{i}$, and is affected by other independent variables $\mathbf{x_i} = (\mathbf{x}_1, \mathbf{x}_2, \ldots, \mathbf{x}_{\mathbf{k}-1})$. The probability density function is as follows:

$$\Pr(\mathbf{Y_i} = \mathbf{y_i} \mid x_i) = \frac{\boldsymbol{\lambda}_\mathbf{i}^{\mathbf{y_i}} \exp(-\boldsymbol{\lambda}_\mathbf{i})}{\mathbf{y_i}!}, \ \mathbf{y_i} = 0, 1, 2, \ldots, \mathbf{u_i} > 0. \quad (1)$$

In this equation, $\lambda_\mathbf{i} > 0$ means that the Poisson arrival rate is affected by the independent variable $\mathbf{x_i}$. Assuming that the expected value is equal to the variance; that is, $\mathbf{E}(\mathbf{Y_i} = \mathbf{y_i} \mid \mathbf{x_i}) = \mathrm{Var}(\mathbf{Y_i} = \mathbf{y_i} \mid \mathbf{x_i})$. In the Poisson distribution, λ represents the average number of events occurring per unit time. As such, the Poisson regression can be defined as follows:

$$\ln[\mathbf{E}(\mathbf{Y_i} = \mathbf{y_i} \mid \mathbf{x_i})] = \ln(\boldsymbol{\lambda}_\mathbf{i}) = \mathbf{x_i'}\boldsymbol{\beta}, \mathbf{i} = 1, 2, \ldots, \mathbf{n}. \quad (2)$$

Assuming that the samples are mutually independent, the likelihood function of the samples can be developed as follows:

$$\mathbf{L}(\boldsymbol{\beta}) = \frac{\exp(-\sum_{i=1}^{n} \boldsymbol{\lambda}_\mathbf{i}) \prod_{i=1}^{n} \boldsymbol{\lambda}_\mathbf{i}^{\mathbf{y_i}}}{\prod_{\mathbf{i}=1}^{\mathbf{n}} \mathbf{y_i}!}. \quad (3)$$

Take the logarithm of equation (3) and we can obtain the following equation:

$$\begin{aligned} \ln \mathbf{L}(\boldsymbol{\beta}) &= \sum_{i=1}^{n} [-\boldsymbol{\lambda}_\mathbf{i} + \mathbf{y_i} \ln \boldsymbol{\lambda}_\mathbf{i} - \ln(\mathbf{y_i}!)] \\ &= \sum_{i=1}^{n} [-\exp(\mathbf{x_i'}\boldsymbol{\beta}) + \mathbf{y_i}\mathbf{x_i'}\boldsymbol{\beta} - \ln(\mathbf{y_i}!)]. \end{aligned} \quad (4)$$

Perform first-order differentiation on equation (4) and we obtain the following:

$$\sum_{i=1}^{n} [\mathbf{y_i} - \exp(\mathbf{x_i}'\boldsymbol{\beta})]\mathbf{x_i} = 0. \quad (5)$$

From the above equation, the estimated coefficient β of each independent variable $\mathbf{x_i}$ with consistency can be deduced. In the above equation, X is an independent variable.

In analyzing empirical data, the influence on the dependent variable is discussed by including various micro- and macrovariables.

In addition, the limitation of Poisson regression is that the mean (expected value) and variance of the distribution are assumed to be equal, resulting in an equidispersion. However, in reality, empirical data often do not have expected values that are equal to variances. To solve this problem, equation (2) can be rewritten as follows:

$$\ln(\boldsymbol{\lambda_i}) = \mathbf{x_i^{'}\beta} + \boldsymbol{\varepsilon_i}, \mathbf{i} = 1, 2, \ldots, \mathbf{n}. \quad (6)$$

In this equation, ε_i represents the unobservable part or the heterogeneity of the individual in the conditional expectation, and the following equation can be obtained:

$$\boldsymbol{\lambda_i} = \mathbf{exp}\left(\mathbf{x_i^{'}\beta}\right)\mathbf{exp}(\boldsymbol{\varepsilon_i}) = \mathbf{u_i v_i}. \quad (7)$$

$\mathbf{u_i}$ is the deterministic function of the independent variable, and $\mathbf{v_i}$ is still a random variable, which belongs to the unobservable part. Therefore, the empirical model still follows the Poisson distribution:

$$\mathbf{P}(\mathbf{Y_i} = \mathbf{y_i} \mid \mathbf{x_i}, \mathbf{v_i}) = \frac{\mathbf{exp}(-\mathbf{u_i v_i})(\mathbf{u_i v_i})^{y_i}}{\mathbf{y_i}!}. \quad (8)$$

As $\mathbf{v_i}$ is usually larger than 0, it is assumed that it follows the Gamma distribution, and it is assumed that $\mathbf{v_i} \sim \text{Gamma}(1/a, a)$ and $a > 0$. Therefore, the expected value of $\mathbf{v_i}$ is 1 and the variance is a. Substitute its probability density into the equation, a negative binomial distribution can be obtained. Perform MLB estimation, and we can get a negative binomial regression. The conditional variance is as follows:

$$\text{Var}(Y_i \mid x_i) = u_i + \alpha \mathrm{u}_i^2 > u_i = E(Y_i \mid x_i). \quad (9)$$

This shows that the conditional variance is larger than expected in the negative binomial regression. The above equation shows that the variance value is an increasing function of α. When α approaches 0, the negative binomial regression and Poisson regression tend to be equal. In addition, if α in the Gamma distribution is transformed into δ/u_i i; that is, $\mathbf{v_i} \sim \text{Gamma}(u_i/\delta, \delta/u_i)$, then equation (9) can be turned into the following equation:

$$\text{Var}(Y_i \mid x_i) = u_i + \left(\frac{\delta}{u_i}\right)u_i^2 = u_i + \delta u_i > u_i. \quad (10)$$

Through the estimation of the approximate function, the analysis can be carried out according to the properties of the empirical data.

If the empirical data contains a large number of 0 values, traditionally the Zero-Inflated Poisson Regression or the Zero-Inflated Negative Binomial Regression is often used. Therefore, the empirical data also assumed that followed the Poisson distribution or negative binomial distribution. Theoretically, the analysis is divided into two parts. First, the decision to take the proportion of 0 or 0 is equivalent to binary choice in econometrics. Second, decide which value group to choose. Assume that the dependent variables follow a mixed distribution:

$$\begin{cases} P(y_i = 0 \mid x_i) = \theta, \\ P(y_i = j \mid x_i) = \dfrac{(1-\theta)\mathbf{exp}(-\boldsymbol{\lambda_i})\boldsymbol{\lambda}_{\boldsymbol{ii}}^{j}}{j!(1-\mathbf{exp}(-\boldsymbol{\lambda_i}))}, \end{cases} (j = 1, 2, \ldots), \quad (11)$$

where $\lambda_i = \mathbf{exp}(\mathbf{x_i'}\beta)$. Similarly, the estimated value of the coefficient of each independent variable x can be further obtained through calculation, and whether it has statistical significance for subsequent analysis can be decided.

Traditionally, when is it appropriate to use the Poisson regression? When is it appropriate to use negative binomial regression? Generally, in addition to looking at the data attribute, it is also a recommended practice to use respective regression analyses and calculate robust standard errors to achieve consistent estimation. This is somewhat similar to the regression estimation using the least-squares method and then getting robust standard error. Generally speaking, these approaches mostly aim to ensure that the estimation results are robust and reliable.

3. Dynamic Count Regression Models

To summarize, this paper first reviewed what kind of theoretical model and approaches are usually used when encountering count data in the process of data analysis. However, these models may produce biased results in estimation when used for analyzing data with time series or autoregressive characteristics. For example, in analyzing the problem of heat energy consumption generated in the production activities of various industrial plants, the heat energy consumption during each working day is related to the production activity plan [24]. As a result, there is a time series phenomenon according to the production planning activities. Failure to take this phenomenon into account in the analysis could lead to biased estimation. Admittedly, when using power supply data of plants, regional differences and autocorrelation issues seem to be negligible in empirical analysis if the research area is Japan, Taiwan, and other small island economies. However, when researchers aim to investigate economics with a large land area, such as China and the United States, it is important to know that these economics have different climatic zones and geographical regions. Therefore, in studying the power supply problem of the power plant, ignoring the impact of time series on the region in data analysis would lead to increased risks in model misspecification and biased estimation. Therefore, some suggestions are provided for researchers. First, the research objects must be limited, such as focusing only on the coastal areas of China or cities on the east coast of the United States, to avoid the potential impact of large variances within a large study area. Second, for data with time series features, an adjustment in the model is required. In order to model the autoregressive process while avoiding the above problems, the model can be rewritten in a way that the logarithm of the lagged dependent variable is taken as the dependent variable. In the regression, there is an infinite number of independent variables and error terms with geometric decay lags. These lag terms are in

exponential functions, constraining the conditional mean to reasonable nonnegative values. Therefore, equation (5) can be rewritten as follows:

$$\begin{aligned}
\mathbf{y_t} &= \mathbf{exp}\left(\mathrm{a}_0 + b_0 x_t + \mathbf{u_t}\right) y_{t-1}^{a_1},\\
\mathbf{y_t} &= \mathbf{exp}\left(\mathrm{a}_0 + b_0 x_t + \mathbf{u_t} + \mathrm{a}_1 \log\left(y_{t-1}\right)\right),\\
\mathbf{y_t} &= \mathbf{exp}\left(\mathrm{a}_0 + b_0 x_t + \mathbf{u_t} + \mathrm{a}_1 \log\left(\mathbf{exp}\left(\mathrm{a}_0 + b_0 x_{t-1} + \mathbf{u_{t-1}}\right)\right)\right.\\
&\quad \left. + \mathrm{a}_1 \log\left(y_{t-2}\right)\right),\\
\mathbf{y_t} &= \mathbf{exp}\left(\mathrm{a}_0 + b_0 x_t + \mathbf{u_t} + \mathrm{a}_0 \mathrm{a}_1 + \mathrm{a}_1 u_{t-1} + a_1^2 a_0 + a_1^2 b_0 x_{t-2}\right.\\
&\quad \left. + a_1^2 u_{t-2} + \ldots\right).
\end{aligned} \tag{12}$$

This generalization of autoregression has a number of desirable properties. The model is stable for $|\,\mathrm{a}_1 < 1\,|$. After simplification, we can use the long-run multiplier for an independent variable LRM $= (b_0 + b_1 + b_2 + \ldots / 1 - a_1 - a_2 - \ldots)$. Although this model is desirable, it encounters problems with data where the observation count is 0. Since the logarithm of 0 cannot be calculated, this value will result in model nonconvergence in model estimation. Theoretically, the data generation process in equation (12) assumes that zero is a convergent state, once a value of zero is observed in a series, the series will continue to remain zero. However, this is not the case in all settings. Therefore, this model has to be abandoned in favour of a more flexible model. Applying the concept of Zeger and Qaqish (1998), we add a constant to the time series so that no value is equal to 0 ($y_{ts}^{+} = y_{ts} + c$). We also add a constant to the observed zero values of the time series ($y_{\mathrm{ts}}^{+} = \max y_{\mathrm{ts}}, c,\ c \le 1$). Then equation (12) can be described as follows:

$$\mathbf{y_t} = \mathbf{exp}\left(\mathrm{a}_0 + b_0 x_t + \mathbf{u_t} + \mathrm{a}_1 \log\left(y_{t-1}^{+}\right)\right). \tag{13}$$

Compared with equation (12), equation (13) produces an econometric model that can still proceed to model estimation when the data contain values of 0. In this case, the count regression can be performed on the data with autocorrelation characteristics according to equation (13). Secondly, to further analyze the autoregressive problem, equation (12) can be further rewritten as follows:

$$\mathbf{y_t} = \mathbf{exp}\left(\mathrm{a}_0 + b_0 x_t + \mathbf{u_t} + \mathrm{a}_1 \log\left(y_{t-1}^{+}\right) + \theta d_{t-1}\right), \tag{14}$$

where $d_{t-1} = 1$ if $y_{t-1} = 0$, $d_{t-1} = 0$ if otherwise. Equation (14) takes into account the intertemporal influence on autoregression, so the count regression model can be further extended to statistical data analysis with time series characteristics and autoregressive properties with equations (13) and (14).

4. Conclusions

In reality, observed data often have the nature of time series or autoregression. In this case, analyzing with count regression models will result in biased estimation, because the count regression models cannot handle the problem of autoregression and possible heteroscedasticity. Therefore, this study proposed an improved autoregressive model for dynamic count data. This model has advantages over the Poisson Regression, Zero-Inflated Poisson Regression, and Negative Binominal Regression used in general econometric analysis, which cannot take into account time series and autoregression. The regression model proposed in this paper points out that it is possible to apply a link function to a lagging dependent variable and use it in the generalized linear model, which further expands this model to analyze various types of data. In this study, the revised econometric model has desirable theoretical properties and can be easily incorporated into existing models used for analyzing count data, especially for some specific policy analyses.

At the end of the article, we explain the application of the revised model. As mentioned above, to analyze the heat energy consumption generated in the production activities of each industrial plant, it is important to consider that the heat energy consumption during each working day is related to the production activity plan, so that the production planning activities have time series. Through the revised econometric model, we can further discuss how to model thermal energy data with the time series nature and analyze the influence of independent variables on the dependent variables. Secondly, the model setting of this paper can be further combined with the panel data model in the future to discuss whether the single root problem should be dealt with in data under the control of regional difference attributes and random variable characteristics under the dynamic situation to facilitate empirical application or model construction. In addition, in analyzing policies and research projects, such as thermal policies, the revised model can be extended to discuss the impact of changes in the number of projects in different regions and different periods. For instance, it can be used to analyze the thermal energy dispersal status of incinerators and power plants. Furthermore, the influence of the marginal rate of change of each time on the thermal energy dissipated scale can be analyzed under the first-order difference. In terms of empirical analysis, the revised model can also further discuss power supply issues in large regions such as China, Russia, and the United States and can be used to conduct follow-up analysis.

Data Availability

Requests for access to the data used to support the findings of this study should be made to Jiliang Hu (jilianghucentral@outlook.com).

Conflicts of Interest

The authors declare that they have no conflicts of interest regarding the publication of this paper.

Authors' Contributions

Yixin Yan and Jiliang Hu performed conceptualization, developed the methodology, and wrote the original draft. Xiding Chen performed the formal analysis. A.P.Senthil Kumar performed the formal analysis, wrote the final draft, and performed the supervision.

References

[1] G. K. F. Tso and K. K. W. Yau, "Predicting electricity energy consumption: a comparison of regression analysis, decision tree and neural networks," *Energy*, vol. 32, no. 9, pp. 1761–1768, 2007.

[2] E. W. Steyerberg, A. J. Vickers, N. R. Cook et al., "Assessing the performance of prediction models," *Epidemiology*, vol. 21, no. 1, pp. 128–138, 2010.

[3] R. A. Sian and C.-C. Wang, "A generalized log-linear Poisson-modeled correlation to predict the optimal heat rejection pressure of transcritical CO2 systems," *Science and Technology for the Built Environment*, vol. 24, no. 8, pp. 897–907, 2018.

[4] Y. Zhang, J. Dai, B. Chen, and K. Chen, "Correlation between economic and industrial demand and scientific innovation: a case study of thermodynamics discipline statistics of National Natural Science Foundation of China," *Journal of Thermal Analysis and Calorimetry*, vol. 144, no. 6, pp. 2347–2355, 2021.

[5] S. Li and Q. Shao, "Exploring the determinants of renewable energy innovation considering the institutional factors: a negative binomial analysis," *Technology in Society*, vol. 67, Article ID 101680, 2021.

[6] Y. Bai, L. Chou, and W. Zhang, "Industrial innovation characteristics and spatial differentiation of smart grid technology in China based on patent mining," *Journal of Energy Storage*, vol. 43, Article ID 103289, 2021.

[7] F. Castellares, S. L. P. Ferrari, and A. J. Lemonte, "On the Bell distribution and its associated regression model for count data," *Applied Mathematical Modelling*, vol. 56, pp. 172–185, 2018.

[8] E. Altun, "A new model for over-dispersed count data: Poisson quasi-Lindley regression model," *Mathematical Sciences*, vol. 13, no. 3, pp. 241–247, 2019.

[9] M. El-Morshedy, E. Altun, and M. S. Eliwa, "A new statistical approach to model the counts of novel coronavirus cases," *Mathematical Sciences*, vol. 16, no. 1, pp. 37–50, 2021.

[10] G. Luo, X. Zhang, S. Liu, E. Dan, and Y. Guo, "Demand for flexibility improvement of thermal power units and accommodation of wind power under the situation of high-proportion renewable integration-taking North Hebei as an example," *Environmental Science and Pollution Research*, vol. 26, no. 7, pp. 7033–7047, 2019.

[11] S. Han, Y.-h. Qiao, J. Yan, Y.-q. Liu, L. Li, and Z. Wang, "Mid-to-long term wind and photovoltaic power generation prediction based on copula function and long short term memory network," *Applied Energy*, vol. 239, pp. 181–191, 2019.

[12] D. Yang and Z. Dong, "Operational photovoltaics power forecasting using seasonal time series ensemble," *Solar Energy*, vol. 166, pp. 529–541, 2018.

[13] Y. Zou, R. V. Donner, N. Marwan, J. F. Donges, and J. Kurths, "Complex network approaches to nonlinear time series analysis," *Physics Reports*, vol. 787, pp. 1–97, 2019.

[14] C.-L. Liu, W.-H. Hsaio, and Y.-C. Tu, "Time series classification with multivariate convolutional neural network," *IEEE Transactions on Industrial Electronics*, vol. 66, no. 6, pp. 4788–4797, 2019.

[15] G. L. Simpson, "Modelling palaeoecological time series using generalised additive models," *Frontiers in Ecology and Evolution*, vol. 6, p. 149, 2018.

[16] W. Fan and Y. Hao, "An empirical research on the relationship amongst renewable energy consumption, economic growth and foreign direct investment in China," *Renewable Energy*, vol. 146, pp. 598–609, 2020.

[17] M. B. Shrestha and G. R. Bhatta, "Selecting appropriate methodological framework for time series data analysis," *The Journal of Finance and Data Science*, vol. 4, no. 2, pp. 71–89, 2018.

[18] B. K. Sovacool, J. Axsen, and S. Sorrell, "Promoting novelty, rigor, and style in energy social science: towards codes of practice for appropriate methods and research design," *Energy Research & Social Science*, vol. 45, pp. 12–42, 2018.

[19] P. T. Brandt, J. T. Williams, B. O. Fordham, and B. Pollins, "Dynamic modeling for persistent event-count time series," *American Journal of Political Science*, vol. 44, no. 4, pp. 823–843, 2000.

[20] P. T. Brandt and J. T. Williams, "A linear Poisson autoregressive model: the Poisson AR(p) model," *Political Analysis*, vol. 9, no. 2, pp. 164–184, 2001.

[21] T. L. Davis, B. Dirks, E. A. Carnero et al., "Chemical oxygen demand can be converted to gross energy for food items using a linear regression model," *Journal of Nutrition*, vol. 151, no. 2, pp. 445–453, 2021.

[22] A. C. Cameron and P. K. Trivedi, *A Companion to Theoretical Econometrics*, p. 331, Wiley, New Jersey, USA, 2001.

[23] W. Chen, L. Qian, J. Shi, and M. Franklin, "Comparing performance between log-binomial and robust Poisson regression models for estimating risk ratios under model misspecification," *BMC Medical Research Methodology*, vol. 18, no. 1, pp. 63–12, 2018.

[24] J. S. Randhawa and I. S. Ahuja, "An investigation into manufacturing performance achievements accrued by Indian manufacturing organization through strategic 5S practices," *International Journal of Productivity and Performance Management*, vol. 67, no. 4, pp. 754–787, 2018.

Hindawi
Mathematical Problems in Engineering
Volume 2022, Article ID 6488571, 9 pages
https://doi.org/10.1155/2022/6488571

Research Article

Deep Neural Network-Based Intrusion Detection System through PCA

Shoayee Dlaim Alotaibi,[1] Kusum Yadav,[1] Arwa N. Aledaily,[1] Lulwah M Alkwai,[1] Alaa Kamal Yousef Dafhalla,[1] Shahad Almansour,[1] and Velmurugan Lingamuthu[2]

[1]*College of Computer Science and Engineering, University of Ha'il, Kingdom of Ha'il, Saudi Arabia*
[2]*Department of Computer Science, School of Informatics and Electrical Engineering, Hachalu Hundesa Campus, Ambo University, Ambo, Ethiopia*

Correspondence should be addressed to Velmurugan Lingamuthu; velmurugan.lingamuthu@ambou.edu.et

Received 3 March 2022; Revised 2 April 2022; Accepted 8 April 2022; Published 9 May 2022

Academic Editor: Amandeep Kaur

Today, challenges such as a high false-positive rate, a low detection rate, a slow processing speed, and a big feature dimension are all part of intrusion detection. To address these issues, decision trees (DTs), deep neural networks (DNNs), and principal component analysis (PCA) are available. Through a higher detection rate and a lower false-positive rate, the research-based intrusion detection model DT-PCA-DNN increases the processing speed of intrusion detection systems (IDSs). To minimize the overall data volume and accelerate processing, DT is used to initially differentiate the data. Differentiate DTs save the temporary training sample set for intrusion data in order to retrain and optimize the DT and DNN, treat the DT judges as standard data, and delete the added average data. After signing, we should lower the dimension of the data using PCA and then submit the data to DNN for secondary discrimination. However, DT employs a shallow structure in order to prevent an excessive quantity of average numbers from being interpreted as intrusion data. As a result, additional DNN secondary processing cannot effectively increase the accuracy. DNN accelerates data processing by utilizing the ReLU activation function from the simplified neural network calculation approach and the faster convergence ADAM optimization algorithm. Class two and five trials on the NSL-KDD dataset demonstrate that the proposed model is capable of achieving high detection accuracy when compared to other deep learning-based intrusion detection approaches. Simultaneously, it has a faster detection rate, which effectively solves the real-time intrusion detection problem.

1. Introduction

Communication systems and network entrances are always faced with network attacks from the outside or even within their systems and are not like single attacks in the immature period of the network. Today, most of the intrusion behaviors are of various types and are developing in a mixed situation. Development is getting harder. According to the relevant literature, the Yahoo data breach caused a loss of 350 million US dollars and the "Bitcoin" breach caused a loss of about 70 million US dollars [1]. Based on intrusion behavior, the intrusion detection can be divided into network-based intrusion detection system (NIDS) and host-based intrusion detection system (HIDS) [2].

Various log files, disk resource information, and system information are used to detect intrusion behavior, while NIDS judges whether there is intrusion behavior by detecting the data packets in and out of the local network data flow. Machine learning, as a very popular algorithm tool in recent years, deserves experts and scholars to try its application in intrusion detection [3]. Especially in recent years, the application of machine learning in intrusion detection has appeared in people's field of vision; the support vector machine (SVM) to neural network (NN) to random forest (RF) has their applications in intrusion detection.

Machine learning has a long history in intrusion detection. In 2003, the literature [4] demonstrated that decision trees (DTs) could detect intrusions faster than the Snort detection engine [5] at the time. The proposed method of joint optimization of feature selection and SVM training model is demonstrated using the intrusion detection dataset. The results indicate that the joint optimization method outperforms the SVM in terms of performance and convergence speed. The literature [6] used support vector machines to identify intrusions and explored the real-time problem; however, the accuracy rate was low. The literature [7] suggested reducing dimensionality by principal component analysis (PCA) and then detecting intrusions with support vector machines (SVMs).

The self-optimization technology increases the classifier's accuracy and decreases training and testing time [8]. In 2019, the literature [9] developed an intrusion detection model based on an upgraded convolution neural network that has a high intrusion detection accuracy and true positive rate, while exhibiting a low false-positive rate. In the same year, Fernandez et al. proposed training an intrusion detection system using a feedforward fully connected deep neural network (DNN) (IDS). Due to the fact that DNN demonstrated robustness in the scenario of dynamic IP address allocation, the model they developed has a broader variety of real-world applications [10]. Still in 2019, the literature introduced the ICA-DNN intrusion detection model [11], which is based on ICA (independent component analysis) and DNN and has a higher feature learning capability than some shallow machine learning models. This has increased classification accuracy, but the algorithm's prediction time is not particularly tested and the model performs poorly in real time. According to the intrusion detection models proposed by the aforementioned scholars, it is discovered that the majority of research studies pay insufficient attention to real-time intrusion detection, while a few intrusion detection models with more in-depth real-time performance research suffer from low detection accuracy. To thoroughly investigate the real-time problem that is critical for intrusion detection and to ensure intrusion detection accuracy, this research offers the DT-PCA-DNN model. The trained DT is basically a series of if-else statements that handle huge batches of data quickly but with insufficient precision; the DNN network has a slow real-time performance but high precision when processing vast volumes of high-dimensional data. By combining the two, data are prefiltered using DT and then fed to DNN following PCA. The experimental results demonstrate that the model significantly accelerates training and detection while maintaining a high detection rate. Researchers are proposing different security protocols [12–15] for providing confidentiality and privacy against security attacks.

2. Basic Theory

2.1. Principal Component Analysis. PCA is a very commonly used linear dimensionality reduction algorithm as shown in Figure 1. It is generally used to extract the main components of high-dimensional data and simplify them into low-dimensional data, but the integrity of the data can be adjusted according to the requirements. Specifically, PCA hopes to map the original feature space into another orthogonal space and hopes to use a hyperplane that satisfies the nearest reconstruction and maximum separability to properly describe all the data in the dataset.

The projections of different points on the dataset on this hyperplane should be as far away as possible.

2.2. Decision Tree. The decision tree model is a tree structure that describes the classification of instances. It consists of nodes and directed edges. There are two types of nodes. Internal nodes represent a feature or attribute [12]. The decision tree starts from the root node and continuously splits according to the characteristics of the data, until all the data reach the leaf nodes. The attributes used as the basis for splitting must be discrete attributes, and for continuous attributes, they can be discretized according to experimental requirements. A sales office wants to judge whether the surveyed object has a house purchase demand based on the object's identity information, age, and whether he is married. The survey results are shown in Table 1.

From this, the corresponding decision tree can be generated as shown in Figure 2. When an object "ω" is a company employee, is married, and is 29 years old, it can be known that he has a housing demand according to the decision tree.

In the above example, the feature selection order of the survey objects is different and different decision trees can be generated. According to the selection of different splitting features, there are three judgment bases, namely, information gain, gain rate, and Gini index. The core of the ID3 (iterative dichotomiser 3) algorithm is to apply the information gain criterion on each node of the decision tree to select features, the C4.5 algorithm uses the information gain ratio to select features, and the CART (classification and regression tree) uses the Gini index as the selection feature in accordance. The decision tree pruning and specific feature selection will not be repeated due to space reasons. Reference [16] is sufficient.

2.3. Deep Neural Networks. A neural network is a large parallel interconnected network composed of simple adaptive units that can be used to simulate the interactive response of the biological nervous system to real-world objects [17], where machine learning is used to interact with neural networks in a broader sense.

In a neural network, the most fundamental structure is the neuron model, which is a simple unit by definition. Each neuron in a biological neural network is connected to other neurons, and when it is "stimulated," it releases neurotransmitters to the related neurons, altering their potential. When a neuron's potential crosses a "threshold" and the neuron becomes activated, or "excited," and begins delivering neurotransmitters to its associated neurons [18].

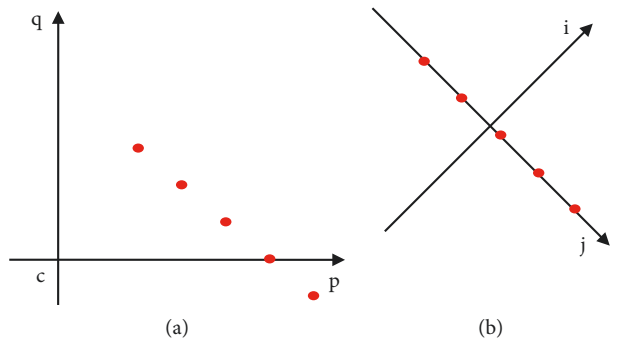

Figure 1: Diagram of data dimensionality reduction. (a) Before transformation. (b) After transformation.

Table 1: Respondent information and willingness.

Object	Identity	Age	Are you married	Whether to buy a house
A	Student	27	Yes	None
B	Staff	29	No	None
Γ	Staff	25	Yes	Have
Δ	Student	21	No	None
Λ	Staff	43	Yes	None

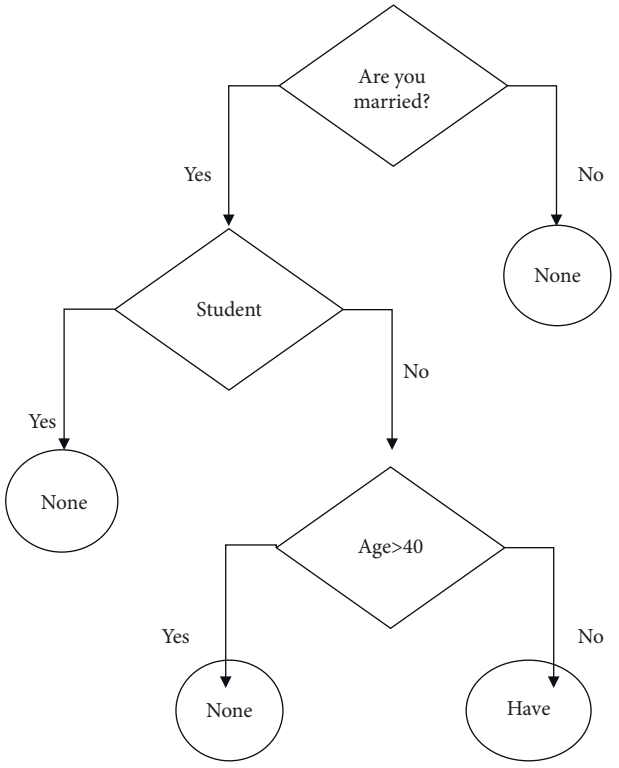

Figure 2: Decision chart of the respondent.

Foreign scholars abstracted the above situation in 1943 into the simple model depicted in Figure 3, dubbed the "M-P neuron model" [19].

In this model, ai denotes the input from the ith neuron, wi is the ith neuron's connection weight, and θ is the threshold. The neuron receives input signals from n other neurons. The signals are transmitted via weighted

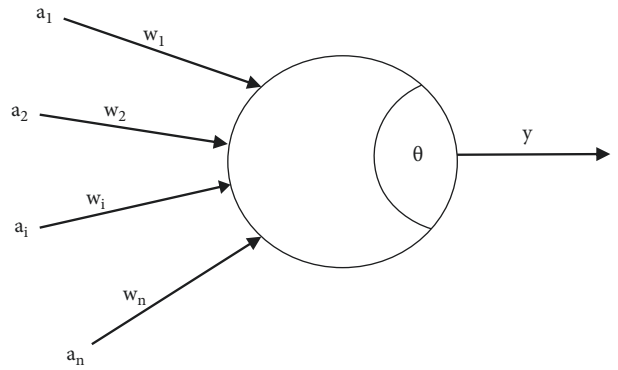

Figure 3: M-P neuron model.

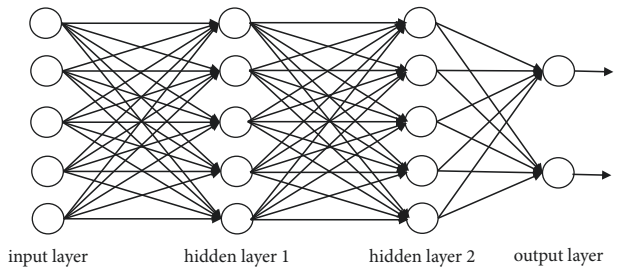

Figure 4: Double hidden layers of fully connected DNN.

connections, and neurons receive them. The resulting total input is compared, and the neuron's output y is obtained by processing the activation function $f(a)$ as specified in

$$o = f\left(\sum_{i=1}^{n} aiwi - \theta\right). \quad (1)$$

The sigmoid function, the tanh function, and the ReLU function are all frequently used activation functions [20]. A neural network is formed by connecting many neurons [21–23]. The term "deep neural network" refers to a neural network with more than two layers and more than two hidden layers. A neural network with input and output layers is only capable of solving linear problems. The hidden layer is introduced to address the nonlinear separable problem. Figure 4 illustrates a fully connected neural network, which means that any neuron in the preceding layer

must be connected to any neuron in the next layer. The neurons in the input layer accept only information and do not process functions. The neural network's learning process is fundamentally one of continuously adjusting the connection weights and thresholds of neurons in order to approach the output outcomes of the training samples. Among them, the most remarkable method is the error back-propagation (BP) algorithm, which is used for the majority of neural network training today.

3. System Design

The overall design of the system is shown in Figure 5. The first step is to preprocess the overall dataset. Data preprocessing first normalizes continuous data and secondly performs one-hot encoding on discrete valued data. The dataset after data preprocessing is divided into training dataset and test dataset.

The processed training dataset builds DT and trains DNN at the same time. PCA is unsupervised learning and does not need to be trained. After the DT and DNN training is completed, the DT-PCA-DNN model is established. At this time, the established intrusion detection model is tested with the preprocessed test dataset and the relevant parameters are adjusted and perfected. The trained DT is actually a series of if-else statements, processing large batches of data at high speed, but with insufficient processing precision; DNN network has poor real-time performance when processing large amounts of high-dimensional data, but high precision; PCA just happens to solve the problem caused by the high data dimension. Combining the three, firstly use DT to prefilter the data, then use PCA, and then send them to DNN for secondary classification, and use DT to filter out the intrusion data that is easy to judge and lighten the workload of DNN. PCA solves the problem that DNN network encounters high-dimensional data and slow training.

The three methods make up for the shortcomings of each other and ensure the accuracy of detection while having good real-time performance.

3.1. Data Processing. The data processing should be divided into two parts. First, the continuous data are normalized, and then the discrete valued data are encoded.

3.1.1. Data Normalization. In this study, the normalization process of the experiment adopts min-max normalization. The normalization method is to perform linear transformation on the original data and the transformed data falls within the [0, 1] interval. The transformation function used is as

$$x^* = \frac{x - \min}{\max - \min}. \quad (2)$$

Assume the dataset contains m items and each item has n-dimensional features, where x is the jth eigenvalue of the ith item prior to normalization and min is the jth dimension of the m items prior to normalization. min is the feature's minimum value, max is the feature's maximum value in the j-th dimension before normalization, and x^* is the feature's j-th dimension value in the ith piece of data after normalization.

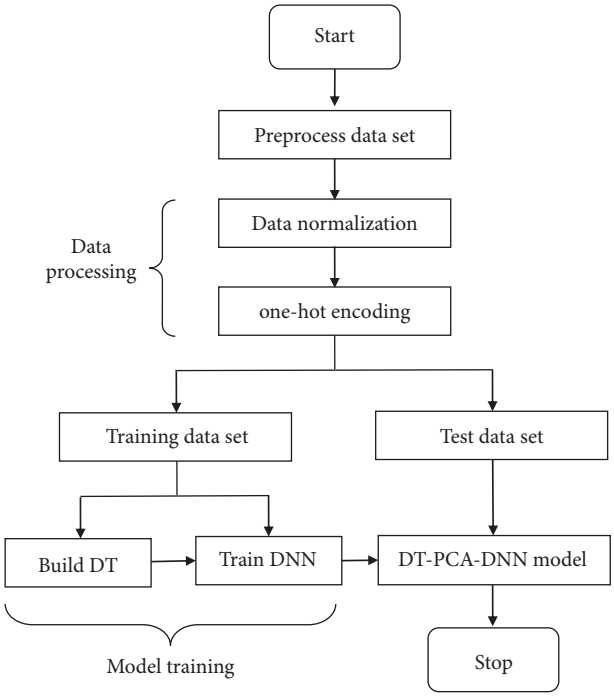

Figure 5: System flowchart.

3.1.2. One-Hot Encoding. For discrete data encoding, one-hot encoding, also known as one-bit efficient encoding, is utilised. N states are encoded using an N-bit status register; each state has its own register bit, and only one bit is valid at any time. Table 2 summarises the present sample set.

The sample feature dimension in Table 2 is 3, feature 1 has two values [0, 1], feature 2 has four values [0, 1, 2, 3], and feature 3 has three values [0, 1, 2].

Feature 1 has two values, so the encoding rule should be as follows:

(i) $0 \longrightarrow 10$

(ii) $1 \longrightarrow 01$

The corresponding feature 2 has four values, so the encoding rule should be as follows:

(i) $0 \longrightarrow 1000$

(ii) $1 \longrightarrow 0100$

(iii) $2 \longrightarrow 0010$

(iv) $3 \longrightarrow 0001$

The coding rule of feature 3 is the same as given above and will not be repeated.

The results of samples X, Y, and Z after one-hot encoding are shown in Table 3.

Table 2: Feature distribution of the sample set.

Sample	Feature 1	Feature 2	Feature 3
X	0	1	1
Y	1	0	2
Z	1	3	0

Table 3: One-hot encoded result of sample set.

Sample	Feature 1	Feature 2	Feature 3
X	10	0100	010
Y	01	1000	001
Z	01	0001	100

3.2. Model Training

3.2.1. Establishing DT. First, select the type of decision tree to be used because the information gain used by the ID3 algorithm has a preference for attributes with a large number of possible values, and the model used uses DT before the experimental data are dimensionally reduced. The data dimension is high, so this paper selects the ID3 algorithm. Followed by the depth of DT since the function of DT is not to identify as much intrusion data as possible but to misjudge average data as intrusion data as little as possible, the depth of DT should not be too deep. If the depth of DT is too deep, the accuracy of the first classification will be improved, but it has been judged as an entry. Invasive but average data will affect the final accuracy.

3.2.2. Training DNN. Because DNN requires a relatively large number of hidden layers to analyze high-dimensional data, the underfitting phenomena will be severe if the number of hidden layers is too low. As the number of hidden layers increases, the time spent training DNN grows exponentially, which is incompatible with the real-time needs of this work. When PCA pair data are introduced after the dimensionality reduction process, the connection between data feature dimensions and data redundancy is reduced, DNN training is faster, and DNN accuracy is ensured.

DNN uses the BP algorithm for training, ReLU as the activation function to simplify the calculation process of the neural network, and the "Adam" optimization algorithm, which occupies fewer resources and has a faster model convergence to shorten the training time.

3.2.3. DT-PCA-DNN Model Optimization. As shown in Figure 6, the preprocessed test dataset is first classified with the trained DT. Next, the data whose classification result is intrusion are judged as intrusion and stored in the temporary training sample. The information whose classification result is typical is removed from this DT classification. Given the label, prepare for the second judgment type of data. The DT layer is equivalent to a filter screen, which filters out the intrusion data easy to filter. Since the trained DT is a series of if-else statements, and the processing speed of large batches of data is extremely high, which significantly reduces the workload of DNN and improves the running speed of the algorithm.

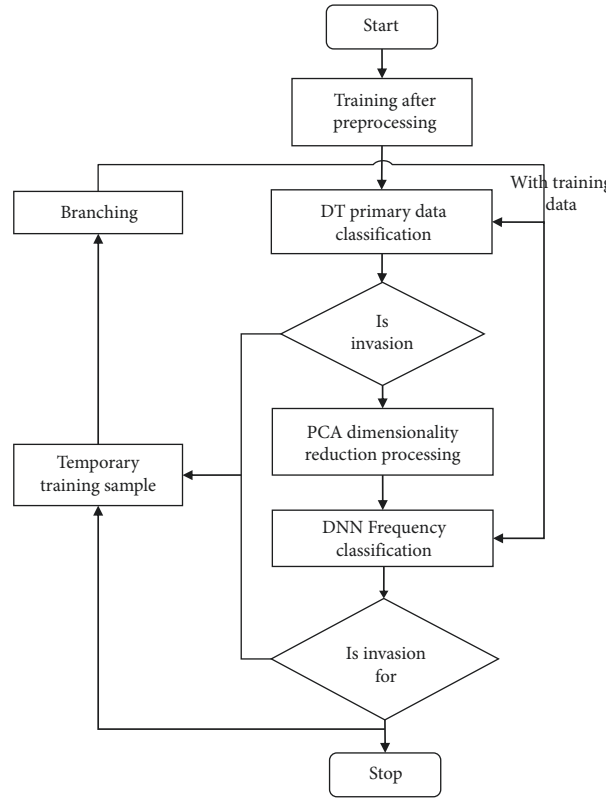

Figure 6: DT-PCA-DNN model optimization.

The second step is to perform PCA dimensionality reduction on the data judged by DT to be expected, but the labels have been removed. The trained DNN classifies the low-dimensional data output after PCA processing for the second time. If the classification result is an intrusion, the intrusion label is added, and the temporary training sample is stored. The standard classification result adds standard labels and stores temporary training samples. Since DT and DNN belong to supervised learning, the tags assigned to the data need to be used when using the brief training sample set for retraining. Since the intrusion detection process is carried out one by one, the method can quantify the comparison results between the original data type of the test dataset and the label added to the corresponding data during the detection process. After the quantified value is accumulated to the threshold set, the collected data can be used. Then, do a retraining fine-tuning of DT and DNN. After several fine-tuning, the designed model reaches the optimum.

4. Experimental Simulation

4.1. Dataset. The NSL-KDD [24] dataset was employed in this experiment, which augments the KDD 99 dataset. In comparison to the KDD 99 dataset, this dataset is devoid of duplicate records. The number of selected records is inversely related to the percentage of records in the original dataset, allowing for more efficient evaluation of the

developed model [25]. The training set has 125,937 items while the test set contains 22,544 items. Table 4 details the various data kinds.

The NSL-KDD dataset contains 41 features, which are classified into four major feature categories: basic TCP connection features, operating features on hosts, time-based network traffic statistical features, and host-based network traffic statistical features. The first three of the 41 features are described in the following. The types are distinct features and include protocol type (there are three types of protocols: TCP, UDP, and ICMP), service (there are 70 values in the training set and 64 in the test set), take two (big value), and flag (connection normal or error status, a total of 11 values). After normalizing the data, one-hot encoding is conducted. The data dimension increases to 43 after encoding the protocol type, then to 112 after encoding the service, and finally to 122 after encoding the flag. After one-hot encoding, the final NSL-KDD dataset has a data dimension of 122.

4.2. Metrics. First, the confusion matrix is listed as shown in Table 5. TP represents the number of data pieces whose real data type is normal. The model prediction result is still normal; TN represents the number of data pieces whose real data type is an intrusion. The model prediction result is also intrusion. FP indicates the number of data pieces whose real data type is an intrusion. Still, the model prediction result is normal. FN represents the number of data pieces whose real data type is normal, but the model prediction result is an intrusion. Of course, the size of different data bars is not enough as a standard for evaluating the experimental results. Therefore, a relatively reasonable evaluation standard is established based on the above parameters: the accuracy rate (AC), detection rate (DR), precision rate (PR), and false alarm rate (FAR), and the definitions are as follows:

$$\begin{aligned} \mathrm{AC} &= \frac{\mathrm{TP}+\mathrm{TN}}{\mathrm{TP}+\mathrm{FP}+\mathrm{FN}+\mathrm{TN}}, \\ \mathrm{DR} &= \frac{\mathrm{TP}}{\mathrm{TP}+\mathrm{FN}}, \\ \mathrm{FAR} &= \frac{\mathrm{FP}}{\mathrm{FP}+\mathrm{TN}}, \\ \mathrm{PR} &= \frac{\mathrm{TP}}{\mathrm{TP}+\mathrm{FP}}. \end{aligned} \tag{3}$$

4.3. Parameter Setting. After preprocessing the data, including one-hot encoding and normalization, all data values are located in the interval [0, 1]. After discretizing each dimension of the data with 0.5 as the standard, we use DT to perform the first test on all training data. For the secondary screening, the main parameters of the DT used are shown in Tables 6–8 and then the PCA dimensionality reduction is carried out. Because the designed system is linear, all parameters can be obtained one by one by fixing other parameters to obtain the optimal parameters.

Table 4: Data distribution of NSL-KDD dataset.

Type		The amount of training set data	Test set data volume
Normal		66945	9641
Attack	DoS	44623	6758
	U2R	48	187
	R2L	886	2247
	Probe	10649	2148
Total		123151	20981

Table 5: Data confusion matrix.

Confusion matrix		Actual value	
		Normal data	Intrusion data
Predictive value	Normal data	TN	FN
	Intrusion data	FP	TP

Table 6: DT main parameters.

Main parameters	Value
Criterion	Entropy
Splitter	Best
max_depth	5
random_state	392

Table 7: PCA main parameters.

Main parameters	Value
*n*_components	11
Whiten	True
svd_solver	Auto

Table 8: DNN main parameters.

Main parameters	Value
hidden_layer_sizes	[140, 70]
Activation	ReLU
Solver	Adam

For Criterion (attribute segmentation criterion), the value is a string type. There are two criteria to choose from: "gini" and "entropy." For Splitter (segmentation point), the value is a string type; there are two standards to choose from, "best" and "random," where "best" means that in all features finding the optimal segmentation point in the "random" means to find the optimal segmentation point in the randomly selected part of the features—max_depth (the constructed decision tree), which can be an integer or none. max_features is the number of features to consider when finding the best segmentation. random_state (multiple states used to generate random numbers) can be an integer, an instance of random state, or none. Experiments have shown that the best effect is achieved when the value is 392.

*n*_components (feature dimension after dimension reduction) can be the number of dimensions reduced or the percentage of data retained; whiten (whether whitening) reduces the correlation between features and all features

have the same variance; svd_solver (singular value decomposer) is a string when its value is "auto," and certain conditions are met, the complete singular value decomposition function is called hidden_layer_sizes (hidden layer sizes), tuple type. The number of hidden layers and the number of neurons in the hidden layer are determined by adjusting this value. Two hidden layers are introduced here, with 140 neurons in the first layer and 70 neurons in the second layer; activation is the activation function; solver (weight optimization function) is selected by selecting different strings of the corresponding weight optimization function.

4.4. Experimental Results. The experiment uses a Windows10 system and 64 bit operating system, the processor version is Intel® CoreTMi7-9750H CPU@2.60 GHz, the total physical memory is 16.0 GB, the development language is Python3.5, and the software package used is sklearn.

4.4.1. Experiment 1. This experiment mainly studies the detection time of binary classification, the real-time problem of detection under binary classification. This experiment primarily compared the two-class prediction accuracy and training time of FC [13], DT, PCA-DNN, EDF [20], CNN [26], and DT-PCA-DNN models. To reflect the characteristics of DT-PCA-DNN, the test data used are all the data in the NSL-KDD test dataset. For the convenience of observation, Figure 7 is obtained from Table 9. In the figure, because the FC training time is too long, the impact on the selected vertical axis interval is too significant, so it is not listed.

Observing Figure 7, we can see that the accuracy AC of PCA-DNN and FC is the same, but the training time of FC is much higher than that of PCA-DNN, the prediction time is slightly longer, and the real-time detection is poor. On the other hand, the training time of the EDF algorithm is marginally more extended than that of PCA-DNN, and the accuracy AC is the same as that of PCA-DNN.

The training time of the CNN algorithm is as long as 90 s, and the accuracy rate is slightly lower than that of EDF and PCA-DNN, which is inferior to both. On the other hand, although the training speed of DT is breakneck, the accuracy rate is four percentage points lower than that of EDF and PCA-DNN.

Compared with PCA-DNN without DT, DT-PCA-DNN takes 1.32 s longer to train 125973 pieces of data and takes about 10 ms more to predict 22544 pieces of data, but the accuracy AC has improved by nearly ten percentage points remarkably. The introduction of DT has minimal impact on training time and prediction time but significantly improves prediction accuracy.

4.4.2. Experiment 2. This experiment mainly studies the five-category detection time of the DT-PCA-DNN model, the real-time detection problem under five categories. Mark normal samples as 0, DoS samples as 1, probe samples as 2, U2R samples as 3, and R2L samples as 4. The analysis in

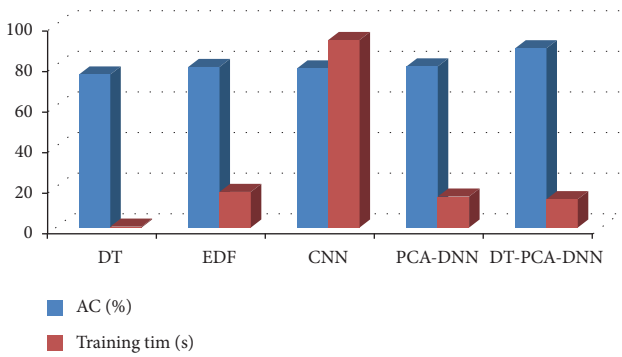

Figure 7: Results of experiment 1.

Table 9: Results of experiment 1.

Algorithm	AC%	DR%	Training time per second	Prediction time/ms
FC	79.49	N/A	1856.31	221.05
DT	75.68	65.74	0.67	58.84
EDF	79.32	64.33	17.79	N/A
CNN	78.63	68.77	92.64	N/A
PCA-DNN	79.61	66.69	15.55	47.84
DT-PCA-DNN	88.64	84.56	14.15	57.86

Table 10: Total results of experiment 2.

Algorithm	Five classification training time/s	Total accuracy/%
DT	0.67	78.82
EDF	41.31	87.28
CNN	93.39	87.01
PCA-DNN	14.48	77.06
DT-PCA-DNN	17.36	83.29

Table 11: Five classification results of experiment 2.

Algorithm	Evaluation criteria	Normal	DoS	Probe	R2L	U2R
DT	PR	67.01	91.84	26	71.49	52
	DR	95.31	84.18	0.41	61.99	4
	FAR	34.38	3.15	0.16	2.62	0.04
EDF	AC	91.62	98.9	88.15	59.59	15.39
CNN	AC	92.56	98.47	92.58	35.5	26.56
PCA-DNN	PR	64.78	95.62	96.67	82.45	0
	DR	98.19	75.48	16.08	67.5	0
	FAR	39.24	1.51	0.08	1.70	0
DT-PCA-DNN	PR	71	92.21	91.09	78.92	0
	DR	98.81	83.26	36.95	61.66	0
	FAR	26.11	4.1	0.39	1.5	0

Table 10 shows that the speed advantage of DT-PCA-DNN in the five classifications is undeniable. Still, the overall accuracy is slightly inferior to EDF and CNN, and we compare DT and PCA-DNN. However, the training time is relatively short. The overall accuracy is low, and the performance is poor. Comparing PCA-DNN and DT-PCA-

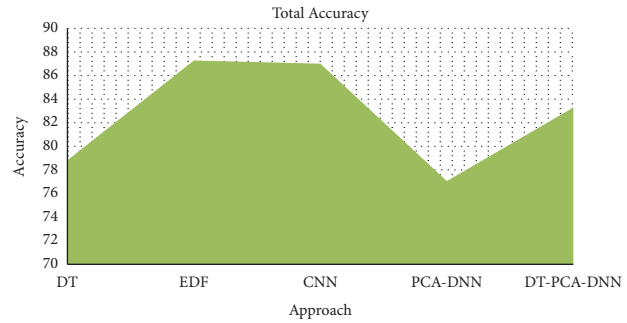

Figure 8: Comparison of accuracy of the model.

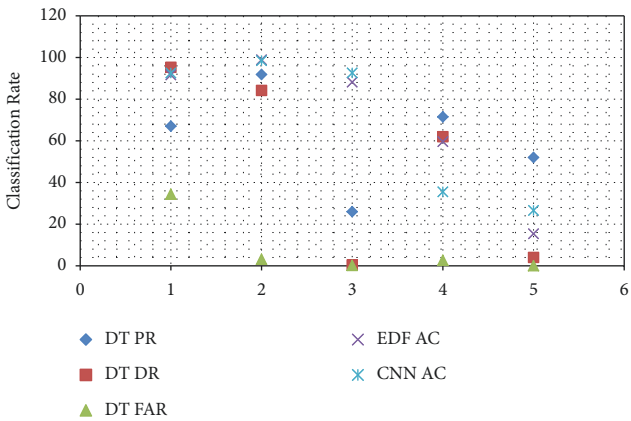

Figure 9: Classification performance over different attack scenarios for benchmark algorithm.

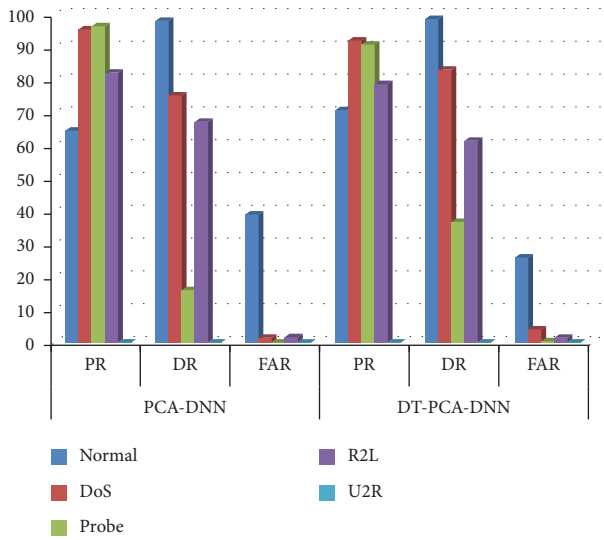

Figure 10: Classification performance over different attack scenarios for the proposed algorithm.

DNN in the five-category experiment, the training time is 3 s longer. The accuracy rate is improved by six percentage points, proving that the introduction of DT does not cause much time while ensuring the accuracy rate loss.

The analysis of Table 11 and Figures 8–10 shows that DT-PCA-DNN may have processed part of the data during DT prescreening, resulting in no U2R results (small U2R sample size).

The advantages of DT-PCA-DNN are mainly reflected in the ability to recognize R2L, but because of its small proportion in the dataset.

As a result, the overall accuracy rate is lower than EDF and CNN. At the same time, the model has a relatively high false alarm rate for normal data when the detection rate is relatively high. This is a problem that needs to be pointed out.

5. Conclusion

The DT-PCA-DNN intrusion detection model described in this study greatly improves the training and detection speed while preserving accuracy. The model employs DT to do a preliminary screening of the preprocessed data to be detected before employing PCA as an input to perform a secondary judgment via DNN. The addition of DT causes a small increase in training time but a large boost in accuracy. Simultaneously, DT prescreening reduces future DNN burden, which has a considerable effect on overall training pace. The following study focus is mostly on overcoming the issue of the DT-PCA-DNN model having a high false alarm rate for normal data in the five-classification experiment while also increasing the DT-PCA-DNN model's five-classification capability. [27].

Data Availability

The data used to support the findings of this study are available from the author Kusum Yadav upon request (kusumasyadav0@gmail.com).

Conflicts of Interest

The authors declare that they have no conflicts of interest.

Authors' Contributions

Shoayee Dlaim Alotaibi proposed the method, Kusum Yadav wrote the paper, Arwa Naser Mohammed Aledaily developed the methodology, Luluah Dhaifullah Al-Quwai proofread the paper, Alaa Kamal Yousef Dafhalla simulated the work, and Shahad Almansour and Velmurugan Lingamuthu analyzed the results.

References

[1] I. Sembiring, "Implementation of honeypot to detect and prevent distributed denial of service attack," in *Proceedings of the 3rd International Conference on Information Technology, Computer, and Electrical Engineering (ICITACEE)*, pp. 345–350, Semarang, Indonesia, October 2016.

[2] A. Phadke, M. Kulkarni, P. Bhawalkar, and R. Bhattad, "A review of machine learning methodologies for network intrusion detection," in *Proceedings of the2019 3rd International Conference on Computing Methodologies and Communication (ICCMC)*, pp. 272–275, Erode, India, March 2019.

[3] K. Shaukat, S. Luo, V. Varadharajan, I. A. Hameed, and M. Xu, "A survey on machine learning techniques for cyber

security in the last decade," *IEEE Access*, vol. 8, pp. 222310–222354, 2020.

[4] G. Vigna, E. Jonsson, and C. Kruegel, Eds., *RAID 2003, LNCS 2820*, pp. 173–191, c Springer-Verlag, Berlin Heidelberg, 2003.

[5] M. Crosbie and G. Spafford, "Defending a Computer System Using Autonomous Agents," Technical Report No. 95-022, Department of Computer Sciences, Purdue University, West Lafayette, Indiana, March 1996.

[6] Y. Li, J. Xia, S. Zhang, J. Yan, X. Ai, and K. Dai, "An efficient intrusion detection system based on support vector machines and gradually feature removal method," *Expert Systems with Applications*, vol. 39, no. 1, pp. 424–430, 2012.

[7] N. P. Moorthi and V. Mathivanan, "Hybrid optimization for feature selection in opinion mining," *International Journal of Engineering & Technology*, vol. 7, no. 1.3, p. 112, 2017.

[8] G. Liu, Z. Yi, and S. Yang, "A hierarchical intrusion detection model based on the PCA neural networks," *Neurocomputing*, vol. 70, no. 7-9, pp. 1561–1568, 2007.

[9] J. Cao, C. Wu, L. Chen, H. Cui, and G. Feng, *Hindawi Computational Intelligence and Neuroscience*, vol. 2019, Article ID 2060796, 12 pages, 2019.

[10] L. Ashiku and C. Dagli, "Network intrusion detection system using deep learning," *Procedia Computer Science*, vol. 185, pp. 239–247, 2021.

[11] Y. Gu, B. Zhou, and J. Zhao, "PCA-ICA ensembled intrusion detection system by pareto-optimal optimization," *Information Technology Journal*, vol. 7, no. 3, pp. 510–515, 2008.

[12] M. Soni and D. K. Singh, "privacy preserving authentication and key management protocol for health information system," *Data Protection and Privacy in Healthcare: Research and Innovations*, CRC Publication, vol. 37, , 2021.

[13] M. Soni and D. K. Singh, "LAKA: Lightweight Authentication and Key Agreement Protocol for Internet of Things Based Wireless Body Area Network," *Wireless Personal Communication*, 2021.

[14] M. Soni and D. K. Singh, "Blockchain Implementation for Privacy Preserving and Securing the Healthcare Data," in *Proceedings of the 2021 10th IEEE International Conference on Communication Systems and Network Technologies (CSNT)*, pp. 729–734, Bhopal, India, June 2021.

[15] M. Soni, G. Dhiman, B. S. Rajput, R. Patel, and N. K. Tejra, "Energy-Effective and Secure Data Transfer Scheme for Mobile Nodes in Smart City Applications," *Wireless Pers Commun*, 2021.

[16] R. Nian, G. Ji, and M. Verleysen, "An unsupervised Gaussian mixture classification mechanism based on statistical learning analysis," in *Proceedings of the 2008 Fifth International Conference on Fuzzy Systems and Knowledge Discovery*, pp. 14–18, Shandong, China, October 2008.

[17] R. Aggarwal and Y. Song, "Artificial neural networks in power systems. Part 1: general introduction to neural computing," *Power Engineering Journal*, vol. 11, no. 3, pp. 129–134, June 1997.

[18] Z.-H. Zhou, *Machine Learning*, Springer Nature Singapore Pte Ltd, Singapore, 2021.

[19] V. R. Sargsyan, "Formation of human higher nervous activity and new biological theories, HSOA journal of brain & neuroscience research, sargsyan VR," *J Brain Neursci*, vol. 2, p. 004, 2018.

[20] S. Albawi, T. A. Mohammed, and S. Al-Zawi, "Understanding of a convolutional neural network," *2017 International Conference on Engineering and Technology (ICET)*, in *Proceedings of the 2017 International Conference on Engineering and Technology (ICET)*, pp. 1–6, Antalya, Turkey, August 2017.

[21] V. K. Gupta, S. K. Shukla, and R. S. Rawat, "Crime tracking system and people's safety in India using machine learning approaches," *International Journal of Modern Research*, vol. 2, no. 1, pp. 1–7, 2022.

[22] P. K. Vaishnav, S. Sharma, and P. Sharma, "Analytical review analysis for screening COVID-19 disease," *International Journal of Modern Research*, vol. 1, no. 1, pp. 22–29, 2021.

[23] I. Chatterjee, "Artificial intelligence and patentability: review and discussions," *International Journal of Modern Research*, vol. 1, no. 1, pp. 15–21, 2021.

[24] UNB, "NSL-KDD Data Set," https://www.unb.ca/research/iscx/dataset/iscx-NSL-KDDdataset.html.

[25] T. Brugger, "KDD Cup'99 Dataset (Network Intrusion) Considered Harmful," KDNuggets, Sept. 2007, https://www.kdnuggets.com/news/2007/n18/4i.html.

[26] X. Gao, C. Shan, C. Hu, Z. Niu, and Z. Liu, "An adaptive ensemble machine learning model for intrusion detection," *IEEE Access*, vol. 7, pp. 82512–82521, 2019.

[27] Q. Qin, K. Poularakis, K. K. Leung, and L. Tassiulas, "Line-speed and scalable intrusion detection at the network edge via federated learning," in *Proceedings of the 2020 IFIP Networking Conference (Networking)*, pp. 352–360, Paris, France, June 2020.

Hindawi
Mathematical Problems in Engineering
Volume 2022, Article ID 4008472, 13 pages
https://doi.org/10.1155/2022/4008472

Research Article

Accessibility of Rehabilitation Facility: Evaluation Based on Spatial Big Data in Xiamen

Tingting Qiu,[1] **Daliang Zhou**,[2] **Jie Wang**,[3] **and Velmurugan Lingamuthu**[4]

[1]*College of Physical Education, Huaqiao University, Quanzhou 362021, China*
[2]*School of Physical Education, Nanjing Xiaozhuang University, Nanjing 211171, China*
[3]*School of Continuing Education, Wenzhou Business College, Wenzhou, China*
[4]*Department of Computer Science, Ambo University, Ambo, Ethiopia*

Correspondence should be addressed to Jie Wang; jie.wang.13@outlook.com and Velmurugan Lingamuthu; velmurugan.lingamuthu@ambou.edu.et

Received 13 March 2022; Revised 6 April 2022; Accepted 13 April 2022; Published 7 May 2022

Academic Editor: Amandeep Kaur

With the help of spatial calculation and numerical analysis, this paper reveals the spatial distribution of rehabilitation infrastructures and the accessibility difference in the city Xiamen. The calculation of Moran's *I*, *Z* value, and *P* value are, respectively, −0.229787, −0.122751, and 0.902304 for health facilities and −0.159235, 0.186166, and 0.852315 for fitness facilities. Such calculation results indicate an uneven pattern and varied accessibility numerical values. The reasons for this influence are diverse, but it is worth noting that the two-step floating catchment area (2SFCA) calculation shows that compared to fitness facilities, the standard deviation of accessibility numerical value of health facilities decreased significantly, which indicates that the accessibility of health service facilities is becoming better, while the change of accessibility of fitness facilities is not obvious. It is pointed out this is due to society's insufficient attention and education on daily health. For better rehabilitation under the pandemic, the importance of fitness facilities should be noticed.

1. Introduction

Currently, with the spread of COVID-19, improving individual immunity is one of the main measures to fight the virus [1]. At the same time, mankind is also facing the pressure of climate change and energy transition [2–5]. Rehabilitation infrastructures such as stadiums play an important role in improving the immunity of individuals, as well as providing important physical facilities for the recovery and rehabilitation of people infected with COVID-19 [6, 7]. Over the past two years, China's COVID-19 prevention efforts have added a lot of rehabilitation infrastructure, both for physical health and routine medical care. A large number of rehabilitation facilities or buildings are also facing new requirements for siting, that is, in a more environmentally friendly way. Specifically, future rehabilitation facilities will need to be built more low-carbon to reduce pressure on energy and transport systems. This is because the starting point of the construction of rehabilitation facilities is to provide convenient and easily accessible services for people, which in essence requires less transportation time. Shorter travel time also means lower carbon emissions. Therefore, the Chinese government has put "accessibility" and "low-carbon (or sustainability)" as the requirements for future rehabilitation facility construction.

The spatial distribution and accessibility of rehabilitation facilities are directly related to the opportunity and convenience of residents to obtain health services and affect the health level and quality of life of residents. The lower accessibility of public leisure and sports facilities will increase the time and cost for residents to obtain health. Especially for vulnerable groups, it will not only increase their living burden but also may reduce the frequency of their access to health, affecting their quality of life [8–12]. In recent years, China's investment in the health service industry continues to increase, but due to the acceleration of urbanization, the

new population in medium-sized and large cities continues to increase, making the existing health resources difficult to meet the needs of citizens, and the contradiction between supply and demand becomes more prominent. Therefore, how to carry out accessible and sustainable planning and layout of rehabilitation facilities, improve their accessibility, and resolve the pressures on energy systems has become the research purpose of this paper. According to Wu and Lu [13], the rehabilitation facilities studied in this paper are limited to medical and health facilities and sports and fitness facilities closest to residents' health among rehabilitation facilities. It mainly includes: (1) large and medium-sized rehabilitation facilities within the street scope, such as large and medium-sized hospitals, parks, and squares; (2) health facilities residents can access around the living area, such as clinics, pharmacies, fitness clubs, and so on; and (3) public welfare health and sports centres at all levels, such as public health service centres (stations) and public sports centres (as shown in Tables 1 and 2).

Research on accessibility needs to make use of the concept proposed by Hansen [14]. Accessibility refers to the opportunity for interaction between nodes in the transportation network. Following this concept, there are abundant research on accessibility at present, among which spatial accessibility is the most noted. Spatial accessibility takes distance (space distance or time) as the influence factor and measures the convenience of obtaining facilities and services through relevant calculation models. It can intuitively reveal the balance of spatial distribution of facilities and identify the area of facilities' supply and configuration. At present, most of the emerging research attempts to integrate big data, mobile Internet, and other new technologies. The reason is that a large number of real-time, multidimensional, and spatiotemporal observation data in cities are increasing, such as network review data, POI data, mobile phone positioning data, real-time internet map data, and so on. Compared with traditional data, POI data has the advantages of large data volume, strong timeliness, and high accuracy, which greatly improves the convenience and scientificity of relevant research [15]. For example, Hou and Chen [16] believe that land use data are greatly limited by timeliness, so it adopts POI data provided by Baidu and the kernel density method to consider commercial-road intersection points, which ultimately improves the accuracy of identifying commercial centres in Nanjing. Wang et al. [17] used POI data to study the distribution of stadiums and gymnasiums in Nanjing, found that the accessibility and fairness indices of public sports facilities in Nanjing differed greatly, and verified this conclusion with LISA and Moran index. The analysis of W. Wang and M. Wang [18] and other studies on finance, tourism, and rural settlements also used POI data and related concepts of geographical accessibility, which ultimately provided a good reference for local policymaking. The use of such emerging data sources makes it possible to study the situation of individuals or populations at microcosmic and spatial scales, including their daily behaviour, disease or health status, choice of health services, and relationship with various environmental factors.

There are many research results available in this field, and the techniques used are sufficiently diverse. However, due to differences in time and space, it is not known whether the research results obtained are applicable to some rapidly developing regions, such as the chosen study area Xiamen in this paper. Xiamen city is located in east China and southeast of Fujian Province. From the island (Xiamen Island), Gulangyu island, west Coast Haicang Peninsula, North Jimei Peninsula, East Coast Xiang'an Peninsula, Dadeng Island, Xiaodeng Island, inland Tongan, Jiulong River, and other components. By 2020, Xiamen has six districts under its jurisdiction, with a total land area of 1,700.61 square kilometres and a sea area of more than 390 square kilometres. The built-up area covers 397.84 square kilometres (Figure 1). According to the 7th National Census, Xiamen has a permanent population of 5,163,970 as of midnight on November 1, 2020. In 2020, Xiamen achieved a GDP of 638.402 billion RMB. Xiamen, as an excellent tourist city in China, is rich in tourist resources. In 2019, it received 100,128,700 domestic and foreign tourists, an increase of 12.5% over the previous year. However, Xiamen, as an important coastal city in China, is also one of the regions where the virus is most likely to spread, despite its economic growth and rapid urbanization due to its abundant tourism resources. The health of residents in the region plays an important role in the prevention and control of the epidemic in inland China and other neighbouring provinces, which is why Xiamen has become one of the regions with the most health policies for residents. In the plans of livelihood facilities announced in 2020, there are four major livelihood plans: Xiamen's near-term construction plan for educational facilities (2019–2023), Xiamen's medical and health facilities plan (2020–2035), Xiamen's recreation and sports facilities plan, and Xiamen's regional tourism plan. Among them, the concept of "Healthy Xiamen" is emphasized in the planning of health and sports facilities.

Considering the importance of Xiamen, we believe that it is necessary to investigate the situation of rehabilitation facilities in this area with spatial methods. Previous studies have proved that advanced big data technologies based on Python and other platforms provide great data collection assistance for spatial analysis. This enables our research to refer to previous studies, such as Hou and Chen [16] and Wang et al. [17]. This paper therefore argues that by conducting a study of rehabilitation facilities closely related to residents' health in this representative region, the spatial distribution and accessibility differences of rehabilitation services can be visually revealed, so as to provide a reference for policymakers to optimize the layout. The second part of this paper is the introduction of our spatial analysis methods; the third part is the analysis and discussion of this paper; and the fourth part is the conclusion.

2. Materials and Methods

2.1. Spatial Autocorrelation Method. Common methods to measure spatial clustering characteristics of geographic point data include the spatial autocorrelation method and variation coefficient of the Voronoi polygon area, among

Table 1: Quantity distribution of rehabilitation facilities in Xiamen.

Districts	Medical	Sports	Total	Proportion (%)
Siming District	1,885	1,499	3,384	31.42
Haicang District	579	399	978	9.08
Huli District	1,263	802	2,065	19.18
Jimei District	1,057	789	1,846	17.14
Tong'an District	1,016	493	1,509	14.01
Xiang'an District	617	370	987	9.17
Total	6,417	4,352	10,769	100.00

Table 2: Components of rehabilitation facilities in Xiamen.

Classifications	Subclassifications	Quantity	Total	Proportion (%)
Medical facilities	Emergency centre	7	6,420	59.49
	Disease prevention agency	10		
	Health care service places	1,504		
	Medical and health care sales shop	2,600		
	Clinic	1,216		
	Specialized subject hospital	771		
	The general hospital	183		
	Other medical facilities	129		
Sports facilities	Vacation and health resort	78	4,372	40.51
	Large outdoor stadium	13		
	Park plaza	31		
	Sports and leisure service places	720		
	Leisure and rehabilitation places	523		
	Commercial fitness facilities	1,205		
	Sports venues	1,648		
	Other sport-related facilities	154		

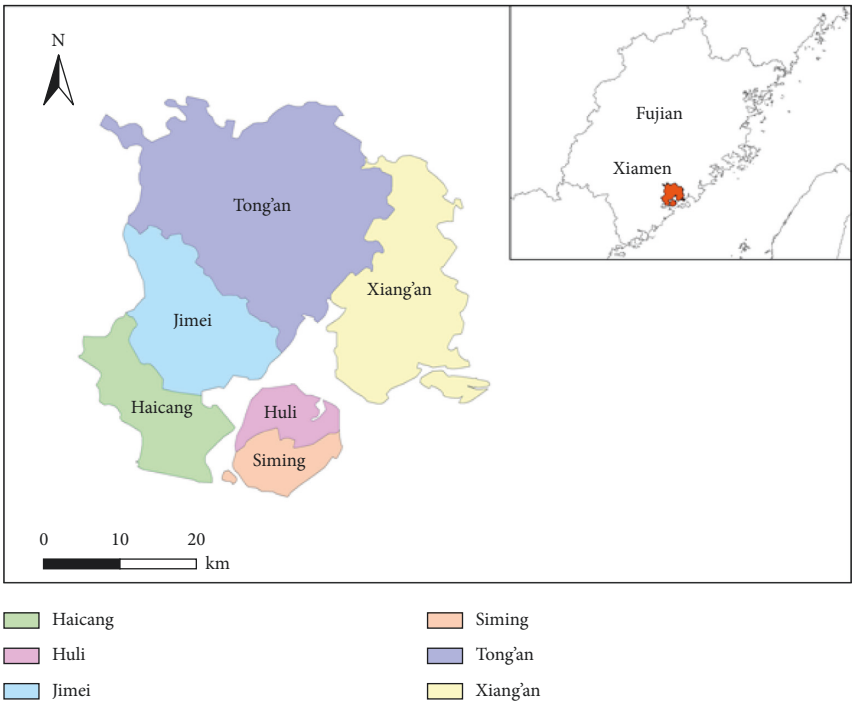

Figure 1: Location of Xiamen city.

which the spatial autocorrelation method is a relatively mature research method [19, 20]. The spatial autocorrelation method is used as an indicator for exploratory spatial analysis to test spatial correlation and agglomeration problems, which can reflect the similarity between individual geographical units and neighbouring geographical units throughout the study area. As the main objective of this study is to provide statistics on the accessibility of urban recreational and sports facilities to the residents of Xiamen, the Moran index of urban facilities using the spatial autocorrelation method is the simplest and most accurate way to calculate the relationship between spatial distance and the influence of facilities. In order to analyze the spatial clustering degree of public recreation and sports facilities in Xiamen, Moran's I index, a commonly used global autocorrelation index, was used to test whether the public recreation and sports facilities in Xiamen had the clustering characteristics as a whole. The following calculation formula of Moran's I index is adapted from Xue et al. [21]:

$$\text{Moran's } I = \frac{\sum_{i=1}^{n}\sum_{j=1}^{n}(Xi-\overline{X})(Xj-\overline{X})}{S^2\sum_{i=1}^{n}\sum_{j=1}^{n}w_{ij}}, \tag{1}$$

where $S^2 = 1/n\sum_{i=1}^{n}(Xi-\overline{X})^2$; $\overline{x} = 1/n\sum_{i=1}^{n}x_i$; Xi and Xj are the numbers of public rehabilitation facilities in the i and j streets respectively; Wij represents the spatial weight matrix of each street; and n is the total number of streets.

The value range of Moran's I is [−1, 1]. If global Moran's $I > 0$, it indicates that there is a spatial positive correlation between the research objects, that is, the values of the research objects in space are high-high adjacent or low-low adjacent. Moran's $I < 0$ indicates that there is a spatial negative correlation phenomenon, that is, the value distribution of the research object is high-low adjacent in space. Moran's $I = 0$ indicates that there is no correlation between research objects. According to the above analysis, this paper uses GeoDa to calculate Moran's I of "medical and health" facilities and "sports and fitness" facilities in Xiamen.

2.2. Kernel Density. Spatial autocorrelation analysis can only distinguish the spatial clustering degree of geographic point data but cannot identify its distribution. According to the research findings of scholars, the kernel density method is more advantageous than other density expression methods (such as Voronoi diagram density, etc.) in the characterization of POI characteristics due to the location influence of Tobler's First Law of Geography. In view of this, the kernel density estimation method is used to analyze the spatial distribution of public recreation and sports facilities in Xiamen. The kernel density method was first proposed by Rosenblatt in 1995 and Emanuel Parzen in 1962. The calculation principle is to obtain the graph of the continuous change of the density of the research object by assigning different weights to the research elements. According to Bai et al. [22], its expression is

$$f_n(x) = \frac{1}{nh}\sum_{i=1}^{n}K\left(\frac{x-x_I}{h_n}\right), \tag{2}$$

where n is the number of samples, h_n is the bandwidth, and $K(X - x_i/h_n)$ is the kernel function. In this paper, Kernel density estimation under the Spatial Analyst tool of ArcGIS 10.2 is used to measure and analyze the Kernel density of Xiamen's public rehabilitation facilities, and finally, the spatial distribution characteristics of Xiamen's public recreation and sports facilities are obtained.

2.3. The Two-Step Floating Catchment Area (2SFCA) Method. The two-step floating catchment area method calculates the accessibility of public service facilities in two steps based on supply place and demand place. In terms of calculating accessibility, 2SFCA has been proved to be a spatial computing method with high accuracy. We use it mainly because the purpose of this article fits the concept of 2SFCA. Specifically, the attenuation of facility service capacity with distance is considered, and the effective search radius is increased [23]. The specific calculation steps are as follows:

Step 1: Take the centre of gravity of each supply place j, select or assume a space distance d_0, form its space scope, and calculate the number of demanders at each demand point k within this scope. By referring to the Gauss equation and adding up the weights, the number of potential demanders of supply place j can be obtained, and then the area of supply place is divided by the total number of potential demanders to calculate the supply-demand ratio R_j as follows:

$$R_j = \frac{S_j}{\sum_{k\in\{d_{kj}\leqslant d_0\}}G\left(d_{kj},d_0\right)P_k}, \tag{3}$$

where d_{kj} is the distance between demand point k and supply point j, d_0 is the space distance set by the supply ground, P_k is the number of demanders (i.e., $d_{kj}\leqslant d_0$) in the search area, S_j is the total supply of point j, and $G(d_{kj}, d_0)$ is the distance decay function of the influence of point source elements on space elements, namely Gaussian equation, and the calculation method is shown in the following equation:

$$G\left(d_{kj},d_0\right) = \begin{cases} \dfrac{e^{-\frac{1}{2}\times\left(\frac{d_{kj}}{d_0}\right)^2} - e^{-\frac{1}{2}}}{}, & d_{kj}\leqslant d_0 \\ 1 - e^{-\frac{1}{2}}, & d_{kj} > d_0 \end{cases} \tag{4}$$

Step 2: For each demand place i, given space distance d_0, its space scope is formed. The supply-demand ratio R_l of supply place l falling within this scope is weighted by the Gaussian equation, and then the weighted ratio is added up to obtain the spatial accessibility A_i^F of demand place i.

$$A_i^F = \sum_{l\in\{d_{il}\leqslant d_0\}}G\left(d_{kj},d_0\right)R_l, \tag{5}$$

where R_l is the supply-demand ratio of supply point i in the search area ($d_{il} \leqslant d_0$) of demand place (l) and d_{il} is the distance between the demand point i and the supply centre of gravity l. Other indicators are the same as equation (3). The larger A_i^F is, the more accessible it is. The spatial accessibility then was calculated by such Gaussian 2SFCA method. The two-step floating catchment area method can be interpreted as the number of rehabilitation facilities per capita in the research unit.

3. Results and Discussion

3.1. Overall Characteristics. In this paper, GIS spatial analysis was used to analyze the kernel density of 10,769 rehabilitation facilities in Xiamen. A total of 10,769 items of data in this paper were obtained from China AutoNavi Map by Python, and all data are open source. This method of data acquisition has been widely adopted by geographical literature in recent years, mainly because of its timeliness and accuracy. The present study followed Wang et al. [24] to realize the data acquisition from China AutoNavi Map. As shown in Figure 2, the calculation of Moran's I, Z value, and P value are, respectively, −0.229787, −0.122751, and 0.902304 for health facilities and −0.159235, 0.186166, and 0.852315 for fitness facilities. Such calculation results indicate an uneven pattern and varied accessibility numerical values. Apart from Moran's I, one of the main factors affecting the estimated kernel density is the distance threshold. After several tests, the distance threshold (bandwidth) was selected as 1 km to generate the kernel density distribution map of rehabilitation facilities in Xiamen (Figure 3). According to the analysis, the number of clustering areas of rehabilitation facilities in Xiamen are divided into five levels: extremely high density, high density, medium density, low density, and extremely low density. Among them, the intersection area of Huli District and Siming District belongs to extremely high-density and high-density area of quantity distribution. The agglomeration areas of urban business centres in other administrative regions, such as Haicang, Jimei, Tong'an, and Xiang'an, are high- and medium-density distribution areas of rehabilitation facilities. As the distance from the commercial centre increases, rehabilitation facilities outside the city are mostly distributed in low-density and extremely low-density areas. In general, the kernel density distribution of rehabilitation facilities in Xiamen is "high in the south and low in the north, high on the island, and low on the coast." There is a serious imbalance in spatial distribution, and the distribution of nucleus density of rehabilitation facilities on the island is much higher than that in inland areas.

Considering that rehabilitation facilities include medical and health facilities and sports and fitness facilities and the nature and spatial distribution of each type of facility are quite different, the accessibility results of these two types of rehabilitation facilities are analyzed.

4. Spatial Accessibility of Medical Type

4.1. Shortest Space Distance. The calculation results of spatial accessibility of medical and health facilities in urban areas of Xiamen are shown in Figure 4(a). The spatial distance between the centroid of each street and the point of public medical and health facilities in the main urban area of Xiamen is 0.261642~207.0575 km. Among them, Xinglin Station, Xiamen North Railway Station, Xiamen North Railway Station, Xiamen Gaoqi Station, and Xiamen Gaoqi International Airport have the shortest distance to public medical facilities, indicating that they have the best spatial accessibility. The accessibility to public medical facilities in Haicang, Jimei, Tong'an, and the northern part of Xiang'an was the worst, with the average space distance exceeding 50 km.

4.2. Shortest Time Distance. The calculation results of the time accessibility of public medical and health facilities in the main urban area of Xiamen are shown in Figure 4(b). The time from the centroid of each street to the point of public medical and health facilities in the main urban area of Xiamen is between 0.34 and 58.73 min. Among them, the medical and health centre in Huli Street and Fengnan Farm in Tong'an District have the shortest time and the best accessibility. The least accessible is Tingxi Town Medical and Health Center in Tong'an District, which takes 58.73 minutes.

To sum up, it can be seen from Figures 4(a) and 4(b) that the spatial accessibility of medical and health facilities in Xiamen is unevenly distributed. Medical and health facilities with high spatial and temporal accessibility are evenly distributed in the central part of Xiamen city and Siming District and Huli District in the south. Low accessibility is distributed in the eastern, northern, and western peripheral areas of Xiamen city. From the results of spatial distance accessibility and temporal distance accessibility, the spatial similarity between them is relatively high. The results show that the medical facilities themselves are the main factors affecting accessibility. This is mainly due to the convenient transportation in the central urban area and the shorter distance for residents to travel.

5. Spatial Accessibility of Sports Type

5.1. Shortest Space Distance. The calculation results of spatial distance accessibility of sports and fitness facilities in Xiamen are shown in Figure 5(a). It can be concluded from calculation results that the spatial distance between the centroid of each street in Xiamen and the points of rehabilitation facilities is between 0.043607 and 34.50959 km. The spatial accessibility is the best in the central part of Xiamen city, the southern part of Xiang'an District, and the border area between Siming District and Huli District, while the accessibility is the worst in Jimei District, the northern part of Tong'an District, and the north-eastern part of Xiang'an District.

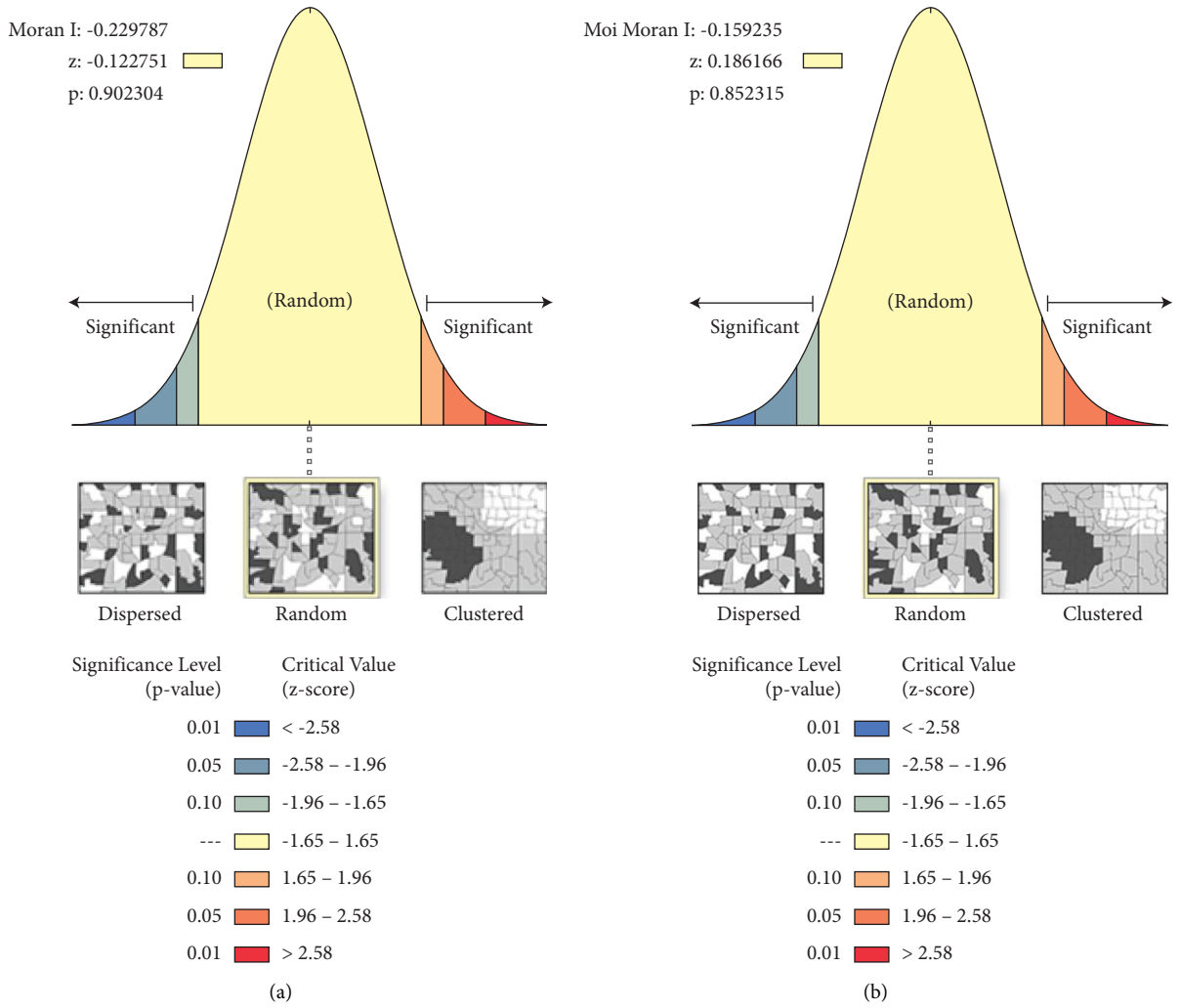

Figure 2: Spatial autocorrelation results: (a) medical and (b) sports.

5.2. Shortest Time Distance. The calculation results of the time accessibility of public sports and fitness facilities in Xiamen are shown in Figure 5(b). It can be seen from calculation results that the time from the centroid of each street to the point of public sports and fitness facilities in Xiamen ranges from 0.26 min to 136.19 min. Among them, Siming District and Huli District, the two main island areas of Xiamen, have the best time accessibility, basically meeting the standard of 15 min life circle. The worst time accessibility is the public sports and fitness facilities in the peripheral areas of Xiamen city.

Combined with Figures 5(a) and 5(b), it can be found that the spatial accessibility distribution of public sports facilities in Xiamen presents obvious spatial heterogeneity: public sports and fitness facilities with high spatial distance accessibility and time accessibility are evenly distributed in Siming and Huli Districts, the main island in the south of Xiamen. The areas with low accessibility are distributed in the peripheral areas of land cities in Xiamen. The results of spatial accessibility and temporal accessibility of sports and fitness facilities are similar to those of medical and health facilities, that is, they are almost the same in space, which also indicates that the factors of sports and fitness facilities themselves are the main factors affecting accessibility. The spatial similarity of public sports and fitness facilities is high, which indicates that the main factor affecting accessibility results is public sports and fitness facilities themselves. This is mainly because the distribution area of sports and fitness facilities are located in the economically developed, convenient transportation, and densely populated urban centre; therefore, its accessibility is high.

5.3. Accessibility of Public Medical Facilities. According to the results of spatial accessibility calculated with a travel limit time of 15 min (as shown in Figure 6(a)), it is obvious that the spatial accessibility of public health service facilities in Xiamen varies greatly with low continuity and uneven distribution. The values of accessibility ranged from 0.000025 to 0.779099, with an average value of 0.155825. The most accessible streets were Wucun Street and Yundang Street in Siming District, Huli Street in Huli District, and Haicang Street in Haicang District. The streets in Xiang'an and Tong'an Districts and some streets in Jimei District are the worst in accessibility.

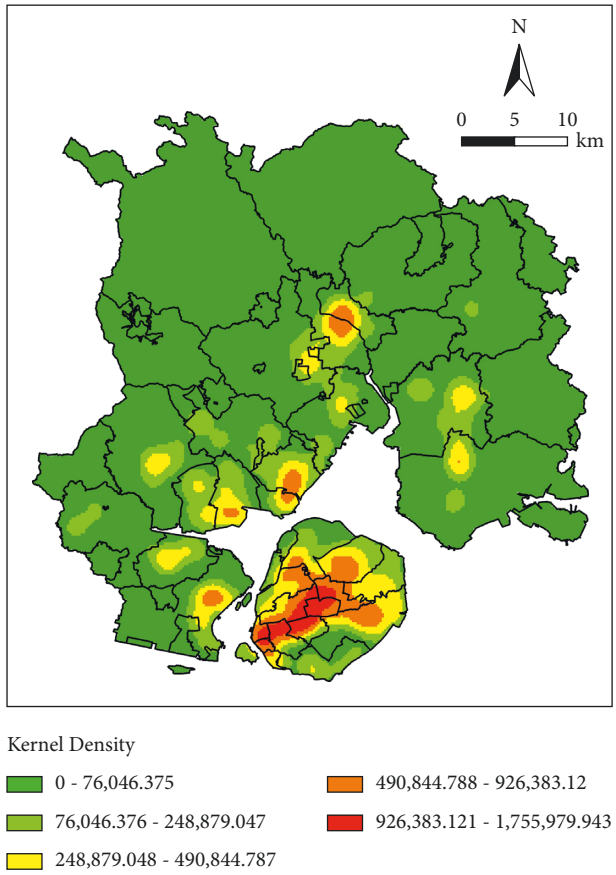

Figure 3: Kernel density.

As shown in Figure 6(b), the spatial accessibility of public health service facilities in Xiamen is distributed between 0 and 0.165415, with an average value of 0.033083, according to the results of spatial accessibility calculated with 30 min as travel limit time (Figure 6(b)). Yuandang in Siming District had the highest accessibility value (0.165415). The street with the worst accessibility has an accessibility value of 0, which is Lianhua Town in Tong'an District.

A comparative analysis of Figures 6(a) and 6(b) shows that: (1) with the increase in time distance, spatial accessibility of public health service facilities in Xiamen becomes better. As travel time increases and the range of public health services expands, residents have more opportunities to choose medical treatment. (2) The accessibility of marginal streets in Xiamen decreases with the increase of time distance. On the contrary, some streets in the central urban area showed a trend of improvement, and the accessibility increased significantly from 15 min to 30 min. (3) With the increase of time distance, the change of accessibility value tends to be slow, and the difference in spatial accessibility of public health service facilities becomes smaller. The standard deviation of accessibility decreases from 0.010300 for 15 min to 0.009707 for 30 min, indicating that the spatial difference of accessibility decreases with time and the degree of spatial smoothness increases.

5.4. Accessibility of Public Sports Facilities. The spatial distribution of accessibility of public fitness facilities in Xiamen is uneven and different in each district according to the results of spatial accessibility calculation based on the travel limit time of 15 min. The values of time accessibility ranged from 0 to 0.600522, with an average value of 0.120104. According to Figure 7(a), the streets with the best accessibility were Wucun Street in Siming District and Huli Street in Yundang District. The streets with the worst accessibility were Lianhua Town in Tong'an District, Fengnan Farm, and Xindian Street in Xiang'an District.

According to the results of spatial accessibility calculated by taking 30 min as travel limit time, the accessibility of public fitness facilities in Xiamen is characterized by uneven spatial distribution and great difference. The values of time accessibility ranged from 0 to 0.480081, with an average of 0.096016. As can be seen from Figure 7(b), Wucun Street in Siming District and Dianqian Street in Huli District have the

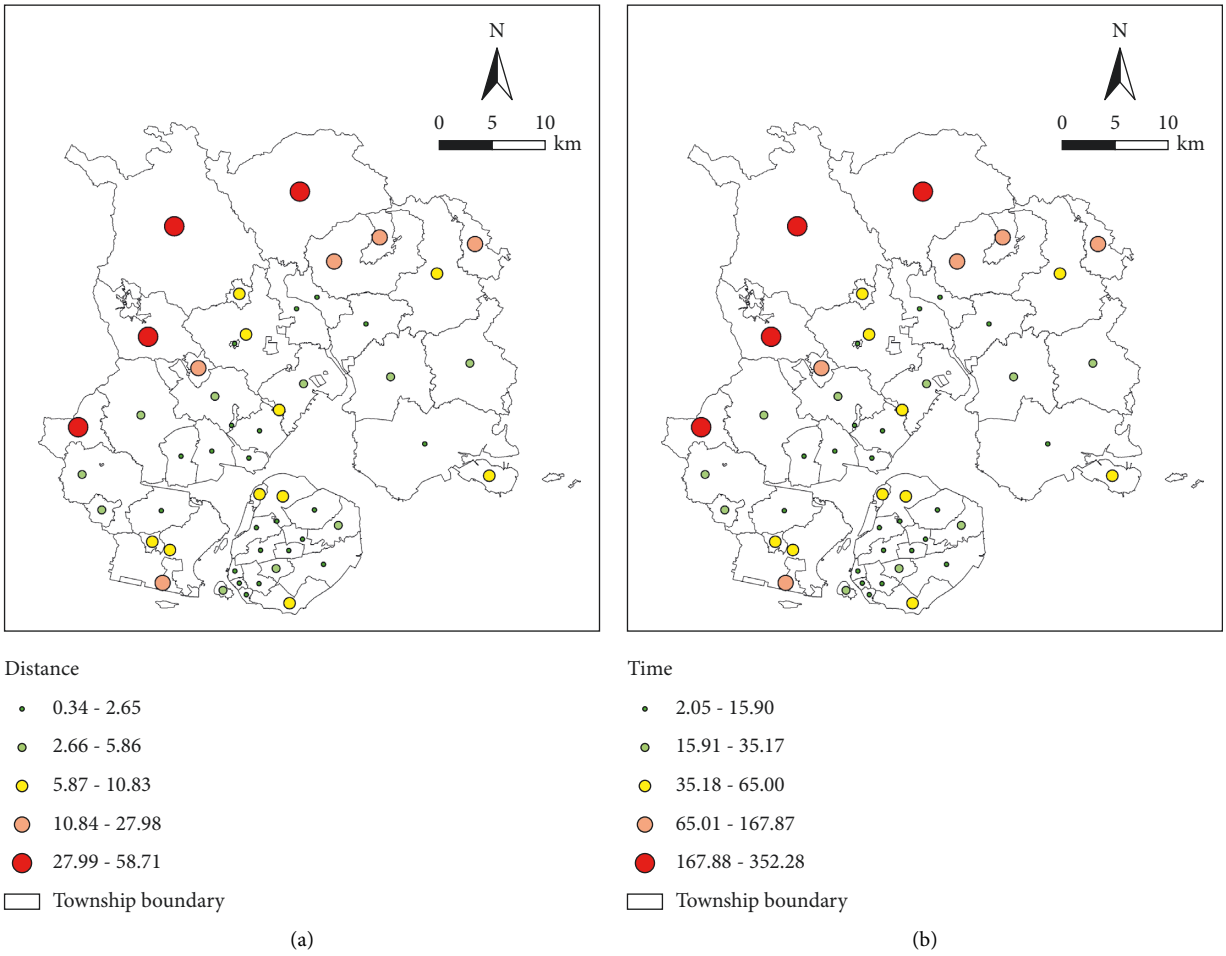

Figure 4: Accessibility of public medical facilities: (a) distance accessibility and (b) time accessibility.

best accessibility, while Lianhua Town, Fengnan Farm, and Xindian Street in Xiang'an District have the worst accessibility. It shows that the accessibility of fitness clubs in Xiamen city has obvious spatial differentiation.

By comparing Figures 7(a) and 7(b), it can be seen that: (1) overall, the spatial accessibility of public fitness facilities in Xiamen has a little change, and even some streets have no change. For example, the accessibility of Lianhua Town, Fengnan Farm, and Xindian Street in Xiang'an District is always the worst, indicating that the accessibility is greatly affected by the number and spatial location of fitness clubs. (2) The accessibility of the marginal streets in Xiamen becomes worse with the increase of time, while the accessibility of some streets in the central city increases. (3) With the decrease in accessibility, the spatial accessibility difference of public fitness facilities tends to narrow. According to the calculation results of accessibility for 15 min and 30 min, the standard deviation of accessibility decreased from 0.007316 for 15 min to 0.004251 for 30 min, indicating that the spatial difference of accessibility had a narrowing trend, but this trend was not obvious in space.

5.5. Discussion: Causal Relationship. Based on the above results, it can be found that in Xiamen, compared with public fitness facilities, the standard deviation of the accessibility of public health service facilities is significantly lower, indicating that the accessibility of public health service facilities is improving, while the accessibility of public fitness facilities does not change significantly. This result raises concerns about rehabilitation in the context of the pandemic. Although the importance of health care facilities is obvious, urban planning is often closely related to the needs of the public. Therefore, exploring the inadequacy of fitness facilities requires more consideration of residents. Understanding the reasons why residents do not like to exercise will help us provide more detailed guidelines for action. In order to test, this study contacted a university in Xiamen and tentatively conducted interviews with 20 residents around the school and collected their opinions on fitness facilities. Please note that this supplementary study is only for a preliminary exploration of the reasons, and we will discuss this issue separately in the follow-up study. The average age of the people who participated in the pilot survey

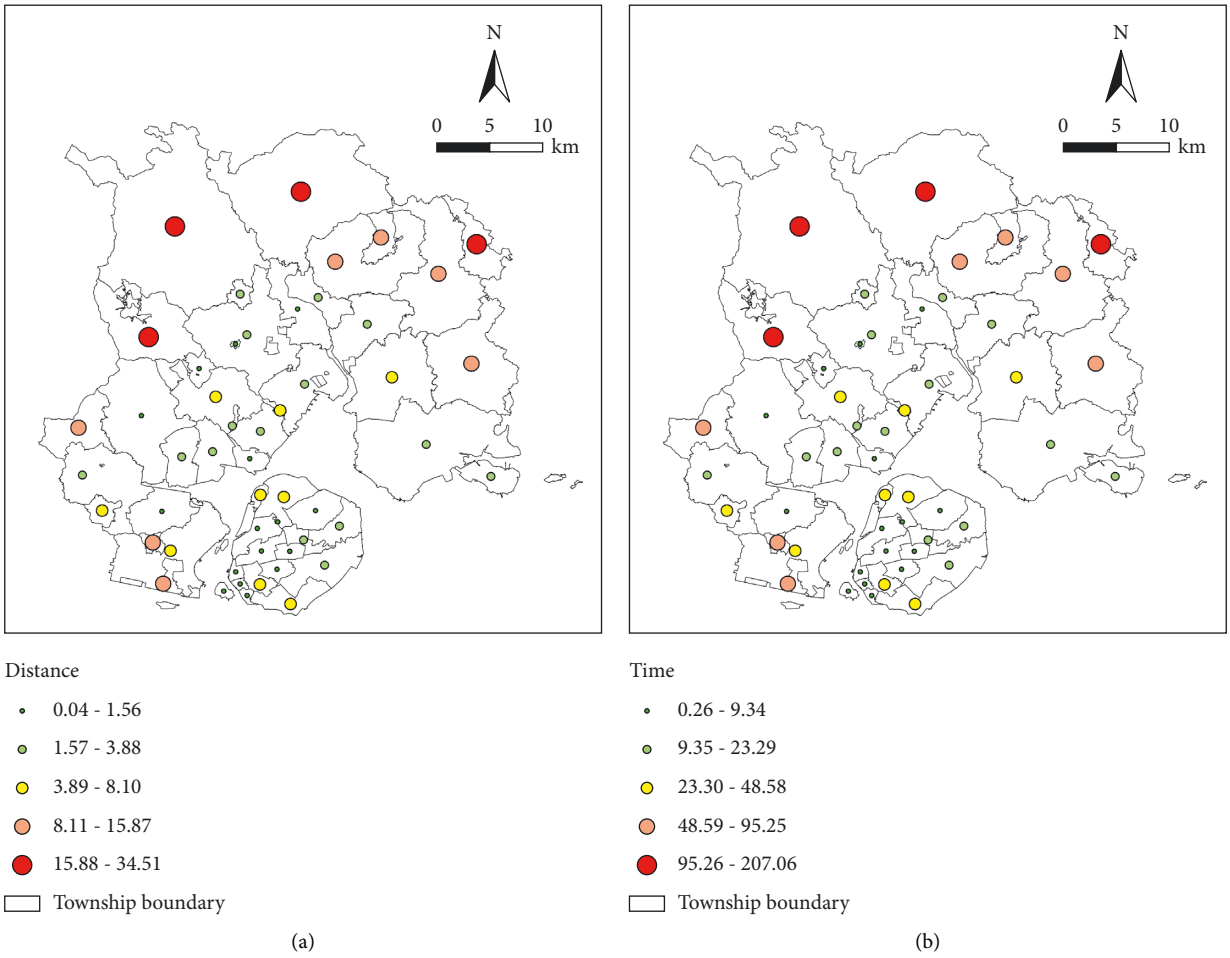

Figure 5: Accessibility of public sports and fitness facilities: (a) distance accessibility and (b) time accessibility.

was 35 years old, mainly due to the general youth of the people around the school. But it is enough as an exploratory pilot study. Finally, the analysis of the text of the interviews shows that the main factors affecting the fitness activities of community residents are as follows: laziness, lack of guidance, lack of interest, busy work, lack of confidence, lack of facilities, and fear of injury. Based on this preliminary understanding, we believe that the lack of facilities is not the main reason affecting residents' fitness, but the influence of psychological factors and knowledge factors is the leading factor causing the lack of fitness, which in turn affects residents' actual demand. Based on the practice theory, material accessibility is only one of the components of practice, and the rest also need the joint action of "meaning" and "competence" elements to achieve the final "practice." Therefore, although the study in this paper is a discussion about facilities, combined with this survey, we believe that further research is needed in the future to determine the psychological factors that affect residents' fitness needs. On the whole, it is certain that the realization of fitness practice must improve the overall awareness of residents and health education.

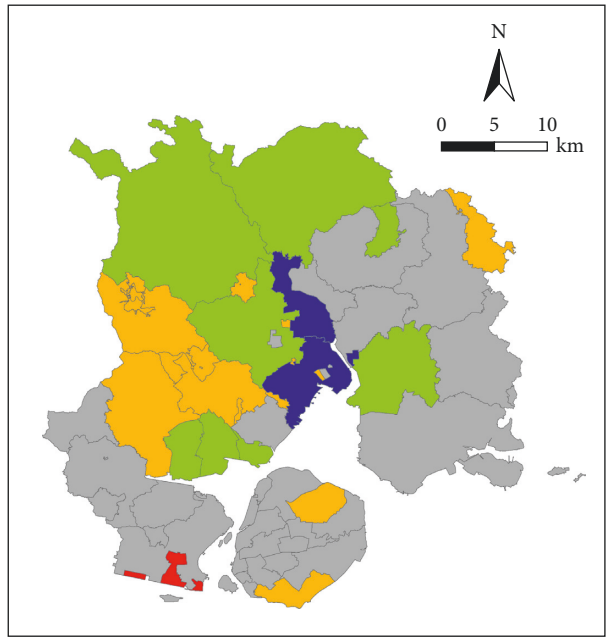

Accessibility of medical facilities (min)

- 0.000025 - 0.012245
- 0.012246 - 0.048279
- 0.048280 - 0.106150
- 0.106151 - 0.170231
- 0.170232 - 0.779099
- Township boundary

(a)

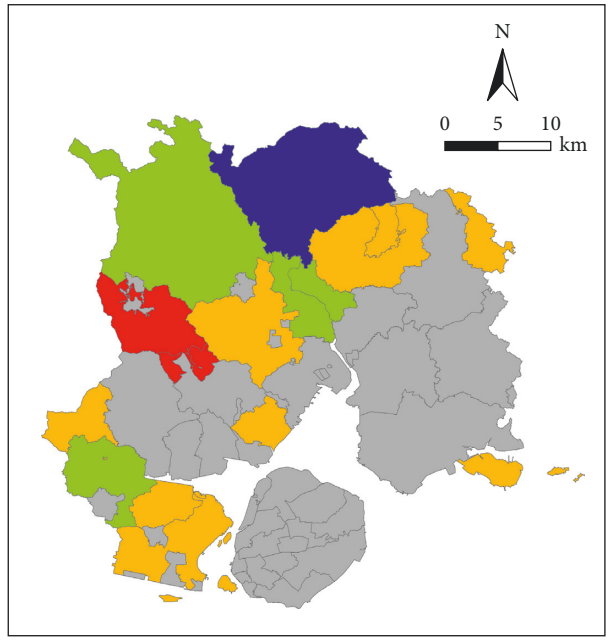

Accessibility of medical facilities (min)

- 0.000000 - 0.002892
- 0.002893 - 0.013732
- 0.013733 - 0.032412
- 0.032413 - 0.092355
- 0.092356 - 0.165415
- Township boundary

(b)

Figure 6: Accessibility of public medical facilities: (a) 15 min and (b) 30 min.

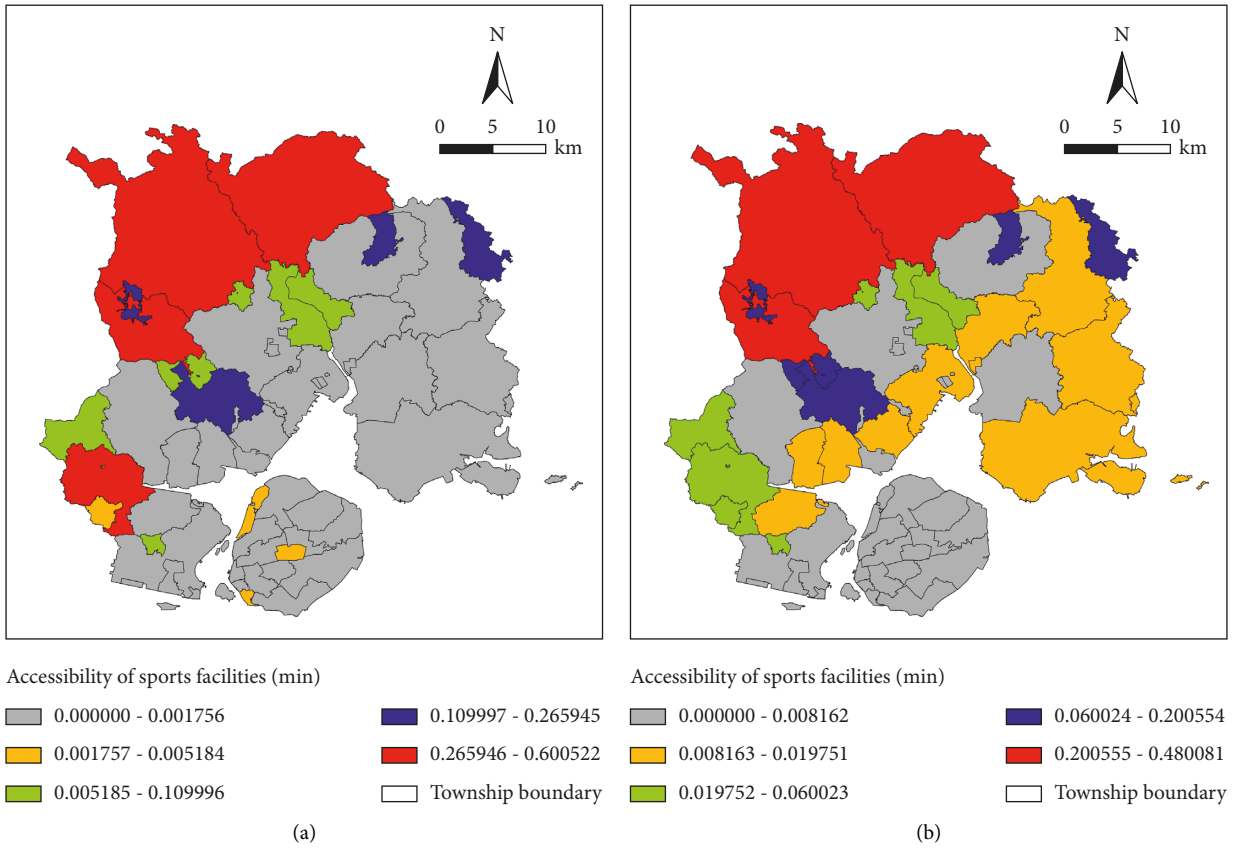

Figure 7: Accessibility of public sports facilities: (a) 15 min and (b) 30 min.

6. Conclusions

In this study, the accessibility of rehabilitation facilities in Xiamen was analyzed by using the nearest distance method and the 2SFCA method, and the following conclusions were drawn:

(1) The spatial distribution of accessibility of rehabilitation facilities in Xiamen is uneven, and accessibility varies greatly among streets.

(2) Under the nearest distance method, the highest accessibility was Yundang, Wuncun, and Wundang in Siming District; Huli, Dianqian, and Haicang in Huli District; and Haicang in Haicang District. The streets with the lowest accessibility are Lianhua Town, Fengnan Farm, and Xindian Street in Xiang'an District. This is due to the fact that the streets with high accessibility are close to the centre of the main urban area and the road traffic network is relatively perfect, while the streets with low accessibility are far away from the main urban area and the traffic accessibility is poor. This indicates that the accessibility of rehabilitation facilities is related to distance and transportation networks.

(3) According to the calculation results of the two-step floating catchment area (2SFCA), there are the following similarities and differences in the spatial accessibility of public health service facilities and public fitness facilities in Xiamen. Similarities: The spatial accessibility of the two facilities is not evenly distributed, and the accessibility of different streets varies greatly. With the increase of time, the spatial accessibility difference of public health service facilities and public fitness facilities becomes smaller. In both cases, street accessibility near the main urban centre increased, while street accessibility at the edge of the main urban area decreased. Differences: Compared with public fitness facilities, the standard deviation of accessibility of public health service facilities decreased significantly, indicating that the street accessibility of public health service facilities became better, while the street accessibility of public fitness facilities did not change significantly. The results of our further pilot interviews showed that residents' awareness may be an important factor potentially leading to this result, and further research is needed to analyze the driving factors of residents' fitness practice in the future.

(4) From the results of accessibility, there are some differences between the calculation results of the nearest distance method and 2SFCA because the distance is the main factor in the calculation of the

nearest distance method, while the two-step mobile search method not only considers the distance factor, but the factors of service capacity and population demand of rehabilitation facilities are also considered. In real life, residents' choice of rehabilitation facilities is not only affected by travel distance but also affected by the service capacity of rehabilitation facilities. Therefore, for the accessibility analysis of rehabilitation facilities in Xiamen, the 2SFCA method is more accurate and effective than the nearest distance method, which is more in line with the actual situation.

The traditional accessibility calculation method, accessibility index, through subjective investigation and measurement of public facilities, carries out spatial quantification of accessibility; the quantification results contain a great subjectivity. In this paper, the 2SFCA calculation is completed based on POI data, user access data, and GIS software. This method not only considers the service capacity of rehabilitation facilities but also takes into account a large amount of sample data so that the analysis results can more accurately and clearly indicate the accessibility of rehabilitation facilities in each street. However, there are still deficiencies in the calculation of accessibility of rehabilitation facilities in this paper. For example, in reality, residents' demands for community rehabilitation facilities are also affected by multiple factors such as population age, education level, income level, and living environment. Therefore, the above factors can be incorporated into the accessibility analysis in further studies to study the influence of these factors on residents' preference in selecting community-based rehabilitation facilities.

Data Availability

Requests for access to the data used to support the findings of this study should be made to Jie Wang (jie.wang.13@outlook.com).

Conflicts of Interest

The authors declare that there are no conflicts of interest regarding the publication of this paper.

References

[1] W. Wang and J. Shen, "Deep visual attention prediction," *IEEE Transactions on Image Processing*, vol. 27, no. 5, pp. 2368–2378, 2018.

[2] M. Esmaeili, A. Bahrini, and S. Shayanrad, "Using game theory approach to interpret stable policies for Iran's oil and gas common resources conflicts with Iraq and Qatar," *Journal of Industrial Engineering International*, vol. 11, no. 4, pp. 543–554, 2015.

[3] H. Wei, J. Dai, I. Maharik, A. Ghasemi, A. Mouldi, and A. Brahmia, "Simultaneous synthesis of H2, O2, and N2 via an innovatory energy system in coronavirus pandemic time: design, techno-economic assessment, and optimization approaches," *International Journal of Hydrogen Energy*, 2021.

[4] L. Chou, J. Dai, X. Qian, A. Karimipour, and X. Zheng, "Achieving sustainable soil and water protection: the perspective of agricultural water price regulation on environmental protection," *Agricultural Water Management*, vol. 245, Article ID 106583, 2021.

[5] H. Lin, L. Chou, and W. H. Zhang, "Cross-Strait Climate Change and Agricultural Product Loss," *Environmental Science and Pollution Research*, vol. 96, no. sp1, pp. 1–14, 2019.

[6] D. Ivanov, "Predicting the impacts of epidemic outbreaks on global supply chains: a simulation-based analysis on the coronavirus outbreak (COVID-19/SARS-CoV-2) case," *Transportation Research Part E: Logistics and Transportation Review*, vol. 136, Article ID 101922, 2020.

[7] P. Zhang, C. Liu, and Q. Li, "Application of gray relational analysis for chloride permeability and freeze-thaw resistance of high-performance concrete containing nanoparticles," *Journal of Materials in Civil Engineering*, vol. 23, no. 12, pp. 1760–1763, 2011.

[8] Y. Xu and X. Dou, "From Empowerment to Encapsulation: Sanitation Workers' Struggles and Sources of Power in South China," *Labour History*, vol. 62, pp. 1–21, 2021.

[9] R. Eisler, "Health risks of gold miners: a synoptic review," *Environmental Geochemistry and Health*, vol. 25, no. 3, pp. 325–345, 2003.

[10] H. Zhang and E. Friedman, "Informality and working conditions in China's sanitation sector," *The China Quarterly*, vol. 238, pp. 375–395, 2019.

[11] H. Ning, Y. Zhou, Z. Zhou et al., "Challenges to improving occupational health in China," *Occupational and Environmental Medicine*, vol. 74, no. 12, pp. 924-925, 2017.

[12] B. M. Quaney, L. A. Boyd, J. M. McDowd et al., "Aerobic exercise improves cognition and motor function poststroke," *Neurorehabilitation and Neural Repair*, vol. 23, no. 9, pp. 879–885, 2009.

[13] R. Wu and J. Lu, "Dynamic information acquisition technology system of urban recreation and sports facilities based on RS and GIS," *World of Sports*, vol. 2, 2018.

[14] W. G. Hansen, "How accessibility shapes land use," *Journal of the American Institute of Planners*, vol. 25, no. 2, pp. 73–76, 1959.

[15] K. Hur, W.-S. Sohn, J.-K. Kim, and Y. Lee, "Novel MAC protocol and middleware designs for wearable sensor-based systems for health monitoring," *International Journal of Distributed Sensor Networks*, vol. 2013, no. 4, 15 pages, Article ID 404168, 2013.

[16] G. Hou and L. Chen, "Regional commercial center identification based on POI big data in China," *Arabian Journal of Geosciences*, vol. 14, no. 14, pp. 1360–1414, 2021.

[17] J. Wang, J. Li, and Y. Pan, "Retracted article: the spatial effect of Nanjing's fitness strategy: considering citizens' fitness status," *Arabian Journal of Geosciences*, vol. 14, no. 16, pp. 1607–1609, 2021.

[18] W. Wang and M. Wang, "Retracted article: convenience analysis of financial services: GIS-based distribution of ATM network in Hangzhou City," *Arabian Journal of Geosciences*, vol. 14, no. 17, pp. 1755–1810, 2021.

[19] Y. Song, Y. Long, P. Wu, and X. Wang, "Are all cities with similar urban form or not? Redefining cities with ubiquitous points of interest and evaluating them with indicators at city and block levels in China," *International Journal of Geographical Information Science*, vol. 32, no. 12, pp. 2447–2476, 2018.

[20] X. Dong, A. B. Murray, and J. B. Heffernan, "Competition among limestone depressions leads to self-organized regular

patterning on a flat landscape," *Journal of Geophysical Research: Earth Surface*, vol. 126, no. 5, Article ID e2021JF006072, 2021.

[21] B. Xue, X. Xiao, and J. Li, "Identification method and empirical study of urban industrial spatial relationship based on POI big data: a case of Shenyang City, China," *Geography and Sustainability*, vol. 1, no. 2, pp. 152–162, 2020.

[22] Y. Bai, L. Chou, and W. Zhang, "Industrial innovation characteristics and spatial differentiation of smart grid technology in China based on patent mining," *Journal of Energy Storage*, vol. 43, Article ID 103289, 2021.

[23] H. Shao, C. Jin, J. Xu, Y. Zhong, and B. Xu, "Supply-demand matching of medical services at a city level under the background of hierarchical diagnosis and treatment - based on Didi Chuxing Data in Haikou, China," *BMC Health Services Research*, vol. 22, no. 1, pp. 354–412, 2022.

[24] Z. Wang, D. Ma, D. Sun, and J. Zhang, "Identification and analysis of urban functional area in Hangzhou based on OSM and POI data," *PLoS One*, vol. 16, no. 5, Article ID e0251988, 2021.

Hindawi
Mathematical Problems in Engineering
Volume 2022, Article ID 5782587, 17 pages
https://doi.org/10.1155/2022/5782587

Review Article

Evolution of Software Development Effort and Cost Estimation Techniques: Five Decades Study Using Automated Text Mining Approach

Anil Jadhav,[1] Mandeep Kaur,[2,3] and Farzana Akter[4]

[1]*Symbiosis Centre for Information Technology, Pune, Maharashtra, India*
[2]*Department. of Computer Science, Savitribai Phule Pune University, Pune, Maharashtra, India*
[3]*Permtech Research Solutions, Pune, Maharashtra, India*
[4]*Department of ICT, Bangabandhu Sheikh Mujibur Rahman Digital University, Kaliakair, Gazipur, Bangladesh*

Correspondence should be addressed to Farzana Akter; farzana@ict.bdu.ac.bd

Received 28 February 2022; Accepted 6 April 2022; Published 2 May 2022

Academic Editor: Amandeep Kaur

Software development effort and cost estimation (SDECE) is one of the most important tasks in the field of software engineering. A large number of research papers have been published on this topic in the last five decades. Investigating research trends using a systematic literature review when such a large number of research papers are published is a very tedious and time-consuming task. Therefore, in this research paper, we propose a generic automated text mining framework to investigate research trends by analyzing the title, author's keywords, and abstract of the research papers. The proposed framework is used to investigate research trends by analyzing the title, keywords, and abstract of select 1015 research papers published on SDECE in the last five decades. We have identified the most popular SDECE techniques in each decade to understand how SDECE has evolved in the past five decades. It is found that artificial neural network, fuzzy logic, regression, analogy-based approach, and COCOMO methods are the most used techniques for SDECE followed by optimization, use case point, machine learning, and function point analysis. The NASA and ISBSG are the most used dataset for SDECE. The MMRE, MRE, and PRED are the most used accuracy measures for SDECE. Results of the proposed framework are validated by comparing it with the outcome of the previously published review work and we found that the results are consistent. We have also carried out a detailed bibliometric analysis and metareview of the review and survey papers published on SDECE. This research study is significant for the development of new models for cost and effort estimations.

1. Introduction

Software development effort and cost estimation (SDECE) is a process of estimating the effort and cost required for software development and is one of the most important activities of software engineering. There exist several research papers on this topic. Some papers talk about the software development effort estimation (SDEE) [1–9] and the others talk about the software development cost estimation (SDCE) [10–15]. It is very common that the terms "software effort estimation" and "software cost estimation" have been used interchangeably in the literature. However, software cost estimation is an outcome of software effort estimation [16]. The ability of sales consultants, presales consultants, project managers, delivery managers, and delivery heads to determine accurate costs depends on the amount of detailing and care that has been taken to estimate efforts. Estimating accurate effort and cost have an important role in the success of the software project. Over the past five decades, there has been a significant increase in the complexity of software projects. This has led to the design and implementation of numerous techniques for estimating the effort and cost of the software development and its consequent discussion in literature.

Initial papers published on this topic discussed techniques such as COCOMO, SEER, PRICE-S, Checkpoint,

SLIM, Delphi Technique, and COCOMO II [17]. There also exist techniques based on function point analysis (FPA) [18–21], use case point analysis (UCP) [22–24], and Work Breakdown Structure (WBS) [25]. Several research papers discussed analogy-based approach [26–32] and case-based reasoning (CBR) approach [33, 34]. The techniques such as regression [35–37], artificial neural network (ANN) [38–41], and Fuzzy logic [31, 42–45] have become more popular in the recent past. Machine learning (ML) based techniques have also been used very widely in the literature [3, 16, 46–49]. A large number of research papers also discussed the optimization techniques used for SDECE [50–54].

Thus, there exist several studies on SDEE, SDCE, systematic reviews on SDEE, and systematic reviews on SDCE. However, there is a lack of research that analyzes research trends and techniques that have evolved in the last five decades. There is also a need to do a systematic bibliometric analysis of articles published on SDECE in the last five decades. Analyzing such vast research papers published on this topic in the last five decades is a very tedious and time-consuming task. Considering this fact, in this research paper, we proposed a generic text-mining-based framework to analyze a vast range of articles and investigate research trends and techniques used for SDECE in the last five decades. The framework is based on natural language processing and it is an automated process. The advantage of using a text-mining approach is that it significantly reduces manual efforts required to investigate research trends and patterns from the corpus of the documents on specific topics like SDECE [55, 56]. This has motivated us to conduct this research study based on the text mining mechanism. The proposed framework is very generic and can be used in any other domain where a large number of research articles are published and need to be investigated in a manner that may be similar to this study. In this study, we analyzed 1015 research articles indexed in the Scopus database. The objectives, research questions, and contributions of this study are as follows.

1.1. Research Objectives

(1) To propose a generic automated text-mining framework to analyze a large number of research papers, for identifying changing research trends in technologies, methodologies, frameworks, tools, and techniques in an identified area or topic of any scientific or social science field. This paper was carried out to understand how SDECE techniques have evolved in the last five decades.

(2) To investigate frequently used techniques, accuracy measures, and datasets for SDECE using the proposed text mining framework

(3) To validate the proposed framework to ensure consistent outcomes

(4) To do a systematic bibliometric analysis of studies on SDECE

(5) To do a comprehensive metareview of the review and survey papers on SDECE

1.2. Research Questions (RQ).

We attempt to address following research questions in this study.

RQ1: What are the most frequently used SDECE techniques? What is research trend? How have SDECE techniques evolved in the last five decades?

RQ2: What are the most frequently used datasets in SDECE studies?

RQ3: What are the most frequently used accuracy measures in SDECE studies?

RQ4: What is the distribution of SDECE papers and their citations by document type?

RQ5: How many research papers are published on SDECE each year and in each decade since 1970?

RQ6: What is the distribution of citations of SDECE papers? This research question is further divided into sub-questions as follows:

RQ6.1: What is the distribution of journal and conference papers with zero citation and papers with one or more than one citation?

RQ6.2: What are highly cited papers?

RQ7: Who are the top authors in terms of the number of papers and number of citations?

1.3. Research Contributions

(1) We propose a generic text mining framework to investigate research trends by analysis title, keywords, and abstract of the research papers. This will help researchers from any domain to investigate research trends and patterns in an identified topic of the study.

(2) We have used a proposed framework to investigate the most frequently used techniques, datasets, and accuracy measures for SDECE in the last five decades. Decade-wise analysis is also done to understand the evolution of SDECE techniques in the last five decades.

(3) The study presents a comprehensive metareview of the review and survey papers on SDECE, which enables researchers to understand research trends and the contribution of researchers in this field.

(4) The study presents a comprehensive citation analysis of select 1015 Scopus indexed research papers published on SDECE during the period between the year 1974 and 2020.

The paper is organized as follows: in the second section, we present the research method. The third section presents a metareview of the review and survey papers. Results of the automated text mining framework and bibliometric analysis are presented in the fourth section. In the fifth section, we validate the results of the proposed text mining framework. The threats to the validity of the study are explained in the sixth section. Finally, we conclude paper in the seventh section.

2. Research Method

To achieve the stated objectives of this study we have analyzed select 1015 articles from the Scopus database. We had three options to select articles on SDECE from indexing databases including Scopus, Web of Science, and Google scholar. These are the three most popular and widely used online indexing databases by researchers. We decided to use the Scopus database because we could download all required data about research articles, such as the title of study, year of publication, the number of citations, source of the article (Journal, conference, etc.), author's keywords, abstract, document type, and authors information in CSV file format.

The search string used for finding the documents from Scopus database was decided by taking into account the objectives and research questions of the study. The search terms used were "software effort estimation" OR "software cost estimation". We used this search string because it was needed to limit the study to the research papers that discuss software effort estimation and software cost estimations. The search of documents was done on 23 May 2020. We exported the search results in CSV (excel) file format. In the title column of the extracted data, we found that some of the titles were not research papers but the titles belonged to conferences, symposiums, and workshops. So, we decided to remove those titles from our list. We removed the following type of titles from the search results: (i) 48 conference titles; (ii) 6 symposium titles; (iii) 2 annual conventions titles; (iv) 6 international work-shop titles; (v) 1 conference review title; and (vi) 1 conference note. We also found that in search results there were 26 non-English papers, so we removed those papers from the list. Thus, in total we removed 90 titles from the original search results and selected 1015 papers for purpose of this study. Later, by reading the title of the research papers, we checked whether all selected 1015 research papers are on SDECE and we found that all of them were relevant. Thus, other than the criteria that the paper should be on SDECE and written in the English language, we did not use any exclusion criteria.

The analysis to investigate research trends and techniques used for SDECE was done separately for title, keywords, and abstract of the research papers. We did the analysis separately because we wanted to check whether the results of the analysis based on the title, abstract, and keywords of the research papers are consistent or not. We used "wordcloud" and "tm" packages in "R" programming language for the text mining task. The bibliometric analysis of 1015 is done using the following information of the research papers: title; authors; year of publication; source title; cited by; affiliation; and document type. The detailed results of both bibliometric analysis and text mining are presented in Section 4.

3. Metareview of Review and Survey Papers on SDECE and Related Work

Several studies have been published on the topic SDECE in the last five decades. In this section, we present a detailed metareview of review and survey papers. Out of the selected 1015 articles, we found 39 review/survey papers, which include 13 journal articles, 25 conference papers, and one book chapter. Among the 39 review/survey papers, 9 papers that were published in year 2018 and 2019 did not receive any citation till May 2020. The remaining 30 papers received a total 1636 citations. The main findings of the 39 review/survey papers are presented in Table 1. For some studies, data such as duration of the study and number of papers reviewed were not available so we could not include those details in Table 1.

Some existing studies have used a text mining approach for identifying research trends in different areas. Garousi and Mantyala [55] used text mining to identify research themes, hot and cold topics in software engineering. The study conducted by Nie and Sun [85] used text mining to identify major academic branches and identify research trends in design research. Sehra et el. [56] conducted a study to identify research patterns and trends in software effort estimation using a text mining approach. The study was conducted by applying text mining on articles published during the period between 1996 and 2016. In all these studies, it is found that usage of the text mining is an adequate choice for better assessment when large number of articles needs to be assessed to understand the research trends, research themes, hot and cold topics in an identified research area. However, we found that there is a lack of research on (i) investigating research trend in SDECE in the last five decades; (ii) identifying the most popular SDECE techniques in each decade to understand how SDECE techniques have evolved in the last five decades; (iii) investigating research trends by analyzing title, keywords, and abstract of research papers separately to understand whether results are consistent or different; (iv) metareview of the review and survey papers published on SDECE in the last five decades; and (v) bibliometric analysis of the papers published in the last five decades. Therefore, in this study, we attempt to fill these gaps.

Based on a metareview of the review and survey papers, we have identified the most used (i) SDECE techniques, (ii) datasets, and (iii) accuracy measures for SDECE. The most used SDECE techniques are shown in Figure 1. The most used datasets and accuracy measures are given in Table 2.

The strengths and weaknesses of the commonly used SDECE techniques:

Based on the review of literature and our understanding about SDECE techniques, we present the strengths and weaknesses of the most used SDECE techniques.

(A) Linear regression: The strengths are as follows: (i) easy to understand, implement, interpret, and explain; (ii) can work well with small datasets; (iii) computationally not very expensive. The weaknesses are as follows: (i) assumes linear relationship and therefore not suitable when nonlinear relationship exists in the data; (ii) multicollinearity issue needs to be resolved, if it exists; (iii) sensitive to the outliers.

(B) Artificial neural network: The strengths are as follows: (i) it can learn complex relationship in the

Table 1: Findings of review and survey papers on SDECE.

Research paper	Findings
	Journal papers
[17]	This study classifies cost estimation models into five different categories along with detailed explanation of each category. The techniques are classified as i) Model based approaches: SLIM, COCOMO, checkpoint, SEER; ii) expertise based models: Delphi, rule based; iii) learning based models: ANN, robust; iv) regression models: OLS and robust; and v) composite models: Bayesian and COCOMO II
[10]	The study reviewed 304 papers from 76 journals. Research papers published before April 2004 were included in the study by manual search. Focus of the review was to classify papers based on research topic, research approach, SDEE technique, and datasets used for the study. The study also listed important cost estimation journals, research topics, research approaches, estimation approaches, context of the study.
[16]	The study reviewed 84 articles during the period 1991 to 2010. Four different aspects of ML models were reviewed: ML technique; accuracy of estimation using ML technique; comparison of ML models; and estimation context. Finding of study are that accuracy of ML models is better than non-ML models/techniques.
[37]	Conducted systematic empirical analysis of 10 local and global models of SEE. Study found that the results obtained are different for local and global methods of SDEE because of different experiment design and datasets.
[41]	Reviewed 21 articles describing neural network based models for SEE. The study reports range of features used for SDEE using ANN. The important finding of the study are as follows: i) ANN gives better results compared to regression, classic COCOMO model, SLIM FPA; ii) most of the researcher used COCOMO dataset; iii) the most used accuracy measures are MMRE, MdMRE, MRE, pred, MMER; iv) the most used neural network is feed forward neural network;
[57]	The study reviewed 129 articles during the period 2000 to 2014 and discussed usefulness and limitations of the ISBSG dataset used for SEE. About 70% papers used ISBSG dataset for SDEE and 36% papers used ISBSG dataset to study its properties. 55% papers used ISBSG dataset and others used complementary datasets for SEE. The study also highlighted that the most common methods used for SDEE are regression, machine learning, and estimation by analogy.
[58]	Review period of this study was from 1991 to 2016. The study reported that because of changing nature of the software development and its complexity several estimation techniques are evolved. The study also reported that for improved results several data mining and machine learning techniques are used along with conventional methods of SEE.
[59]	The study reviewed 101 articles during the period 2006 to 2015. The study reviewed papers related to cost estimation using agile software development. The study reported most popular SDEE techniques, accuracy measures, and project success rate over the years. ANN and expert judgment are the most used techniques for agile SDECE. MRE, MMRE, MdMRE, and pred are most used accuracy measures.
[60]	Review period was from 2000 to 2017. The articles are reviewed with respect to type of soft computing or machine learning techniques used for SEE. The study reported that COCOMO, NASA, ISBSG, DEHANAI are the most used datasets and MMRE and PRED are most used evaluation metrics. It is also reported that ANN is most used estimation technique.
[61]	The study analyzed 20 papers on SDCE tools. The review concluded that most of the tools are based on COCOMO model.
[3]	The study reviewed models built using ML techniques for SEE. The study reviewed 75 papers during the period 1991 to 2017. The study found that i)ANN is widely used ML technique; ii) MMRE is widely used accuracy measure; iii)ANN and SVM outperformed the other techniques; iv) Regression is non-ML technique widely used for effort estimation.
[62]	The study reviewed 74 articles from the period 2000 to 2017. Eight types of techniques found to be used for SEE. The study found that i) most used datasets are ISBSG, COCOMO, NASA93, NASA, desharnias, albercht, sdr, China, kemerer, miyaki, maxwell, Finnish. ii) Most widely used methods are ANN, CBR, linear regression, fuzzy logic, GA, kNN, support vector regression, logistic regression, and decision tree. iii) Most used accuracy measures are MMRE, MdMRE, PRED.
[63]	Discussed issues of estimating cost of software projects.
	Conference papers
[64]	Paper reports survey results on SDEE technique used in JPL laboratory. It is found that i) most technical staff use informal analogy and high level partitioning of requirements, and ii) staff was better in estimating effort than size.
[5]	The findings are based on surveys on SDEE and the findings are as follows: i) 60–70% projects encounter effort or schedule overrun; ii)30–40% projects encounter cost overrun; iii) frequent method used for estimation is expert's judgment.
[65]	The study analyzed 112 projects from Chinese software industry. The survey investigated estimation methods, accuracy of method, and factors influencing adoption of certain method. The main findings are as follows: i) The large projects are prone to cost and schedule overrun, and ii) about 15% organizations used model based methods.
[66]	Paper provides compressive overview of analogy based SEE. Paper also discussed analogy based tool and systems, dataset quality and its relevance in predicting SEE.
[67]	This study reports the review of three parametric models used for SDEE namely: SLIM-putnam 1979, SEER-SEM 1989, SPR-knowledge plan 1999.
[68]	This study reports result of survey analysis on SDEE from industry perspective such as abilities of software organizations to apply SDEE technique and actually use techniques for effort estimation. The study also reports requirement of SDEE identified on the basis of survey and are compared with the requirements of existing methods.

Table 1: Continued.

Research paper	Findings
[69]	This study reports cost and schedule estimation approaches for component-based software development. Analysis of published work is done with respect to modeling techniques, data requirement, type of estimation, and lifecycle activities.
[70]	This survey reports results of reliability of expert's judgment for SDCE in a medium sized software company. The study also reported that cost estimation based on expert's judgment is unreliable.
[71]	The study reports overview and usefulness of ANN for SDEE and its accuracy. The study reviewed 19 articles from the period 2000 to 2014.
[72]	The focus of review was to determine whether use of feature weighting technique (FWT) in CBR improves SDEE prediction accuracy. The study concluded that use of FWT in CBR improves SDEE prediction accuracy.
[73]	The study reviewed articles pertaining to SDEE and concluded that every technique has its own advantages and disadvantages and there is no globally accepted single technique for SEE. The study reviewed 167 papers from the period 2000 to 2013.
[74]	The study reports statistics about usage of variables in ISBSG dataset for SEE. The study found that variables with missing values are less frequently used.
[75]	The study reviewed 16 articles only. Reviewed articles were classified using nine criteria for global software development (GSD). It is found that the dominant contribution of GSD research was the models and software development cost.
[76]	The study reviewed article on the tools and frameworks developed for SDEE using use case point model.
[59]	This study reviewed various soft computing techniques such as genetic algorithm, neural networks, fuzzy systems, particle swarm optimization used for SDEE in agile software development. The study found that soft computing techniques provide better accuracy estimation.
[77]	The study reviewed 15 articles. The findings of the study are as follows: i) company's use expert's judgment for SDEE; ii) need to improve algorithms and prediction techniques.
[78]	The study reports 8 common approaches used to find k value for analogy based SDEE techniques. It is reported that due to varied performance of different approaches in finding k values resulted in conflicting results.
[79]	The study conducted review of article to find which estimation method is best. It is found that use case point analysis approach is better that function point analysis and COCOMO model.
[80]	The study reviewed 10 articles. The survey analyzed contribution of papers in estimating effort with respect time, cost, and test. The study found that supervised learning algorithms are most popular for effort estimation.
[81]	The study reviewed 41 papers on ML based SDEE from the period between 2000 and 2017. The study discussed ML techniques, size metrics, benchmark datasets, and validation methods for SEE. It is found that i) most used techniques: Fuzzy logic, ANN, GA, anlogy based, SVR, bayesian network, regression tree, CBR; ii) dataset used: NASA, ISBSG, albrecth, COCOMO, desharnais, kemerer, kotengray, maxwell; iii) performance measures: MRE, MMRE, pred, MdMre, MMER, MSE, RMSE, standard deviation.
[82]	The review was conducted to understand importance of nonfunctional requirement in SDEE. The study identified nonfunctional requirements used in SDEE and how they are used. It is also found that use of nonfunctional requirements in SDEE brings down error by 30%.
[83]	The study reviews cost estimation techniques and presents strength and weakness of the techniques.
[4]	The study reviewed use case-based effort estimation methods and provides factors contributing to use case effort estimation. Provides inputs on criteria to evaluate accuracy and effectiveness of the models.
[3]	The study reviewed 30 articles on 'bio-inspired feature selection algorithms' during the period 2007 to 2018. It is fount that genetic algorithm (GA) and particle swarm optimization (PSO) are widely used bio-inspired algorithms. Results of GA and PSO are better than baseline estimation techniques.
[21]	The study discussed limitations and accuracy of the function point analysis method.
[84]	The study: i) Reviewed papers that describes models, processes, and practices and ii) proposed a general prediction process and framework for selecting predictive measures.

data; (ii) feature engineering is not required to be done. The weaknesses are as follows: (i) large amount of data is required for training, therefore it is computationally expensive; (ii) it is difficult to understand the reasoning behind the results, so interpretation of the results is difficult; (iii) it may suffer from over-fitting problem; (iv) cannot deal with missing values; (v) categorical values need to be converted to the numeric type.

(C) Analogy-based approaches: the strengths are as follows: (i) Easy to understand the reasoning behind the outcome; (ii) can deal with outliers. The weaknesses are as follows: (i) computationally intensive; (ii) sensitive to the similarity function; (iii) categorical variables need to be converted to numeric type; (iv) cannot handle missing values; (v) difficult to get the solution if similar work has not been done in the past.

(D) Fuzzy logic: The strengths are as follows: (i) It is based on the theory of classes with soft boundaries so it can deal with uncertainty in the data caused by measurement error during data collection; (ii) it can also deal with uncertainty in the model; (iii) gives improved performance if combined with ML or non-ML models; (iv) it is similar to human reasoning process. Its only weakness is that it becomes computationally intensive when combined with ML or non-ML models.

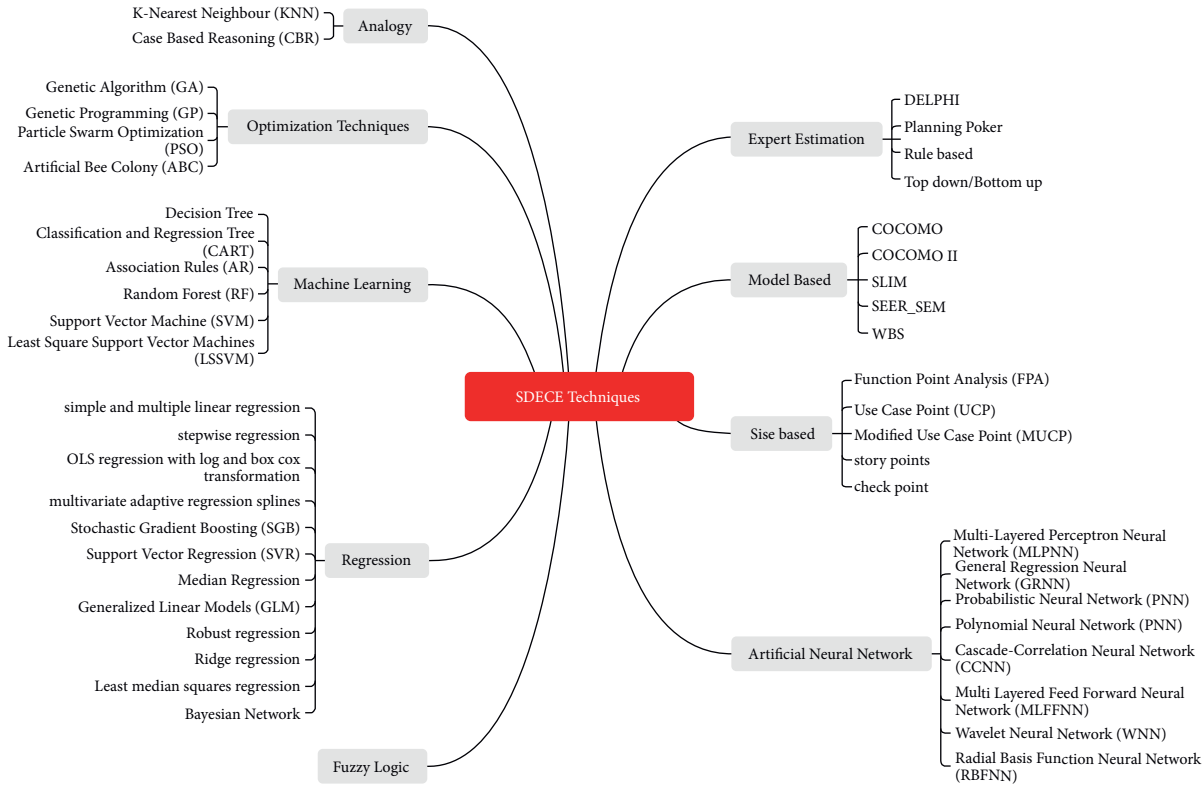

Figure 1: The SDECE techniques based on review.

Table 2: The datasets and accuracy measures.

The most commonly used accuracy measures: magnitude of relative error (MRE), mean magnitude relative error (MMRE), median magnitude relative error (MdMRE), percentage relative error deviation (PRED)
The most commonly used datasets: NASA, ISBSG, COCOMO, albrecht, desharnais, kemerer

(E) ML (Machine learning) techniques: Tree-based model and SVM are the most used ML techniques for SDECE. Each ML technique has its own strengths and weaknesses. The decision tree (DT), CART, and RF techniques fall under tree-based ML models, and its strengths are as follows: (i) intuitive, so easy to understand and interpret the results of model; (ii) can handle both categorical and numeric data; (iii) suitable when nonlinear relation exists in the data; (iv) robust with the outliers or we can say it has the capability to deal with the outliers. Its weaknesses are as follows: (i) DT is prone to overfitting if the dataset is small; (ii) cannot deal with missing values; (iii) time complexity is high for a large dataset; (iv) a small change in data can have a large change in the model.

The strengths of SVM are as follows: (i) It is suitable for high dimensional data; (ii) learns nonlinear relationship in the data. The weaknesses are as follows: (i) memory intensive; (ii) may not scale well with large datasets.

(F) Optimization techniques: the strengths are as follows: (i) it is useful for feature weighting and feature selection; (ii) accuracy of the estimation improves if used in combination with ML or non-ML techniques. The weaknesses are as follows: (i) it is a nondeterministic approach, the so results may vary each time; (ii) computationally expensive.

(G) Model and size-based estimation: The strength is that it is very useful for project planning, control, and budgeting. Its weakness is that it is based on calibration of the past experience. Difficulty in estimation arises with unprecedented situation.

(H) Expertise-based estimation: Its strengths are that it is very useful when no quantifiable or empirical data is available. Its weakness is that it is purely based on knowledge and experience of the expert, so estimation is just opinion and it can be biased and may go wrong.

4. The Generic Automated Text-Mining Framework and Bibliometric Analysis

This section is divided into two parts: first part explains the generic automated text-mining framework to study the evolution of SDECE in the last five decades and the second part presents a bibliometric analysis of the selected 1015 research papers.

4.1. The Generic Automated Text-Mining Framework for Identifying Research Trends and Patterns. In this section, we present the generic automated text-mining framework and use it to investigate research trends and techniques used for SDECE by analyzing the title, abstract, and author's keywords of the selected 1015 research papers published in the last five decades. The framework is shown diagrammatically in Figure 2.

The text mining is applied to (i) title, (ii) abstract, and (iii) authors' keywords of research papers. We have used "tm," "RWeka," and "wordcloud" package in the "R" tool. The steps used for text mining are as follows:

Step 1: The title of research papers was first loaded in "R" from the CSV file downloaded from the Scopus database

Step 2: We then created a corpus of the documents, where each title is treated as a separate document

Step 3: The third step was text cleaning, and we performed following text cleaning tasks:

(i) Converting text to lower case

(ii) Removing punctuations, whitespace, numbers, and special characters from the text

(iii) Removing the stopwords. Stopwords are the words that occur very frequently in the document, such as "the," "this," "and", but do not help in extracting any meaningful insights from the text data

Step 4: The next step was to create tokens of the words and find their frequency using "NgramTokenizer" function in "Rweka" package in 'R'

Step 5: The last step was to create WordCloud using word-frequency table created in the third step

We repeated the above process for the abstracts and authors' keywords of the selected 1015 papers. We also performed decade-wise analysis using title, abstract, and keywords of the research papers published in each decade. We stored the results of Step 3 (word frequency table) in CSV file format so that we could cross-check WordCloud and word-frequency table.

We address the following research questions using the proposed framework:

RQ1: What are the most frequently used SDECE techniques? What is research trend and how SDECE techniques have evolved in the last five decades?

RQ2: What are the most frequently used datasets in SDECE studies?

RQ3: What are the most frequently used accuracy measures in SDECE studies?

Results of the text mining (i) using all 1015 papers and (ii) papers published in each decade are shown in Table 3. The first column in the table shows WordCloud using title, second column shows WordCloud using authors' keywords, and the third column shows WordCloud using the abstract of the research papers. The prominent words in each WordCloud are given just below the WordCloud for better understanding. These prominent words indicate the most commonly used/referred/discussed techniques for SDECE. The first row in Table 3 shows WorldCloud of the papers published between the year 1971 and May 2020. The other rows in Table 3 show WordCloud of research papers published in each decade.

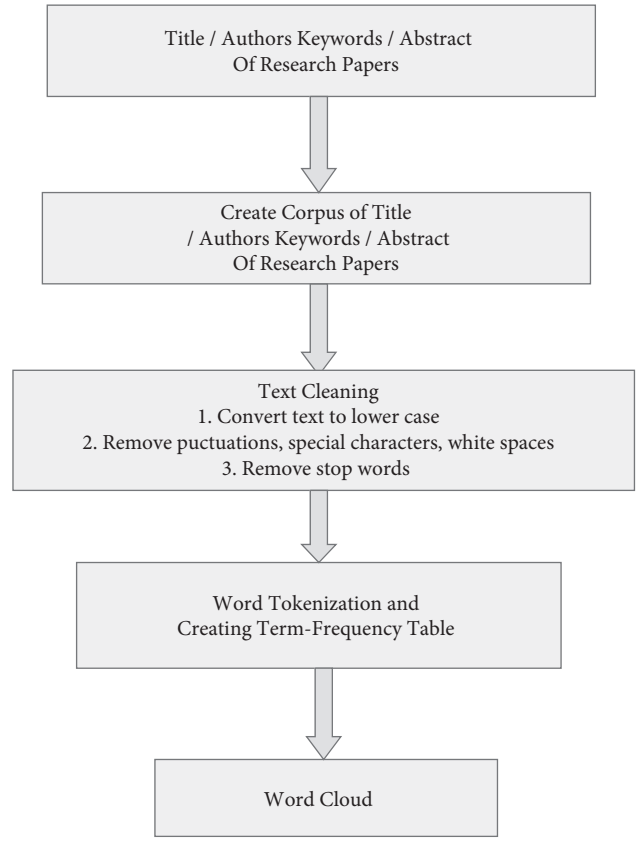

Figure 2: A Generic Text-Mining Framework to investigate changing research trends.

From Table 3, it is observed that the five most common techniques used for SDECE in the last five decades (1971 to May 2000) are fuzzy logic, artificial neural network, regression, analogy-based approach, and COCOMO model. The results also show that the other commonly used techniques are optimization, use case points, function point analysis, machine learning, COCOMO II, and CBR. There is a small variation in the most common techniques identified based on the analysis of the title, keywords, and abstract of the research papers. The SDECE technique mentioned in the title of the research paper generally indicates that the technique is proposed or used in the research paper for SDECE, whereas the techniques listed in the authors' keywords and abstract of the research paper may indicate that the technique is either proposed/used/referred/discussed in the paper or compared with other existing techniques. Therefore, we strongly believe that the title-based text mining approach gives us information about the technique proposed/used by the researcher for SDECE, whereas, the keywords- and abstract-based text mining results give us information about the most discussed/proposed/used/referred technique or it is compared with the other techniques.

Table 3: The text-mining results using the title, keywords, and abstracts of the research papers.

Title	Keywords	Abstract
Papers between period 1971 and 2020 (number of papers: 1015)		
	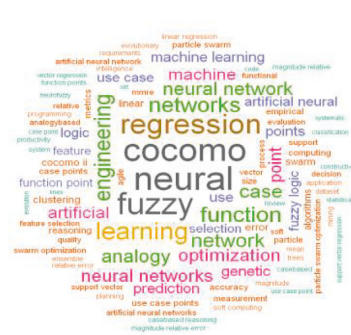	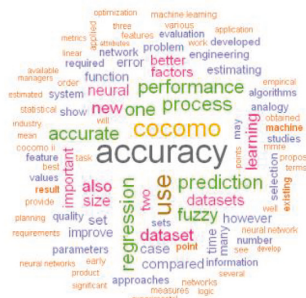
Techniques: Fuzzy logic, ANN, regression, analogy based approach, cocomo, optimization, use case points, machine learning, function point analysis, cocomo ii, CBR, particle swarm optimization, feature selection, support vector.	Techniques: ANN, cocomo, fuzzy logic, regression, analogy based approach, optimization, ML, use case points, function point analysis, cocomo ii, clustering, particle swarm optimization, CBR, support vector, feature selection, soft computing, trees, ensemble, support vector, Dataset:NASA, metrics: MMRE, MRE	Techniques:cocomo, regression, fuzzy logic, ANN, analogy based apporach, ML, cocomo ii, optimization, use case points, clustering, feature selection, function point analysis, CBR, ensemble, particle swarm optmization, trees, support vector, dataset: ISBSG, NASA, Metrics:MMRE, pred, MRE
Papers between period 2011 and 2020 (number of papers: 629)		
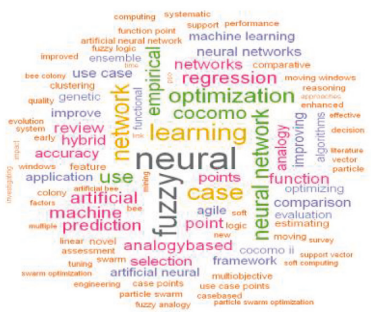	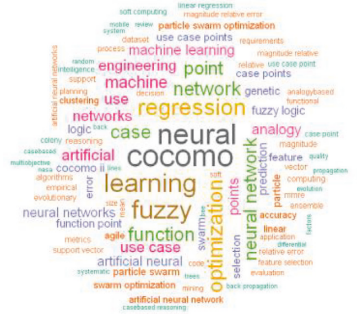	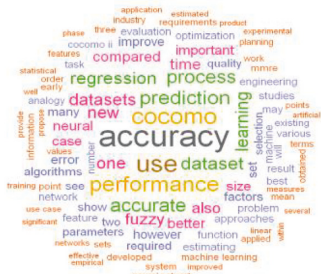
Techniques: ANN, fuzzy approach, optmization, cocomo, regression, analogy based, approach, use case points, ML, cocomo ii, GA, ensemble, function point, particle swarm optimization, CBR, artificial bee colony, dataset: ISBSG	Techniques: Cocomo, ANN, fuzzy approach, regression, optimization, use case points, analogy, machine learning, function point analysis, GA, cocmo ii, particle swarm optimization, clustering, support vector, metrics: MMRE, MRE, dataset: ISBSG, NASA	Techniques: Cocomo, regression, fuzzy approach, neural, optimization, cocomo ii, analogy based approach, machine learning, use case points, swarm, function point, Metrics: MMRE, pred, Dataset:ISBSG, NASA

Table 3: Continued.

Title	Keywords	Abstract
Papers between period 2001 and 2010 (number of articles: 306)		
Title	Keywors	Abstract
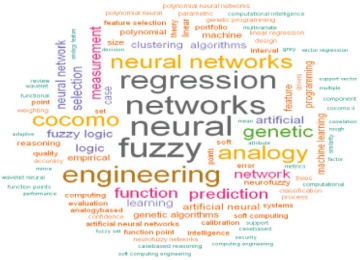		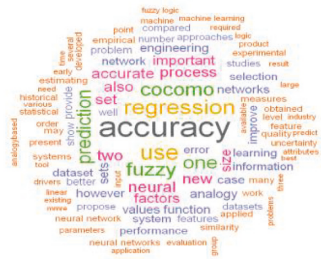
Techniques: Fuzzy, ANN, regression, analogy based, cocomo, clustering, function point, soft computing, GP, GRA, machine learning, radial basis function, use case point, cocomo ii, CBR, metrics: MMRE	Techniques: ANN, fuzzy approach, regression, analogy, cocomo, GA, clustering, ML, function point, soft computing, genetic programming, linear regresion, polynomial NN, CBR, cocomo ii, SVR, metrics: MMRE, dataset: ISBSG	Techniques: Regression, fuzzy, cocomo, neural, analogy, ML, cocomo ii, function point, use case point, metrics: MMRE, dataset: ISBSG, NASA
Papers between period 1991 and 2000 (number of articles: 57)		
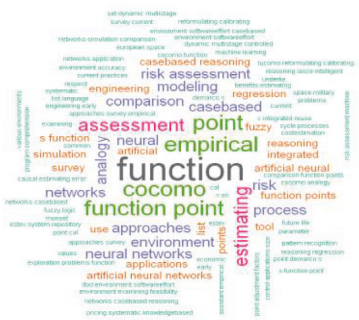	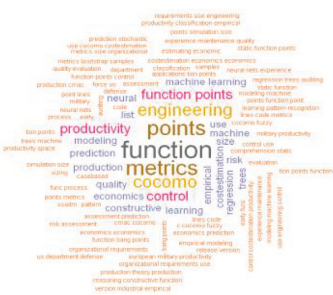	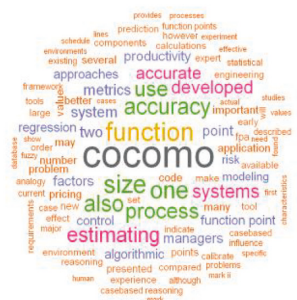
Techniques: Cocomo, function point, analogy, case based, ANN, fuzzy, regression	Techniques: COCOMO, function point, ML, ANN, regression, trees	Techniques:Cocomo, function point, regression, analogy, case based, fuzzy logic, cocomo ii
Papers between period 1981 to 1990 (number of articles-21)		
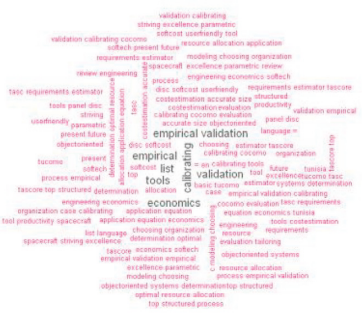	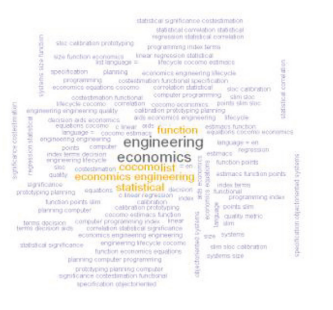	
Techniques: Calibrating, economics, empirical	Techniques: Economics, engineering, cocomo	Techniques: Process, productivity, tool, cocomo, calibration

However, the top five techniques based on the text analysis of the title, authors' keywords, and abstract of the research paper are the same.

4.2. Evolution of SDECE Techniques. The text-mining results based on the title of the research papers published during the period between 2011 and May 2020 show that ANN, fuzzy approach, optimization, COCOMO, and regression are the most used techniques. The text-mining results based on keywords and the abstract of the research papers show that COCOMO is the most discussed technique. The other widely used techniques are analogy-based approach, use case point, function point analysis, machine learning, COCOMO II, and GA.

The text-mining results for the period between 2001 and 2010 show that fuzzy approach, ANN, regression, analogy-based, and COCOMO are the most used techniques. It is also observed that regression is the most discussed technique based on text analysis of the abstract. The title-based text mining results show that fuzzy-based approach is the most used technique, which is followed by ANN, regression, analogy, and COCOMO. The other widely used techniques during this period are clustering, function point analysis, soft computing, GP, machine learning, use case point, and COCOMO II.

The text-mining results for the period between 1991 and 2000 show that COCOMO and function point analysis are the most used techniques followed by analogy, CBR, ANN, regression, fuzzy logic, and ML techniques. As there exist very few select research papers (21) in our study for the period between 1981 and 1990, the WordCloud does not have a large set of words. However, the results show that COCOMO was the most popular method during this period. We did not apply text mining to the research papers published during the period between 1971 and 1980 because out of the total 1015 selected papers, we had only two papers for that period. The number of research papers published during this period may be large but we found only two papers in the set out of the selected 1015 papers.

Thus, the text mining results show that (i) for the initial period between 1981 and 1990 focus of the research was on calibration and productivity and COCOMO was the most used technique; (ii) during the period between 1991 and 2000 COCOMO became more popular and researchers also proposed functions point analysis, regression, analogy-based approach, CBR, and fuzzy-based techniques; (iii) fuzzy approach, ANN, and regression-based approaches became more popular during the period between 2001 and 2010 followed by COCOMO, analogy-based approach, clustering and ML techniques; (iv) during the period between 2011 and 2020, ANN-based approach was more popular followed by fuzzy logic, optimization, COCOMO, regression, and analogy based approach. Use case point, function point analysis, and machine learning were other popular techniques during that period; (v) for the last fifty years, i.e., for the period between 1971 and May 2020, the most popular technique based on analysis of the studied research papers are fuzzy logic, ANN, regression, analogy-based approach, COCOMO followed by optimization, use case point, function point, ML, COCOMO II, clustering, and CBR-based approaches.

We can map the evolution of SDECE techniques with the evolution of the programming languages. In the initial period (1970 to 1990) COCOMO was the most popular model because software systems were being developed using the assembly and procedure-oriented programming languages and COCOMO model is based on a number of lines of code written to develop the software system.

In the later stage (1991–2000), function point analysis, regression, analogy-based approaches became more popular because by that time a large number of software projects data was recorded and available for the estimation of the newly developed software systems. Regression is a statistical technique, which is used to estimate efforts and cost using historical software projects data, whereas in analogy-based approach, efforts are estimated by considering efforts required for similar systems/projects developed in the past. Function point analysis also became more popular because software systems were being developed using functional programming languages.

Later, during the period between 2001 and 2010, fuzzy logic and ANN techniques became more popular. Fuzzy logic was popular because it takes into account vagueness and imprecise information, and ANN was popular because some researchers were of the opinion that ANN gives more accurate estimation than the existing techniques. During the same period due to the emergence of machine learning techniques and the availability of the existing projects' data, people also started using different ML techniques for effort and cost estimation. Since researchers started using ML techniques, optimization also became more popular as it helped in selecting the most appropriate features. Also, as systems were being developed using object-oriented programming language, scholars started using use case point techniques for SDECE.

For the period between 2010 and 2020, researchers started using existing techniques in combination with the other existing techniques for better estimation. In the recent past, scholars have used deep learning techniques for prediction in other domains, but there is a lack of research in using deep learning techniques for SDECE. Therefore, we recommend that scholars should explore this option for SDECE.

We have also identified the most common datasets and accuracy measures used for SDECE. As researchers rarely use the dataset name and accuracy measures in the title of the research article, finding the most frequently used datasets and accuracy measures by applying text mining to the title of the research papers is difficult. However, researchers use the dataset name and accuracy measures in authors' keywords and abstract of the research papers. Therefore, we could find the most frequent datasets and accuracy measures by applying text mining on authors' keywords and the abstracts of the research papers. The most frequently used datasets and accuracy measures for each decade and for the period between 1974 to May 2020 are also given in Table 3. It is observed that (i) NASA and ISBSG are the most used datasets; and (ii) MMRE, MRE, and PRED are the most used accuracy measures for the period between

1971 and May 2020, and also for each decade starting from 1970s to 2020.

Using the text mining, we have also identified whether focus of the research was on the SDEE or SDCE. The results of the text mining for the same are presented in Table 4. The results show that (i) for the initial period from 1981 to 1990 focus of the research papers was on the cost estimation; (ii) for the period between 1991 to 2000 and 2001 to 2010 the focus was on cost estimation followed by effort estimation; (iii) for the period between 2011 and 2020 most studies discussed effort estimation than the cost estimation; (iv) for the past five decades, from 1974 to May 2020 most studies discussed effort estimation than the cost estimation. However, it is important to note that some researchers use these two terms interchangeably.

4.3. Bibliometric Analysis. In this section, we present the bibliometric analysis of select 1015 research papers published during the period between 1974 and May 2020 to address the research questions from RQ4 to RQ7.

RQ4: What is the distribution of SDECE papers and its citations by document type?

The distribution of the selected papers by document type is given in Table 5. The contribution of the journal and conference documents is 39.11% and 59.41%, respectively. However, in terms of the number of citations, journal papers received more citations (68.62%) as compared to the conference papers (31.04%). The contribution of the books and book chapters in terms of the number of papers as well as citations is very less.

RQ5: How many research papers are published on SDECE each year and each decade since 1970?

The distribution of papers published in the last five decades is given in Table 6. It is observed that about 92% of the papers were published in the last 2 decades. Figure 3 shows the graph of a number of papers published in each year since 1974. As we have included paper till May 2020, the number of papers published in the year 2020 is less as compared to the year 2019.

RQ6: What is the distribution of citations of SDECE papers?

This research question is further divided into five subquestions as follows.

RQ6.1: What is the distribution of journal and conference papers with zero citation and with one or more than one citation?

The number of citations of the research paper plays an important role in deciding the influence or impact of the research paper. Based on articles selected for this study, the count of citations for journal and conference articles is given in Table 7. It is observed that 22.36% of the papers have received zero citations. The proportion of the journal and conference articles having zero citations is 19.89% and 23.21%, respectively.

RQ6.2: What are highly cited papers?

We have identified highly cited papers using an average annual number of citations received by the paper per year since its publication. The top 5 articles based on the average annual number of citations are shown in Figure 4. The top five articles are published in the journal. It is also found that out of the top 10 articles, all articles were from the journal except one at the seventh position.

RQ7: Who are the top authors in terms of the number of papers and number of citations?

The contribution of authors is measured using two metrics: (i) number of articles published by the author and (ii) number of citations received by the author for all his articles selected in this study. The top ten authors based on these two metrics are given in Table 8. We have also created a WordCloud of authors using the authors column of the CSV file of select 1015 papers. The resulting WordCloud (Figure 5) of the author's contribution based on the number of papers matches with the manual calculations of the number of papers published by the top author (Refer Table 8).

The bibliometric analysis of select 1015 papers shows that (i) impact of journal papers in terms of the number of citations is more than the conference papers, though the number of conference papers is more than the journal papers; (ii) IEEE transaction on software engineering, Information and Software technology, Journal of Systems and Software are the top journal sources for the research on software development effort and cost estimation; (iii) Jorgensen, Boehm, and Shepperd are the most cited researchers whereas Idri, Angeles, and Keung have published the maximum number of research papers on SDECE.

5. Validation of the Framework

In this section, we validate the results of the proposed automated text mining framework by comparing it with the (i) results/outcome of the comprehensive systematic literature reviews (SLRs) done in the past; and (ii) results obtained manually by reading the title of all selected 1015 research papers.

5.1. Validation Using past SLRs. A summary of the results based on five selected comprehensive systematic literature reviews conducted in the past is shown diagrammatically in Figure 6.

The five SLRs conducted in the past show that (i) regression, ANN, fuzzy logic, analogy-based approach, CBR, DT, SVR, GA, and GP are the most used techniques; (ii) MRE, MMRE, Pred, and MdMRE are the most used accuracy measures; and (iii) NASA, ISBSG, and COCOMO are the most used datasets for SDECE.

Out of five comprehensive SLRs, three studies show that regression is the most used non-ML technique for SDECE. Two studies that reviewed research papers published between the year 2000 and 2017 show that (i) the most used SDECE techniques are regression, ANN, DT, fuzzy logic, analogy, and CBR-based approaches; (ii) the most used datasets are NASA, ISBSG, and COCOMO; and (iii) the most used accuracy measures are MRE, MMRE, and Pred.

5.2. Validation by Reading Title of the Research Papers. The results obtained manually by reading the title of the selected 1015 research papers are shown in Figure 7. The

Table 4: What is research focus: effort or cost estimation?

Period: 1974–2020	Period: 2011–2020	Period: 2001–2010
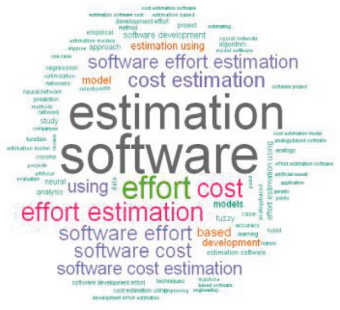	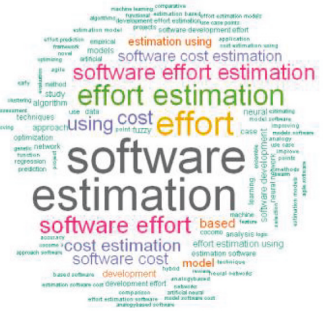	
Effort estimation, cost estimation	Effort estimation, cost estimation	Cost estimation, effort estimation
Period: 1991–2000	Period: 1981–1990	
		
Cost estimation, effort estimation	Cost estimation	

Table 5: Distribution of papers and citations by document type.

Document type	Articles	Citations
Journal articles	397 (39.11%)	11646 (68.62%)
Conference papers	603 (59.41%)	5267 (31.04%)
Book chapters	14 (1.38%)	48 (0.28%)
Books	1 (0.10%)	10 (0.06%)
Total	1015	16971

Table 6: Distribution of the papers published in each decade.

Decade	Conference articles	Journal articles	Book and book chapters	Total
2011–2020	383	236	10	629 (61.97%)
2001–2010	196	106	4	306 (30.14%)
1991–2000	17	39	1	57 (05.61%)
1981–1990	7	14	0	21 (02.06%)
1971–1980	2	0	0	2 (0.19%)

results show that fuzzy logic, analogy-based approach, ANN, regression, and optimization techniques are the most used techniques for SDECE. We did not validate the most-used datasets and accuracy measures by reading the title of the research papers because usually it is not mentioned in the title of the research paper.

Thus, the careful examination of the results obtained manually by reading the title of research papers and the outcome of the five selected SLRs shows that these results are almost similar with the results obtained using the proposed text-mining approach. Therefore, we strongly believe that the proposed automated text-mining framework is very useful to investigate research trends in an identified research area and makes our job easy compared to amount of time and efforts required to do so by systematic literature review method.

6. Discussions

We have used the following search strings to search literature from the Scopus database: "software effort estimation" OR "software cost estimation". The search string was designed by considering the objectives and research questions of the study. As papers are selected only from the

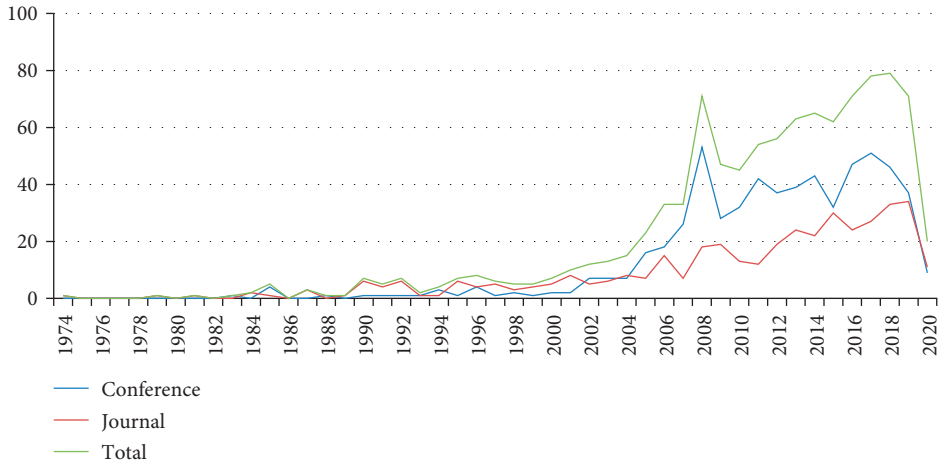

Figure 3: No. of papers per year.

Table 7: Distribution of papers with zero and with one or more than one citation.

	Journal articles	Conference articles	Book chapters	Books	Total
Papers with one or more than one citations	318	463	6	1	788
Papers with zero citations	79	140	8	0	227
Total	397	603	14	1	1015

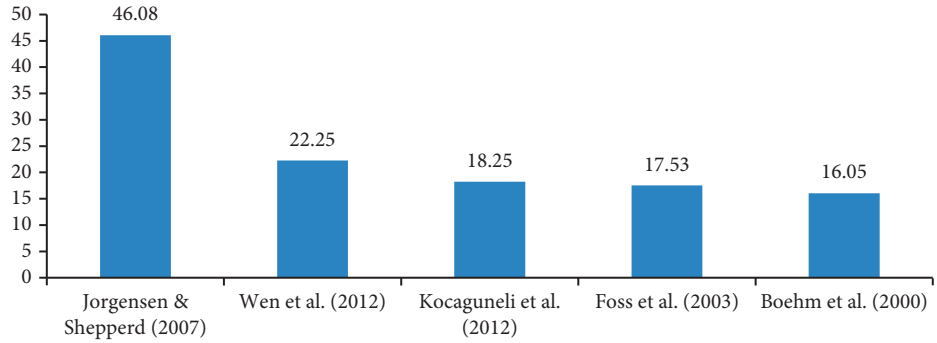

Figure 4: Highly cited papers.

Table 8: Contribution of the authors by the number of papers and citations.

Authors by number of papers		Authors by no. of citations	
Author name	No. of papers	Author name	No. of citations
Idri	35	Jorgensen	1378
Angelis	32	Boehm	1227
Keung	30	Shepperd	875
Mitts	23	Kitchenham	831
Boehm	20	Angelis	808
Azzeh	20	Menzies	671
Abran	20	Keung	658
Lokan	18	Kocaguneli	553
Jorgensen	17	Kemerer	523
Nassif	17	Stamelos	472

Figure 5: Contribution of authors by the number of papers.

Scopus database, there is a possibility that we may have missed some relevant papers which could be a potential threat to this study. However, as Scopus is the largest abstract and citation database for peer-reviewed literature, it can offer the widest coverage of literature that one can achieve using a single search engine and it also mitigates the exclusion of relevant important papers [86, 87]. Further, we did not apply any exclusion criteria on the searched results except that the paper should be written in English language, and the focus of the study should be on SDECE. Therefore, we believe that there was no bias in the paper selection process. When we checked the final list of selected papers

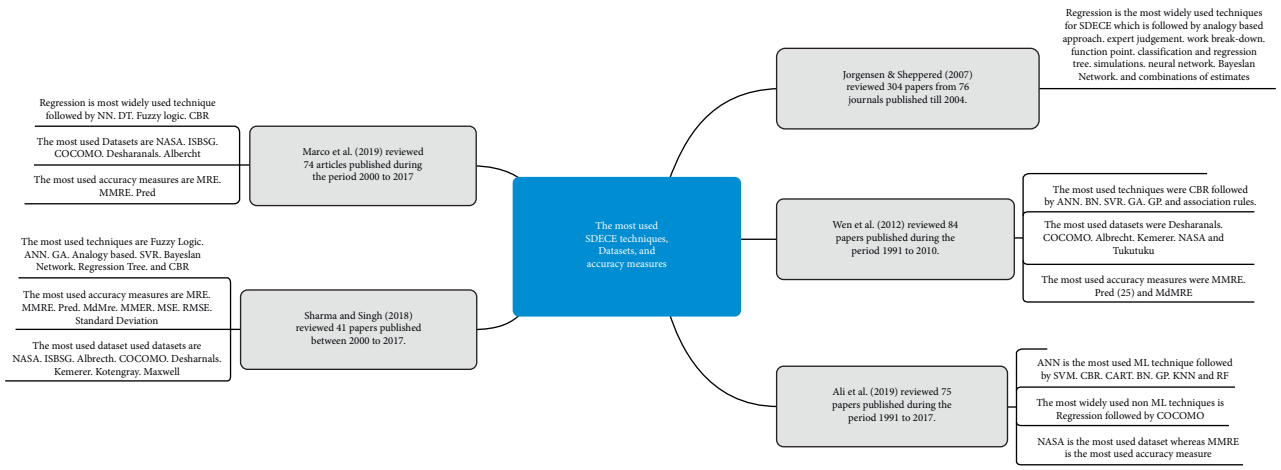

Figure 6: Outcomes of the past five SLRs.

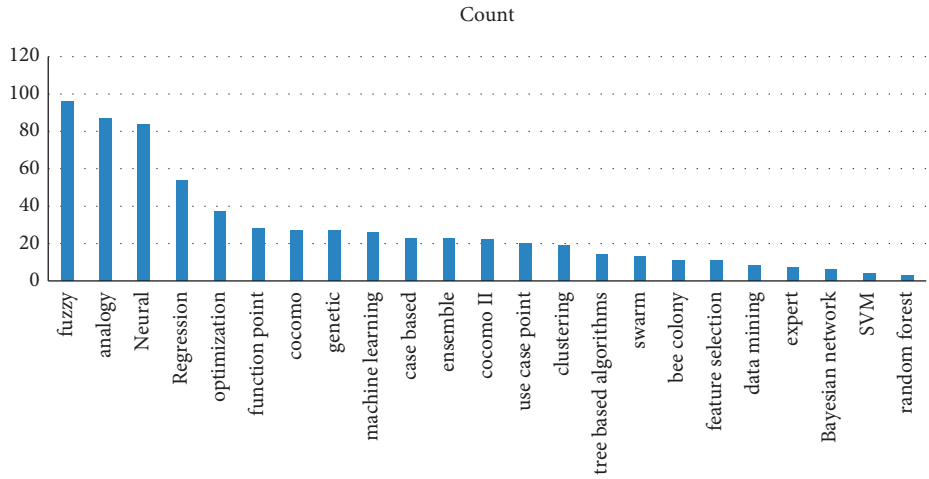

Figure 7: Most used SDECE techniques identified by reading the title of the papers.

and found that all the selected papers were relevant to meet the objectives of the study. We strongly believe that our analysis results would not be much different had we included more papers from the Scopus or other indexing databases because the number of papers selected in the study is 1015, which is a very good number to achieve research objectives. Another threat to the study with respect to using text mining for investigating the most popular technique in each decade is that if scholars use the name of the technique in a slightly different way than the usual one, then that technique would be treated as a different one. However, in most manuscripts, the techniques are named/referred in the same manner barring a few cases. Therefore, that will not affect much in capturing the overall research trend.

7. Conclusion

In this research article, a generic automated text mining framework is proposed to investigate the research trends by analyzing the title, keywords, and abstract of research papers published in an identified area. The proposed framework is used to investigate research trends by analyzing select 1015 research papers published on SDECE in the last five decades. It is found that fuzzy logic, artificial neural networks (ANN), regression, analogy, and COCOMO are the most popular techniques followed by use case point, function point analysis, and machine learning-techniques. The NASA and ISBSG are the most used datasets while MMRE, MRE, and PRED are the most used accuracy measures. It is observed that there is a lack of research on using deep learning techniques for software effort and cost estimation. Therefore, we recommend research scholars to explore deep learning techniques for software development effort and cost estimation. The analysis is also carried out to investigate the most used techniques, datasets, and accuracy measures in each decade to understand how SDECE techniques have evolved in the last five decades.

The results of the proposed framework are validated by comparing it with the outcome of previously published review work, and we have found that the results are consistent. Therefore, the proposed text mining framework is beneficial for futuristic study and can reduce the efforts required to investigate research trends on the topic of an identified research area. To uncover research trends, we have

analyzed the titles, keywords, and abstracts of the research papers separately and found that there is no significant difference in the outcome except slight change in the rank of the most popular SDECE techniques. The detailed bibliometric analysis is also performed along with the metareview of the survey papers, which aids to determine the most relevant papers, venues, authors, and contributions of researchers in the field of the proposed research. A study is recommended to uncover the research patterns and trends by analyzing numerous research papers collected from different electronic databases as this study is limited to research papers collected only from the Scopus database.

Data Availability

The data are available for the experimental study.

Conflicts of Interest

The authors have nothing to declare as conflicts of interest with respect to this manuscript.

References

[1] S. Di Martino, F. Ferrucci, C. Gravino, and F. Sarro, "Assessing the effectiveness of approximate functional sizing approaches for effort estimation," *Information and Software Technology*, vol. 123, Article ID 106308, 2020.

[2] A. B. Nassif, M. Azzeh, A. Idri, and A. Abran, "Software development effort estimation using regression fuzzy models," *Computational Intelligence and Neuroscience*, vol. 2019, Article ID 8367214, 17 pages, 2019.

[3] A. Ali and C. Gravino, "A systematic literature review of software effort prediction using machine learning methods," *Journal of Software: Evolution and Process*, vol. 31, no. 10, 2019.

[4] H. L. T. K. Nhung, H. T. Hoc, and V. V. Hai, "A review of use case-based development effort estimation methods in the system development context," in *Intelligent Systems Applications in Software Engineering*, pp. 484–499, Springer, Scam, Switcherland, 2019.

[5] K. Molokken and M. Jorgensen, "A review of software surveys on software effort estimation," in *Proceedings of the 2003 International Symposium on Empirical Software Engineering, ISESE*, Rome, Italy, September, 2003.

[6] E. Kocaguneli, T. Menzies, and J. W. Keung, "On the value of ensemble effort estimation," *IEEE Transactions on Software Engineering*, vol. 38, no. 6, pp. 1403–1416, 2011.

[7] K. Dejaeger, W. Verbeke, D. Martens, and B. Baesens, "Data mining techniques for software effort estimation: a comparative study," *IEEE Transactions on Software Engineering*, vol. 38, no. 2, pp. 375–397, 2011.

[8] Y. Shan, R. I. McKay, C. J. Lokan, and D. L. Essam, "Software project effort estimation using genetic programming," *IEEE 2002 International Conference on Communications, Circuits and Systems and West Sino Expositions*, vol. 2, pp. 1108–1112, 2002.

[9] B. Alsaadi and K. Saeedi, "Data-driven effort estimation techniques of agile user stories: a systematic literature review" Artificial Intelligence Review," vol. 1-32, 2022.

[10] M. Jorgensen and M. Shepperd, "A systematic review of software development cost estimation studies," *IEEE Transactions on Software Engineering*, vol. 33, no. 1, pp. 33–53, 2006.

[11] C. F. Kemerer, "An empirical validation of software cost estimation models," *Communications of the ACM*, vol. 30, no. 5, pp. 416–429, 1987.

[12] B. Boehm, B. Clark, E. Horowitz, C. Westland, R. Madachy, and R. Selby, "Cost models for future software life cycle processes: cocomo 2.0," *Annals of Software Engineering*, vol. 1, no. 1, pp. 57–94, 1995.

[13] N. Mittas and L. Angelis, "Ranking and clustering software cost estimation models through a multiple comparisons algorithm," *IEEE Transactions on Software Engineering*, vol. 39, no. 4, pp. 537–551, 2012.

[14] C. Pareta, N. S. Yaadav, A. Kumar, and A. K. Sharma, "Predicting the accuracy of machine learning algorithms for software cost estimation," in *Advances in Intelligent Systems and Computing*, pp. 605–615, Springer, Singapore, 2019.

[15] A. A. Fadhil, R. G. H. Alsarraj, and A. M. Altaie, "Software cost estimation based on dolphin algorithm," *IEEE Access*, vol. 8, Article ID 75279, 2020.

[16] J. Wen, S. Li, Z. Lin, Y. Hu, and C. Huang, "Systematic literature review of machine learning based software development effort estimation models," *Information and Software Technology*, vol. 54, no. 1, pp. 41–59, 2012.

[17] B. Boehm, C. Abts, and S. Chulani, "Software development cost estimation approaches—a survey," *Annals of Software Engineering*, vol. 10, no. 1-4, pp. 177–205, 2000.

[18] G. R. Finnie, G. E. Wittig, and J.-M. Desharnais, "A comparison of software effort estimation techniques: using function points with neural networks, case-based reasoning and regression models," *Journal of Systems and Software*, vol. 39, no. 3, pp. 281–289, 1997.

[19] R. Betteridge, "Successful experience of using function points to estimate project costs early in the life-cycle," *Information and Software Technology*, vol. 34, no. 10, pp. 655–658, 1992.

[20] A. J. Albrecht and J. E. Gaffney, "Software function, source lines of code, and development effort prediction: a software science validation," *IEEE Transactions on Software Engineering*, vol. SE-9, no. 6, pp. 639–648, 1983.

[21] V. Van Hai, H. Le Thi Kim Nhung, and H. T. Hoc, "A review of software effort estimation by using functional points analysis," in *Computational Statistics and Mathematical Modeling Methods in Intelligent Systems*, pp. 408–422, Springer, Cham, Switcherland, 2019.

[22] M. Ochodek, J. Nawrocki, and K. Kwarciak, "Simplifying effort estimation based on use case points," *Information and Software Technology*, vol. 53, no. 3, pp. 200–213, 2011.

[23] A. B. Nassif, L. F. Capretz, and D. Ho, "Estimating software effort based on use case point model using sugeno fuzzy inference system," in *Proceedings of the 2011 IEEE 23rd International Conference on Tools with Artificial Intelligence*, pp. 393–398, Boca Raton, FL, USA, November, 2011.

[24] M. Azzeh and A. B. Nassif, "A hybrid model for estimating software project effort from Use Case Points," *Applied Soft Computing*, vol. 49, pp. 981–989, 2016.

[25] W. T. Lee, K. H. Hsu, J. Lee, and J. Y. Kuo, "Applying software effort estimation model based on work breakdown structure," in *Proceedings of the 2012 Sixth International Conference on Genetic and Evolutionary Computing*, pp. 192–195, IEEE, Kitakyushu, Japan, August, 2012.

[26] F. Walkerden and R. Jeffery, "An empirical study of analogy-based software effort estimation," *Empirical Software Engineering*, vol. 4, no. 2, pp. 135–158, 1999.

[27] M. Shepperd, C. Schofield, and B. Kitchenham, "Effort estimation using analogy," in *Proceedings of IEEE 18th International Conference on Software Engineering*, pp. 170–178, IEEE, Berlin, Germany, March, 1996.

[28] L. Angelis and I. Stamelos, *Empirical Software Engineering*, vol. 5, no. 1, pp. 35–68, 2000.

[29] E. Kocaguneli, T. Menzies, A. Bener, and J. W. Keung, "Exploiting the essential assumptions of analogy-based effort estimation," *IEEE Transactions on Software Engineering*, vol. 38, no. 2, pp. 425–438, 2011.

[30] J. Li, G. Ruhe, A. Al-Emran, and M. M. Richter, "A flexible method for software effort estimation by analogy," *Empirical Software Engineering*, vol. 12, no. 1, pp. 65–106, 2007.

[31] M. Azzeh, D. Neagu, and P. I. Cowling, "Analogy-based software effort estimation using Fuzzy numbers," *Journal of Systems and Software*, vol. 84, no. 2, pp. 270–284, 2011.

[32] I. Myrtveit and E. Stensrud, "A controlled experiment to assess the benefits of estimating with analogy and regression models," *IEEE Transactions on Software Engineering*, vol. 25, no. 4, pp. 510–525, 1999.

[33] Y. F. Li, M. Xie, and T. N. Goh, "A study of mutual information based feature selection for case based reasoning in software cost estimation," *Expert Systems with Applications*, vol. 36, no. 3, pp. 5921–5931, 2009.

[34] D. Wu, J. Li, and C. Bao, "Case-based reasoning with optimized weight derived by particle swarm optimization for software effort estimation," *Soft Computing*, vol. 22, no. 16, pp. 5299–5310, 2018.

[35] P. Sentas, L. Angelis, I. Stamelos, and G. Bleris, "Software productivity and effort prediction with ordinal regression," *Information and Software Technology*, vol. 47, no. 1, pp. 17–29, 2005.

[36] A. B. Nassif, D. Ho, and L. F. Capretz, "Towards an early software estimation using log-linear regression and a multilayer perceptron model," *Journal of Systems and Software*, vol. 86, no. 1, pp. 144–160, 2013.

[37] O. Fedotova, L. Teixeira, and H. Alvelos, "Software effort estimation with multiple linear regression: review and practical application," *Journal of Information Science and Engineering*, vol. 29, no. 5, pp. 925–945, 2013.

[38] H. Park and S. Baek, "An empirical validation of a neural network model for software effort estimation," *Expert Systems with Applications*, vol. 35, no. 3, pp. 929–937, 2008.

[39] I. F. de Barcelos Tronto, J. D. S. da Silva, and N. Sant'Anna, "An investigation of artificial neural networks based prediction systems in software project management," *Journal of Systems and Software*, vol. 81, no. 3, pp. 356–367, 2008.

[40] N. Tadayon, "Neural network approach for software cost estimation," *IEEE International Conference on Information Technology: Coding and Computing (ITCC'05)-Volume II*, vol. 2, pp. 815–818, 2005.

[41] V. S. Dave and K. Dutta, "Neural network based models for software effort estimation: a review," *Artificial Intelligence Review*, vol. 42, no. 2, pp. 295–307, 2014.

[42] M. A. Ahmed, M. Omolade Saliu, and J. AlGhamdi, "Adaptive fuzzy logic-based framework for software development effort prediction," *Information and Software Technology*, vol. 47, no. 1, pp. 31–48, 2005.

[43] C. S. Reddy and K. V. S. N. Raju, "An improved fuzzy approach for COCOMO's effort estimation using Gaussian membership function," *Journal of Software*, vol. 4, no. 5, pp. 452–459, 2009.

[44] C. López-Martín, C. Yáñez-Márquez, and A. Gutiérrez-Tornés, "Predictive accuracy comparison of fuzzy models for software development effort of small programs," *Journal of Systems and Software*, vol. 81, no. 6, pp. 949–960, 2008.

[45] X. Huang, D. Ho, J. Ren, and L. F. Capretz, "Improving the COCOMO model using a neuro-fuzzy approach," *Applied Soft Computing*, vol. 7, no. 1, pp. 29–40, 2007.

[46] K. Srinivasan and D. Fisher, "Machine learning approaches to estimating software development effort," *IEEE Transactions on Software Engineering*, vol. 21, no. 2, pp. 126–137, 1995.

[47] B. Baskeles, B. Turhan, and A. Bener, "Software Effort Estimation Using Machine Learning Methods," in *Proceedings of the 22nd International Symposium on Computer and Information Sciences*, pp. 1–6, IEEE, Ankara, Turkey, November, 2007.

[48] F. A. Amazal and A. Idri, "Estimating software development effort using fuzzy clustering-based analogy," *Journal of Software: Evolution and Process*, vol. 33, no. 4, 2021.

[49] R. R. Sinha and R. K. Gora, "Software effort estimation using machine learning techniques," in *Proceedings of the Advances in Information Communication Technology and Computing*, pp. 65–79, Noida, India, January, 2021.

[50] A. L. I. Oliveira, P. L. Braga, R. M. F. Lima, and M. L. Cornélio, "GA-based method for feature selection and parameters optimization for machine learning regression applied to software effort estimation," *Information and Software Technology*, vol. 52, no. 11, pp. 1155–1166, 2010.

[51] S.-J. Huang and N.-H. Chiu, "Optimization of analogy weights by genetic algorithm for software effort estimation," *Information and Software Technology*, vol. 48, no. 11, pp. 1034–1045, 2006.

[52] C. V. M. K. Hari and P. V. G. D. Reddy, "A fine parameter tuning for COCOMO 81 software effort estimation using particle swarm optimization," *Journal of Software Engineering*, vol. 5, no. 1, pp. 38–48, 2011.

[53] S. Chalotra, S. K. Sehra, Y. S. Brar, and N. Kaur, "Tuning of cocomo model parameters by using bee colony optimization," *Indian Journal of Science and Technology*, vol. 8, no. 14, 2015.

[54] D. K. K. Reddy and H. S Behera, "Software effort estimation using particle swarm optimization: advances and challenges," in *Computational Intelligence in Pattern Recognition"*, pp. 243–258, Springer, Singapore, 2020.

[55] V. Garousi and M. V. Mäntylä, "Citations, research topics and active countries in software engineering: a bibliometrics study," *Computer Science Review*, vol. 19, pp. 56–77, 2016.

[56] S. K. Sehra, Y. S. Brar, N. Kaur, and S. S. Sehra, "Research patterns and trends in software effort estimation," *Information and Software Technology*, vol. 91, pp. 1–21, 2017.

[57] M. Fernández-Diego and F. González-Ladrón-De-Guevara, "Potential and limitations of the ISBSG dataset in enhancing software engineering research: a mapping review," *Information and Software Technology*, vol. 56, no. 6, pp. 527–544, 2014.

[58] S. Rajper and Z. A. Shaikh, "Software development cost estimation: a survey," *Indian Journal of Science and Technology*, vol. 9, no. 31, 2016.

[59] S. Bilgaiyan, S. Sagnika, S. Mishra, and M. Das, "A systematic review on software cost estimation in agile software," *Development" Journal of Engineering Science & Technology Review*, vol. 10, no. 4, 2017.

[60] V. Venkataiah, M. Ramakanta, and M. Nagaratna, "Review on intelligent and soft computing techniques to predict software cost estimation," *IJAER*, vol. 12, no. 22, Article ID 12665, 2017.

[61] H. Hakimi, M. Kamalrudin, A. Pradana, and S. Sidek, "A review of using software cost estimation tools in software development process," *Journal of Advanced Research in Dynamical and Control Systems*, vol. 119, 2018.

[62] R. Marco, N. Suryana, and S. S. S. Ahmad, "A systematic literature review on methods for software effort estimation," *Journal of Theoretical and Applied Information Technology*, vol. 97, no. 2, 2019.

[63] M. A. Saleem, T. Alyas, R. Asfandayar Ahmad et al., "Systematic literature review of identifying issues in software cost estimation techniques," *International Journal of Advanced Computer Science and Applications*, vol. 10, no. 8, 2019.

[64] J. Hihn and H. Houabib-agahi, "Cost estimation of software intensive projects: a survey of current practices," in *Proceedings of the 13th International Conference on Software Engineering*, pp. 276–287, Austin, TX, USA, May, 1991.

[65] D. Yang, Q. Wang, M. Li, Y. Yang, K. Ye, and J. Du, "A survey on software cost estimation in the Chinese software industry," in *Proceedings of the Second ACM-IEEE International Symposium on Empirical Software Engineering and Measurement*, pp. 253–262, Kaiserslautern, Germany, January, 2008.

[66] J. Keung, "Software Development Cost Estimation Using Analogy: A Review," in *Proceedings of the Australian Software Engineering Conference*, pp. 327–336, Gold Coast, QLD, Australia, April, 2009.

[67] P. Rodríguez-Soria, J. J. Cuadrado-Gallego, J. A. G. de Mesa, and B. Martín-Herrera, "A Review of Parametric Effort Estimation Models for the Software Project Planning Process," in *Proceedings of the 22nd International Conference on Software Engineering & Knowledge Engineering SEKE*, pp. 135–140, San Francisco, CA, USA, January, 2010.

[68] A. Trendowicz, J. Münch, and R. Jeffery, "State of the practice in software effort estimation: a survey and literature review," in *Proceedings of the IFIP Central and East European Conference on Software Engineering Techniques*, pp. 232–245, Springer, Berlin, Heidelberg, Germany, September, 2008.

[69] T. Wijayasiriwardhane, R. Lai, and K. C. Kang, "Effort estimation of component-based software development - a survey," *IET Software*, vol. 5, no. 2, pp. 216–228, 2011.

[70] P. Faria and E. Miranda, "Expert Judgment in Software Estimation during the Bid Phase of a Project--An Exploratory Survey," in *Proceedings of the 2012 Joint Conference of the 22nd International Workshop on Software Measurement and the 2012 Seventh International Conference on Software Process and Product Measurement*, pp. 126–131, IEEE, Nagoya, Japan, Octobar, 2012.

[71] H. Hamza, A. Kamel, and K. Shams, "Software effort estimation using artificial neural networks: a survey of the current practices," in *Proceedings of the 2013 10th International Conference on Information Technology: New Generations*, pp. 731–733, IEEE, Las Vegas, NV, USA, April, 2013.

[72] B. Sigweni and M. Shepperd, "Feature weighting techniques for CBR in software effort estimation studies: a review and empirical evaluation," in *Proceedings of the 10th International Conference on Predictive Models in Software Engineering*, pp. 32–41, Torino, Italy, 2014, September.

[73] H. Rastogi, S. Dhankhar, and M. Kakkar, "A survey on software effort estimation techniques," in *Proceedings of the 2014 5th International Conference-Confluence the Next Generation Information Technology Summit*, pp. 826–830, IEEE, Noida, India, September, 2014.

[74] F. González-Ladrón-de-Guevara and M. Fernández-Diego, "ISBSG variables most frequently used for software effort estimation: a mapping review," in *Proceedings of the 8th ACM/IEEE International Symposium on Empirical Software Engineering and Measurement*, pp. 1–4, New York, USA, September, 2014.

[75] M. El Bajta, A. Idri, J. L. Fernández-Alemán, J. N. Ros, and A. Toval, "Software cost estimation for global software development a systematic map and review study," in *Proceedings of the 2015 International Conference on Evaluation of Novel Approaches to Software Engineering (ENASE)*, pp. 197–206, Barcelona, Spain, April, 2015.

[76] M. Saroha and S. Sahu, "Tools & methods for software effort estimation using use case points model—a review," in *Proceedings of the International Conference on Computing, Communication & Automation*, pp. 874–879, Barcelona, Spain, April, 2015.

[77] K. Usharani, V. V. Ananth, and D. Velmurugan, "A survey on software effort estimation," in *Proceedings of the 2016 International Conference on Electrical, Electronics, and Optimization Techniques (ICEEOT)*, pp. 505–509, Chennai, India, March, 2016.

[78] B. Chinthanet, P. Phannachitta, Y. Kamei et al., "A review and comparison of methods for determining the best analogies in analogy-based software effort estimation," in *Proceedings of the 31st Annual ACM Symposium on Applied Computing*, pp. 1554–1557, Pisa, Italy, April, 2016.

[79] T. Arnuphaptrairong, "A literature survey on the accuracy of software effort estimation models," *Proceedings of the International MultiConference of Engineers and Computer Scientists*, vol. 2, pp. 16–18, 2016.

[80] A. Saeed, W. H. Butt, F. Kazmi, and M. Arif, "Survey of software development effort estimation techniques," in *Proceedings of the 2018 7th International Conference on Software and Computer Applications*, pp. 82–86, Kuantan, Malaysia, Febrauary, 2018.

[81] P. Sharma and J. Singh, "Systematic Literature Review on Software Effort Estimation Using Machine Learning Approaches," in *Proceedings of the 2017 International Conference on Next Generation Computing and Information Systems (ICNGCIS)*, pp. 43–47, IEEE, Jammu, India, December, 2017.

[82] S. Silva and C. Mario, "Use of non-functional requirements in software effort estimation: systematic review and experimental results," in *Proceedings of the 2017 5th International Conference in Software Engineering Research and Innovation (CONISOFT)*, pp. 1–9, IEEE, Merida, Mexico, Octobar, 2017.

[83] B. Sharma and R. Purohit, "Review of current software estimation techniques," in *Proceedings of the International Conference on Recent Developments in Science, Engineering and Technology*, pp. 380–399, Bangalore, India, April, 2017.

[84] F. Walkerden and R. Jeffery, "Software cost estimation: a review of models, process, and practice," *Advances in Computers*, vol. 44, pp. 59–125, 1997.

[85] B. Nie and S. Sun, "Using text mining techniques to identify research trends: a case study of design research," *Applied Sciences*, vol. 7, no. 4, p. 401, 2017.

[86] p. Mongeon and A. Paul-Hus, "The journal coverage of web of science and scopus: a comparative analysis," *Scientometrics*, vol. 106, no. 1, pp. 213–228, 2016.

[87] L. S. Adriaanse and C. Rensleigh, "Web of science, scopus and Google scholar," *The Electronic Library*, vol. 31, no. 6, pp. 727–744, 2013.